



PB96-136940

Development and Experimental Study of Semi-Active
Fluid Damping Devices for Seismic Protection of Structures

by

M.D. Symans and M.C. Constantinou

State University of New York at Buffalo
Department of Civil Engineering
Buffalo, New York 14260

Technical Report NCEER-95-0011

August 3, 1995

REPRODUCED BY: **NTIS**
U.S. Department of Commerce
National Technical Information Service
Springfield, Virginia 22161


This research was conducted at the State University of New York at Buffalo and was partially supported by the National Science Foundation under Grant No. BCS 90-25010 and the New York State Science and Technology Foundation under Grant No. NEC-91029.

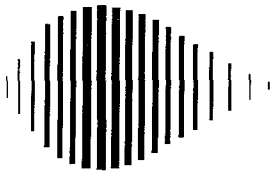
NOTICE

This report was prepared by the State University of New York at Buffalo as a result of research sponsored by the National Center for Earthquake Engineering Research (NCEER) through grants from the National Science Foundation, the New York State Science and Technology Foundation, and other sponsors. Neither NCEER, associates of NCEER, its sponsors, the State University of New York at Buffalo, nor any person acting on their behalf:

- a. makes any warranty, express or implied, with respect to the use of any information, apparatus, method, or process disclosed in this report or that such use may not infringe upon privately owned rights; or
- b. assumes any liabilities of whatsoever kind with respect to the use of, or the damage resulting from the use of, any information, apparatus, method, or process disclosed in this report.

Any opinions, findings, and conclusions or recommendations expressed in this publication are those of the author(s) and do not necessarily reflect the views of NCEER, the National Science Foundation, the New York State Science and Technology Foundation, or other sponsors.

REPORT DOCUMENTATION PAGE	1. REPORT NO. NCEER-95-0011	2.	3. 
4. Title and Subtitle Development and Experimental Study of Semi-Active Fluid Damping Devices for Seismic Protection of Structures		5. Report Date August 3, 1995	6.
7. Author(s) M.D. Symans and M.C. Constantinou		8. Performing Organization Rept. No.	
9. Performing Organization Name and Address State University of New York at Buffalo Department of Civil Engineering Buffalo, New York 14260		10. Project/Task/Work Unit No.	
		11. Contract(C) or Grant(G) No. (C) BCS 90-25010 (G) NEC-91029	
12. Sponsoring Organization Name and Address National Center for Earthquake Engineering Research State University of New York at Buffalo Red Jacket Quadrangle Buffalo, NY 14261		13. Type of Report & Period Covered Technical Report	
		14.	
15. Supplementary Notes This research was conducted at the State University of New York at Buffalo and was partially supported by the National Science Foundation under Grant No. BCS 90-25010 and the New York State Science and Technology Foundation under Grant No. NEC-91029.			
16. Abstract (Limit: 200 words) This report describes the development and testing of semi-active fluid damping devices for the control of structures subjected to seismic excitation. The semi-active dampers operate on the principle of fluid orificing and have mechanical properties which are controllable through modulation of fluid flow within the device. The experimental testing and analytical modeling of two different semi-active fluid damping devices is described. Furthermore, shaking table tests have been performed on a one-story and three-story model structure both with and without the semi-active damping system. The effectiveness of various control algorithms and time delay compensation methods is discussed. Analytical predictions of the shaking table test results are presented and shown to compare reasonably well with the experiments. It is concluded that, for the tested control algorithms, the semi-active control system afforded a substantial reduction of response in comparison to the response without the control system.			
17. Document Analysis a. Descriptors b. Identifiers/Open-Ended Terms Fluid damping devices. Semi-active control. Shaking table tests. Fluid orificing. Analytical models. Control algorithms. Time delay compensation methods. Earthquake engineering. c. COSATI Field/Group			
18. Availability Statement Release Unlimited		19. Security Class (This Report) Unclassified	21. No. of Pages 270
		20. Security Class (This Page) Unclassified	22. Price



PB96-136940



Development and Experimental Study of Semi-Active Fluid Damping Devices for Seismic Protection of Structures

by

M.D. Symans¹ and M.C. Constantinou²

August 3, 1995

Technical Report NCEER-95-0011

NCEER Task Numbers 93-5120 and 94-5103A

NSF Master Contract Number BCS 90-25010

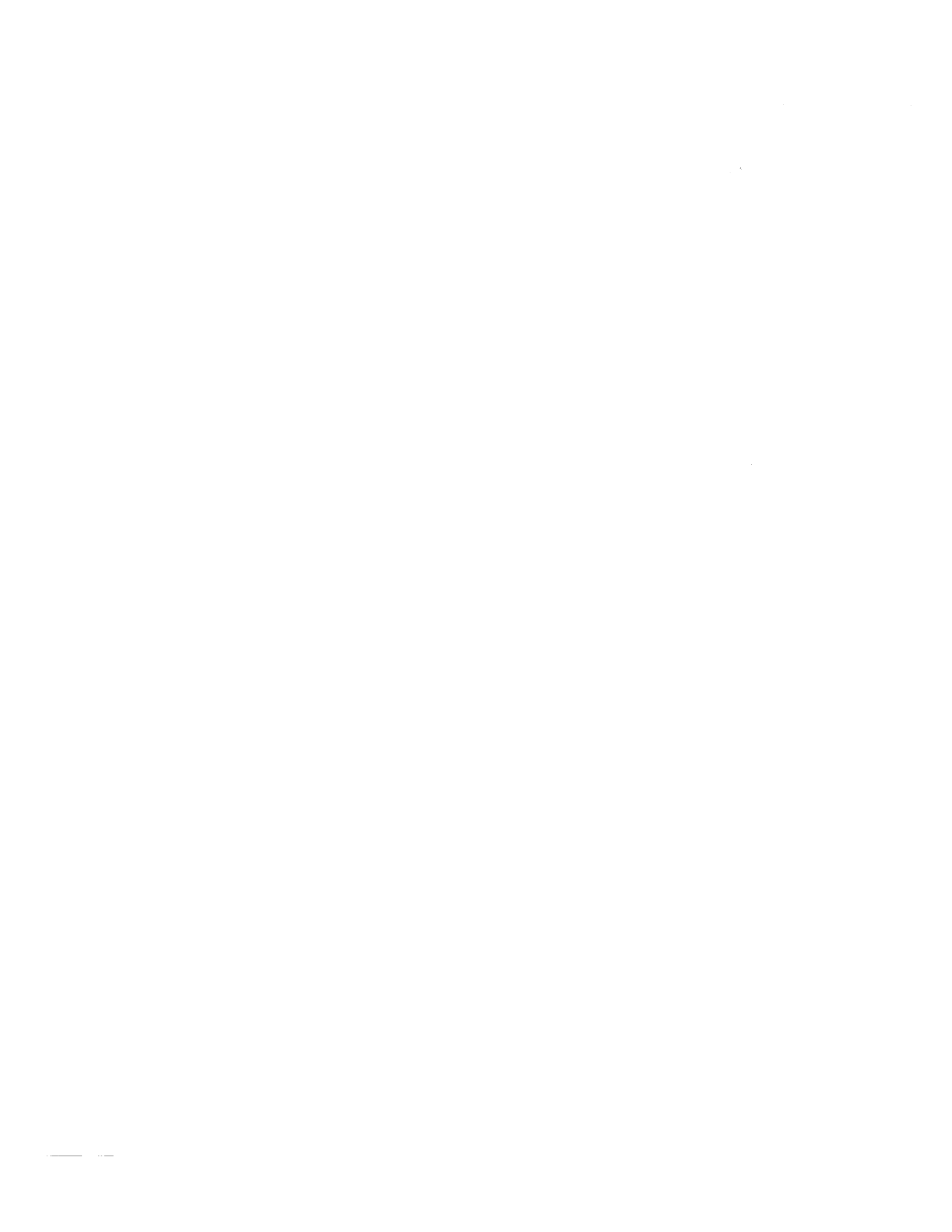
and

NYSSTF Grant Number NEC-91029

- 1 Assistant Professor, Department of Civil and Environmental Engineering, Washington State University
- 2 Professor, Department of Civil Engineering, State University of New York at Buffalo

NATIONAL CENTER FOR EARTHQUAKE ENGINEERING RESEARCH
State University of New York at Buffalo
Red Jacket Quadrangle, Buffalo, NY 14261

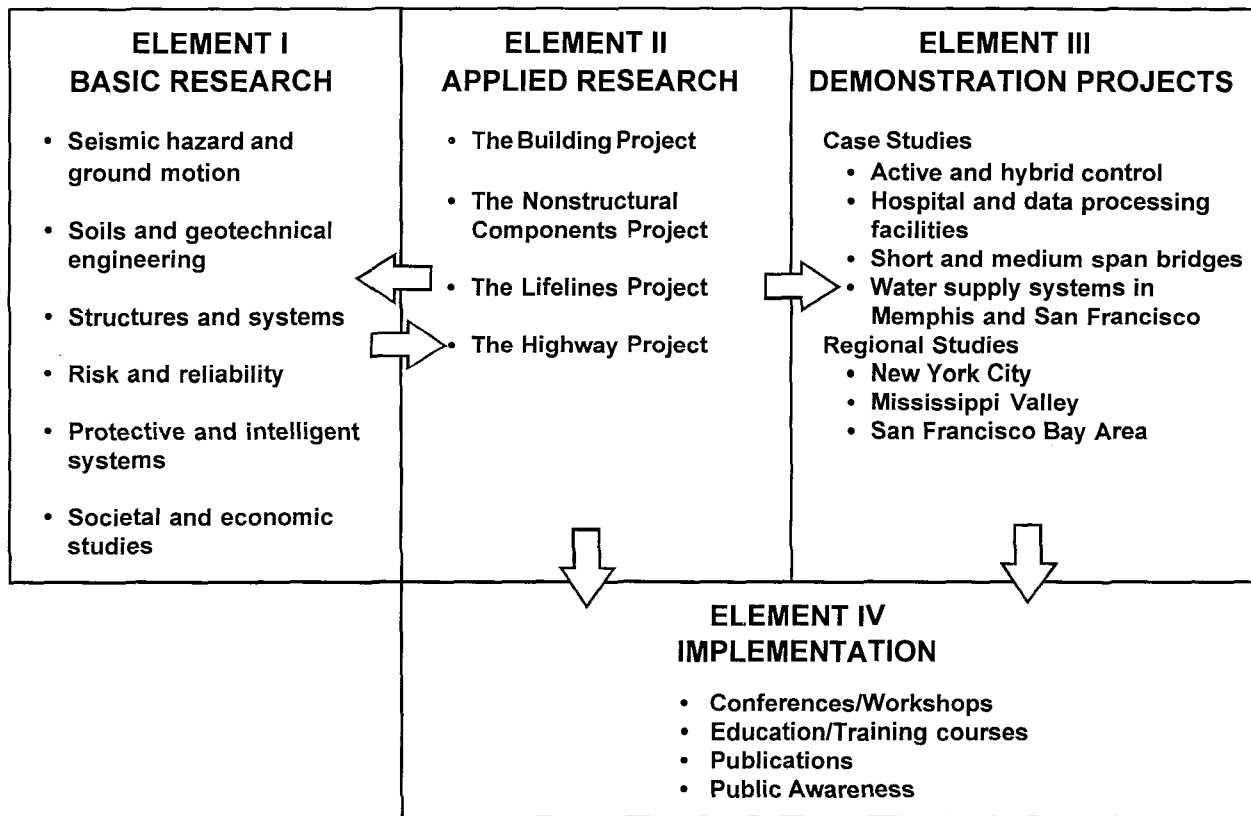
PROTECTED UNDER INTERNATIONAL COPYRIGHT
ALL RIGHTS RESERVED.
NATIONAL TECHNICAL INFORMATION SERVICE
U.S. DEPARTMENT OF COMMERCE



PREFACE

The National Center for Earthquake Engineering Research (NCEER) was established to expand and disseminate knowledge about earthquakes, improve earthquake-resistant design, and implement seismic hazard mitigation procedures to minimize loss of lives and property. The emphasis is on structures in the eastern and central United States and lifelines throughout the country that are found in zones of low, moderate, and high seismicity.

NCEER's research and implementation plan in years six through ten (1991-1996) comprises four interlocked elements, as shown in the figure below. Element I, Basic Research, is carried out to support projects in the Applied Research area. Element II, Applied Research, is the major focus of work for years six through ten. Element III, Demonstration Projects, have been planned to support Applied Research projects, and will be either case studies or regional studies. Element IV, Implementation, will result from activity in the four Applied Research projects, and from Demonstration Projects.



Research in the **Building Project** focuses on the evaluation and retrofit of buildings in regions of moderate seismicity. Emphasis is on lightly reinforced concrete buildings, steel semi-rigid frames, and masonry walls or infills. The research involves small- and medium-scale shake table tests and full-scale component tests at several institutions. In a parallel effort, analytical models and computer programs are being developed to aid in the prediction of the response of these buildings to various types of ground motion.

Two of the short-term products of the **Building Project** will be a monograph on the evaluation of lightly reinforced concrete buildings and a state-of-the-art report on unreinforced masonry.

The **protective and intelligent systems program** constitutes one of the important areas of research in the **Building Project**. Current tasks include the following:

1. Evaluate the performance of full-scale active bracing and active mass dampers already in place in terms of performance, power requirements, maintenance, reliability and cost.
2. Compare passive and active control strategies in terms of structural type, degree of effectiveness, cost and long-term reliability.
3. Perform fundamental studies of hybrid control.
4. Develop and test hybrid control systems.

In the passive control area, considerable work has been carried out at NCEER in research and development of supplemental fluid viscous dampers (e.g., Technical Report NCEER-92-0032). In this report, passive fluid viscous dampers are modified to operate as semi-active devices and the development and testing of these devices are reported. They operate on the principle of fluid orificing and have mechanical properties which are controllable through modulation of fluid flow within the device. Analytical and experimental results show that structural response reduction achieved by using such devices is comparable to that using a properly designed passive energy dissipation system. With further improvements, they are expected to provide better protection of structures than passive systems.

ABSTRACT

The research reported herein involves the development and testing of semi-active fluid damping devices for the control of structures subjected to seismic excitation. These devices may be utilized as part of a seismic isolation system or within the lateral bracing of a structure. The semi-active dampers operate on the principle of fluid orificing and have mechanical properties which are controllable through modulation of fluid flow within the device. The control forces acting on the structural system are developed as a result of the motion of the structure itself through appropriate adjustment of the mechanical properties of the device.

The experimental testing and analytical modeling of two different semi-active fluid damping devices is described in this report. Furthermore, shaking table tests have been performed on a one-story and three-story model structure both with and without the semi-active damping system. The effectiveness of various control algorithms and time delay compensation methods is discussed. Analytical predictions of the shaking table test results are presented and shown to compare reasonably well with the experiments.

It is concluded that, for the tested control algorithms, the semi-active control system afforded a substantial reduction of response in comparison to the response without the control system. Furthermore, the response reduction achieved by the semi-active control system was comparable to that afforded by a properly designed passive energy dissipation system. However, given the limitations of the tested hardware and control algorithms, it is not difficult to envision that the semi-active control system may be improved to the extent that it provides a further reduction of response beyond that afforded by the passive system.

ACKNOWLEDGMENTS

Financial Support for this project was provided by the National Center for Earthquake Engineering Research (Project Numbers 93-5120 and 94-5103A), Taylor Devices, Inc., and Moog Inc.

The fluid dampers used in the experiments were manufactured by Taylor Devices, Inc., North Tonawanda, New York. The assistance of Mr. Douglas P. Taylor, President, and Mr. Michael Muchow, Research Engineer, is appreciated.

The direct-drive servovalves used in the experiments were manufactured by Moog Inc., East Aurora, New York. The assistance of Mr. Kenneth D. Garnjost, Vice President of Engineering, and Mr. Michael P. Brooks, Senior Development Engineering Technician, is appreciated.

Professor Andrei M. Reinhorn of the State University of New York at Buffalo assisted in the development of the control algorithms used in the shaking table tests. Further, Dr. Panagiotis Tsopelas of the State University of New York at Buffalo assisted in the analytical predictions of the shaking table test results.

The assistance of the National Center for Earthquake Engineering Research laboratory staff in carrying out the experimental portion of this project is appreciated. In particular, acknowledgments are due to Mr. Mark Pitman, Instructional Support Specialist, Mr. Daniel Walch, Instructional Support Specialist, Mr. Richard Cizdziel, Senior Research Support Specialist, and Mr. Xiaoqing Gao, Electronics Specialist.



TABLE OF CONTENTS

SECTION	TITLE	PAGE
1	INTRODUCTION	1-1
1.1	Structural Control Strategies	1-1
1.1.1	Passive Control Systems	1-3
1.1.2	Active Control Systems	1-5
1.1.3	Semi-Active Control Systems	1-6
1.2	Objectives	1-7
2	LITERATURE REVIEW OF SEMI-ACTIVE CONTROL SYSTEMS	2-1
2.1	Vibration Isolation Applications	2-1
2.2	Automotive Vibration Control	2-3
2.3	Structural Vibration Control	2-6
2.3.1	Tuned Mass Dampers	2-8
2.3.2	Stiffness Control Devices	2-8
2.3.3	Electrorheological Dampers	2-10
2.3.4	Friction Dampers	2-15
2.3.5	Fluid Dampers	2-18
3	MECHANICAL PROPERTIES OF TESTED SEMI-ACTIVE FLUID DAMPERS	3-1
3.1	Description and Principles of Operation	3-1
3.1.1	Two-Stage Damper	3-6
3.1.2	Variable Damper	3-10
3.2	Component Testing Procedure	3-20
3.2.1	General Testing Arrangement	3-20
3.2.2	Two-Stage Damper	3-23
3.2.3	Variable Damper	3-25
3.3	Mechanical Properties	3-28
3.3.1	Theoretical Considerations	3-28
3.3.2	Two-Stage Damper	3-32
3.3.3	Variable Damper	3-42
3.4	System Response to Saturated Command Signal	3-63
3.4.1	Two-Stage Damper	3-66
3.4.2	Variable Damper	3-71

TABLE OF CONTENTS (Cont'd)

SECTION	TITLE	PAGE
4	ANALYTICAL MODELS OF SEMI-ACTIVE FLUID DAMPERS	
		4-1
4.1	Viscous Dashpot Model	4-1
4.2	Viscoelastic Maxwell Model	4-1
4.3	Fluid Mechanics Based Model	4-3
4.3.1	Analytical Predictions	4-8
5	STRUCTURAL MODEL FOR SEISMIC SIMULATION TESTING	
		5-1
5.1	Description of Model and Testing Configurations	5-1
5.1.1	One-Story Structure	5-1
5.1.2	Three-Story Structure	5-4
5.2	Test Program	5-12
5.3	Shaking Table Motions Used in Test Program	5-15
5.4	Measurement Instrumentation and Data Acquisition	5-21
5.5	Control Systems and Hardware	5-26
6	IDENTIFICATION OF STRUCTURAL PROPERTIES	
		6-1
6.1	Introduction	6-1
6.2	Method of Identification	6-1
6.3	Identification of One-Story Structure	6-3
6.3.1	Equation of Motion	6-3
6.3.2	Transfer Functions	6-4
6.3.3	Eigenvalue Problem	6-5
6.4	Identification of Multi-Story Structure	6-7
6.4.1	Equations of Motion	6-7
6.4.2	Construction of Stiffness and Damping Matrix	6-8
6.4.3	Transfer Functions of Structure without Fluid Dampers	6-9
6.4.4	Transfer Functions of Structure with Fluid Dampers	6-11
6.4.5	Eigenvalue Problem	6-12
6.5	Properties of One-Story and Three-Story Structure	6-13
6.6	Comparison of Experimental and Analytical Transfer Functions	6-17
7	CONTROL ALGORITHMS FOR SEISMIC SIMULATION TESTING	
		7-1
7.1	Introduction	7-1
7.2	One-Story Structure with Two-Stage Dampers	7-2
7.2.1	Base Shear Coefficient Control	7-2
7.2.2	Force Transfer Control	7-3

TABLE OF CONTENTS (Cont'd)

SECTION	TITLE	PAGE
7.3	One-Story Structure with Variable Dampers	7-4
7.3.1	Introduction	7-4
7.3.2	Feedforward Control	7-6
7.3.3	Skyhook Damping Control	7-8
7.4	Three-Story Structure with Variable Dampers	7-13
7.4.1	Linear Quadratic Regulator Optimal Control	7-13
7.4.2	Sliding Mode Control	7-21
8	SYSTEM TIME DELAYS AND METHODS OF COMPENSATION	8-1
8.1	Introduction	8-1
8.2	Kinematic Compensation	8-3
8.2.1	One-Story Structure	8-3
8.3	Harmonic Compensation	8-5
8.3.1	One-Story Structure	8-5
8.3.2	Three-Story Structure	8-6
8.4	Experimentally Measured Time Delays	8-8
8.4.1	Response Measurement Time Delay	8-8
8.4.2	Control Force Time Delay	8-11
9	SEISMIC SIMULATION TEST RESULTS	9-1
9.1	One-Story Structure	9-1
9.2	Three-Story Structure	9-17
9.3	Effectiveness of Semi-Active Control	9-32
9.3.1	Reduction of Peak Response	9-36
9.3.1.1	One-Story Structure	9-39
9.3.1.2	Three-Story Structure	9-47
9.3.2	Time Delay Compensation	9-59
9.3.2.1	One-Story Structure	9-59
9.3.2.2	Three-Story Structure	9-68
9.4	Comparison with an Active Control System	9-73
10	ANALYTICAL PREDICTION OF SEISMIC SIMULATION TEST RESULTS	10-1
10.1	Instantaneous Control Predictions	10-1
10.2	Predictions Including the Effect of Time Delays	10-1
10.3	Time History Response Analysis	10-2
10.3.1	One-Story Structure	10-4
10.3.2	Three-Story Structure	10-5

TABLE OF CONTENTS (Cont'd)

SECTION	TITLE	PAGE
10.4	Comparison of Experimental Results and Analytical Predictions	10-7
10.4.1	One-Story Structure	10-7
10.4.2	Three-Story Structure	10-28
11	CONCLUSIONS	11-1
12	REFERENCES	12-1
APPENDIX A: Data Acquisition and Instrumentation Specifications		A-1
Shaking Table Test Results		
Appendix B: One-Story Structure with No Dampers (Bare Frame)		B-1
Appendix C: One-Story Structure with Two-Stage Dampers		C-1
Appendix D: One-Story Structure with Variable Dampers		D-1
Appendix E: Three-Story Structure with No Dampers (Bare Frame)		E-1
Appendix F: Three-Story Structure with Variable Dampers		F-1

LIST OF ILLUSTRATIONS

FIGURE	TITLE	PAGE
1-1	Elements of a Passive Control System	1-2
1-2	Elements of an Active Control System	1-2
1-3	Elements of a Semi-Active Control System	1-4
2-1	Semi-Active Damper Described by Karnopp (1974)	2-2
2-2	Schematic of Semi-Active Variable Damper Experimentally Tested by Hamilton (1985)	2-4
2-3	Semi-Active Damper with Piston Head Solenoid Valve (from Wylie 1989)	2-5
2-4	An All-Mechanical Control System with Adjustable Damping Characteristics (from Ivers 1991)	2-7
2-5	Schematic of (a) SDOF Model with a Semi-Active Tuned Mass Damper Control System and (b) Semi-Active Variable Fluid Damper (from Hrovat 1983)	2-9
2-6	Semi-Active Stiffness Control Device (from Kobori 1993)	2-11
2-7	Testing Arrangement and Typical Hysteresis Loops For Semi-Active Electrorheological Damper at Two Electric Field Strengths (from Gavin 1994)	2-13
2-8	Electrorheological Fluid Damper Tested by Makris (1995)	2-14
2-9	Semi-Active Friction Damper (from Akbay 1991)	2-16
2-10	Cross-Sectional and Plan View of Semi-Active Friction Control Bearing (from Feng 1992)	2-17
2-11	Semi-Active Adjustable Force Device Tested by Kawashima (1992)	2-19
2-12	Hysteresis Loops of Semi-Active Fluid Damper Subjected to Constant Amplitude Sinusoidal Motion at a Frequency of 0.1 Hz (from Kawashima 1992)	2-20
2-13	Construction of Semi-Active Fluid Viscous Damper Described by Shinozuka (1992)	2-22
2-14	Schematic of Semi-Active Fluid Damper Described by Sack (1993)	2-24
3-1	Construction of Passive Fluid Viscous Damper	3-2
3-2	Construction of Semi-Active Fluid Viscous Damper	3-4
3-3	Photograph of Semi-Active Two-Stage Damper	3-8
3-4	Geometric and other Characteristics of Semi-Active Two-Stage Damper	3-9
3-5	Cross-Sectional View of Solenoid Valve Used in Semi-Active Two-Stage Damping System	3-11
3-6	Photograph of Semi-Active Variable Damper	3-13

LIST OF ILLUSTRATIONS (Cont'd)

FIGURE	TITLE	PAGE
3-7	Geometric and Other Characteristics of Semi-Active Variable Damper	3-14
3-8	Cross-Sectional View of Direct-Drive Servovalve Used in Semi-Active Variable Damper System	3-15
3-9	Schematic of a Typical Electrohydraulic Nozzle Flapper Servovalve	3-15
3-10	Recorded Values of Variable Damper Spool Displacement Due to Pseudo-Statically Applied Command Signal for a) Unit VAR-A and b) Unit VAR-B	3-17
3-11	Recorded Values of Direct-Drive Servovalve Flow Rate Due to Pseudo-Statically Applied Command Signal for a) Unit VAR-A and b) Unit VAR-B	3-18
3-12	Photograph of Testing Arrangement	3-21
3-13	Schematic of Testing Arrangement	3-22
3-14	Block Diagram of Two-Stage Damper Component Testing	3-24
3-15	Schematic of Semi-Active Two-Stage Damper Computer Control Circuit	3-26
3-16	Block Diagram of Variable Damper Component Testing	3-27
3-17	Experimental and Analytical Values of Damping Coefficient and Storage Stiffness of a Passive Fluid Viscous Damper (from Constantinou 1992b)	3-31
3-18	Diagram Describing Method of Extracting Damper Mechanical Properties From Component Test Results	3-36
3-19	Hysteresis Loops for Two-Stage Damper Switching from High Damping to Low Damping and Subjected to Sinusoidal Motion at a Frequency of a) 1 Hz and b) 2 Hz	3-38
3-20	Hysteresis Loop and Corresponding Command Signal for Two-Stage Damper	3-39
3-21	Hysteresis Loops for Two-Stage Damper Subjected to Constant Velocity Motion at a Frequency of 1 Hz and with Damping Switching from a) High to Low and b) Low to High	3-40
3-22	Experimental Values of Peak Force Versus Peak Velocity for Two-Stage Damper Unit a) 2ST-A and b) 2ST-B	3-41
3-23	Typical Force-Displacement Loops Under Constant Velocity Motion for the Variable Damper with Damping Switching from High to Low and Input Frequencies of a) 1 Hz and b) 0.5 Hz	3-48
3-24	Typical Force-Displacement Loops Under Constant Velocity Motion for the Variable Damper with Damping Switching from Low to High and Input Frequencies of a) 1 Hz and b) 0.5 Hz	3-49
3-25	Hysteresis Loop and Corresponding Command Signal and Spool Displacement for Variable Damper Two-Stage Test	3-50

LIST OF ILLUSTRATIONS (Cont'd)

FIGURE	TITLE	PAGE
3-26	Typical Force-Displacement Loops for Variable Damper Subjected to Constant Velocity Motion in a Multi-Stage Test with Damping Switching from a) High to Low and b) Low to High	3-57
3-27	Hysteresis Loops and Corresponding Command Signal and Spool Displacement for Variable Damper Multi-Stage Test	3-58
3-28	Typical Force-Displacement Loops for Variable Damper Subjected to Sinusoidal Motion in a Multi-Stage Test with Damping Switching from High to Low and Input Frequencies of a) 1 Hz and b) 2 Hz	3-59
3-29	Experimental Values of Peak Force Versus Peak Velocity for Variable Damper Under Three Different Command Signals for a) Unit VAR-A and b) Unit VAR-B	3-60
3-30	Experimental and Analytical Values of Damping Coefficient Versus Command Signal for Variable Damper a) Unit VAR-A and b) Unit VAR-B	3-62
3-31	Typical Constant Velocity Test from Which System Response Time is Evaluated	3-64
3-32	Example of Two-Stage Damper Test from Which Response Times were Extracted	3-67
3-33	Response Times for Two-Stage Damper Unit 2ST-A	3-68
3-34	Response Times for Two-Stage Damper Unit 2ST-B	3-69
3-35	Example of Variable Damper Test from Which Response Times were Extracted	3-72
3-36	Response Times for Variable Damper Unit VAR-A	3-73
3-37	Response Times for Variable Damper Unit VAR-B	3-74
4-1	Schematic of Semi-Active Damper Used to Generate Analytical Fluid Mechanics Based Model	4-4
4-2	Comparison of Analytical and Experimental Force-Displacement Loops for a Variable Damper Component Test With Sinusoidal Input at a Frequency of 1 Hz	4-12
5-1	Schematic of Model Structure (1 in = 25.4 mm)	5-2
5-2	Photograph of Model Structure on Shaking Table	5-3
5-3	Test Configurations for One-Story Structure (1 in = 25.4 mm)	5-5
5-4	Schematic of Damper Connection Details (1 in = 25.4 mm)	5-6
5-5	Photograph of One-Story Structure with No Dampers (Bare Frame)	5-7
5-6	Photograph of One-Story Structure with Two Semi-Active Two-Stage Dampers in the First Story	5-8

LIST OF ILLUSTRATIONS (Cont'd)

FIGURE	TITLE	PAGE
5-7	Close-Up View of Semi-Active Two-Stage Dampers Installed in First Story of Model Structure	5-9
5-8	Close-Up View of Semi-Active Variable Dampers Installed in First Story of Model Structure	5-10
5-9	Test Configurations for Three-Story Structure	5-11
5-10	Photograph of Three-Story Structure with No Dampers (Bare Frame)	5-13
5-11	Photograph of Three-Story Structure with Two Semi-Active Variable Dampers in the First Story	5-14
5-12	Time Histories of Displacement, Velocity, and Acceleration and Acceleration Spectrum of Shaking Table Excited by 75% of El Centro Motion	5-17
5-13	Time Histories of Displacement, Velocity, and Acceleration and Acceleration Spectrum of Shaking Table Excited by 100% of Hachinohe Motion	5-18
5-14	Time Histories of Displacement, Velocity, and Acceleration and Acceleration Spectrum of Shaking Table Excited by 100% of Modified Hachinohe Motion	5-19
5-15	Time Histories of Displacement, Velocity, and Acceleration and Acceleration Spectrum of Shaking Table Excited by 0.2g 5 Hz Harmonic Motion	5-20
5-16	Schematic of Model Structure Showing Location of Measurement Instrumentation	5-25
5-17	Block Diagram of Closed-Loop Shaking Table Tests with Semi-Active Two-Stage Dampers	5-27
5-18	Block Diagram of Closed-Loop Shaking Table Tests with Semi-Active Variable Dampers	5-28
5-19	Photograph of Control Computers and Associated Equipment for Semi-Active Two-Stage Dampers (right) and Variable Dampers (left)	5-31
6-1	Comparison of Experimental and Analytical Transfer Functions of One-Story Stiff Structure with No Dampers and with Two-Stage Dampers	6-18
6-2	Comparison of Experimental and Analytical Transfer Functions of One-Story Flexible Structure with No Dampers and with Two-Stage Dampers	6-19
6-3	Comparison of Experimental and Analytical Transfer Functions of One-Story Flexible Structure with No Dampers and with Variable Dampers	6-20

LIST OF ILLUSTRATIONS (Cont'd)

FIGURE	TITLE	PAGE
6-4	Comparison of Experimental and Analytical Transfer Functions of Three-Story Structure with No Dampers	6-21
6-5	Comparison of Experimental and Analytical Transfer Functions of Three-Story Structure with Variable Dampers Set to Low Damping	6-22
6-6	Comparison of Experimental and Analytical Transfer Functions of Three-Story Structure with Variable Dampers Set to High Damping	6-23
7-1	Relationship Between Experimental Damping Coefficient and Command Signal for Variable Dampers. Dashed Line Represents Approximate Relationship Used in Shaking Table Tests.	7-5
7-2	Comparison of Conventional and Skyhook Damping Displacement Transmissibilities	7-11
7-3	Diagram of Error Phase Plane Used in Sliding Mode Control Algorithm	7-24
8-1	Diagram For Analysis of Time Delays	8-2
8-2	Transfer Function and Phase Angle for Signal Conditioning Amplifier Subjected to Banded (0 - 20 Hz) White Noise	8-12
8-3	Transfer Function and Phase Angle for Analog Low-Pass Filter (Cut-Off Frequency = 25 Hz) Subjected to Banded (0 to 50 Hz) White Noise	8-13
8-4	Transfer Function and Phase Angle for Analog Differentiator Subjected to Banded (0 to 40 Hz) White Noise	8-14
8-5	Transfer Function and Phase Angle for Control Computation (Feedforward Control Algorithm) Subjected to Banded (0 to 20 Hz) White Noise	8-15
9-1	Base Shear-Drift Loops of One-Story Flexible Structure with Two-Stage Dampers Subjected to 25% El Centro and Controlled by Low and High Damping Passive Systems	9-12
9-2	Test Results for One-Story Flexible Structure with Two-Stage Dampers Subjected to Harmonic Motion and Controlled by Base Shear Coefficient Control Algorithm	9-13
9-3	Test Results for One-Story Flexible Structure with Variable Dampers Subjected to 100% Modified Hachinohe Motion and Controlled by Skyhook Control Algorithm	9-16

LIST OF ILLUSTRATIONS (Cont'd)

FIGURE	TITLE	PAGE
9-4	Test Results for Three-Story Structure with Variable Dampers Subjected to 25% El Centro Motion and Controlled by Low and High Damping Passive Control Systems	9-30
9-5	Test Results for Three-Story Structure with Variable Dampers Subjected to 125% Modified Hachinohe Motion and Controlled by Optimal Control Algorithm with High Gains and Harmonic Compensation	9-31
9-6	Base Shear-Drift Loop of One-Story Flexible Structure with Two-Stage Dampers Subjected to 50% Hachinohe and Controlled by High Damping Passive Control System and Semi-active Damping Control System	9-33
9-7	Base Shear-Drift Loops of One-Story Stiff Structure with Two-Stage Dampers Subjected to 25% El Centro Motion and Controlled by High Damping Passive Control System and Base Shear Coefficient Control Algorithm	9-35
9-8	Base Shear-Drift Loops of One-Story Flexible Structure with Variable Dampers Subjected to Two Different Ground Motions and Controlled by High Damping Passive Control System and Skyhook Control Algorithm	9-37
9-9	Comparisons of Peak Response of the Stiff One-Story Structure with Two-Stage Dampers Subjected to 25% El Centro Motion	9-40
9-10	Comparisons of Peak Response of the Flexible One-Story Structure with Two-Stage Dampers Subjected to a) 25% El Centro Motion and b) 50% Hachinohe Motion	9-41
9-11	Comparisons of Peak Response of Flexible One-Story Structure with Two-Stage Dampers Subjected to a) 100% Modified Hachinohe Motion and b) Harmonic Motion	9-42
9-12	Comparisons of Peak Response of Flexible One-Story Structure with Variable Dampers Subjected to a) 25% El Centro Motion and b) 50% Hachinohe Motion	9-43
9-13	Comparisons of Peak Response of Flexible One-Story Structure with Variable Dampers Subjected to a) 100% Modified Hachinohe Motion and b) Harmonic Motion	9-44
9-14	Comparison of Response of One-Story Flexible Structure with Two-Stage Dampers Subjected to Harmonic Motion and Controlled by a) Low Damping Passive Control System, b) High Damping Passive Control System, and c) Base Shear Coefficient Control Algorithm	9-46

LIST OF ILLUSTRATIONS (Cont'd)

FIGURE	TITLE	PAGE
9-15	Comparison of Peak Response Profiles for Three-Story Structure Subjected to 25% El Centro Motion and Controlled by Various Control Systems	9-48
9-16	Comparison of Peak Response Profiles for Three-Story Structure Subjected to 50% Hachinohe Motion and Controlled by Various Control Systems	9-49
9-17	Comparison of Peak Response Profiles for Three-Story Structure Subjected to 100% Modified Hachinohe Motion and Controlled by Various Control Systems	9-50
9-18	Comparison of Peak Response Profiles for Three-Story Structure Subjected to Harmonic Motion and Controlled by Various Control Systems	9-51
9-19	Comparison of Peak Response Profiles for Three-Story Structure Subjected to 25% El Centro Motion and Controlled by Various Control Systems	9-52
9-20	Comparison of Peak Response Profiles for Three-Story Structure Subjected to 50% Hachinohe Motion and Controlled by Various Control Systems	9-53
9-21	Peak Response of One-Story Flexible Structure with Two-Stage Dampers Subjected to 25% El Centro and 50% Hachinohe Motions and Controlled with and without Kinematic Compensation Applied to Control Algorithms	9-60
9-22	Peak Response of One-Story Flexible Structure with Two-Stage Dampers Subjected to 100% Modified Hachinohe Motion and Harmonic Motion and Controlled with and without Kinematic Compensation Applied to Control Algorithms	9-61
9-23	Peak Response of One-Story Flexible Structure with Two-Stage Dampers Subjected to Various Ground Motions and Controlled with and without Harmonic Compensation Applied to the Control Algorithms	9-62
9-24	Effect of Time Delay Compensation on Response of One-Story Structure Subjected to 25% El Centro	9-64
9-25	Comparison of Response of One-Story Structure Subjected to Harmonic Motion and Controlled with and without Time Delay Compensation	9-65
9-26	Test Results for One-Story Structure with Two-Stage Dampers Subjected to Harmonic Motion and Controlled by Base Shear Coefficient Control Algorithm with Kinematic Compensation	9-67

LIST OF ILLUSTRATIONS (Cont'd)

FIGURE	TITLE	PAGE
9-27	Comparison of Peak Response Profiles of Three-Story Structure Subjected to 25% El Centro and Controlled by Optimal Control Algorithm with and without Harmonic Compensation	9-69
9-28	Comparison of Peak Response Profiles of Three-Story Structure Subjected to 50% Hachinohe Motion and Controlled by Optimal Control Algorithm with and without Harmonic Compensation	9-70
9-29	Comparison of Peak Response Profiles of Three-Story Structure Subjected to 100% Modified Hachinohe Motion and Controlled by Optimal Control Algorithm with and without Harmonic Compensation	9-71
9-30	Comparison of Peak Response Profiles of Three-Story Structure Subjected to Harmonic Motion and Controlled by Optimal Control Algorithm with and without Harmonic Compensation	9-72
9-31	Comparison of Peak Response Profiles for Three-Story Structure Subjected to 25% El Centro Ground Motion and Controlled by Active Control System and Semi-Active Control System	9-75
9-32	Comparison of Semi-Active Optimal Control Test Results with High Damping Passive Control Test Results for Three-Story Structure Subjected to 50% El Centro Motion	9-77
10-1	Comparison of Experimental and Analytical Base Shear Versus Drift Loops of the One-Story Flexible Structure with Two-Stage Dampers Set to Low and High Damping	10-8
10-2	Comparison of Experimental and Analytical Base Shear Versus Drift Loops of One-Story Flexible Structure with Two-Stage Dampers Subjected to 25% El Centro Motion and Controlled by Base Shear Coefficient Control Algorithm	10-9
10-3	Comparison of Experimental and Analytical Base Shear Versus Drift Loops of One-Story Flexible Structure with Two-Stage Dampers Subjected to 50% Hachinohe Motion and Controlled by Base Shear Coefficient Control Algorithm	10-10
10-4	Comparison of Experimental and Analytical Base Shear Versus Drift Loops of One-Story Flexible Structure with Two-Stage Dampers Subjected to Harmonic Motion and Controlled by Base Shear Coefficient Control Algorithm	10-11

LIST OF ILLUSTRATIONS (Cont'd)

FIGURE	TITLE	PAGE
10-5	Comparison of Experimental and Analytical Base Shear Versus Drift Loops of One-Story Flexible Structure with Two-Stage Dampers Subjected to 25% El Centro Motion and Controlled by Force Transfer Control Algorithm	10-12
10-6	Comparison of Experimental and Analytical Base Shear Versus Drift Loops of One-Story Flexible Structure with Two-Stage Dampers Subjected to 50% Hachinohe Motion and Controlled by Force Transfer Control Algorithm	10-13
10-7	Comparison of Experimental and Analytical Base Shear Versus Drift Loops of One-Story Flexible Structure with Two-Stage Dampers Subjected to Harmonic Motion and Controlled by Base Shear Coefficient Control Algorithm with Kinematic Compensation	10-14
10-8	Comparison of Experimental and Analytical Base Shear Versus Drift Loops of One-Story Flexible Structure with Two-Stage Dampers Subjected to 50% Hachinohe Motion and Controlled by Force Transfer Control Algorithm with Kinematic Compensation	10-15
10-9	Comparison of Experimental and Analytical Base Shear Versus Drift Loops of One-Story Flexible Structure with Two-Stage Dampers Subjected to 50% Hachinohe Motion and Controlled by Force Transfer Control Algorithm with Kinematic Compensation	10-16
10-10	Comparison of Experimental and Analytical Base Shear Versus Drift Loop of One-Story Flexible Structure with Two-Stage Dampers Subjected to 100% Modified Hachinohe Motion and Controlled by Force Transfer Control Algorithm with Harmonic Compensation	10-17
10-11	Comparison of Experimental and Analytical Base Shear Versus Drift Loops of One-Story Flexible Structure with Two-Stage Dampers Subjected to Harmonic Motion and Controlled by Force Transfer Control Algorithm with Harmonic Compensation	10-18
10-12	Experimental and Analytical Time Histories of Various Response Quantities of One-Story Flexible Structure with Two-Stage Dampers Subjected to Harmonic Motion and Controlled by Base Shear Coefficient Control Algorithm	10-21
10-13	Comparisons of Experimental and Analytical Response of One-Story Flexible Structure with Two-Stage Dampers Subjected to Harmonic Motion and Controlled by Base Shear Coefficient Control Algorithm	10-22

LIST OF ILLUSTRATIONS (Cont'd)

FIGURE	TITLE	PAGE
10-14	Comparison of Experimental and Analytical Base Shear Versus Drift Loops of the One-Story Flexible Structure with Variable Dampers Set to Low and High Damping	10-24
10-15	Comparison of Experimental and Analytical Base Shear Versus Drift Loops of One-Story Flexible Structure with Variable Dampers Subjected to 25% El Centro Motion and Controlled by Skyhook Damping Algorithm	10-25
10-16	Comparison of Experimental and Analytical Base Shear Versus Drift Loops of One-Story Flexible Structure with Variable Dampers Subjected to 75% Hachinohe Motion and Controlled by Feedforward Control Algorithm	10-26
10-17	Comparison of Experimental and Analytical Results for One-Story Flexible Structure with Variable Dampers Subjected to 75% Hachinohe Motion and Controlled by Feedforward Control Algorithm	10-27
10-18	Comparison of Experimental and Analytical Story Shear Versus Story Drift Loops for Three-Story Structure Subjected to 25% Hachinohe Motion with Variable Dampers Set to Low Damping	10-29
10-19	Comparison of Experimental and Analytical Story Shear Versus Story Drift Loops for Three-Story Structure Subjected to 50% El Centro Motion with Variable Dampers Set to High Damping	10-30
10-20	Comparison of Experimental and Analytical Story Shear Versus Story Drift Loops for Three-Story Structure Subjected to 50% El Centro Motion with Variable Dampers Controlled by Optimal Control Algorithm with Low Gains	10-31
10-21	Comparison of Experimental and Analytical Story Shear Versus Story Drift Loops for Three-Story Structure Subjected to 50% El Centro Motion with Variable Dampers Controlled by Optimal Control Algorithm with High Gains	10-32
10-22	Comparison of Experimental and Analytical Story Shear Versus Story Drift Loops for Three-Story Structure Subjected to 50% El Centro Motion with Variable Dampers Controlled by Optimal Control Algorithm with Low Gains and Harmonic Compensation	10-33
10-23	Comparison of Experimental and Analytical Story Shear Versus Story Drift Loops for Three-Story Structure Subjected to Harmonic Motion with Variable Dampers Controlled by Optimal Control Algorithm with High Gains and Harmonic Compensation	10-34

LIST OF ILLUSTRATIONS (Cont'd)

FIGURE	TITLE	PAGE
10-24	Comparison of Experimental and Analytical Story Shear Versus Story Drift Loops for Three-Story Structure Subjected to 75% El Centro Motion with Variable Dampers Controlled by Sliding Mode Control Algorithm	10-36
10-25	Comparison of Experimental and Analytical Story Shear Versus Story Drift Loops for Three-Story Structure Subjected to 75% Hachinohe Motion with Variable Dampers Controlled by Sliding Mode Control Algorithm	10-37
10-26	Comparison of Experimental and Analytical Story Shear Versus Story Drift Loops for Three-Story Structure Subjected to Harmonic Motion with Variable Dampers Set to Low Damping and Analytical Predictions Based on Alternate Model of Structure	10-40
10-27	Comparison of Experimental and Analytical Results for Three-Story Structure Subjected to 75% Hachinohe Motion with Variable Dampers Controlled by Sliding Mode Control Algorithm	10-41

LIST OF TABLES

TABLE	TITLE	PAGE
3-I	Experimentally Tested Semi-Active Damper Systems	3-7
3-II	Notation for Semi-Active Damper Units Tested	3-7
3-III	Summary of Two-Stage Damper Component Tests	3-33
3-IV	Summary of Variable Damper Component Tests (Two-Stage Tests)	3-43
3-V	Summary of Variable Damper Component Tests (Multi-Stage Tests)	3-52
3-VI	Average System Response Times for Two-Stage Damper	3-70
3-VII	Average System Response Times for Variable Damper	3-75
4-I	Values of Parameters Used in Fluid Mechanics Based Model	4-11
5-I	Earthquake Motions Used in Shaking Table Test Program and Characteristics in Prototype Scale	5-16
5-II	Data Acquisition Channels (with reference to Figure 5-16)	5-22
6-I	Properties of One-Story Model Structure at Small Amplitude of Vibration	6-14
6-II	Properties of Three-Story Model Structure at Small Amplitude of Vibration	6-16
7-I	Values of Parameters Used in Control Algorithms for Shaking Table Tests with Variable Dampers	7-12
8-I	Experimentally Measured Time Delays	8-9
9-I	Summary of Experimental Results for Bare Frame One-Story Structure	9-2
9-II	Summary of Experimental Results for One-Story Structure with Two-Stage Dampers	9-3
9-III	Summary of Experimental Results for One-Story Structure with Variable Dampers	9-7
9-IV	Summary of Experimental Results for Bare Frame Three-Story Structure	9-18
9-V	Summary of Experimental Results for Three-Story Structure with Variable Dampers	9-19
9-VI	Notation for Shaking Table Test Results	9-38
9-VII	Comparison of Experimental Results from Active and Semi-Active Control Tests	9-74

LIST OF TABLES (Cont'd)

TABLE	TITLE	PAGE
10-I	Time Delays for Numerical Analysis of Response of One-Story Structure with Two-Stage Dampers (with reference to Figure 8-1)	10-3
10-II	Time Delays for Numerical Analysis of Response of One-Story and Three-Story Structure with Variable Dampers (with reference to Figure 8-1)	10-3
A-I	Data Acquisition Channel Specifications	A-2
A-II	Instrumentation Specifications for Transducers Located on the Model Structure (with reference to Figure 5-16)	A-4
A-III	Strain Gage Signal Conditioner Specifications	A-5

SECTION 1

INTRODUCTION

1.1 Structural Control Strategies

The control of structures subjected to seismic excitation represents a challenging task for the civil engineering profession. The traditional approach to seismic hazard mitigation is to design structures with sufficient strength capacity and the ability to deform in a ductile manner. Alternatively, newer concepts of structural control, including both passive and active control systems, have been growing in acceptance and may preclude the necessity of allowing for inelastic deformations in the structural system. A compromise between passive and active control systems has been developed recently in the form of semi-active control systems. Semi-active control systems maintain the reliability of passive control systems while taking advantage of the adjustability of an active control system.

The three basic approaches to structural control may be defined as follows:

Passive Control Systems

A passive control system may be defined as a system which does not require an external power source for operation and utilizes the motion of the structure to develop the control forces. Control forces are developed as a function of the response of the structure at the location of the passive control system (see Figure 1-1).

Active Control Systems

An active control system may be defined as a system which requires a large power source for operation of electrohydraulic actuators which supply control forces to the structure. Control forces are developed based on feedback from

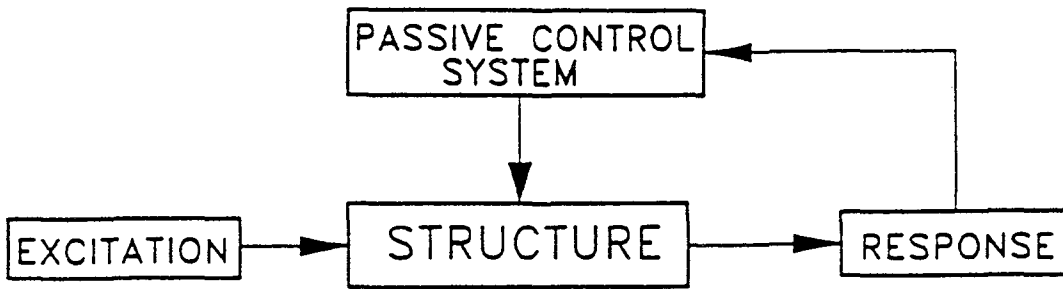


Figure 1-1 Elements of a Passive Control System

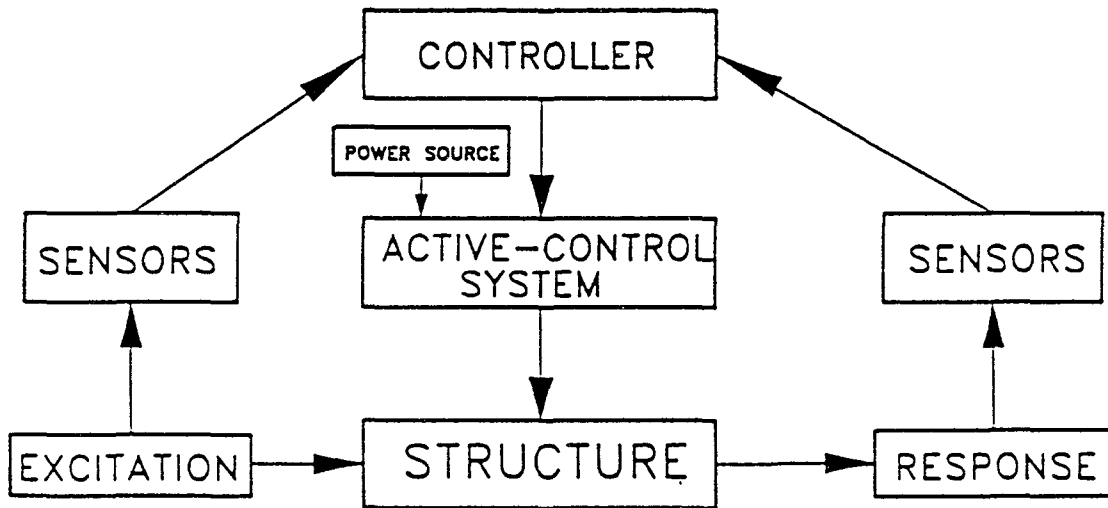


Figure 1-2 Elements of an Active Control System

sensors that measure the excitation and/or the response of the structure. The feedback from the structural response may be measured at locations remote from the location of the active control system (see Figure 1-2).

Semi-Active Control Systems

A semi-active control system may be defined as a system which typically requires a small external power source for operation (e.g., a battery) and utilizes the motion of the structure to develop the control forces. Control forces are developed based on feedback from sensors that measure the excitation and/or the response of the structure. The feedback from the structural response may be measured at locations remote from the location of the semi-active control system (see Figure 1-3).

1.1.1 Passive Control Systems

A passive control system may be used to increase the energy dissipation capacity of a structure through localized, discrete energy dissipation devices located either within a seismic isolation system or over the height of the structure. Such systems may be referred to as supplemental energy dissipation systems and have been reviewed by Soong (1994), ATC (1994 and 1993), EERI (1993), and Constantinou (1993a and 1992b). The objective of these systems is to absorb a significant amount of the seismic input energy, thus reducing the demand on the structural system. Depending on their construction, these systems may also increase the stiffness and strength of the structure to which they are attached (ATC 1994). A passive control system does not require an external power source for operation. Rather, the motion of the structure is utilized to produce relative motion within the passive control devices which, in turn, dissipates energy. Supplemental

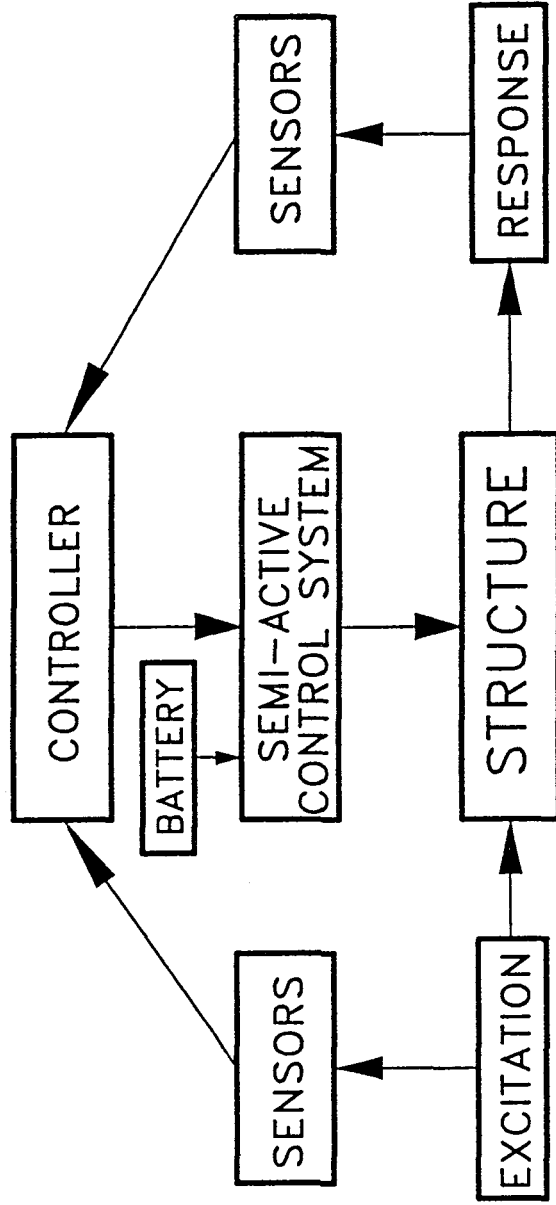


Figure 1-3 Elements of a Semi-Active Control System

energy dissipation devices may take many forms and dissipate energy through a variety of mechanisms including the yielding of mild steel, viscoelastic action in rubber-like materials, shearing of viscous fluid, orificing of fluid, and sliding friction. A discussion on the operation and performance of supplemental energy dissipation devices has been presented by Constantinou (1993a and 1992b), Soong (1994), and ATC (1994).

Seismic isolation systems represent another form of passive control systems. In these systems, a flexible isolation system is introduced between the foundation and superstructure so as to increase the natural period of the system. The increase in flexibility typically results in the deflection of a major portion of the earthquake energy; reducing accelerations in the superstructure while permitting an increase in displacement across the isolation level. Seismic isolation systems are discussed by Soong (1994), Kelly (1993), Skinner (1993), EERI (1990), and ATC (1993).

1.1.2 Active Control Systems

The control forces within an active control system are generated by electrohydraulic actuators based on feedback from the excitation and/or from the measured response of the structure. The feedback measurements are monitored by a controller (a computer) which, based on a pre-determined control algorithm, determines the appropriate control signal for operation of the actuators. The generation of control forces by electrohydraulic actuators requires large power sources, which are on the order of tens of kilowatts for small structures and may reach several megawatts for large structures (Reinhorn, 1992). Active

control systems may also be designated as active energy dissipation systems since the primary effect of an active control system is to modify the level of damping with a minor modification of stiffness (Dyke 1994 and Soong 1990). An overview of active structural control is provided by Soong (1994 and 1991) and numerous papers on the subject are available (e.g., International Association for Structural Control (1994) and ATC (1993)).

1.1.3 Semi-Active Control Systems

Semi-active control systems have only very recently been considered for structural control applications. A semi-active control system generally originates from a passive control system which has been subsequently modified to allow for the adjustment of mechanical properties. Specifically, supplemental energy dissipation devices which dissipate energy through shearing of viscous fluid, orificing of fluid, and sliding friction have been modified to behave in a semi-active manner (a more detailed discussion of these devices is provided in Section 2.3). The mechanical properties of these systems may be adjusted based on feedback from the excitation and/or from the measured response. As in an active control system, a controller monitors the feedback measurements and generates an appropriate command signal for the semi-active devices. As in a passive control system, however, the control forces are developed as a result of the motion of the structure itself. The control forces are developed through appropriate (based on a pre-determined control algorithm) adjustment of the mechanical properties of the semi-active control system. Furthermore, the control forces in a semi-active control system are always in a direction which opposes the motion of the structural system and therefore promote the overall stability of the

structure. Semi-active control systems generally require a small amount of external power for operation (on the order of tens of watts).

1.2 Objectives

The objectives of this research included the following:

- a) Development of semi-active fluid dampers in cooperation with two industry partners.
- b) Testing and identification of mechanical properties of the developed semi-active fluid dampers.
- c) Development of analytical models to describe the dynamic behavior of semi-active fluid dampers.
- d) Selection of appropriate control algorithms for operation of semi-active fluid dampers.
- e) Seismic simulation testing of a one-story and three-story model structure with and without semi-active fluid dampers.
- f) Evaluation of the effects of time delays and methods of time delay compensation.
- g) Comparison of experimental performance of structural systems with a semi-active damper control system, a passive high damping control system, and no control system.
- h) Comparison of experimental shaking table results with results obtained from time history analysis.
- i) Interpretation of results.

SECTION 2

LITERATURE REVIEW OF SEMI-ACTIVE CONTROL SYSTEMS

Semi-active control systems were proposed as early as the 1920's when a patent was issued for automobile shock absorbers which utilized a seismic mass to activate hydraulic valving (no power required) or utilized a solenoid valve for directing fluid flow (small amount of power required) (Karnopp 1974). Within the field of structural engineering, Hrovat (1983) was apparently the first to discuss the concept of semi-active structural control for systems subjected to environmental loads. A large amount of research on semi-active control systems has been performed in other fields of engineering (primarily automotive and mechanical).

2.1 Vibration Isolation Applications

Analytical studies on semi-active damper systems for general vibration isolation applications have been performed by, for example, Karnopp (1990, 1974), Rakheja (1985), and Alanoly (1987). Karnopp (1974) investigated semi-active damping devices such as that shown in Figure 2-1 which resembles a conventional hydraulic shock absorber except that the hydraulic pressure is controlled by a pair of poppet valves. Two valves are used to independently control the damping during compression and during tension. The relative merits of "skyhook" control (output force proportional to absolute velocity) and conventional control (output force proportional to relative velocity) for vibration isolation were examined. Rakheja (1985) analytically studied the vibration and shock isolation

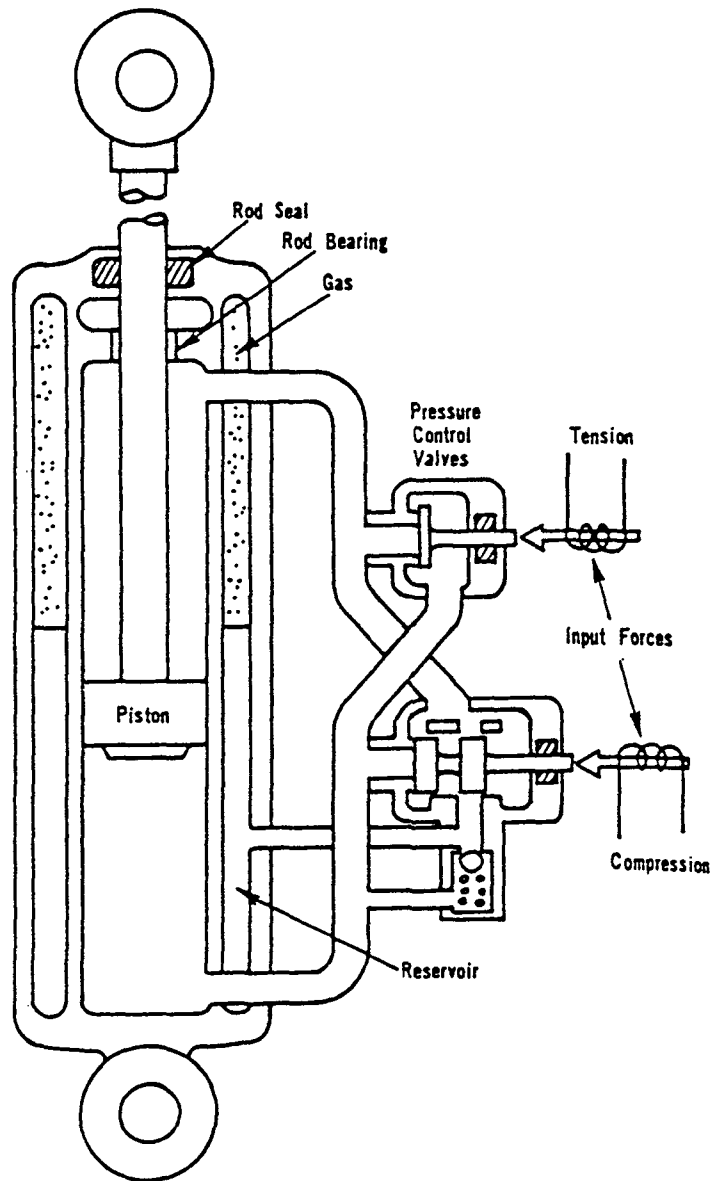


Figure 2-1 Semi-Active Damper Described by Karnopp (1974)

performance of a SDOF (single-degree-of-freedom) spring-mass-damper system in which the damper was a two-stage (high damping or low damping) semi-active device. The control algorithm utilized directly measurable quantities (relative displacement and relative velocity of the mass) to determine the appropriate command signal for the semi-active damper. One conclusion of the study was that time delays associated with operation of solenoid valves can significantly affect semi-active damper behavior. Alanoly (1987) performed a study similar to Rakheja (1985) in which the semi-active damper fluid flow orifices could be continuously modulated (i.e., a variable damper).

2.2 Automotive Vibration Control

Within the automotive engineering field, semi-active control devices have been studied extensively. A majority of the studies on semi-active dampers for automotive applications have been of an analytical nature. In contrast, Hamilton (1985) experimentally investigated the performance of a semi-active suspension system consisting of an electronically controlled damping device (see Figure 2-2). The damping device uses a control valve in combination with two pressure regulators to provide variable damping in compression and in tension. An experimental investigation of a semi-active control system used within a full-scale vehicle is discussed by Crolla (1987).

A semi-active damper containing a solenoid-actuated piston valve (contained within the piston head) is described by Wylie (1989). A schematic of the device is shown in Figure 2-3. A mathematical model based on fundamental mechanics principles was developed to

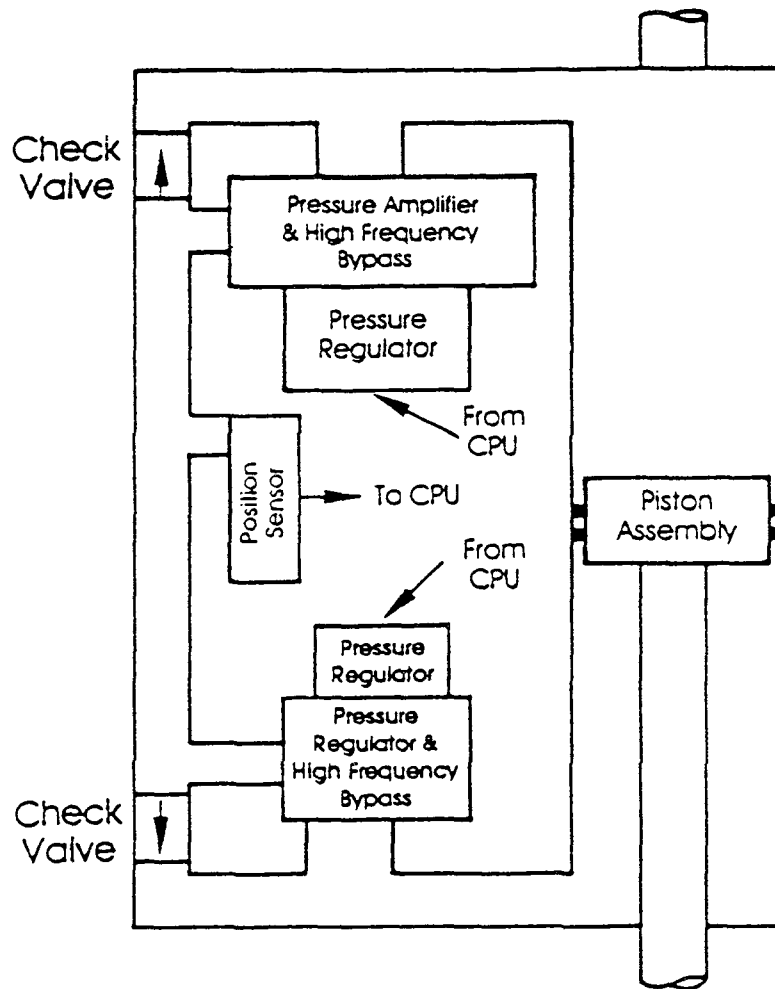


Figure 2-2 Schematic of Semi-Active Variable Damper Experimentally Tested by Hamilton (1985)

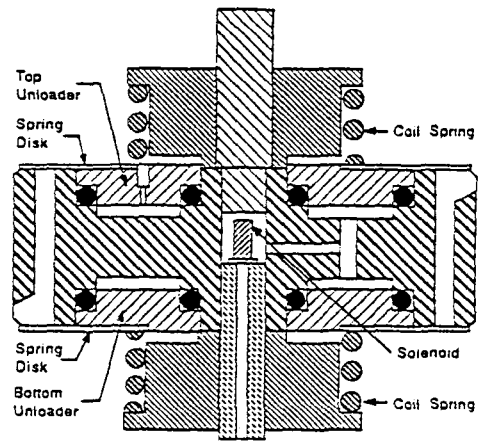
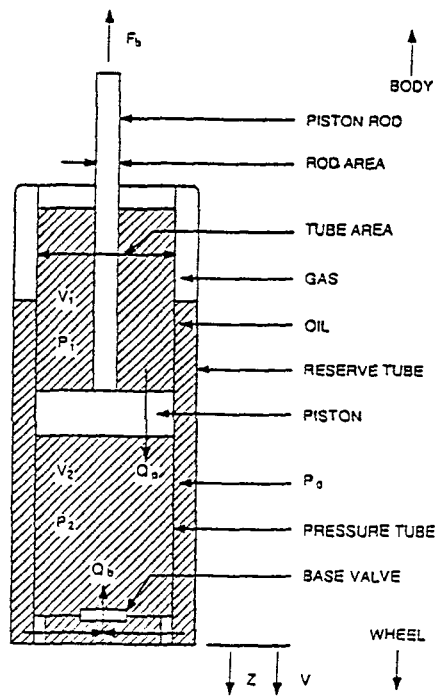


Figure 2-3 Semi-Active Damper with Piston Head Solenoid Valve (from Wylie 1989)

describe the damper behavior and numerical results were compared with experimental measurements. The piston valve response time was reported to be on the order of 10 to 15 msec.

Duchnowski (1989) provides a detailed hydraulic model of a two-stage semi-active solenoid-operated shock absorber. The hydraulic model is based on the principles of mass conservation and force equilibrium. The device contains a normally open voice coil solenoid valve within the wall of a hollow piston rod. The author discusses the need for an extremely fast valve response time and reports a control valve close time of about 7 msec and an open time of about 20 msec for actual valve hardware. Furthermore, time lags in the building up of hydraulic forces in the shock absorbers were shown to significantly affect system performance.

The evolution of semi-active suspension technology is presented by Ivers (1991). A discussion on hardware and control algorithms is presented. Of particular interest is the description of an all-mechanical semi-active control system (see Figure 2-4). These systems eliminate the requirement for sensors and microprocessors through the use of hydraulic circuitry and mechanical feedback.

2.3 Structural Vibration Control

The development and experimental testing of semi-active control systems for applications in structural response control has only been pursued in the recent past (5 years or less).

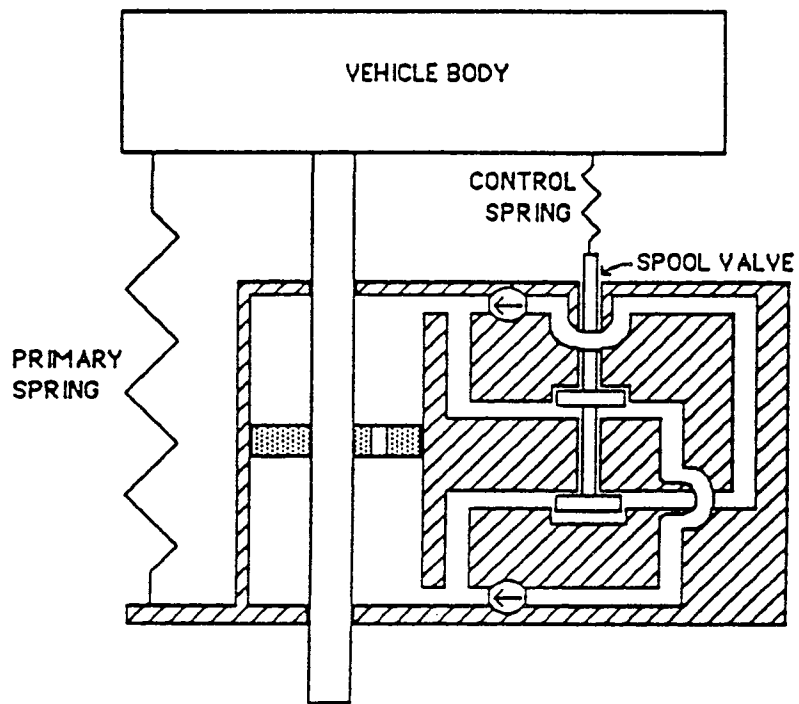


Figure 2-4 An All-Mechanical Control System with Adjustable Damping Characteristics (from Ivers 1991)

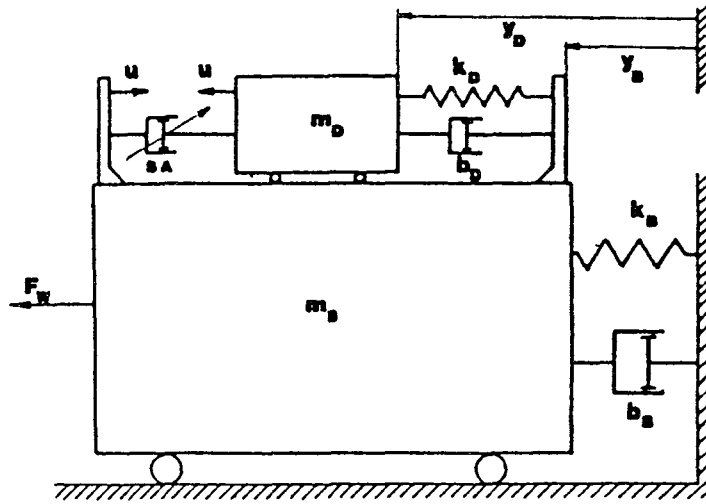
Therefore, many of these systems are quite primitive and a comparison among various systems may not be appropriate as it would be in a subject which has seen a more mature level of research. With that in mind, the following review of semi-active control systems for structural vibration control focuses on a description of semi-active control hardware, principles of operation of the hardware, and some results from small-scale component testing.

2.3.1 Tuned Mass Dampers

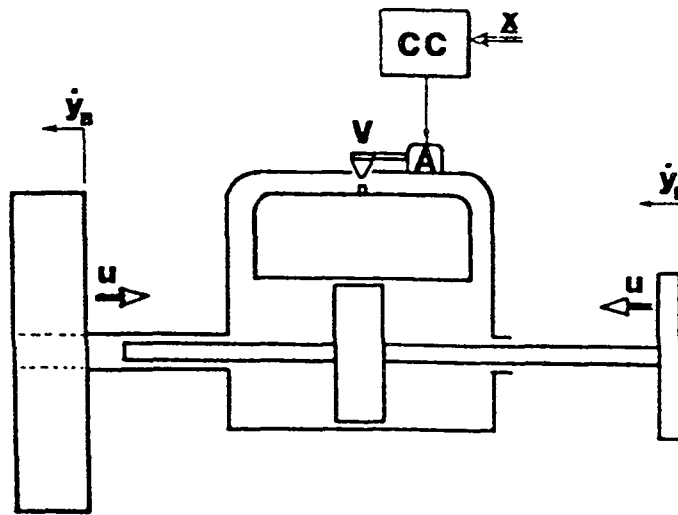
Hrovat (1983) examined a semi-active tuned mass damper (TMD) for control of wind induced vibrations in tall buildings (see Figure 2-5). A small amount of external power is required to modulate the damping within the semi-active fluid damper. Simulation studies were performed to demonstrate that the semi-active TMD is superior to the passive TMD and comparable to an active TMD. The authors note that the extension of the semi-active control concept from the vehicle vibration isolation field to the structural control of buildings is extremely promising in view of the relatively low bandwidth requirements (less than about 5 Hz) compared with that of vehicle suspensions (up to about 50 Hz).

2.3.2 Stiffness Control Devices

A semi-active stiffness system for seismic response control of structures has been described by Kobori (1993). The authors refer to the semi-active stiffness device as a "variable stiffness device" and this notation will be followed. The variable stiffness system primarily controls the stiffness of a building to establish a non-resonant condition during



(a)



(b)

Figure 2-5 Schematic of (a) SDOF Model with a Semi-Active Tuned Mass Damper Control System and (b) Semi-Active Variable Fluid Damper (from Hrovat 1983)

earthquakes. The variable stiffness devices are engaged or released so as to include or not include, respectively, the stiffness of the bracing system of the structure. A schematic of the variable stiffness device is shown in Figure 2-6. The device is composed of a balanced (double-acting piston rod) hydraulic cylinder with a normally closed solenoid control valve inserted in the tube connecting the two cylinder chambers. The solenoid valve can either be on or off, thus opening or closing, respectively, the fluid flow path through the tube. When the valve is closed (off), the fluid can not flow and effectively locks the beam to the braces below. When the valve is open (on), the fluid flows freely and disengages the beam/brace connection. The operation of each device consumes approximately 20 W of power. The system also offers fail-safe characteristics in that the interruption of power causes the variable stiffness devices to automatically engage, thus increasing the stiffness of the structure. According to the behavior described above, this device may be more appropriately designated as a "two-stage" stiffness device. Note that each two-stage stiffness device within a structure can be controlled independently and therefore the combination of the two-stage stiffness devices and the structure may be designated as a semi-active variable stiffness system.

2.3.3 Electrorheological Dampers

Electrorheological dampers contain dielectric particles suspended within a fluid (typically oil). In the presence of an adjustable electric field, the behavior of the electrorheological material can be regulated. As the electric field surrounding the damper increases, the behavior of the electrorheological material changes from that of a viscous fluid to that of a

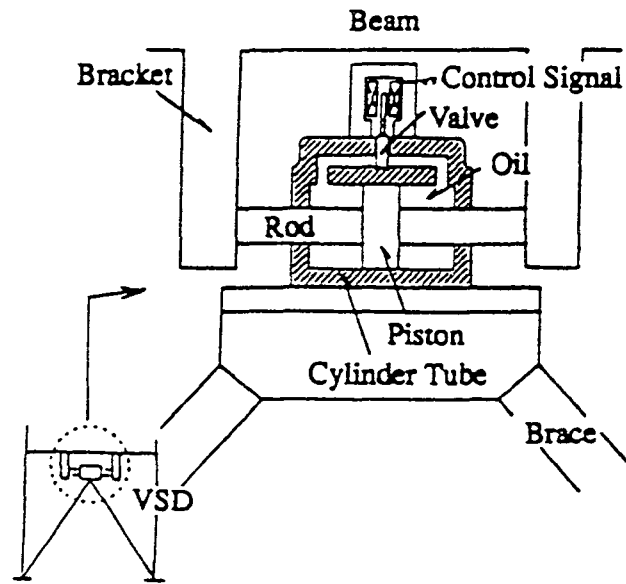


Figure 2-6 Semi-Active Stiffness Control Device (from Kobori 1993)

yielding solid. Currently available electrorheological materials are capable of resisting shear stresses of up to 7 kPa (\approx 0.1 psi) before yielding.

Experimental component tests have been performed by Gavin (1994) on an electrorheological damper using the arrangement shown in Figure 2-7. An actuator is used to impose the motion of a single prismatic plunger through electrorheological fluid contained within an open box. The electric field is generated by charging the plunger and connecting the open box to ground. The range of electric field strength used in the tests was 0 kV/mm to 3.2 kV/mm. Typical hysteresis loops are shown in Figure 2-7 in which the imposed displacement was a sinusoidal function with a frequency of 0.83 Hz and steadily increasing amplitudes. The maximum power required during the tests shown in Figure 2-7 was 5 W. Note, however, that the peak force developed in the device is only 40 N.

Makris (1995) has tested an electrorheological fluid damper which consists of a cylinder containing a balanced piston rod and a piston head that pushes electrorheological fluid through an annular duct (see Figure 2-8). Damping forces are developed as the result of both shearing of the fluid (electrorheological effect) and orificing of the fluid (viscous effect). Results indicate that the average fluid velocity within the electrorheological duct must be relatively small so that viscous stresses do not dominate over yield stresses associated with electrorheological fluid behavior.

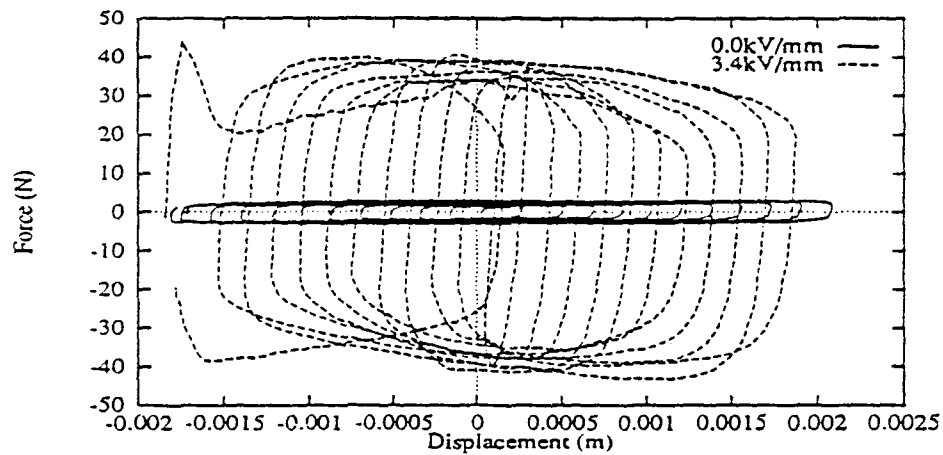
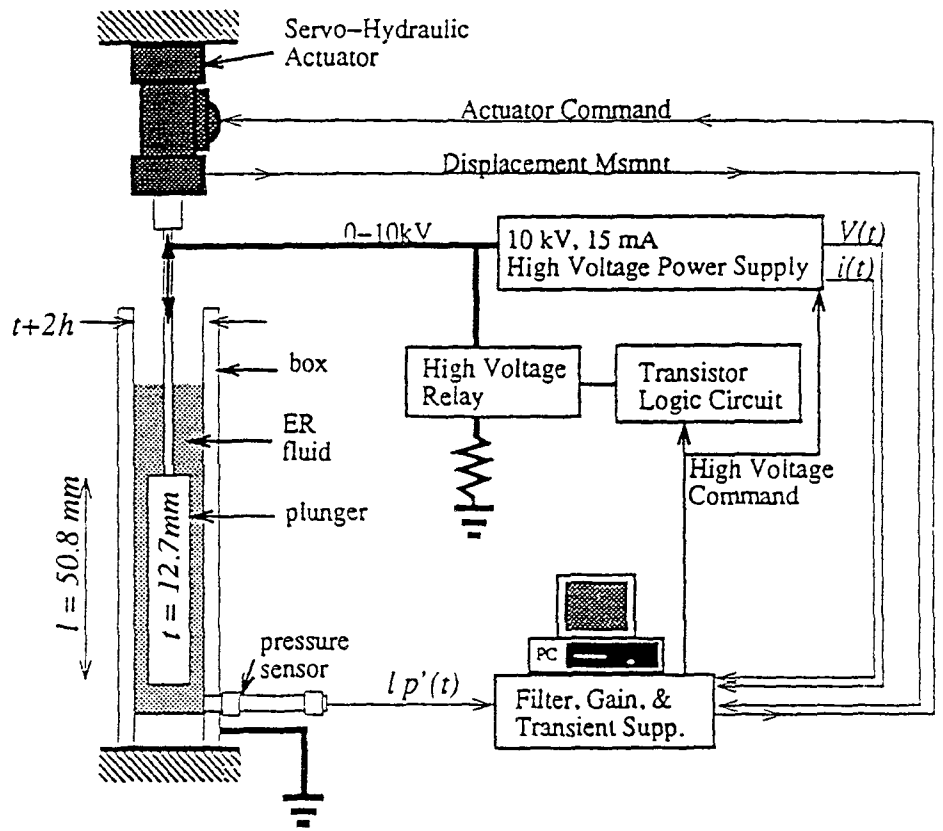


Figure 2-7 Testing Arrangement and Typical Hysteresis Loops For Semi-Active Electrorheological Damper at Two Electric Field Strengths (from Gavin 1994)

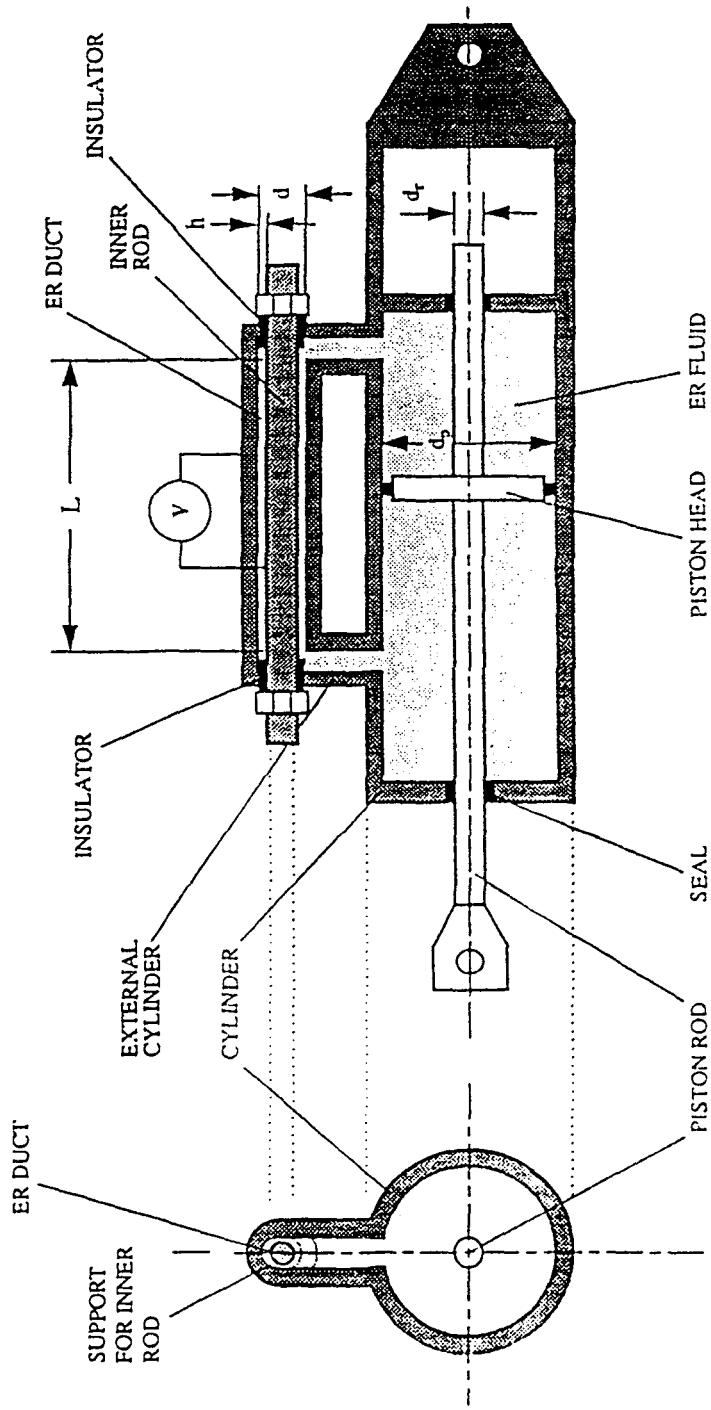


Figure 2-8 Electro-rheological Fluid Damper Tested by Makris (1995)

2.3.4 Friction Dampers

Akbay (1991) describes an energy dissipation system which is based on the control of friction within the bracing of a structure. A schematic of the semi-active friction control device is shown in Figure 2-9. The friction force is modified by the adjustment of the clamping force (normal force) on the friction interface of the device. When the axial force in the brace exceeds the friction force, the brace slips axially through the friction interface resulting in the dissipation of energy in an amount equal to the brace axial force multiplied by the slip displacement. Note that the axial brace force may be controlled within the range of zero force to the buckling or yield strength of the brace.

An isolation system incorporating semi-active friction controllable sliding bearings has been analytically and experimentally investigated by Feng (1992). The friction force on the sliding interface between the superstructure and the foundation is controlled so as to limit the sliding displacement and minimize the transfer of seismic force to the superstructure. A cross-sectional and plan view of the semi-active friction control bearing is shown in Figure 2-10. Each bearing has a fluid chamber in which the pressure can be modified through a pressure control system composed of a servovalve, an accumulator, and a computer. The normal force at the sliding bearing interface is controlled by modulation of the fluid pressure which, in turn, regulates the friction force. The computer control signal for fluid pressure is determined as a function of the response of the structure. Two control algorithms were developed for controlling the friction force in a sliding isolation system. The first was based on instantaneous optimal control in which a

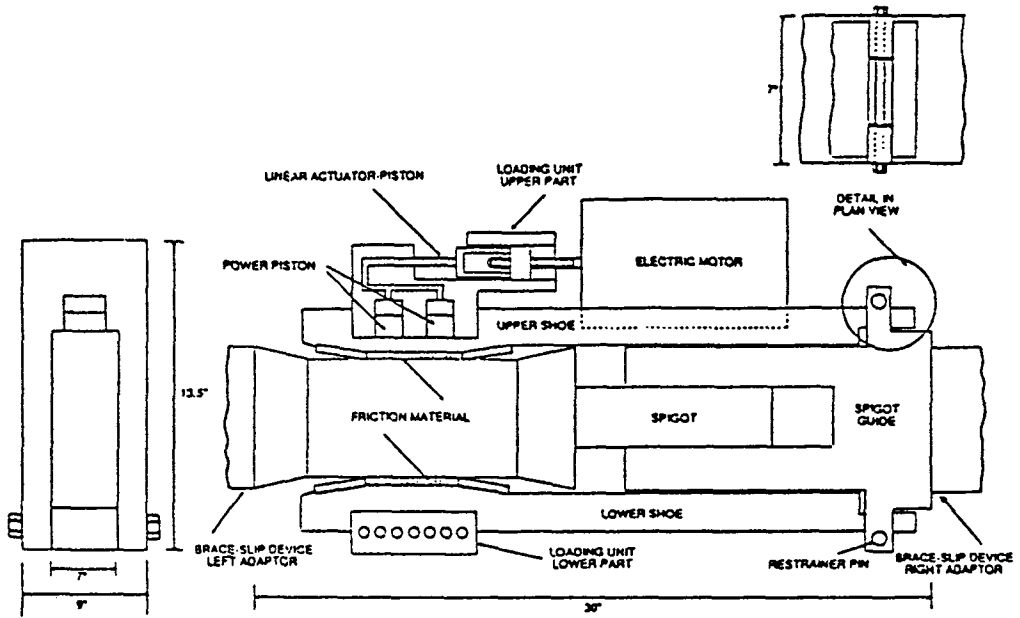
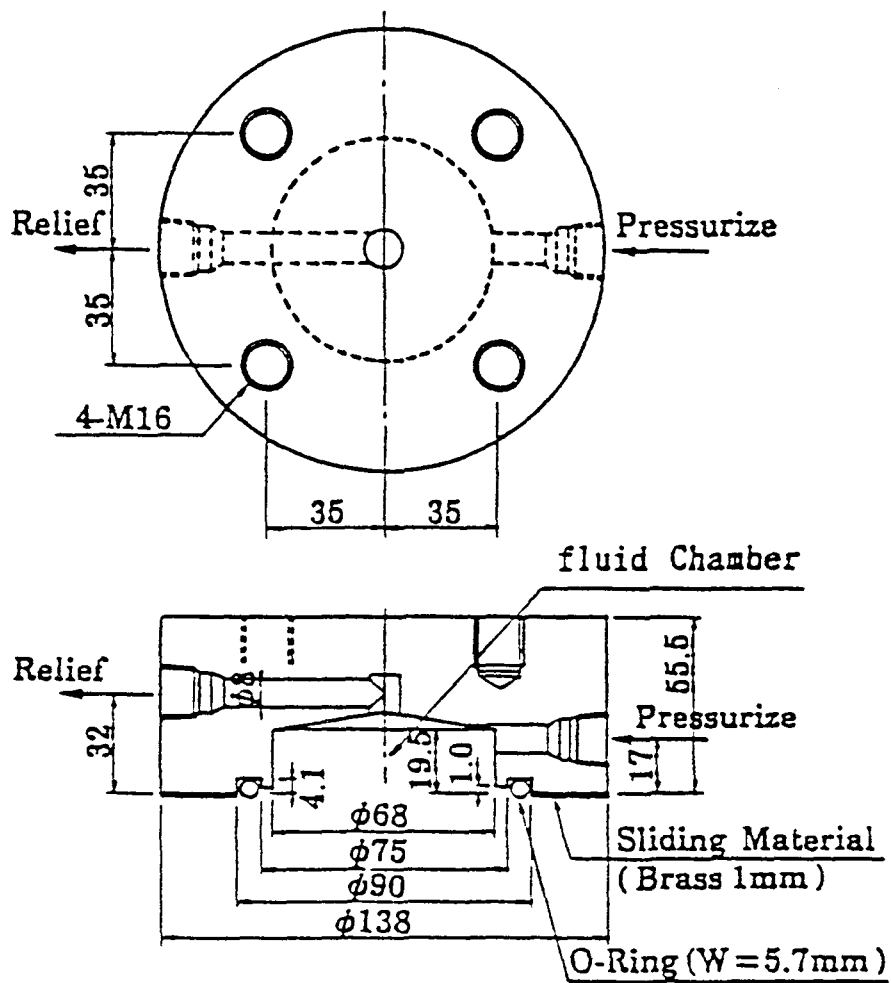


Figure 2-9 Semi-Active Friction Damper (from Akbay 1991)



UNITS: mm

Figure 2-10 Cross-Sectional and Plan View of Semi-Active Friction Control Bearing (from Feng 1992)

performance index is minimized at every time step during the excitation. Under this control, the friction controlled sliding bearings behave as semi-active devices in which the friction force is continuously modulated. The second control algorithm was based on bang-bang control in which only two distinct control signals are sent to the friction controlled sliding bearing. This results in a semi-active device in which the friction force at the foundation/superstructure interface is limited to two distinct values.

2.3.5 Fluid Dampers

An analytical and experimental study of semi-active fluid dampers for control of highway bridges has been presented by Kawashima (1992). The device consists of a fluid damper combined with an external bypass loop containing a servovalve. Damping characteristics are controlled by varying the amount of flow passing through the bypass loop. A model of the semi-active damper having a rated output force of 200 kN, a stroke of ± 13 cm, and a length of about 1.2 m was tested (see Figure 2-11). The power required for valve operation was 50 W. The device utilizes two servovalves which independently control the fluid flow for relative piston head motion to the left or right. The servovalves are actually pressure relief valves which open when the oil pressure through the valve exceeds a specified value. The damping force is developed by a pressure differential across the piston head. Therefore, the damping force increases until the pressure in the servovalve reaches a specified value after which the damping force becomes constant. Experimental hysteresis loops for the semi-active damper are shown in Figure 2-12 for constant amplitude sinusoidal input and servovalve command voltage of 0 volts (fully closed) to 3.5

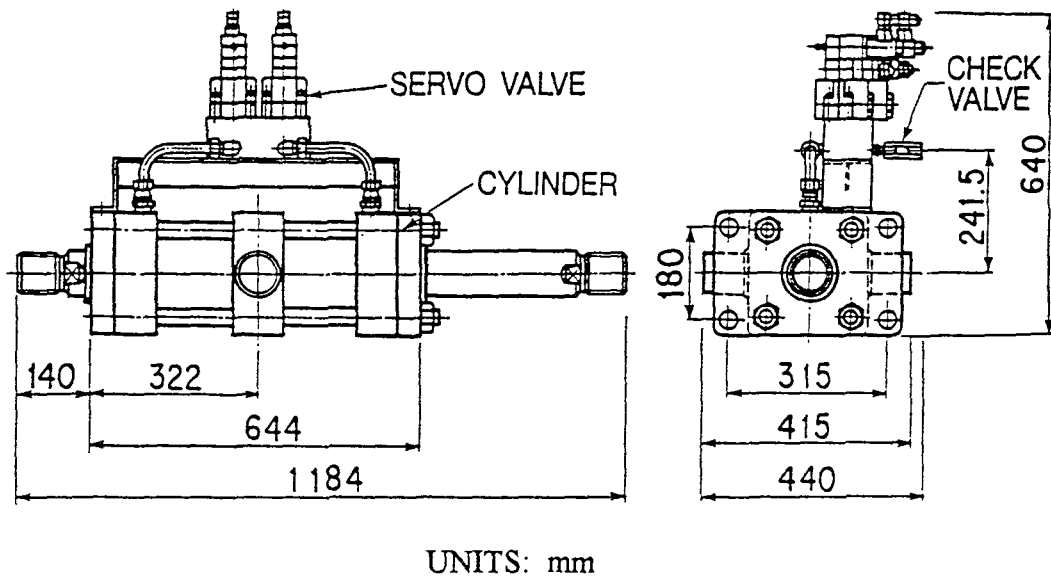
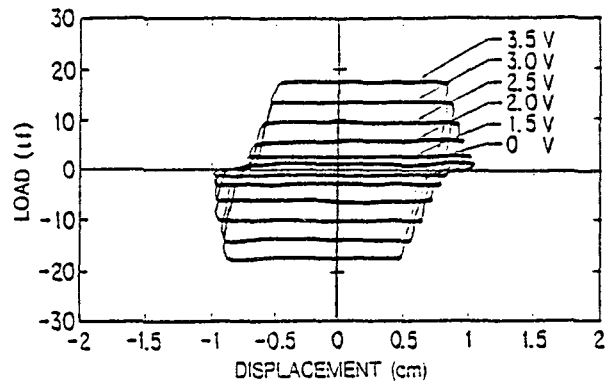
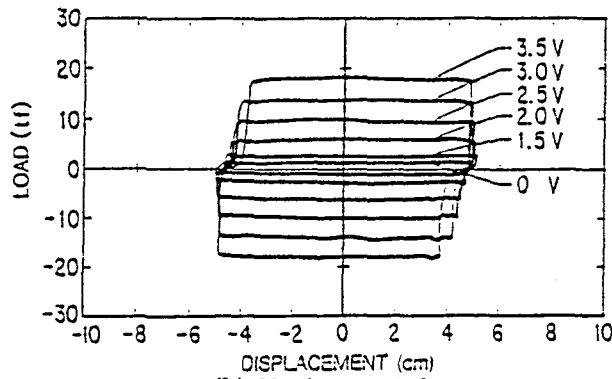


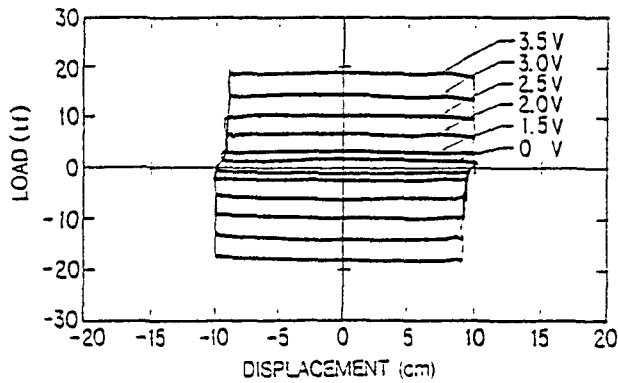
Figure 2-11 Semi-Active Adjustable Force Device Tested by Kawashima (1992)



(a) Displacement 1cm



(b) Displacement 5cm



(c) Displacement 10cm

Figure 2-12 Hysteresis Loops of Semi-Active Fluid Damper Subjected to Constant Amplitude Sinusoidal Motion at a Frequency of 0.1 Hz (from Kawashima 1992)

volts (partially open). Note that the three graphs shown in Figure 2-12 are for tests with different sinusoidal inputs (i.e., the frequency of testing is same in each case (0.1 Hz) but the peak displacement is different). However, the peak force at a given voltage level is nearly the same for each graph which shows that the device is behaving as an adjustable force device. The authors appropriately describe the output force of the semi-active damper as a friction type damping force.

An analytical study of the utility of semi-active fluid dampers for structural control is presented by Shinozuka (1992). A simple two-stage semi-active fluid damper was described and is shown in Figure 2-13. This device uses a normally closed solenoid valve to open or close a secondary orifice which controls the fluid flow through a bypass loop. Damping forces are developed as a result of a pressure differential across the piston head. When the valve is closed, the device delivers high linear viscous damping. When the valve is opened, the device delivers a very small level of linear viscous damping. Further, a multi-stage semi-active fluid damper is proposed which is capable of producing several distinct damping levels by introducing several solenoid valves rather than the single one shown in Figure 2-13. Finally, a semi-active damper is proposed in which the solenoid valve shown in Figure 2-13 is replaced by a servovalve allowing for continuous modulation of the damping properties between two prescribed levels.

An experimental study of a semi-active fluid damper for seismic response control has been presented by Patten (1994). The configuration of the damper includes a balanced piston

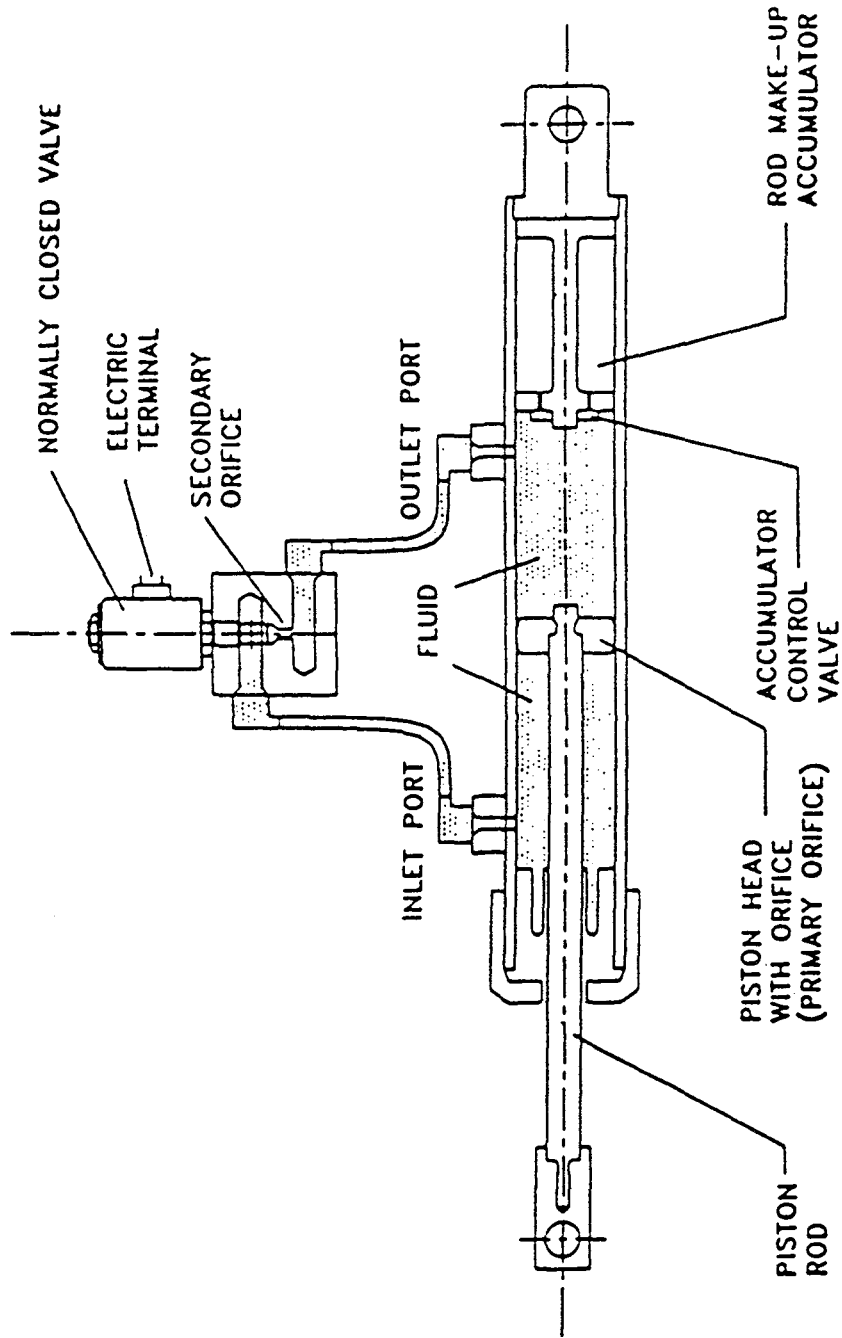


Figure 2-13 Construction of Semi-Active Fluid Viscous Damper
 Described by Shinozuka (1992)

rod and an external control valve containing an orifice which is modulated by a small motor. A mathematical model is developed to describe the behavior of the damper including the effects of fluid compressibility. Apparently, the tested damper is capable of storing energy and thus the issue of stability is addressed.

Sack (1993) describes a semi-active fluid damper in which standard orifice flow equations are utilized in the development of the mathematical model of the device (see Figure 2-14). The use of standard orifice equations indicate that the damper behaves as a Bernoullian damper which delivers a force output proportional to the square of the relative velocity. A control algorithm is described in which the control of the adjustable orifice involves the "linearization" of the dynamics of the damper. Through this process of dynamic linearization, the variable orifice is adjusted in such a way that the damper delivers a force which is directly proportional to relative velocity. In effect, a Bernoullian damper is made to behave as a linear viscous damper.

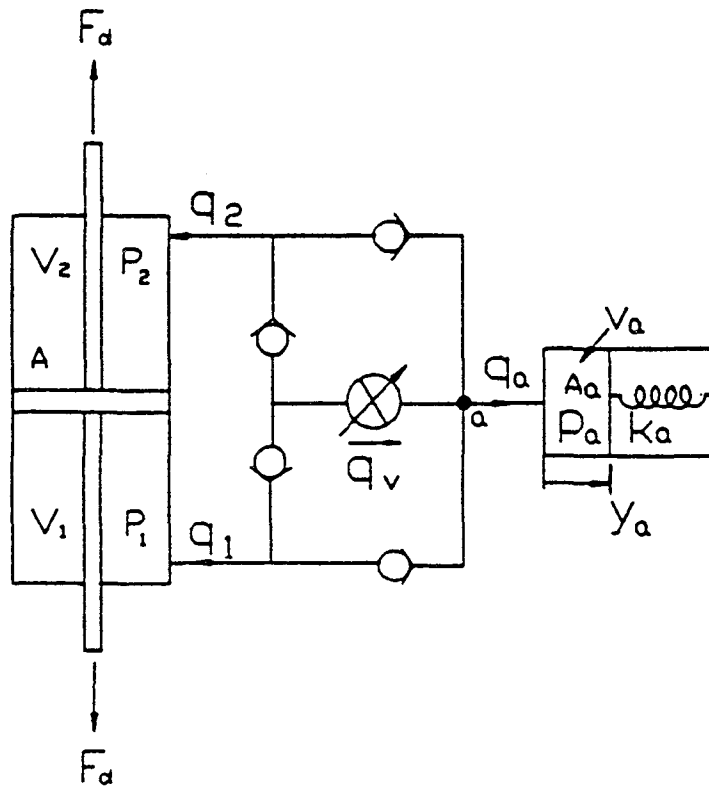


Figure 2-14 Schematic of Semi-Active Fluid Damper Described by Sack (1993)

SECTION 3

MECHANICAL PROPERTIES OF TESTED SEMI-ACTIVE FLUID DAMPERS

3.1 Description and Principles of Operation

The semi-active fluid dampers described in this report are based on the design of a passive fluid damping device which has been studied by Constantinou (1993b, 1992a, 1992b) for seismic energy dissipation and seismic isolation (see Figure 3-1). The passive portion of the semi-active fluid damper consists of a stainless steel piston rod, a bronze piston head, and a piston rod make-up accumulator. The damper is filled with a thin silicone oil (kinematic viscosity =100 cSt, specific weight = 9.78 kN/m³). The piston head orifices are designed such that the fluid flow is altered according to the fluid speed resulting in a force output which is proportional to the relative velocity of the piston head with respect to the damper housing. Such orifices are known as "fluidic" control orifices, "fluidic" coming from the concatenation of the words "fluid" and "logic" (i.e., logical operations using fluids).

The force generated by the damper is a result of a pressure differential across the piston head. When the damper is subjected to a compressive force, the fluid volume is reduced by the product of travel and piston rod area. Since the fluid is nearly incompressible, the reduction in fluid volume results in the development of a restoring force. This is prevented by the use of a rod make-up accumulator and control valve. Under compression and tension forces, the control valve opening is adjusted to permit the

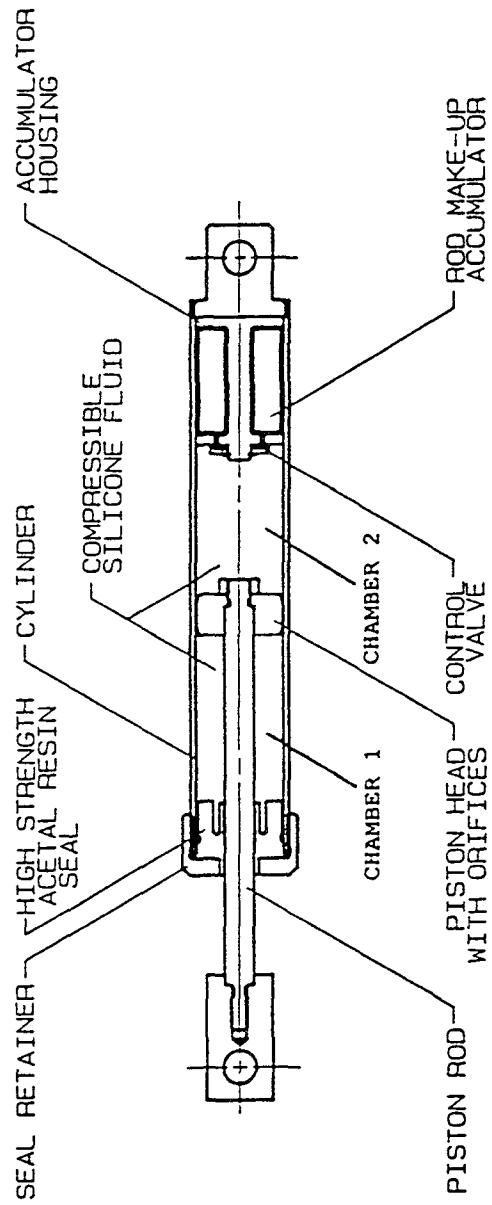


Figure 3-1 Construction of Passive Fluid Viscous Damper

appropriate amount of fluid to pass in and out of the rod make-up accumulator, respectively. An alternate construction of this device is with a balanced piston rod. A balanced piston rod is one in which the rod enters the damper, is connected to the piston head, and then continues out through the opposite end of the damper. This arrangement avoids changes in fluid volume and therefore prevents the development of restoring force.

The orifice flow around the piston head is compensated according to the temperature such that the mechanical properties remain relatively stable over a wide temperature range (-40°C to 70°C). This is accomplished passively through the use of an orifice design which utilizes a bi-metallic thermostat. Note that the dampers may be described as "inertial" dampers since the behavior is primarily governed by the speed of fluid through the orifices and secondarily by the mechanical properties of the fluid. Therefore, any effect of temperature on the fluid viscosity will not significantly alter the behavior of the damper.

The passive fluid damper shown in Figure 3-1 was modified to create a semi-active fluid damper as shown in Figure 3-2. This configuration represents one possible modification of the passive fluid damper in which only damping can be modulated. Alternate modifications can be developed. For example, a restoring force/semi-active damping device can be developed by removing the accumulator in Figure 3-2 to allow for the development of stiffness. Another possible configuration involves the construction of an external accumulator with its own control valve to obtain a semi-active restoring

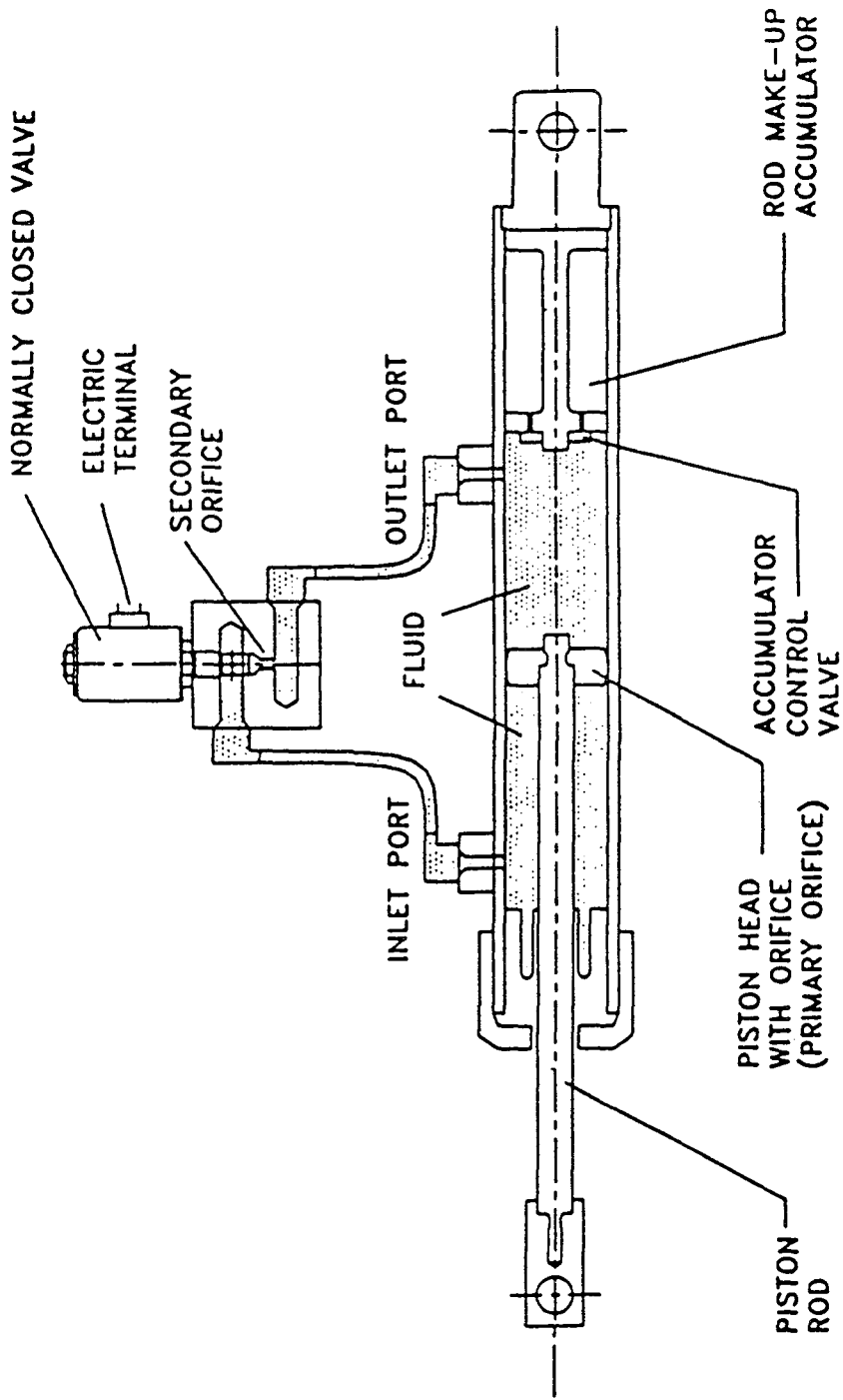


Figure 3-2 Construction of Semi-Active Fluid Viscous Damper

force/damping device which is capable of independent adjustment of both stiffness and damping.

Semi-active fluid damping and stiffness devices have been used in numerous applications within the U.S. military. Examples of applications include the suspension system of armored vehicles, the suspension system of self-propelled Howitzers, and the Sikorsky Flying Crane Helicopter. The design of a semi-active stiffness device for the suspension system of a U.S. Marine Corps armored amphibious vehicle is described by Taylor Devices (1991). The semi-active devices are capable of providing two levels of stiffness which are controlled by the operator of the vehicle (i.e., no microprocessors or external sensors are utilized). During the 1960's, the Sikorsky Flying Crane Helicopter used a semi-active stiffness device on the winch mechanism to isolate the lifted load from the airframe. The device accepted sensor inputs and altered its output to suit different loads and load environments. This device was entirely successful and many of these helicopters are still in service with the Air National Guard and various commercial firms. In the late 1960's, the U.S. Navy experimented with an isolated ship deck utilizing a semi-active damping and stiffness device. The intent of the isolation system was to allow high speed patrol craft to operate in severe sea states without injury to the crew. An experimental patrol boat with the semi-active isolators proved highly successful, but was never produced in quantity. The U.S. military has recently specified a semi-active stiffness device for use within a missile guidance system. This application was prompted by the research reported herein.

The semi-active fluid dampers described in this report were developed, constructed, and tested over a period of 19 months. A total of 767 tests were conducted on five different semi-active damper systems (see Table 3-I). Of the five semi-active damper systems, two were selected for extensive evaluation and are described in detail in this report:

- 1) Two-Stage damper with normally closed solenoid spool valve (system 3 in Table 3-I)
- 2) Variable damper with normally closed direct-drive servovalve (system 5 in Table 3-I)

In anticipation of future shaking table studies, two damping units were tested for each of the above damping systems. The notation for each damping unit tested is given in Table 3-II.

3.1.1 Two-Stage Damper

The tested two-stage fluid damper is of the form depicted in Figure 3-2. The passive fluid damper of Figure 3-1 was modified by including an external bypass loop containing a control valve. Damping characteristics are controlled by varying the amount of flow passing through the bypass loop. The control valve is an A.C. (alternating current) controlled normally closed solenoid valve. The solenoid valve can either be turned on (solenoid coil energized and valve open) or off (solenoid coil de-energized and valve closed). Therefore, only two levels of damping are available from the system and hence the designation, two-stage damper. A photograph of the semi-active two-stage damper is shown in Figure 3-3. Geometrical and other characteristics of the semi-active damper are shown in Figure 3-4.

Table 3-I Experimentally Tested Semi-Active Damper Systems

SYSTEM	VALVE TYPE	DAMPER CONFIGURATION
1	2 normally closed solenoid spool valves	3 stage damper
2	1 normally open solenoid spool valve	2 stage damper
3	1 normally closed solenoid spool valve	2 stage damper
4	1 normally closed solenoid poppet valve	2 stage damper
5	1 normally closed direct-drive servovalve	variable damper

Table 3-II Notation For Semi-Active Damper Units Tested

SEMI-ACTIVE DAMPER SYSTEM	DAMPING UNIT	NOTATION
Two-Stage Damper	1	2ST-A
	2	2ST-B
Variable Damper	1	VAR-A
	2	VAR-B

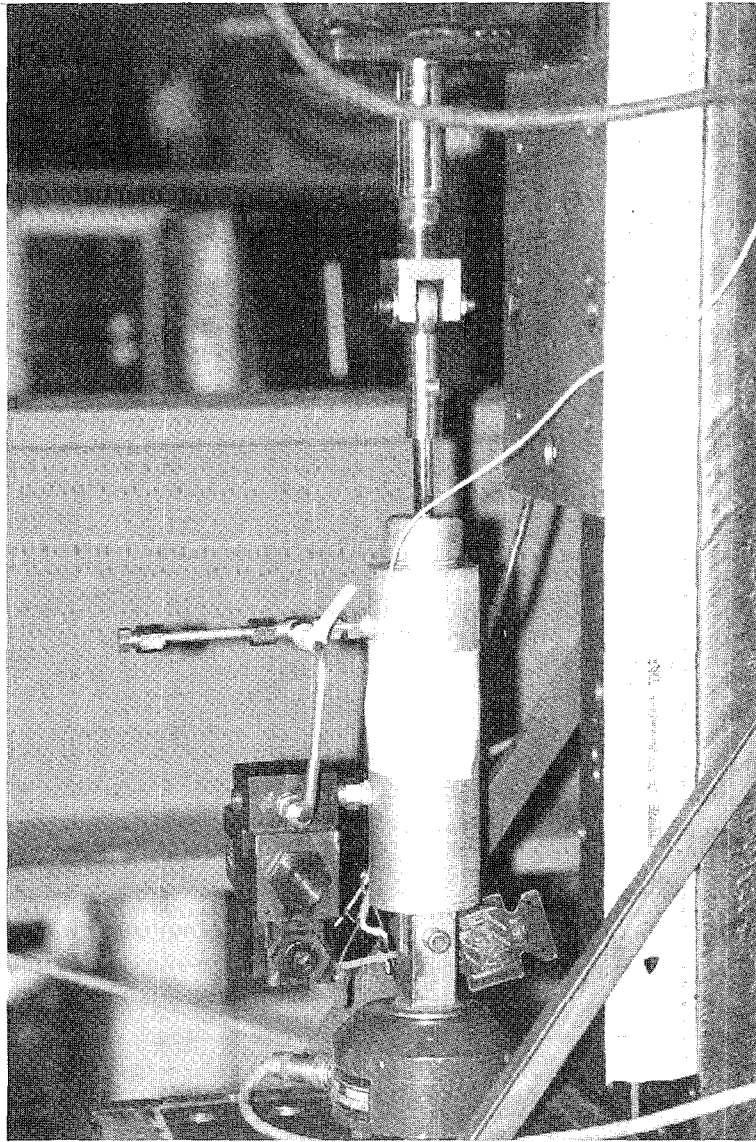
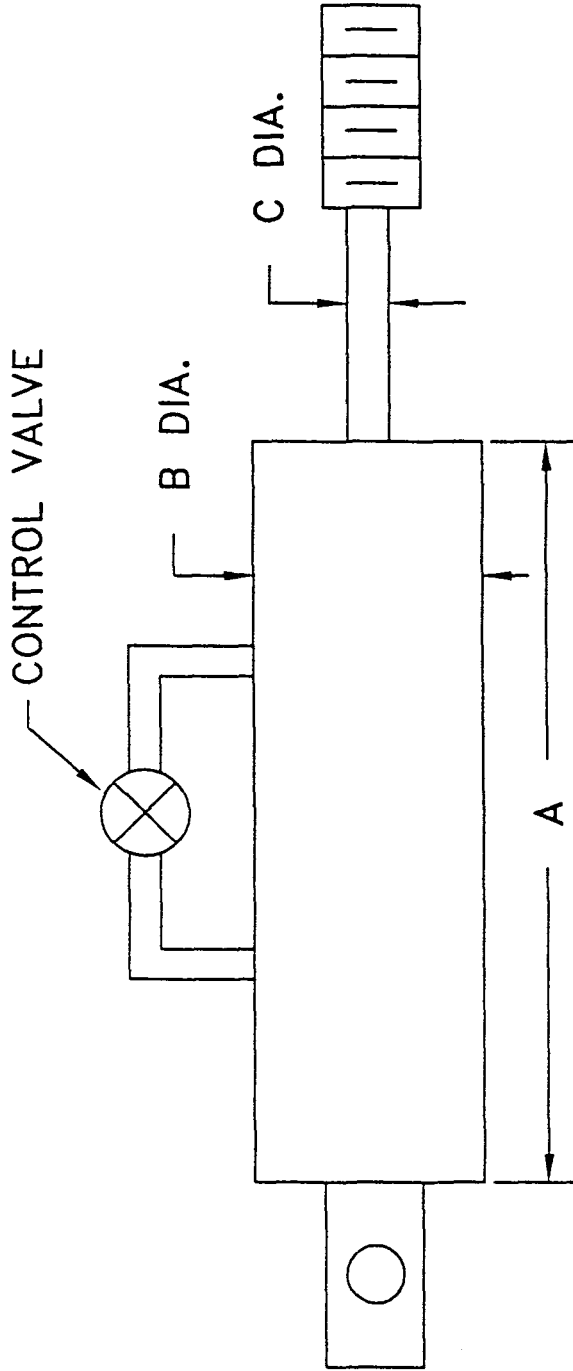


Figure 3-3 Photograph of Semi-Active Two-Stage Damper



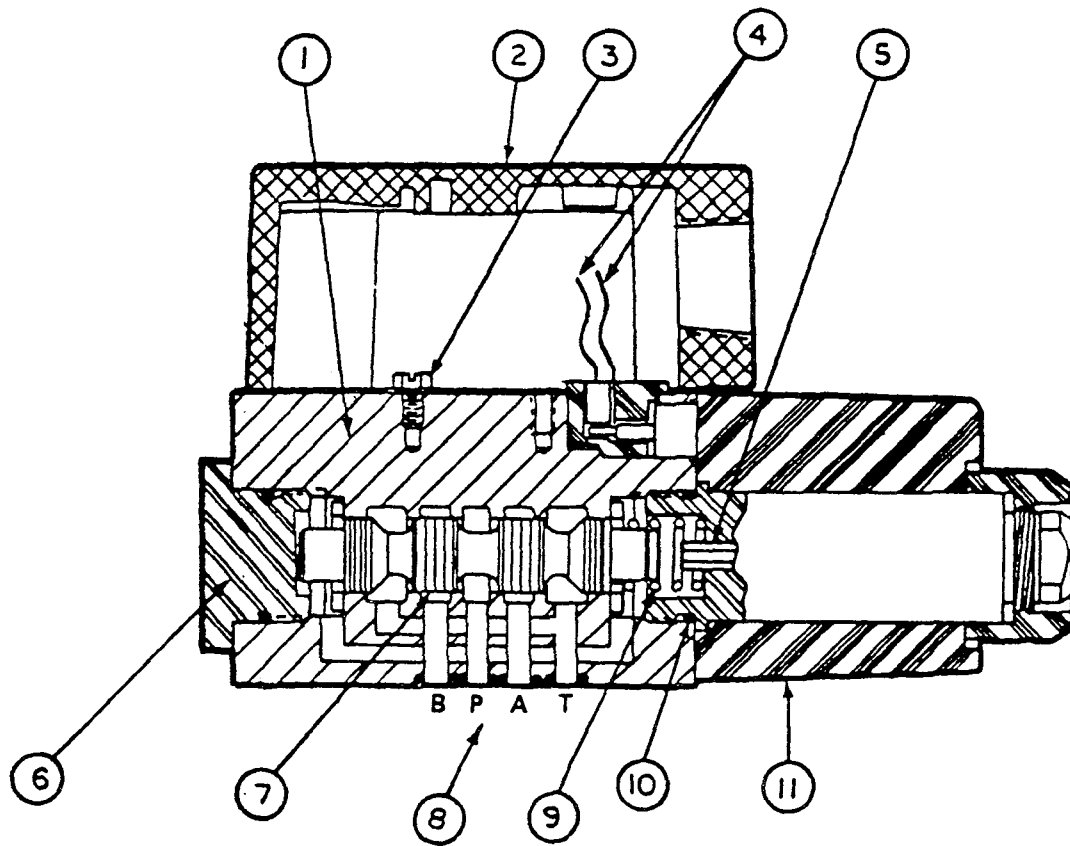
SEMI-ACTIVE TWO-STAGE DAMPER CHARACTERISTICS						
Max. Force (N)	Stroke (mm)	Weight (N)	A (mm)	B (mm)	C (mm)	Average Power Required (W)
8,900	76.2	61.6	192.09	63.50	11.11	55

Figure 3-4 Geometric and Other Characteristics of Semi-Active Two-Stage Damper

A cross-sectional view of the solenoid valve is shown in Figure 3-5. The valve may be described as a spool type, two-stage (on-off), normally closed solenoid valve. Although the valve was manufactured with four ports, only two are used in this application. Normally, when there is no voltage applied across the leads, fluid flow is blocked across the two remaining ports: P and B. In this mode, all fluid flow in the damper is through the piston head fluid orifices and its damping performance is simply that of a standard passive fluid viscous damper. When voltage is applied across the leads, the solenoid coil moves the spool to an open position with an electromagnetically induced force. This force must overcome the force of the reset spring which moves the spool back to a closed position following removal of the voltage. When the spool is in the open position, a majority of the fluid flow in the damper is through the external bypass loop and the damping level is much lower than when the spool is in the closed position. The average power required to operate the A.C. controlled solenoid valve is approximately 55 W and the valve can therefore operate on the power of batteries which is critical during an earthquake when the main power source of a structure may fail. The solenoid valve offers fail-safe characteristics in that the loss of power to the device causes the valve to become fully closed which in turn causes the semi-active damper to behave as a passive device with high damping characteristics.

3.1.2 Variable Damper

The tested variable damper is also of the form depicted in Figure 3-2 in which the passive fluid damper of Figure 3-1 was modified by including an external bypass loop containing a



NO.	DESCRIPTION
1	HOUSING
2	JUNCTION BOX
3	GROUND SCREW
4	POWER LEADS
5	SOLENOID PIN
6	END PLUG
7	SPOOL
8	PORTS
9	RETURN SPRING
10	SEAL
11	SOLENOID COIL

Figure 3-5 Cross-Sectional View of Solenoid Valve Used in Semi-Active Two-Stage Damping System

control valve. The control valve is a normally closed direct-drive servovalve. The servovalve can be off (no voltage to coils - valve closed), fully on (sufficient voltage to fully energize coils - valve open), or between off and fully on (sufficient voltage to partially energize coils - valve partially open). Therefore, a full range of damping levels are available from the system and hence the designation, variable damper. A photograph of the semi-active variable damper is shown in Figure 3-6 and geometrical and other characteristics of the variable damper are shown in Figure 3-7.

The variable damper utilized a direct-drive servovalve for control of the fluid flow through the external bypass loop. A cross-sectional view of the direct drive servovalve is shown in Figure 3-8. The direct-drive servovalve was originally developed for control of the primary flight control servo-actuation system on the U.S. Air Force B-2 Stealth Bomber. The valve was designed to replace the conventional hydraulic amplifier pilot stage with a high-force, high-response drive motor acting directly on the valve spool. The operation of a conventional electrohydraulic servovalve (see Figure 3-9) requires a pilot stage in which a torque motor is utilized to adjust the position of a flapper which diverts flow to the ends of a spool. The pilot stage effectively controls the pressure on each side of the spool and as a result of a pressure differential the spool slides in its bushing. The bushing contains slots which allow fluid to flow to the control ports. The fluid flow to the control ports may be used to drive an actuator. In contrast, the direct-drive servovalve is ideally applicable to semi-active control in that the valve spool is driven by an electric drive motor, eliminating the need for a source of hydraulic pressure to operate a pilot stage.

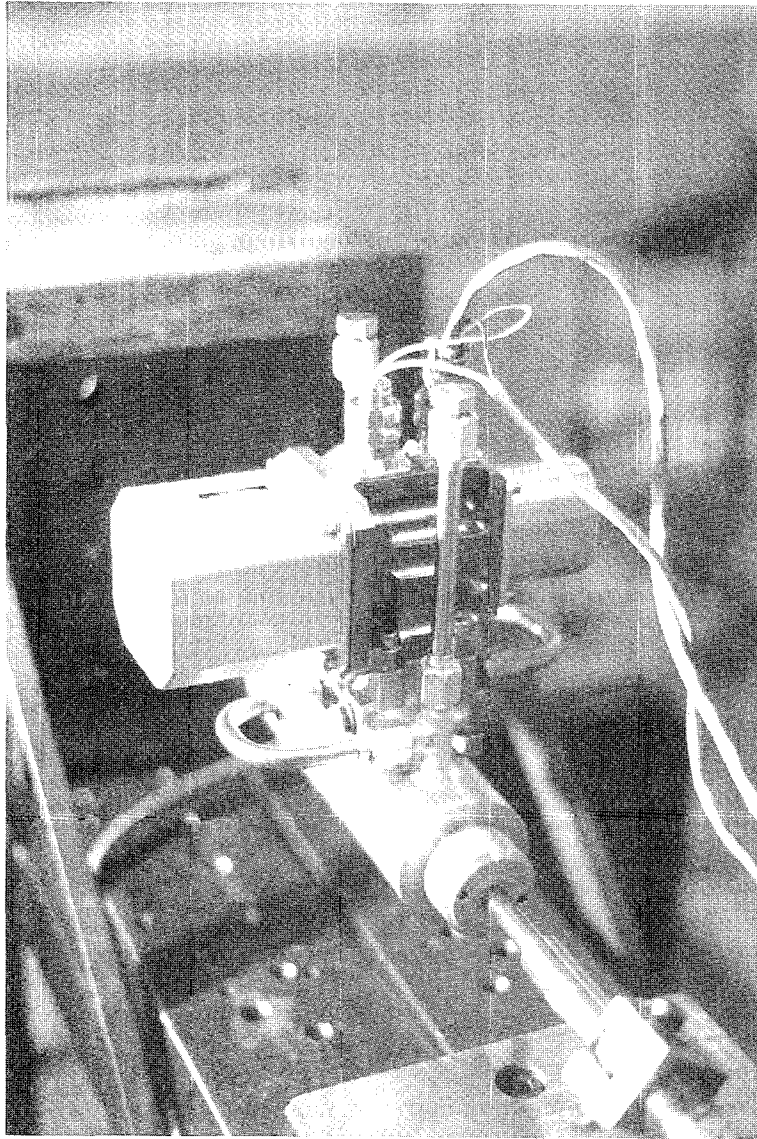
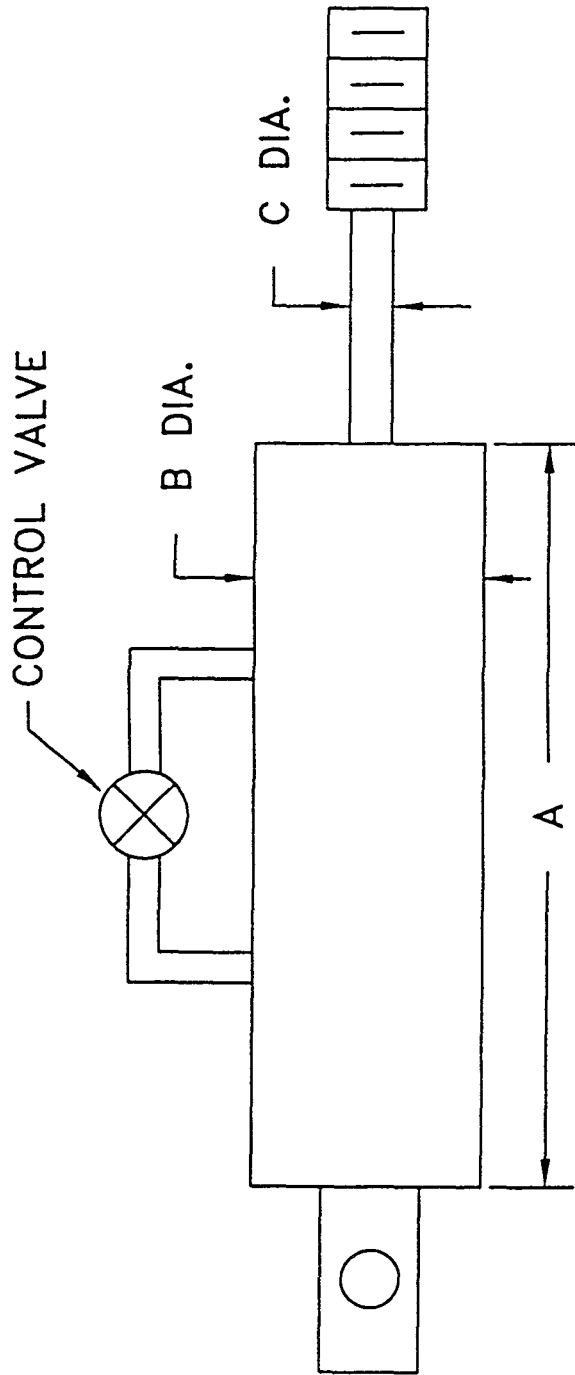


Figure 3-6 Photograph of Semi-Active Variable Damper



SEMI-ACTIVE VARIABLE DAMPER CHARACTERISTICS						
Max. Force (N)	Stroke (mm)	Weight (N)	A (mm)	B (mm)	C (mm)	Peak Power Required (W)
8,900	76.2	79.5	192.09	63.50	11.11	3.5

Figure 3-7 Geometric and Other Characteristics of Semi-Active Variable Damper

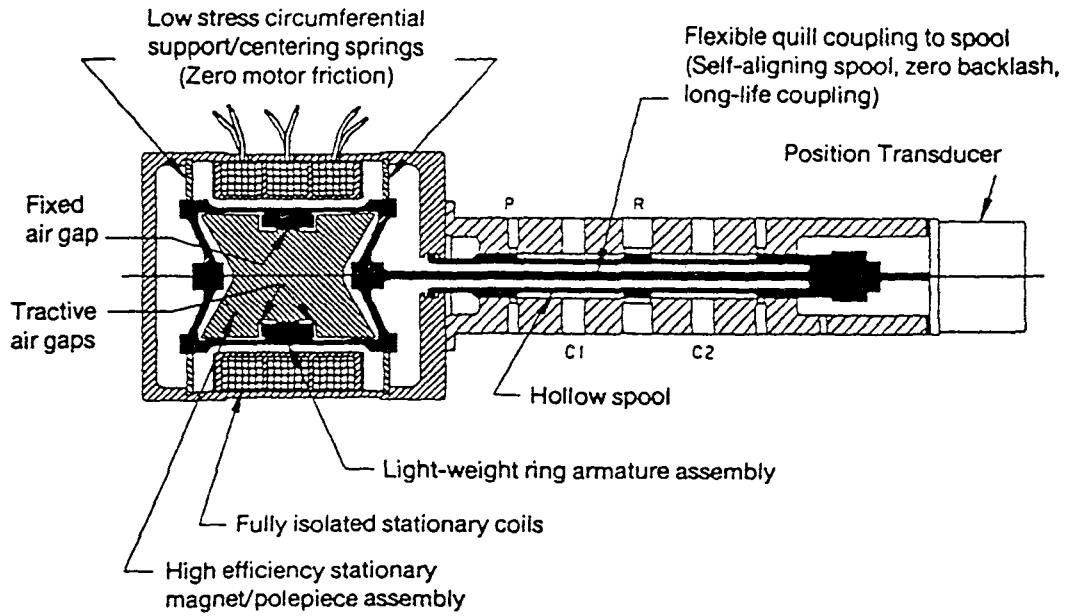


Figure 3-8 Cross-Sectional View of Direct-Drive Servovalve Used in Semi-Active Variable Damper System

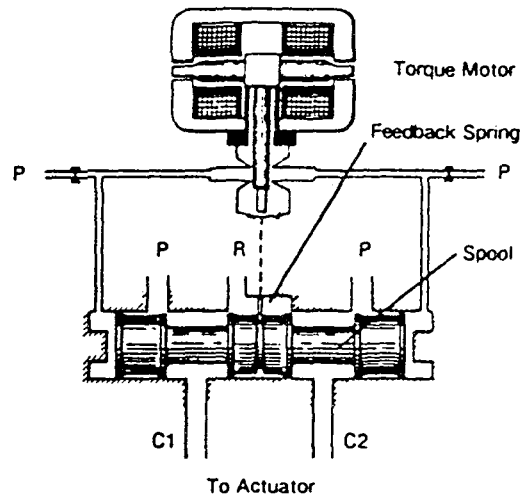


Figure 3-9 Schematic of a Typical Electrohydraulic Nozzle Flapper Servovalve

The direct-drive servovalve may be described as a spool type, continuously adjustable, normally closed servovalve. Although the valve was manufactured with four ports, only two are used in this application. Normally, when there is no command voltage to the coils, fluid flow is blocked across the two ports. In this mode, all fluid flow in the semi-active damper system is through the piston head orifices and its damping performance is simply that of a standard passive fluid viscous damper. When a command voltage is sent to the coils, a D.C. (direct current) drive motor is used to impose a spool displacement in proportion to the command voltage (see Figure 3-10). The hysteretic behavior in Figure 3-10 is related to the friction between the spool seals and the spool bushing. Neglecting the dead-zone due to spool land overlap, the linear motion of the spool opens up a circumferential fluid flow area which is directly proportional to the spool displacement. When the spool is in the full open position, a majority of the fluid flow in the damper is through the external bypass loop and the damping level is much lower than when the spool is in the full closed position.

Note that for a given command signal voltage, the spool displacement in the two variable damper units is not the same (see Figure 3-10). However, there was no attempt made to match the slope of these curves. Instead, since the behavior of the variable dampers is directly related to the flow rate of fluid through the control valves, the relationship between the command signal and the flow rate through each valve was matched (see Figure 3-11). The curves in Figure 3-11 match very well except at low command signal voltage levels where unit VAR-A allows more fluid flow than unit VAR-B. Apparently,

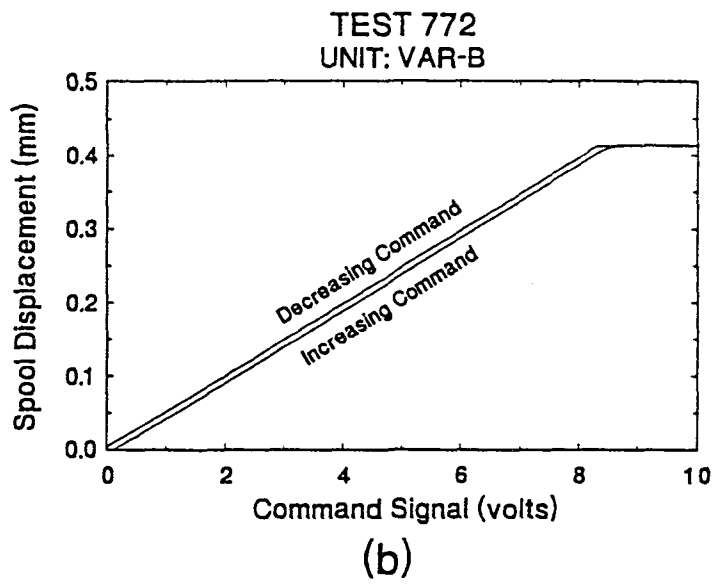
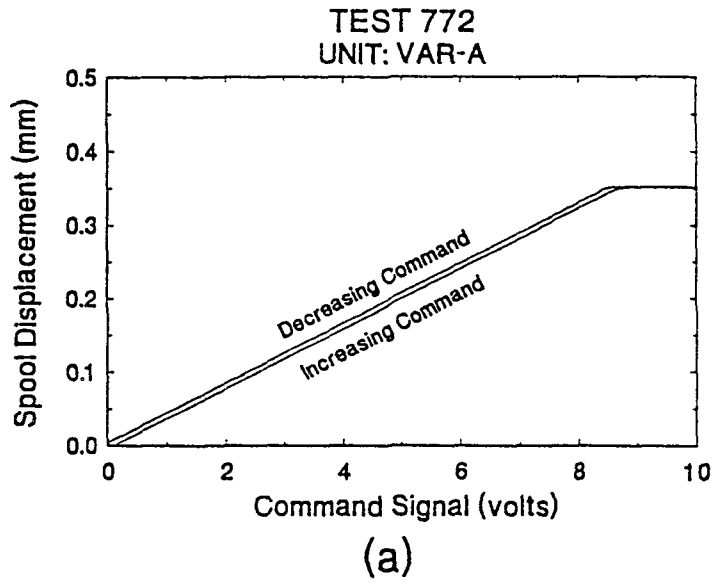


Figure 3-10 Recorded Values of Variable Damper Spool Displacement Due to Pseudo-Statically Applied Command Signal for a) Unit VAR-A and b) Unit VAR-B

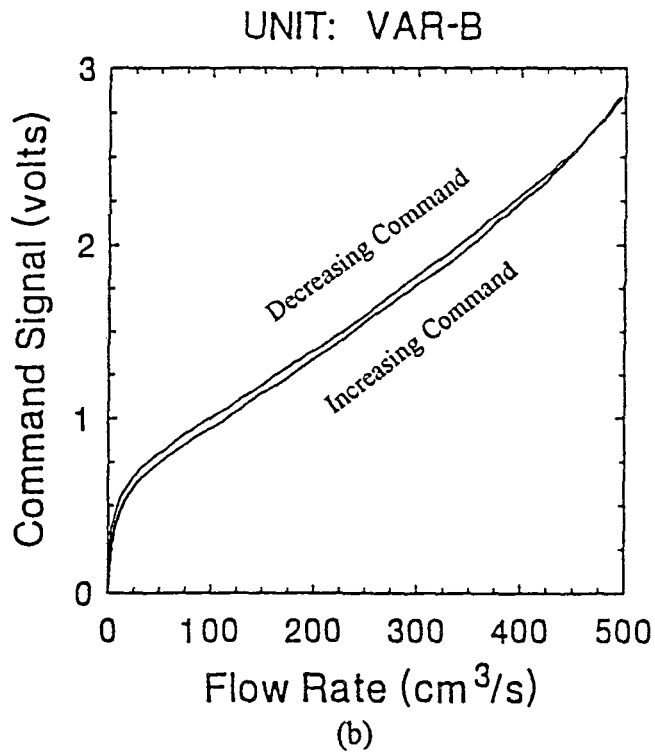
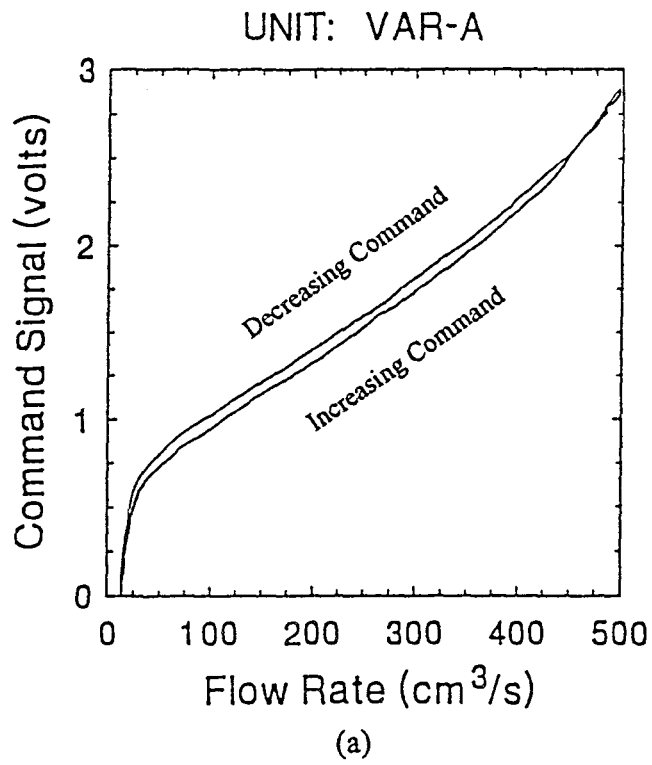


Figure 3-11 Recorded Values of Direct-Drive Servovalve Flow Rate Due to Pseudo-Statically Applied Command Signal for a) Unit VAR-A and b) Unit VAR-B

the spool seals that restrict flow at low command signal voltage levels in the two units were not functioning identically. The effect of this difference in flow rate on the damping coefficient of the two variable damper units will be demonstrated in Section 3.3.3.

Figure 3-11 also shows that the flow rate does not change appreciably until the command signal voltage level exceeds about 0.5 volts. This is the result of spool land overlap which restricts fluid flow until the spool moves beyond the length of the spool land overlap. Furthermore, the flow rate becomes saturated at command signal voltage levels beyond about 3 volts. This is the result of flow restrictions within the external tubing manifold ports and valve internal passages which are smaller than the maximum valve orifice opening. For command signals between about 0.5 volts and 3 volts, the flow rate is essentially a linear function of the command signal since the spool displacement is linearly related to the command signal (see Figure 3-10).

The command signal corresponding to the desired spool position is in the form of a voltage signal. The voltage signal is delivered to a current driver/amplifier which drives the linear motor (i.e., the valve is current controlled). The advantage of using current control to drive the valve is that the sluggish performance associated with direct voltage control (due to the direct drive motor coil resistance and inductance) is drastically improved to the extent that the dynamics of current build-up can usually be neglected (Watton 1989). This is critical for applications in which minimal system response times are required.

As a result of a command signal, the drive motor forces the spool to move. An oscillator excites a spool position transducer (LVDT - Linear Variable Differential Transformer) producing an electrical signal proportional to spool position. The demodulated spool position signal is compared with the desired spool position and the resulting spool position error causes current to flow in the drive motor coil until the spool has moved to its commanded position and the spool position error is reduced to zero. This spool position feedback loop results in a precise positioning of the spool for a given command signal.

The direct-drive servovalve offers fail-safe characteristics in that the loss of power to the device causes the valve to become fully closed which in turn causes the semi-active damper to behave as a passive device with high damping characteristics. Furthermore, the direct-drive servovalve requires a peak power of 3.5 W and can therefore operate on the power of batteries which is critical during an earthquake when the main power source of a structure may fail.

3.2 Component Testing Procedure

3.2.1 General Testing Arrangement

The testing arrangement shown in Figure 3-12 was used for testing the semi-active fluid dampers. A schematic of the testing arrangement is shown in Figure 3-13. A 10 kN capacity servo hydraulic actuator with a ± 50.8 mm stroke and a 37 l/min servovalve was utilized to provide dynamic excitation to the dampers. The force in the damper is measured by a 10 kN capacity load cell placed between the damper and reaction frame.

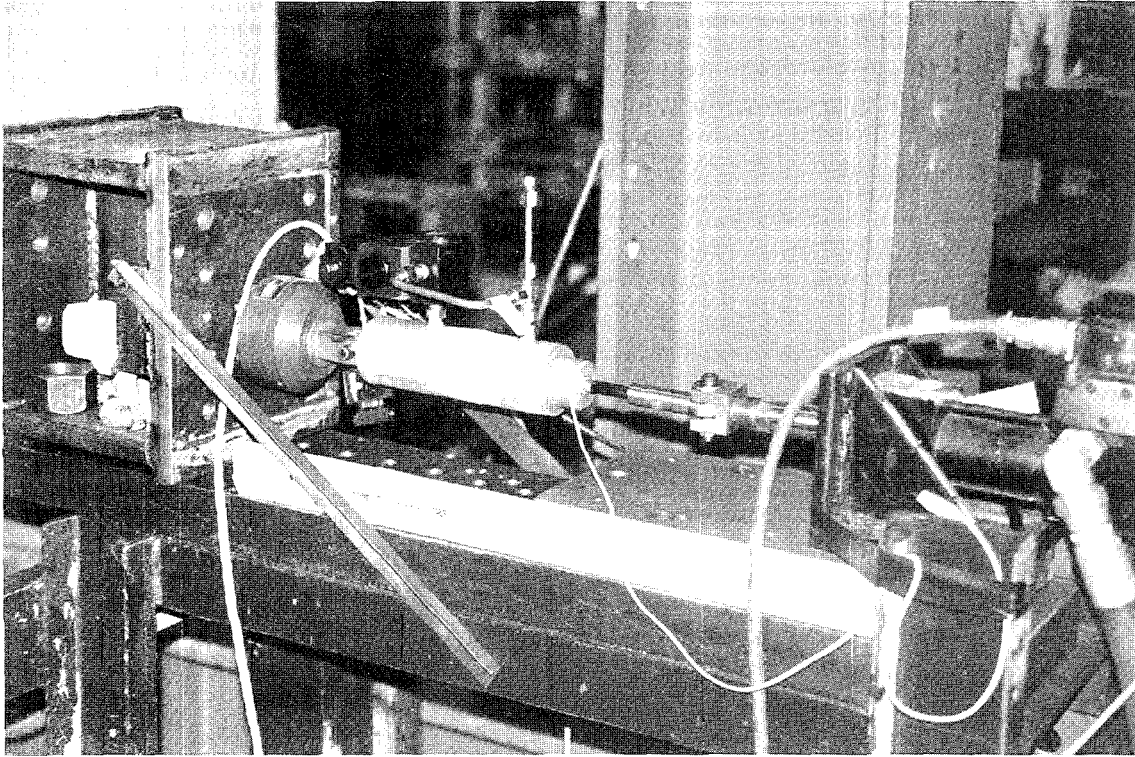


Figure 3-12 Photograph of Testing Arrangement

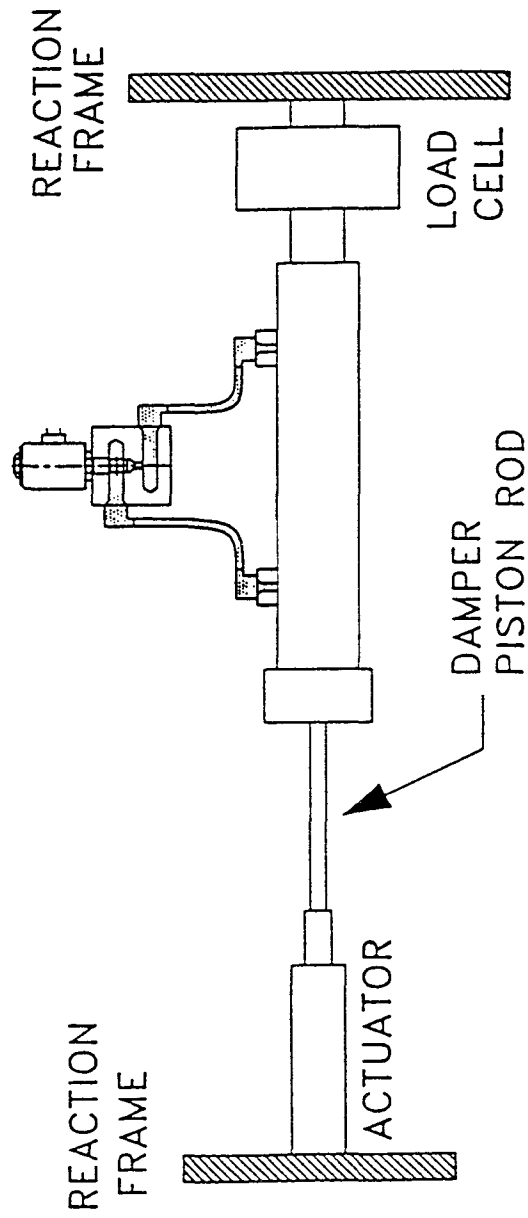


Figure 3-13 Schematic of Testing Arrangement

The position of the piston rod of the damper with respect to the damper housing is measured using an LVDT (Linear Variable Differential Transformer) located within the actuator. Data acquisition was performed using Labtech Notebook™ data acquisition software running on a PC with an INTEL™ 80386/33 MHz processor and a 12 bit data acquisition board having 8 channels of analog-to-digital conversion and 2 channels of digital-to-analog conversion. All recorded signals were filtered using six pole low-pass butterworth filters with a cut-off frequency of 10 Hz. The sampling rate was selectively varied depending on the type of test performed.

3.2.2 Two-Stage Damper

A block diagram describing the two-stage damper component testing is presented in Figure 3-14. Component testing of the two-stage damper required a switch to open and close the 110 volt A.C. (alternating current) solenoid valve. In order to measure the response time of the solenoid valve/damper system, the data acquisition computer was also used to control the solenoid valve. However, a direct connection between the solenoid valve 110 V A.C. power circuit and the computer 5 volt TTL logic circuit is not possible. Therefore, an optoisolator was used to connect the two circuits. An optoisolator contains an emitter which is optically coupled to a photo-detector through an insulating medium. This arrangement permits the passage of information from the low voltage computer circuit, which contains the emitter, to the high voltage power circuit, which contains the detector. A low digital output signal from the computer causes the

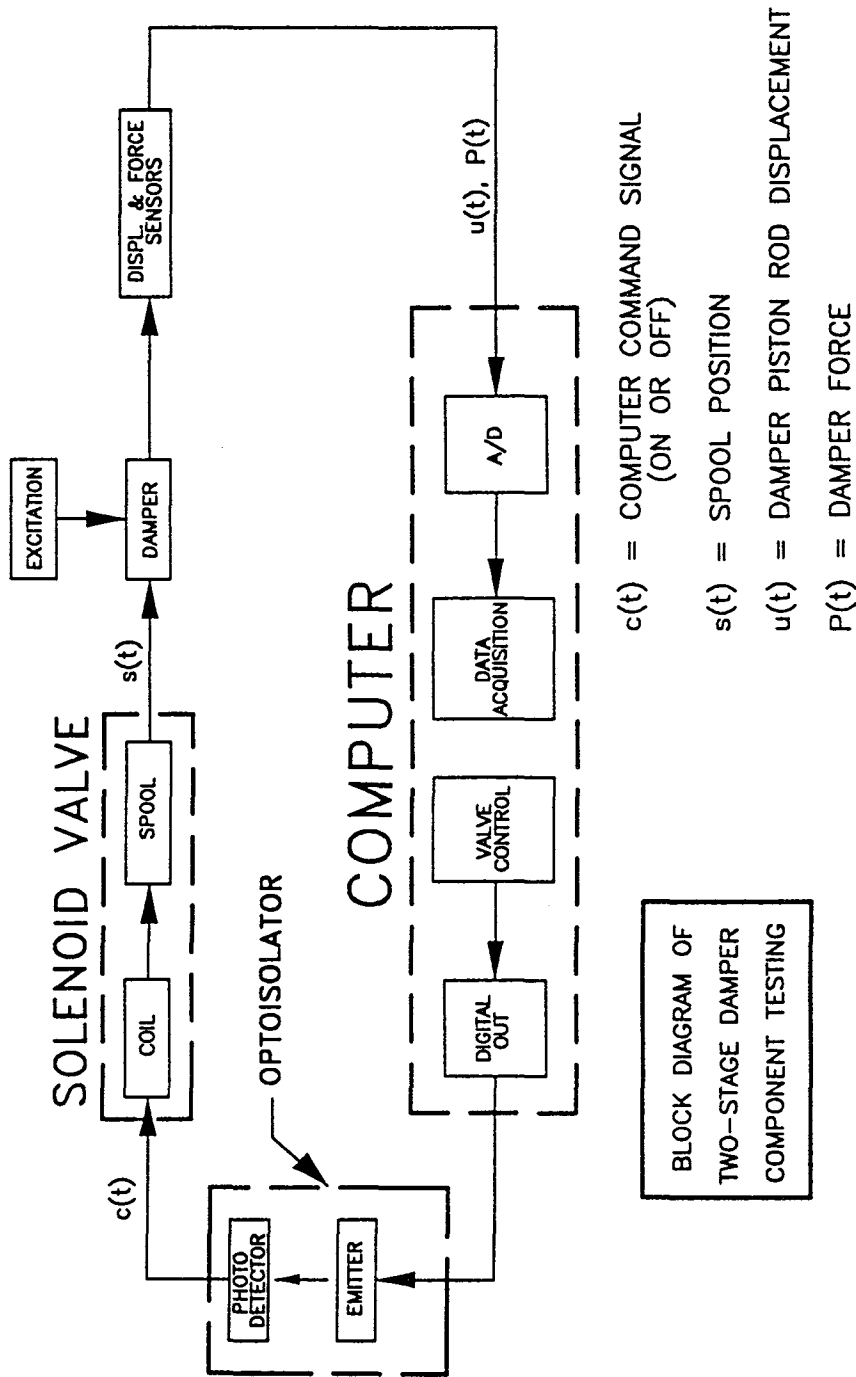


Figure 3-14 Block Diagram of Two-Stage Damper Component Testing

detector to close the 110 V A.C. circuit whereas a high digital output signal opens the 110 V A.C. circuit. A schematic of the computer control circuit is shown in Figure 3-15.

3.2.3 Variable Damper

A block diagram describing the variable damper component testing is presented in Figure 3-16. The semi-active variable damper required special electronic equipment for operation of the direct-drive servovalve. Two electronic circuits were constructed for precise positioning of the valve spool. A voltage controlled (current is very low) spool position feedback circuit determines the difference (error) between the actual spool position (measured by an LVDT located within the valve) and the computer commanded spool position. This error is expressed as a voltage signal. A current driver/amplifier circuit receives the voltage signal from the spool position feedback circuit and converts it to a proportional current signal. The current signal is delivered to the coils of the drive motor which controls the spool position. The servovalve spool position feedback circuit and the current driver/amplifier circuit require a 3.5 W capacity power supply. Furthermore, while the command voltage corresponding to the full spool displacement travel is about 8.5 volts (see Figure 3-10), the power supply delivers 40 volts to the two electronic circuits that control the valve. For dynamic applications, the inductance of the coil increases with frequency and therefore a high voltage power supply is required to drive the spool at high speeds.

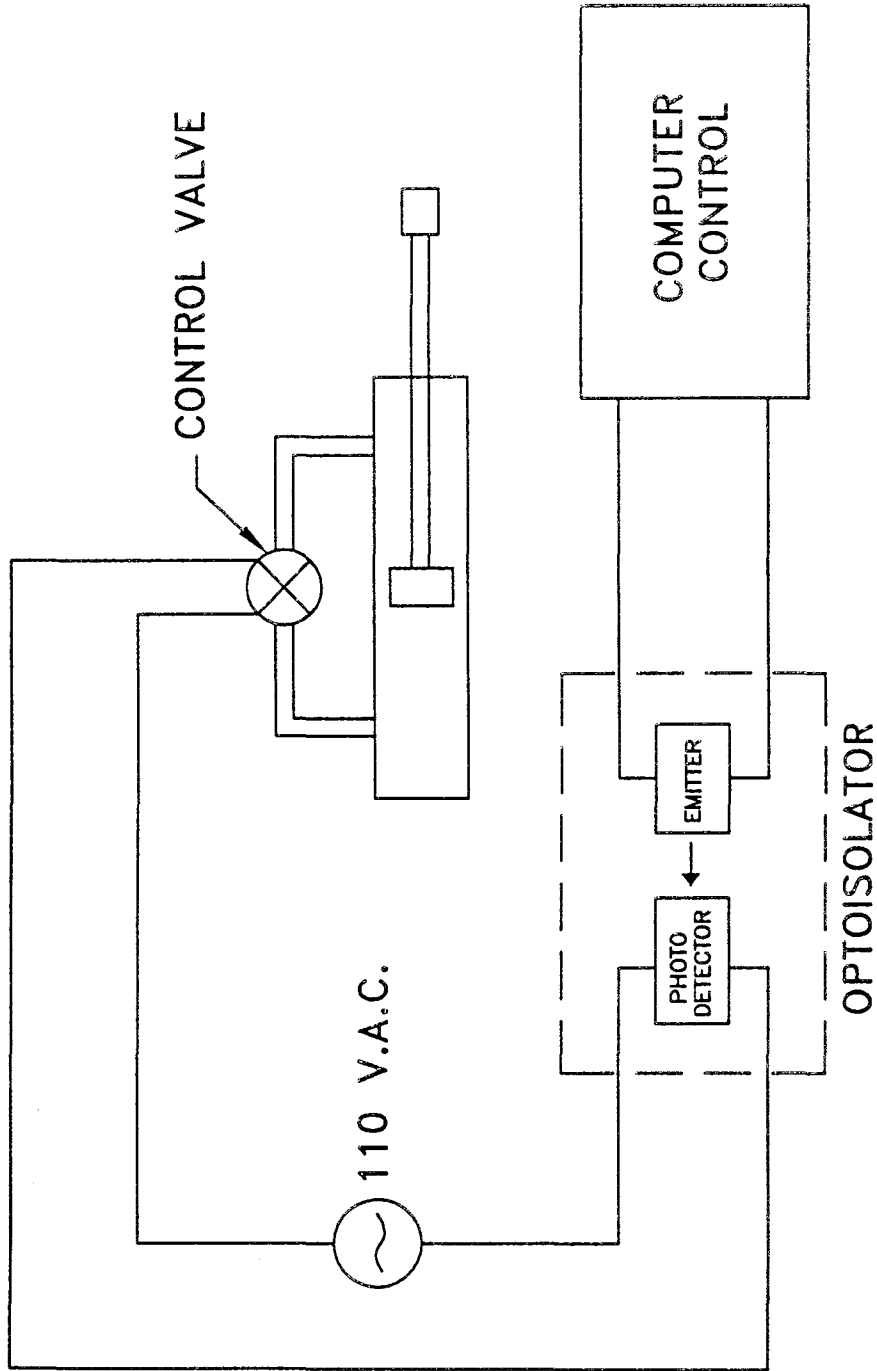


Figure 3-15 Schematic of Semi-Active Two-Stage Damper Computer Control Circuit

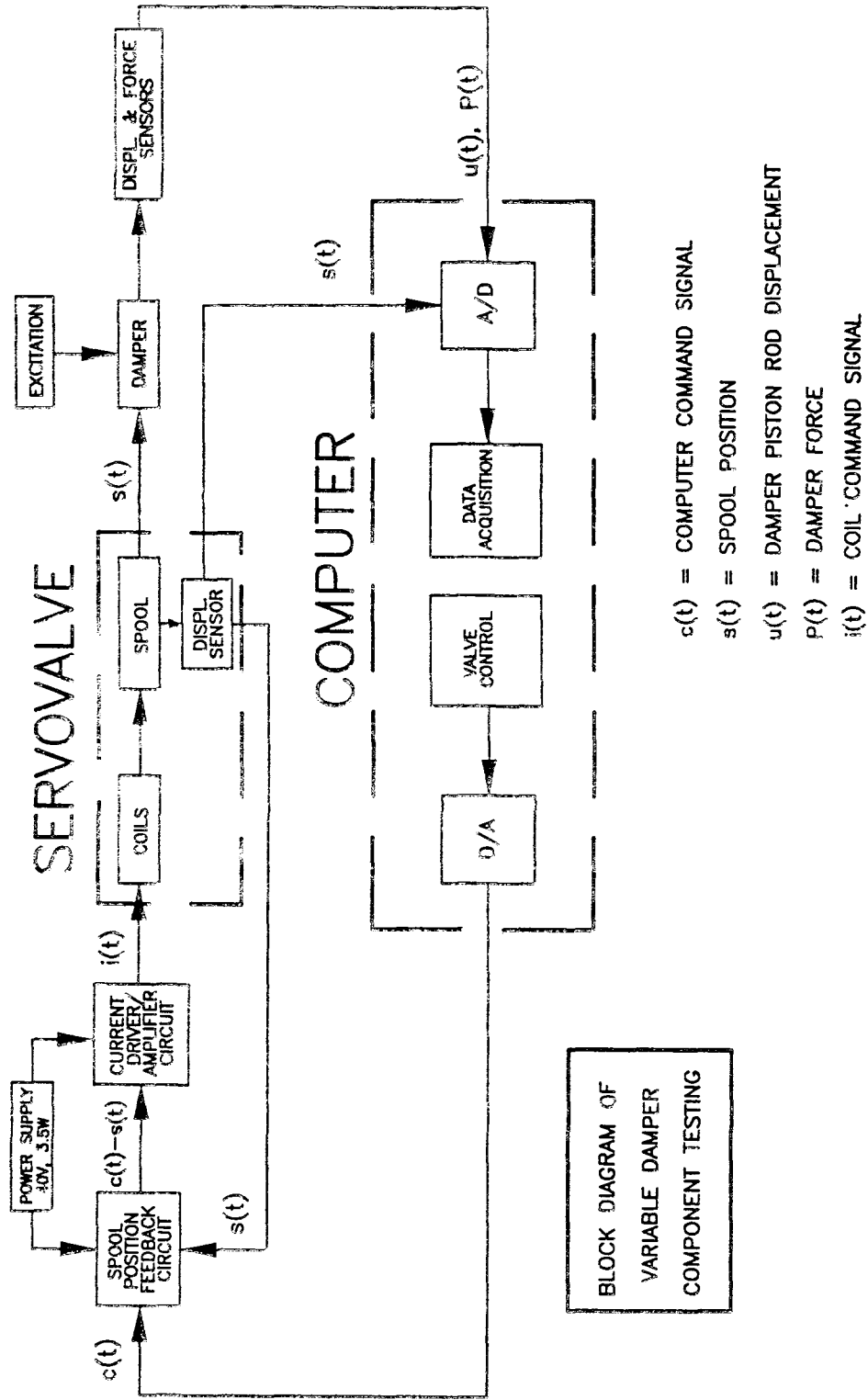


Figure 3-16 Block Diagram of Variable Damper Component Testing

3.3 Mechanical Properties

3.3.1 Theoretical Considerations

The mechanical properties of the semi-active fluid dampers were obtained by imposing cyclic motion to the dampers using the testing arrangement shown in Figure 3-12. For each test, the frequency and amplitude of motion of the piston was specified. The actuator motion was run under displacement control. For sinusoidal input, the damper motion is given by

$$u = u_o \sin(\omega t) \quad (3-1)$$

where u_o is the amplitude of the displacement, ω is the frequency of motion, and t is the time. For steady-state conditions, the force needed to maintain this motion is

$$P = P_o \sin(\omega t + \delta) \quad (3-2)$$

where P_o is the amplitude of the force, and δ is the phase angle between the imposed displacement and the resulting force. The area within the recorded force-displacement loops can be measured to determine the energy dissipated in a single cycle of motion

$$W_d = \oint P du = \pi P_o u_o \sin(\delta) \quad (3-3)$$

Expanding Equation (3-2),

$$P = P_o \sin(\omega t) \cos(\delta) + P_o \cos(\omega t) \sin(\delta) \quad (3-4)$$

and introducing the quantities

$$K_1 = \frac{P_o}{u_o} \cos(\delta) \quad (3-5)$$

$$K_2 = \frac{P_o}{u_o} \sin(\delta) \quad (3-6)$$

where K_1 is the storage stiffness (associated with recoverable (stored) energy) and K_2 is the loss stiffness (associated with irrecoverable (lost) energy), one obtains

$$P = K_1 u_o \sin(\omega t) + K_2 u_o \cos(\omega t) \quad (3-7)$$

Equation (3-6) may also be written in the form

$$P = K_1 u + \frac{K_2}{\omega} \dot{u} \quad (3-8)$$

where the overdot indicates differentiation with respect to time. It is clear that the first term in Equation (3-8) represents the force due to the stiffness of the damper which is in-phase with the motion and the second term represents the force in the damper due to the viscosity of the damper which is 90° out-of-phase with the motion. The damping coefficient is obtained from Equation (3-8) as

$$C = \frac{K_2}{\omega} \quad (3-9)$$

Combining Equation (3-3) and (3-6),

$$K_2 = \frac{W_d}{\pi u_o^2} \quad (3-10)$$

and rearranging Equation (3-6)

$$\delta = \sin^{-1} \left(\frac{K_2 u_o}{P_o} \right) \quad (3-11)$$

Equations (3-5) and (3-9) through (3-11) can now be used to obtain the mechanical properties of the damper from experimentally measured values of W_d , P_o , and u_o . First the loss stiffness is determined from Equation (3-10). Knowing the imposed frequency, ω , the

damping coefficient is determined from Equation (3-9). Equation (3-11) is used to compute the phase angle. Finally, the storage stiffness is computed using Equation (3-5).

Previous testing on the passive portion of the semi-active fluid dampers (see Figure 3-1) revealed that, below a certain cut-off frequency, the damping coefficient was nearly constant while the storage stiffness was negligible (Constantinou 1993b and 1992b). This is clearly demonstrated in the experimental data of Figure 3-17 which was obtained using Equations (3-5) and (3-9). The mechanical properties of the semi-active fluid dampers were therefore obtained by assuming linear viscous dashpot behavior

$$P = C\dot{u} \quad (3-12)$$

where C is the damping coefficient. For each semi-active damper test, the damping coefficient was determined by dividing the measured peak force by the measured peak velocity.

In addition to the harmonic tests, tests were performed with constant velocity motion (sawtooth displacement). Finally, tests were performed to determine the friction force between the semi-active damper piston rod and piston rod seal. In these tests, the damper piston rod was fully compressed and the damper was supported such that its longitudinal axis was in the vertical direction. Known masses were attached to the piston rod until motion was observed. The measured friction force was approximately 110 N.

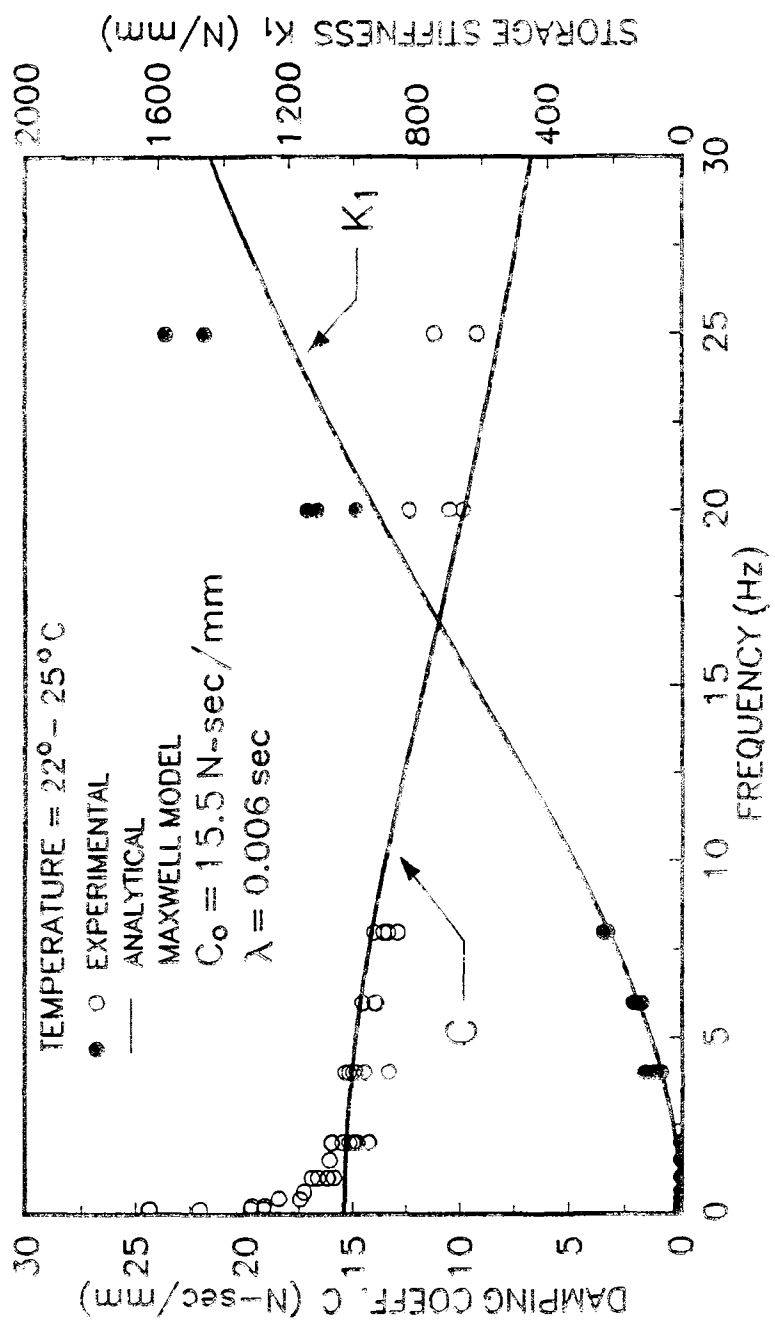


Figure 3-17 Experimental and Analytical Values of Damping Coefficient and Storage Stiffness of a Passive Fluid Viscous Damper (from Constantinou 1992b)

3.3.2 Two-Stage Damper

A total of 45 tests were conducted in the frequency range of 0.5 to 5 Hz and peak velocity range of 49 to 465 mm/s. The results are summarized in Table 3-III. In each test, three cycles of motion were imposed at either high (H) or low (L) damping, followed by three cycles of motion at the opposite level of damping. The column in Table 3-III labeled "stage" refers to whether the damping is switched from high to low (stage HL) or from low to high (stage LH). In all tests, the sampling rate was 400 pt/sec. For each test the maximum and minimum damping coefficient were obtained as follows:

$$C_{\max} = \frac{F_{\max}}{\dot{u}_o} \quad , \quad C_{\min} = \frac{F_{\min}}{\dot{u}_o} \quad (3-13)$$

where F_{\max} is the measured average peak force with the valve closed (high damping), F_{\min} is the measured average peak force with the valve opened (low damping), and \dot{u}_o is the measured average peak velocity (see Figure 3-18).

The response times shown in Table 3-III refer to the amount of time elapsed while the damper force changes from either high to low or low to high. Response times for the two-stage damper will be discussed in detail in Section 3.4.1.

The temperature is also provided in Table 3-III for the start and end of each test. The ambient temperature was measured by attaching a thermocouple to the cylindrical housing of the damper. The temperature was recorded immediately prior to a test (initial temperature) and again at the completion of the test (final temperature). For all tests, the increase in temperature during testing was less than or equal to 1°C.

TABLE 3-III Summary of Two-Stage Damper Component Tests

TEST	UNIT	STAGE	INPUT	FREQ. (Hz)	AMPL. (mm)	PEAK VEL. (mm/s)	MAX. FORCE (N)	MIN. FORCE (N)	C _{max} (N-s/mm)	C _{min} (N-s/mm)	RESPONSE TIME (ms)			TEMP (°C)	
											t ₁	t ₂	TOTAL	INITIAL	FINAL
561	2ST-A	HL	CV	0.5	24.52	49.04	828.20	126.40	16.89	2.58	---	---	---	25	25
567	2ST-A	HL	CV	0.5	24.85	49.71	798.30	122.53	16.06	2.46	9.58	5.36	14.94	25	25
566	2ST-A	LH	CV	0.5	24.41	48.82	792.70	117.80	16.24	2.41	---	---	---	25	25
568	2ST-A	LH	CV	0.5	24.87	49.74	788.88	121.58	15.86	2.44	27.35	23.02	50.37	25	26
575	2ST-A	HL	S	0.5	24.92	78.28	1257.10	183.60	16.06	2.35	---	---	---	23	24
583	2ST-A	HL	CV	0.75	24.86	74.57	1193.50	179.40	16.01	2.41	9.85	7.17	17.02	24	24
584	2ST-A	LH	CV	0.75	24.83	74.49	1186.40	178.00	15.93	2.39	40.11	14.88	54.99	24	24
560	2ST-A	HL	CV	1	24.03	96.11	1623.40	244.80	16.89	2.55	---	---	---	24	24
565	2ST-A	HL	CV	1	23.96	95.86	1562.70	230.00	16.30	2.40	---	---	---	25	25
569	2ST-A	HL	CV	1	24.78	99.11	1573.99	228.09	15.88	2.30	7.31	6.97	14.28	25	26
591	2ST-A	HL	CV	1	24.75	98.99	1619.60	244.80	16.36	2.47	9.98	4.69	14.67	23	23
592	2ST-A	HL	CV	1	24.78	99.11	1609.43	241.51	16.24	2.44	7.30	4.89	12.19	23	23
593	2ST-A	HL	CV	1	24.78	99.11	1618.87	241.51	16.33	2.44	7.37	4.83	12.20	23	23
564	2ST-A	LH	CV	1	23.96	95.86	1577.80	228.10	16.46	2.38	---	---	---	24	25
570	2ST-A	LH	CV	1	24.77	99.07	1545.71	239.40	15.60	2.42	24.95	13.68	38.63	25	26
594	2ST-A	LH	CV	1	24.78	99.11	1624.53	245.28	16.39	2.47	37.22	14.29	51.51	23	23
595	2ST-A	LH	CV	1	24.82	99.27	1621.11	245.05	16.33	2.47	35.01	14.89	49.90	23	23
596	2ST-A	LH	CV	1	24.80	99.19	1623.00	246.94	16.36	2.49	37.20	15.08	52.28	23	23
576	2ST-A	HL	S	1	24.89	156.41	2483.10	398.30	15.88	2.55	---	---	---	24	24
585	2ST-A	HL	CV	1.25	24.75	123.76	1956.20	317.80	15.81	2.57	7.14	6.04	13.18	24	25
586	2ST-A	LH	CV	1.25	24.75	123.74	1981.60	327.50	16.01	2.65	40.04	12.07	52.11	23	24

Table 3-III Cont'd

TEST	UNIT	STAGE	INPUT	FREQ. (Hz)	AMPL. (mm)	PEAK VEL. (mm/s)	MAX. FORCE (N)	MIN. FORCE (N)	Cmax (N-s/mm)	Cmin (N-s/mm)	RESPONSE TIME (ms)			TEMP (°C)	
											t ₁	t ₂	TOTAL	INITIAL	FINAL
587	2ST-A	HL	CV	1.5	24.75	148.49	2378.50	395.50	16.02	2.66	7.38	6.64	14.02	23	23
588	2ST-A	LH	CV	1.5	24.73	148.37	2372.90	415.30	15.99	2.80	40.11	13.28	53.39	24	24
577	2ST-A	HL	S	1.5	24.75	233.28	3597.00	674.20	15.42	2.89	---	---	---	24	24
589	2ST-A	HL	CV	1.75	24.49	171.41	2754.20	477.40	16.07	2.79	7.37	5.76	13.13	23	24
590	2ST-A	LH	CV	1.75	24.73	173.10	2740.10	491.50	15.83	2.84	40.14	12.88	53.02	23	23
562	2ST-A	HL	CV	2	23.10	184.80	3013.20	531.10	16.31	2.87	---	---	---	25	25
571	2ST-A	HL	CV	2	24.41	195.29	3016.02	539.11	15.44	2.76	7.94	6.53	14.47	25	26
563	2ST-A	LH	CV	2	23.11	184.86	2978.30	561.70	16.11	3.04	---	---	---	25	25
572	2ST-A	LH	CV	2	24.50	195.98	2978.32	539.11	15.20	2.75	22.61	10.65	33.26	25	26
578	2ST-A	HL	S	2	24.75	311.04	4562.60	987.80	14.67	3.18	---	---	---	24	24
579	2ST-A	HL	S	2.5	24.88	390.86	5254.20	1299.40	13.44	3.32	---	---	---	24	25
573	2ST-A	HL	CV	3	24.15	289.80	4377.90	900.10	15.11	3.11	---	---	---	25	26
574	2ST-A	LH	CV	3	24.25	290.90	4231.90	942.50	14.55	3.24	35.37	15.81	51.18	25	26
580	2ST-A	HL	S	3	24.66* 24.38*	464.83* 459.48*	5587.60	1632.80	12.16	3.51	---	---	---	24	25
581	2ST-A	HL	S	4	12.26	308.06	4548.40	940.70	14.76	3.05	---	---	---	24	24
582	2ST-A	HL	S	5	12.09* 11.86*	379.83* 372.58*	5242.90	1214.70	14.07	3.20	---	---	---	24	24
597	2ST-B	HL	CV	0.5	24.93	49.86	792.10	133.60	15.89	2.68	9.91	7.36	17.27	22	22
598	2ST-B	LH	CV	0.5	24.90	49.80	782.08	134.91	15.70	2.71	30.14	19.19	49.33	22	22

Table 3-III Cont'd

TEST	UNIT	STAGE	INPUT	FREQ. (Hz)	AMPL. (mm)	PEAK VEL. (mm/s)	MAX. FORCE (N)	MIN FORCE (N)	C _{max} (N-s/mm)	C _{min} (N-s/mm)	RESPONSE TIME (ms)		TEMP (°C)		
											t ₁	t ₂	TOTAL	INITIAL FINAL	
599	2ST-B	HL	CV	1	24.72	98.86	1542.80	257.80	15.61	2.61	7.37	5.03	12.40	22	22
600	2ST-B	LH	CV	1	24.82	99.27	1515.09	266.04	15.26	2.68	30.04	13.97	44.01	22	22
601	2ST-B	HL	CV	1.5	24.61	147.65	2238.70	419.00	15.16	2.84	7.37	6.70	14.07	22	22
602	2ST-B	LH	CV	1.5	24.72	148.31	2219.34	445.75	14.96	3.01	29.76	13.14	42.90	22	22
603	2ST-B	HL	CV	2	24.55	196.41	2930.30	576.30	14.92	2.93	7.94	6.94	14.88	22	23
604	2ST-B	LH	CV	2	24.60	196.77	2867.92	607.55	14.57	3.09	34.92	13.11	48.03	22	23

Notes:

* = low damping

= high damping

--- = response measurements low-pass filtered ; therefore response time not measured

HL = High to Low damping test

LH = Low to High damping test

CV = Constant velocity test

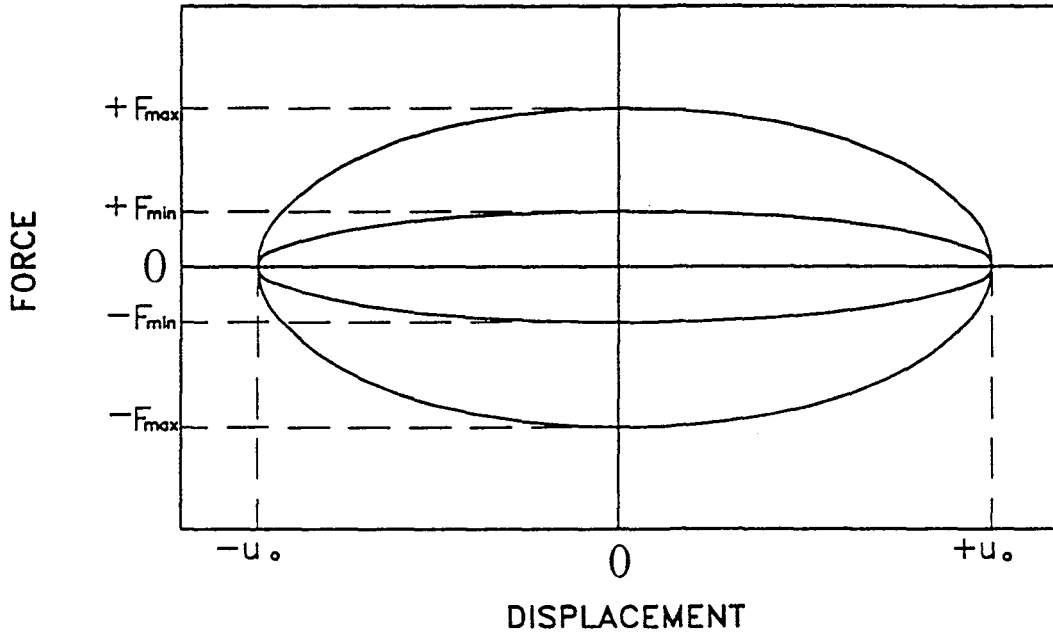
S = Sinusoidal test

t₁ = Static response time

t₂ = Dynamic response time

Data acquisition sampling rate for all tests = 400 pt/sec

TYPICAL TEST RESULT UNDER SINUSOIDAL MOTION



$$\dot{u}_o = f(\omega, u_o)$$

$$C_{max} = F_{max} / \dot{u}_o$$

$$C_{min} = F_{min} / \dot{u}_o$$

$$u_o = \frac{|+u_o| + |-u_o|}{2}$$

$$F_{max} = \frac{|+F_{max}| + |-F_{max}|}{2}$$

$$F_{min} = \frac{|+F_{min}| + |-F_{min}|}{2}$$

Figure 3-18 Diagram Describing Method of Extracting Damper Mechanical Properties from Component Test Results

Figure 3-19 shows typical force-displacement loops under two different sinusoidal motions and with the damping switching from high to low. Note that the elliptical shape of the force-displacement loops is an indication of linear viscous damping. The force-displacement loop of Figure 3-19(a) is shown again in Figure 3-20 along with its corresponding command signal time history. Recall that the command signal is a digital output signal with values of 0 (valve off) or 1 (valve on). Figure 3-21 shows typical force-displacement loops under two different constant velocity motions and with the damping switching from high to low (Figure 3-21(a)) and from low to high (Figure 3-21(b)). The nearly constant output force is an indication of linear viscous damping.

The relationship between the peak velocity and peak force for both of the tested two-stage damper units is shown in Figure 3-22. Two sets of data are plotted in each graph. One set corresponds to the closed solenoid valve (high damping) while the other set corresponds to the open solenoid valve (low damping). Clearly, the two sets of data can be fit with straight lines having slopes equal to the corresponding damping coefficient (i.e., C_{\max} or C_{\min}). Note that the data shown in Figure 3-22 corresponds to tests run at frequencies of 4 Hz or less. Recall that the dampers begin to develop stiffness for frequencies above the cut-off frequency (see Figure 3-17). As a result, for frequencies beyond about 4 Hz, the data begins to deviate from the linearity shown in Figure 3-22.

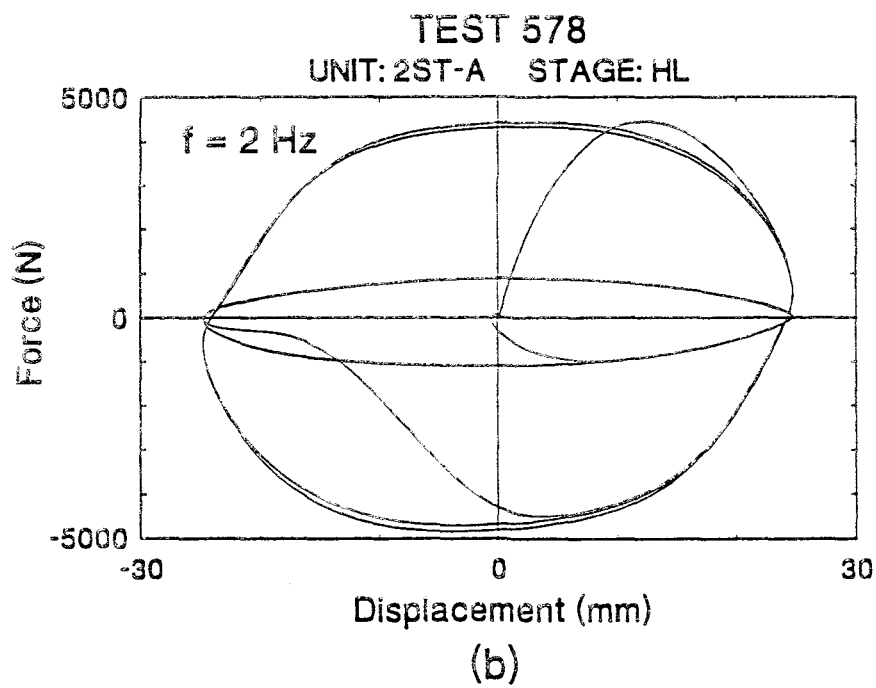
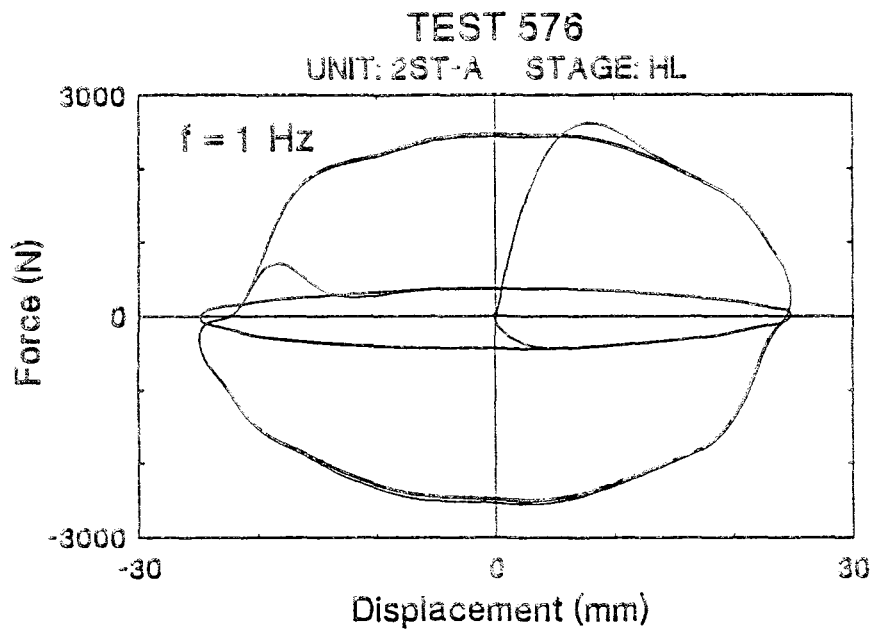


Figure 3-19 Hysteresis Loops for Two-Stage Damper Switching from High Damping to Low Damping and Subjected to Sinusoidal Motion at a Frequency of a) 1 Hz and b) 2 Hz

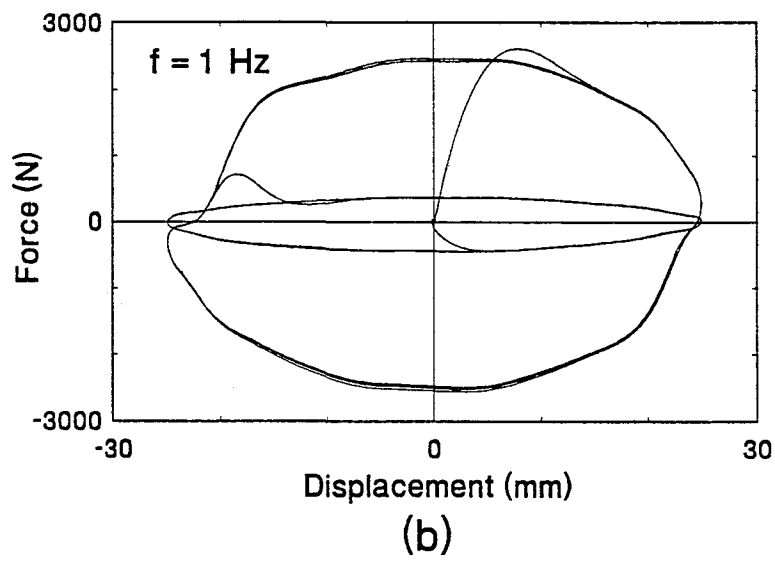
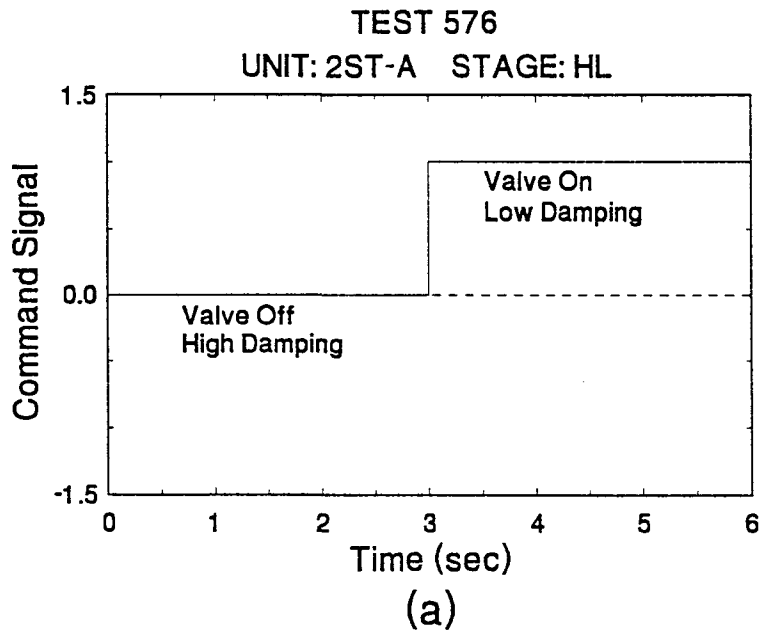


Figure 3-20 Hysteresis Loop and Corresponding Command Signal for Two-Stage Damper

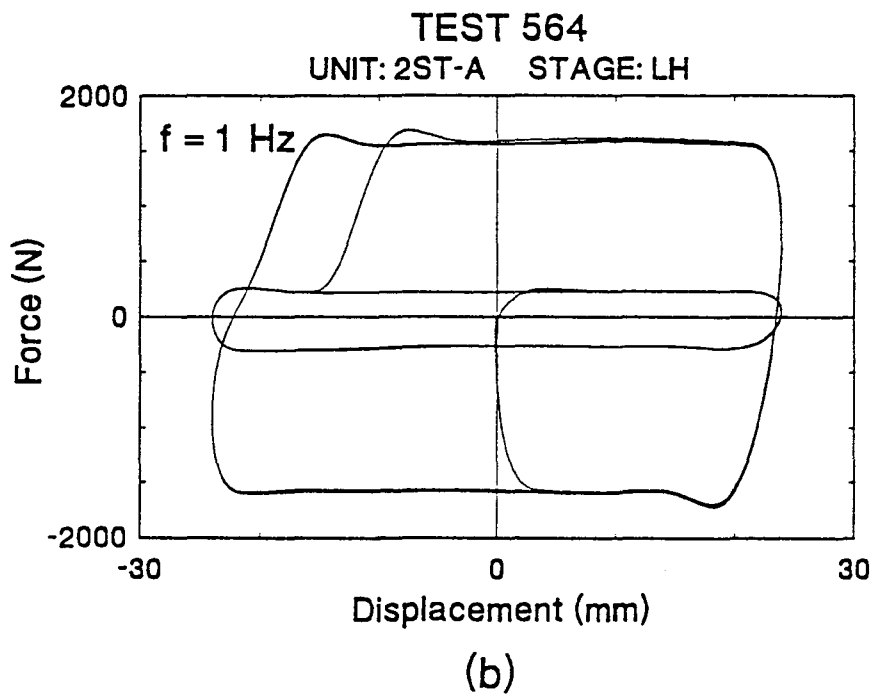
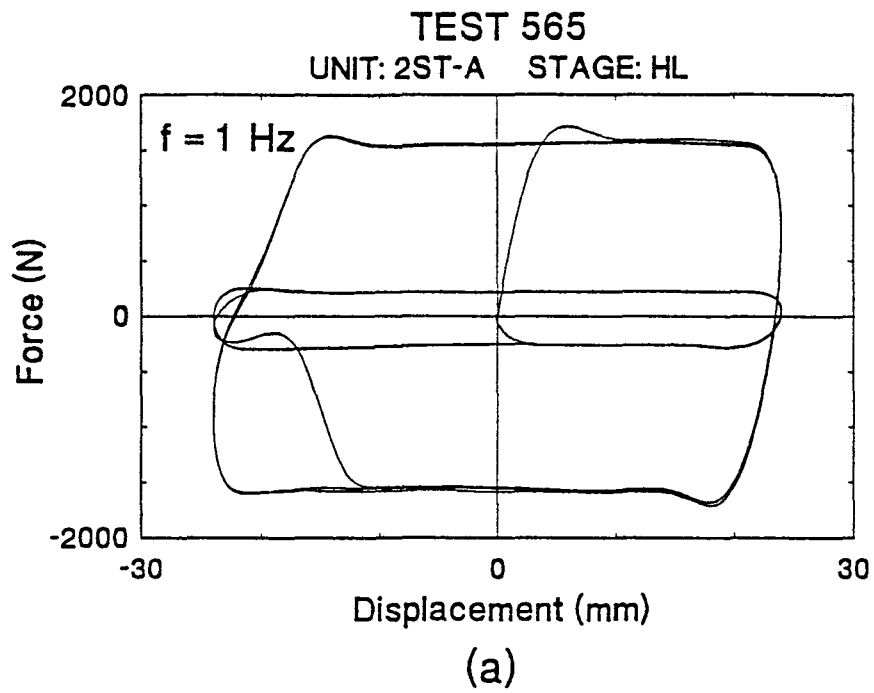
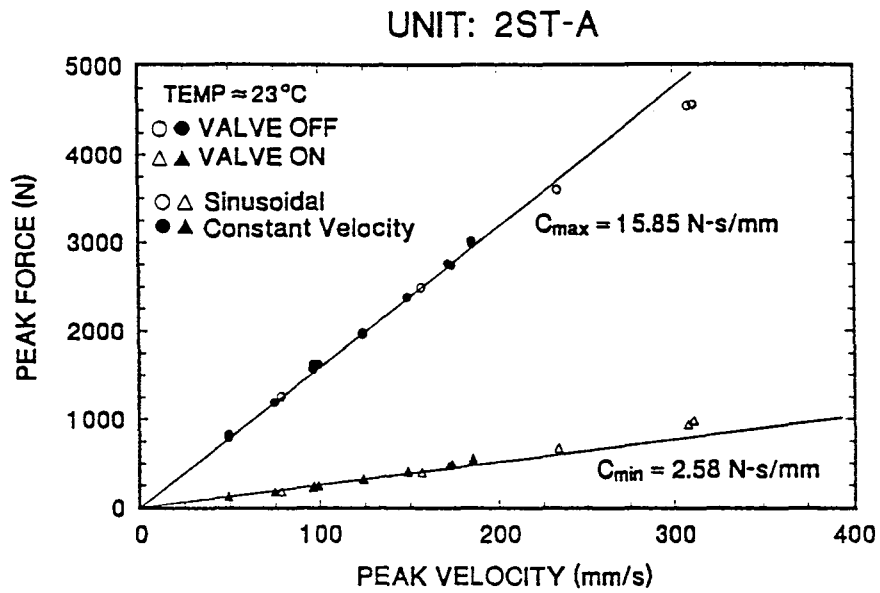
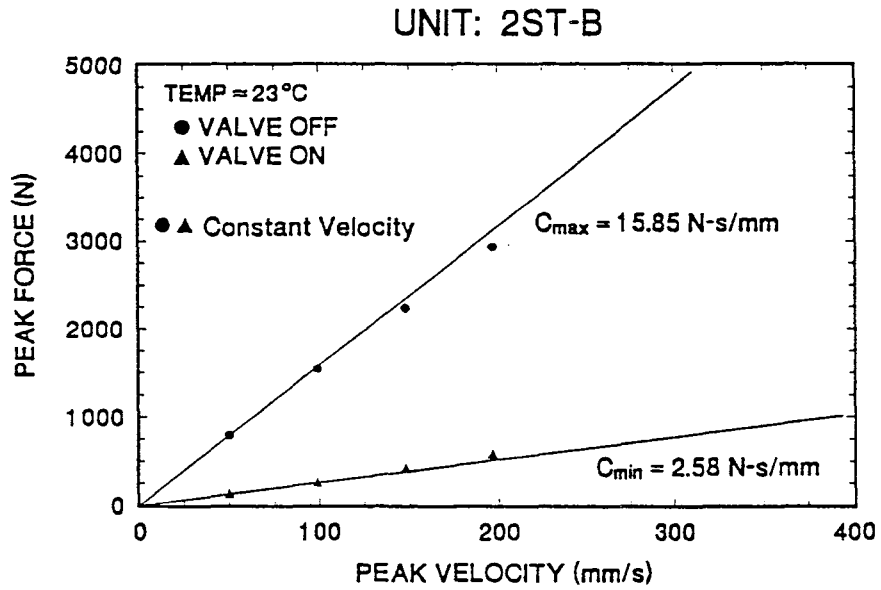


Figure 3-21 Hysteresis Loops for Two-Stage Damper Subjected to Constant Velocity Motion at a Frequency of 1 Hz and with Damping Switching from a) High to Low and b) Low to High



(a)



(b)

Figure 3-22 Experimental Values of Peak Force Versus Peak Velocity for Two-Stage Damper Unit a) 2ST-A and b) 2ST-B

3.3.3 Variable Damper

A total of 92 tests were conducted in the frequency range of 0.25 to 4 Hz and peak velocity range of 39 to 603 mm/s. Two basic tests were performed on the variable dampers. The first test was one in which the valve was operated from either a full closed position (high damping, 0 volt command signal) to a full open position (low damping, 3 volt command signal) or from a full open position to a full closed position. This type of test is designated as a two-stage test (not to be confused with the two-stage dampers) and a total of 58 of these tests were performed. The test results for the two-stage tests are presented in Table 3-IV. In each test, three cycles of motion were imposed at either high (H) or low (L) damping, followed by three cycles at the opposite level of damping. In all of the two-stage tests, the sampling rate was 400 pt/sec. For each test, the maximum and minimum damping coefficient were found by the same method described in Section 3.3.2 for tests on the two-stage damper.

The response times shown in Table 3-IV refer to the amount of time elapsed while the damper force changes from either high to low or low to high. Response times for the variable damper will be discussed in detail in Section 3.4.2.

The temperature is also provided in Table 3-IV for the start and end of each test. For all of the two-stage tests, the increase in temperature during testing was less than or equal to 2°C. Note that the temperature was not recorded for approximately 20% of the two-stage tests.

Table 3-IV Summary of Variable Damper Component Tests (Two-Stage Tests)

TEST	UNIT	STAGE	INPUT	FREQ. (Hz)	AMPL. (mm)	PEAK VEL. (mm/s)	MAX. FORCE (N)	MIN. FORCE (N)	C _{max} (N-s/mm)	C _{min} (N-s/mm)	RESPONSE TIME (ms)			TEMP (°C)	
											t ₁	t ₂	TOTAL	INITIAL	FINAL
678	VAR-A	HL	CV	0.5	24.76	49.51	884.53	118.94	17.87	2.40	7.34	4.84	12.18	X	X
700	VAR-A	HL	CV	0.5	24.50	48.99	890.69	130.87	18.18	2.67	---	---	---	X	X
710	VAR-A	HL	CV	0.5	25.24	50.48	764.43	128.56	15.14	2.55	9.84	4.68	14.52	21	21
679	VAR-A	LH	CV	0.5	24.87	49.73	887.99	116.63	17.85	2.35	7.98	35.21	43.19	X	X
711	VAR-A	LH	CV	0.5	25.13	50.27	762.89	123.94	15.18	2.47	7.35	20.19	27.54	21	21
701	VAR-A	HL	S	0.5	24.14	75.83	1387.99	192.84	18.30	2.54	---	---	---	X	X
712	VAR-A	HL	CV	0.75	25.12	75.35	1131.64	196.30	15.02	2.61	10.32	4.68	15.00	21	22
713	VAR-A	LH	CV	0.75	25.14	75.41	1137.13	192.99	15.08	2.56	10.16	15.56	25.72	21	22
676	VAR-A	HL	CV	1	24.80	99.19	1722.86	277.14	17.37	2.79	7.42	6.94	14.36	X	X
699	VAR-A	HL	CV	1	24.01	96.05	1755.20	252.50	18.27	2.63	---	---	---	X	X
714	VAR-A	HL	CV	1	25.04	100.16	1508.85	277.14	15.06	2.77	10.00	4.84	14.84	21	22
726	VAR-A	HL	CV	1	25.09	100.35	1523.08	276.92	15.18	2.76	7.89	6.36	14.25	20	21
727	VAR-A	HL	CV	1	25.09	100.35	1523.08	275.38	15.18	2.74	7.96	6.35	14.31	20	21
764	VAR-A	HL	CV	1	25.04	100.18	1504.62	261.54	15.02	2.61	10.29	8.49	18.78	21	21
765	VAR-A	HL	CV	1	25.04	100.18	1503.08	267.69	15.00	2.67	10.29	7.14	17.43	20	21
766	VAR-A	HL	CV	1	25.16	100.63	1603.08	261.54	15.93	2.60	9.98	6.01	15.99	20	21
767	VAR-A	HL	CV	1	25.00	100.02	1601.54	263.08	16.01	2.63	9.78	4.95	14.73	20	21
677	VAR-A	LH	CV	1	24.78	99.13	1729.00	275.60	17.44	2.78	7.34	12.83	20.17	X	X
715	VAR-A	LH	CV	1	25.10	100.40	1493.46	266.36	14.87	2.65	7.42	15.32	22.74	21	22
728	VAR-A	LH	CV	1	25.06	100.22	1530.77	263.08	15.27	3.14	5.00	13.87	18.87	20	20
729	VAR-A	LH	CV	1	25.06	100.24	1516.92	281.54	15.13	2.81	7.25	13.04	20.29	20	20

Table 3-IV Cont'd

TEST	UNIT	STAGE	INPUT	FREQ. (Hz)	AMPL. (mm)	PEAK VEL. (mm/s)	MAX. FORCE (N)	MIN. FORCE (N)	C _{max} (N-s/mm)	C _{min} (N-s/mm)	RESPONSE TIME (ms)			TEMP (°C)	
											t ₁	t ₂	TOTAL	INITIAL	FINAL
716	VAR-A	HL	CV	1.25	24.98	124.90	1876.44	363.74	15.02	2.91	10.00	6.45	16.45	21	22
717	VAR-A	LH	CV	1.25	24.97	124.86	1850.92	346.69	14.82	2.78	7.90	13.71	21.61	21	21
718	VAR-A	HL	CV	1.5	24.97	149.83	2234.62	442.31	14.91	2.95	7.63	7.63	15.27	21	21
719	VAR-A	LH	CV	1.5	24.86	149.18	2230.77	442.31	14.95	2.96	7.53	12.58	20.11	20	21
720	VAR-A	HL	CV	1.75	24.80	173.60	2661.54	553.85	15.33	3.19	9.50	6.29	15.79	20	21
721	VAR-A	LH	CV	1.75	24.94	174.55	2672.31	553.85	15.31	3.17	9.67	8.70	18.37	20	20
722	VAR-A	HL	CV	2	24.80	198.40	3070.77	649.23	15.48	3.27	10.19	5.26	15.45	20	21
723	VAR-A	LH	CV	2	24.81	198.52	3043.08	643.08	15.33	3.24	7.59	13.78	21.37	20	20
724	VAR-A	HL	CV	3	24.56* 24.04#	294.72* 288.48#	4569.23	1153.85	15.84	3.92	7.59	11.86	19.45	20	21
725	VAR-A	LH	CV	3	24.62* 24.32#	295.44* 291.84#	4169.23	1157.69	14.29	3.92	7.59	11.86	19.45	21	23
690	VAR-B	HL	CV	0.5	24.91	49.81	922.25	130.87	18.51	2.63	10.17	7.18	17.35	X	X
744	VAR-B	HL	CV	0.5	25.28	50.56	944.62	130.77	18.68	2.59	12.72	4.66	17.38	20	20
691	VAR-B	LH	CV	0.5	24.94	49.89	917.63	131.64	18.39	2.64	10.25	37.13	47.38	X	X
745	VAR-B	LH	CV	0.5	25.17	50.34	939.95	130.10	18.67	2.58	9.66	20.13	29.79	20	20
746	VAR-B	HL	CV	0.75	25.10	75.31	1383.46	174.23	18.37	2.31	10.47	6.36	16.83	20	21
747	VAR-B	LH	CV	0.75	25.28	75.85	1397.23	180.14	18.42	2.38	9.98	19.97	29.95	20	20
688	VAR-B	HL	CV	1	24.83	99.32	1816.78	249.42	18.29	2.51	10.32	6.77	17.09	X	X
698	VAR-B	HL	CV	1	23.97	95.90	1799.85	230.95	18.77	2.41	---	---	---	X	X

Table 3-IV Cont'd

TEST	UNIT	STAGE	INPUT	FREQ. (Hz)	AMPL. (mm)	PEAK VEL. (mm/s)	MAX. FORCE (N)	MIN. FORCE (N)	C _{max} (N-s/mm)	C _{min} (N-s/mm)	RESPONSE TIME (ms)			TEMP (°C)	
											t ₁	t ₂	TOTAL	INITIAL	FINAL
748	VAR-B	HL	CV	1	24.94	99.74	1855.27	235.57	18.60	2.36	9.76	6.53	16.29	20	20
760	VAR-B	HL	CV	1	25.01	100.05	1812.31	229.23	18.11	2.29	10.19	6.02	16.21	20	21
761	VAR-B	HL	CV	1	25.06	100.22	1830.77	235.38	18.27	2.35	10.37	5.55	15.92	20	21
689	VAR-B	LH	CV	1	24.94	99.77	1790.61	254.04	17.94	2.55	10.24	20.16	30.40	X	X
749	VAR-B	LH	CV	1	25.10	100.42	1833.72	246.34	18.26	2.45	9.81	17.20	27.01	20	20
762	VAR-B	LH	CV	1	25.10	100.42	1841.54	244.62	18.34	2.44	9.74	17.63	27.37	20	21
763	VAR-B	LH	CV	1	25.02	100.10	1827.69	240.00	18.26	2.40	9.76	17.74	27.50	20	20
750	VAR-B	HL	CV	1.25	24.90	124.48	2255.58	306.00	18.12	2.46	10.37	6.35	16.72	20	21
751	VAR-B	LH	CV	1.25	24.90	124.48	2215.17	306.00	17.80	2.46	10.06	16.83	26.89	20	21
752	VAR-B	HL	CV	1.5	24.94	149.66	2688.22	371.82	17.96	2.48	9.78	6.67	16.45	20	21
753	VAR-B	LH	CV	1.5	24.98	149.90	2655.89	385.68	17.72	2.57	9.81	14.33	24.14	20	21
754	VAR-B	HL	CV	1.75	24.84	173.87	3110.08	458.81	17.89	2.64	9.65	6.67	16.32	20	22
755	VAR-B	LH	CV	1.75	24.88	174.15	3076.92	464.62	17.67	2.67	9.65	13.75	23.40	20	20
756	VAR-B	HL	CV	2	24.74	197.94	3538.11	554.27	17.87	2.80	10.09	7.40	17.49	20	21
757	VAR-B	LH	CV	2	24.77	198.20	3485.76	554.27	17.59	2.80	9.89	14.62	24.51	19	20
696	VAR-B	HL	S	2	24.94	313.40	5224.02	1103.93	16.67	3.52	---	---	---	21	22
758	VAR-B	HL	CV	3	24.64* 23.76#	295.28* 285.12#	4984.62	964.62	17.48	3.27	9.61	7.51	17.12	21	23
759	VAR-B	LH	CV	3	24.42* 23.94#	293.01* 287.28#	4933.85	978.46	17.17	3.34	8.55	21.37	29.92	20	20

Table 3-IV Cont'd

TEST	UNIT	STAGE	INPUT	FREQ. (Hz)	AMPL. (mm)	PEAK VEL. (mm/s)	MAX. FORCE (N)	MIN. FORCE (N)	C _{max} (N-s/mm)	C _{min} (N-s/mm)	RESPONSE TIME (ms)		TEMP (°C)	
											t ₁	t ₂	TOTAL	INITIAL
697	VAR-B	HL	S	4	24.01* 18.68#	603.44* 469.48#	6146.27	2155.50	10.19	4.59	---	---	22	23

Notes:

- * = low damping
- # = high damping
- = response measurements low-pass filtered ; therefore response time not measured
- X = temperature not recorded
- HL = High to Low damping test
- LH = Low to High damping test
- CV = Constant velocity test
- S = Sinusoidal test
- t₁ = Static response time
- t₂ = Dynamic response time
- Data acquisition sampling rate for all tests = 400 pt/sec

Figure 3-23 and 3-24 show typical force-displacement loops under two different constant velocity motions and with the damping switching from high to low (Figure 3-23) and low to high (Figure 3-24). The force-displacement loops of these figures were obtained from experimental data which was not low pass filtered. These tests therefore have a lower signal-to-noise ratio compared to the two-stage damper tests of Figure 3-21.

The force-displacement loop of Figure 3-23(a) is shown again in Figure 3-25 along with its corresponding command signal and spool displacement time history. The command signal is in the form of a step function from 0 volts to 3 volts (see Figure 3-25(a)). However, the spool displacement is not able to follow the step function and exhibits an overshoot in displacement (see Figure 3-25(b)). This is the result of the inertia of the spool as well as a possible overshoot in the current command signal from the current driver circuit (see Figure 3-16). The effect of the spool displacement overshoot on the damper behavior is shown in part (c) of Figure 3-25 where the measured force exhibits an overshoot as well. The spool displacement and damper force overshoot can both be reduced at the expense of increased response times. A number of tests were performed in which the current driver/amplifier circuit was adjusted to control the amount of spool overshoot. Furthermore, the size of the spool seals (and, therefore, the friction between the spool seals and the spool bushing) was adjusted to control the amount of spool overshoot, the response time, and the flow leakage at low command signal voltage levels (recall discussion in Section 3.1.2 related to spool seals and valve behavior at low

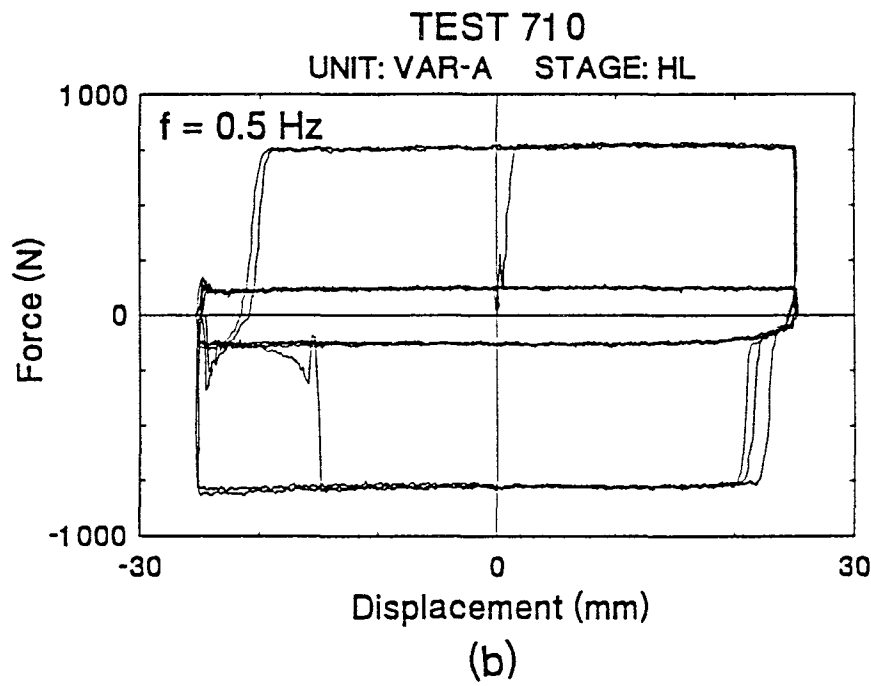
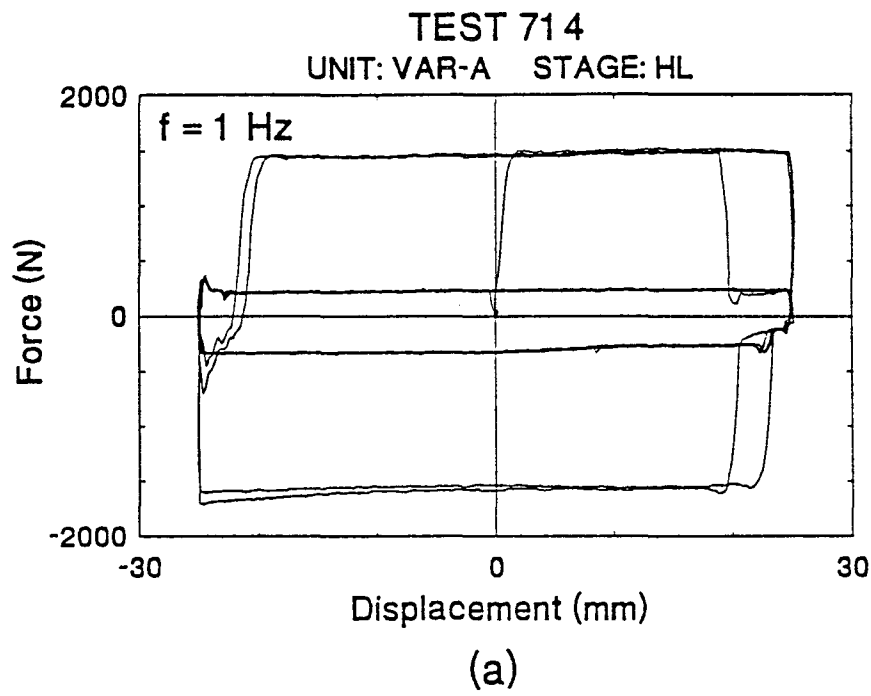


Figure 3-23 Typical Force-Displacement Loops Under Constant Velocity Motion for the Variable Damper with Damping Switching from High to Low and Input Frequencies of a) 1 Hz and b) 0.5 Hz

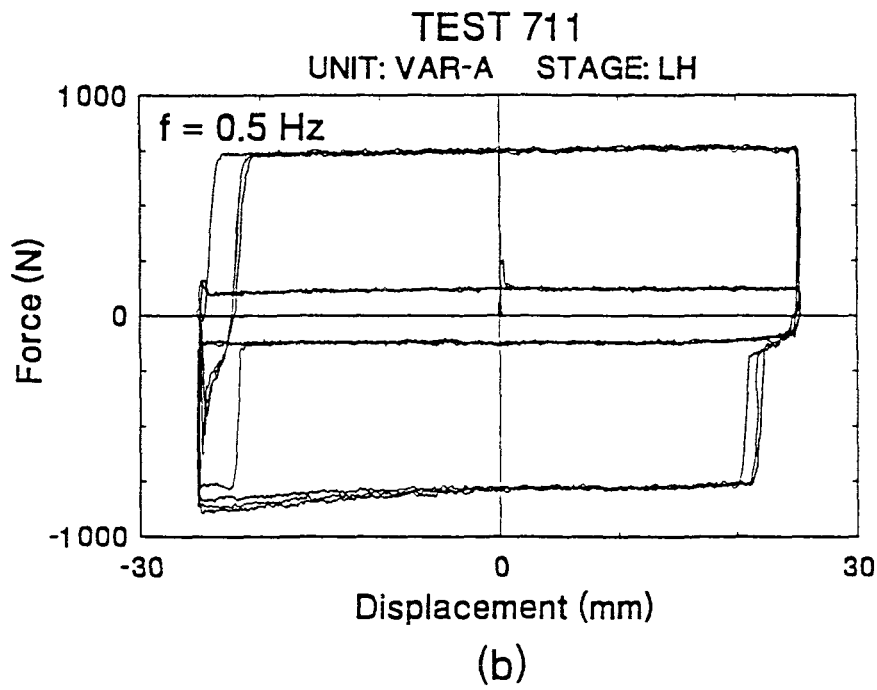
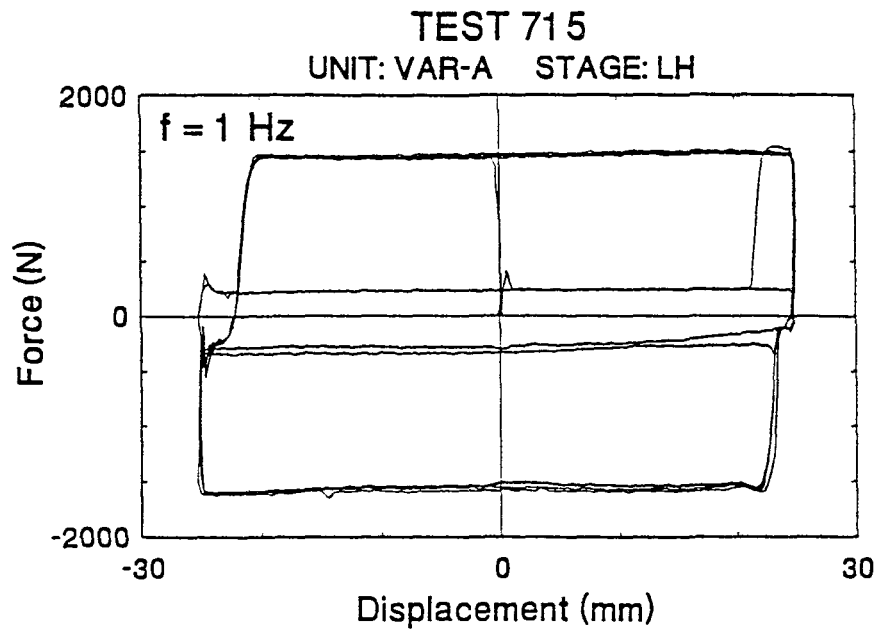
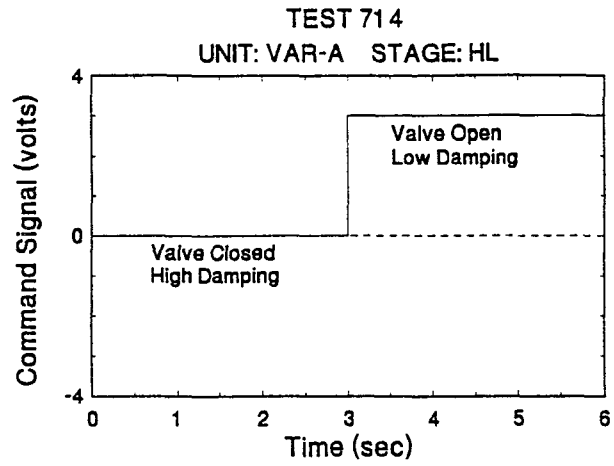
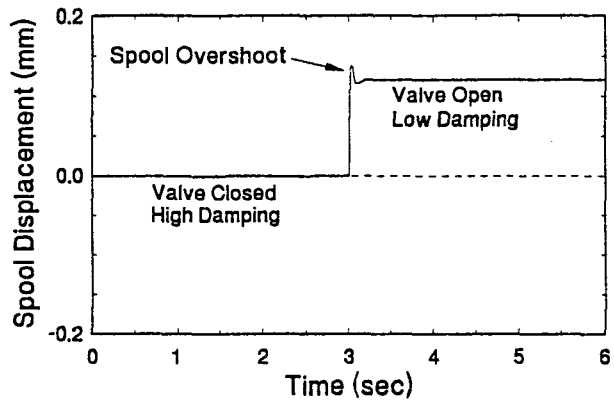


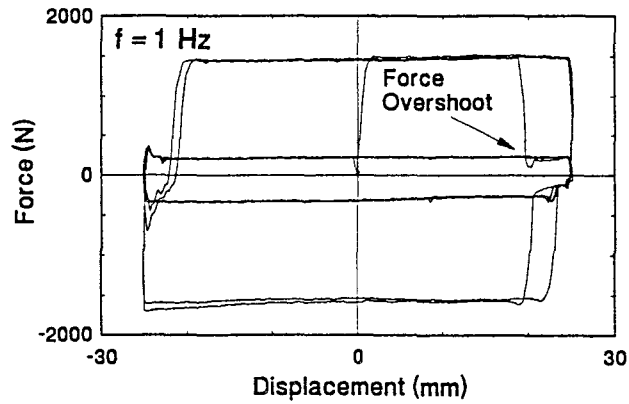
Figure 3-24 Typical Force-Displacement Loops Under Constant Velocity Motion for the Variable Damper with Damping Switching from Low to High and Input Frequencies of a) 1 Hz and b) 0.5 Hz



(a)



(b)



(c)

Figure 3-25 Hysteresis Loop and Corresponding Command Signal and Spool Displacement for Variable Damper Two-Stage Test

command signal voltage levels). A compromise was reached in which the response times (see Section 3.4.2) and damper force overshoot were acceptable.

As mentioned previously, two basic tests were performed on the variable dampers. The second test was one in which the valve position was incrementally changed from either a full closed position (high damping) to a full open position (low damping) or from a full open to a full closed position. This type of test is designated as a multi-stage test and a total of 34 of these tests were performed. In each test, 2 cycles of motion were imposed at each damping level. The test results for the multi-stage tests are presented in Tables 3-V(a) and 3-V(b). Note that the peak force and damping coefficient are given at seven different voltage levels in Table 3-V(a) and 3-V(b), respectively. The voltage levels correspond to the command signal from the computer. A 0 volt command signal corresponds to a fully closed valve (high damping) and a 3.0 volt command signal corresponds to a fully open valve (low damping). The damping coefficient given in Table 3-V (b) is calculated for the i -th level of voltage by

$$C_i = \frac{(F_o)_i}{(\dot{u}_o)_i} \quad , \quad i = 1 \text{ to } 7 \quad (3-14)$$

where $(F_o)_i$ and $(\dot{u}_o)_i$ are the peak force and peak velocity for the i -th level of voltage, respectively (e.g., $i = 1$ corresponds to a 0 volt command signal and $i = 7$ corresponds to a 3.0 volt command signal).

The temperature is also provided in Tables 3-V(a) and 3-V(b) for the start and end of each test. For all tests, the increase in temperature during testing was less than or equal to

Table 3-V(a) Summary of Variable Damper Component Tests (Multi-Stage Tests)

TEST	UNIT	STAGE	INPUT	FREQ. (Hz)	AMPL. (mm)	PEAK VEL. (mm/s)	PEAK FORCE (N)								TEMP (°C)	
							0 volts	0.75 volts	1.0 volts	1.25 volts	1.5 volts	2.0 volts	3.0 volts	INITIAL	FINAL	
702	VAR-A	HL	S	0.25	25.00	39.27	689.76	689.76	625.10	504.39	375.06	216.78	103.46	22	22	
730	VAR-A	HL	S	0.25	25.16	39.52	627.08	627.08	579.08	488.00	380.92	233.85	116.92	20	20	
680	VAR-A	HL	CV	0.5	24.43	48.86	877.60	877.60	779.45	610.85	437.64	254.04	127.02	X	X	
734	VAR-A	HL	CV	0.5	24.72	49.45	776.15	756.15	702.31	576.92	435.38	263.85	131.54	21	21	
681	VAR-A	LH	CV	0.5	24.41	48.82	877.60	877.60	782.91	612.01	438.80	254.04	127.02	X	X	
682	VAR-A	HL	S	0.5	24.76	77.77	1385.68	1356.43	1214.78	919.17	660.51	386.45	184.76	X	X	
731	VAR-A	HL	S	0.5	25.10	78.87	1270.38	1234.62	1149.23	934.62	696.92	430.38	219.23	20	21	
683	VAR-A	LH	S	0.5	24.81	77.95	1383.08	1355.38	1198.46	907.69	653.85	383.08	187.69	X	X	
735	VAR-A	HL	CV	1	24.24	96.96	1523.08	1463.08	1335.38	1030.77	755.38	483.08	276.92	21	22	
674	VAR-A	HL	CV	1	24.02	96.08	1653.00	1627.10	1415.40	1039.60	750.20	467.00	257.70	X	X	
675	VAR-A	LH	CV	1	24.01	96.04	1663.80	1631.50	1403.20	1050.10	771.00	464.10	259.10	X	X	
684	VAR-A	HL	S	1	24.81	155.92	2750.58	2639.72	2214.78	1706.70	1309.47	831.41	436.49	X	X	
732	VAR-A	HL	S	1	25.10	157.74	2466.92	2397.69	2130.00	1650.00	1250.77	807.69	438.46	20	22	
685	VAR-A	LH	S	1	24.81	155.92	2609.70	2584.30	2173.21	1720.55	1332.56	836.03	441.11	X	X	
736	VAR-A	HL	CV	1.5	23.67	142.03	2231.54	2125.38	1850.77	1451.54	1103.08	738.46	436.15	21	23	
703	VAR-A	HL	S	1.5	24.90	234.64	4080.06	3775.98	3113.93	2501.92	2040.03	1385.68	731.33	22	25	
733	VAR-A	HL	S	1.5	25.06	236.19	3630.77	3421.54	2920.00	2375.38	1938.46	1323.08	738.46	20	22	
708	VAR-A	HL	CV	2	23.13	185.04	2800.00	2680.00	2307.69	1840.00	1480.00	993.85	569.23	22	26	
709	VAR-A	LH	CV	2	23.15	185.20	2676.92	2643.08	2375.38	1969.23	1553.85	1052.31	615.38	22	25	
704	VAR-A	HL	S	2	24.97	313.81	5085.45	4678.98	3944.57	3288.68	2729.79	1981.52	1108.55	22	27	
707	VAR-A	LH	S	2	24.98	313.91	3884.62	3826.92	3426.92	2992.31	2538.46	1865.38	1076.92	22	27	
705	VAR-A	HL	S	3	24.96	470.56	4993.07	4928.41	4448.04	3967.67	3533.49	2729.79	1806.00	22	30	

Table 3-V(a) Cont'd

TEST	UNIT	STAGE	INPUT	FREQ. (Hz)	AMPL. (mm)	PEAK VEL. (mm/s)	PEAK FORCE (N)								TEMP (°C)			
							0 volts	0.75 volts	1.0 volts	1.25 volts	1.5 volts	2.0 volts	3.0 volts	INITIAL	FINAL			
							**	4076.92	3523.08	2961.54	2500.00	1846.15	1053.85	22	25			
706	VAR-A	HL	S	4	12.40	311.65												
737	VAR-B	HL	CV	0.5	24.65	49.03	946.15	909.23	783.46	568.85	393.46	230.77	125.77	21	21			
738	VAR-B	HL	S	0.5	25.11	78.89	1433.85	1381.54	1186.15	844.62	573.85	338.46	183.08	21	22			
692	VAR-B	HL	CV	1	23.97	95.90	1812.93	1751.35	1501.15	1079.68	737.11	427.25	234.80	21	21			
739	VAR-B	HL	CV	1	24.11	96.45	1828.85	1734.62	1459.62	1036.54	713.46	438.46	232.69	21	23			
694	VAR-B	LH	CV	1	23.92	95.68	1738.26	1710.55	1464.20	1034.64	720.55	417.24	241.72	21	22			
693	VAR-B	HL	S	1	24.89	156.40	2815.24	2672.06	2194.00	1637.41	1189.38	739.03	392.61	21	21			
740	VAR-B	HL	S	1	25.14	157.97	2843.08	2673.85	2243.08	1670.77	1215.38	707.69	396.92	21	23			
695	VAR-B	LH	S	1	24.84	156.07	2729.79	2609.70	2233.26	1662.82	1221.71	720.55	404.16	21	22			
741	VAR-B	HL	CV	1.5	23.82	142.90	2683.08	2501.54	2076.92	1510.77	1095.38	646.15	369.23	21	23			
742	VAR-B	HL	S	1.5	25.10	236.57	4076.92	3807.69	3200.00	2503.85	1961.54	1192.31	653.85	20	24			
743	VAR-B	HL	CV	2	23.26	186.06	3518.09	3237.11	2698.23	2078.52	1555.04	950.73	538.88	20	24			

Notes:

** = Value not available from measured data

X = Temperature not measured

HL = High to Low damping test (incrementally changed between high and low)

LH = Low to High damping test (incrementally changed between low and high)

CV = Constant velocity test

S = Sinusoidal test

Table 3-V(b) Summary of Variable Damper Component Tests (Multi-Stage Tests)

TEST	UNIT	STAGE	INPUT	FREQ. (Hz)	AMPL. (mm)	PEAK VEL. (mm/s)	DAMPING COEFFICIENT (N-s/mm)								TEMP (°C)	
							0 volts	0.75 volts	1.0 volts	1.25 volts	1.5 volts	2.0 volts	3.0 volts	INITIAL	FINAL	
702	VAR-A	HL	S	0.25	25.00	39.27	17.56	17.56	15.92	12.84	9.55	5.52	2.63	22	22	
730	VAR-A	HL	S	0.25	25.16	39.52	15.87	15.87	14.65	12.35	9.64	5.92	2.96	20	20	
680	VAR-A	HL	CV	0.5	24.43	48.86	17.96	17.96	15.95	12.50	8.96	5.20	2.60	X	X	
734	VAR-A	HL	CV	0.5	24.72	49.45	15.70	15.29	14.20	11.67	8.81	5.34	2.66	21	21	
681	VAR-A	LH	CV	0.5	24.41	48.82	17.97	17.97	16.04	12.53	8.99	5.20	2.60	X	X	
682	VAR-A	HL	S	0.5	24.76	77.77	17.82	17.44	15.62	11.82	8.49	4.97	2.38	X	X	
731	VAR-A	HL	S	0.5	25.10	78.87	16.11	15.65	14.57	11.85	8.84	5.46	2.78	20	21	
683	VAR-A	LH	S	0.5	24.81	77.95	17.74	17.39	15.37	11.64	8.39	4.91	2.41	X	X	
735	VAR-A	HL	CV	1	24.24	96.96	15.71	15.09	13.77	10.63	7.79	4.98	2.86	21	22	
674	VAR-A	HL	CV	1	24.02	96.08	17.20	16.93	14.73	10.82	7.81	4.86	2.68	X	X	
675	VAR-A	LH	CV	1	24.01	96.04	17.32	16.99	14.61	10.93	8.03	4.83	2.70	X	X	
684	VAR-A	HL	S	1	24.81	155.92	17.64	16.93	14.20	10.95	8.40	5.33	2.80	X	X	
732	VAR-A	HL	S	1	25.10	157.74	15.64	15.20	13.50	10.46	7.93	5.12	2.78	20	22	
685	VAR-A	LH	S	1	24.81	155.92	16.74	16.57	13.94	11.03	8.55	5.36	2.83	X	X	
736	VAR-A	HL	CV	1.5	23.67	142.03	15.71	14.96	13.03	10.22	7.77	5.20	3.07	21	23	
703	VAR-A	HL	S	1.5	24.90	234.64	17.39	16.09	13.27	10.66	8.69	5.91	3.12	22	25	
733	VAR-A	HL	S	1.5	25.06	236.19	15.37	14.49	12.36	10.06	8.21	5.60	3.13	20	22	
708	VAR-A	HL	CV	2	23.13	185.04	15.13	14.48	12.47	9.94	8.00	5.37	3.08	22	26	
709	VAR-A	LH	CV	2	23.15	185.20	14.45	14.27	12.83	10.63	8.39	5.68	3.32	22	25	
704	VAR-A	HL	S	2	24.97	313.81	16.21	14.91	12.57	10.48	8.70	6.31	3.53	22	27	
707	VAR-A	LH	S	2	24.98	313.91	12.37	12.19	10.92	9.53	8.09	5.94	3.43	22	27	
705	VAR-A	HL	S	3	24.96	470.56	10.61	10.47	9.45	8.43	7.51	5.80	3.84	22	30	

Table 3-V(b) Cont'd

TEST	UNIT	STAGE	INPUT	FREQ. (Hz)	AMPL. (mm)	PEAK VEL. (mm/s)	DAMPING COEFFICIENT (N-s/mm)								TEMP (°C)			
							0 volts	0.75 volts	1.0 volts	1.25 volts	1.5 volts	2.0 volts	3.0 volts	INITIAL	FINAL			
							**	13.08	11.30	9.50	8.02	5.92	3.38	22	25			
706	VAR-A	HL	S	4	12.40	311.65												
737	VAR-B	HL	CV	0.5	24.65	49.03	19.19	18.44	15.89	11.54	7.98	4.68	2.55	21	21			
738	VAR-B	HL	S	0.5	25.11	78.89	18.18	17.51	15.04	10.71	7.27	4.29	2.32	21	22			
692	VAR-B	HL	CV	1	23.97	95.90	18.90	18.26	15.65	11.26	7.69	4.46	2.45	21	21			
739	VAR-B	HL	CV	1	24.11	96.45	18.96	17.98	15.13	10.75	7.40	4.55	2.41	21	23			
694	VAR-B	LH	CV	1	23.92	95.68	18.17	17.88	15.30	10.81	7.53	4.36	2.53	21	22			
693	VAR-B	HL	S	1	24.89	156.40	18.00	17.08	14.03	10.47	7.60	4.73	2.51	21	21			
740	VAR-B	HL	S	1	25.14	157.97	18.00	16.93	14.20	10.58	7.69	4.48	2.51	21	23			
695	VAR-B	LH	S	1	24.84	156.07	17.49	16.72	14.31	10.65	7.83	4.62	2.59	21	22			
741	VAR-B	HL	CV	1.5	23.82	142.90	18.78	17.51	14.53	10.57	7.67	4.52	2.58	21	23			
742	VAR-B	HL	S	1.5	25.10	236.57	17.23	16.10	13.53	10.58	8.29	5.04	2.76	20	24			
743	VAR-B	HL	CV	2	23.26	186.06	18.91	17.40	14.50	11.17	8.36	5.11	2.90	20	24			

NOTES: ** = Value not available from measured data

X = Temperature not measured

HL = High to Low damping test (incrementally changed between high and low)

LH = Low to High damping test (incrementally changed between low and high)

CV = Constant velocity test

S = Sinusoidal test

5°C except in one test in which the temperature increased by 8°C. Note that the temperature was not recorded for approximately 25% of the multi-stage tests.

Figure 3-26 shows typical force displacement loops under constant velocity motion and with damping switching incrementally from high to low (Figure 3-26(a)) and low to high (Figure 3-26(b)). The force-displacement loop of Figure 3-26(a) is shown again in Figure 3-27 along with its corresponding command signal and spool displacement time history. Each time the command signal is adjusted, a corresponding spool displacement overshoot is observed (see Figure 3-27(b)). Figure 3-28 shows typical force-displacement loops under sinusoidal motion and with damping switching from high to low at input frequencies of 1 Hz (Figure 3-28(a)) and 2 Hz (Figure 3-28(b)).

The relationship between peak velocity and peak force for both variable damper units is shown in Figure 3-29 for three different command signal voltages. The data for each command signal voltage level can be fit with straight lines having a slope equal to the corresponding damping coefficient. Note that when the command signal voltage is 0 volts, the damping coefficient of the two units is not the same (Unit VAR-A has $C_{\max} = 16.67$ N-s/mm and Unit VAR-B has $C_{\max} = 18.51$ N-s/mm). Under a command signal of 0 volts, the valves are theoretically closed and should result in the same damping coefficient for each damper unit. Recall Figure 3-11 which shows that the flow rate in unit VAR-A is higher than in unit VAR-B at low command signal voltages. This explains the difference in the maximum damping coefficient for the two variable damper units. Note that the data

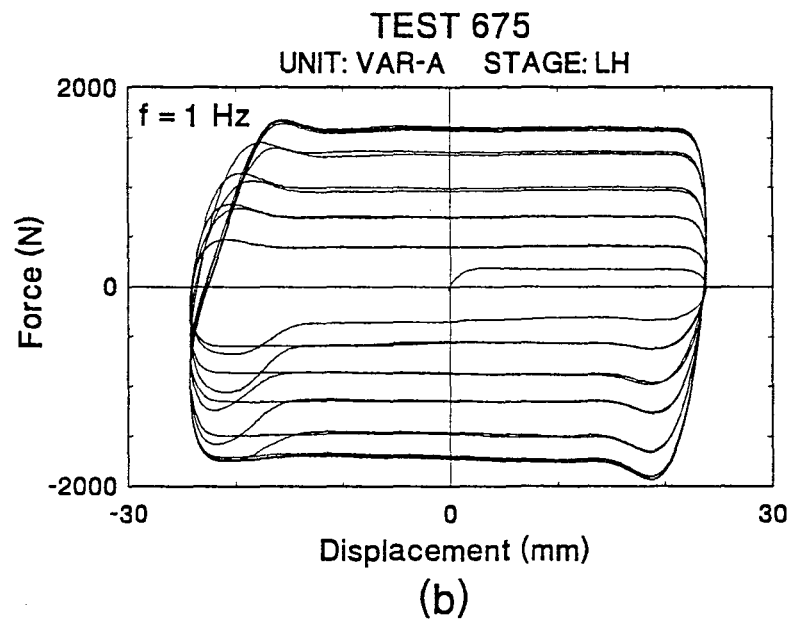
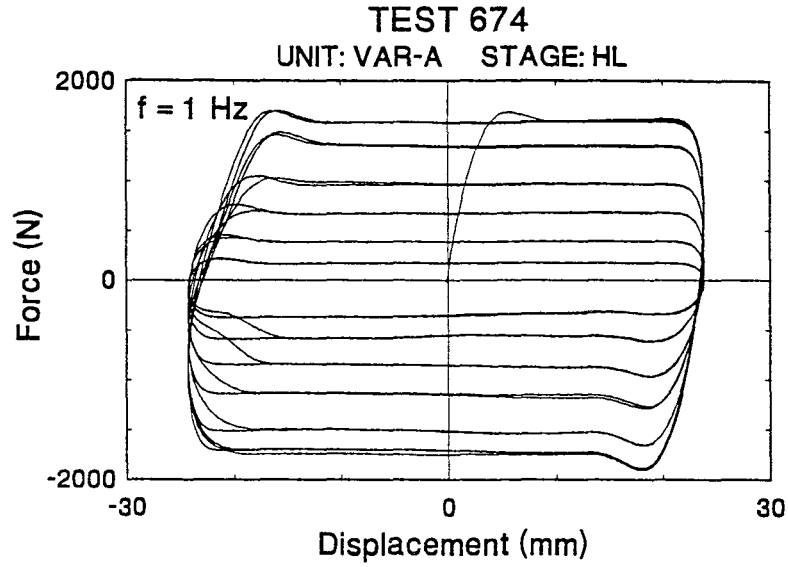


Figure 3-26 Typical Force-Displacement Loops for Variable Damper Subjected to Constant Velocity Motion in a Multi-Stage Test with Damping Switching from a) High to Low and b) Low to High

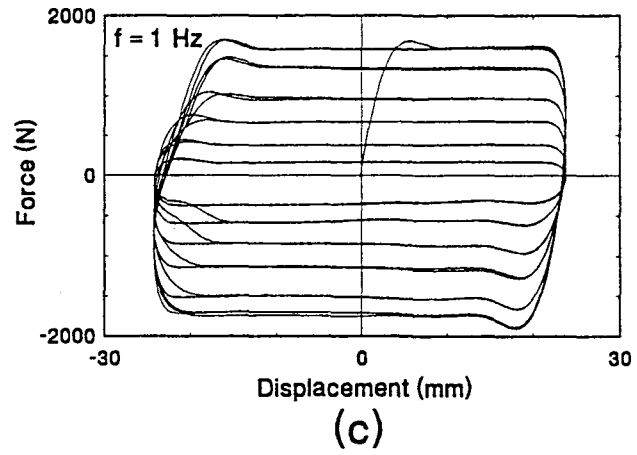
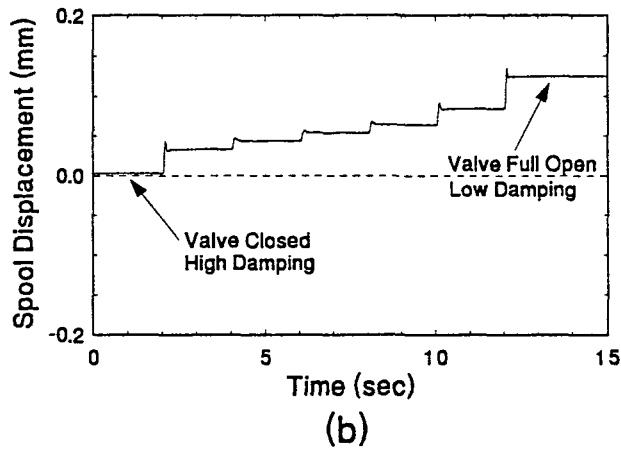
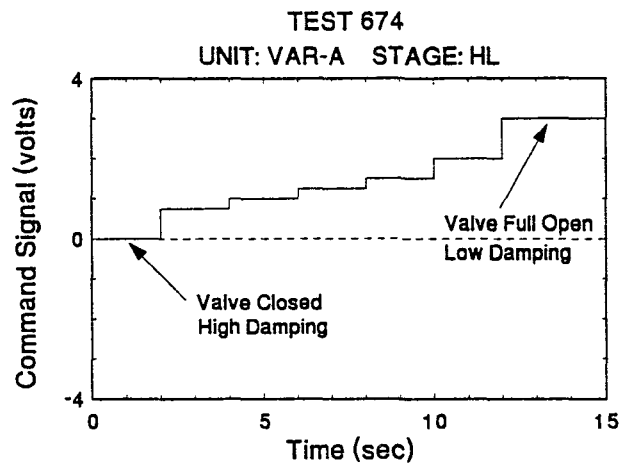


Figure 3-27 Hysteresis Loops and Corresponding Command Signal and Spool Displacement for Variable Damper Multi-Stage Test

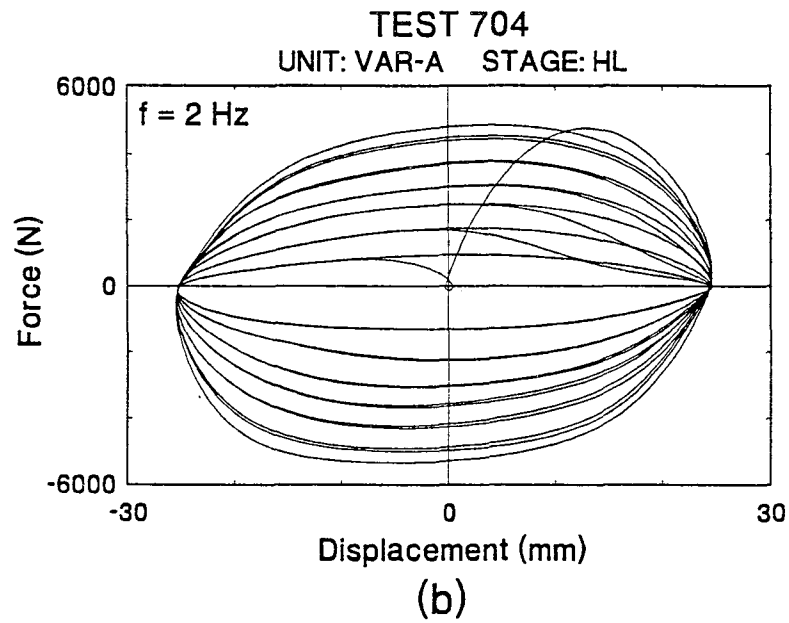
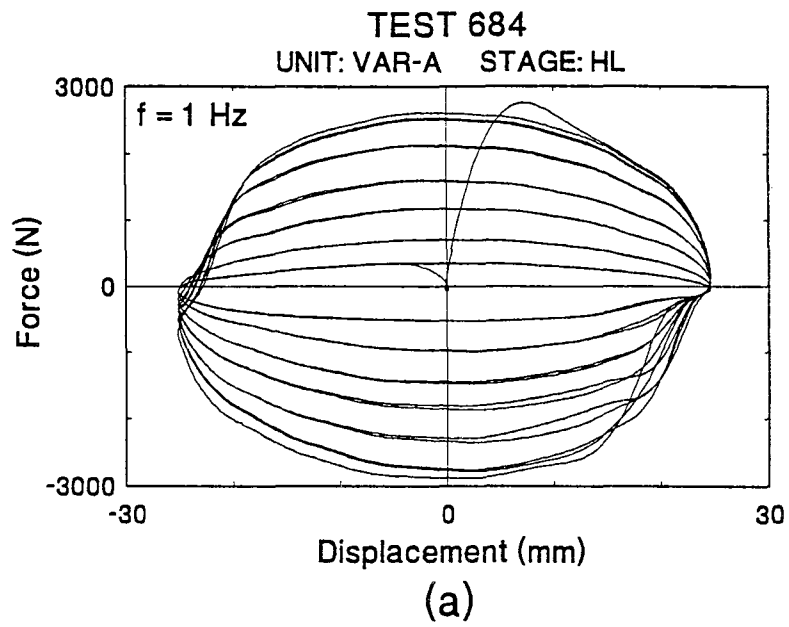
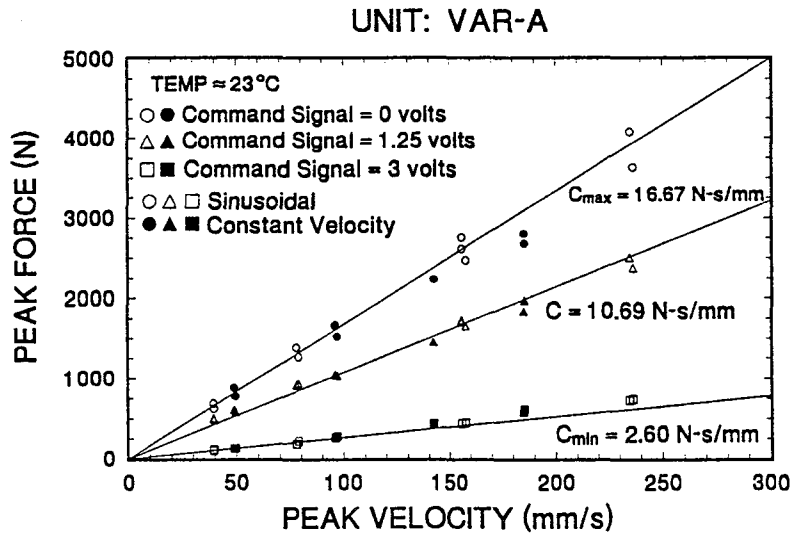
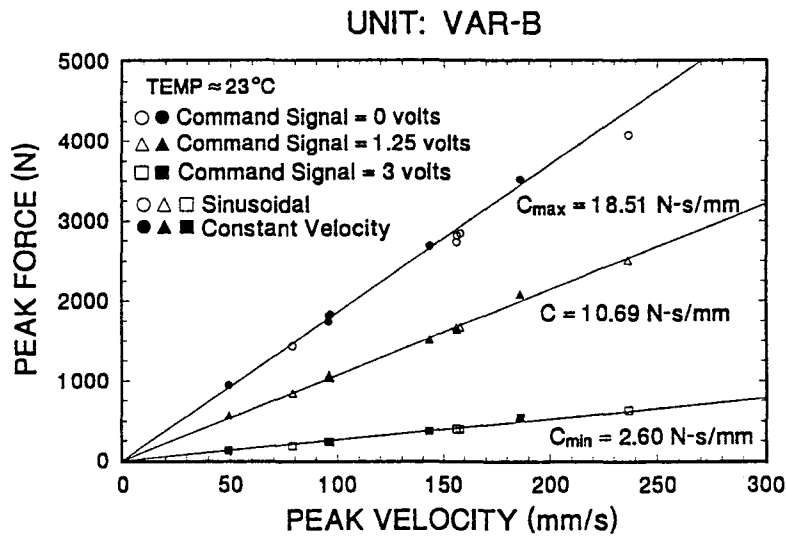


Figure 3-28 Typical Force-Displacement Loops for Variable Damper Subjected to Sinusoidal Motion in a Multi-Stage Test with Damping Switching from High to Low and Input Frequencies of a) 1 Hz and b) 2 Hz



(a)



(b)

Figure 3-29 Experimental Values of Peak Force Versus Peak Velocity for Variable Damper Under Three Different Command Signals for a) Unit VAR-A and b) Unit VAR-B

shown in Figure 3-29 is for tests run at frequencies of 2 Hz or less. Recall that the dampers begin to develop stiffness for frequencies above the cut-off frequency. As a result, for frequencies beyond about 4 Hz, the data begins to deviate from the linearity shown in Figure 3-29.

For the variable damper system, the damping coefficient is dependent on the command signal voltage. This is demonstrated in Figure 3-30 which shows experimental data for both sinusoidal and constant velocity tests at input frequencies of 4 Hz or less. The scatter in the data at a given command signal voltage is primarily due to differences in the frequency of testing (e.g., compare the values of damping coefficient of test 702 (frequency = 0.25 Hz) and test 706 (frequency = 4 Hz) in Table 3-V(b)). The nonlinearity of the experimental data in Figure 3-30 is the result of the nonlinear relationship between the command signal and the flow rate through the valve due to saturating flow conditions and spool land overlap (see Figure 3-11). Note that beyond about 3 volts, the spool is still in motion (see Figure 3-10) while the damping coefficient remains essentially constant (see Figure 3-30). As mentioned in Section 3.1.2, this is the result of flow restrictions within the external tubing manifold ports and valve internal passages which are smaller than the maximum valve orifice opening and, as a result, saturate the flow beyond a command voltage of 3 volts. Furthermore, the nearly constant value of damping coefficient at voltage levels below about 0.25 volts is due to spool land overlap which does not permit fluid flow through the servovalve until the spool moves beyond the length of the spool

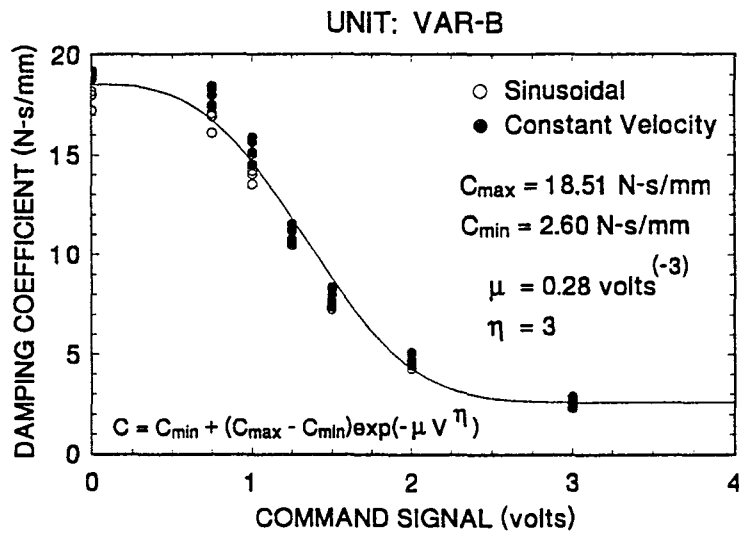
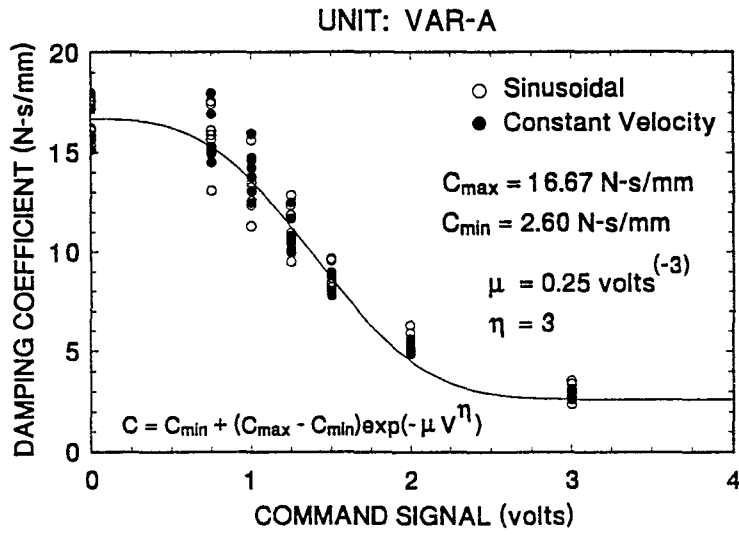


Figure 3-30 Experimental and Analytical Values of Damping Coefficient Versus Command Signal for Variable Damper a) Unit VAR-A and b) Unit VAR-B

land overlap. An analytical expression for the damping coefficient has been fit through the experimental data of Figure 3-30 and is given by

$$C = C_{\min} + (C_{\max} - C_{\min}) \exp(-\mu V^\phi) \quad (3-15)$$

where C_{\min} is the damping coefficient at the full open valve position, C_{\max} is the damping coefficient at the full closed valve position, and μ and ϕ are parameters which are evaluated through curve fitting. The basic form of Equation (3-15) is utilized in Section 4.3.1 for analytical predictions of semi-active variable damper component tests.

3.4 System Response to Saturated Command Signal

An important response time to be measured for a semi-active damper with an adjustable damping coefficient is the time required to modify the damping coefficient from its maximum to its minimum value and vice-versa. Assuming purely viscous damping, tests which are run under constant velocity motion provide damper forces which are directly proportional to the corresponding damping coefficient and can therefore be used to obtain system response times. The response time of the semi-active fluid dampers was evaluated under saturated command signals. A saturated command signal is defined to be a command signal which opens the valve fully or closes the valve fully (thus modifying the damping coefficient from its maximum to its minimum value and vice-versa).

A typical constant velocity test from which system response times can be obtained is shown in Figure 3-31 where the system is switched from a fully open valve condition (low damping, minimum damping coefficient) to a fully closed valve condition (high damping,

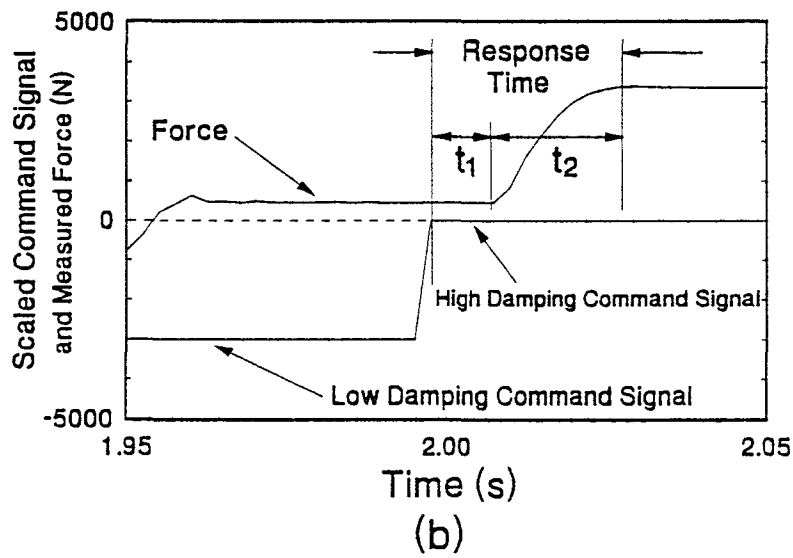
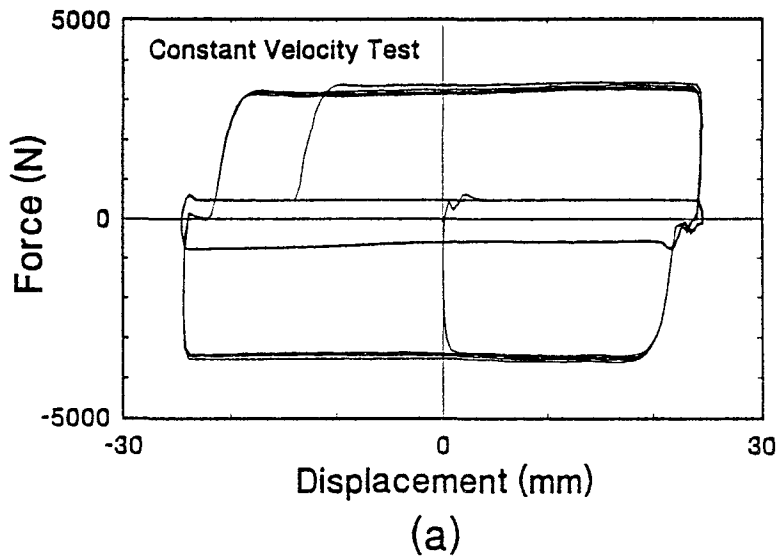


Figure 3-31 Typical Constant Velocity Test from Which System Response Time is Evaluated

maximum damping coefficient). The response time may be extracted from the time history of the measured force and scaled command signal (Figure 3-31(b)). The response time is measured from the point at which the command signal is sent to the control valve to the point at which the damping coefficient (or, correspondingly, force) reaches its target value. The target value was either the maximum damping coefficient, C_{\max} , or the minimum damping coefficient, C_{\min} . Note that all signals were unfiltered to eliminate the effect of filters on the measurement of response time.

The response time is a non-zero quantity as a result of a combination of valve dynamics and hydraulic system dynamics and can be separated into two distinct parts. The first part of the response time is designated as t_1 and is measured from the point at which the command signal is sent to the control valve to the point at which the damping coefficient (force) begins to change. Therefore, response time t_1 is also designated as the static response time. The length of time t_1 is dependent on many factors including spool static friction (stiction), spool driver electronics (variable damper only), and the time it takes to build-up or collapse the electromagnetic field of the valve coil. The second part of the response time is designated as t_2 and is measured from the point at which the damping coefficient (force) begins to change to the point at which the damping coefficient (force) first reaches its target value. Therefore, response time t_2 is also designated as the dynamic response time. The length of time t_2 is dependent on many factors including the dynamics of the valve (e.g., spool inertia), spool sliding friction, spool driver electronics (variable damper only), and the dynamics of the hydraulic system (e.g., fluid inertia).

Note that there was no clear dependency of response time on the frequency of testing. The sampling rate used in all tests in which response times were measured was 400 pt/sec (2.5 ms/pt).

A general agreement or standard defining the appropriate method of measuring time delays associated with active or semi-active control system components does not exist. Therefore, one must be careful in using reported time delays for comparing the relative merits of different control systems.

3.4.1 Two-Stage Damper

A total of 29 tests were performed on the two-stage semi-active fluid dampers for which response times could be measured. These tests are listed in Table 3-III which includes response time t_1 , t_2 , and the total response time, $t_1 + t_2$. A typical test from which response times were extracted is shown in Figure 3-32. A summary of response time data for the two-stage dampers is provided in Figures 3-33 (unit 2ST-A) and 3-34 (unit 2ST-B) with average system response times shown in Table 3-VI. Note that the response time varies significantly depending upon the direction of motion of the spool (i.e., high to low (HL) or low to high (LH) damping). The observed difference in system response is the result of the difference in the mode of operation of the solenoid valve in the two directions (recall the discussion on two-stage damper valve operation in Section 3.1.1).

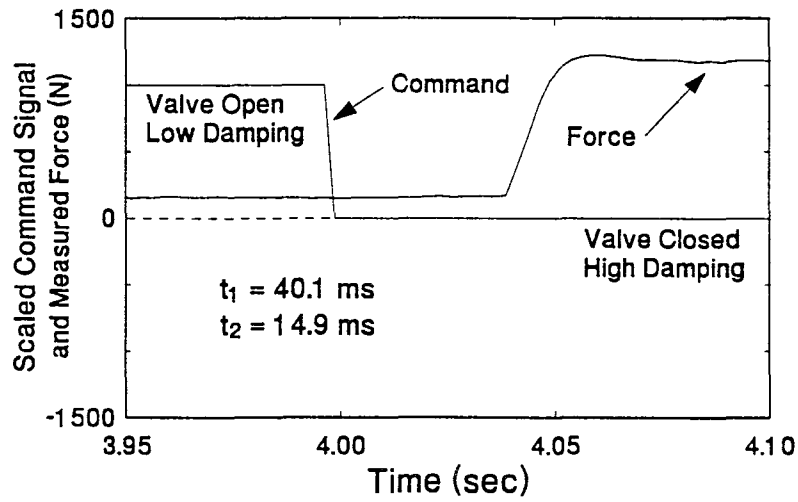
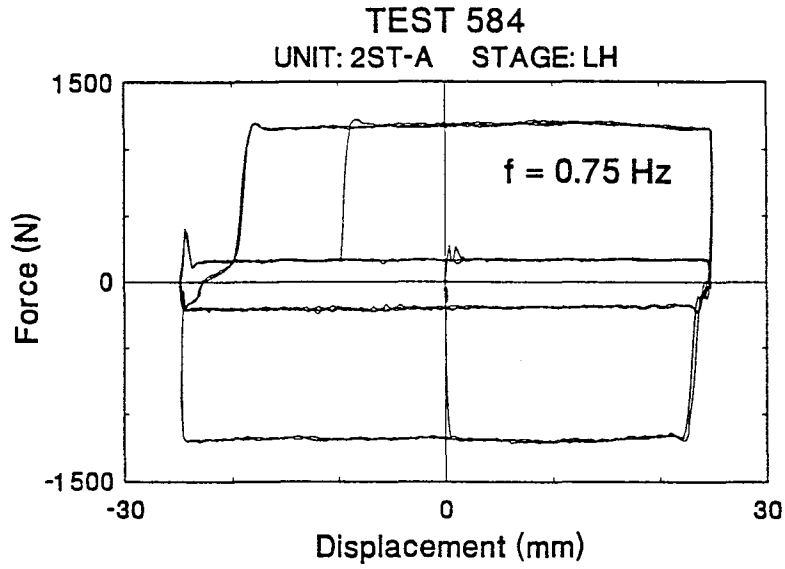


Figure 3-32 Example of Two-Stage Damper Test from Which Response Times were Extracted

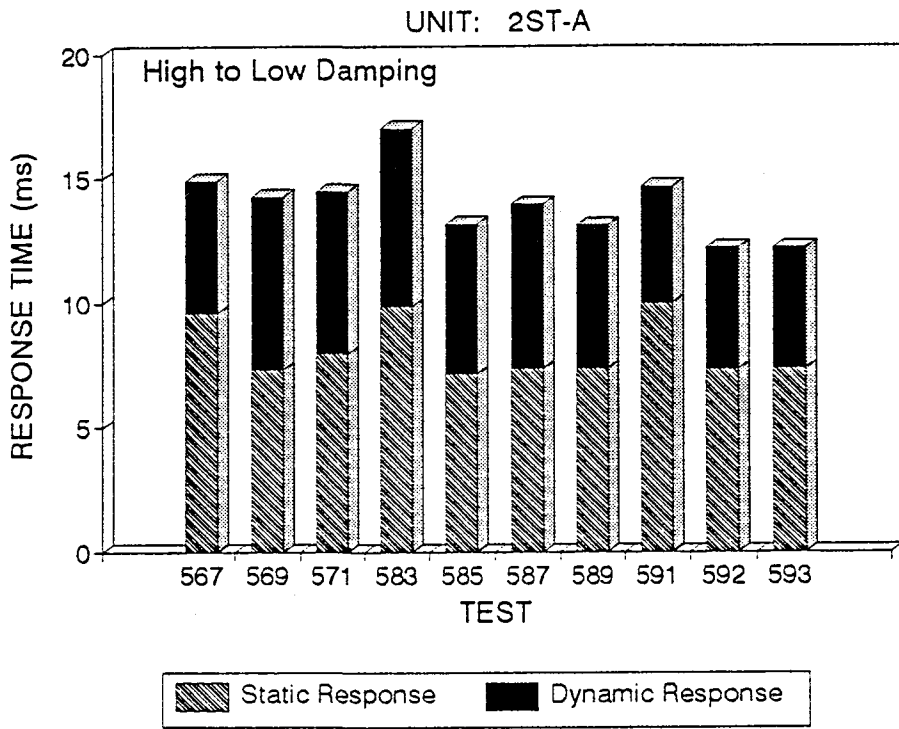
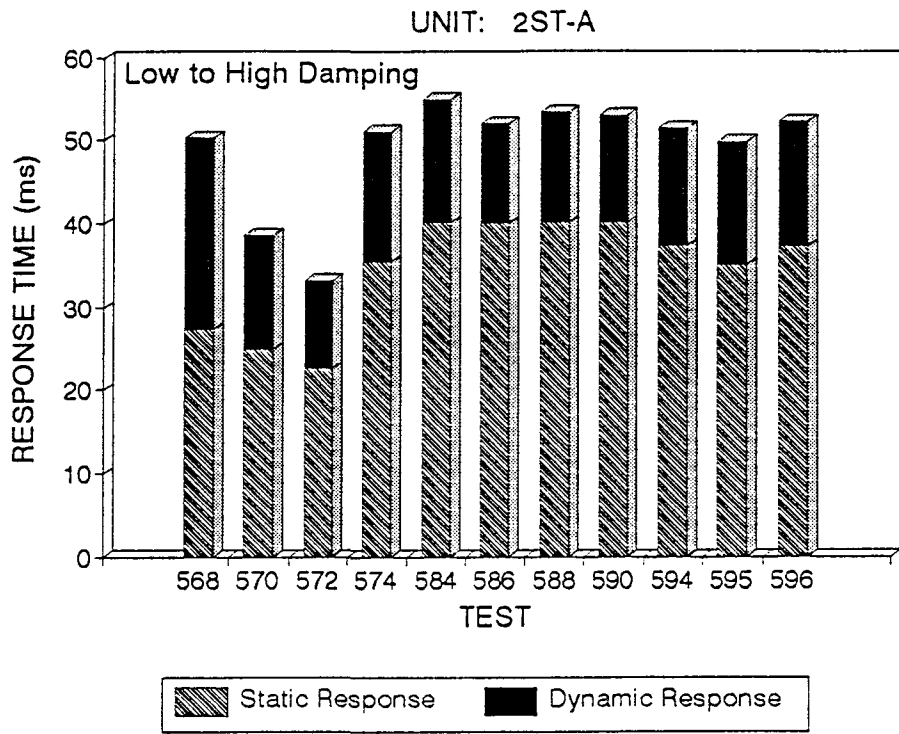


Figure 3-33 Response Times for Two-Stage Damper Unit 2ST-A

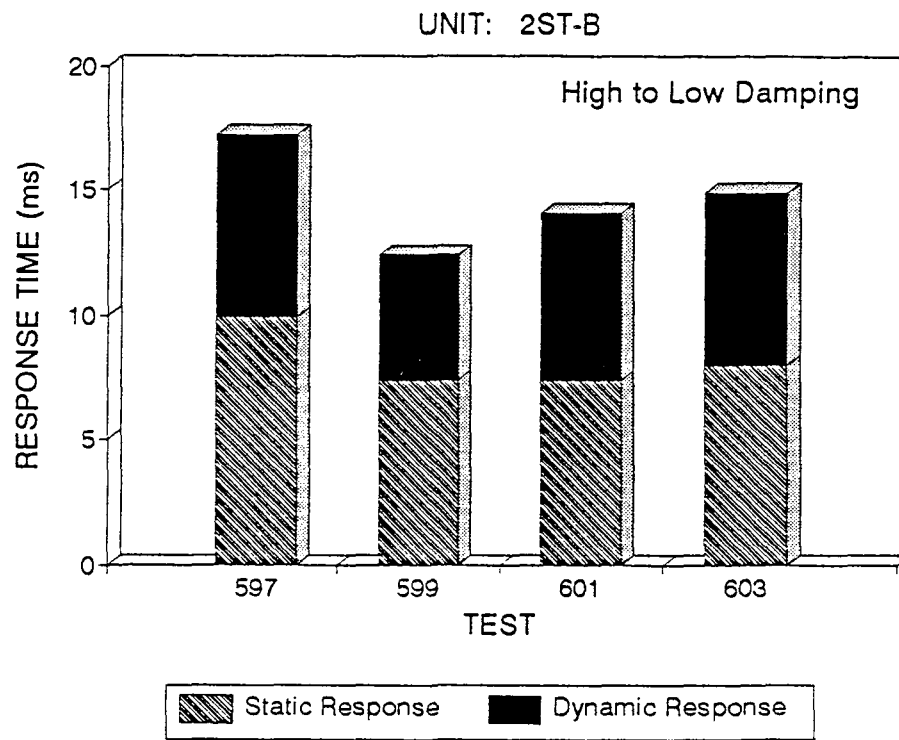
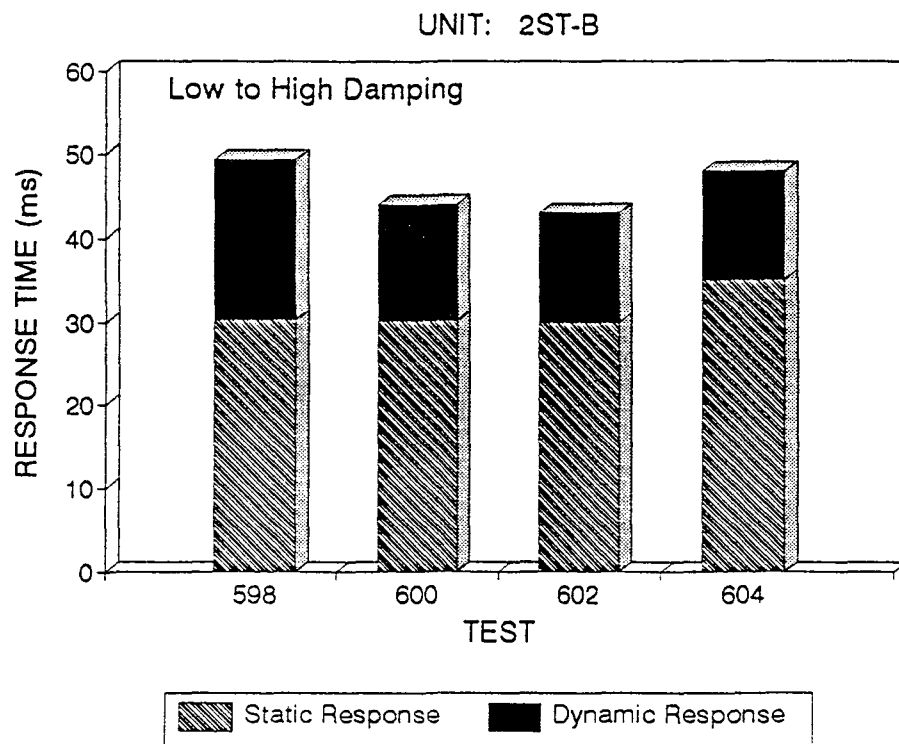


Figure 3-34 Response Times for Two-Stage Damper Unit 2ST-B

Table 3-VI Average System Response Times for Two-Stage Damper

System	Unit	Stage	AVERAGE RESPONSE TIME (ms)		
			t ₁	t ₂	Total
Two-Stage Damper	2ST-A	HL	8.1	5.9	14.0
		LH	34.6	14.6	49.2
	2ST-B	HL	8.1	6.5	14.6
		LH	31.2	14.9	46.1

3.4.2 Variable Damper

A total of 52 tests were performed on the variable dampers for which response times could be measured. These tests are listed in Table 3-IV which includes response time t_1 , t_2 , and the total response time, $t_1 + t_2$. A typical test from which response times were extracted is shown in Figure 3-35. A summary of response time data for the variable dampers is provided in Figures 3-36 (unit VAR-A) and 3-37 (unit VAR-B) with average system response times shown in Table 3-VII. Note that the response time is approximately the same for both directions of spool motion. This is because the mode of operation of the valve is essentially the same for either direction of spool motion (recall the discussion on variable damper valve operation in Section 3.1.2).

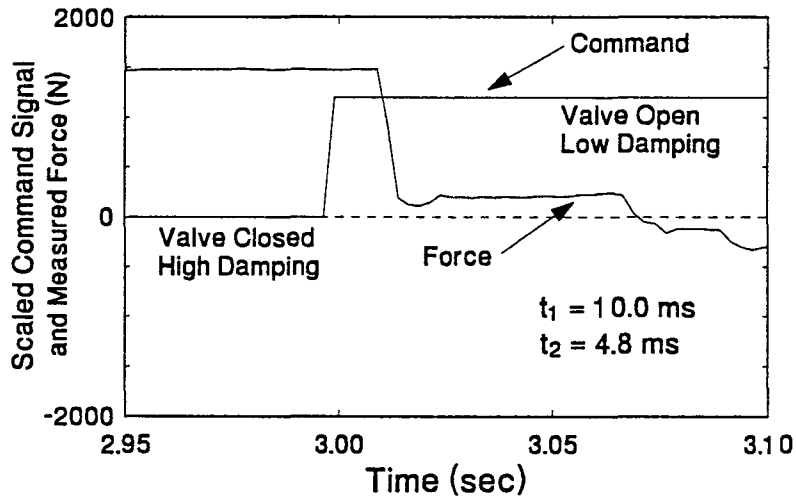
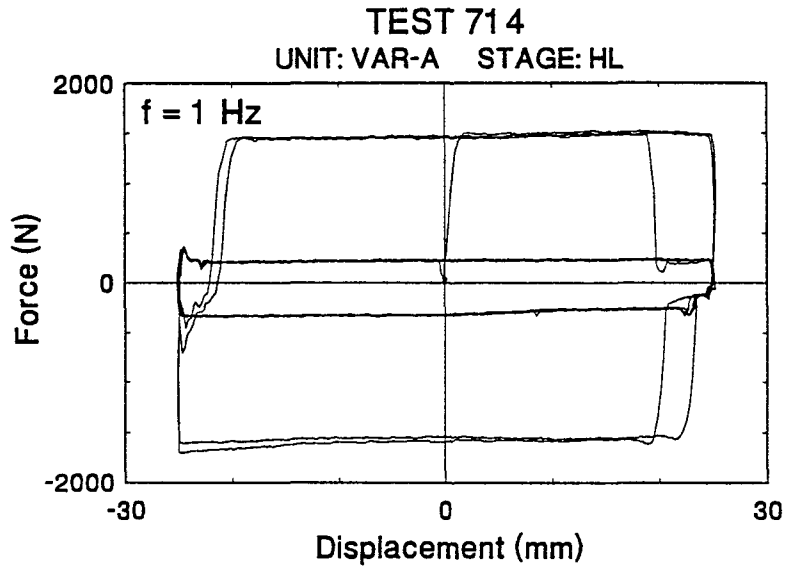


Figure 3-35 Example of Variable Damper Test from which Response Times were Extracted

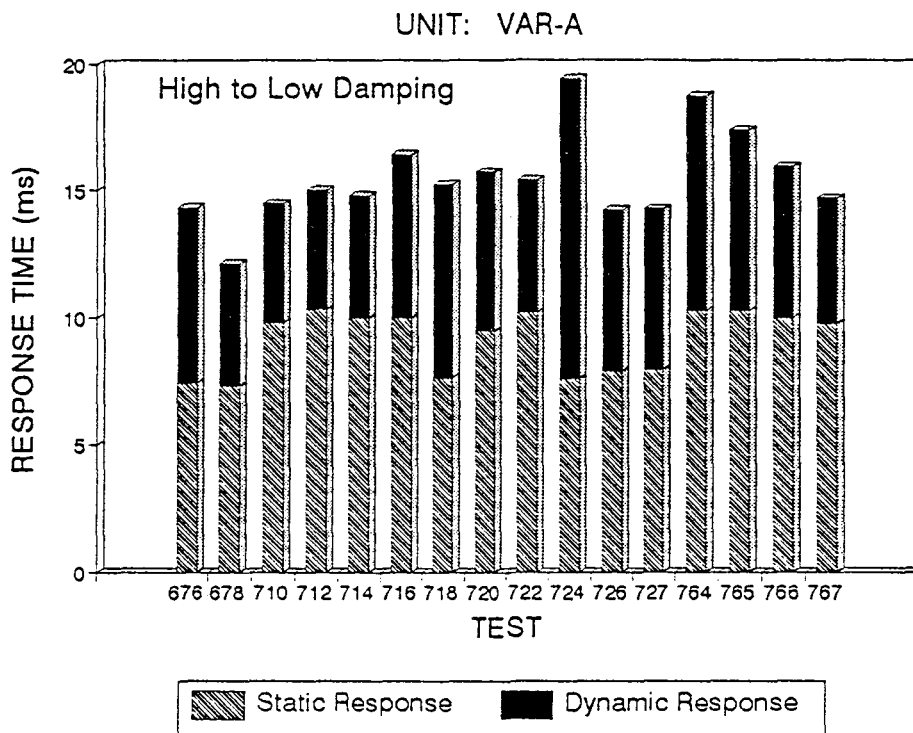
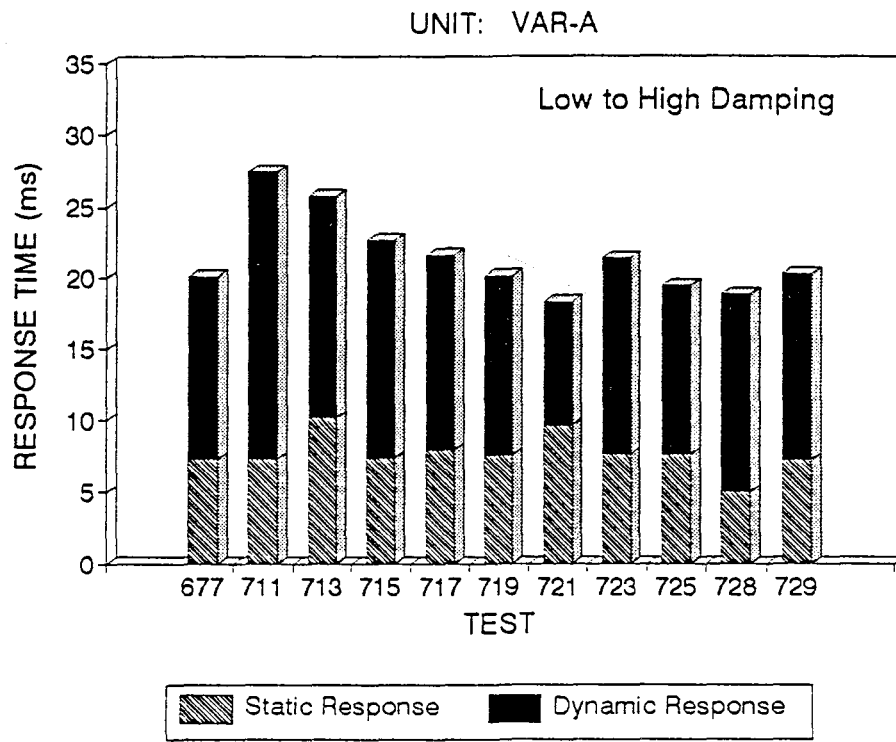


Figure 3-36 Response Times for Variable Damper Unit VAR-A

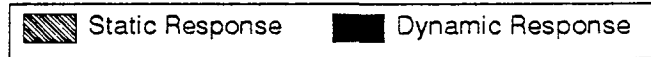
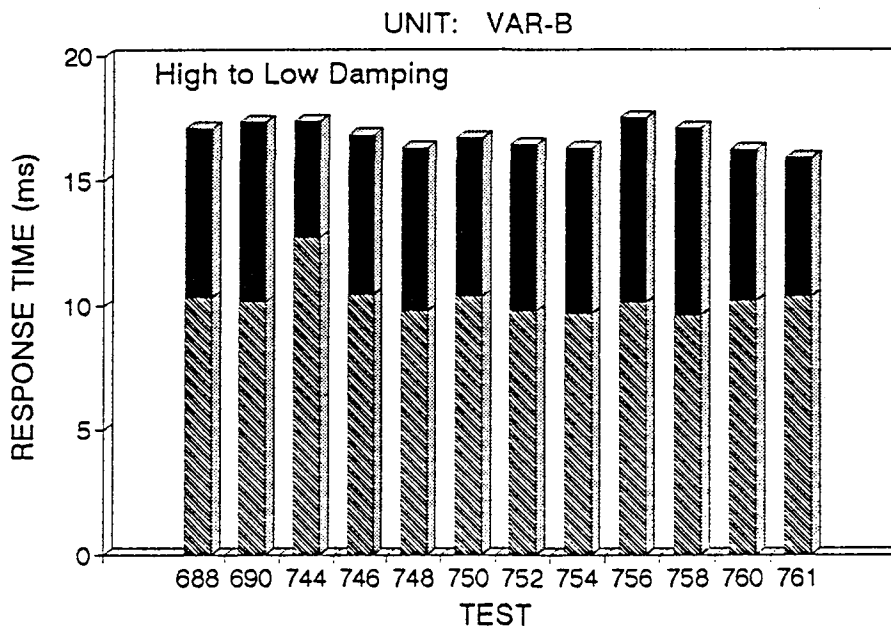
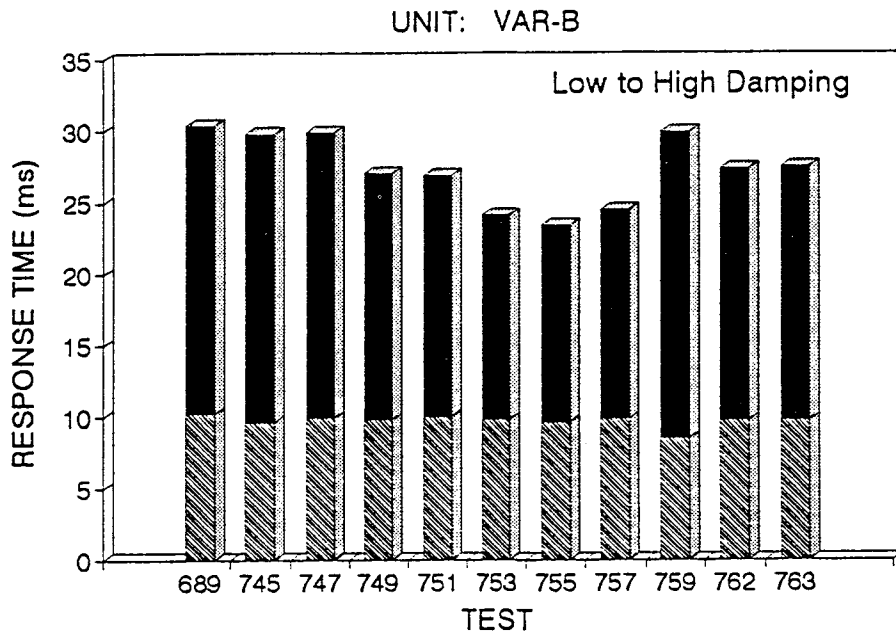


Figure 3-37 Response Times for Variable Damper Unit VAR-B

Table 3-VII Average System Response Times for Variable Damper

System	Unit	Stage	AVERAGE RESPONSE TIME (ms)		
			t ₁	t ₂	Total
Variable Damper	VAR-A	HL	9.1	6.4	15.5
		LH	7.7	13.8	21.5
	VAR-B	HL	10.3	6.5	16.8
		LH	9.7	17.6	27.3

SECTION 4

ANALYTICAL MODELS OF SEMI-ACTIVE FLUID DAMPERS

4.1 Viscous Dashpot Model

Recalling the discussion in Section 3.3.1, the passive portion of the semi-active fluid dampers exhibits viscoelastic fluid behavior over a wide frequency range. However, for frequencies below the cut-off frequency (about 4 Hz), the passive portion of the damper behaves as a linear viscous dashpot governed by Equation (3-12)

$$P(t) = C \dot{u}(t) \quad (4-1)$$

where C is the damping coefficient. Realizing that a semi-active fluid damper may be thought of as a passive fluid damper with an adjustable damping coefficient, the following linear viscous dashpot model is proposed in which the damping coefficient, C , is now a function of time

$$P(t) = C(t) \dot{u}(t) \quad , \quad C_{\min} \leq C(t) \leq C_{\max} \quad (4-2)$$

where C_{\max} and C_{\min} are the damping coefficients of the semi-active damper with the valve fully closed and fully open, respectively. The viscous dashpot model would be valid for a wider range of frequencies when the damper construction includes a balanced piston rod rather than a piston rod make-up accumulator.

4.2 Viscoelastic Maxwell Model

Recall Figure 3-17 which shows experimental data representing the damping coefficient and storage stiffness of a passive fluid damper which was previously tested by

Constantinou (1993b and 1992b) and has an identical design to the passive portion of the semi-active fluid dampers tested herein. Clearly, the mechanical properties of the passive fluid damper were frequency dependent over a wide range of frequencies. The simplest model to account for this viscoelastic fluid behavior is the Maxwell model which is given by

$$P(t) + \lambda \dot{P}(t) = C_0 \dot{u}(t) \quad (4-3)$$

where λ is the relaxation time and C_0 is the damping constant at zero frequency. The Maxwell model was calibrated for the passive fluid damper resulting in the analytical curves shown in Figure 3-17 and the parameters $C_0 = 15.5 \text{ N-s/mm}$ and $\lambda = 0.006 \text{ sec}$. As mentioned in Section 4.1, the primary effect of converting a passive fluid damper to a semi-active fluid damper is to create a device having adjustable damping properties with little or no modification in stiffness properties. Therefore, the following viscoelastic Maxwell model is proposed for the semi-active fluid damper in which the damping constant is now a function of time

$$P(t) + \lambda \dot{P}(t) = C(t) \dot{u}(t) \quad , \quad C_{\min} \leq C(t) \leq C_{\max} \quad (4-4)$$

The viscoelastic Maxwell model will be used in Section 6 for analytical identification of the structure and in Section 9 to obtain analytical predictions of shaking table test results.

4.3 Fluid Mechanics Based Model

A general model to describe the dynamic behavior of semi-active fluid dampers has been developed using principles of fluid mechanics. A schematic of a semi-active damper used for generating the analytical model is shown in Figure 4-1.

The general mass flow rate continuity for a fluid volume is given by (Watton 1989)

$$\frac{d}{dt}(m) = \frac{d}{dt}(\rho V) = \rho_i Q_i - \rho_o Q_o \quad (4-5)$$

where t is time, m is the mass of fluid within the fluid volume, ρ is the fluid mass density, V is the fluid volume, and Q is the flow rate. The subscripts i and o refer to input and output, respectively.

For incompressible flows and a fluid volume with rigid boundaries, Equation (4-5) may be set equal to zero. However, these conditions are not satisfied for chambers 1 and 2 shown in Figure 4-1. Expanding the center portion of Equation (4-5)

$$\frac{d}{dt}(\rho V) = \rho \frac{dV}{dt} + \frac{d\rho}{dt} V = \rho \frac{dV}{dt} + V \frac{d\rho}{dP} \frac{dP}{dt} \quad (4-6)$$

where P is the pressure within the fluid volume. From the definition of bulk modulus

$$dP = -\beta \frac{dV}{V} \quad (4-7)$$

where β is the bulk modulus of the fluid which is generally dependent on temperature and pressure. Considering a vanishingly small mass element

$$dm = d(\rho V) = \rho dV + V d\rho \quad (4-8)$$

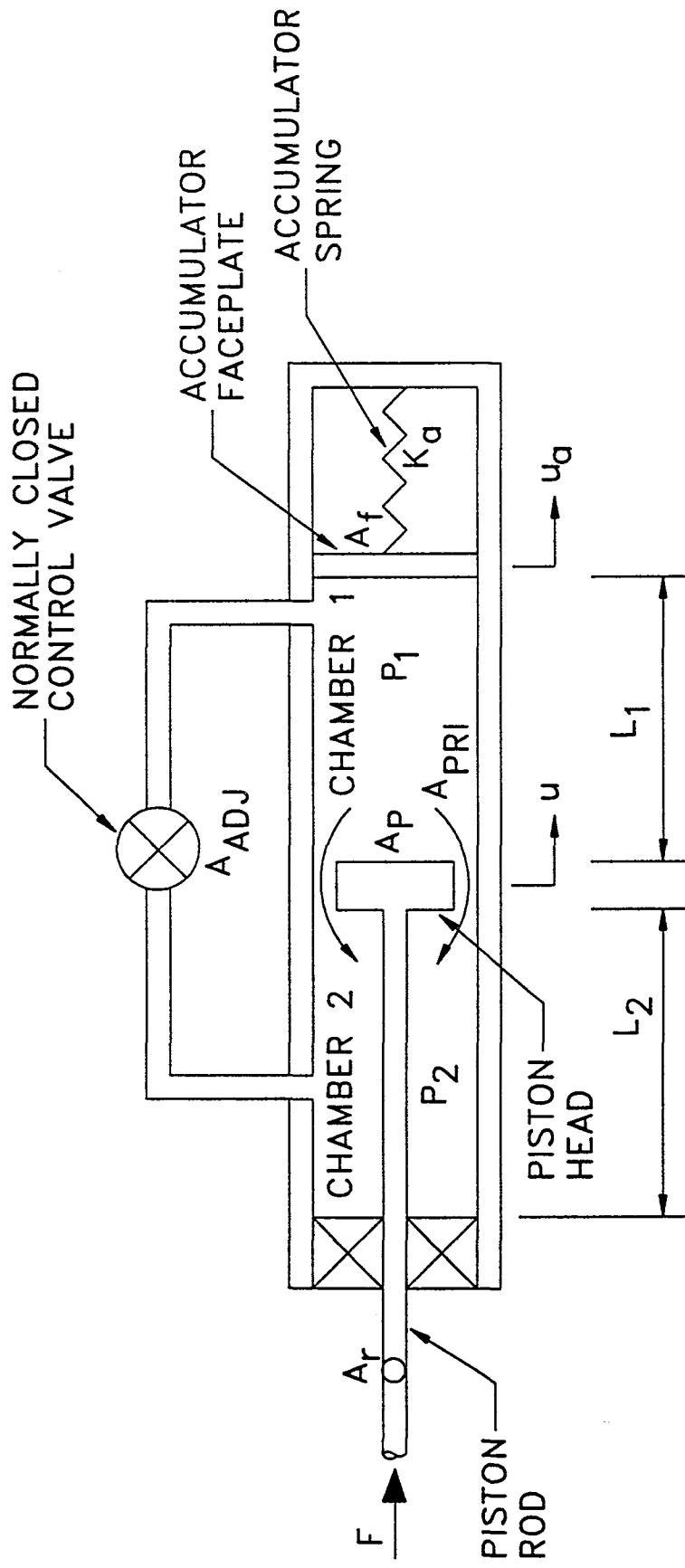


Figure 4-1 Schematic of Semi-Active Damper Used to Generate Analytical Fluid Mechanics Based Model

from which

$$\frac{dV}{V} = -\frac{d\rho}{\rho} \quad (4-9)$$

Combining Equations (4-6), (4-7), and (4-9)

$$\frac{d}{dt}(\rho V) = \rho \left(\frac{dV}{dt} + \frac{V d\rho}{\rho dt} \right) \quad (4-10)$$

where the first term on the right hand side of Equation (4-10) is related to the boundary deformations and the second term is related to the fluid compressibility. Combining Equations (4-5) and (4-10) and assuming a constant fluid density

$$\frac{dV}{dt} + \frac{V d\rho}{\rho dt} = Q_i - Q_o \quad (4-11)$$

which is the general mass flow rate continuity equation accounting for boundary deformation and fluid compressibility.

Under the assumed compression force of Figure 4-1, the flow continuity equation for volume 1 is given by

$$\frac{dV_1}{dt} + \frac{V_1 d\rho_1}{\rho_1 dt} = Q_i - Q_o \quad (4-12)$$

where the subscript 1 indicates chamber one. In this case, Q_i is zero and Q_o is given by

$$Q_o = k_{pri} A_{pri} v_{pri} + k_{adj} A_{adj} v_{adj} \quad (4-13)$$

where the subscript "pri" refers to the primary orifice across the piston head, subscript "adj" refers to the adjustable orifice contained within the control valve, k is a general

orifice discharge coefficient, A is the orifice area, and v is the average velocity of the fluid through the orifice. Utilizing conservation of energy, mass flow rate continuity, and assuming an incompressible, inviscid fluid (pressure forces on fluid particles dominate over viscous forces), it can be shown that the average velocity of fluid through a small orifice is related to the pressure drop, ΔP , across the orifice by (McCloy 1980)

$$v = \left(\frac{2\Delta P}{\rho} \right)^{\frac{1}{2}} \quad (4-14)$$

This relationship is applicable to the orifice contained within the control valve. However, the orifice across the piston head does not follow this relation. Recall that the piston head orifice is shaped in a special way so as to obtain a force output which is linearly related to the relative velocity of the piston head. For this reason, the following empirical pressure-velocity relationship was utilized for the primary orifice

$$v_{\text{pri}} = \delta \left(\frac{2\Delta P}{\rho} \right)^1 \quad (4-15)$$

where the exponent of unity is explicitly shown for emphasis and δ is a factor which is used to maintain dimensional equivalence. The mass conservation equation for chamber one may be written as

$$\frac{dV_1}{dt} + \frac{V_1}{\beta_1} \frac{dP_1}{dt} = -k_{\text{pri}} A_{\text{pri}} \delta \left[\frac{2(P_1 - P_2)}{\rho} \right]^1 - k_{\text{adj}} A_{\text{adj}} \left[\frac{2|P_1 - P_2|}{\rho} \right]^{\frac{1}{2}} \text{sgn}(P_1 - P_2) \quad (4-16)$$

where $\text{sgn}(\bullet)$ is the signum function and $|\bullet|$ indicates the magnitude of the enclosed quantity. For chamber two, a similar equation results

$$\frac{dV_2}{dt} + \frac{V_2}{\beta_2} \frac{dP_2}{dt} = k_{\text{pri}} A_{\text{pri}} \delta \left[\frac{2(P_1 - P_2)}{\rho} \right]^1 + k_{\text{adj}} A_{\text{adj}} \left[\frac{2|P_1 - P_2|}{\rho} \right]^{\frac{1}{2}} \text{sgn}(P_1 - P_2) \quad (4-17)$$

Note that it has been assumed that fluid is not able to enter the accumulator chamber. In reality, fluid enters the accumulator through a small control valve (orifice) and compresses a cylindrical foam element. To account for the effect of the accumulator, it has been assumed that the fluid in chamber one is in direct contact with an accumulator face plate which is supported by a linear elastic spring (see Figure 4-1). The spring stiffness and face plate area can be adjusted to properly account for the accumulator behavior. Equating the spring force to the fluid pressure force

$$K_a u_a = P_1 A_f \quad (4-18)$$

where K_a is the accumulator spring stiffness, u_a is the accumulator faceplate relative displacement, and A_f is the faceplate area. The total volume of fluid in chamber one is

$$V_1 = (L_1 - u + u_a) A_p \quad (4-19)$$

where L_1 is the length of chamber one measured from the piston head (at center position) to the accumulator faceplate (at undeformed position), u is the piston head relative displacement, and A_p is the piston head area. The total volume of fluid in chamber two is

$$V_2 = (L_2 + u)(A_p - A_r) \quad (4-20)$$

where L_2 is the length of chamber two measured from the piston head (at center position) to the cap of the damper and A_r is the piston rod area. Note that the values of L_1 and L_2 are modified to account for the volume of fluid contained within the external bypass loop tubing. The combination of Equations (4-16) , (4-18), and (4-19) and Equations (4-17) and (4-20) leads to the following two first order nonlinear differential equations, respectively

$$\frac{dP_1}{dt} = \frac{\left\{ A_p \dot{u} - k_{pri} A_{pri} \delta \left[\frac{2(P_1 - P_2)}{\rho} \right]^1 - k_{adj} A_{adj} \left[\frac{2|P_1 - P_2|}{\rho} \right]^{\frac{1}{2}} \text{sgn}(P_1 - P_2) \right\}}{\left[\left(L_1 - u + \frac{P_1 A_r}{K_a} \right) \frac{A_p}{\beta_1} + \frac{A_r A_p}{K_a} \right]} \quad (4-21)$$

$$\frac{dP_2}{dt} = \left\{ (A_r - A_p) \dot{u} + k_{pri} A_{pri} \delta \left[\frac{2(P_1 - P_2)}{\rho} \right]^1 + k_{adj} A_{adj} \left[\frac{2|P_1 - P_2|}{\rho} \right]^{\frac{1}{2}} \text{sgn}(P_1 - P_2) \right\} \left\{ \frac{\beta_2}{(A_p - A_r)(L_2 + u)} \right\} \quad (4-22)$$

The bulk modulus of the silicone fluid, β_i , is governed by the following empirical relationship which is valid for units of Newtons and millimeters

$$\beta_i = 864 + 4.166 P_i \quad (4-23)$$

where P_i is the pressure in chamber i . Finally, the force output of the semi-active damper is primarily a result of a pressure differential across the piston head and is given by

$$F = P_1 A_p - P_2 (A_p - A_r) + F_f \text{sgn}(\dot{u}) \quad (4-24)$$

where F_f is the magnitude of the force required to overcome the friction between the piston rod and oil seals. Equations (4-21) and (4-22) may be solved for the pressure in each chamber. The solution requires knowledge of the displacement history, $u(t)$, the velocity history, $\dot{u}(t)$, and the adjustable orifice area history, $A_{adj}(t)$. Note that the fluid mechanics based model presented above does not account for the dynamic characteristics of the external control valve.

4.3.1 Analytical Predictions

Analytical predictions of experimental force-displacement loops were obtained for the semi-active variable damper using the fluid mechanics based mathematical model. Recall

from Section 3.1.2 that, neglecting spool land overlap, the linear motion of the spool opens up a circumferential fluid flow area which is directly proportional to the spool displacement

$$A_{\text{adj}}(t) = \pi d s(t) \quad (4-25)$$

where d is the diameter of the spool and $s(t)$ is the spool displacement. However, to model the control valve adjustable orifice area appropriately, the nonlinearity between the spool position and the fluid flow rate must be accounted for (recall discussion in Section 3.1.2 regarding nonlinearities due to spool land overlap and fluid flow saturation). The relationship between the command voltage and the damping coefficient is given by Equation (3-15). This equation implicitly includes the nonlinear effects discussed above. Examining Equation (3-15), it is apparent that the effective valve orifice area may be more appropriately written as

$$A_{\text{adj}}(\varepsilon) = A_{\text{max}}[1 - \exp(-\gamma\varepsilon^\zeta)] \quad (4-26)$$

where ε is the command voltage, γ and ζ are parameters to be determined empirically, and A_{max} is the maximum adjustable orifice area of the variable dampers. Note that Equation 4-26 is implicitly a function of time as required by Equations (4-21) and (4-22).

All parameters of the fluid mechanics based model were either measured or determined through analytical calibration. Specifically, the primary orifice discharge coefficient, k_{pri} , was determined through calibration of the model for the closed valve condition. The adjustable orifice discharge coefficient, k_{adj} , was assumed to be constant and was

determined by comparing experimental and analytical results for a command voltage of 3 volts (full open valve). Finally, parameters γ and ζ of Equation (4-26) were determined by comparing experimental and analytical results for command voltages over the range of 3 volts (full open valve) to 0 volts (full closed valve). The values of the model parameters used in the numerical simulations are given in Table 4-I.

A comparison of experimental and analytical results is shown in Figure 4-2 for a sinusoidal test at a frequency of 1 Hz. The analytical results were obtained by numerically solving the differential equations describing the pressure in each chamber of the damper (Equations (4-21) and (4-22)) and substituting the results into Equation (4-24) to obtain the force output. As demonstrated in Figure 4-2, the fluid mechanics model appears to adequately describe the semi-active variable damper behavior.

TABLE 4-I Values of Parameters Used in Fluid Mechanics Based Model

PARAMETER	VALUE
β_i	$864 + 4.166P_i$
ρ	$9.96 \times 10^{-10} \text{ N}\cdot\text{s}^2/\text{mm}^4$
A_r	96.94 mm^2
A_p	859.0 mm^2
A_f	859.0 mm^2
K_a	10.0 N/mm
A_{pri}	17.24 mm^2
k_{pri}	1×10^{-6} (unitless)
k_{adi}	0.25 (unitless)
L_1	96.81 mm
L_2	52.94 mm
F_f	89.0 N
γ	$0.15 \text{ (volts)}^{-3}$
ζ	3.0 (unitless)
A_{max}	16.28 mm^2
δ	1 s/mm

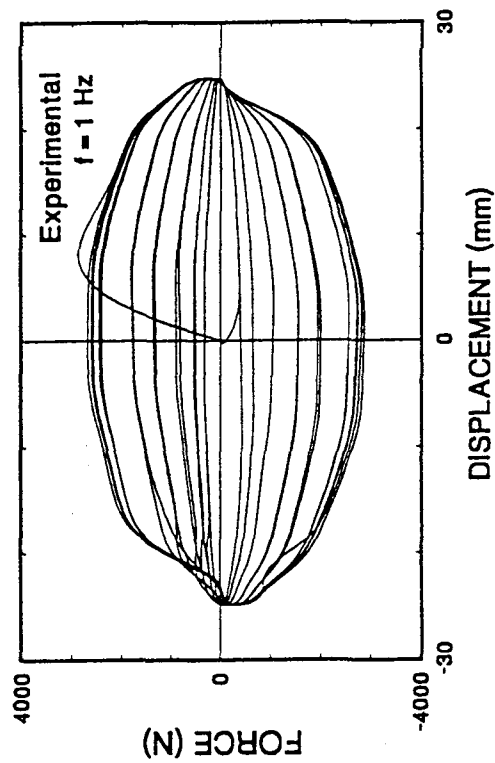
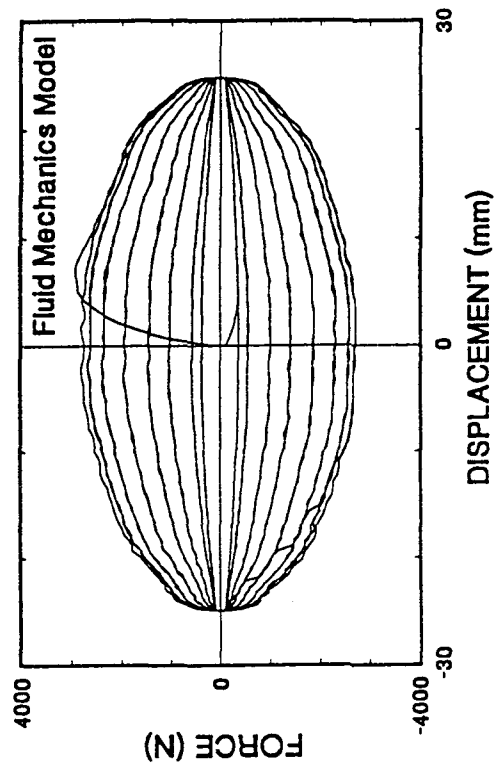


Figure 4-2 Comparison of Analytical and Experimental Force-Displacement Loops for a Variable Damper Component Test with Sinusoidal Input at a Frequency of 1 Hz

SECTION 5

STRUCTURAL MODEL FOR SEISMIC SIMULATION TESTING

5.1 Description of Model and Testing Configurations

A three-story model structure was used for seismic simulation testing. The structure was a 1:4 scale steel moment-resisting frame which modeled a shear building by the method of artificial mass simulation (Soong 1987). The model does not represent a similitude-scaled replica of a full-scale building. Rather, the test structure was designed as a small structural system. The structure has been used in a number of previous earthquake simulation studies.

The structure was bolted to the center of a concrete block which was in turn bolted to the shaking table such that the main frames of the model were parallel to the motion of the table. The two frames of the structure which are perpendicular to the direction of motion were rigidly braced for all tests and ensured that there was no motion of the structure perpendicular to the direction of table motion (see Figures 5-1 and 5-2). This resulted in the reduction of a three dimensional structural system to, essentially, a planar frame.

5.1.1 One-Story Structure

For some of the tests, the structure was modified by rigidly bracing the second and third stories so that the frame would act as a one-story structure. The one-story structure had a mass of 2925 kg. The structure was tested with no dampers (bare frame structure) and with two semi-active dampers placed within the diagonal bracing of the first story (see

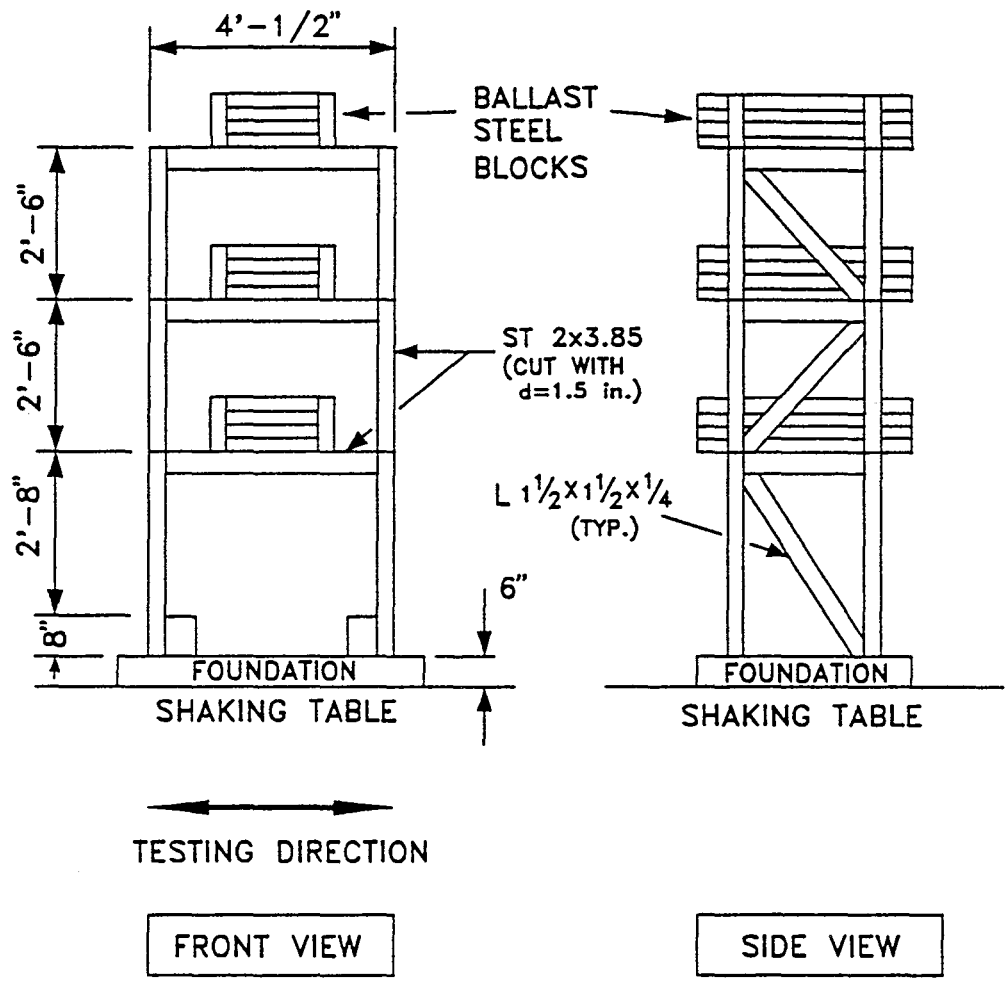


Figure 5-1 Schematic of Model Structure (1 in = 25.4 mm)

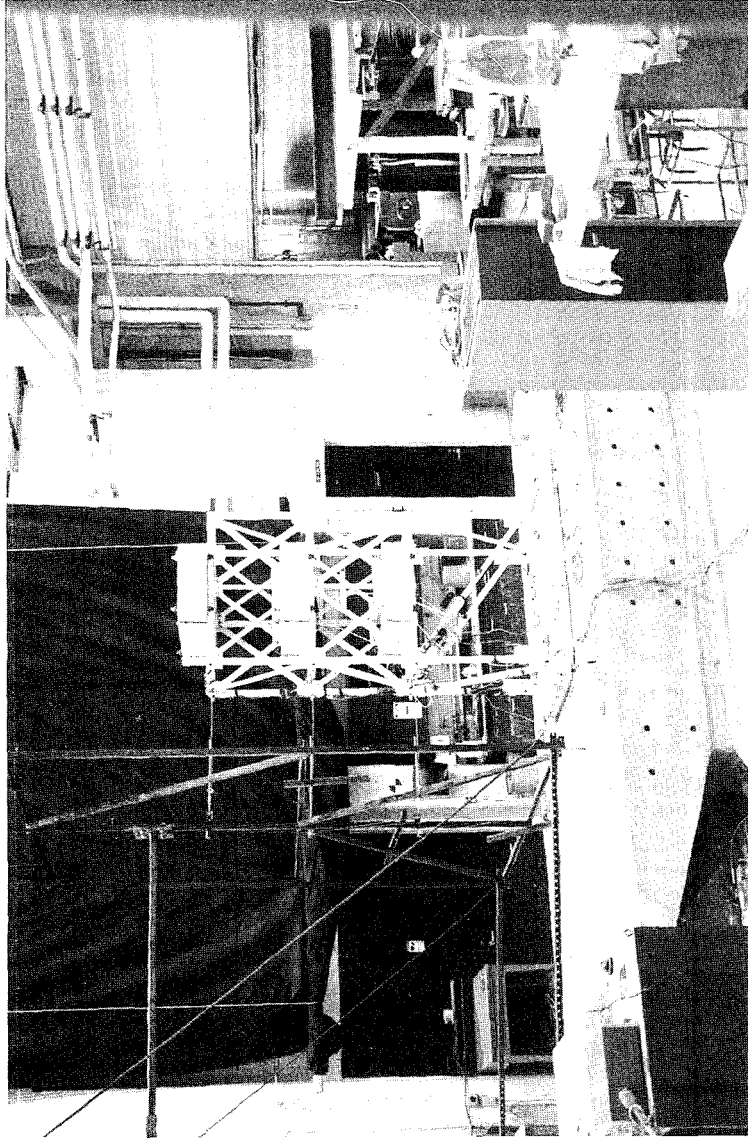


Figure 5-2 Photograph of Model Structure on Shaking Table

Figure 5-3). The semi-active dampers were attached to the structure as shown schematically in Figure 5-4. Special non-slip bushings were designed and constructed for the two ends of the diagonal bracing/damper system. The bushings allowed the joints to rotate freely while reducing the slipping that had occurred in previous testing on the same structure (Constantinou 1993b and 1992b). A photograph of the one-story structure with no dampers (bare frame) and with two semi-active two-stage dampers in the first story is shown in Figures 5-5 and 5-6, respectively. A close-up view of the semi-active two-stage dampers and the semi-active variable dampers installed in the first story of the structure is shown in Figures 5-7 and 5-8, respectively. Note the large elastic rubber cords that are used to support the dampers. These cords support part of the weight of the dampers while maintaining flexibility along the axis of the damper. The purpose of the cords was to reduce the friction between the damper piston rod and the piston rod oil seal. The effect of friction in the dampers will be demonstrated in Section 9 where shaking table test results are presented.

5.1.2 Three-Story Structure

The mass of the three-story structure was 2868 kg, each floor having an equal mass of 956 kg. The structure was tested with no dampers (bare frame) and with two semi-active dampers placed within the diagonal bracing of the first story (see Figure 5-9). The dampers were attached to the structure as shown in Figure 5-4. The non-slip bushings described in Section 5.1.1 were also used in tests on the three-story structure. A photograph of the three-story structure with no dampers (bare frame) and with two

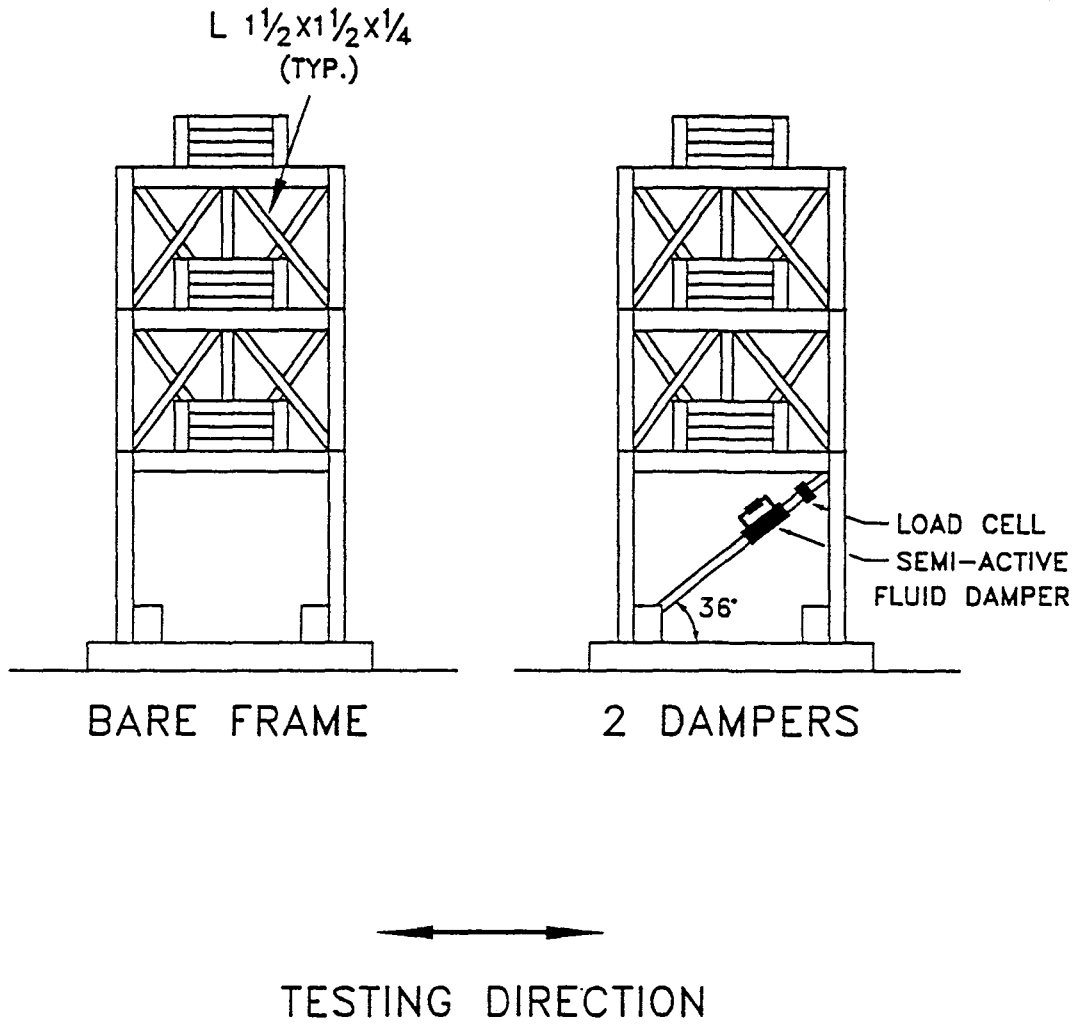
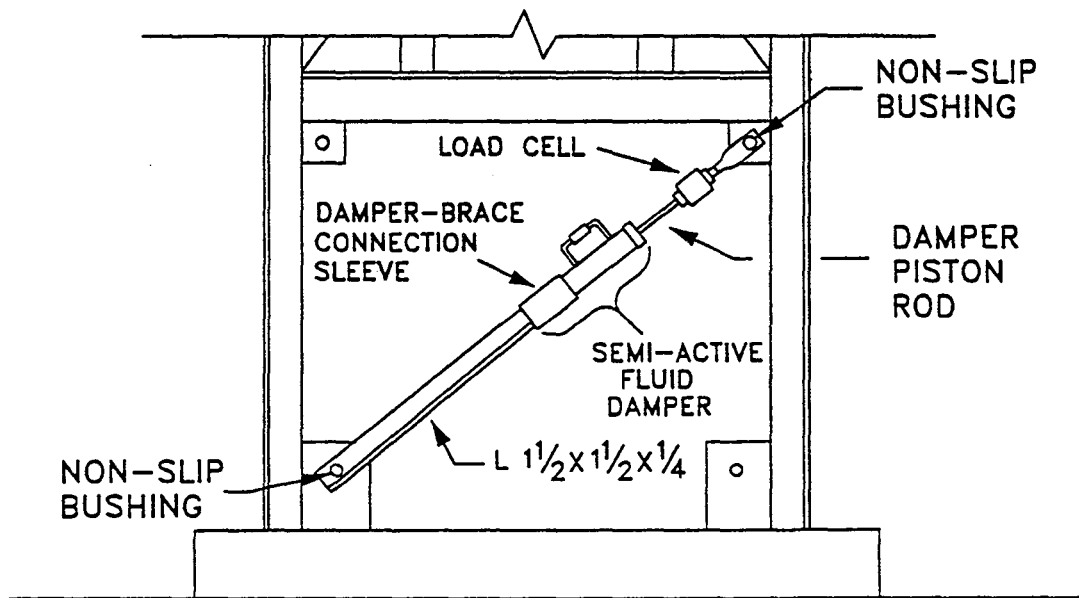


Figure 5-3 Test Configurations for One-Story Structure (1 in = 25.4 mm)



SHAKING TABLE

Figure 5-4 Schematic of Damper Connection Details (1 in = 25.4 mm)

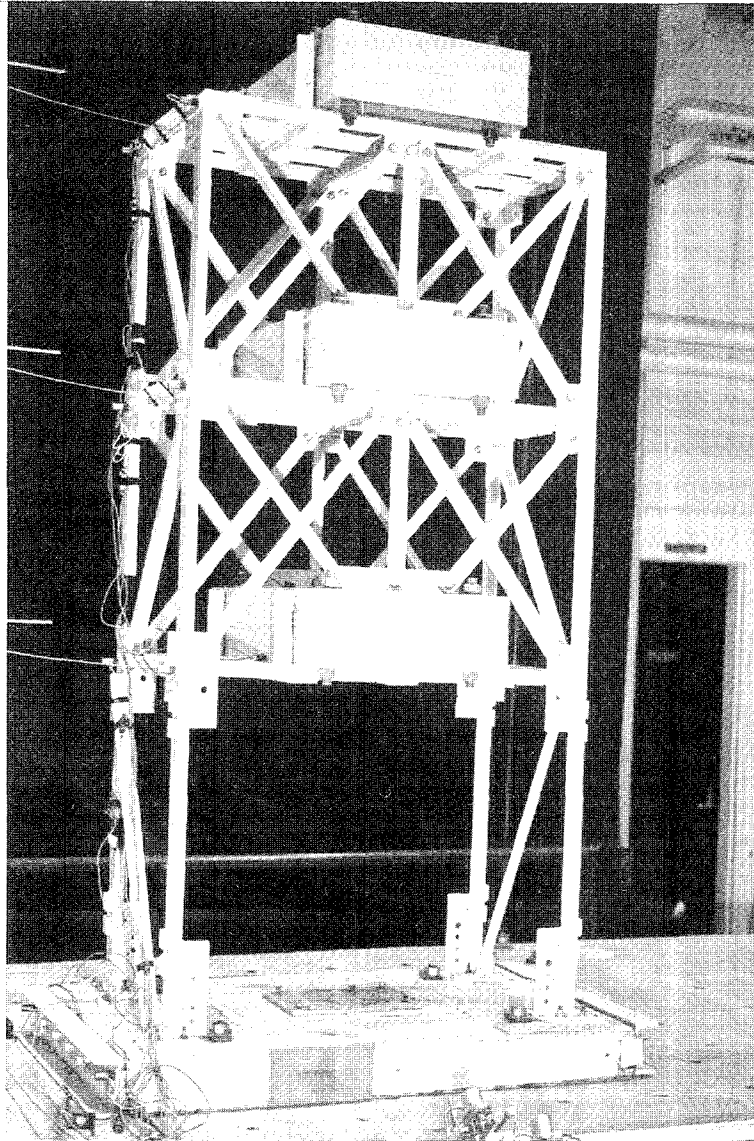


Figure 5-5 Photograph of One-Story Structure with No Dampers (Bare Frame)

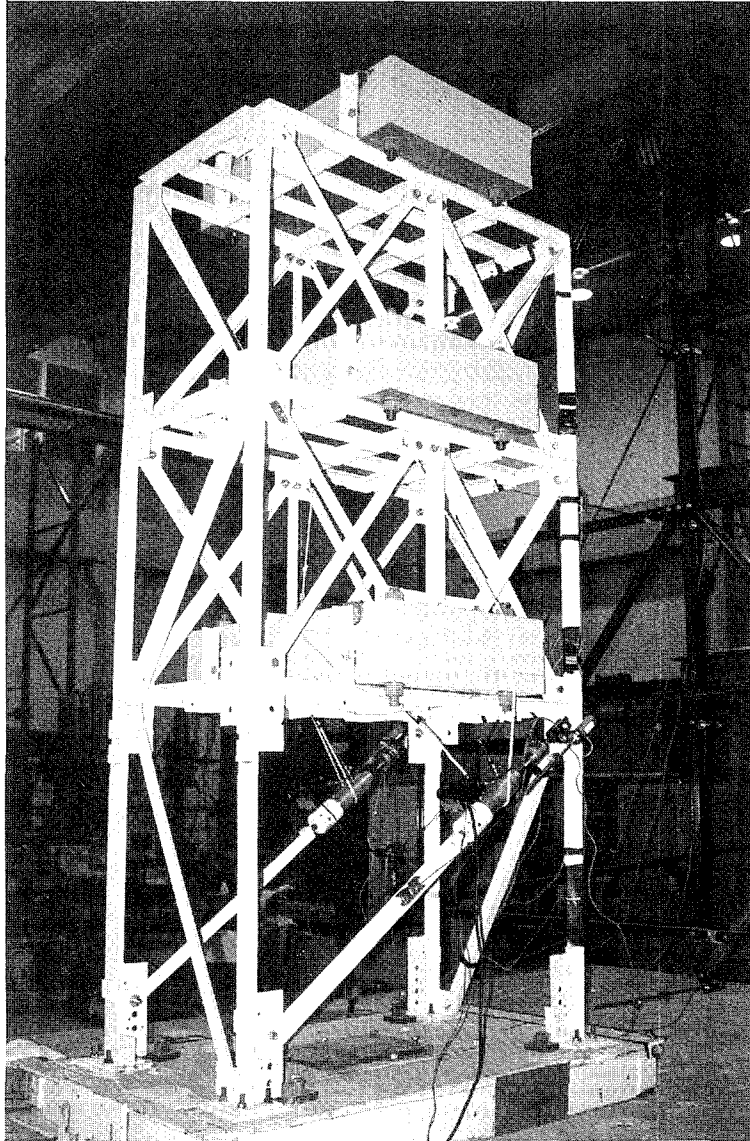


Figure 5-6 Photograph of One-Story Structure with Two Semi-Active Two-Stage Dampers in the First Story

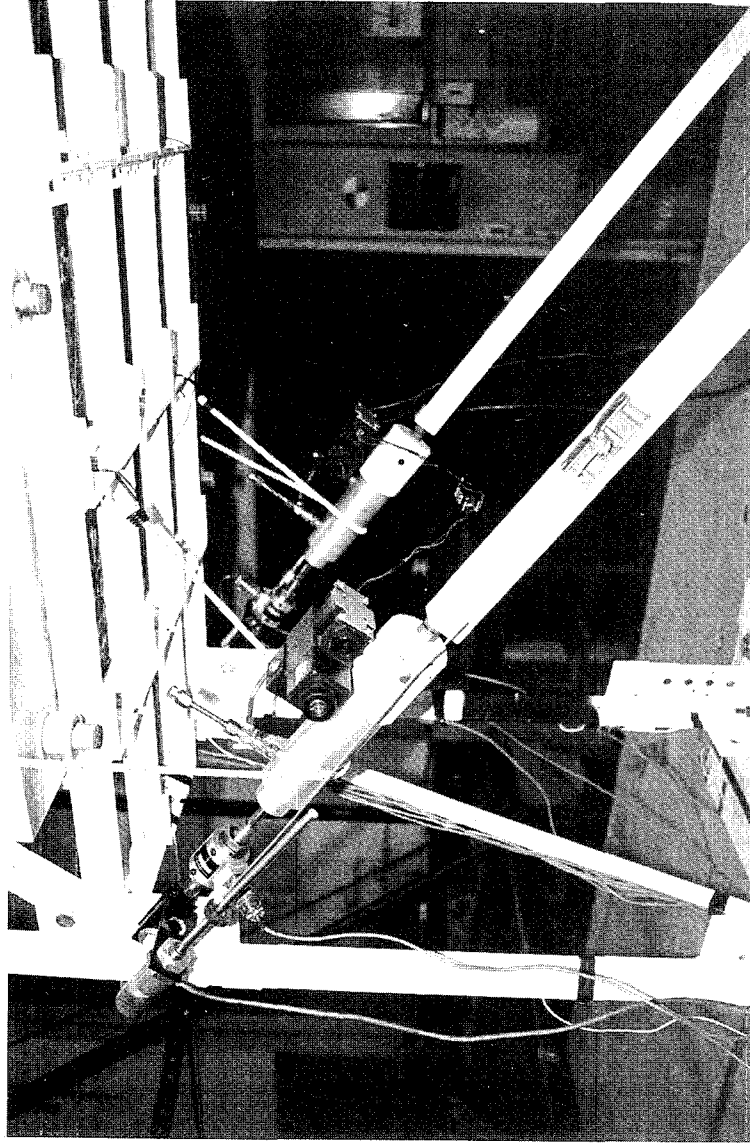


Figure 5-7 Close-Up View of Semi-Active Two-Stage Dampers Installed in First Story of Model Structure

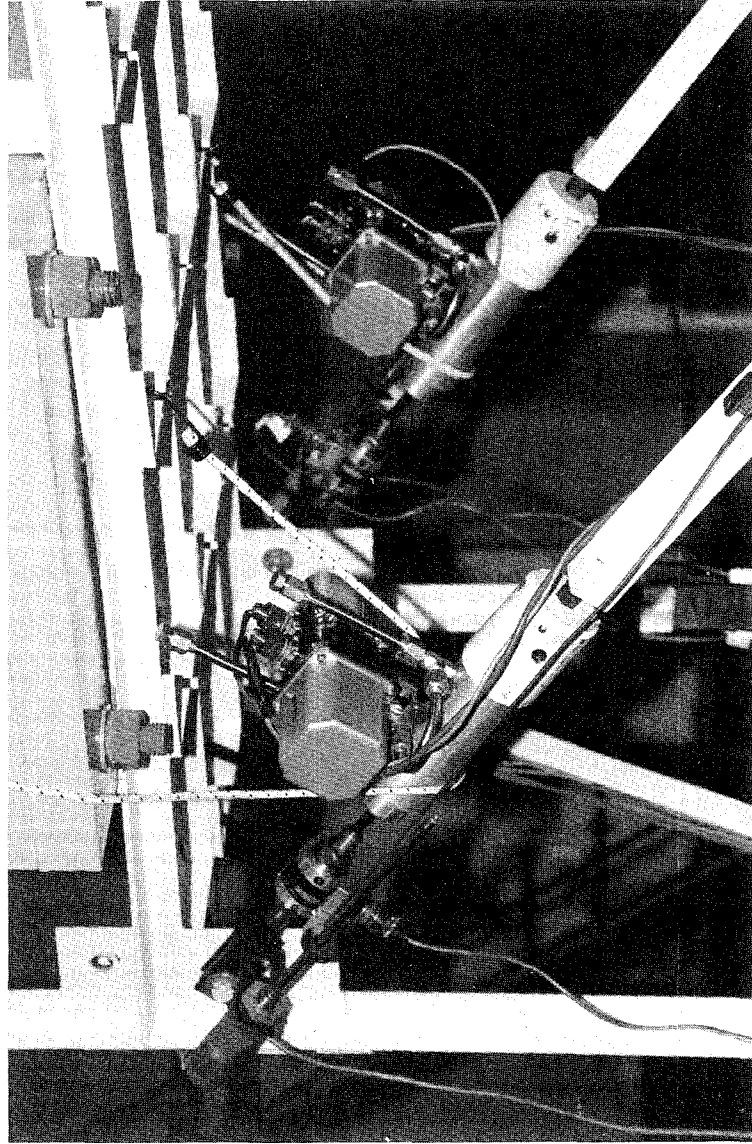


Figure 5-8 Close-Up View of Semi-Active Variable Dampers Installed in First Story of Model Structure

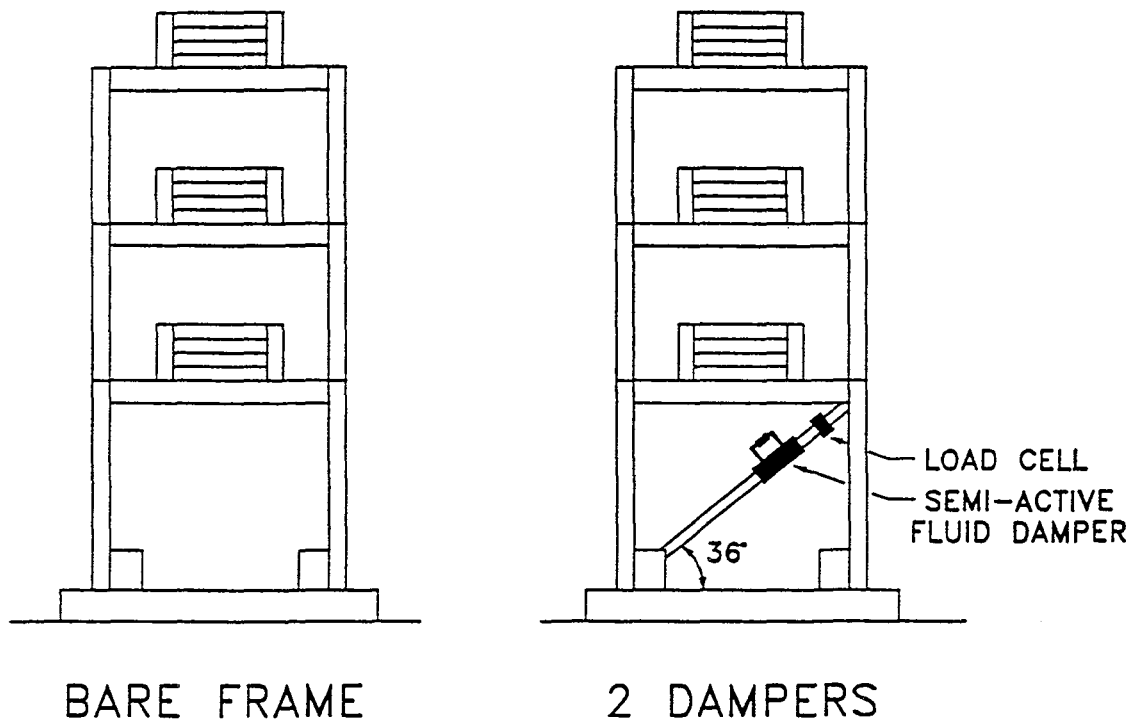


Figure 5-9 Test Configurations for Three-Story Structure

semi-active variable dampers in the first story is shown in Figures 5-10 and 5-11, respectively.

5.2 Test Program

Testing proceeded in the following sequence. First the one-story structure was tested without and with semi-active fluid dampers. In the semi-active damper tests, both the two-stage dampers and the variable dampers were utilized. The bare frame structure was identified to have, at small amplitudes of vibration, a frequency of 2.8 Hz and a damping ratio of 0.74%. An unexpectedly large response occurred during one of the semi-active control tests (described in Section 9.3.1.1) which caused damage to the structural frame. Cracks developed on the webs of the structural tees forming the first story columns. Propagation of the cracks was prevented by drilling small holes at the tip of each crack. Backing plates were then welded to the flange in an attempt to restore the moment of inertia of the structural tees to their pre-cracked value. After the repair, the one-story bare frame structure was identified to have, at small amplitudes of vibration, a frequency of 2.4 Hz and a damping ratio of 1.47%. In seismic excitation, the damping ratio was estimated to be 2.5%. For the pre-repaired condition, the structure is designated as the stiff one-story structure. For the post-repaired condition, the structure is designated as the flexible one-story structure.

The three-story structure was tested next both without and with semi-active dampers. In the semi-active damper tests, only the variable dampers were utilized. The bare frame

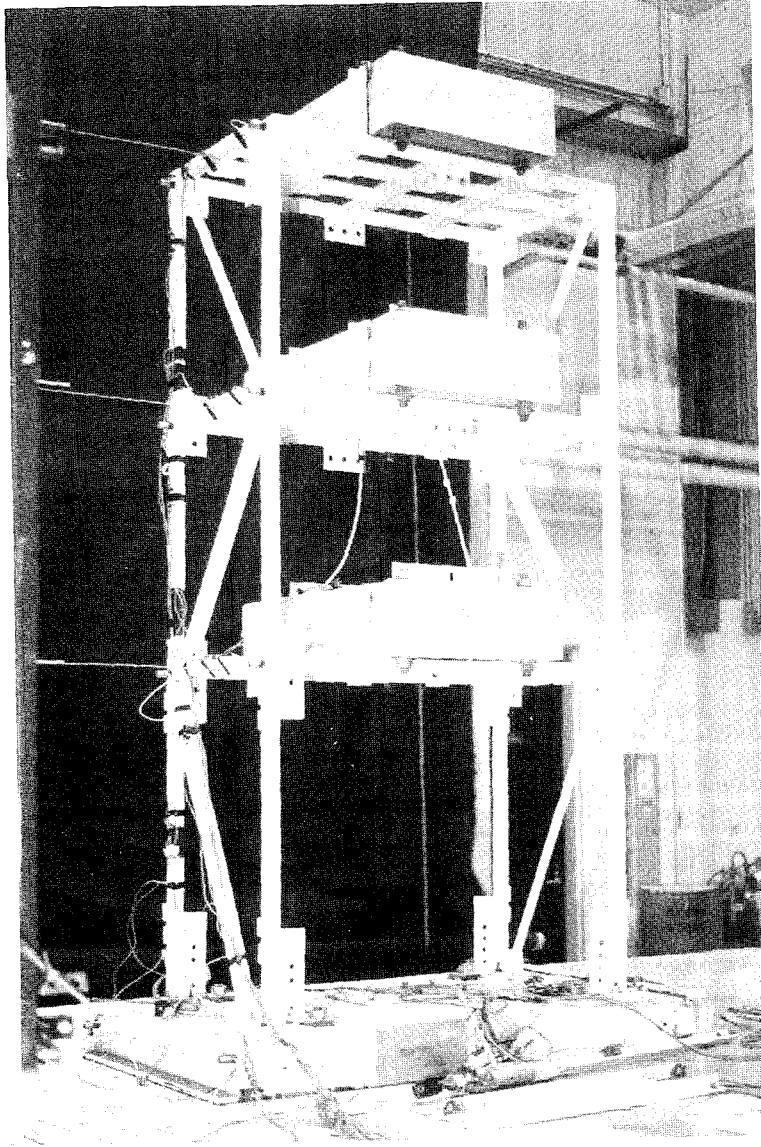


Figure 5-10 Photograph of Three-Story Structure with No Dampers (Bare Frame)

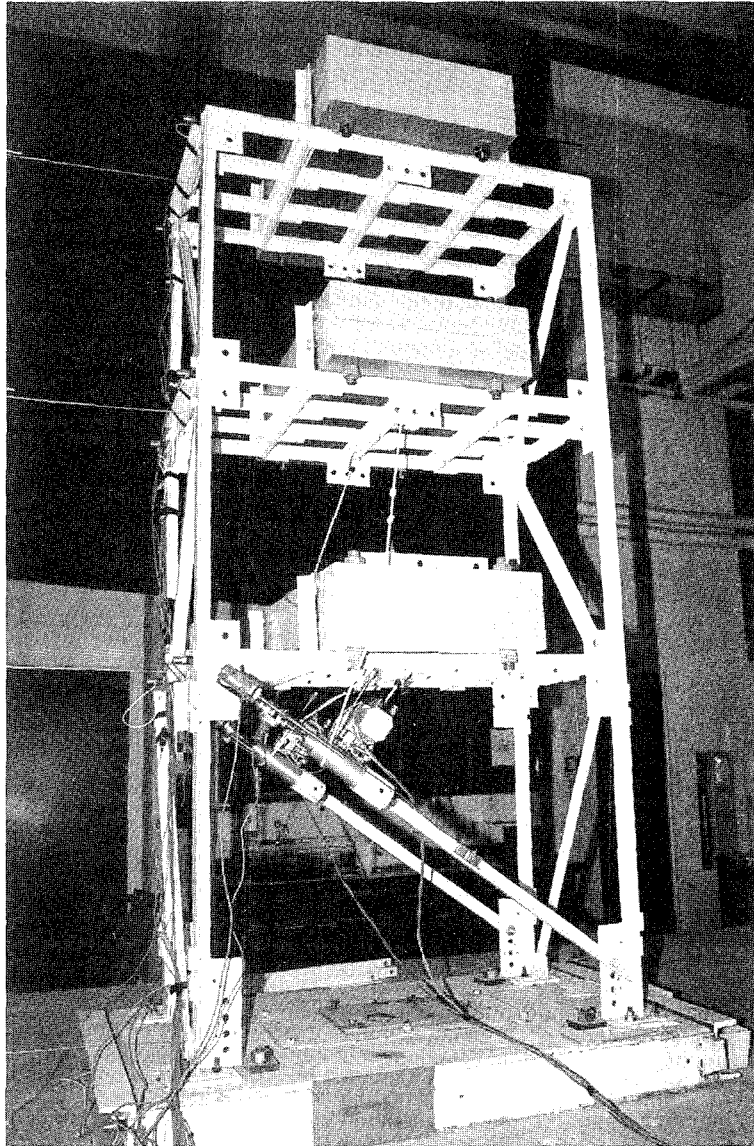


Figure 5-11 Photograph of Three-Story Structure with Two Semi-Active Variable Dampers in the First Story

structure was identified to have, at small amplitudes of vibration, a fundamental frequency of 1.8 Hz and a corresponding damping ratio of 1.74%.

A total of 451 shaking table tests were performed on the model structure. Of these, 253 were deemed useful for reporting.

5.3 Shaking Table Motions Used in Test Program

Four different motions were used as input to the shaking table. Two of the motions were historical earthquake records (El Centro and Hachinohe), one motion was a high frequency version of a historical earthquake record (Hachinohe), and one motion was a harmonic signal of constant frequency and amplitude.

Characteristics of the two historical earthquake records are provided in Table 5-I in prototype scale. These records were compressed in time by a factor of two to satisfy the similitude requirements of the quarter length scale model. Further, the historical Hachinohe earthquake record was compressed in time by a factor of four to create a high frequency version of the record. This high frequency motion is designated as the Modified Hachinohe earthquake (Hachinohe-M). Figures 5-12 through 5-15 show recorded time histories of the shaking table motion for 75% of the El Centro earthquake record, 100% of the Hachinohe earthquake record, 100% of the Modified Hachinohe earthquake record, and a harmonic signal having a frequency of 5 Hz and an amplitude of 0.2g, respectively. The acceleration and displacement records were directly measured whereas the velocity

Table 5-1 Earthquake Motions Used in Shaking Table Test Program and Characteristics in Prototype Scale

NOTATION	RECORD	MAGNITUDE	PREDOMINANT FREQUENCY RANGE (Hz)	PEAK ACCELERATION (g)	PEAK VELOCITY (cm/sec)	PEAK DISPLACEMENT (cm)
El Centro S00E	Imperial Valley, May 18, 1940, component S00E	6.7	1-4	0.34	33.45	10.87
Hachinohe	Tokachi-Oki earthquake, Japan, May 16, 1968, component NS	7.9	0.25 - 1.5	0.23	35.71	11.89

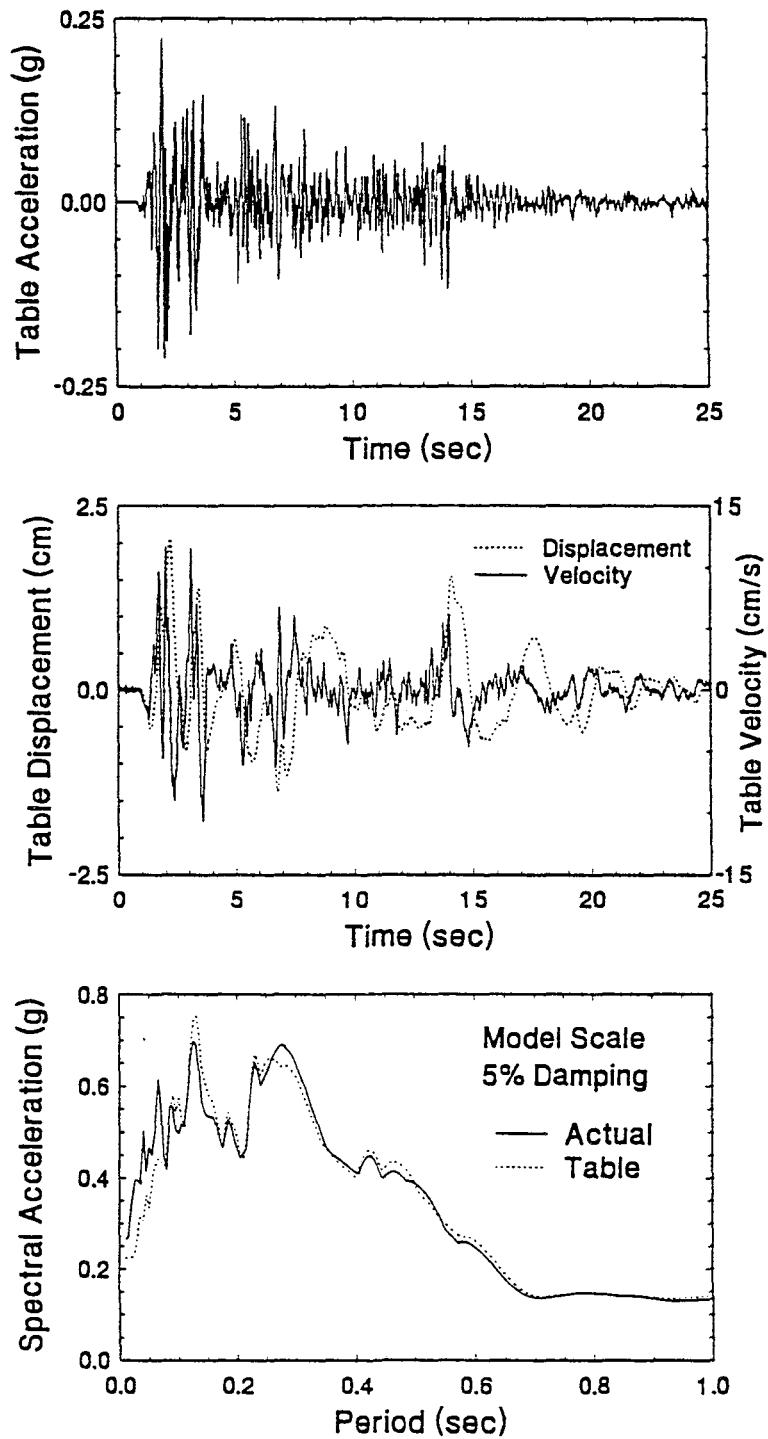


Figure 5-12 Time Histories of Displacement, Velocity, and Acceleration and Acceleration Spectrum of Shaking Table Excited by 75% of El Centro Motion

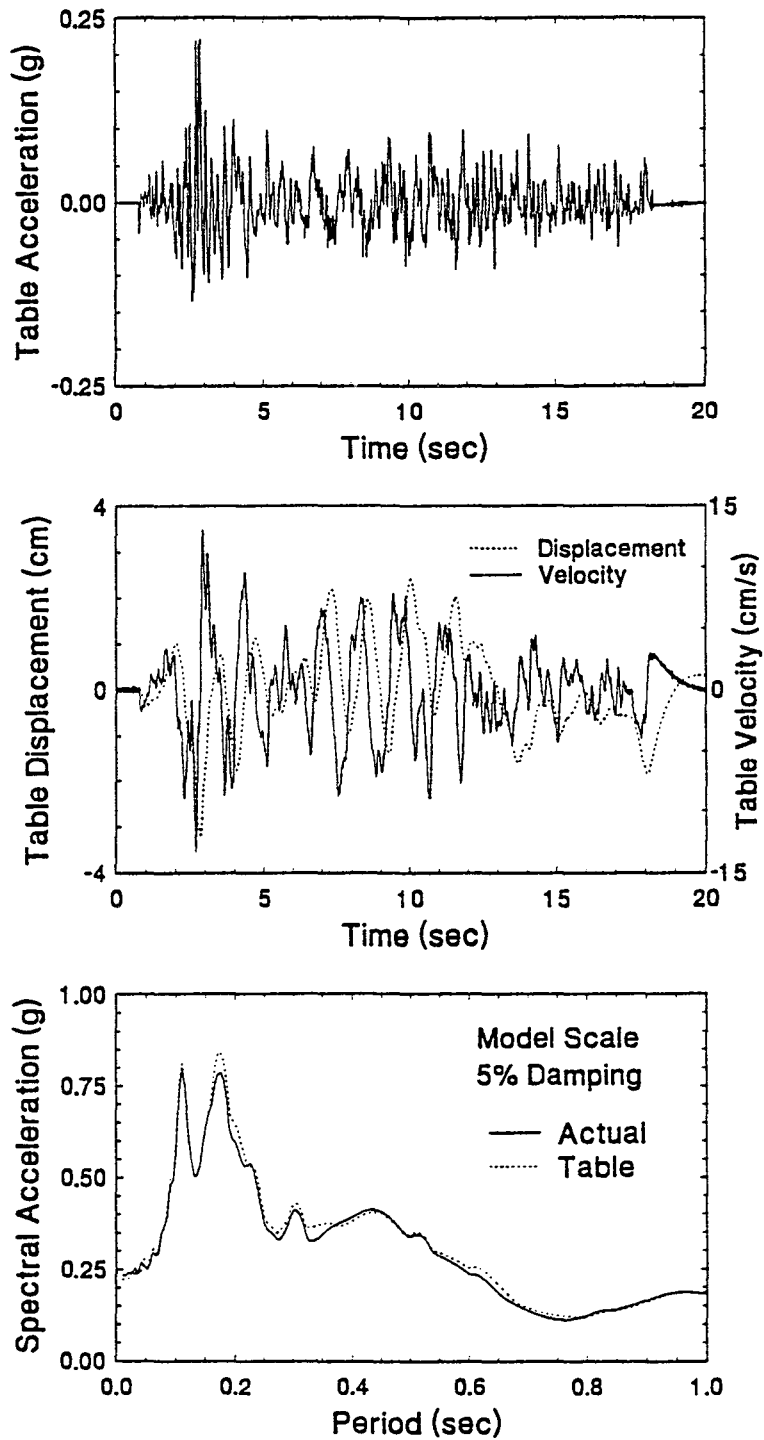


Figure 5-13 Time Histories of Displacement, Velocity, and Acceleration and Acceleration Spectrum of Shaking Table Excited by 100% of Hachinohe Motion

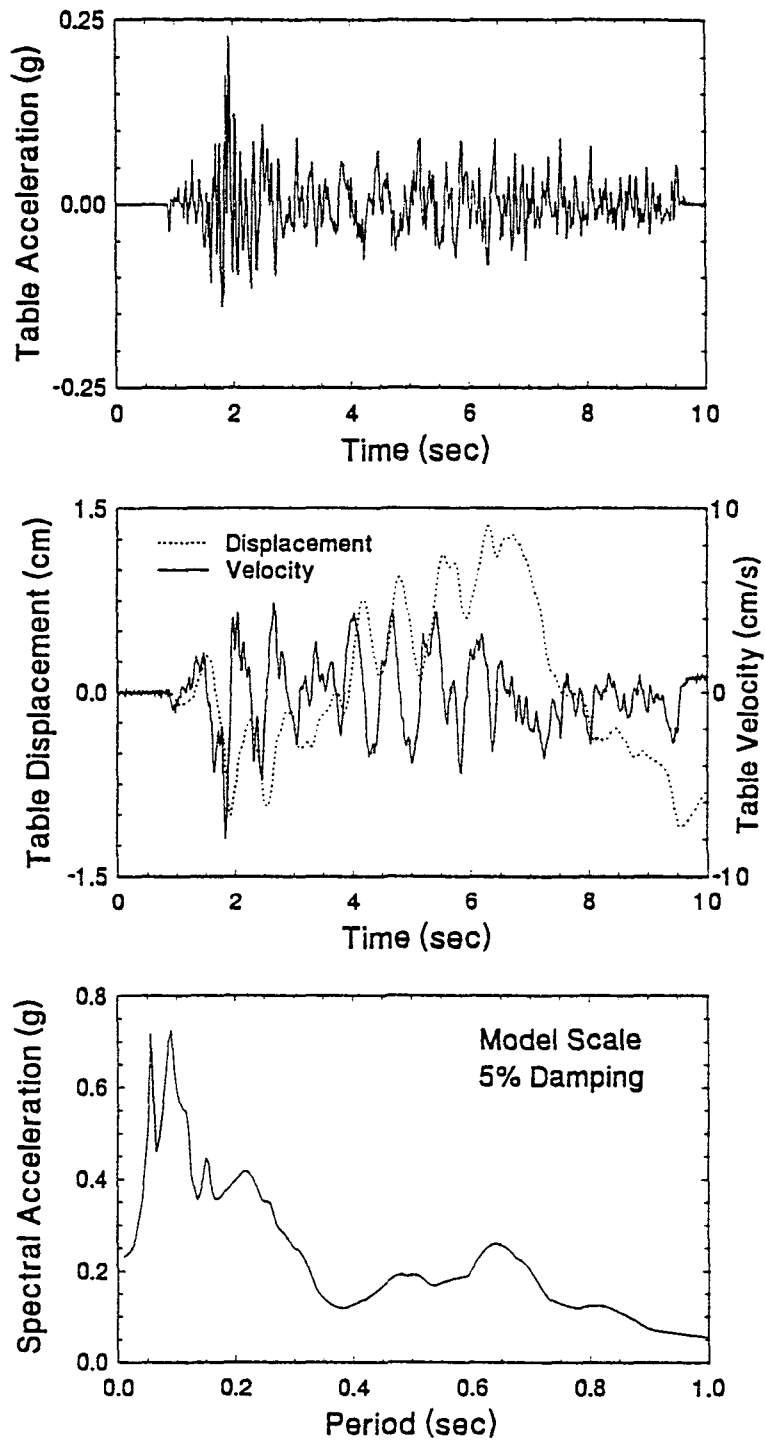


Figure 5-14 Time Histories of Displacement, Velocity, and Acceleration and Acceleration Spectrum of Shaking Table Excited by 100% of Modified Hachinohe Motion

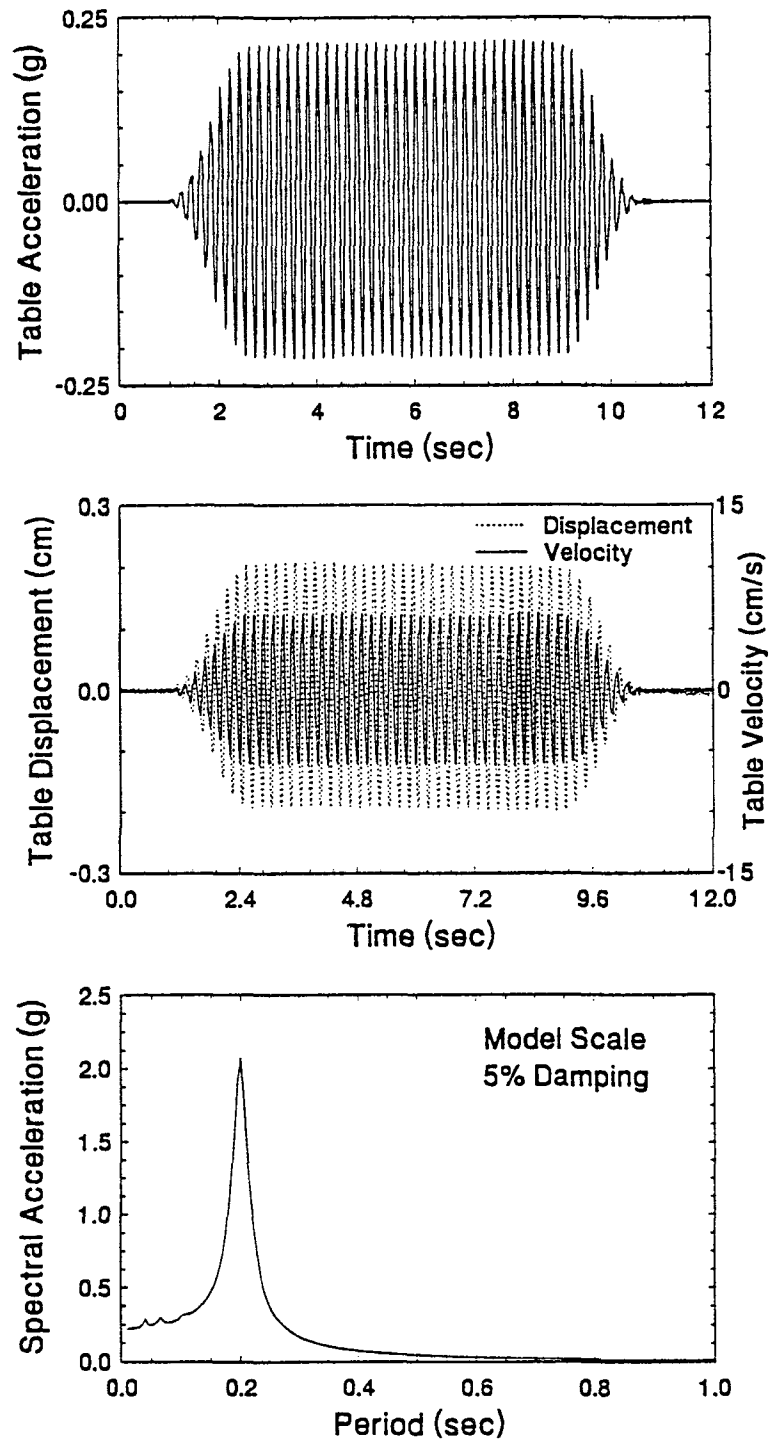


Figure 5-15 Time Histories of Displacement, Velocity, and Acceleration and Acceleration Spectrum of Shaking Table Excited by 0.2g 5 Hz Harmonic Motion

record was obtained by numerical differentiation of the displacement record. It may be observed that for the two historical ground motions, the peak ground motion was reproduced well, but not exactly, by the table generated motion. Figures 5-12 through 5-15 also show the response spectra of acceleration (exact, not pseudo-acceleration) of the shaking table motion. For the two historic ground motions, the 5% damped acceleration spectra is compared to the spectra of the actual record to demonstrate the good reproduction by the shaking table.

For tests on the one-story structure, the frequency of the harmonic signal was selected to be approximately twice the natural frequency of the structure. In the case of the one-story stiff structure (natural frequency = 2.8 Hz), the frequency of the harmonic signal was 5.6 Hz and in the case of the one-story flexible structure (natural frequency = 2.4 Hz), the frequency of the harmonic signal was 5 Hz. The harmonic loading was also utilized in shaking table tests on the three-story model. In this case, the driving frequency of the harmonic input was selected to be 5 Hz which is near the frequency of the second mode of the three-story structure (5.8 Hz).

5.4 Measurement Instrumentation and Data Acquisition

A total of 34 data acquisition channels were utilized for the shaking table tests. A list of these channels and a description of the response measured is given in Table 5-II. Of the 34 channels recorded, 23 were used to measure data from transducers located on the model structure. A schematic of the model structure showing the location of 17 of the

Table 5-II Data Acquisition Channels (with reference to Figure 5-16)

CHANNEL	TRANSDUCER	NOTATION	RESPONSE MEASURED
1	ACCEL	AFHE	FOUNDATION HORIZ. ACCELERATION - EAST
2	ACCEL	AFHW	FOUNDATION HORIZ. ACCELERATION - WEST
3	ACCEL	A1HE	FLOOR 1 HORIZ. ACCELERATION - EAST
4	ACCEL	A1HW	FLOOR 1 HORIZ. ACCELERATION - WEST
5	ACCEL	A2HE	FLOOR 2 HORIZ. ACCELERATION - EAST
6	ACCEL	A2HW	FLOOR 2 HORIZ. ACCELERATION - WEST
7	ACCEL	A3HE	FLOOR 3 HORIZ. ACCELERATION - EAST
8	ACCEL	A3HW	FLOOR 3 HORIZ. ACCELERATION - WEST
9	LDT	DFHC	FOUNDATION HORIZ. DISPLACEMENT - CENTER
10	LDT	D1HC	FLOOR 1 HORIZ. DISPLACEMENT - CENTER
11	LDT	D2HC	FLOOR 2 HORIZ. DISPLACEMENT - CENTER
12	LDT	D3HC	FLOOR 3 HORIZ. DISPLACEMENT - CENTER
13	LDT	DDAE	AXIAL DAMPER DISPLACEMENT - EAST
14	LDT	DDAW	AXIAL DAMPER DISPLACEMENT - WEST
15	LOAD CELL	LCAE	AXIAL DAMPER FORCE - EAST
16	LOAD CELL	LCAW	AXIAL DAMPER FORCE - WEST
17	STRAIN GAGE	DIHW	FLOOR 1 HORIZ. RELATIVE DISPLACEMENT - WEST
18	LVDT	DLAT	TABLE HORIZ. DISPLACEMENT
19	ACCEL	ALAT	TABLE HORIZ. ACCELERATION
20	LVDT	DROL	TABLE ROLL DISPLACEMENT
21	ACCEL	AROL	TABLE ROLL ACCELERATION
22	LVDT	VAR-A	VARIABLE DAMPER - A SPOOL DISPLACEMENT
23	LVDT	VAR-B	VARIABLE DAMPER - B SPOOL DISPLACEMENT

Table 5-II Cont'd

CHANNEL	TRANSDUCER	NOTATION	RESPONSE MEASURED
24	---	VFHC	FOUNDATION HORIZ. VELOCITY - CENTER
25	---	V1HC	FLOOR 1 HORIZ. VELOCITY - CENTER
26	---	V2HC	FLOOR 2 HORIZ. VELOCITY - CENTER
27	---	V3HC	FLOOR 3 HORIZ. VELOCITY - CENTER
28	---	DCOM	DAMPER COMMAND SIGNAL
29	---	DCOM2	UNFILTERED DAMPER COMMAND SIGNAL
30	---	MEST	MASS ESTIMATE
31	---	KEST	STIFFNESS ESTIMATE
32	---	CEST	DAMPING COEFFICIENT ESTIMATE
33	---	CUNB	UNBOUNDED DAMPING COEFFICIENT
34	---	JERK	FLOOR 1 HORIZ. RATE OF ACCELERATION - EAST

NOTES: ACCEL = Accelerometer
LDT = Linear Displacement Transducer
LVDT = Linear Variable Differential Transformer

transducers is shown in Figure 5-16. The 6 transducers which are not shown in Figure 5-16 are those which measured the table motion and the LVDT's which measured the spool position of the variable dampers.

The following description of the measurement instrumentation is given with reference to Table 5-II. An accelerometer was located on the east and west frame at each floor level so that the effect of torsion could be evaluated. The displacement transducers at each floor measured the displacement of the floor with respect to an inertial reference frame. The displacement transducer located along the axis of each damper measured the displacement of the piston rod with respect to the damper housing. The velocity measurements were obtained by passing the floor displacement signals through a bank of analog differentiators. The damper command signal from the control computer was measured both as a filtered and unfiltered signal. Channels 30 to 32 were calculated by the control computer for the control algorithm described in Section 7.4.2 and Channel 33 was calculated by the control computer for the control algorithm described in Section 7.4.1. Finally, the jerk of the first floor was obtained by passing the signal from the first floor east frame accelerometer through an analog differentiator.

All of the data acquisition channels were recorded at a sampling rate of 100 points/sec on a PC computer with an INTEL™ 80486/50 MHz processor interfaced with an OPTIM™ Megadac 16 bit data acquisition system having 168 channels of analog-to-digital conversion and running the program Test Control Software (TCS). All channels were

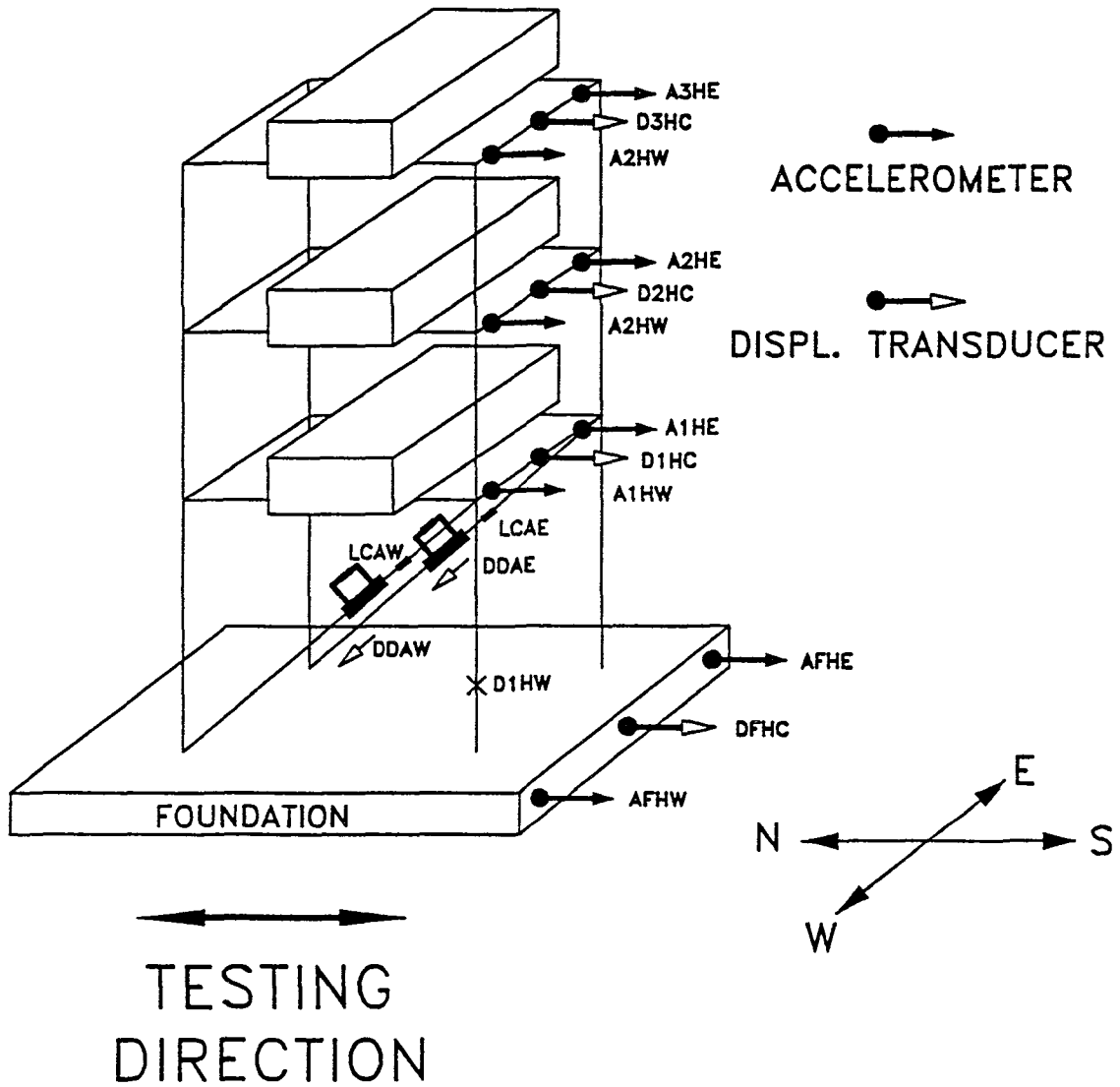


Figure 5-16 Schematic of Model Structure Showing Location of Measurement Instrumentation

passed through the Megadac's programmable 8 pole low-pass butterworth filters. The cut-off frequency for all channels was set to 30 Hz except for the unfiltered command signal which was set to "bypass".

The calibration factor, full-scale voltage, full-scale measurement, and minimum resolution of each data acquisition channel is provided in Appendix A, Table A-I. Specifications related to the transducers located on the model structure (see Figure 5-16) are provided in Appendix A, Table A-II. Specifications related to the 11 strain gages (8 within accelerometers, 2 within load cells, and one located on a first story column) and corresponding signal conditioners are provided in Appendix A, Table A-III.

5.5 Control Systems and Hardware

During the shaking table tests in which semi-active dampers were attached to the model structure, a computer was used for control of the dampers. A block diagram showing the closed-loop shaking table tests with the semi-active two-stage dampers and with the semi-active variable dampers is shown in Figures 5-17 and 5-18, respectively. The control computer received signals from the measured response of the structure, processed the signals according to a pre-determined control algorithm, and sent an appropriate command signal to the semi-active damper valves. The response measurements were passed through six pole low-pass butterworth filters (cut-off frequency = 25 Hz) prior to entering the control computer. In addition to the control computer, a computer for data acquisition was used as described in Section 5.4.

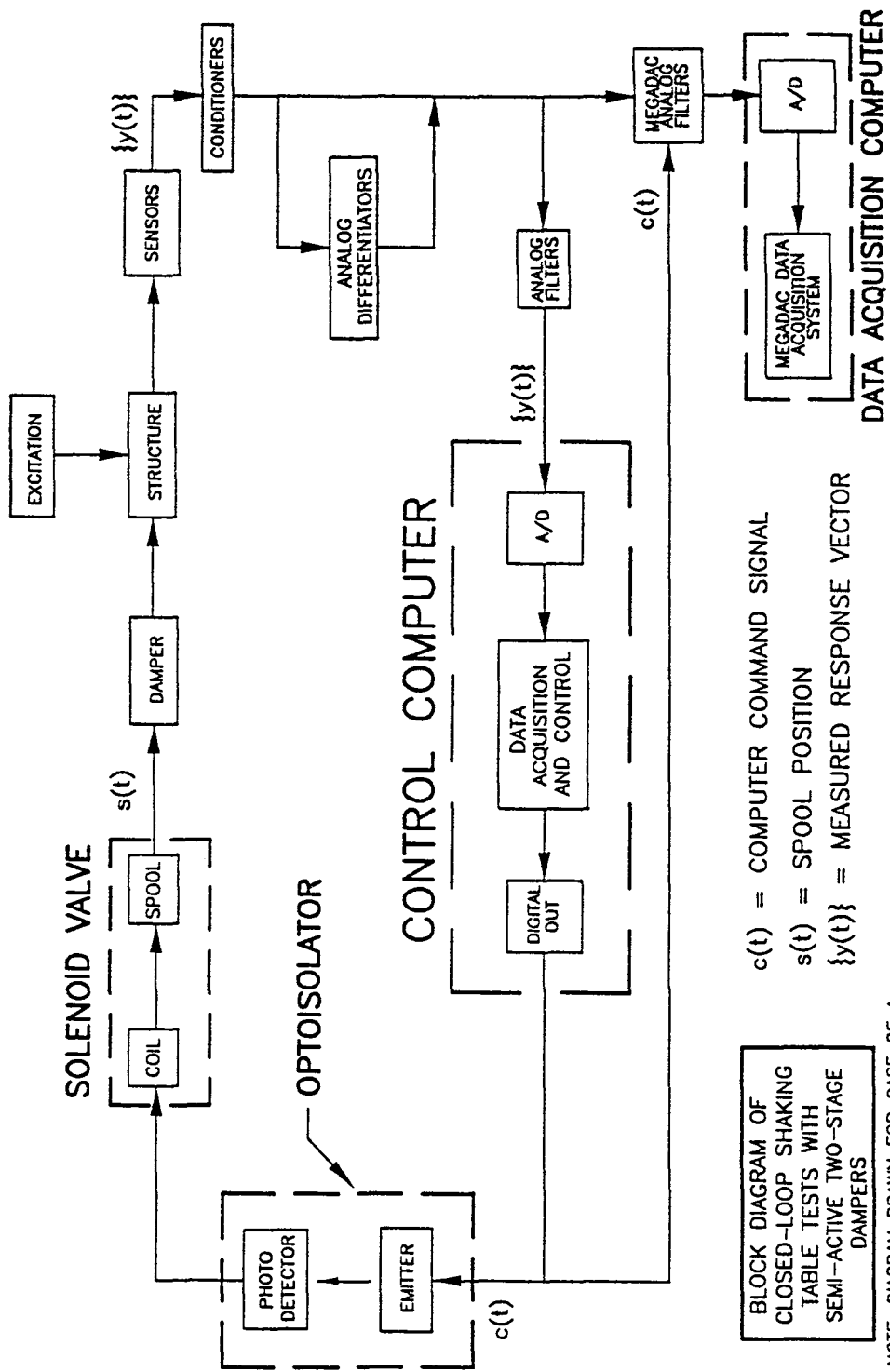


Figure 5-17 Block Diagram of Closed-Loop Shaking Table Tests with Semi-Active Two-Stage Dampers

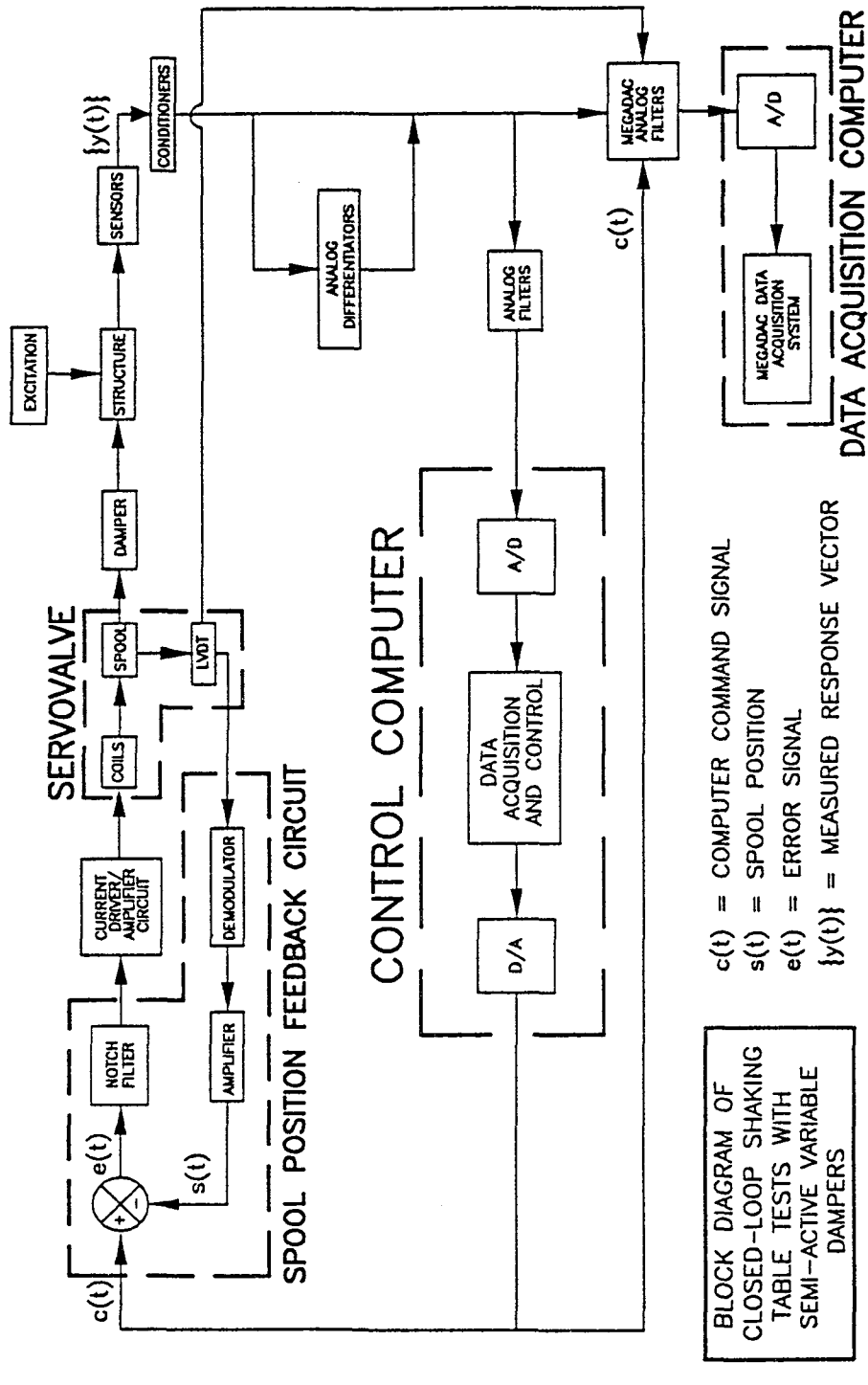


Figure 5-18 Block Diagram of Closed-Loop Shaking Table Tests with Semi-Active Variable Dampers

The function of the optoisolator shown in the block diagram for the shaking table tests with two-stage dampers (Figure 5-17) has been described previously in Section 3.2.2. Recall that two semi-active dampers were placed in the first story of the structure for the shaking table tests. In the case of the two-stage dampers, the two solenoid valves corresponding to each two-stage damper unit were on the same circuit and were controlled by a single optoisolator and thus the command signal was identical for each solenoid valve. The average power required for the simultaneous control of the solenoid valves was about 110 W.

The spool position feedback circuit and current driver circuit shown in the block diagram for the variable damper shaking table tests (Figure 5-18) has been described previously in Section 3.2.3. With reference to Figure 5-18, each servovalve of the two variable damper units located within the first story of the structure had its own spool position feedback circuit and current driver/amplifier circuit which were supplied power simultaneously by a dual-tracking power supply. A single command signal was sent from the control computer to the spool position feedback circuit corresponding to each variable damper unit and thus the command signal was identical for each servovalve. The peak power required for the simultaneous control of the servovalves was 7 W.

Two different control computers and control software were used over the course of the testing program. During the initial portion of testing (Tests 1 through 190), relatively simple control algorithms were utilized for control of the semi-active two-stage dampers

(see Section 7.2). The control computer was a PC with an INTEL™ 80486/33 MHz processor and a 12 bit data acquisition board having 8 channels of analog-to-digital conversion and 2 channels of digital-to-analog conversion. A commercially available data acquisition and control software program (Labtech Notebook™, version 7.2) was sufficient for implementation of the simple control algorithms used in controlling the semi-active two-stage dampers. The sampling rate for control of the two-stage dampers was 200 pt/sec.

More sophisticated control algorithms were developed for use with the semi-active variable dampers (see Sections 7.3 and 7.4). These control algorithms were implemented on a PC computer with an INTEL™ 80386/25 MHz processor with two 12 bit data acquisition boards, each board having 8 channels of analog-to-digital conversion and 2 channels of digital-to-analog-conversion. Computer programs written in the Quickbasic computer language (Microsoft Quickbasic extended version 7.1) were used for implementation of the control algorithms. The sampling rate for control of the variable dampers was dependent on the control algorithm and ranged from about 160 pt/sec to about 530 pt/sec. Sampling rate data was obtained from measurements of the computational time delay associated with each control algorithm (see Section 8.4.1).

A photograph showing the computer control systems and associated equipment for the semi-active two-stage dampers and variable dampers is provided in Figure 5-19.

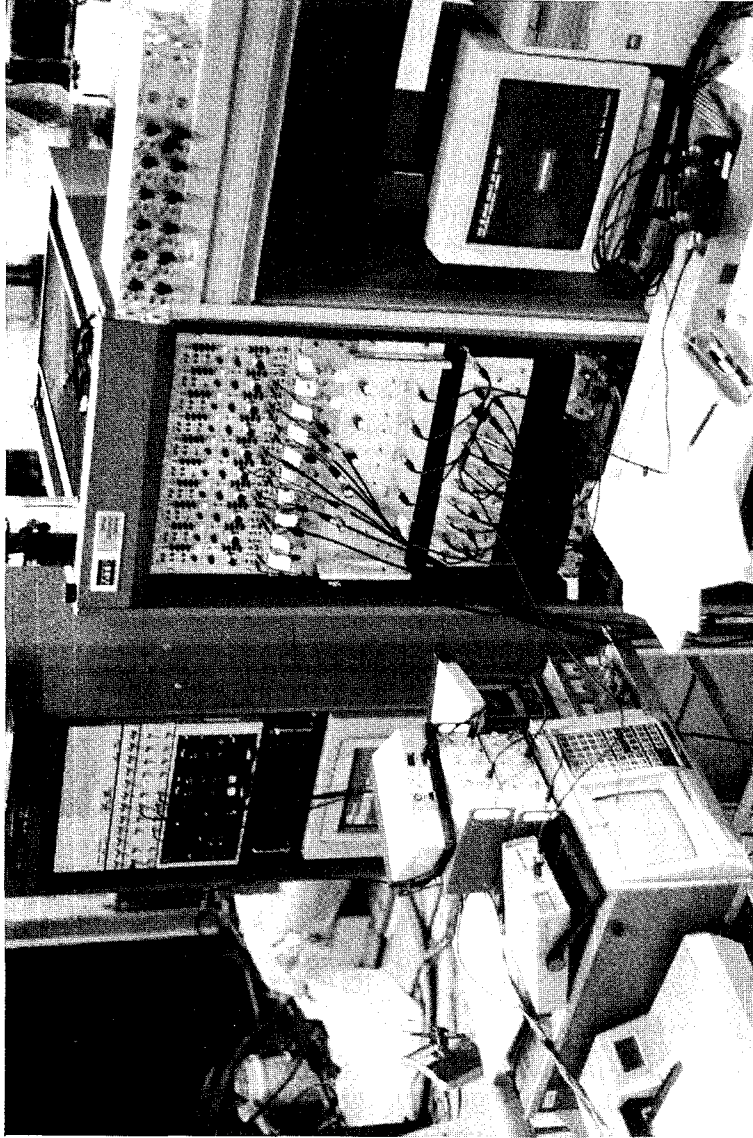


Figure 5-19 Photograph of Control Computers and Associated Equipment for Semi-Active Two-Stage Dampers (right) and Variable Dampers (left)

SECTION 6

IDENTIFICATION OF STRUCTURAL PROPERTIES

6.1 Introduction

The structural properties of the one-story and three-story structures were identified in the bare frame configuration and with semi-active fluid dampers attached to the structure. For identification of the structure with semi-active fluid dampers, the damping was set to either low or high.

6.2 Method of Identification

The method of identification involved exciting the foundation of the structure with a banded, 0 to 20 Hz white noise excitation having an acceleration amplitude of 0.05 to 0.2g. For each structural system (i.e., bare frame, semi-active dampers set to low damping, and semi-active dampers set to high damping) the acceleration amplitude of the white noise excitation was selected based on two criteria. The excitation must be small enough to prevent inelastic behavior in the structure and, in the case of the structural system with semi-active dampers, must be large enough to induce viscous damping behavior. If the excitation is too low, the friction between the damper piston rod and piston rod seal is the primary source of damping. Therefore, a relatively large amplitude white noise excitation must be used to excite the structural system with semi-active dampers so that the measured properties related to damping are primarily a result of viscous behavior of the dampers.

The banded white noise excitation is used to excite the structure over a wide range of frequencies. The amplitude and phase angle of the total acceleration transfer function is then obtained for each degree of freedom. The amplitude of the total acceleration transfer function of the j -th degree of freedom is calculated as the ratio of the Fourier amplitude of the total acceleration of the j -th degree of freedom to the Fourier amplitude of the harmonic ground acceleration. For the structure without fluid dampers (lightly damped system), the amplitudes of the total acceleration transfer functions contain sharp and narrow peaks which reveal frequencies, damping ratios, and mode shapes. For highly damped structures, the amplitudes of the total acceleration transfer functions do not usually contain well defined peaks and identification of the structural properties requires a more refined analytical method.

The equations of motion of the structure combined with an equation describing the semi-active damper behavior may be utilized to 1) obtain analytical expressions for the amplitudes of transfer functions and 2) to solve the associated eigenvalue problem. The analytically determined transfer functions may then be compared with experimental transfer functions to determine the validity of the mathematical models describing the structure and damper behavior.

6.3 Identification of One-Story Structure

6.3.1 Equation of Motion

The equation of motion of a base excited single-degree-of-freedom (SDOF) lumped mass structure with fluid dampers can be written as

$$m\ddot{u} + c_u\dot{u} + k u + \eta P_d = -m\ddot{u}_g \quad (6-1)$$

where m is the mass of the structure, k is the linear elastic stiffness of the undamped structure, c_u is the damping coefficient of the structure without dampers, η is the number of dampers, P_d is the horizontal component of force in a single damper, \ddot{u}_g is the ground acceleration; and \ddot{u} , \dot{u} , and u are the relative acceleration, velocity, and displacement, respectively, of the mass. The viscoelastic Maxwell model for describing semi-active fluid damper behavior was utilized in the identification of both the one-story and three-story structure (see Equation (4-4)). Note that the symbol \dot{u} used in Equation (4-4) represents the axial velocity of the piston head with respect to the damper housing whereas, in this section, \dot{u} represents the relative velocity of the mass of the structure. For a single damper inclined at an angle θ with respect to the horizontal axis, the equation describing the damper force in the horizontal direction is given by

$$P_d + \lambda \dot{P}_d = C_{SA} \cos^2 \theta \dot{u} \quad (6-2)$$

where C_{SA} is the damping coefficient of the semi-active dampers. For identification purposes, the semi-active dampers are set to either low or high damping and therefore the time dependent damping coefficient of Equation (4-4) has been set equal to a constant value ($C_{SA} = C_{\max}$ or C_{\min}).

In the case of the one-story structure without dampers, $\eta = 0$ and Equation (6-1) assumes the following form

$$m\ddot{u} + c_u\dot{u} + ku = -m\ddot{u}_g \quad (6-3)$$

6.3.2 Transfer Functions

The amplitude of the total acceleration transfer function of the one-story structure with dampers is obtained by applying the Fourier transform to Equation (6-1) and (6-2) and obtaining the ratio of the Fourier amplitude of the total acceleration to the Fourier amplitude of the ground acceleration

$$T = \left| 1 + \omega^2 \left[-\omega^2 + \omega_n^2 + 2i\omega\omega_n\xi_u + \frac{i\eta\omega C_{SA}\cos^2\theta}{m(1+i\omega\lambda)} \right]^{-1} \right| \quad (6-4)$$

where ω_n is the natural frequency of the undamped structure, i is the imaginary unit, ξ_u is the damping ratio of the structure without dampers, and $|\bullet|$ indicates the modulus of the contained complex quantity.

In the case of the one-story structure without dampers, $\eta = 0$ and Equation (6-4) assumes the following form

$$T = \left| 1 + \omega^2 [-\omega^2 + \omega_n^2 + 2i\omega\omega_n\xi_u]^{-1} \right| \quad (6-5)$$

For lightly damped structures ($\xi_u < 10\%$), the position and magnitude of the single sharp peak in the transfer function determines the structural properties. Specifically, at frequency $\omega = \omega_n$ the transfer function has the value

$$T(\omega_n) = \frac{(1 + 4\xi_u^2)^{\frac{1}{2}}}{2\xi_u} \quad (6-6)$$

which nearly coincides with the peak value of the transfer function. Thus, for lightly damped structures the position of the peak value in the transfer function reveals the natural frequency, whereas the damping ratio can be obtained from Equation (6-6)

$$\xi_u = \frac{1}{2} (T^2(\omega_n) - 1)^{-\frac{1}{2}} \quad (6-7)$$

6.3.3 Eigenvalue Problem

For highly damped structures, the amplitudes of the transfer functions do not contain well defined peaks and identification of the structural properties is not as simple as in the case of a lightly damped structure. However, the properties can be determined by solving the associated eigenvalue problem, having first verified the analytical model of the system by comparing some analytical and experimental responses, such as transfer functions. The eigenvalue problem of the structure with semi-active fluid dampers requires a numerical procedure. Equation (6-1) and (6-2), with \ddot{u}_g set equal to zero, can be written in matrix form, having first introduced a new vector $\{Z\}$:

$$\{Z\} = \begin{Bmatrix} \dot{u} \\ u \\ P_d \end{Bmatrix} \quad (6-8)$$

where

$$[B]\{\dot{Z}\} + [A]\{Z\} = \{0\} \quad (6-9)$$

$$[B] = \begin{bmatrix} 1 & 0 & 0 \\ 0 & 1 & 0 \\ 0 & 0 & \lambda \end{bmatrix} \quad (6-10)$$

$$[A] = \begin{bmatrix} 2\xi_u \omega_n & \omega_n^2 & m^{-1} \\ -1 & 0 & 0 \\ -\eta C_{SA} \cos^2 \theta & 0 & 1 \end{bmatrix} \quad (6-11)$$

For a solution of the form

$$\{Z\} = \{Z_o\} \exp(\mu t) \quad (6-12)$$

Equation (6-9) reduces to

$$[A]\{Z_o\} = -\mu [B]\{Z_o\} \quad (6-13)$$

Equation (6-13) describes a generalized eigenvalue problem. The solution of this problem (e.g., IMSL 1987) will result in values of the complex eigenvalue μ .

The frequency, ω_n , and damping ratio, ξ_u , are determined by recalling the expression for the characteristic roots of the equation of free vibration of a viscously damped SDOF system:

$$\mu = -\xi_1 \omega_1 \pm i \omega_1 \sqrt{1 - \xi_1^2} \quad (6-14)$$

Accordingly,

$$\omega_1 = |\mu| \quad (6-15)$$

$$\xi_1 = -\frac{\Re(\mu)}{\omega_1} \quad (6-16)$$

where $\Re(\bullet)$ indicates the real part of the contained complex quantity.

6.4 Identification of Multi-Story Structure

6.4.1 Equations of Motion

The equations of motion of a base excited multi-degree-of-freedom (MDOF) lumped mass structure with fluid dampers may be written as

$$[M]\{\ddot{u}\} + [C_u]\{\dot{u}\} + [K]\{u\} + \{P_d\} = -[M]\{R\} \ddot{u}_g \quad (6-17)$$

where $[M]$ is the mass matrix, $[C_u]$ is the damping matrix of the structure without fluid dampers, $[K]$ is the stiffness matrix, $\{P_d\}$ is a vector containing the horizontal components of damper forces acting on the degrees of freedom; and $\{\ddot{u}\}$, $\{\dot{u}\}$, and $\{u\}$ are the vectors of relative acceleration, velocity, and displacement of the degrees of freedom, respectively. For a structure with one degree of freedom per floor, $\{R\}$ is a vector containing units. The vector of damper forces may be written as

$$\{P_d\} = \left\{ \begin{array}{c} \eta_N P_N \\ \vdots \\ \eta_j P_j - \eta_{j+1} P_{j+1} \\ \vdots \\ \eta_1 P_1 - \eta_2 P_2 \end{array} \right\} \quad (6-18)$$

where η_j is the number of dampers at the j -th story and P_j is the horizontal component of force in a single damper at the j -th story. It is assumed here that all dampers at a story are identical.

The constitutive equation describing the damper force P_j is of the same form as Equation (6-2) wherein the viscoelastic Maxwell model is utilized

$$P_j + \lambda \dot{P}_j = (C_{SA})_j \cos^2 \theta_j \frac{d}{dt} (u_j - u_{j-1}) \quad (6-19)$$

where $(C_{SA})_j$ is the damping coefficient of the semi-active dampers in the j th story, θ_j is the angle of placement of damper j with respect to the horizontal, and $u_0 = 0$ ($j = 1$).

In the case of the three-story structure without fluid dampers, Equation (6-17) reduces to

$$[M]\{\ddot{u}\} + [C_u]\{\dot{u}\} + [K]\{u\} = -[M]\{R\}\ddot{u}_g \quad (6-20)$$

6.4.2 Construction of Stiffness and Damping Matrix

The stiffness matrix, $[K]$, and the damping matrix, $[C_u]$, are constructed from the experimentally determined frequencies, damping ratios, and mode shapes (for the structure without fluid dampers) using a procedure described by Clough (1975). The undamped eigenvalue problem is given by

$$\omega_k^2 [M]\{\phi_k\} = [K]\{\phi_k\} \quad (6-21)$$

where ω_k and $\{\phi_k\}$ are the frequency and mode shape corresponding to the k -th mode of vibration. The generalized mass and stiffness matrices are given by

$$[M^*] = [\Phi]^T [M] [\Phi] \quad (6-22)$$

$$[K^*] = [\Phi]^T [K] [\Phi] \quad (6-23)$$

where $[\Phi]$ is the mode shape matrix containing the mode shapes $\{\phi_k\}$. The orthogonality of the mode shapes relative to the mass matrix can be used to obtain the following relationship

$$[\Phi]^{-1} = [M^*]^{-1} [\Phi]^T [M] \quad (6-24)$$

Using Equations (6-23) and (6-24), the stiffness matrix, $[K]$, can be determined as

$$[K] = [M][\Phi][M^*]^{-1}[K^*][M^*]^{-1}[\Phi]^T[M] \quad (6-25)$$

The matrix $[M^*]$ is diagonal with elements m_k^* given by

$$m_k^* = \{\phi_k\}^T [M] \{\phi_k\} \quad (6-26)$$

Equations (6-25) and (6-26) are combined to give

$$[K] = [M] \left[\sum_{k=1}^N \frac{\omega_k^2}{m_k^*} \{\phi_k\} \{\phi_k\}^T \right] [M] \quad (6-27)$$

where N is the number of modes.

In a similar way, the damping matrix is evaluated as

$$[C_u] = [M] \left[\sum_{k=1}^N \frac{2\xi_k \omega_k}{m_k^*} \{\phi_k\} \{\phi_k\}^T \right] [M] \quad (6-28)$$

where ξ_k is the damping ratio corresponding to the k -th mode.

6.4.3 Transfer Functions of Structure without Fluid Dampers

Recall the equations of motion of the structure without semi-active fluid dampers

(Equation (6-20))

$$[M]\{\ddot{u}\} + [C_u]\{\dot{u}\} + [K]\{u\} = -[M]\{R\} \ddot{u}_g \quad (6-29)$$

The relative displacement vector may be expressed in modal form as

$$\{u\} = [\Phi]\{y\} \quad (6-30)$$

where $\{y\}$ is the modal coordinate vector. The equation of motion can be transformed into the modal domain by substituting Equation (6-30) into (6-29). Upon application of Fourier transform to the result, one may, after considerable manipulations, obtain the amplitude of the transfer function of degree of freedom j with contributions from all modes as

$$T_j = \left| \sum_{k=1}^N \frac{-\Gamma_k (2i\omega \xi_k \omega_k + \omega_k^2)}{\omega_k^2 - \omega^2 + 2i\xi_k \omega \omega_k} \phi_{jk} \right| \quad (6-31)$$

where ϕ_{jk} is the component of mode shape $\{\phi_k\}$ corresponding to degree of freedom j and Γ_k is the k -th modal participation factor given by

$$\Gamma_k = \frac{-\{\phi_k\}^T [M] \{R\}}{\{\phi_k\}^T [M] \{\phi_k\}} \quad (6-32)$$

For a lightly damped structure ($\xi_k < 10\%$), the k -th peak of the amplitude of the transfer function of the j -th degree of freedom occurs at frequency ω_k . Furthermore, if we assume well separated modes, the term in front of ϕ_{jk} in Equation (6-31) is equal to a negligible value for all frequencies $\omega \neq \omega_k$. Accordingly, Equation 6-31 simplifies to

$$T_j(\omega_k) \approx \frac{\Gamma_k (1 + 4\xi_k^2)^{\frac{1}{2}}}{2\xi_k} \phi_{jk} \quad (6-33)$$

It should be noted that the term in front of ϕ_{jk} in Equation (6-33) is a constant. Therefore, the magnitude of the peak of T_j at frequency ω_k is proportional to the magnitude of the k -th mode shape corresponding to the j -th degree of freedom. Thus, for lightly damped

structures the position and magnitude of the peaks of experimental transfer functions of all degrees of freedom directly yield the frequencies and mode shapes. Equations 6-32 and 6-33 can be used to determine the corresponding damping ratios

$$\xi_k = \left[\left(\frac{2T_j(\omega_k)}{\Gamma_k \phi_{jk}} \right)^2 - 4 \right]^{-\frac{1}{2}} \quad (6-34)$$

6.4.4 Transfer Functions of Structure with Fluid Dampers

Applying the Fourier transform to the equation of motion (Equation (6-17)) and to the equation describing the fluid damper behavior (Equation (6-19)) results in

$$[S(\omega)]\{\bar{u}\} = -[M]\{1\} \bar{u}_g \quad (6-35)$$

where the overbar denotes the Fourier transform and $[S(\omega)]$ represents the dynamic stiffness matrix:

$$[S(\omega)] = -\omega^2[M] + i\omega[C_u] + [K] + [D(\omega)] \quad (6-36)$$

where $[D(\omega)]$ contains the contribution of the damper forces to the dynamic stiffness matrix and is given by

$$[D(\omega)] = \frac{i\omega}{1+i\omega\lambda}[C] \quad (6-37)$$

and in the case of two dampers at the first story

$$[C] = \begin{bmatrix} 0 & 0 & 0 \\ 0 & 0 & 0 \\ 0 & 0 & 2C_{SA}\cos^2\theta \end{bmatrix} \quad (6-38)$$

Defining the inverse of $[S(\omega)]$ as $[H(\omega)]$, Equation (6-35) may be solved for $\{\bar{u}\}$. Upon multiplication by $-\omega^2$, the Fourier transform of the relative acceleration vector is obtained:

$$\{\bar{\ddot{u}}\} = \omega^2 [H(\omega)] [M] \{1\} \bar{\ddot{u}}_g \quad (6-39)$$

The amplitude of the transfer function of the j-th degree of freedom is by definition

$$T_j = \left| \frac{\bar{\ddot{u}}_g + \bar{\ddot{u}}_j}{\bar{\ddot{u}}_g} \right| \quad (6-40)$$

or

$$T_j = \left| 1 + \omega^2 \sum_{k=1}^N H_{jk}(\omega) m_k \right| \quad (6-41)$$

where $H_{jk}(\omega)$ are elements of matrix $[H(\omega)]$ and m_k is the lumped mass at the k-th degree of freedom.

6.4.5 Eigenvalue Problem

The eigenvalue problem is formulated and solved in the same way as that of the one story structure (Section 6.3.3).

Vector $\{Z\}$ is defined as

$$\{Z\} = \begin{Bmatrix} \{\dot{u}\} \\ \{u\} \\ \{P_d\} \end{Bmatrix} \quad (6-42)$$

Equation (6-9) is valid with matrix $[A]$ and $[B]$ given, in the case of the tested structure,

by

$$[B] = \begin{bmatrix} [M] & [0] & [0] \\ [0] & [I] & [0] \\ [0] & [0] & \lambda[I] \end{bmatrix} \quad (6-43)$$

$$[A] = \begin{bmatrix} [C_u] & [K] & [I] \\ -[I] & [0] & [0] \\ -[C] & [0] & [I] \end{bmatrix} \quad (6-44)$$

where [I] is the identity matrix.

It should be noted that the solution of Equation (6-9) will result in the eigenvectors $\{Z_o\}$, a portion of which contains the complex-valued mode shapes. The physical interpretation of the complex-valued mode shapes is that, for each mode of vibration, the degrees of freedom are phase-shifted and therefore reach their maximum amplitude at different times.

6.5 Properties of One-Story and Three-Story Structure

The properties of the one-story model structure are presented in Table 6-I. The properties of the one-story bare frame structure were determined from the position and magnitude of the single sharp peak in the experimental transfer function. The properties of the one-story structure with semi-active fluid dampers were determined by solving the eigenvalue problem described in Section 6.3.3 using the identified properties of the bare frame and the calibrated model of the fluid dampers (see Section 4.2).

The structural properties of the flexible bare frame structure were also identified from seismic tests. Recorded base shear-drift loops were used to obtain the stiffness, energy dissipated in a full cycle of motion, W_d , and elastic energy stored at maximum drift, W_s . The frequency was calculated from the measured stiffness and the known mass. The damping ratio was calculated according to (Clough 1975)

$$\xi = \frac{W_d}{4\pi W_s} \quad (6-45)$$

Table 6-1 Properties of One-Story Model Structure at Small Amplitude of Vibration

Stiff Structure	Bare Frame	Two-Stage Dampers: Low Damping	Two-Stage Dampers: High Damping
Frequency (Hz)	2.80	2.81	2.86
Damping Ratio (%)	0.74	4.00	21.13

Flexible Structure	Bare Frame	Bare Frame: Seismic Motion	Two-Stage Dampers: Low Damping	Two-Stage Dampers: High Damping	Variable Dampers: Low Damping	Variable Dampers: High Damping
Frequency (Hz)	2.40	2.40	2.41	2.46	2.41	2.46
Damping Ratio (%)	1.47	2.50	5.29	25.35	5.91	25.58

The properties of the three-story model are presented in Table 6-II. The three-story bare frame model was not directly identified from the experimental transfer functions as described in Section 6.4.3. The experimental transfer functions of the bare frame structure did not exhibit sharp narrow peaks as expected (see Figure 6-4). For each degree of freedom, there is a closely spaced double peak in the transfer function of the bare frame structure at approximately 2 Hz. This is an indication of torsional motion which may have been induced by the first story structural repairs discussed in Section 5.2.

An alternate method was utilized to obtain structural properties of the three-story bare frame structure. This method did not explicitly account for the presence of the torsional mode. The frequencies were estimated from the experimental transfer functions. A stiffness matrix was constructed assuming a shear type structure and extracting story stiffnesses from the slope of experimental story shear versus story drift loops (see Appendix E). Using the known mass matrix and the shear type structure stiffness matrix, the undamped eigenvalue problem was solved to obtain modal frequencies and mode shapes (see Equation 6-21). The experimentally obtained values of modal frequencies were thought to be very good estimates and therefore the modal frequencies from the shear type structure eigenvalue analysis were discarded. Finally, the damping ratios were taken to be identical to those values obtained in previous testing of the model by Constantinou (1993b and 1992b). The identified properties of the bare frame structure are verified in Section 10 where analytical and experimental shaking table test results are compared.

Table 6-II Properties of Three-Story Model Structure at Small Amplitude of Vibration

		Bare Frame			Variable Dampers: Low Damping			Variable Dampers: High Damping		
		1	2	3	1	2	3	1	2	3
Mode		1.80	5.80	11.40	1.80	5.84	11.43	1.85	6.04	11.48
Frequency (Hz)		1.74	0.76	0.34	4.13	3.90	1.07	14.41	18.79	4.83
Damping Ratio (%)		1.000	1.000	1.000						
Mode Shapes	Floor 3	0.830	-0.425	-2.116						
	Floor 2	0.507	-1.275	1.491						
	Floor 1									

The properties of the three-story structure with semi-active fluid dampers were determined by solving the eigenvalue problem of Section 6.4.5 using the identified properties of the bare frame structure and the calibrated model of the fluid dampers (see Section 4.2).

The results in Tables 6-I and 6-II demonstrate the following:

- a) The flexible one-story structure exhibits, under seismic motion, damping of approximately 2.5 percent of critical. This shows that the structure was realistically damped.
- b) The semi-active fluid dampers had a primary effect of increasing damping. The effect on the fundamental frequency is, as expected, small and amounts to an increase of stiffness of generally less than 6 percent.
- c) The semi-active fluid dampers are capable of increasing the damping ratio of the one-story structure by a factor of between 2 and 10. For the three-story structure, the damping ratio in the fundamental mode is increased by a factor of between 2.4 and 8.3.

6.6 Comparison of Experimental and Analytical Transfer Functions

The accuracy of the analytical models described in Section 6.3 and 6.4 is demonstrated in Figures 6-1 through 6-6 which compare analytical and experimental transfer functions.

SDOF STIFF STRUCTURE

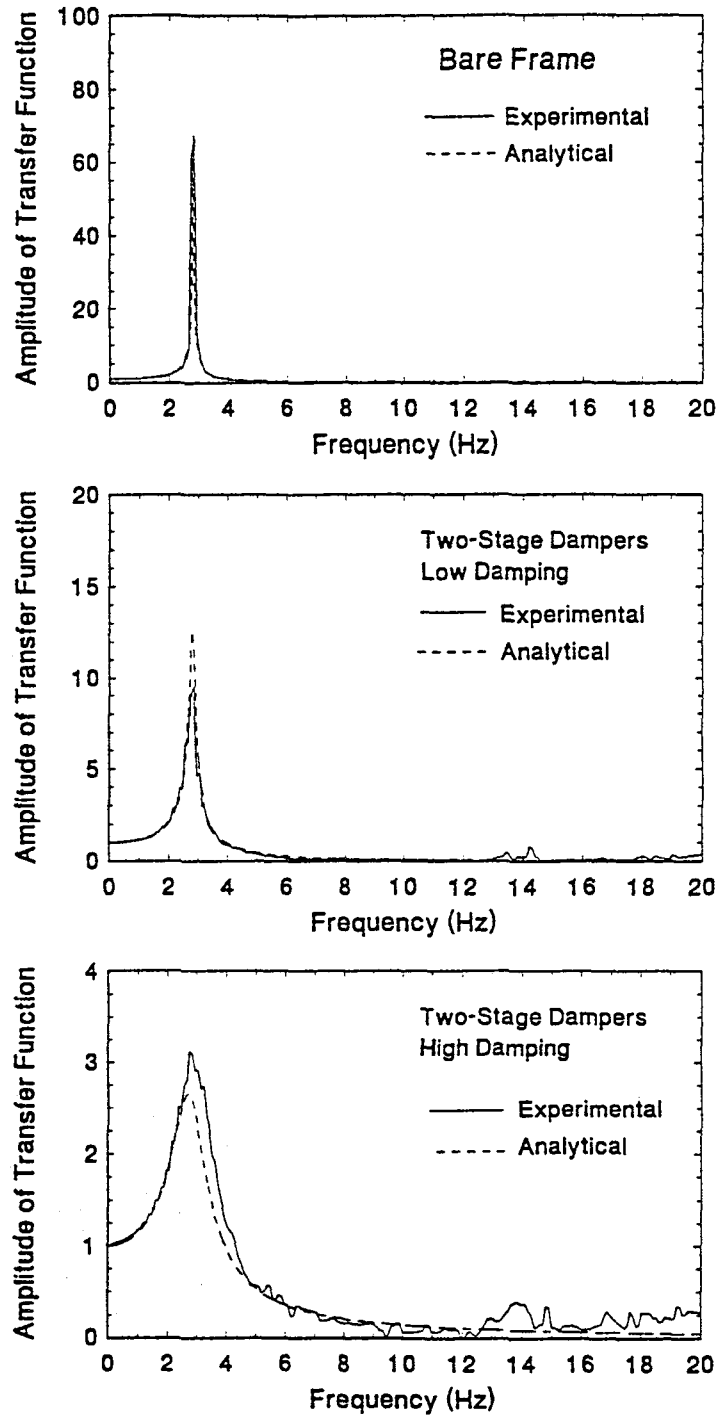


Figure 6-1 Comparison of Experimental and Analytical Transfer Functions of One-Story Stiff Structure with No Dampers and with Two-Stage Dampers

SDOF FLEXIBLE STRUCTURE

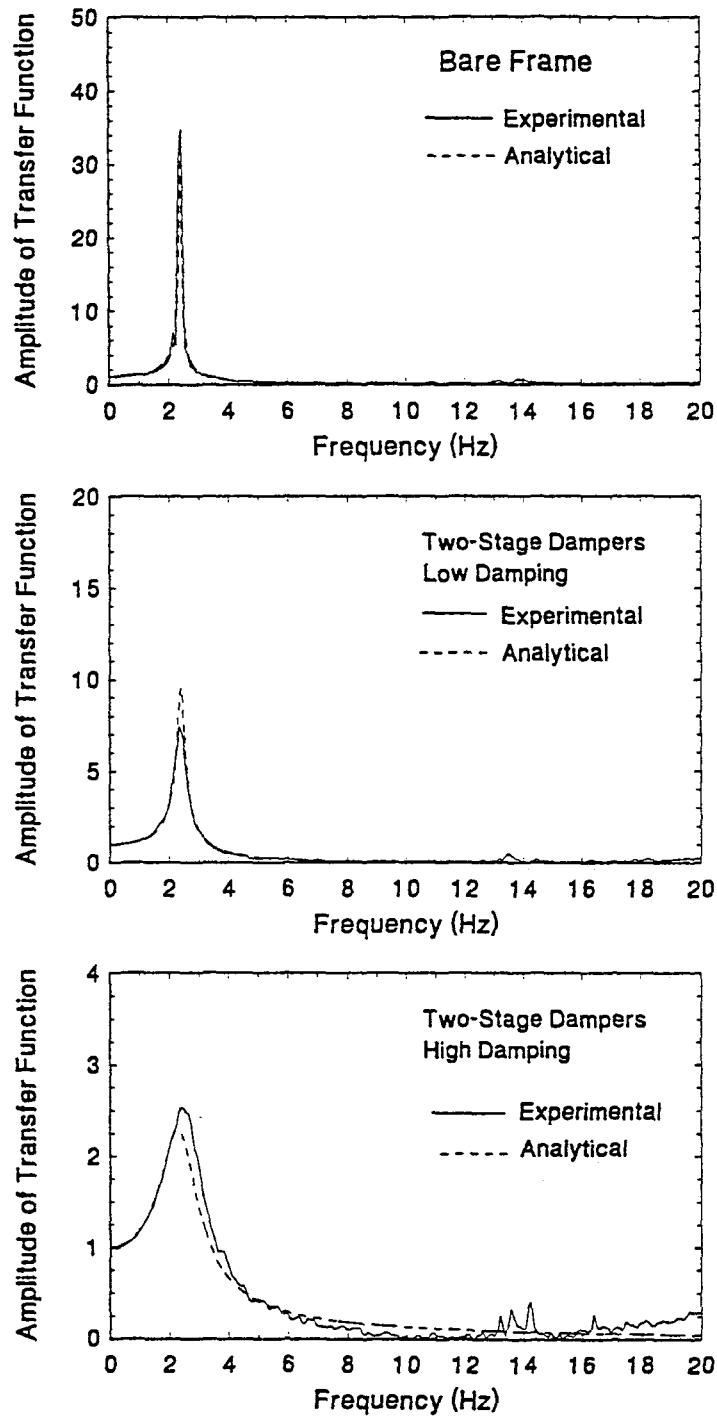


Figure 6-2 Comparison of Experimental and Analytical Transfer Functions of One-Story Flexible Structure with No Dampers and with Two-Stage Dampers

SDOF FLEXIBLE STRUCTURE

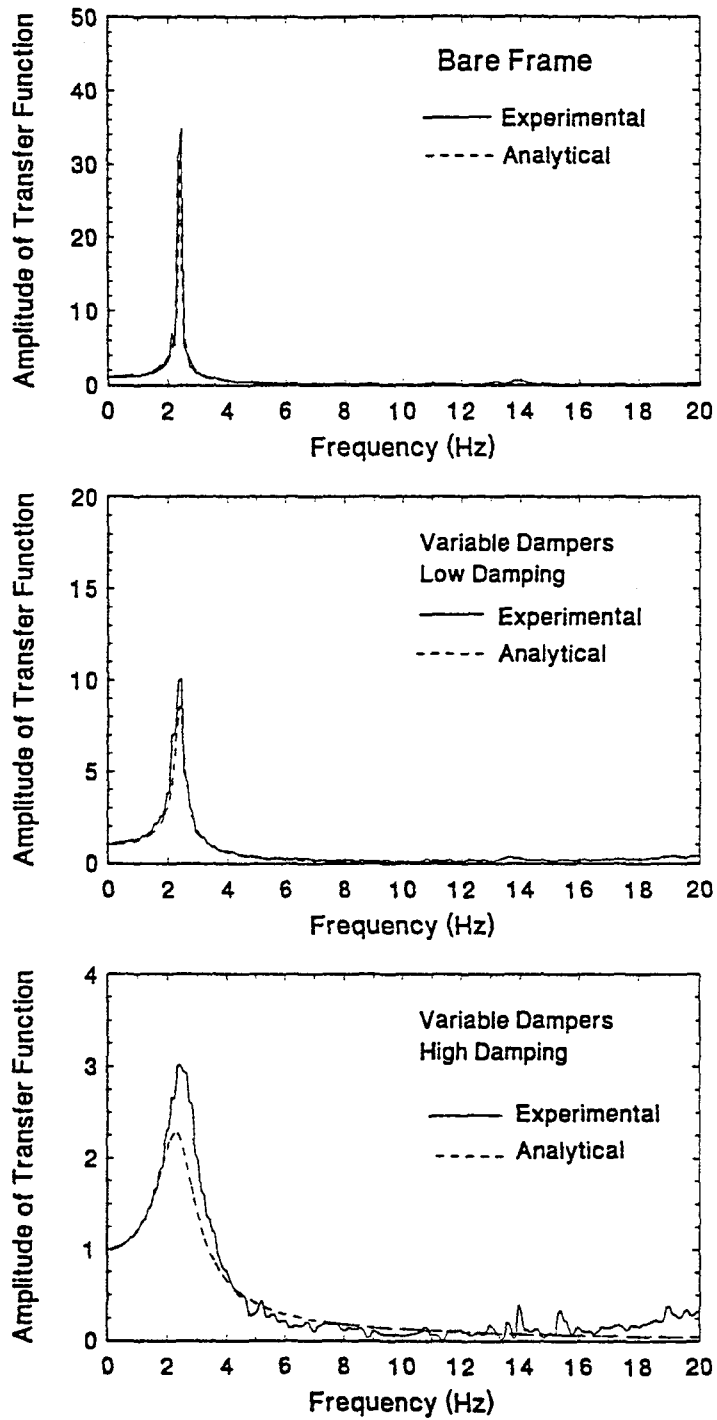


Figure 6-3 Comparison of Experimental and Analytical Transfer Functions of One-Story Flexible Structure with No Dampers and with Variable Dampers

MDOF STRUCTURE

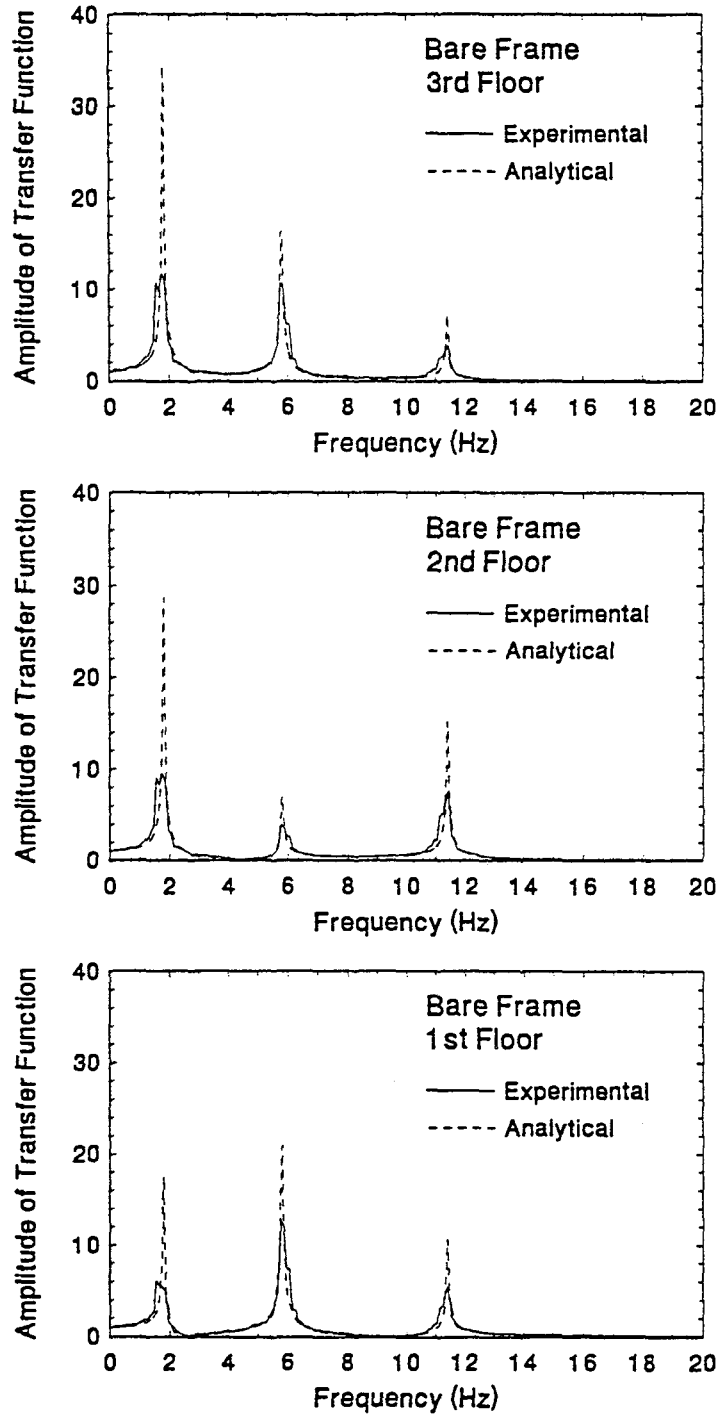


Figure 6-4 Comparison of Experimental and Analytical Transfer Functions of Three-Story Structure with No Dampers

MDOF STRUCTURE

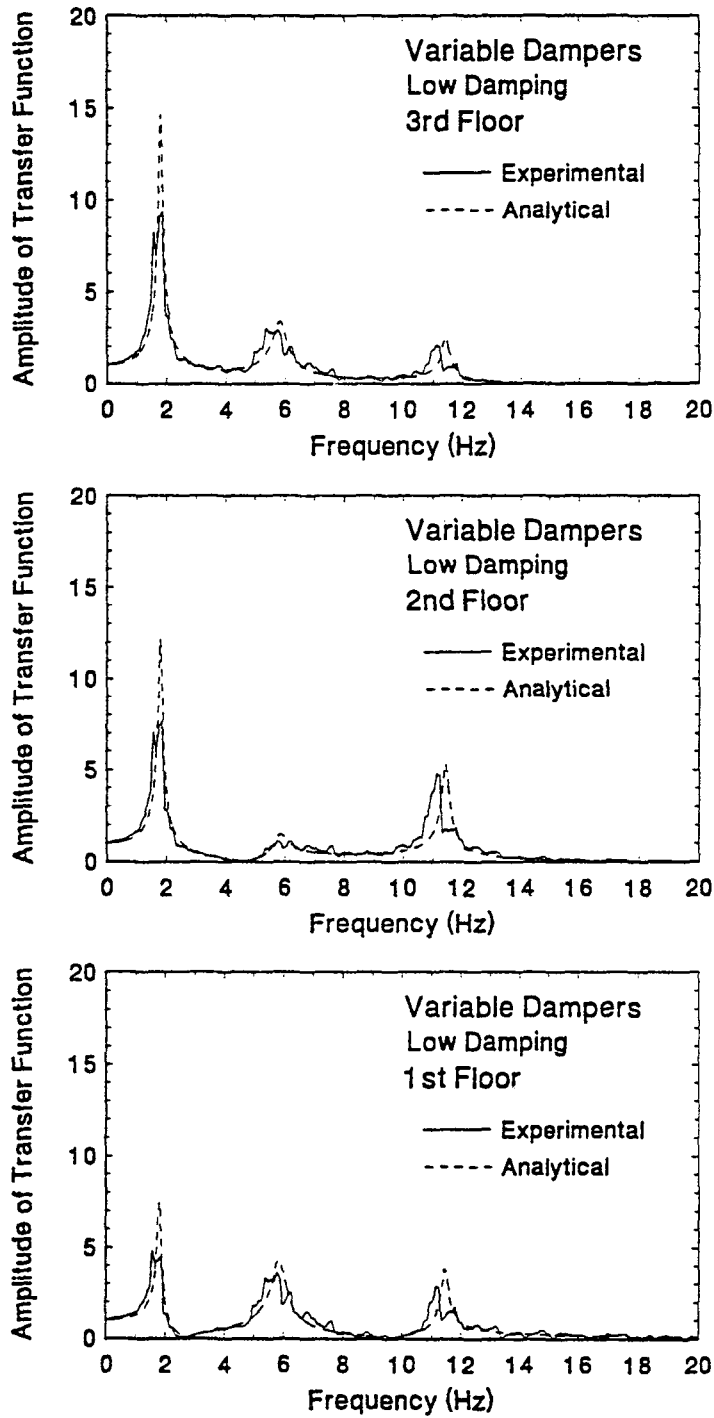


Figure 6-5 Comparison of Experimental and Analytical Transfer Functions of Three-Story Structure with Variable Dampers Set to Low Damping

MDOF STRUCTURE

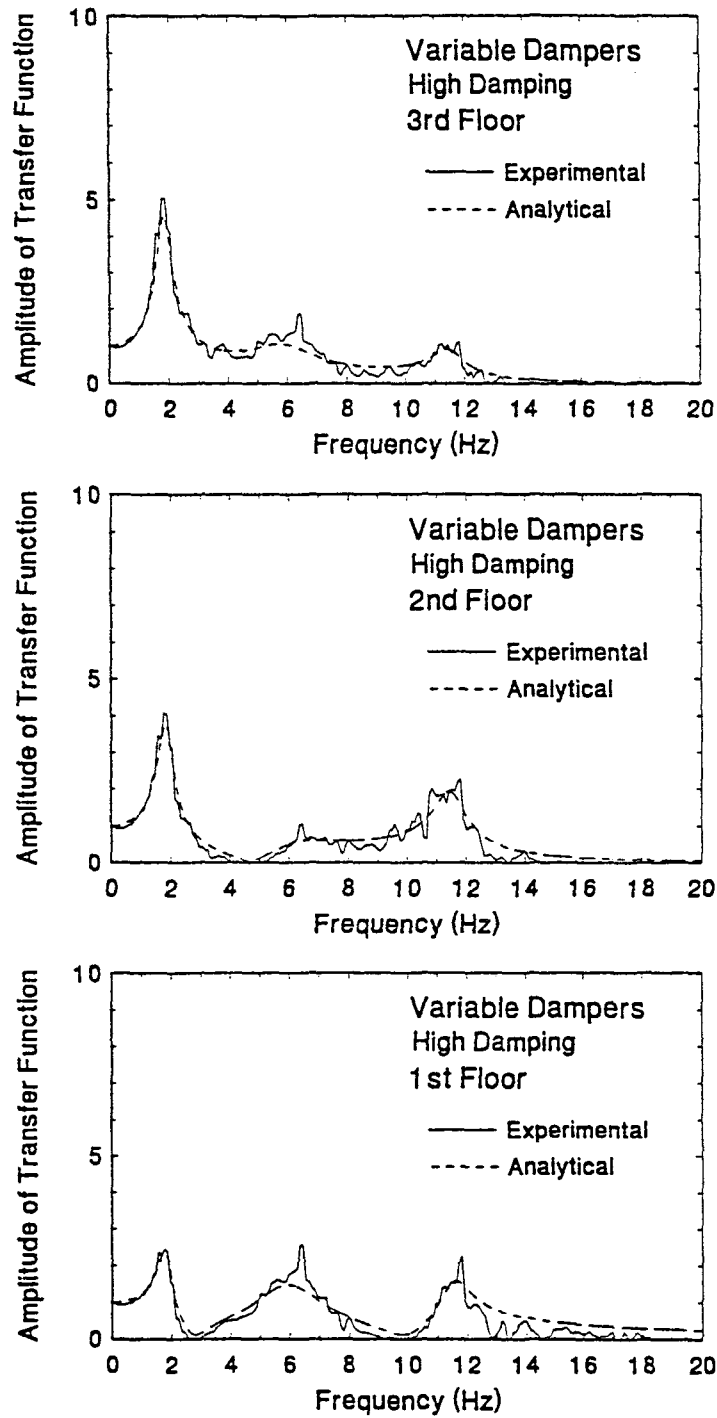


Figure 6-6 Comparison of Experimental and Analytical Transfer Functions of Three-Story Structure with Variable Dampers Set to High Damping

The results for the one-story bare frame compare very well (see Figures 6-1 through 6-3). Further, as shown in the same figures, the one-story low damping and high damping results compare reasonably well except for differences in the amplitude and width of the peaks of the transfer functions. These differences in experimental and analytical transfer functions are related to the effect of damper friction (between the piston rod and piston rod seals) on the experimental transfer functions. Recalling Section 6.2, the amplitude of white noise excitation for the low damping tests was set at a low value so as to prevent inelastic behavior in the structure. As a result, the dampers were not stroked sufficiently to exhibit strong viscous behavior. Rather, friction was the dominate source of damping. The analytical transfer function, on the other hand, does not explicitly include the effect of friction (see Equation (6-4)). This explains the difference in the experimental and analytical transfer functions of the one-story model with semi-active dampers set at low damping. An improvement is observed in the comparisons of the one-story high damping transfer function since the white noise excitation was of larger amplitude and viscous damper behavior controlled the damper response.

The comparison between the experimental and analytical transfer functions of the three-story bare frame structure do not compare well in terms of the magnitude of the peaks but do compare reasonably well in terms of the location of the peaks (see Figure 6-4). The observed differences in amplitudes are the result of the presence of a torsional mode of vibration as discussed in Section 6.5. As the damping is increased, the comparisons of transfer functions improve (see Figure 6-5 (low damping) and 6-6 (high

damping)). Specifically, the high damping transfer functions of Figure 6-6 compare very well, indicating that high damping may be effective in controlling the response of any torsional modes.

SECTION 7

CONTROL ALGORITHMS FOR SEISMIC SIMULATION TESTING

7.1 Introduction

Control algorithms were developed for the two-stage semi-active dampers which are simple and directly implementable using a commercial data acquisition and control program (see Section 5.5). Furthermore, control algorithms were developed for the variable dampers in which the constraint on the damping coefficient (i.e., $C_{\min} \leq C(t) \leq C_{\max}$) was not directly taken into account. Rather, during experimental application of the control algorithms, the damping coefficient was clipped at the upper and lower bounds. In general, the control algorithms for the variable dampers may require that the dampers perform work on the structure such that the energy within the structural system is increased. The effect of clipping the damping coefficient at the lower bound is to account for the inability of the semi-active dampers to perform this type of work on the structure (i.e., the dampers are only capable of absorbing energy).

The issue of stability was not explicitly considered in the development of the control algorithms since the semi-active fluid dampers can only absorb energy; they are not capable of storing energy and thus inducing instability.

7.2 One-Story Structure with Two-Stage Dampers

7.2.1 Base Shear Coefficient Control

This algorithm was originally explored analytically by Shinozuka (1992). The objective is to control the base shear coefficient of a one-story structure through modulation of the damping. The equation of motion of the one-story structure is given by Equation (6-1). For an undamped structure ($c_u = 0$) with linear viscous semi-active dampers, the magnitude of the base shear coefficient (BSC) (magnitude of the ratio of inertia force to weight) is

$$\text{BSC} = \frac{|m\ddot{u}_t|}{W} = \frac{|\eta P_d + ku|}{W} \quad (7-1)$$

where \ddot{u}_t is the total acceleration of the mass and W is the weight of the structure. Clearly, the base shear coefficient is dependent on both the damping force and the restoring force.

The base shear coefficient control algorithm may be given as

$$C_{SA} = \begin{cases} C_{\min} & , \text{ if } \text{BSC} > \text{BSCLIM} \\ C_{\max} & , \text{ if } \text{BSC} < \text{BSCLIM} \end{cases} \quad (7-2)$$

where BSCLIM is a pre-selected base shear coefficient limit, C_{SA} is the time dependent damping coefficient of each semi-active damper, and C_{\min} and C_{\max} are the minimum and maximum damping coefficient, respectively, available from each semi-active damper. In essence, when the force transmitted to the mass (as measured by the base shear coefficient) exceeds a pre-determined fraction of the weight of the structure, the damping coefficient is reduced, which in turn reduces the damping force and hence, the total force

transmitted to the mass. However, the reduction in damping may result in an increase in drift which correspondingly increases the elastic restoring force and hence, the total force transmitted to the mass. Therefore, in attempting to control the base shear coefficient, a penalty may be paid in terms of increased drift. As demonstrated analytically by Shinozuka (1992), the two-stage solenoid valve must be capable of responding instantaneously to the command signal in order to achieve the control described by Equation (7-2). Note that experimental implementation of this algorithm only requires measurements from a single accelerometer.

7.2.2. Force Transfer Control

This algorithm has been described by Ivers (1991) for applications in automotive vibration control. For applications in structural control, the objective is to control the total force (or, equivalently, the total acceleration) transferred to the mass of the structure through modulation of the damping. Note that this objective is essentially the same as that described in the previous section for the base shear coefficient control algorithm. Neglecting the inherent damping in the structure, the total force applied to the mass is equal to the sum of the restoring force from the columns and the damping force from the semi-active dampers. The column force and damper force are directly proportional to the drift, u , and drift velocity, \dot{u} , respectively. If the damper and column force, or correspondingly, the drift and drift velocity, have the same sign, the total force acting on the mass tends to be larger than when they have the opposite sign. Therefore, the

following algorithm may be suitable for minimizing the total force (total acceleration) applied to the mass

$$C_{SA} = \begin{cases} C_{\min} & , \text{ if } \ddot{u} > 0 \\ C_{\max} & , \text{ if } \ddot{u} < 0 \end{cases} \quad (7-3)$$

7.3 One-Story Structure with Variable Dampers

7.3.1 Introduction

The variation in damping coefficient for the variable dampers may be taken to vary with command voltage according to Equation (3-15). However, the damping coefficient does not vary significantly at voltage levels below about 0.75 volts and above about 2.25 volts (see Figure 3-30). Furthermore, the variation in damping coefficient with command voltage is approximately linear between 0.75 volts and 2.25 volts. Therefore, for the shaking table tests with variable dampers, the damping coefficient of both variable damper units was taken to vary linearly with command voltage. A linear curve was fit through the experimental values of damping coefficient for both variable damper units (see Figure 7-1 which contains the experimental data of Figure 3-30). The linear curve was expressed by the same equation for both variable damper units (i.e., the dashed lines in Figure 7-1(a) and 7-1(b) are identical). The linear equation describing the damping coefficient is given by

$$C_{SA}(t) = \frac{C_{\max} - C_{\min}}{V_1 - V_2} V(t) + \frac{C_{\max} V_2 - C_{\min} V_1}{V_2 - V_1} \quad (7-4)$$

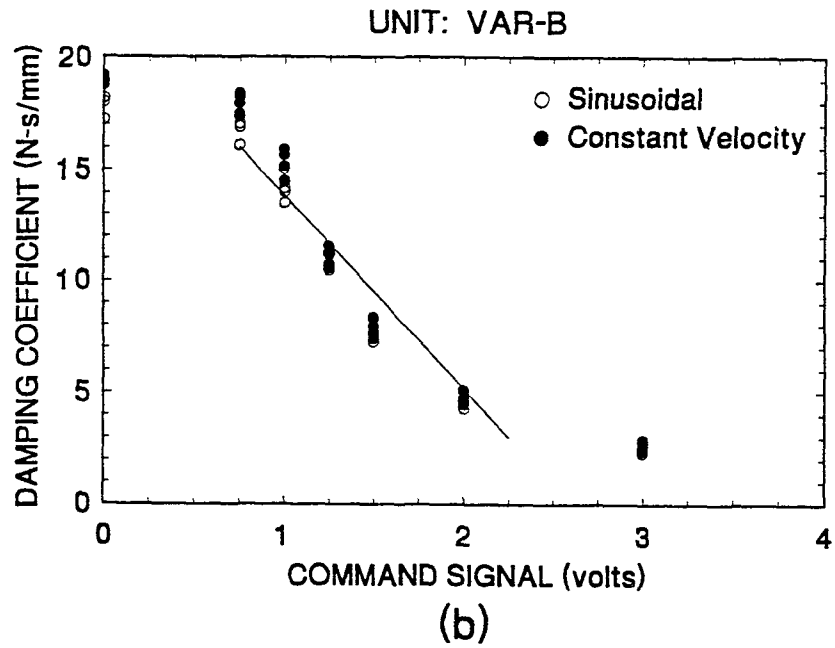
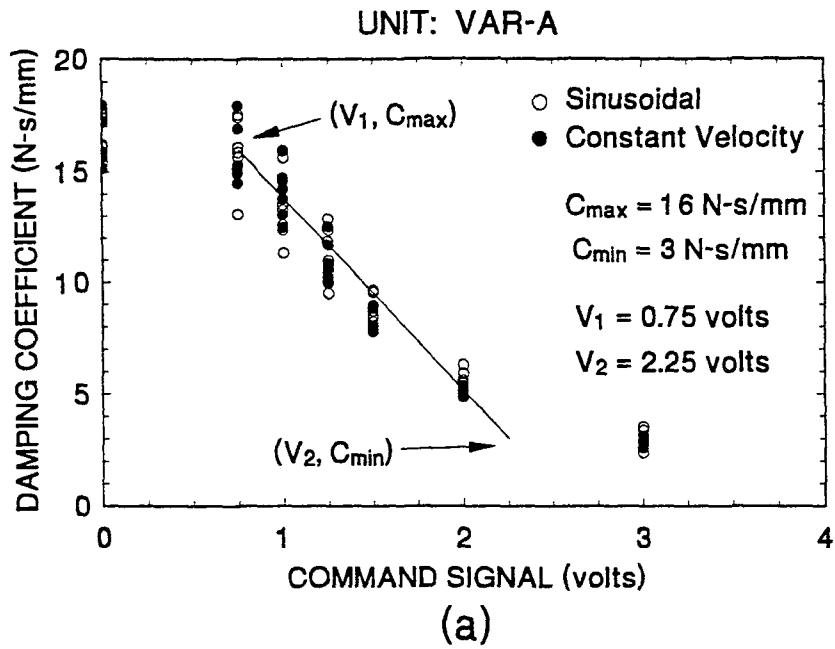


Figure 7-1 Relationship Between Experimental Damping Coefficient and Command Signal for Variable Dampers. Dashed Line Represents Approximate Relationship Used in Shaking Table Tests.

where $V(t)$ is the command voltage, V_2 is the command voltage corresponding to C_{\min} ($V_2 = 2.25$ volts), V_1 is the command voltage corresponding to C_{\max} ($V_1 = 0.75$ volts), and C_{\min} and C_{\max} have values of 3 N-s/mm and 16 N-s/mm, respectively. Solving Equation (7-4) for the command voltage, $V(t)$, we obtain

$$V(t) = \frac{C_{SA}(t)(V_1 - V_2) + C_{\max}V_2 - C_{\min}V_1}{C_{\max} - C_{\min}} \quad (7-5)$$

In the control algorithms described in the following sections, the objective is to determine the damping coefficient which satisfies a given control objective and upon substitution into Equation (7-5), the appropriate command voltage is determined. The damping coefficient determined by each control algorithm is bounded according to

$$C_{\min} \leq C_{SA} \leq C_{\max} \quad (7-6)$$

and therefore Equation (7-5) is bounded by V_1 and V_2 .

7.3.2 Feedforward Control

A feedforward control algorithm utilizes feedback measurements from the input. In the case of structural control, the application of a feedforward control algorithm requires that the ground motion be a measurable quantity. In theory, the absolute motion of a structure can be brought to zero if a control force can be applied which completely negates the effect of the measured ground motion. Experimental and analytical work on absolute motion control of sliding isolation systems using an active control system has been described by Riley (1994).

The equation of motion of the one-story structure may be rewritten as (see Equation (6-1))

$$m\ddot{u} + c_v \dot{u} + ku = -m\ddot{u}_g - \eta P_d \quad (7-7)$$

Clearly, the effective input is zero if the horizontal force from each semi-active damper has the value

$$P_d = \frac{-m\ddot{u}_g}{\eta} \quad (7-8)$$

Assuming that the variable dampers behave according to the linear viscous dashpot model of Equation (4-2), Equation (7-8) is rewritten as

$$P_d = \left[\frac{-m\ddot{u}_g}{\eta\dot{u}} \right] \dot{u} = C_d \dot{u} \quad (7-9)$$

where C_d is the required damping coefficient related to the horizontal damping force, P_d .

The horizontal component of force from each semi-active damper is given by

$$P_d = C_{SA} \cos^2\theta \dot{u} \quad (7-10)$$

Equating Equations (7-9) and (7-10)

$$C_{SA} = -\frac{m\ddot{u}_g}{\eta \cos^2\theta \dot{u}} \quad (7-11)$$

which describes the necessary variation in the damping coefficient of each semi-active damper to negate the effect of the input. However, the damping coefficient of the semi-active variable dampers is constrained according to Equation (7-6). The feedforward control algorithm is then obtained by combining Equations (7-6) and (7-11)

$$C_{SA} = \begin{cases} C_{\min} & , \text{ if } C^* \leq C_{\min} \\ -m \ddot{u}_g (\eta \cos^2 \theta \dot{u})^{-1} & , \text{ if } C_{\min} < C^* < C_{\max} \\ C_{\max} & , \text{ if } C^* \geq C_{\max} \end{cases} \quad (7-12)$$

where

$$C^* = \frac{-m \ddot{u}_g}{\eta \cos^2 \theta \dot{u}} \quad (7-13)$$

Note that the calculation of C^* requires division by the relative velocity. To avoid division by zero, the value of the relative velocity was set equal to a small constant, ϵ , when the absolute value of the measured relative velocity was below this constant. The value of the parameter ϵ was selected to be 1×10^{-4} cm/sec for all of the control algorithms developed for control of the variable dampers.

7.3.3 Skyhook Damping Control

A passive linear viscous damper system within a one-story structure produces forces which are proportional to the relative velocity of the mass. An alternative control approach, which can not be achieved with a passive device, is to control the structure with a force which is proportional to the total velocity of the mass. This type of control has been proposed by Karnopp (1974) and Ivers (1991) for applications in general vibration isolation and automotive vibration control. The term "skyhook" damping control is associated with the fact that, in order to obtain a damping force proportional to total velocity, the damper must be connected between the mass and an inertial reference frame.

The advantage of skyhook damper control over conventional damper control for steady-state harmonic excitation is made clear by examining the associated displacement transmissibilities. The equation of motion of a SDOF structure subjected to base excitation, \ddot{u}_g , may be written as

$$m\ddot{u} + k u + f_d = -m\ddot{u}_g \quad (7-14)$$

where f_d represents the damping force. In the case of harmonic base excitation and conventional damping force ($f_d = c\dot{u}$), the displacement transmissibility is given by

$$TR = \sqrt{\frac{1 + (2\xi r)^2}{(1 - r^2)^2 + (2\xi r)^2}} \quad (7-15)$$

where r is the ratio of the driving frequency, ω , to the natural frequency, ω_n , and ξ is the damping ratio of the conventional damping system given by

$$\xi = \frac{c}{2 m \omega_n} \quad (7-16)$$

In the case of skyhook damper control, the damping force is given by

$$f_d = C_{SH}\dot{u}_t \quad (7-17)$$

where C_{SH} is the damping coefficient of the skyhook damper and \dot{u}_t is the total velocity of the mass. The damping ratio of the structure with skyhook damping is denoted by

$$\xi_{SH} = \frac{C_{SH}}{2 m \omega_n} \quad (7-18)$$

and the displacement transmissibility is given by

$$TR_{SH} = \sqrt{\frac{1}{(1 - r^2)^2 + (2\xi_{SH}r)^2}} \quad (7-19)$$

A comparison of the conventional and skyhook displacement transmissibilities is shown in Figure 7-2. Near resonance, $r = 1$, both the conventional and skyhook damping systems reduce the transmissibility as the corresponding damping ratio is increased. Beyond resonance, both systems begin to isolate the mass from the ground motion. However, as the damping ratio of the skyhook damper system is increased, the response near the resonance frequency decreases and the high frequency response decreases marginally while, in the conventionally damped system, an increase in damping ratio reduces the response near resonance while increasing the response at high frequencies. Apparently, skyhook control would prove particularly advantageous in vibration isolation of systems subjected to a wide range of input frequencies.

The application of skyhook control for the one-story model structure was explored in shaking table tests with both steady-state harmonic excitation and transient earthquake excitation. Furthermore, two different values of the skyhook damper damping coefficient were selected for use in the shaking table test program and are given in Table 7-I. The implementation of this algorithm requires that Equation (7-17) be rewritten as

$$P_d = \left(\frac{C_{SH} \dot{u}_t}{\eta \dot{u}} \right) \dot{u} = C_d \dot{u} \quad (7-20)$$

where f_d was replaced by ηP_d and linear viscous dashpot behavior is assumed. The horizontal component of force from each semi-active damper is described by Equation (7-10). Equating Equations (7-10) and (7-20)

$$C_{SA} = \frac{C_{SH} \dot{u}_t}{\eta \cos^2 \theta \dot{u}} \quad (7-21)$$

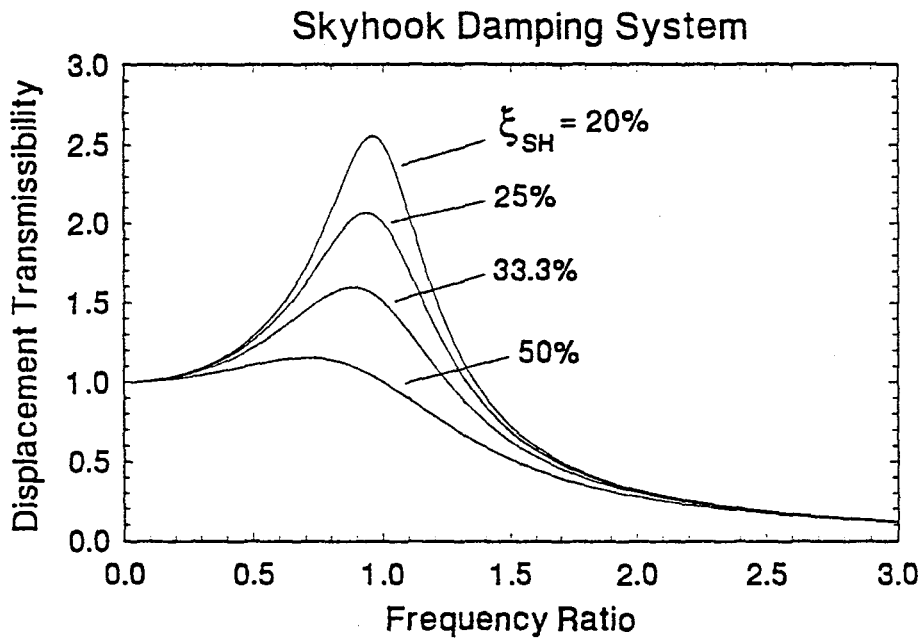
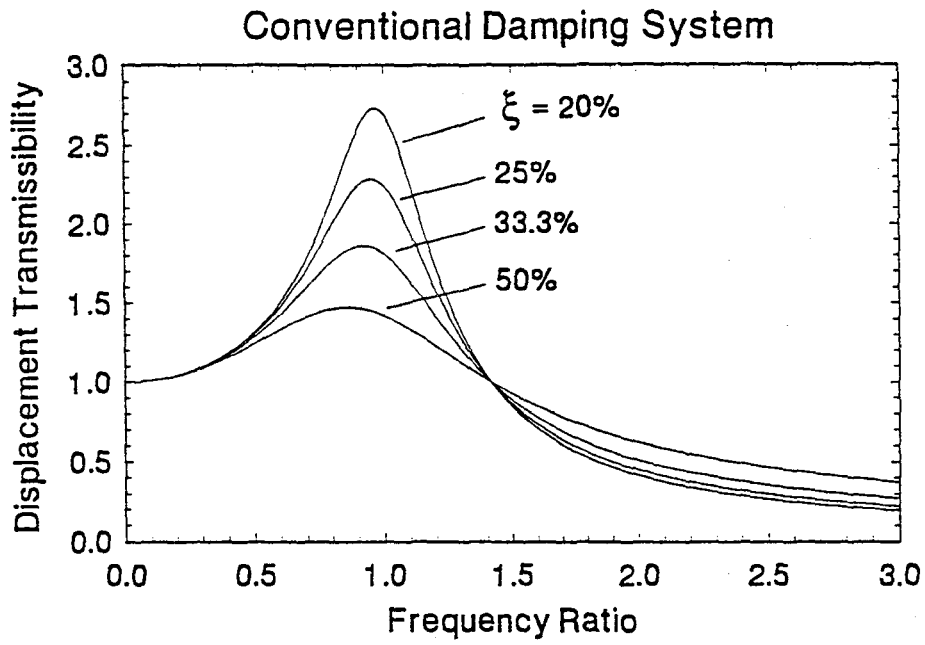


Figure 7-2 Comparison of Conventional and Skyhook Damping Displacement Transmissibilities

TABLE 7-1 Values of Parameters Used in Control Algorithms for Shaking Table Tests with Variable Dampers

CONTROL ALGORITHM	PARAMETER	VALUE
Skyhook	C_{SH}	200 N-s/cm
		400 N-s/cm
Optimal Control (Low Gains)	$g_{1,1}$	2316.2 N/cm
	$g_{1,2}$	-1638.4 N/cm
	$g_{1,3}$	471.1 N/cm
	$g_{1,4}$	205.8 N-s/cm
	$g_{1,5}$	23.2 N-s/cm
	$g_{1,6}$	60.3 N-s/cm
Optimal Control (High Gains)	$g_{1,1}$	9382.4 N/cm
	$g_{1,2}$	-6869.6 N/cm
	$g_{1,3}$	1961.5 N/cm
	$g_{1,4}$	321.8 N-s/cm
	$g_{1,5}$	73.3 N-s/cm
	$g_{1,6}$	101.1 N-s/cm
Sliding Mode Control	$\hat{m}_{initial}$	2587.5 kg
	$\hat{c}_{initial}$	10.2 N-s/cm
	$\hat{k}_{initial}$	3309.7 N/cm
	γ	0.1 (units vary)
	λ	1.0 sec ⁻¹
	μ	10.0 N-s/cm
	Δt	0.00625 sec

which describes the necessary variation in the damping coefficient of each semi-active damper to obtain skyhook damping control. Recall that the damping coefficient of the semi-active dampers is constrained according to Equation (7-6). The skyhook damping control algorithm is then obtained by combining Equations (7-6) and (7-21)

$$C_{SA} = \begin{cases} C_{\min} & , \text{ if } C^* \leq C_{\min} \\ C_{SH} \dot{u}_t (\eta \cos^2 \theta \dot{u})^{-1} & , \text{ if } C_{\min} < C^* < C_{\max} \\ C_{\max} & , \text{ if } C^* \geq C_{\max} \end{cases} \quad (7-22)$$

where

$$C^* = \frac{C_{SH} \dot{u}_t}{\eta \cos^2 \theta \dot{u}} \quad (7-23)$$

7.4 Three-Story Structure with Variable Dampers

The discussion in Section 7.3.1 regarding the approximate damping coefficient/command signal relationship for the one-story structure with variable dampers (Equation (7-4)) also applies to the three-story structure with variable dampers.

7.4.1 Linear Quadratic Regulator Optimal Control

The linear quadratic regulator (LQR) control algorithm has been investigated by a number of researchers for applications to semi-actively controlled structures (e.g., Fujita 1994, Sack 1993, Hasegana 1992, Mizuno 1992, and Hrovat 1983) and to actively controlled structures (e.g., Soong 1994 and 1990). The general optimal control problem may be stated as: given a system subjected to external inputs, find the control which minimizes a

certain measure of the performance of the system. The system is therefore optimized only with respect to that specific performance measure.

Consider the equation of motion of a linear MDOF structure having n degrees of freedom

$$[M]\{\ddot{u}\} + [C_v]\{\dot{u}\} + [K]\{u\} = [D]\{d\} + [E]\{f\} \quad (7-24)$$

where $[M]$ is an $n \times n$ mass matrix, $[C_v]$ is an $n \times n$ damping coefficient matrix, $[K]$ is an $n \times n$ stiffness matrix, $[D]$ is an $n \times m$ matrix describing the location of the control forces, $[E]$ is a $n \times r$ matrix describing the location of the input, $\{d\}$ is an $m \times 1$ control force vector, $\{f\}$ is a $r \times 1$ input vector; and $\{\ddot{u}\}$, $\{\dot{u}\}$, and $\{u\}$ are the $n \times 1$ vectors of relative acceleration, velocity and displacement. The $2n \times 1$ state vector is given by

$$\{Z\} = \begin{Bmatrix} \{u\} \\ \{\dot{u}\} \end{Bmatrix} \quad (7-25)$$

which, when substituted into the equation of motion (Equation (7-24)) leads to

$$\{\dot{Z}\} = [A]\{Z\} + [B]\{d\} + [F]\{f\} \quad (7-26)$$

which represents a system of first order differential equations where

$$[A] = \begin{bmatrix} [0] & [I] \\ -[M]^{-1}[K] & -[M]^{-1}[C_v] \end{bmatrix} \quad (7-27)$$

is a $2n \times 2n$ system matrix and

$$[B] = \begin{bmatrix} [0] \\ [M]^{-1}[D] \end{bmatrix} \quad \text{and} \quad [F] = \begin{bmatrix} [0] \\ [M]^{-1}[E] \end{bmatrix} \quad (7-28)$$

are $2n \times m$ and $2n \times r$ location matrices specifying the locations of the control forces and the input in the state space, respectively. The performance index for the LQR problem is given by the following scalar quantity

$$J = \int_0^{t_f} \left(\{Z\}^T [Q] \{Z\} + \{d\}^T [R] \{d\} \right) dt \quad (7-29)$$

where t_f is the final time of the control interval, $[Q]$ is a $2n \times 2n$ positive semi-definite state weighting matrix, and $[R]$ is an $m \times m$ positive definite control force weighting matrix. The relative values assigned to the state and control weighting matrices reflect the importance attached to minimization of the state variables and control forces, respectively. The optimal control problem is to minimize the scalar functional J subject to the constraint equation given by (7-26). The Lagrangian, L , is formed by adjoining Equations (7-26) and (7-29) with a time dependent Lagrange multiplier, $\{\lambda\}$:

$$L = \int_0^{t_f} \left(\{Z\}^T [Q] \{Z\} + \{d\}^T [R] \{d\} + \{\lambda\}^T \left[[A] \{Z\} + [B] \{d\} + [F] \{f\} - \dot{\{Z\}} \right] \right) dt \quad (7-30)$$

where the integrand is defined as the Hamiltonian, H . The necessary conditions for the extremization process are derived from the calculus of variations and result in the Euler-Lagrange equations:

$$\frac{\partial H}{\partial \{d\}} - \frac{d}{dt} \frac{\partial H}{\partial \{\dot{d}\}} = 0 \quad (7-31)$$

$$\frac{\partial H}{\partial \{Z\}} - \frac{d}{dt} \frac{\partial H}{\partial \{\dot{Z}\}} = 0 \quad (7-32)$$

Equations (7-31) and (7-32) lead to

$$\{d\} = -\frac{1}{2}[R]^{-1}[B]^T\{\lambda\} \quad (7-33)$$

$$\{\dot{\lambda}\} = -[A]^T\{\lambda\} - 2[Q]\{Z\} \quad (7-34)$$

The transversality conditions are given by (Sage 1977)

$$\left(\frac{\delta H}{\delta \{\dot{Z}\}} \delta \{Z\} \right)_{t=0} = 0 \quad (7-35)$$

and

$$\left(\frac{\delta H}{\delta \{\dot{Z}\}} \delta \{Z\} \right)_{t=t_f} = 0 \quad (7-36)$$

where δ is the variational operator. Equation (7-35) is satisfied due to the boundary condition

$$\{Z(0)\} = 0 \quad (7-37)$$

which implies that $(\delta\{Z\})_{t=0} = 0$. Since $(\delta\{Z\})_{t=t_f}$ is open, Equation (7-36) reduces to

$$\left(\frac{\delta H}{\delta \{\dot{Z}\}} \right)_{t=t_f} = 0 \quad (7-38)$$

and we therefore obtain

$$\{\lambda(t_f)\} = \{0\} \quad (7-39)$$

The system of equations given by (7-26), (7-33), (7-34), (7-37), and (7-39) define a two-point boundary value problem.

The control vector becomes a linear function of the state vector (closed-loop control) when the Lagrange multiplier is written as

$$\{\lambda\} = [P]\{Z\} \quad (7-40)$$

where $[P]$ is a $2n \times 2n$ time dependent matrix. Substitution of Equation (7-40) into (7-33) leads to

$$\{d\} = -\frac{1}{2}[R]^{-1}[B]^T[P]\{Z\} \quad (7-41)$$

The derivative of Equation (7-40) gives

$$\{\dot{\lambda}\} = [\dot{P}]\{Z\} + [P]\{\dot{Z}\} \quad (7-42)$$

which can be combined with Equation (7-34) and (7-40) to yield

$$[\dot{P}]\{Z\} + [P]\{\dot{Z}\} = -[A]^T[P]\{Z\} - 2[Q]\{Z\} \quad (7-43)$$

Substituting Equation (7-26) into (7-43) leads to

$$[\dot{P}]\{Z\} + [P]([A]\{Z\} + [B]\{d\} + [F]\{f\})\{\dot{Z}\} = -[A]^T[P]\{Z\} - 2[Q]\{Z\} \quad (7-44)$$

Substituting Equation (7-41) into (7-44) gives

$$\left([\dot{P}] + [P][A] - \frac{1}{2}[P][B][R]^{-1}[B]^T[P] + [A]^T[P] + 2[Q] \right) \{Z\} + [P][F]\{f\} = \{0\} \quad (7-45)$$

At the end of the control interval, $t = t_f$, and Equation (7-40) becomes

$$\{\lambda(t_f)\} = [P(t_f)]\{Z(t_f)\} \quad (7-46)$$

According to Equation (7-39), $\{\lambda(t_f)\} = \{0\}$. Further, we have $\{Z(t_f)\} = \text{open}$ and therefore conclude from Equation (7-46) that

$$[P(t_f)] = [0] \quad (7-47)$$

In summary, the optimal control force is given by Equation (7-41) with matrix [P] satisfying Equation (7-45) (a first order matrix differential equation) and Equation (7-47). Since [P] is specified at the terminal time, t_f , Equation (7-45) must be solved backwards in time.

In the case of earthquake input, the input vector {f} in Equation (7-45) is unknown and is typically taken as a null vector. Furthermore, matrix [P] has been shown to be essentially constant over the entire control interval and we may therefore let $\dot{[P]} = 0$ (Soong 1994 and 1990). With these simplifications, Equation (7-45) reduces to

$$[P][A] - \frac{1}{2}[P][B][R]^{-1}[B]^T[P] + [A]^T[P] + 2[Q] = [0] \quad (7-48)$$

which is known as the algebraic matrix Ricatti equation in which [P] is the Ricatti matrix. Equation (7-48) is easily solved using commercial mathematical analysis software (e.g., MATLAB 1990). The control force vector given in Equation (7-41) may now be written as

$$\{d\} = -\frac{1}{2}[R]^{-1}[B]^T[P]\{Z\} = [G]\{Z\} \quad (7-49)$$

where [G] is an $m \times 2n$ constant control gain matrix which is dependent on the system matrix, [A], defining the dynamic characteristics of the structure, the control force location matrix, [B], and the state and control force weighting matrices [Q] and [R]. Note that in both experimental and analytical studies, the values assigned to the weighting matrices are typically obtained through parametric studies that include the seismic

excitation. If the full state vector is measurable (or can be estimated), Equation (7-49) can be used to determine the control force vector.

The control force vector is linear in the state vector (Equation (7-49)), the performance index is quadratic in the state and in the control (Equation (7-29)), and the performance index regulates the state of the system as opposed to tracking a specified trajectory. The control algorithm is therefore defined to be a linear quadratic regulator optimal control algorithm.

The three-story model structure was tested with semi-active dampers in the first story only. In this case, the control force location matrix, $[D]$, and the control force vector, $\{d\}$, of Equation (7-24) become a 3×1 vector and a scalar, respectively. Furthermore, with reference to Equation (7-24), the mass matrix, $[M]$, was known while the damping matrix of the structure without dampers, $[C_d]$, and the stiffness matrix, $[K]$, were calculated as described in Section 6.4.2. The state weighting matrix $[Q]$, and control weighting matrix, $[R]$, were selected to be identical to those used by previous researchers (Soong 1994 and 1990) in the study of an active tendon system on the same three-story model structure subjected to 25% of the El Centro ground motion. The algebraic Riccati Equation (7-48) was solved to obtain the Riccati matrix, $[P]$, which was then substituted into Equation (7-49) to obtain the 1×6 control gain matrix. In the case of the three-story model structure with the control force applied at the first floor only, the control force vector becomes a scalar given by

$$d = \sum_{n=1}^3 (g_{1,n} u_n) + \sum_{n=1}^3 (g_{1,n+3} \dot{u}_n) \quad (7-50)$$

where g_{ij} is the component of matrix $[G]$ in the i -th row and the j -th column and u_n and \dot{u}_n are the relative displacement and relative velocity, respectively, of the n -th floor. Assuming linear viscous behavior, the horizontal component of the semi-active damper force output is proportional to the relative velocity of the first floor

$$P_d = \left(\frac{d}{\eta \dot{u}_1} \right) \dot{u}_1 = C_d \dot{u}_1 \quad (7-51)$$

The horizontal component of force acting on the first floor from each semi-active damper is given by

$$P_d = C_{SA} \cos^2 \theta \dot{u}_1 \quad (7-52)$$

Equating Equations (7-51) and (7-52)

$$C_{SA} = \frac{1}{\eta \cos^2 \theta \dot{u}_1} \left[\sum_{n=1}^3 (g_{1,n} u_n) + \sum_{n=1}^3 (g_{1,n+3} \dot{u}_n) \right] \quad (7-53)$$

which describes the necessary variation in the damping coefficient of each semi-active damper to achieve the LQR optimal control. However, the damping coefficient of the semi-active dampers is constrained according to Equation (7-6). The LQR optimal control algorithm is then obtained by combining Equations (7-6) and (7-53):

$$C_{SA} = \begin{cases} C_{\min} & , \text{ if } C^* \leq C_{\min} \\ (\eta \cos^2 \theta \dot{u}_1)^{-1} \left[\sum_{n=1}^3 (g_{1,n} u_n) + \sum_{n=1}^3 (g_{1,n+3} \dot{u}_n) \right] & , \text{ if } C_{\min} \leq C^* \leq C_{\max} \\ C_{\max} & , \text{ if } C^* \geq C_{\max} \end{cases} \quad (7-54)$$

where

$$C^* = \frac{1}{\eta \cos^2 \theta \dot{u}_1} \left[\sum_{n=1}^3 (g_{1,n} u_n) + \sum_{n=1}^3 (g_{1,n+3} \dot{u}_n) \right] \quad (7-55)$$

Note that Equation (7-53) is considered to be the optimal damping coefficient while Equation (7-54) is a suboptimal damping coefficient since the damping coefficient constraint equation (Equation (7-6)) was not considered in the optimization process. Furthermore, it may be argued that, for a semi-active damper control system, the control force weighting matrix, [R], should be set equal to the null matrix since there is no penalty (e.g., excessive power requirements) to be paid for large control forces. This discrepancy was addressed in an approximate way through modification of the control force weighting matrix. In the specific case under study, [R] is a 1 X 1 matrix (i.e., a scalar). This scalar quantity was reduced in value by a factor of 9 with the effect of increasing the values contained within the control gain matrix, [G], by a factor of about 4 for the displacement gains and about 2 for the velocity gains. Shaking table tests were performed using both the "low" and "high" set of feedback gains. The feedback gains for the optimal control algorithm are presented in Table 7-I.

7.4.2 Sliding Mode Control

The objective of the control algorithm described in this section is to track a specified trajectory, and in particular, for the case of stabilization the desired trajectory is identically zero. The combined error in velocity and displacement is used to determine the accuracy

of tracking. Moreover, the algorithm can accommodate uncertainties that may exist in the parameters that define the structural system (e.g., mass, stiffness, and damping properties). The control algorithm is developed based on sliding mode control theory. A major advantage of sliding mode control theory is that the control of the structural system can be designed to be robust with respect to unmodeled dynamics, uncertain parameters, and external inputs. Sliding mode control theory begins with the design of a switching surface so that the response of the structural system has certain prescribed characteristics on the surface (e.g., the design is such that the system is asymptotically stable on the surface). Following the design of the switching surface, a control strategy is developed which directs the response of the structural system onto the switching surface and attempts to maintain it there.

The sliding mode control algorithm discussed in the following has been described by Ghanem (1994) for applications to the control of SDOF systems. The same approach will be used herein, with modifications in the final results to adapt the algorithm for control of the three-story model structure. Consider the equation of motion for a one-story structure with control force $F_c(t)$

$$m\ddot{u} + c_u\dot{u} + ku = -m\ddot{u}_g + F_c(t) \quad (7-56)$$

The tracking error is defined to be the difference between the measured response and the desired response

$$e(t) = u(t) - u_d(t) \quad (7-57)$$

The combined error is defined to be a hyperplane in the $(e(t), \dot{e}(t))$ plane and is given by

$$s(t) = \dot{e}(t) + \lambda e(t) \quad , \quad \lambda \geq 0 \quad (7-58)$$

where λ is a real positive constant which controls the relative weight given to the error in displacement versus the error in velocity. Setting the combined error in Equation (7-58) equal to zero (see Figure 7-3), we obtain

$$e(t) = a \exp(-\lambda t) \quad (7-59)$$

where a is a real constant. Equation (7-59) shows that the tracking error goes exponentially to zero as $t \rightarrow \infty$. A control algorithm, based on sliding mode control theory, is now developed which guarantees the convergence of the combined error to zero as $t \rightarrow \infty$ and, in turn, guarantees that the tracking error goes exponentially to zero as $t \rightarrow \infty$.

For implementation of this algorithm, the desired trajectory was set equal to zero ($u_d(t) = 0$). In this case, the tracking error is equal to the relative displacement and Equation (7-58) becomes

$$s(t) = \dot{u}(t) + \lambda u(t) \quad (7-60)$$

If the combined error converges to zero, then its derivative also converges to zero and we obtain

$$\ddot{u}_r(t) = -\lambda \dot{u}(t) = -\lambda \frac{d}{dt}[e(t)] \quad (7-61)$$

where $\ddot{u}(t)$ has been replaced by $\ddot{u}_r(t)$, the "reference" acceleration. Note that the reference acceleration is simply an estimate of the relative acceleration based on the measured tracking error.

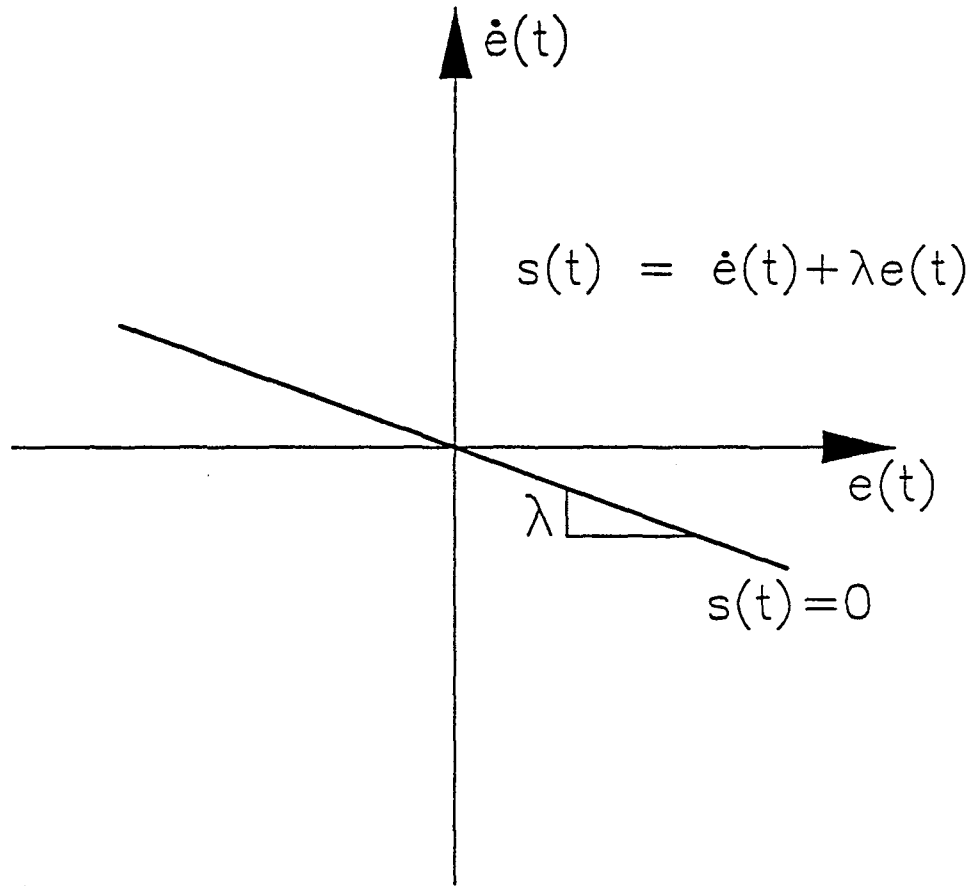


Figure 7-3 Diagram of Error Phase Plane Used in Sliding Mode Control Algorithm

The control force is considered to be of the following form

$$F_c(t) = m\ddot{u}_r - \mu s(t) + c_u \dot{u} + ku + m\ddot{u}_g \quad (7-62)$$

where μ is a positive real constant. Equation (7-62) describes the dynamics of a system where the combined error, $s(t)$, is compensated for by the control force, $F_c(t)$.

Substituting Equation (7-62) into Equation (7-56) leads to

$$m(\ddot{u} + \ddot{u}_r) + \mu s(t) = 0 \quad (7-63)$$

which may be rewritten as

$$m\dot{s}(t) + \mu s(t) = 0 \quad (7-64)$$

The solution of Equation (7-64) is

$$s(t) = b \exp\left(-\frac{\mu}{m} t\right) \quad (7-65)$$

where b is a real constant. Equation (7-65) indicates that, as expected, the combined error, $s(t)$, converges exponentially to zero as $t \rightarrow \infty$. In summary, the control force given by Equation (7-62) guarantees that the tracking error (relative displacement) converges to zero as $t \rightarrow \infty$.

To this point, it has been assumed that the values of the parameters defining the model structure are known with absolute certainty. With the introduction of uncertainty in these parameters, Equation (7-64) is generally not valid (and therefore stability is not ensured). To maintain stable operation of the controlled structural system, conditions on updating the uncertain parameters should be developed. The error in any parameter may be given by

$$\bar{a} = \hat{a} - a \quad (7-66)$$

where \hat{a} is an estimate of the true value of parameter a . Rewriting the control force of Equation (7-62) using estimated parameters

$$F_c(t) = \hat{m}\ddot{u}_r - \mu s(t) + \hat{c}_u \dot{u} + \hat{k}u + \hat{m}\ddot{u}_g \quad (7-67)$$

Substituting Equation (7-67) into the equation of motion (7-56)

$$m(\ddot{u} - \ddot{u}_r) + \mu s(t) = \tilde{m}(\ddot{u}_r + \ddot{u}_g) + \tilde{c}_u \dot{u} + \tilde{k}u \quad (7-68)$$

and using Equation (7-61) and the derivative of Equation (7-60), we obtain

$$m\dot{s} + \mu s = \tilde{m}(\ddot{u}_r + \ddot{u}_g) + \tilde{c}_u \dot{u} + \tilde{k}u \quad (7-69)$$

The convergence of $s(t)$ to zero as $t \rightarrow \infty$ depends on the values of \tilde{m} , \tilde{c}_u , and \tilde{k} in Equation (7-69). Equation (7-69) can be rewritten as

$$m\dot{s} + \mu s = \{g\}^T \{G\} \quad (7-70)$$

where

$$\{g\}^T = [\tilde{m} \quad \tilde{c}_u \quad \tilde{k}] \quad (7-71)$$

and

$$\{G\} = \begin{Bmatrix} \ddot{u}_r + \ddot{u}_g \\ \dot{u} \\ u \end{Bmatrix} \quad (7-72)$$

Equation (7-70) can be represented by

$$s(t) = \frac{1}{mp+k} \{g\}^T \{G\} \quad (7-73)$$

which is of the form

$$s(t) = H(p) [n \{g\}^T \{G\}] \quad (7-74)$$

where $n = 1$ and

$$H(p) = \frac{1}{mp + k} \quad (7-75)$$

Equation (7-74) expresses the combined error $s(t)$ as the output of a stable, positive, and real filter with transfer function $H(p)$ to an input given by the right hand side of Equation (7-70). It may be shown (Slotine 1991) that a sufficient condition for the asymptotic decay of the combined error $s(t)$ (as $t \rightarrow \infty$, $s(t) \rightarrow 0$) is that

$$\{\dot{g}(t)\} = -\text{sgn}(n) \gamma s(t) \{G(t)\} \quad (7-76)$$

where γ is a positive real constant related to the level of uncertainty about the parameters. Equation (7-76) may be rewritten as three separate equations which represent parameter adaptation laws that are proportional to the combined error

$$\dot{\hat{m}}(t) = -\gamma s(t) (\ddot{u}_r + \ddot{u}_g) \quad (7-77)$$

$$\dot{\hat{c}}_u(t) = -\gamma s(t) \dot{u} \quad (7-78)$$

$$\dot{\hat{k}}(t) = -\gamma s(t) u \quad (7-79)$$

In summary, the control force given by Equation (7-67) guarantees the asymptotic decay of the combined error, $s(t)$, when the estimates of the model parameters are updated according to Equations (7-77), (7-78), and (7-79).

The horizontal component of control force from each semi-active damper is given by Equation (7-10). Equations (7-10) and (7-67) may be used to obtain

$$C_{SA} = \frac{-1}{\eta \cos^2 \theta \dot{u}} [\hat{m}(\ddot{u}_r + \ddot{u}_g) - \mu s(t) + \hat{c}_u \dot{u} + \hat{k}u] \quad (7-80)$$

which describes the necessary variation in the damping coefficient of each semi-active damper to achieve the sliding mode control. However, the damping coefficient of the semi-active dampers is constrained by Equation (7-6). The sliding mode control algorithm is then obtained by combining Equations (7-6) and (7-80)

$$C_{SA} = \begin{cases} C_{\min} & , \quad \text{if } C^* \leq C_{\min} \\ -(\eta \cos^2 \theta \dot{u})^{-1} [\hat{m}(\ddot{u}_r + \ddot{u}_g) - \mu s(t) + \hat{c}_u \dot{u} + \hat{k}u] & , \quad \text{if } C_{\min} < C^* < C_{\max} \\ C_{\max} & , \quad \text{if } C^* \geq C_{\max} \end{cases} \quad (7-81)$$

where

$$C^* = \frac{-1}{n \cos^2 \theta \dot{u}} [\hat{m}(\ddot{u}_r + \ddot{u}_g) - \mu s(t) + \hat{c}_u \dot{u} + \hat{k}u] \quad (7-82)$$

with \hat{m} , \hat{c}_u , and \hat{k} obtained from Equations (7-77), (7-78), and (7-79), respectively.

The sliding mode control algorithm for SDOF systems was modified to adapt the algorithm for control of a MDOF system. The MDOF structure is replaced by a SDOF representation, neglecting the effect of structural damping. The SDOF representation has mass m , stiffness k , and height h . These quantities are determined such that the SDOF representation has the same frequency as the fundamental mode of the MDOF structure and the same base shear and overturning moment.

The equations of motion of the MDOF structure in a shear type representation are

$$[M]\{\ddot{u}\} + [K]\{u\} = -[M]\{1\} \ddot{u}_g \quad (7-83)$$

Assuming vibration in the first mode

$$\{u\} = \{\phi_1\} y_1 \quad (7-84)$$

where $\{\phi_1\}$ and y_1 are the mode shape and modal coordinate, respectively, corresponding to the first mode. Substituting Equation (7-84) into (7-83) and pre-multiplying by $\{\phi_1\}^T$ we obtain

$$m_1^* \ddot{y}_1 + k_1^* y_1 = p_1^* \quad (7-85)$$

where

$$m_1^* = \{\phi_1\}^T [M] \{\phi_1\} \quad (7-86)$$

$$k_1^* = \{\phi_1\}^T [K] \{\phi_1\} \quad (7-87)$$

$$p_1^* = -\{\phi_1\}^T [M] [1] \ddot{u}_g \quad (7-88)$$

are the generalized mass, stiffness, and loading, respectively, corresponding to the first mode. Equation (7-85) may be rewritten as

$$\ddot{y}_1 + \omega_1^2 y_1 = - \left[\frac{\sum_j (m_j \phi_j)}{\sum_j (m_j \phi_j^2)} \right] \ddot{u}_g \quad (7-89)$$

where ω_1 is the generalized natural frequency corresponding to the first mode, j is an index representing the floor level, and ϕ_j is the modal amplitude of the j -th floor in the first mode.

The response of the structure is obtained from the spectral displacement, $S_D(\omega_1, \xi_1)$ for frequency ω_1 (and corresponding damping ratio ξ_1) from the response spectrum of the ground motion, \ddot{u}_g . The maximum relative displacement and total acceleration of the j -th

floor are given by

$$(u_j)_{\max} = \phi_j S_D(\omega_1, \xi_1) \left[\frac{\sum_j (m_j \phi_j)}{\sum_j (m_j \phi_j^2)} \right] \quad (7-90)$$

$$(\ddot{u}_j)_{\max} = \omega_1^2 \phi_j S_D(\omega_1, \xi_1) \left[\frac{\sum_j (m_j \phi_j)}{\sum_j (m_j \phi_j^2)} \right] \quad (7-91)$$

The maximum base shear (V) and maximum overturning moment (OTM) are obtained using Equation (7-91)

$$V = \sum_j [m_j (\ddot{u}_j)_{\max}] = \omega_1^2 S_D(\omega_1, \xi_1) \frac{\left[\sum_j (m_j \phi_j) \right]^2}{\sum_j (m_j \phi_j^2)} \quad (7-92)$$

$$\text{OTM} = \sum_j [m_j (\ddot{u}_j)_{\max} h_j] = \omega_1^2 S_D(\omega_1, \xi_1) \frac{\left[\sum_j (m_j \phi_j h_j) \right] \left[\sum_j (m_j \phi_j) \right]}{\sum_j (m_j \phi_j^2)} \quad (7-93)$$

The SDOF representation of the MDOF structure is expressed by (neglecting structural damping)

$$m \ddot{u} + k u = -m \ddot{u}_g \quad (7-94)$$

which may be rewritten as

$$\ddot{u} + \omega_1^2 u = -\ddot{u}_g \quad (7-95)$$

where ω_1 is the frequency of the fundamental mode of the MDOF structure. The maximum response of the SDOF representation is again obtained from the response spectrum of the ground motion, \ddot{u}_g , for frequency ω_1 (and corresponding damping ratio

ξ_1). The maximum relative displacement and total acceleration are given by

$$u_{\max} = S_D(\omega_1, \xi_1) \quad (7-96)$$

$$\ddot{u}_{\max} = \omega_1^2 S_D(\omega_1, \xi_1) \quad (7-97)$$

The maximum base shear V_{SDOF} and maximum overturning moment (OTM_{SDOF}) are obtained using Equation (7-97)

$$V_{\text{SDOF}} = m \ddot{u}_{\max} = \omega_1^2 m S_D(\omega_1, \xi_1) \quad (7-98)$$

$$\text{OTM}_{\text{SDOF}} = m \ddot{u}_{\max} h = \omega_1^2 m h S_D(\omega_1, \xi_1) \quad (7-99)$$

Equating the base shear and overturning moment of the MDOF structure and the SDOF representation (Equations (7-92) and (7-98); Equations (7-93) and (7-99)) we obtain

$$m = \frac{\left[\sum_j (m_j \phi_j) \right]^2}{\sum_j (m_j \phi_j^2)} \quad (7-100)$$

and

$$h = \frac{\sum_j (m_j \phi_j h_j)}{\sum_j (m_j \phi_j)} \quad (7-101)$$

which are the required properties of the SDOF representation from which we obtain $k = \omega_1^2 m$ and $c = 2\xi_1 \omega_1 m$. Relating these properties to the terms required for the sliding mode control described by Equation (7-81)

$$\hat{m} = m \quad (7-102)$$

$$\hat{c}_v = 2\xi_1 \omega_1 m \quad (7-103)$$

$$\hat{k} = \omega_1^2 m \quad (7-104)$$

where m is given by Equation (7-100) and ω_1 and ξ_1 are obtained from the experimental identification of the MDOF structure (see Section 6.5). Note that equations (7-102), (7-103), and (7-104) simply serve as initial parameter estimates for the sliding mode control algorithm. Furthermore, the parameter adaptation laws of Equations (7-77), (7-78), and (7-79) are written in the form of backward finite difference expressions for implementation purposes. The time step of the finite difference expression, Δt , corresponds to the control computation time delay for the sliding mode control algorithm.

The sliding mode control algorithm also requires measurements of relative displacement and velocity of the SDOF representation (see Equation (7-81)). However, only measurements of floor displacements and velocities of the MDOF structure are available. Equations for displacement and velocity in the SDOF representation may be obtained by equating either base shears or overturning moments in the two systems. In this case, the equality of base shears was selected

$$V = V_{\text{SDOF}} \quad (7-105)$$

$$\sum_j [m_j(\ddot{u}_j + \ddot{u}_g)] = m(\ddot{u} + \ddot{u}_g) \quad (7-106)$$

Noting that the mass of each floor of the MDOF structure is the same, we obtain

$$m_j \left[\sum_j (\ddot{u}_j) + 3\ddot{u}_g \right] = m(\ddot{u} + \ddot{u}_g) \quad (7-107)$$

replacing m by Equation (7-100) and introducing the parameter α

$$\alpha = \frac{\left[\sum_j (\phi_j) \right]^2}{\left[\sum_j (\phi_j^2) \right]} \quad (7-108)$$

we obtain the relative acceleration of the SDOF representation

$$\ddot{u} = \alpha^{-1} \left[\sum_j (\ddot{u}_j) \right] + (3\alpha^{-1} - 1)\ddot{u}_g \quad (7-109)$$

which can be integrated to obtain the relative velocity (initial conditions are all zero)

$$\dot{u} = \alpha^{-1} \left[\sum_j (\dot{u}_j) \right] + (3\alpha^{-1} - 1)\dot{u}_g \quad (7-110)$$

and the relative displacement

$$u = \alpha^{-1} \left[\sum_j (u_j) \right] + (3\alpha^{-1} - 1)u_g \quad (7-111)$$

The relative displacement and velocity required for the sliding mode control described in Equation (7-81) are now available from measurements on the MDOF structure using Equations (7-111) and (7-110), respectively.

Finally, we must consider the application of the control force. In the MDOF structure, the control force is applied at the first floor whereas in the SDOF representation, the control force should be applied to the mass, m , located at height h (see Equation (7-101)). Therefore, in general, the two control forces are not equivalent in terms of overturning moments in the two systems. However, the two control forces are equivalent in terms of the base shear in the two systems.

The parameters used in the sliding mode control algorithm for shaking table tests of the three-story model structure are presented in Table 7-I.

SECTION 8

SYSTEM TIME DELAYS AND METHODS OF COMPENSATION

8.1 Introduction

There is a considerable amount of analytical research performed in the area of active and semi-active structural control in which the response of the structure, the control computation, and the application of the control force are assumed to occur instantaneously. However, as a number of experimental studies have shown, time delays exist in the control system and, in general, must be considered to ensure stability of the structural system. Many methods of time delay compensation have been developed and experimentally tested (e.g., Soong 1990, Reinhorn 1992, and McGreevy 1988).

Time delays may be conveniently separated into two components (see Figure 8-1). In the following, it is assumed that the structural control is based on feedback that includes the response quantity $u(t)$ (e.g., displacement, velocity, acceleration, etc.). The first portion of the time delay is designated as τ_1 and represents the time required to obtain measurements of the response. The second portion of the time delay is designated as τ_2 and represents the time required to apply the control force. With reference to Figure 8-1, at time t the control computer determines the response of the structural system. Ideally, the measured response is $u(t)$. However the measured response actually occurred at time t_1 where the response is $u(t_1)$ and is being measured with a time delay due to, for example, signal conditioners, filters, differentiators, integrators, and computer computations. Also,

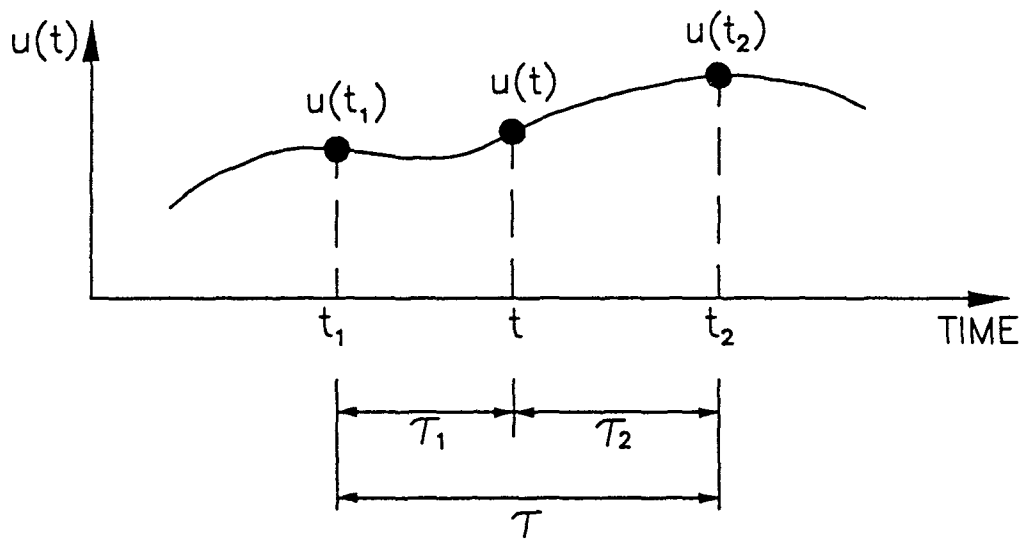


Figure 8-1 Diagram For Analysis of Time Delays

at time t , the control computer determines the appropriate control signal to be sent to the control system. Ideally, the control is applied at time t . However, the control system (e.g., servohydraulic actuator, semi-active fluid dampers, etc.) does not respond instantaneously and actually applies the control force at time t_2 where the response is $u(t_2)$. Clearly, if time delays are not considered, control forces will be applied at time t_2 based on the response at time t_1 .

The approach used herein to account for time delays is as follows: at time t , the controller receives information on the response measured at time t_1 and uses this information to predict the response at time t_2 . The predicted response is based on experimentally measured values of time delays τ_1 and τ_2 . Further, the predicted response is used to determine the appropriate control to be applied at time t_2 . Note that time delay τ_1 is dependent on the response quantity being measured and the control algorithm; it does not depend on the control system. Further, time delay τ_2 is dependent only on the control system; it does not depend on the response quantity being measured or on the control algorithm.

8.2 Kinematic Compensation

8.2.1 One-Story Structure

The kinematic compensation method is based on describing the motion of the system in terms of Taylor series expansions (e.g., Soong 1990, McGreevy 1988, and Abdel-Rohman 1985). Referring to Figure 8-1, the response at time t_2 may be written as

$$u(t_2) = u(t_1) + \tau \dot{u}(t_1) + \frac{\tau^2}{2} \ddot{u}(t_1) + \dots \quad (8-1)$$

Letting $t_1 = 0$ and $t_2 = \tau$ (i.e., starting time at t_1), Equation (8-1) gives the predicted response at time τ

$$u(\tau) = u(0) + \tau \dot{u}(0) + \frac{\tau^2}{2} \ddot{u}(0) + \dots \quad (8-2)$$

If Equation (8-2) is used to predict the displacement, the predicted velocity and acceleration may be obtained by taking derivatives of Equation (8-2) and replacing the total time delay, τ , with a value appropriate for the predicted response quantity. If the total time delay is small in comparison to the natural period of the structure, the series may be truncated after a few terms with minimal error. For the tests on the one-story flexible structure in which kinematic compensation was utilized, the total time delay was approximately 61 msec which is about 15% of the natural period of the structure. In all tests with kinematic compensation, the series of Equation (8-2) was truncated after the second term.

The experimental results obtained by McGreevy on an active control system indicated that the kinematic compensation method worked well for cases in which the excitation represents a well defined smooth function (e.g., a steady-state harmonic motion) and was not as useful for cases in which the excitation was of a random nature (e.g., earthquake motion).

8.3 Harmonic Compensation

The harmonic compensation method is based on the assumption that the structure responds as an undamped system in free vibration during the time interval between measuring the response and applying the control force. Clearly, this assumption is incorrect since the ground motion as well as the semi-active damper control forces act on the system during this time interval. However, if time delays are relatively small, the assumption of harmonic motion may be acceptable.

8.3.1 One-Story Structure

Assuming that variable u in Figure 8-1 represents the relative displacement of the structure, the undamped free vibration response at time t_1 is given by

$$u(t_1) = A \sin(\omega_n t_1) + B \cos(\omega_n t_1) \quad (8-3)$$

where ω_n is the natural frequency of the one-story structure. Similarly, assuming free vibration response between time t_1 and t_2 , the response at time t_2 is given by

$$u(t_2) = A \sin(\omega_n t_2) + B \cos(\omega_n t_2) \quad (8-4)$$

Letting $t_1 = 0$ and $t_2 = \tau$ (i.e., starting time at t_1), Equation (8-3) and its derivative lead to

$$u(0) = B \quad , \quad \dot{u}(0) = A\omega_n \quad (8-5)$$

which are the initial conditions at time t_1 . Combining Equations (8-4) and (8-5), the predicted response at time τ is given by

$$u(\tau) = \frac{\dot{u}(0)}{\omega_n} \sin(\omega_n \tau) + u(0)\cos(\omega_n \tau) \quad (8-6)$$

The predicted velocity and acceleration may be obtained by taking derivatives of Equation (8-6) and replacing the total time delay, τ , with a value appropriate for the predicted response quantity.

8.3.2 Three-Story Structure

The relative displacement response of a MDOF structure may be written in terms of modal coordinates as

$$\{u\} = [\Phi]\{y\} \quad (8-7)$$

where $\{y\}$ is the modal coordinate vector. The contribution to the response from the k -th mode of vibration is given by

$$\{u\}_k = \{\phi_k\} y_k \quad (8-8)$$

where $\{\phi_k\}$ and y_k are the mode shape and modal coordinate of the k -th mode, respectively. The equations of motion of the undamped MDOF structure in free vibration can be decomposed into SDOF equations in modal coordinates for each mode k (Clough 1975):

$$\ddot{y}_k + \omega_k^2 y_k = 0 \quad (8-9)$$

where

$$\omega_k = \sqrt{\frac{k_k^*}{m_k^*}} \quad (8-10)$$

and the generalized mass, m_k^* , and generalized stiffness, k_k^* , for the k -th mode are defined by

$$m_k^* = \{\phi_k\}^T [M] \{\phi_k\} \quad (8-11)$$

and

$$k_k^* = \{\phi_k\}^T [K] \{\phi_k\} \quad (8-12)$$

where $[M]$ and $[K]$ are the mass and stiffness matrix, respectively, of the MDOF structure.

Letting $t_1 = 0$ and $t_2 = \tau$ in Figure 8-1 (i.e., starting time at t_1), the free vibration response corresponding to Equation (8-9) is given by (compare with Equation (8-6))

$$y_k(\tau) = \frac{\dot{y}_k(0)}{\omega_k} \sin(\omega_k \tau) + y_k(0) \cos(\omega_k \tau) \quad (8-13)$$

The relative displacement vector is obtained as the sum of the modal contributions from each mode k

$$\{u\} = \sum_{k=1}^N (\{\phi_k\} y_k) \quad (8-14)$$

where N is the number of modes. At time $t = 0$, Equation (8-7) becomes

$$\{u(0)\} = [\Phi] \{y(0)\} \quad (8-15)$$

from which we obtain

$$\{y(0)\} = [\Phi]^{-1} \{u(0)\} \quad (8-16)$$

Substituting Equation (8-16) and its derivative into Equation (8-13) and the resulting expression into Equation (8-14), we may obtain the predicted relative displacement of the j -th degree of freedom in the following simple form

$$u_j(\tau) = \sum_{i=1}^N [(a_i)_j u_i(0) + (b_i)_j \dot{u}_i(0)] \quad (8-17)$$

where $u_i(0)$ and $\dot{u}_i(0)$ are the relative displacement and relative velocity, respectively, of the i -th degree of freedom at $t = 0$ and $(a_i)_j$, $(b_i)_j$, $(c_i)_j$, and $(d_i)_j$ are constants corresponding to the j -th degree of freedom and are determined from the modal frequencies, mode shapes, and measured time delays. Expressions similar to Equation (8-17) can be developed to predict the relative velocity and relative acceleration of the j -th degree-of-freedom.

8.4 Experimentally Measured Time Delays

The time delays τ_1 and τ_2 of Figure 8-1 were determined from experimental measurements of various time delays. Time delay τ_1 is considered to be the result of the following: signal conditioning, filtering, differentiating, and control computer computations. Further, time delay τ_2 is considered to be the result of delays in operation of the semi-active dampers. The values of the experimentally measured time delays which were used to determine the values of τ_1 and τ_2 are shown in Table 8-I.

8.4.1 Response Measurement Time Delay

The time delays associated with response measurement (signal conditioning, filtering, differentiating) and control computer computations are obtained by passing a white noise signal through each component of the system and obtaining the transfer function between the input signal and the output signal. The white noise input is made up of harmonic signals of the form

Table 8-I Experimentally Measured Time Delays

COMPONENT	TIME DELAY (ms)
Signal Conditioners (wide-band filters)	0.0
Low Pass Filters (25 Hz cut-off)	21.0
Analog Differentiators	3.9
Control Computations (Two-Stage Damper Tests)	5
Control Computations (Variable Damper Tests)	1.9 - 6.3
Two-Stage Damper	31.0
Variable Damper	20.3

$$W_I = A \exp(i\omega t) \quad (8-18)$$

where A is the amplitude of the input and ω is the frequency of the harmonic signal. In components which exhibit a pure time delay, τ_d , the output corresponding to the input at frequency ω is

$$W_o = A \exp[i\omega(t + \tau_d)] \quad (8-19)$$

The transfer function between the input and output signal is given by the ratio of Equation (8-19) and (8-18)

$$T(\omega) = \frac{W_o}{W_I} = \exp(i\omega\tau_d) = \cos(\omega\tau_d) + i \sin(\omega\tau_d) \quad (8-20)$$

and the phase angle is given by

$$\theta(\omega) = \tan^{-1} \left(\frac{\Im [T(\omega)]}{\Re [T(\omega)]} \right) = \omega\tau_d \quad (8-21)$$

where $\Im(\bullet)$ and $\Re(\bullet)$ indicate the imaginary and real parts of the contained complex quantity.

Therefore, in components which exhibit a pure time delay, the amplitude of the transfer function between the input and output signal is unity (Equation (8-20)) and the phase angle is a linear function of frequency (Equation (8-21)). The time delay is obtained from Equation (8-21)

$$\tau_d = \frac{\theta(\omega)}{\omega} \quad (8-22)$$

Figures 8-2 through 8-5 present experimental plots of amplitudes of transfer functions and phase angles between input and output signal for the signal conditioning amplifiers, the low-pass analog filters, the analog differentiators, and one of the control algorithms, respectively.

Clearly, the signal conditioning amplifier introduces negligible time delays (see Figure 8-2). The low-pass analog filters introduce a time delay of 21.0 ms and the amplitude of the transfer function has a value of about -3 db (~70%) at the cut-off frequency of 25 Hz (see Figure 8-3). The analog differentiators have acceptable response characteristics (i.e., linear variation in amplitude of transfer function) over a frequency range of about 0 to 20 Hz and introduce a time delay of about 3.9 ms (see Figure 8-4). Finally, the computer computations introduce time delays of 5 ms for the two-stage damper tests and 1.9 to 6.3 ms for the variable damper tests (recall the discussion in Section 5.5 related to the control computers and control sampling rates). Figure 8-5 shows the white noise test results for the variable damper feedforward control algorithm which exhibits a time delay of 1.9 ms.

8.4.2 Control Force Time Delay

The time delays associated with the development of the semi-active damper control forces were determined by measuring the system response to a saturated command signal (see Section 3.4 and recall that the system response time was composed of both a static and dynamic time delay of duration t_1 and t_2 , respectively). Note that the symbols t_1 and t_2 used in Section 3.4 do not represent the same quantities as those depicted in Figure 8-1.

Signal Conditioning Amplifier

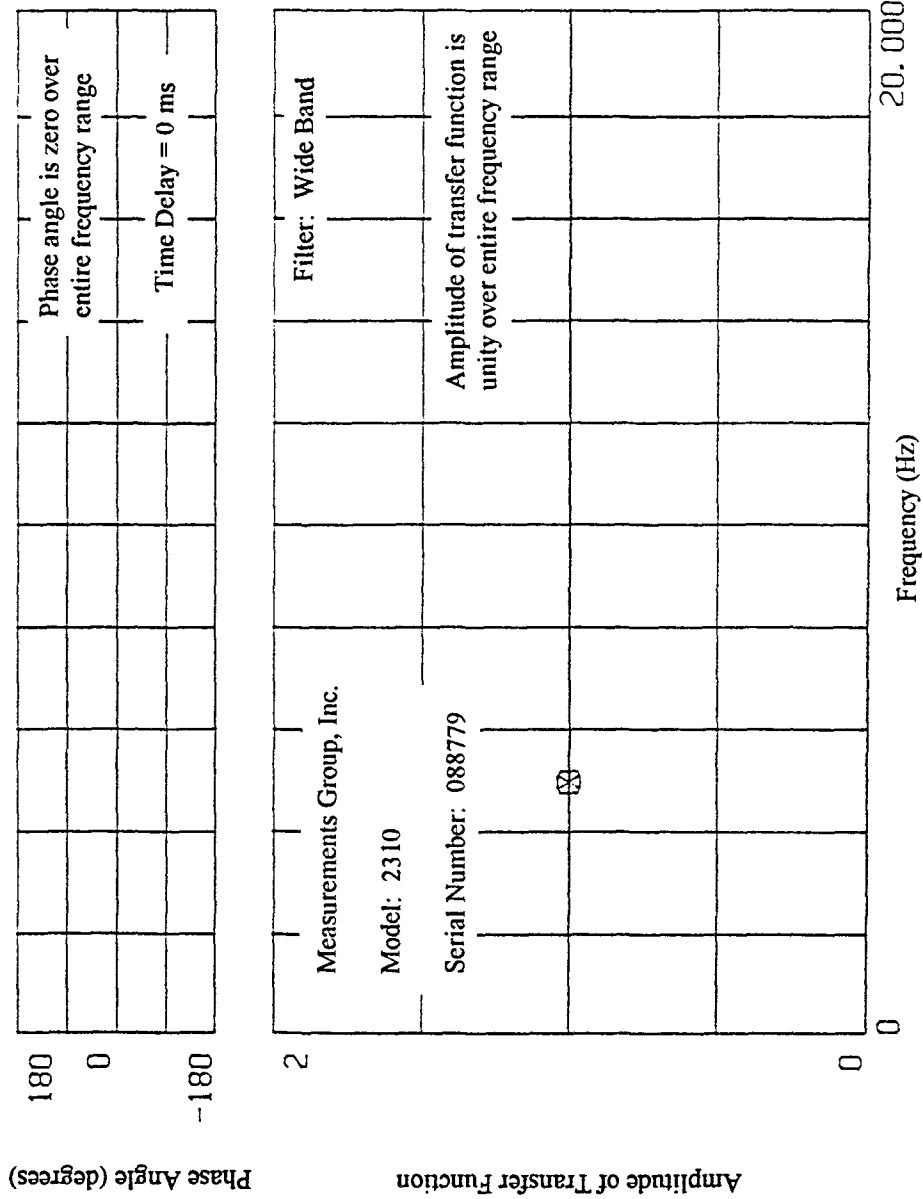


Figure 8-2 Transfer Function and Phase Angle for Signal Conditioning Amplifier Subjected to Banded (0 - 20 Hz) White Noise

Analog Low-Pass Filter

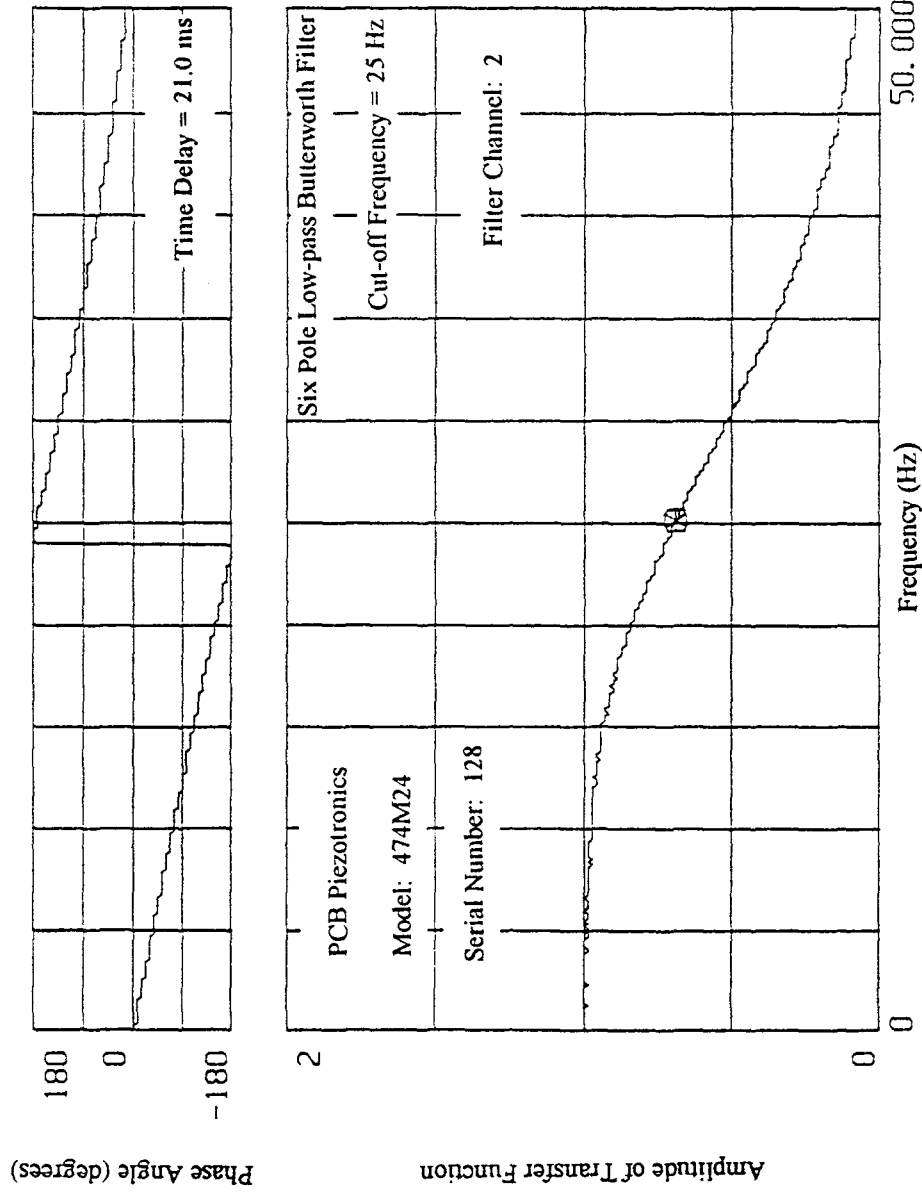


Figure 8-3 Transfer Function and Phase Angle for Analog Low-Pass Filter (Cut-Off Frequency = 25 Hz) Subjected to Banded (0 to 50 Hz) White Noise

Analog Differentiator

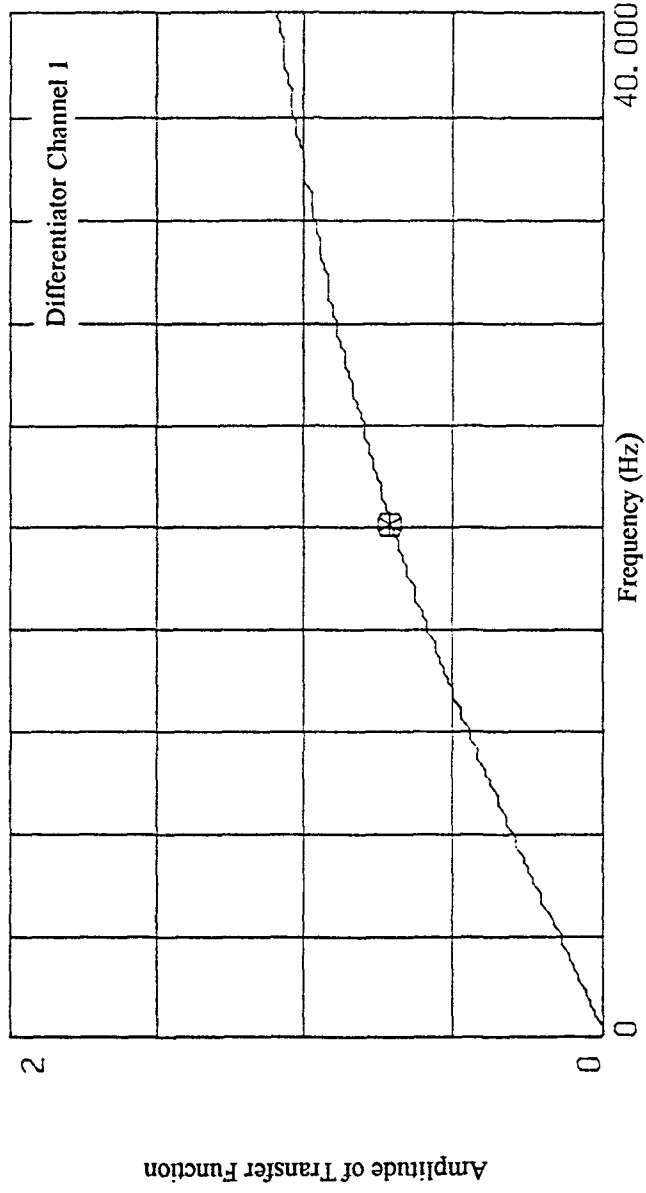
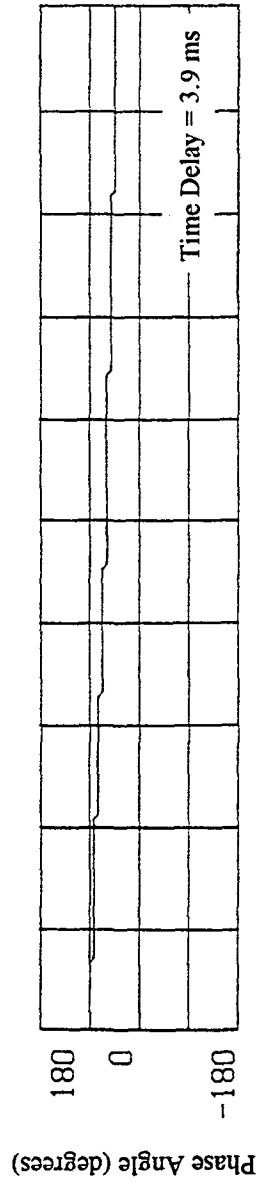


Figure 8-4 Transfer Function and Phase Angle for Analog Differentiator Subjected to Banded (0 to 40 Hz) White Noise

Control Computation

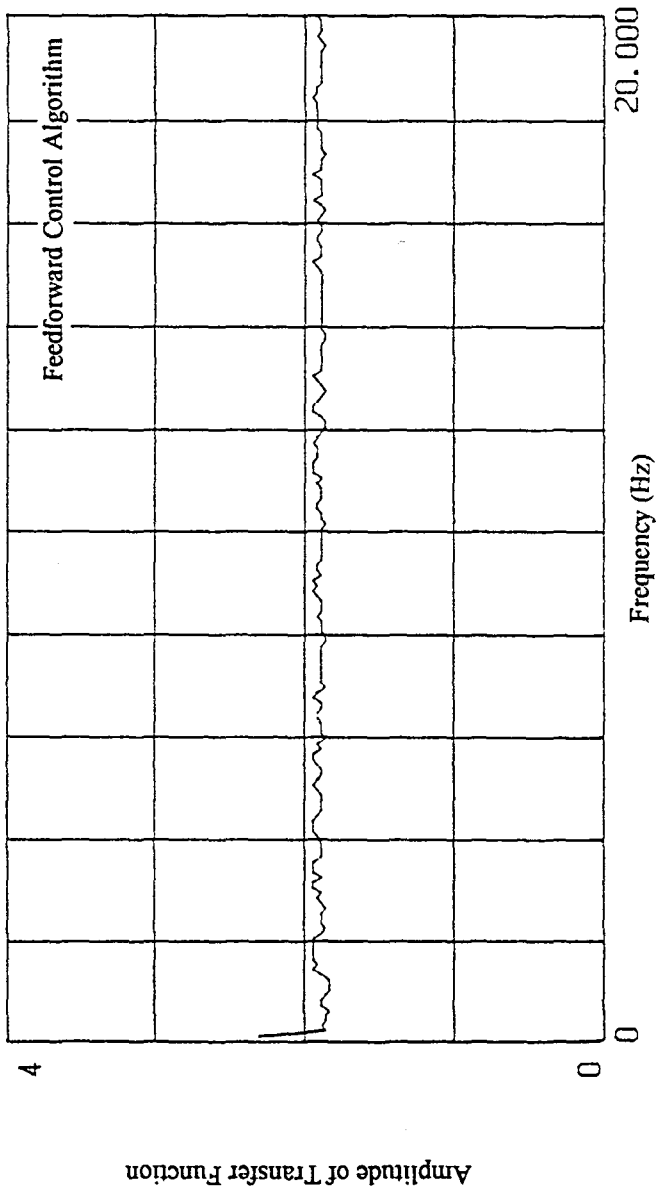
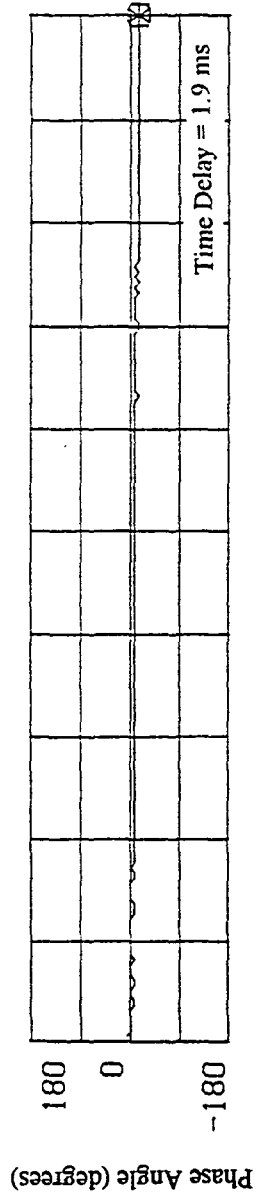


Figure 8-5 Transfer Function and Phase Angle for Control Computation (Feedforward Control Algorithm) Subjected to Banded (0 to 20 Hz) White Noise

The damper time delays presented in Table 8-I represent averages which are used in the compensation methods described in Sections 8.2 and 8.3 (see Table 3-VI and 3-VII for a more detailed description of time delays associated with each individual damper unit).

SECTION 9

SEISMIC SIMULATION TEST RESULTS

9.1 One-Story Structure

The experimental results for the one-story stiff and flexible structure are presented in Tables 9-I, 9-II, and 9-III for the bare frame structure, the structure with two-stage dampers, and the structure with variable dampers, respectively. For each test in which earthquake excitation was used, a percentage figure is included which indicates the degree of magnification as compared to the historical record (e.g., 200% indicates that the historical record was scaled up by a factor of 2). The values of peak table motion in the horizontal direction are also given. The displacement and acceleration were directly measured whereas the velocity was determined by numerical differentiation of the displacement record. The peak shear force was calculated from the known masses and recorded accelerations and is given as a fraction of the total weight (28.7 kN) of the structure. The peak drift is given as a percentage of the story height which was 81.3 cm. Results for all of the tests on the one-story structure are presented in graphical form in Appendix B (bare frame structure), Appendix C (structure with two-stage dampers), and Appendix D (structure with variable dampers). The graphs show recorded loops of base shear over total weight ratio versus story drift over height ratio. Further, in the tests with semi-active dampers, the recorded loops are decomposed into the contribution from the columns and from the semi-active dampers (see page C-2). In all tests, the dampers exhibit essentially no stiffness.

Table 9-1 Summary of Experimental Results for Bare Frame One-Story Structure

TEST	EXCITATION	PEAK TABLE MOTION			PEAK SHEAR FORCE / WEIGHT	PEAK DRIFT / HEIGHT (%)
		Displ. (cm)	Veloc. (cm/s)	Accel. (g)		
3	0.05g White Noise	0.94	3.05	0.05	0.16	0.56
REPAIRED STRUCTURE						
177	0.05g White Noise	0.95	3.05	0.05	0.11	0.59
178	10% El Centro	0.27	1.64	0.04	0.12	0.59
179	15% El Centro	0.05	2.43	0.06	0.17	0.86
180	10% Hachinohe	0.33	1.57	0.03	0.07	0.34
181	20% Hachinohe	0.65	2.69	0.05	0.12	0.64
324	25% Hachinohe	0.80	3.19	0.06	0.15	0.82
182	30% Hachinohe	0.96	3.95	0.07	0.17	0.88
183	20% Hachinohe-M	0.27	1.67	0.04	0.06	0.29
184	40% Hachinohe-M	0.54	3.12	0.09	0.10	0.54
185	50% Hachinohe-M	0.68	4.10	0.11	0.12	0.65
187	0.2g 5Hz Harmonic	0.21	6.38	0.21	0.06	0.34
188	0.3g 5Hz Harmonic	0.31	9.41	0.32	0.10	0.51
189	0.4g 5Hz Harmonic	0.41	12.29	0.44	0.12	0.67
190	0.5g 5Hz Harmonic	0.50	15.57	0.56	0.16	0.84

Table 9-II Summary of Experimental Results for One-Story Structure with Two-Stage Dampers

TEST	EXCITATION	CONTROL ALGORITHM	PEAK TABLE MOTION			PEAK SHEAR FORCE / WEIGHT	PEAK DRIFT / HEIGHT (%)
			Displ. (cm)	Veloc. (cm/s)	Accel. (g)		
43	0.15g White Noise	Low Damping	2.83	8.50	0.15	0.16	0.59
19	10% EI Centro	Low Damping	0.26	1.93	0.05	0.06	0.23
20	25% EI Centro	Low Damping	0.66	4.60	0.10	0.17	0.60
49	25% Hachinohe	Low Damping	0.80	3.33	0.06	0.10	0.35
50	50% Hachinohe	Low Damping	1.59	6.62	0.11	0.20	0.70
34	100% Hachinohe-M	Low Damping	1.36	7.74	0.23	0.15	0.54
48	125% Hachinohe-M	Low Damping	1.70	9.79	0.27	0.18	0.67
37	0.25g 5.6 Hz Harmonic	Low Damping	0.21	6.79	0.25	0.09	0.33
39	0.5g 5.6 Hz Harmonic	Low Damping	0.41	13.31	0.54	0.18	0.66
44	0.15g White Noise	High Damping	2.28	8.57	0.15	0.10	0.30
17	25% EI Centro	High Damping	0.66	4.52	0.10	0.14	0.44
18	33.3% EI Centro	High Damping	0.88	5.83	0.12	0.18	0.57
46	50% Hachinohe	High Damping	1.59	6.55	0.12	0.14	0.48
47	75% Hachinohe	High Damping	2.38	10.24	0.16	0.21	0.74
35	100% Hachinohe-M	High Damping	1.36	7.48	0.23	0.16	0.49
45	125% Hachinohe-M	High Damping	1.70	9.95	0.27	0.19	0.60
40	0.25g 5.6 Hz Harmonic	High Damping	0.21	6.69	0.26	0.14	0.36
42	0.5g 5.6 Hz Harmonic	High Damping	0.41	13.22	0.54	0.25	0.69
29	25% EI Centro	Base Shear Control BSCLIM = 0.05	0.66	4.48	0.10	0.16	0.55

Table 9-II Cont'd

TEST	EXCITATION	CONTROL ALGORITHM	PEAK TABLE MOTION			PEAK SHEAR FORCE / WEIGHT	PEAK DRIFT / HEIGHT (%)
			Displ. (cm)	Veloc. (cm/s)	Accel. (g)		
51	25% El Centro	Base Shear Control BSCLIM = 0.1	0.69	4.43	0.09	0.13	0.44
52	33.3% El Centro	Base Shear Control BSCLIM = 0.15	0.89	6.05	0.12	0.18	0.58
55	50% Hachinohe	Base Shear Control BSCLIM = 0.1	1.59	6.67	0.12	0.15	0.51
56	75% Hachinohe	Base Shear Control BSCLIM = 0.15	2.39	9.79	0.17	0.24	0.82
53	125% Hachinohe-M	Base Shear Control BSCLIM = 0.1	1.70	9.67	0.28	0.18	0.66
54	125% Hachinohe-M	Base Shear Control BSCLIM = 0.15	1.70	9.43	0.28	0.19	0.61
57	0.5g 5.6 Hz Harmonic	Base Shear Control BSCLIM = 0.15	0.40	13.36	0.54	0.32	1.16
REPAIRED STRUCTURE							
59	0.1g White Noise	Low Damping	2.09	5.81	0.11	0.12	0.63
83	10% El Centro	Low Damping	0.28	1.64	0.04	0.05	0.24
84	25% El Centro	Low Damping	0.70	3.88	0.09	0.16	0.79
86	25% Hachinohe	Low Damping	0.80	3.31	0.06	0.10	0.49
85	50% Hachinohe	Low Damping	1.59	6.76	0.12	0.20	1.04
87	50% Hachinohe-M	Low Damping	0.69	3.86	0.11	0.07	0.31
88	100% Hachinohe-M	Low Damping	1.37	7.72	0.23	0.14	0.74
66	0.2g 5Hz Harmonic	Low Damping	0.21	6.31	0.20	0.07	0.34

Table 9-II Cont'd

TEST	EXCITATION	CONTROL ALGORITHM	PEAK TABLE MOTION			PEAK SHEAR FORCE / WEIGHT	PEAK DRIFT / HEIGHT (%)
			Displ. (cm)	Veloc. (cm/s)	Accel. (g)		
62	0.3g 5Hz Harmonic	Low Damping	0.30	9.36	0.31	0.10	0.49
60	0.15g White Noise	High Damping	3.08	8.83	0.16	0.11	0.46
75	25% El Centro	High Damping	0.69	4.02	0.09	0.09	0.37
76	40% El Centro	High Damping	1.11	6.12	0.13	0.14	0.59
77	50% El Centro	High Damping	1.39	7.75	0.15	0.18	0.75
79	25% Hachinohe	High Damping	0.79	3.55	0.06	0.07	0.30
78	50% Hachinohe	High Damping	1.59	6.62	0.12	0.14	0.62
80	50% Hachinohe-M	High Damping	0.68	3.98	0.12	0.07	0.25
81	100% Hachinohe-M	High Damping	1.37	7.60	0.22	0.13	0.51
82	125% Hachinohe-M	High Damping	1.71	9.95	0.28	0.15	0.64
65	0.2g 5Hz Harmonic	High Damping	0.20	6.33	0.21	0.10	0.36
61	0.3g 5 Hz Harmonic	High Damping	0.30	9.19	0.32	0.14	0.52
139	25% El Centro	Base Shear Control BSCLIM = 0.08	0.68	3.83	0.09	0.09	0.38
140	50% Hachinohe	Base Shear Control BSCLIM = 0.1	1.60	6.75	0.12	0.13	0.66
141	100% Hachinohe-M	Base Shear Control BSCLIM = 0.1	1.35	7.74	0.23	0.12	0.54
142	0.2g 5 Hz Harmonic	Base Shear Control BSCLIM = 0.08	0.20	6.26	0.21	0.14	0.66
143	25% El Centro	Base Shear Control - KC BSCLIM = 0.08	0.68	4.02	0.08	0.16	0.78

Table 9-II Cont'd

TEST	EXCITATION	CONTROL ALGORITHM	PEAK TABLE MOTION			PEAK SHEAR FORCE / WEIGHT	PEAK DRIFT / HEIGHT (%)
			Displ. (cm)	Veloc. (cm/s)	Accel. (g)		
144	50% Hachinohe	Base Shear Control - KC BSCLIM = 0.1	1.60	6.67	0.12	0.19	0.99
145	100% Hachinohe-M	Base Shear Control - KC BSCLIM = 0.1	1.35	7.88	0.24	0.14	0.69
146	0.2g 5 Hz Harmonic	Base Shear Control - KC BSCLIM = 0.08	0.20	6.24	0.21	0.07	0.34
135	25% El Centro	Force Transfer Control	0.68	3.98	0.09	0.12	0.60
136	50% Hachinohe	Force Transfer Control	1.60	6.44	0.11	0.18	0.94
137	100% Hachinohe-M	Force Transfer Control	1.34	7.88	0.23	0.13	0.63
138	0.2g 5 Hz Harmonic	Force Transfer Control	0.20	6.41	0.03	0.07	0.35
122	25% El Centro	Force Transfer Control - KC	0.70	3.93	0.09	0.15	0.74
125	50% Hachinohe	Force Transfer Control - KC	1.60	6.57	0.12	0.19	1.01
126	100% Hachinohe-M	Force Transfer Control - KC	1.37	7.76	0.24	0.14	0.72
124	0.2g 5 Hz Harmonic	Force Transfer Control - KC	0.20	6.62	0.20	0.06	0.33
147	25% El Centro	Force Transfer Control - HC	0.68	3.76	0.09	0.12	0.59
148	50% Hachinohe	Force Transfer Control - HC	1.60	6.64	0.12	0.19	1.00
149	100% Hachinohe-M	Force Transfer Control - HC	1.35	7.72	0.23	0.14	0.72
150	0.2g 5 Hz Harmonic	Force Transfer Control - HC	0.20	6.22	0.21	0.07	0.34

Notes: BSCLIM = Base Shear Coefficient Limit
 KC = Kinematic Compensation
 HC = Harmonic Compensation

Table 9-III Summary of Experimental Results for One-Story Structure with Variable Dampers

TEST	EXCITATION	CONTROL ALGORITHM	PEAK TABLE MOTION			PEAK SHEAR FORCE / WEIGHT	PEAK DRIFT / HEIGHT (%)
			Displ. (cm)	Veloc. (cm/s)	Accel. (g)		
153	0.1g White Noise	Low Damping	1.89	5.76	0.10	0.10	0.50
154	0.15g White Noise	Low Damping	2.83	8.55	0.14	0.16	0.84
165	10% El Centro	Low Damping	0.27	1.71	0.04	0.06	0.27
166	25% El Centro	Low Damping	0.68	3.79	0.09	0.19	1.03
167	25% Hachinohe	Low Damping	0.81	3.48	0.06	0.10	0.50
168	40% Hachinohe	Low Damping	1.29	5.24	0.10	0.17	0.87
169	50% Hachinohe	Low Damping	1.60	6.60	0.12	0.21	1.14
170	50% Hachinohe-M	Low Damping	0.67	3.86	0.12	0.08	0.37
171	100% Hachinohe-M	Low Damping	1.35	7.60	0.23	0.16	0.84
172	0.2g 5Hz Harmonic	Low Damping	0.20	6.50	0.21	0.06	0.34
173	0.3g 5Hz Harmonic	Low Damping	0.30	9.26	0.31	0.09	0.49
174	0.5g 5 Hz Harmonic	Low Damping	0.49	15.07	0.55	0.15	0.83
151	0.1g White Noise	High Damping	1.88	5.79	0.10	0.07	0.26
152	0.2g White Noise	High Damping	4.43	11.41	0.19	0.13	0.59
155	25% El Centro	High Damping	0.68	3.91	0.09	0.10	0.39
156	50% El Centro	High Damping	1.37	7.53	0.15	0.19	0.78
158	25% Hachinohe	High Damping	1.03	3.33	0.06	0.07	0.33
157	50% Hachinohe	High Damping	1.60	6.52	0.12	0.15	0.68
159	100% Hachinohe-M	High Damping	1.36	7.55	0.22	0.12	0.54
160	125% Hachinohe-M	High Damping	1.70	9.62	0.27	0.15	0.64
161	150% Hachinohe-M	High Damping	2.04	11.43	0.32	0.18	0.79

Table 9-III Cont'd

TEST	EXCITATION	CONTROL ALGORITHM	PEAK TABLE MOTION			PEAK SHEAR FORCE / WEIGHT	PEAK DRIFT / HEIGHT (%)
			Displ. (cm)	Veloc. (cm/s)	Accel. (g)		
162	0.2g 5 Hz Harmonic	High Damping	0.20	6.22	0.21	0.10	0.36
164	0.3g 5 Hz Harmonic	High Damping	0.30	9.07	0.32	0.15	0.53
175	0.4g 5 Hz Harmonic	High Damping	0.39	12.10	0.43	0.19	0.70
176	0.5g 5 Hz Harmonic	High Damping	0.49	15.07	0.55	0.22	0.87
286	10% El Centro	Skyhook Damping $C_{SH} = 200 \text{ N-s/cm}$	0.28	1.60	0.04	0.04	0.17
287	25% El Centro	Skyhook Damping $C_{SH} = 200 \text{ N-s/cm}$	0.69	3.93	0.09	0.09	0.43
288	50% El Centro	Skyhook Damping $C_{SH} = 200 \text{ N-s/cm}$	1.37	7.62	0.16	0.16	0.79
289	25% Hachinohe	Skyhook Damping $C_{SH} = 200 \text{ N-s/cm}$	0.79	3.31	0.06	0.07	0.36
290	50% Hachinohe	Skyhook Damping $C_{SH} = 200 \text{ N-s/cm}$	1.59	6.72	0.12	0.14	0.70
291	75% Hachinohe	Skyhook Damping $C_{SH} = 200 \text{ N-s/cm}$	2.39	9.81	0.17	0.22	1.15
292	50% Hachinohe-M	Skyhook Damping $C_{SH} = 200 \text{ N-s/cm}$	0.68	3.98	0.12	0.06	0.27
293	100% Hachinohe-M	Skyhook Damping $C_{SH} = 200 \text{ N-s/cm}$	1.36	7.79	0.25	0.11	0.53
294	150% Hachinohe-M	Skyhook Damping $C_{SH} = 200 \text{ N-s/cm}$	2.03	11.95	0.35	0.17	0.77
295	0.2g 5 Hz Harmonic	Skyhook Damping $C_{SH} = 200 \text{ N-s/cm}$	0.20	6.31	0.21	0.08	0.39

Table 9-III Cont'd

TEST	EXCITATION	CONTROL ALGORITHM	PEAK TABLE MOTION			PEAK SHEAR FORCE / WEIGHT	PEAK DRIFT / HEIGHT (%)
			Displ. (cm)	Veloc. (cm/s)	Accel. (g)		
296	0.3g 5 Hz Harmonic	Skyhook Damping $C_{SH} = 200$ N-s/cm	0.30	9.14	0.32	0.11	0.54
297	0.5g 5 Hz Harmonic	Skyhook Damping $C_{SH} = 200$ N-s/cm	0.50	14.98	0.57	0.17	0.88
298	10% El Centro	Skyhook Damping $C_{SH} = 400$ N-s/cm	0.28	1.67	0.04	0.04	0.17
299	25% El Centro	Skyhook Damping $C_{SH} = 400$ N-s/cm	0.69	3.95	0.09	0.09	0.43
300	50% El Centro	Skyhook Damping $C_{SH} = 400$ N-s/cm	1.37	7.74	0.16	0.17	0.77
301	25% Hachinohe	Skyhook Damping $C_{SH} = 400$ N-s/cm	0.79	3.43	0.06	0.08	0.36
302	50% Hachinohe	Skyhook Damping $C_{SH} = 400$ N-s/cm	1.59	6.88	0.11	0.14	0.73
303	75% Hachinohe	Skyhook Damping $C_{SH} = 400$ N-s/cm	2.38	9.91	0.16	0.22	1.14
304	50% Hachinohe-M	Skyhook Damping $C_{SH} = 400$ N-s/cm	0.68	4.02	0.12	0.06	0.27
305	100% Hachinohe-M	Skyhook Damping $C_{SH} = 400$ N-s/cm	1.35	7.91	0.25	0.11	0.53
306	150% Hachinohe - M	Skyhook Damping $C_{SH} = 400$ N-s/cm	2.03	11.93	0.36	0.17	0.75
307	0.2g 5Hz Harmonic	Skyhook Damping $C_{SH} = 400$ N-s/cm	0.21	6.26	0.22	0.09	0.39

Table 9-III Cont'd

TEST	EXCITATION	CONTROL ALGORITHM	PEAK TABLE MOTION			PEAK SHEAR FORCE / WEIGHT	PEAK DRIFT / HEIGHT (%)
			Displ. (cm)	Veloc. (cm/s)	Accel. (g)		
308	0.3g 5Hz Harmonic	Skyhook Damping $C_{SH} = 400$ N-s/cm	0.30	9.14	0.33	0.12	0.55
309	0.5g 5Hz Harmonic	Skyhook Damping $C_{SH} = 400$ N-s/cm	0.50	15.07	0.56	0.19	0.90
310	10% El Centro	Feedforward Control	0.28	1.74	0.04	0.05	0.19
311	25% El Centro	Feedforward Control	0.69	3.95	0.09	0.10	0.48
312	50% El Centro	Feedforward Control	1.38	7.67	0.16	0.19	0.93
313	25% Hachinohe	Feedforward Control	0.80	3.21	0.06	0.08	0.38
314	50% Hachinohe	Feedforward Control	1.59	6.57	0.12	0.17	0.79
315	75% Hachinohe	Feedforward Control	2.38	9.98	0.17	0.25	1.22
316	50% Hachinohe - M	Feedforward Control	0.68	3.98	0.13	0.06	0.27
317	100% Hachinohe - M	Feedforward Control	1.35	7.86	0.24	0.12	0.55
318	125% Hachinohe - M	Feedforward Control	2.03	11.86	0.36	0.18	0.88
319	0.2g 5Hz Harmonic	Feedforward Control	0.21	6.19	0.21	0.09	0.39
320	0.3g 5Hz Harmonic	Feedforward Control	0.31	9.31	0.32	0.13	0.54
321	0.5g 5Hz Harmonic	Feedforward Control	0.51	15.19	0.57	0.20	0.87
322	50% Hachinohe	Feedforward Control - NEG	1.59	6.64	0.12	0.18	0.98
323	50% El Centro	Feedforward Control - NEG	1.37	7.74	0.15	0.22	1.19

Notes: C_{SH} = Skyhook Damping Coefficient
NEG = Negated Control Algorithm

Recall that the damping ratio of the flexible structure with two-stage dampers set to low and set to high damping was about 5% and about 25%, respectively (see Table 6-I). The effect of the low and high damping passive control systems on the structure subjected to the 25% El Centro ground motion is shown in Figure 9-1. Note that friction is clearly present in the low damping test. This friction occurs between the piston rod and the piston rod seal. In the high damping test, the primary source of energy dissipation appears to be through viscous fluid damping. A comparison between the low and high damping response of Figure 9-1 shows that both the base shear and the story drift are reduced by factors of 1.7 and 2.0, respectively. The large increase in damping was clearly beneficial to the structure for this particular input. In Section 9.3.1, it will be shown that for the semi-active control algorithms employed in this study, the response reduction achieved by the semi-active control system was, in general, comparable to that afforded by a high damping passive control system. The semi-active control system with the valves closed represents the "high damping passive control system".

In the shaking table tests on the one-story structure with semi-active control provided by two-stage dampers, the command signal was switched between off (digital 0) and on (digital 1). This is shown in Figure 9-2(d) for the one-story flexible structure subjected to harmonic input motion and controlled according to the base shear coefficient control algorithm. Under this control algorithm, the valve is switched on (low damping) when the base shear coefficient exceeds a specified limit which, in this case, had a value of 0.08. The valve command signal shown in Figure 9-2(d) was low pass filtered prior to data

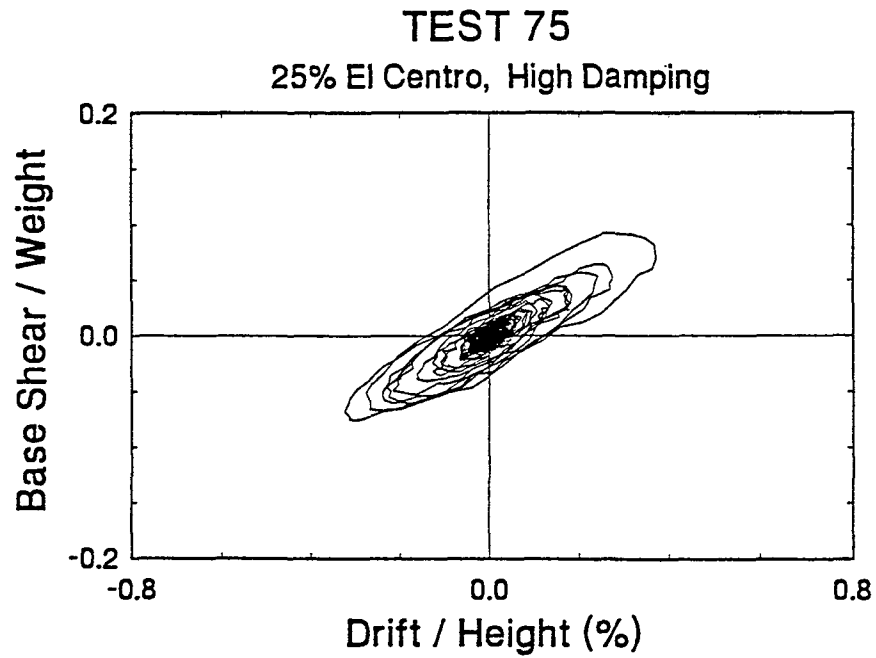
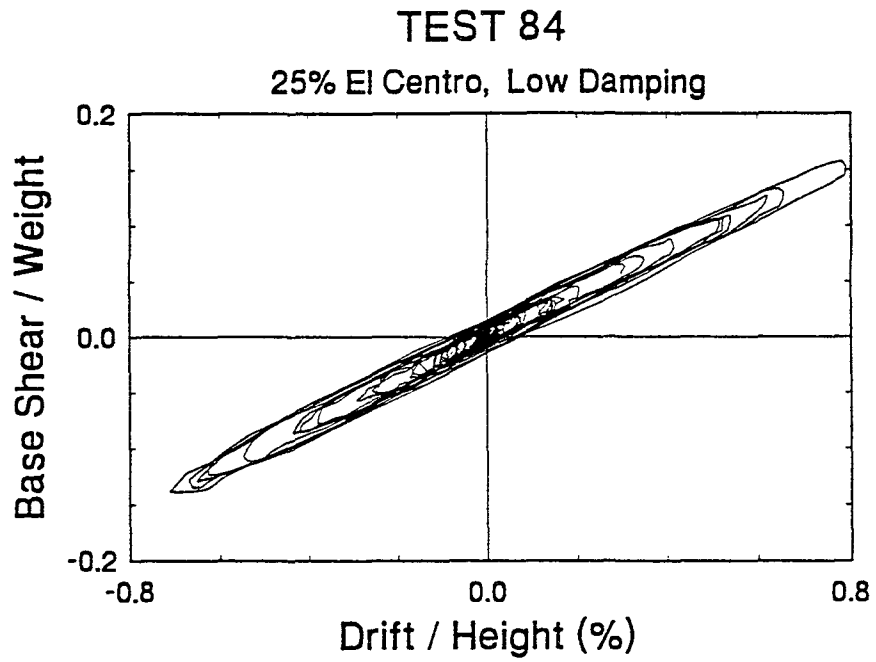


Figure 9-1 Base Shear-Drift Loops of One-Story Flexible Structure with Two-Stage Dampers Subjected to 25% El Centro and Controlled by Low and High Damping Passive Systems

TEST 142

0.2g 5 Hz Harmonic, Base Shear Control

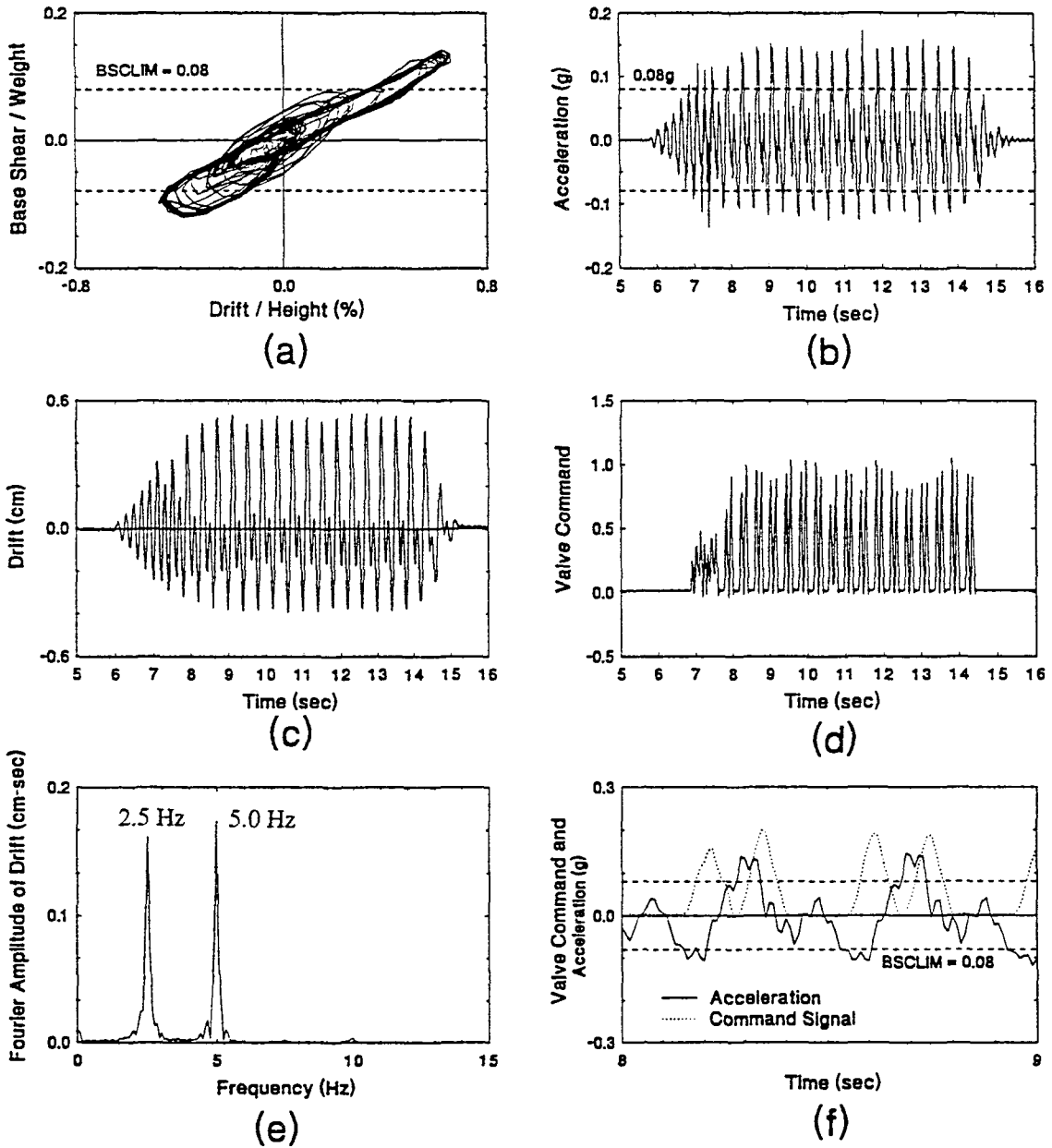


Figure 9-2 Test Results for One-Story Flexible Structure with Two-Stage Dampers Subjected to Harmonic Motion and Controlled by Base Shear Coefficient Control Algorithm

acquisition. Without filtering, the two-stage damper command signal is limited to digital values of 0 (high damping) and 1 (low damping). In Figure 9-2(f), a portion of the acceleration time history of Figure 9-2(b) is shown with the corresponding command signal of Figure 9-2(d) (the command signal was scaled for comparison with the acceleration). Note that, in accordance with the base shear coefficient control algorithm (see Section 7.2.1), the valve command switches on when the base shear coefficient exceeds 0.08 and switches off otherwise.

A careful examination of the base shear and acceleration in Figures 9-2(a) and 9-2(b), respectively, reveals that the peak base shear over weight ratio is not equal to the peak acceleration in g's. The acceleration signal is from a single accelerometer located at the first floor and was used to determine the control signal to the semi-active damper valves. The base shear over weight ratio, on the other hand, was obtained from the measured accelerations at all three floor levels and thus represents the true shear force in the first story columns.

One may note the interesting response of the structure in the test of Figure 9-2. Apparently the response contains two distinct frequencies, one at the driving frequency of the input and the other at the natural frequency of the structure (see Figure 9-2(e)). This bi-harmonic response will be explained further in Section 9.3.1.1.

In the shaking table tests on the one-story structure with variable dampers, the command signal was fully adjustable between 0.75 volts (high damping) and 2.25 volts (low damping) (see Figure 7-1). The command signal to the variable damper valves for the one-story flexible structure subjected to 100% of the modified (high frequency) Hachinohe input and controlled according to the skyhook damping control algorithm is shown in Figure 9-3(b). This command signal was not filtered prior to data acquisition. The damping coefficient corresponding to the valve command signal of Figure 9-3(b) is presented in Figure 9-3(c) and was calculated according to Equation (7-4). In Figure 9-3(d), a portion of the filtered command signal time history is shown with the corresponding filtered spool position signal for one of the variable damper units (unit VAR-A). Note that the spool position signal has been scaled for comparison with the command signal. Apparently, the spool position does not follow the command signal accurately. This is understandable since the spool cannot respond to the command signal instantaneously (see Section 3.4) and therefore follows the general shape of the command signal time history while not being able to follow the high frequency portions of the time history. As will be shown in Section 10.4, the inability of the spool to track the command signal accurately as well as the approximate damping coefficient/command signal relationship (Equation (7-4)) leads to difficulties in predicting the experimental response of the one-story and three-story structure with variable dampers. Finally, Figure 9-3(e) shows a portion of the time history of spool displacement in each of the variable damper units. The pattern of motion of the two spools is very similar except for the distance traveled by each spool. Recall that in the development of the two variable damper units,

TEST 293

100% Hachinohe-M, Skyhook Damping

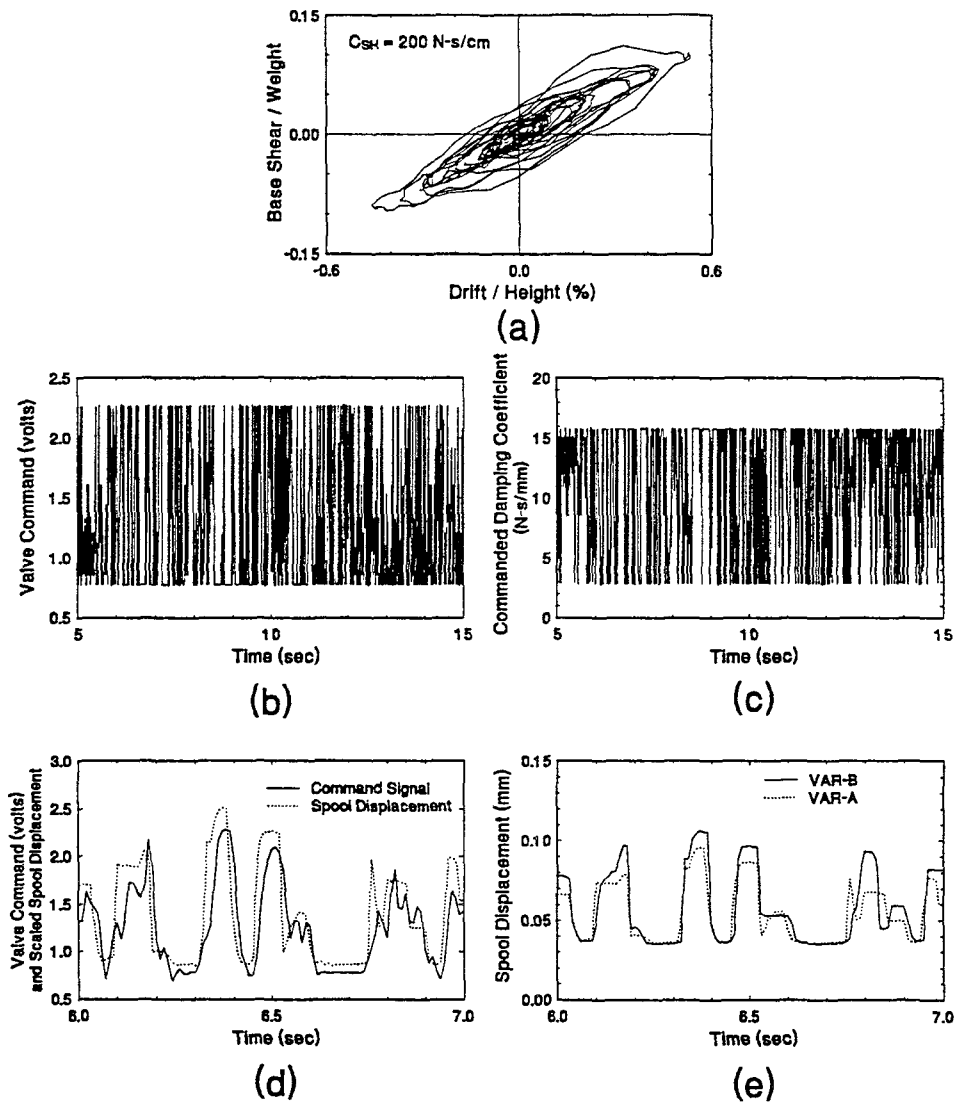


Figure 9-3 Test Results for One-Story Flexible Structure with Variable Dampers Subjected to 100% Modified Hachinohe Motion and Controlled by Skyhook Control Algorithm

there was no attempt to match the spool position versus command signal relationship (see Figure 3-10). Rather, the objective was to match the flow rate versus command signal (see Figure 3-11). This explains the difference in spool displacement of the two damper units shown in Figure 9-3(e).

9.2 Three-Story Structure

The experimental results for the three-story structure are presented in Table 9-IV for the bare frame structure and in Tables 9-V(a) and 9-V(b) for the structure with variable dampers. For each test, the peak table motion in the horizontal direction is given in Tables 9-IV and 9-V(a). The displacement and acceleration were directly measured whereas the velocity was determined by numerical differentiation of the displacement record. The peak acceleration at each floor is given in Tables 9-IV and 9-V(a) and the peak shear force at each story as a fraction of the total weight (28.1 kN) of the structure is given in Tables 9-IV and 9-V(b). Finally the peak drift of each story is given in Tables 9-IV and 9-V(b) as a percentage of the story height which was 81.3 cm for the first story and 76.2 cm for the second and third stories. Results for all of the tests on the three-story structure are presented in graphical form in Appendix E (bare frame structure) and Appendix F (structure with variable dampers). The graphs show recorded story shear force over total weight ratio versus story drift over story height ratio.

Recall that the damping ratio in the fundamental mode of the three-story structure with variable dampers set to low and set to high damping was about 4% and 14%, respectively

Table 9-IV Summary of Experimental Results for Bare Frame Three-Story Structure

TEST	EXCITATION	PEAK TABLE MOTION			PEAK ACCELERATION (g)			PEAK SHEAR FORCE / WEIGHT			PEAK DRIFT / HEIGHT (%)		
		Displ. (cm)	Veloc. (cm/s)	Accel. (g)	1st floor	2nd floor	3rd floor	1st story	2nd story	3rd story	1st story	2nd story	3rd story
191	0.05g White Noise	0.93	3.19	0.05	0.10	0.11	0.13	0.06	0.06	0.04	0.39	0.32	0.22
192	0.1g White Noise	1.88	5.98	0.11	0.18	0.17	0.23	0.11	0.10	0.08	0.69	0.55	0.37
193	10% El Centro	0.28	1.60	0.04	0.07	0.08	0.10	0.07	0.05	0.03	0.43	0.30	0.19
194	20% El Centro	0.55	3.19	0.07	0.12	0.14	0.18	0.12	0.09	0.06	0.79	0.51	0.33
195	25% El Centro	0.69	3.88	0.09	0.16	0.17	0.22	0.15	0.11	0.07	0.96	0.62	0.39
196	10% Hachinohe	0.14	1.50	0.03	0.08	0.07	0.09	0.05	0.04	0.03	0.30	0.23	0.15
197	20% Hachinohe	0.64	2.62	0.05	0.13	0.11	0.15	0.09	0.08	0.05	0.59	0.43	0.28
198	25% Hachinohe	0.80	3.41	0.06	0.16	0.14	0.19	0.11	0.10	0.06	0.74	0.52	0.34
199	30% Hachinohe	0.95	4.10	0.08	0.19	0.16	0.23	0.13	0.11	0.08	0.87	0.61	0.39
200	20% Hachinohe - M	0.30	1.64	0.05	0.07	0.09	0.09	0.06	0.05	0.03	0.37	0.27	0.16
201	40% Hachinohe - M	0.54	3.21	0.10	0.14	0.17	0.17	0.11	0.10	0.06	0.74	0.53	0.29
202	50% Hachinohe - M	0.68	3.95	0.12	0.17	0.21	0.21	0.14	0.12	0.07	0.91	0.64	0.36
203	0.2g 5Hz Harmonic	0.21	6.33	0.21	0.26	0.04	0.24	0.02	0.07	0.08	0.10	0.31	0.34
204	0.4g 5Hz Harmonic	0.41	12.36	0.44	0.52	0.07	0.48	0.04	0.14	0.16	0.16	0.59	0.68
205	0.3g 5Hz Harmonic	0.31	9.41	0.32	0.40	0.06	0.36	0.03	0.11	0.12	0.12	0.44	0.52

Table 9-V(a) Summary of Experimental Results for Three-Story Structure with Variable Dampers

TEST	EXCITATION	CONTROL ALGORITHM	PEAK TABLE MOTION			PEAK ACCELERATION (g)		
			Displ. (cm)	Veloc. (cm/s)	Acccl. (g)	1st floor	2nd floor	3rd floor
209	0.1g White Noise	Low Damping	1.88	5.72	0.11	0.11	0.13	0.14
220	10% El Centro	Low Damping	0.28	1.71	0.04	0.05	0.05	0.07
221	25% El Centro	Low Damping	0.69	3.95	0.09	0.10	0.11	0.15
222	30% El Centro	Low Damping	0.82	4.91	0.11	0.12	0.14	0.18
223	40% El Centro	Low Damping	1.10	6.50	0.13	0.17	0.19	0.25
224	25% Hachinohe	Low Damping	0.80	3.43	0.06	0.10	0.08	0.15
225	40% Hachinohe	Low Damping	1.27	5.26	0.10	0.18	0.15	0.24
226	50% Hachinohe	Low Damping	1.59	7.00	0.12	0.23	0.19	0.31
227	50% Hachinohe-M	Low Damping	0.68	3.88	0.12	0.14	0.16	0.18
228	75% Hachinohe-M	Low Damping	1.01	6.12	0.19	0.22	0.24	0.27
229	0.2g 5 Hz Harmonic	Low Damping	0.20	6.29	0.21	0.25	0.03	0.22
230	0.3g 5 Hz Harmonic	Low Damping	0.31	9.29	0.32	0.41	0.05	0.37
231	0.4g 5 Hz Harmonic	Low Damping	0.40	12.38	0.45	0.57	0.09	0.52
207	0.1g White Noise	High Damping	1.88	5.69	0.11	0.10	0.10	0.09
210	25% El Centro	High Damping	0.68	3.88	0.09	0.08	0.09	0.12
211	50% El Centro	High Damping	1.37	7.62	0.16	0.16	0.18	0.24
212	25% Hachinohe	High Damping	0.80	3.52	0.07	0.10	0.07	0.11
213	50% Hachinohe	High Damping	1.59	6.57	0.12	0.14	0.15	0.20
214	75% Hachinohe	High Damping	2.38	9.95	0.17	0.22	0.20	0.30
285	50% Hachinohe-M	High Damping	0.68	3.88	0.13	0.11	0.15	0.13
215	100% Hachinohe-M	High Damping	1.35	7.98	0.25	0.22	0.29	0.25
216	125% Hachinohe-M	High Damping	1.69	9.95	0.28	0.27	0.36	0.31

Table 9-V(a) Cont'd

TEST	EXCITATION	CONTROL ALGORITHM	PEAK TABLE MOTION			PEAK ACCELERATION (g)		
			Displ. (cm)	Veloc. (cm/s)	Accel. (g)	1st floor	2nd floor	3rd floor
217	0.2g 5 Hz Harmonic	High Damping	0.21	6.43	0.21	0.22	0.03	0.20
218	0.3g 5 Hz Harmonic	High Damping	0.31	9.22	0.32	0.35	0.04	0.31
219	0.4g 5 Hz Harmonic	High Damping	0.40	12.14	0.44	0.48	0.06	0.43
256	10% EI Centro	Optimal Control - LG	0.28	1.76	0.04	0.04	0.04	0.05
257	20% EI Centro	Optimal Control - LG	0.55	3.19	0.08	0.06	0.08	0.10
258	25% EI Centro	Optimal Control - LG	0.69	3.88	0.09	0.08	0.09	0.12
259	30% EI Centro	Optimal Control - LG	0.28	4.76	0.10	0.09	0.11	0.14
260	40% EI Centro	Optimal Control - LG	1.10	6.14	0.12	0.13	0.15	0.19
261	50% EI Centro	Optimal Control - LG	1.38	7.67	0.16	0.15	0.19	0.24
262	75% EI Centro	Optimal Control - LG	2.06	11.62	0.22	0.23	0.29	0.36
263	25% Hachinohe	Optimal Control - LG	0.79	3.29	0.06	0.09	0.07	0.12
264	50% Hachinohe	Optimal Control - LG	1.59	6.67	0.12	0.17	0.15	0.23
265	50% Hachinohe	Optimal Control - LG Signal D2HC Disturbed	1.59	6.38	0.11	0.17	0.14	0.23
266	50% Hachinohe	Optimal Control - LG Random Command	1.59	6.55	0.12	0.19	0.14	0.26
248	75% Hachinohe	Optimal Control - LG	2.39	9.95	0.16	0.21	0.21	0.32
249	50% Hachinohe-M	Optimal Control - LG	0.68	3.98	0.13	0.11	0.15	0.13
250	75% Hachinohe-M	Optimal Control - LG	1.02	5.98	0.18	0.17	0.23	0.20
251	100% Hachinohe-M	Optimal Control - LG	1.36	8.05	0.24	0.22	0.30	0.26
252	125% Hachinohe-M	Optimal Control - LG	1.70	10.10	0.30	0.27	0.35	0.31
253	0.2g 5 Hz Harmonic	Optimal Control - LG	0.20	6.45	0.20	0.23	0.03	0.20

Table 9-V(a) Cont'd

TEST	EXCITATION	CONTROL ALGORITHM	PEAK TABLE MOTION			PEAK ACCELERATION (g)		
			Displ. (cm)	Veloc. (cm/s)	Accel. (g)	1st floor	2nd floor	3rd floor
254	0.3g 5 Hz Harmonic	Optimal Control - LG	0.31	9.17	0.32	0.37	0.05	0.32
255	0.4g 5 Hz Harmonic	Optimal Control - LG	0.41	12.29	0.44	0.50	0.07	0.45
387	25% El Centro	Optimal Control - LG	0.69	4.05	0.09	0.08	0.09	0.12
388	50% El Centro	Optimal Control - LG	1.38	7.62	0.15	0.16	0.19	0.26
389	75% El Centro	Optimal Control - LG	2.06	11.69	0.22	0.27	0.29	0.41
390	25% Hachinohe	Optimal Control - HG	0.80	3.26	0.06	0.11	0.07	0.13
391	50% Hachinohe	Optimal Control - HG	1.59	6.76	0.12	0.23	0.15	0.26
392	75% Hachinohe	Optimal Control - HG	2.38	10.02	0.17	0.30	0.23	0.40
393	50% Hachinohe-M	Optimal Control - HG	0.68	4.02	0.12	0.11	0.14	0.13
394	100% Hachinohe-M	Optimal Control - HG	1.36	8.17	0.22	0.22	0.25	0.27
395	125% Hachinohe-M	Optimal Control - HG	1.70	9.98	0.27	0.26	0.28	0.34
396	0.2g 5 Hz Harmonic	Optimal Control - HG	0.21	6.38	0.22	0.23	0.03	0.20
397	0.3g 5 Hz Harmonic	Optimal Control - HG	0.44	12.24	0.45	0.53	0.07	0.46
398	0.4g 5 Hz Harmonic	Optimal Control - HG	0.51	15.43	0.58	0.66	0.10	0.59
437	25% El Centro	Optimal Control - LG, HC	0.69	3.95	0.09	0.08	0.09	0.12
438	50% El Centro	Optimal Control - LG, HC	1.37	7.74	0.15	0.13	0.18	0.20
439	75% El Centro	Optimal Control - LG, HC	2.06	11.67	0.22	0.18	0.25	0.30
440	25% Hachinohe	Optimal Control - LG, HC	0.80	3.31	0.06	0.10	0.07	0.12
441	50% Hachinohe	Optimal Control - LG, HC	1.59	6.55	0.12	0.15	0.15	0.22
442	75% Hachinohe	Optimal Control - LG, HC	2.39	9.86	0.17	0.23	0.21	0.32
443	100% Hachinohe	Optimal Control - LG, HC	3.18	13.36	0.22	0.35	0.29	0.49
444	50% Hachinohe-M	Optimal Control - LG, HC	0.68	3.95	0.11	0.09	0.13	0.13

Table 9-V(a) Cont'd

TEST	EXCITATION	CONTROL ALGORITHM	PEAK TABLE MOTION			PEAK ACCELERATION (g)		
			Displ. (cm)	Veloc. (cm/s)	Accel. (g)	1st floor	2nd floor	3rd floor
445	100% Hachinohe-M	Optimal Control - LG, HC	1.36	7.98	0.23	0.20	0.25	0.25
446	125% Hachinohe-M	Optimal Control - LG, HC	1.70	10.17	0.30	0.26	0.32	0.33
447	0.2g 5 Hz Harmonic	Optimal Control - LG, HC	0.21	6.41	0.22	0.24	0.03	0.21
448	0.3g 5 Hz Harmonic	Optimal Control - LG, HC	0.32	9.41	0.34	0.39	0.06	0.34
449	0.4g 5 Hz Harmonic	Optimal Control - LG, HC	0.42	12.38	0.45	0.53	0.08	0.46
425	25% EI Centro	Optimal Control - HG, HC	0.69	3.88	0.09	0.07	0.08	0.11
426	50% EI Centro	Optimal Control - HG, HC	1.38	7.74	0.15	0.14	0.17	0.24
427	75% EI Centro	Optimal Control - HG, HC	2.06	11.91	0.22	0.28	0.29	0.35
428	25% Hachinohe	Optimal Control - HG, HC	0.80	3.41	0.07	0.09	0.08	0.11
429	50% Hachinohe	Optimal Control - HG, HC	1.59	6.52	0.12	0.14	0.15	0.21
430	75% Hachinohe	Optimal Control - HG, HC	2.39	9.81	0.17	0.23	0.21	0.32
431	100% Hachinohe	Optimal Control - HG, HC	3.19	13.31	0.22	0.30	0.26	0.44
432	50% Hachinohe-M	Optimal Control - HG, HC	0.68	4.10	0.12	0.08	0.13	0.12
450	100% Hachinohe-M	Optimal Control - HG, HC	1.36	8.05	0.23	0.20	0.25	0.26
451	125% Hachinohe-M	Optimal Control - HG, HC	1.70	10.26	0.28	0.24	0.30	0.33
434	0.2g 5 Hz Harmonic	Optimal Control - HG, HC	0.21	6.45	0.22	0.24	0.03	0.21
435	0.3g 5 Hz Harmonic	Optimal Control - HG, HC	0.31	9.48	0.33	0.38	0.05	0.34
436	0.4g 5 Hz Harmonic	Optimal Control - HG, HC	0.41	13.05	0.45	0.53	0.08	0.46
376	25% EI Centro	Sliding Mode Control	0.70	4.10	0.08	0.09	0.10	0.13
377	50% EI Centro	Sliding Mode Control	1.38	7.72	0.15	0.18	0.19	0.22
378	75% EI Centro	Sliding Mode Control	2.06	11.57	0.22	0.28	0.28	0.30
379	25% Hachinohe	Sliding Mode Control	0.80	3.24	0.06	0.11	0.07	0.14

Table 9-V(a) Cont'd

TEST	EXCITATION	CONTROL ALGORITHM	PEAK TABLE MOTION			PEAK ACCELERATION (g)		
			Displ. (cm)	Veloc. (cm/s)	Accel. (g)	1st floor	2nd floor	3rd floor
380	50% Hachinohe	Sliding Mode Control	1.59	6.83	0.12	0.19	0.14	0.25
381	75% Hachinohe	Sliding Mode Control	2.38	10.00	0.17	0.31	0.25	0.42
382	50% Hachinohe - M	Sliding Mode Control	0.07	4.05	0.11	0.10	0.13	0.15
383	100% Hachinohe - M	Sliding Mode Control	1.36	8.02	0.22	0.24	0.30	0.33
384	0.2g 5 Hz Harmonic	Sliding Mode Control	0.29	6.45	0.21	0.23	0.03	0.20
385	0.3g 5 Hz Harmonic	Sliding Mode Control	0.31	9.50	0.33	0.38	0.05	0.33
386	0.4g 5 Hz Harmonic	Sliding Mode Control	0.41	12.24	0.45	0.52	0.07	0.45

Notes: Test 265 - Displacement Transducer Intentionally Disturbed During Test
 Test 266 - Power Supply to Valves Intentionally Switched On and Off Randomly During Test
 LG = Optimal Control Low Gains
 HG = Optimal Control High Gains
 HC = Harmonic Compensation

Table 9-V(b) Summary of Experimental Results for Three-Story Structure with Variable Dampers

TEST	EXCITATION	CONTROL ALGORITHM	PEAK SHEAR FORCE / WEIGHT			PEAK DRIFT / HEIGHT (%)		
			1st story	2nd story	3rd story	1st story	2nd story	3rd story
209	0.1g White Noise	Low Damping	0.08	0.07	0.05	0.45	0.34	0.23
220	10% El Centro	Low Damping	0.03	0.03	0.02	0.18	0.16	0.11
221	25% El Centro	Low Damping	0.10	0.08	0.05	0.66	0.48	0.29
222	30% El Centro	Low Damping	0.13	0.10	0.06	0.84	0.59	0.35
223	40% El Centro	Low Damping	0.18	0.14	0.08	1.16	0.80	0.47
224	25% Hachinohe	Low Damping	0.07	0.07	0.05	0.42	0.35	0.25
225	40% Hachinohe	Low Damping	0.12	0.11	0.08	0.78	0.58	0.40
226	50% Hachinohe	Low Damping	0.16	0.14	0.10	1.04	0.72	0.51
227	50% Hachinohe-M	Low Damping	0.11	0.10	0.06	0.71	0.52	0.31
228	75% Hachinohe-M	Low Damping	0.17	0.15	0.09	1.11	0.81	0.45
229	0.2g 5 Hz Harmonic	Low Damping	0.02	0.06	0.07	0.06	0.29	0.31
230	0.3g 5 Hz Harmonic	Low Damping	0.03	0.11	0.12	0.12	0.44	0.52
231	0.4g 5 Hz Harmonic	Low Damping	0.04	0.15	0.17	0.16	0.60	0.72
207	0.1g White Noise	High Damping	0.07	0.05	0.03	0.38	0.28	0.17
210	25% El Centro	High Damping	0.07	0.05	0.04	0.38	0.29	0.18
211	50% El Centro	High Damping	0.14	0.11	0.08	0.79	0.58	0.36
212	25% Hachinohe	High Damping	0.06	0.05	0.04	0.29	0.28	0.19
213	50% Hachinohe	High Damping	0.11	0.11	0.07	0.59	0.56	0.36
214	75% Hachinohe	High Damping	0.16	0.16	0.10	0.92	0.84	0.53
285	50% Hachinohe-M	High Damping	0.07	0.05	0.04	0.37	0.28	0.19
215	100% Hachinohe-M	High Damping	0.14	0.11	0.08	0.81	0.58	0.37
216	125% Hachinohe-M	High Damping	0.17	0.14	0.10	1.01	0.73	0.46

Table 9-V(b) Cont'd

TEST	EXCITATION	CONTROL ALGORITHM	PEAK SHEAR FORCE / WEIGHT			PEAK DRIFT / HEIGHT (%)		
			1st story	2nd story	3rd story	1st story	2nd story	3rd story
217	0.2g 5 Hz Harmonic	High Damping	0.02	0.06	0.07	0.03	0.26	0.29
218	0.3g 5 Hz Harmonic	High Damping	0.03	0.09	0.10	0.06	0.41	0.45
219	0.4g 5 Hz Harmonic	High Damping	0.04	0.13	0.14	0.08	0.56	0.61
256	10% El Centro	Optimal Control - LG	0.03	0.02	0.02	0.14	0.13	0.08
257	20% El Centro	Optimal Control - LG	0.06	0.04	0.03	0.30	0.24	0.17
258	25% El Centro	Optimal Control - LG	0.07	0.06	0.04	0.40	0.30	0.19
259	30% El Centro	Optimal Control - LG	0.09	0.07	0.05	0.49	0.36	0.23
260	40% El Centro	Optimal Control - LG	0.11	0.19	0.06	0.65	0.48	0.29
261	50% El Centro	Optimal Control - LG	0.14	0.11	0.08	0.81	0.60	0.35
262	75% El Centro	Optimal Control - LG	0.20	0.16	0.12	1.23	0.86	0.53
263	25% Hachinohe	Optimal Control - LG	0.06	0.05	0.04	0.31	0.28	0.21
264	50% Hachinohe	Optimal Control - LG	0.11	0.11	0.08	0.59	0.57	0.40
265	50% Hachinohe	Optimal Control - LG	0.11	0.11	0.08	0.66	2.16	1.97
266	50% Hachinohe	Optimal Control - LG	0.12	0.11	0.09	0.76	0.60	0.43
248	75% Hachinohe	Optimal Control - LG	0.16	0.17	0.11	0.95	0.87	0.56
249	50% Hachinohe-M	Optimal Control - LG	0.07	0.06	0.04	0.41	0.29	0.19
250	75% Hachinohe-M	Optimal Control - LG	0.11	0.09	0.07	0.61	0.44	0.30
251	100% Hachinohe-M	Optimal Control - LG	0.15	0.12	0.09	0.85	0.63	0.37
252	125% Hachinohe-M	Optimal Control - LG	0.18	0.14	0.10	1.05	0.74	0.47
253	0.2g 5 Hz Harmonic	Optimal Control - LG	0.02	0.06	0.07	0.04	0.27	0.29
254	0.3g 5 Hz Harmonic	Optimal Control - LG	0.03	0.10	0.11	0.07	0.42	0.46
255	0.4g 5 Hz Harmonic	Optimal Control - LG	0.04	0.13	0.15	0.11	0.58	0.64

Table 9-V(b) Cont'd

TEST	EXCITATION	CONTROL ALGORITHM	PEAK SHEAR FORCE / WEIGHT			PEAK DRIFT / HEIGHT (%)		
			1st story	2nd story	3rd story	1st story	2nd story	3rd story
387	25% El Centro	Optimal Control - HG	0.08	0.06	0.04	0.46	0.33	0.19
388	50% El Centro	Optimal Control - HG	0.16	0.13	0.09	0.96	0.70	0.42
389	75% El Centro	Optimal Control - HG	0.22	0.19	0.14	1.15	1.04	0.65
390	25% Hachinohe	Optimal Control - HG	0.06	0.05	0.04	0.31	0.28	0.21
391	50% Hachinohe	Optimal Control - HG	0.11	0.11	0.09	0.69	0.57	0.41
392	75% Hachinohe	Optimal Control - HG	0.17	0.16	0.13	1.08	0.85	0.64
393	50% Hachinohe-M	Optimal Control - HG	0.07	0.06	0.04	0.48	0.34	0.23
394	100% Hachinohe-M	Optimal Control - HG	0.16	0.14	0.09	1.00	0.71	0.44
395	125% Hachinohe-M	Optimal Control - HG	0.20	0.17	0.11	1.26	0.91	0.55
396	0.2g 5 Hz Harmonic	Optimal Control - HG	0.02	0.06	0.07	0.06	0.27	0.29
397	0.3g 5 Hz Harmonic	Optimal Control - HG	0.04	0.14	0.15	0.12	0.59	0.66
398	0.4g 5 Hz Harmonic	Optimal Control - HG	0.05	0.17	0.20	0.16	0.73	0.84
437	25% El Centro	Optimal Control - LG, HC	0.07	0.06	0.04	0.43	0.31	0.19
438	50% El Centro	Optimal Control - LG, HC	0.14	0.11	0.07	0.86	0.61	0.36
439	75% El Centro	Optimal Control - LG, HC	0.23	0.17	0.10	1.42	0.91	0.56
440	25% Hachinohe	Optimal Control - LG, HC	0.06	0.05	0.04	0.31	0.29	0.21
441	50% Hachinohe	Optimal Control - LG, HC	0.11	0.11	0.07	0.59	0.58	0.38
442	75% Hachinohe	Optimal Control - LG, HC	0.15	0.16	0.11	0.94	0.88	0.55
443	100% Hachinohe	Optimal Control - LG, HC	0.20	0.21	0.16	1.31	1.15	0.76
444	50% Hachinohe-M	Optimal Control - LG, HC	0.08	0.06	0.04	0.42	0.31	0.19
445	100% Hachinohe-M	Optimal Control - LG, HC	0.15	0.12	0.08	0.85	0.61	0.38
446	125% Hachinohe-M	Optimal Control - LG, HC	0.21	0.17	0.11	1.42	0.93	0.58

Table 9-V(b) Cont'd

TEST	EXCITATION	CONTROL ALGORITHM	PEAK SHEAR FORCE / WEIGHT			PEAK DRIFT / HEIGHT (%)		
			1st story	2nd story	3rd story	1st story	2nd story	3rd story
447	0.2g 5 Hz Harmonic	Optimal Control - LG, HC	0.02	0.06	0.07	0.06	0.28	0.31
448	0.3g 5 Hz Harmonic	Optimal Control - LG, HC	0.03	0.10	0.11	0.08	0.43	0.48
449	0.4g 5 Hz Harmonic	Optimal Control - LG, HC	0.05	0.13	0.16	0.12	0.58	0.65
425	25% El Centro	Optimal Control - HG, HC	0.07	0.06	0.04	0.39	0.30	0.18
426	50% El Centro	Optimal Control - HG, HC	0.15	0.13	0.08	0.90	0.69	0.43
427	75% El Centro	Optimal Control - HG, HC	0.26	0.18	0.12	1.60	1.08	0.57
428	25% Hachinohe	Optimal Control - HG, HC	0.06	0.05	0.04	0.31	0.28	0.19
429	50% Hachinohe	Optimal Control - HG, HC	0.11	0.11	0.07	0.60	0.58	0.36
430	75% Hachinohe	Optimal Control - HG, HC	0.15	0.16	0.11	0.93	0.85	0.54
431	100% Hachinohe	Optimal Control - HG, HC	0.20	0.21	0.15	1.14	1.13	0.72
432	50% Hachinohe-M	Optimal Control - HG, HC	0.07	0.06	0.04	0.40	0.30	0.18
450	100% Hachinohe-M	Optimal Control - HG, HC	0.16	0.13	0.09	0.98	0.74	0.46
451	125% Hachinohe-M	Optimal Control - HG, HC	0.20	0.17	0.11	1.35	0.96	0.58
434	0.2g 5 Hz Harmonic	Optimal Control - HG, HC	0.02	0.06	0.07	0.06	0.28	0.31
435	0.3g 5 Hz Harmonic	Optimal Control - HG, HC	0.03	0.10	0.11	0.09	0.43	0.48
436	0.4g 5 Hz Harmonic	Optimal Control - HG, HC	0.05	0.13	0.15	0.12	0.59	0.65
376	25% El Centro	Sliding Mode Control	0.08	0.06	0.04	0.46	0.33	0.21
377	50% El Centro	Sliding Mode Control	0.14	0.11	0.07	0.90	0.60	0.35
378	75% El Centro	Sliding Mode Control	0.21	0.16	0.10	1.33	0.84	0.49
379	25% Hachinohe	Sliding Mode Control	0.06	0.06	0.05	0.38	0.31	0.22
380	50% Hachinohe	Sliding Mode Control	0.12	0.11	0.08	0.79	0.59	0.41
381	75% Hachinohe	Sliding Mode Control	0.19	0.17	0.14	1.22	0.90	0.66

Table 9-V(b) Cont'd

TEST	EXCITATION	CONTROL ALGORITHM	PEAK SHEAR FORCE / WEIGHT			PEAK DRIFT / HEIGHT (%)		
			1st story	2nd story	3rd story	1st story	2nd story	3rd story
382	50% Hachinohe - M	Sliding Mode Control	0.09	0.08	0.05	0.57	0.42	0.26
383	100% Hachinohe - M	Sliding Mode Control	0.18	0.15	0.11	1.22	0.83	0.52
384	0.2g 5 Hz Harmonic	Sliding Mode Control	0.02	0.06	0.07	0.06	0.27	0.30
385	0.3g 5 Hz Harmonic	Sliding Mode Control	0.03	0.10	0.11	0.08	0.42	0.47
386	0.4g 5 Hz Harmonic	Sliding Mode Control	0.04	0.13	0.15	0.12	0.57	0.64

Notes: Test 265 - Displacement Transducer Intentionally Disturbed During Test
 Test 266 - Power Supply to Valves Intentionally Switched On and Off Randomly During Test
 LG = Optimal Control Low Gains
 HG = Optimal Control High Gains
 HC = Harmonic Compensation

(see Table 6-II). The effect of the low and high damping on the structure subjected to the 25% El Centro ground motion is shown in Figure 9-4. A comparison between the low and high damping response of Figure 9-4 reveals that the first story shear and first story drift are reduced by factors of 1.5 and 1.8, respectively. Similar reductions are obtained in the second and third stories. The large increase in damping was clearly beneficial to the structure for this particular input. In Section 9.3.1, it will be shown that for the semi-active control algorithms employed in this study, the response reduction achieved by the semi-active control system was, in general, comparable to that afforded by a high damping passive control system. The semi-active control system with the valves closed represents the "high damping passive control system".

In some of the semi-active control tests on the three-story structure, the value of the unbounded damping coefficient for the optimal control algorithm was recorded (see Equation (7-53)). The time history of the unbounded damping coefficient for one of the semi-active control tests is shown in Figure 9-5 along with the corresponding unfiltered valve command signal (command signal is scaled up by a factor of 75). The negative values of the unbounded damping coefficient indicate that the control algorithm requires that energy be supplied to the structure from the dampers. However, the dampers can only extract energy from the structure as implied by the minimum bound on the damping coefficient. Note that the command signal is "clipped" when the unbounded damping coefficient exceeds the maximum available damping coefficient, C_{\max} , or when the unbounded damping coefficient is reduced to values below the minimum available

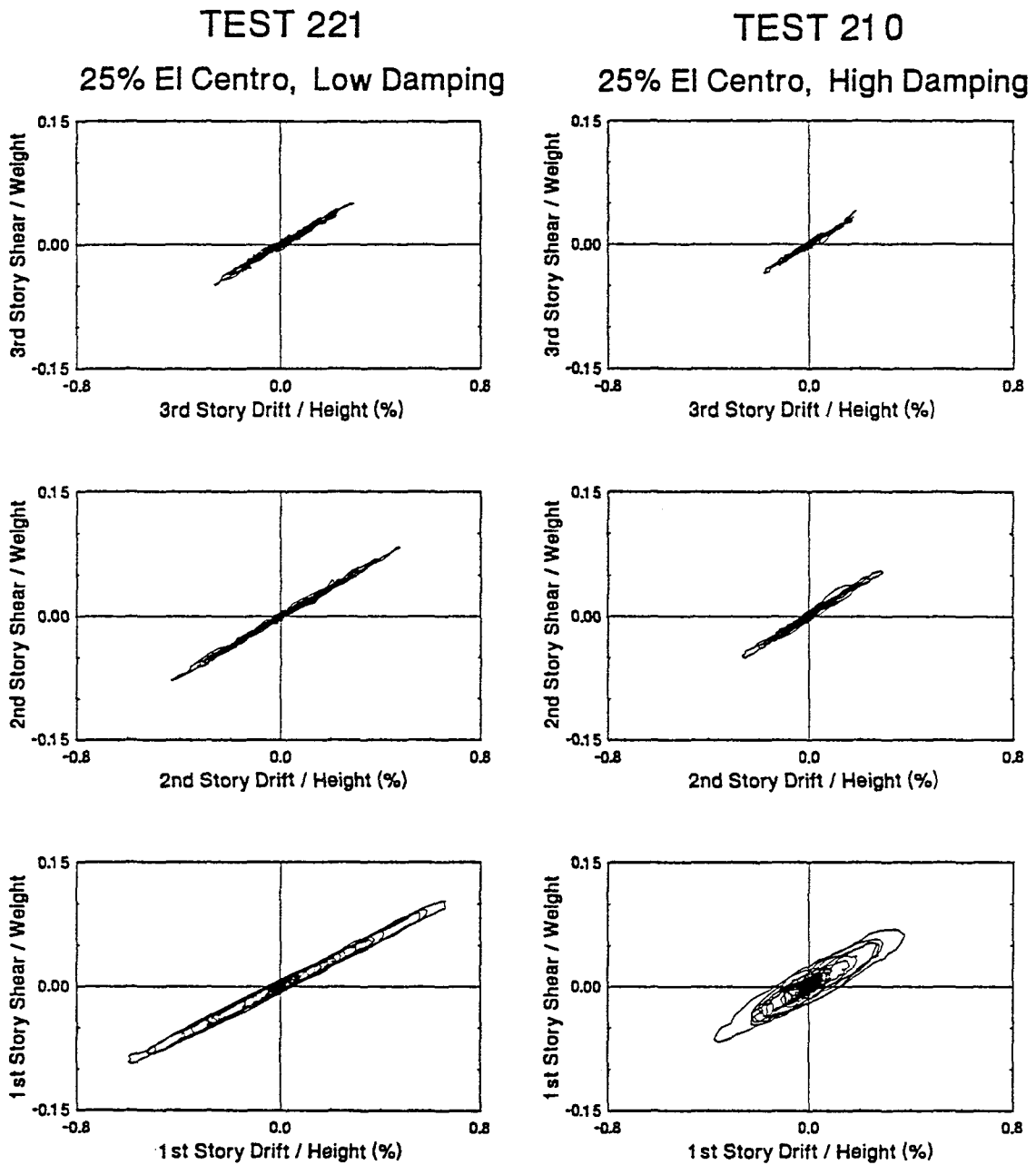


Figure 9-4 Test Results for Three-Story Structure with Variable Dampers Subjected to 25% El Centro Motion and Controlled by Low and High Damping Passive Control Systems

TEST 451

125% Hachinohe-M, Optimal Control - HG,HC

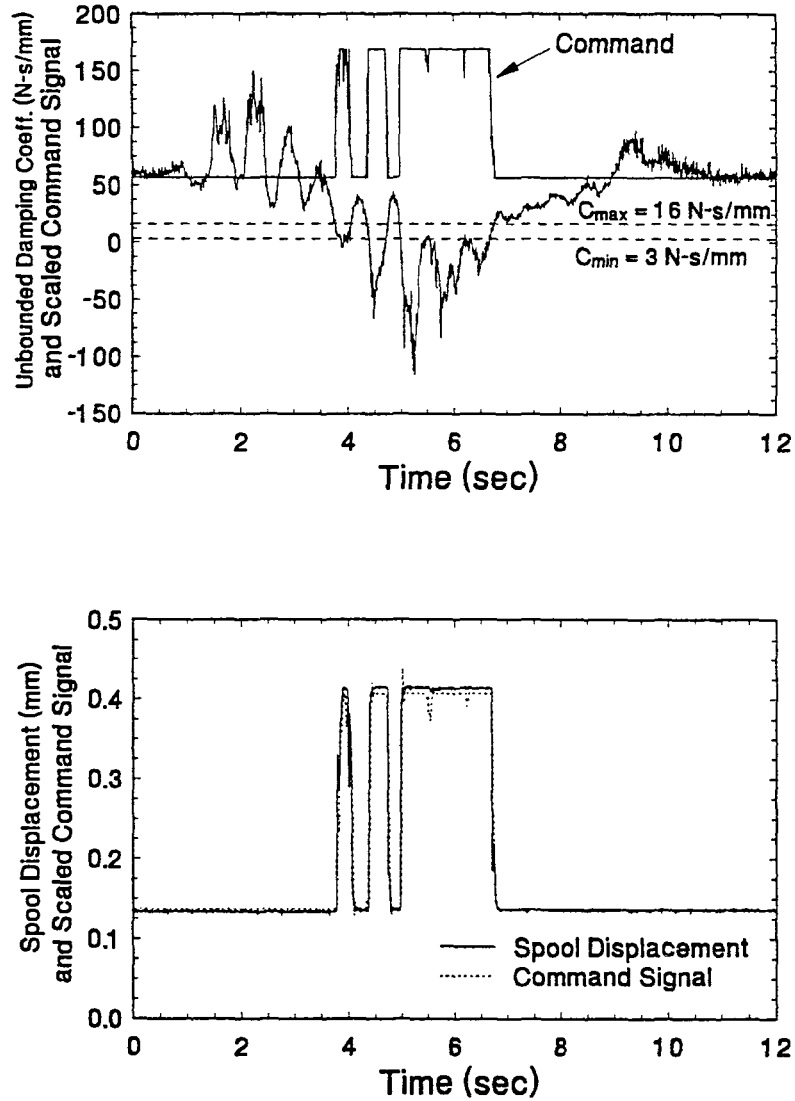


Figure 9-5 Test Results for Three-Story Structure with Variable Dampers Subjected to 125% Modified Hachinohe Motion and Controlled by Optimal Control Algorithm with High Gains and Harmonic Compensation

damping coefficient, C_{\min} . Furthermore, the filtered spool displacement time history of variable damper unit VAR-B is plotted in Figure 9-5 along with the corresponding filtered valve command signal (command signal is scaled down by a factor of about 5.6). The shape of the two sets of data compare quite well since the command signal is relatively smooth. As discussed in Section 9.1, the spool in the variable damper is not capable of accurately following high frequency command signals.

9.3 Effectiveness of Semi-Active Control

A number of shaking table test results were selected for evaluating the effectiveness of semi-active control. Comparisons in terms of peak response reduction for the one-story and three-story structure are presented in Section 9.3.1 in the form of bar charts (one-story structure) and response profiles (three-story structure). In the case of the one-story structure, comparisons are presented in this section in terms of base shear versus drift loops.

Two tests are compared in Figure 9-6 for the one-story flexible structure with two-stage dampers subjected to the 50% Hachinohe ground motion. In one case, the valves are closed to provide high damping while in the second case the base shear coefficient algorithm is employed with a base shear coefficient limit of 0.1. The peak base shear is reduced by about 6% while the peak drift is increased by about 6%. Therefore the semi-active control was marginally effective in meeting the objective of reducing the peak base shear. However, a penalty is paid in terms of an increase in story drift. Note that

TEST 78 & 140
50% Hachinohe

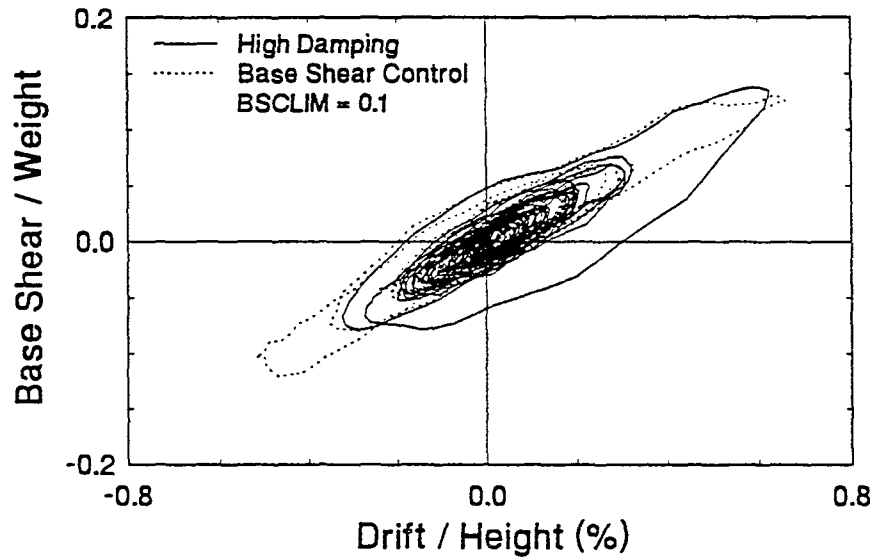


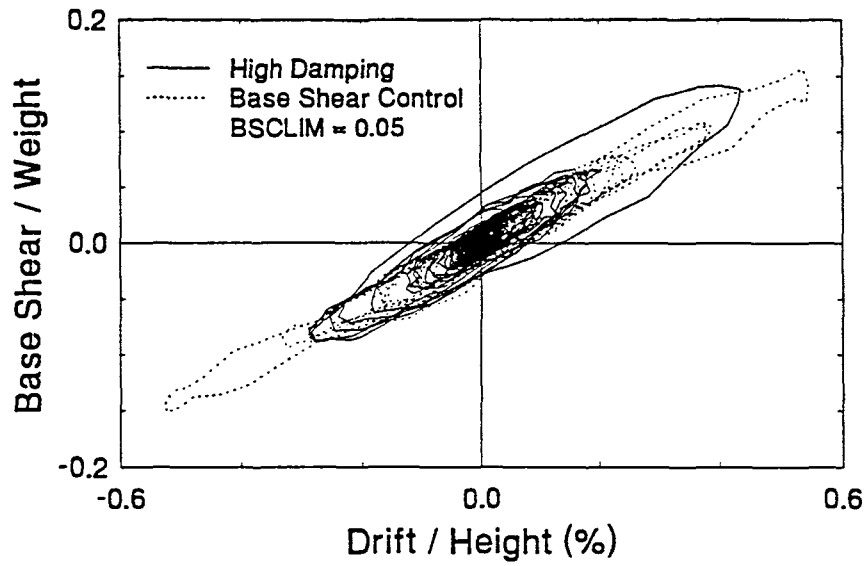
Figure 9-6 Base Shear-Drift Loop of One-Story Flexible Structure with Two-Stage Dampers Subjected to 50% Hachinohe Motion and Controlled by High Damping Passive Control System and Semi-Active Damping Control System

time delay compensation was not utilized in the semi-active control test. Further, note that the effectiveness of the semi-active control system is being evaluated based on comparisons with a high damping passive control system. If comparisons were made with the bare frame response, dramatic reductions in response would be observed with the semi-active control system.

Two comparisons are made in Figure 9-7 for the one-story stiff structure with two-stage dampers subjected to the 25% El Centro ground motion. The base shear coefficient control algorithm is used in both comparisons but with different values of the base shear coefficient limit (BSCLIM). Clearly, the effectiveness of the control depends on the appropriate selection of the value of BSCLIM. In Figure 9-7(a), the value of BSCLIM is relatively low and causes the semi-active damper valves to switch on during a major portion of the earthquake event resulting in an increase in base shear and drift by about 11% and 25%, respectively. Employing a more appropriate value of BSCLIM, Figure 9-7(b) indicates that the peak base shear is reduced by about 9% while the peak drift is essentially unchanged. Note that, once again, the evaluation of the effectiveness of the semi-active control system is based on comparisons with a high damping passive control system.

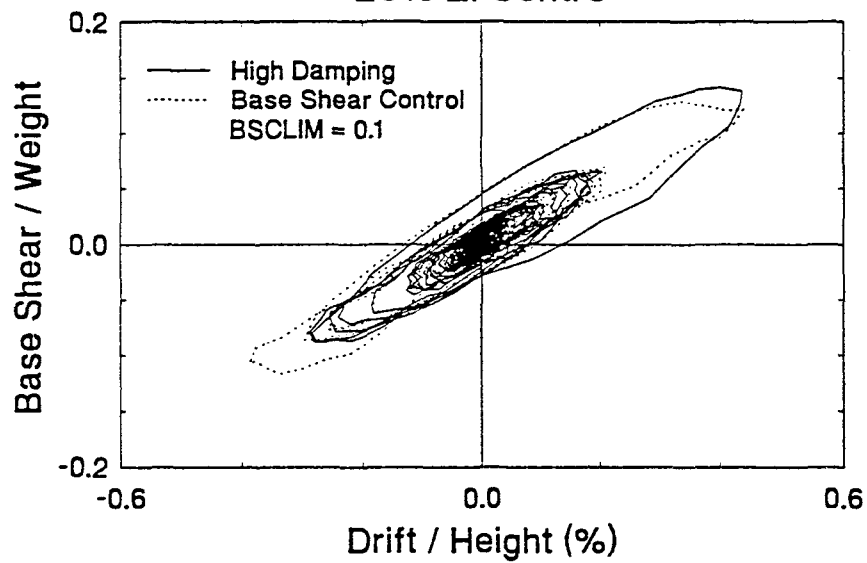
The base shear coefficient control algorithm is impractical for two reasons. First, to limit the base shear coefficient below a prescribed level requires instantaneous control of the two-stage dampers (Shinozuka 1992). Secondly, although improvements were achieved

TEST 17 & 29
25% El Centro



(a)

TEST 17 & 51
25% El Centro



(b)

Figure 9-7 Base Shear-Drift Loops of One-Story Stiff Structure with Two-Stage Dampers Subjected to 25% El Centro Motion and Controlled by High Damping Passive Control System and Base Shear Coefficient Control Algorithm

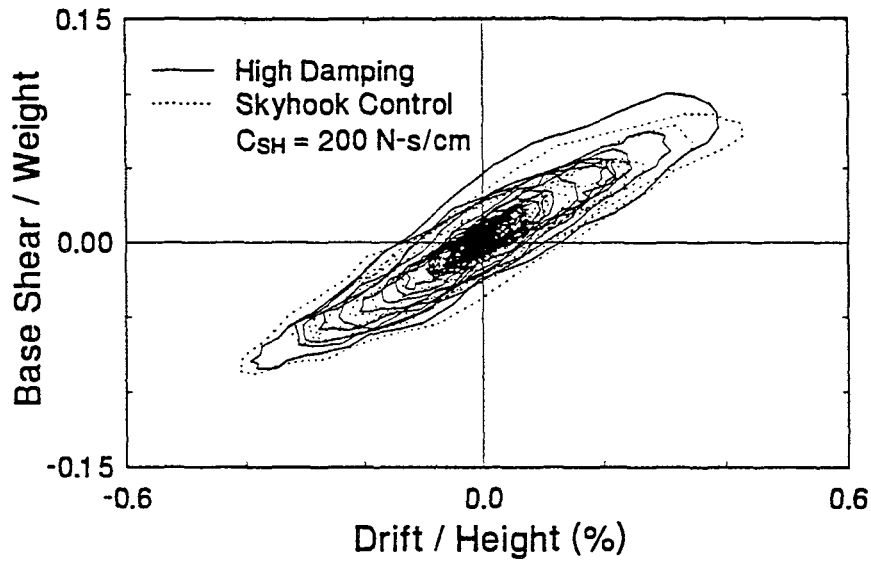
with this control algorithm, previous knowledge of the earthquake input was available and utilized for fine tuning the value of the base shear coefficient limit.

Figure 9-8 shows response comparisons under two different earthquakes and the same control algorithm (skyhook control) applied to the one-story flexible structure with semi-active variable dampers. Under the input of 25% El Centro (Figure 9-8(a)), the peak base shear is reduced by about 13% while the peak drift is increased by about 9%. Under the input of 100% Hachinohe-M (Figure 9-8(b)), the peak base shear is reduced by about 10% while the peak drift is essentially unchanged. Note that, once again, the evaluation of the effectiveness of the semi-active control system is based on comparisons with a high damping passive control system.

9.3.1 Reduction of Peak Response

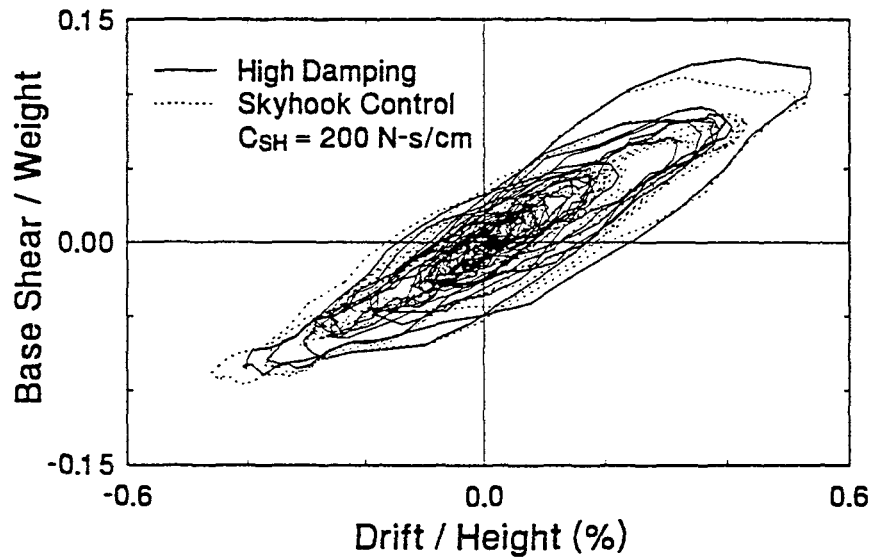
The peak response of selected tests are compared in this section for both the one-story and three-story structure in terms of story shear forces and story drifts. The notation used for comparing the results of these tests is shown in Table 9-VI. The low and high damping cases shown in Table 9-VI refer to the structure with semi-active dampers in which the damper valves are completely open (low damping) or completely closed (high damping).

TEST 155 & 287
25% El Centro



(a)

TEST 159 & 293
100% Hachinohe-M



(b)

Figure 9-8 Base Shear-Drift Loops of One-Story Flexible Structure with Variable Dampers Subjected to Two Different Ground Motions and Controlled by High Damping Passive Control System and Skyhook Control Algorithm

Table 9-VI Notation for Shaking Table Test Results

NOTATION	DESCRIPTION
BF	Bare Frame Structure
BF*	Extrapolated Results for Bare Frame Structure Assuming Linear Elastic Behavior
LD	Low Damping
HD	High Damping
BSC #	Base Shear Control (BSCLIM = #)
FTC	Force Transfer Control
SKY #	Skyhook Control ($C_{SH} = \# \text{ N-s/cm}$)
FF	Feedforward Control
KC	Kinematic Compensation
HC	Harmonic Compensation
OPT	Optimal Control
LG	Low Gains
HG	High Gains

9.3.1.1 One-Story Structure

For tests on the one-story structure, comparisons are made between the semi-active control tests, the low and high damping passive control tests, and the bare frame tests. The results for the one-story bare frame tests are obtained by extrapolating results from bare frame tests subjected to smaller levels of the same earthquake. The extrapolation is based on the assumption that linear elastic behavior is valid under the stronger levels of earthquake motion. In reality, the bare frame structure would have probably yielded at the stronger earthquake levels and therefore the values of peak base shear are overestimated while the values of peak drift are underestimated.

Figures 9-9 through 9-11 show bar charts which compare peak base shear and peak drift of the one-story structure subjected to the four different shaking table motions described in Section 5.3 and controlled by the semi-active two-stage dampers using the control algorithms described in Section 7.2. Furthermore, Figures 9-12 and 9-13 show similar comparisons with the structure controlled by the semi-active variable dampers using the control algorithms described in Section 7.3. The values corresponding to the height of each bar in Figures 9-9 through 9-13 are available in Tables 9-I, 9-II, and 9-III.

A number of observations can be made based on the results shown in Figures 9-9 through 9-13. Under earthquake loading, the peak response for the semi-active control tests is typically between the peak response corresponding to the low and high damping passive

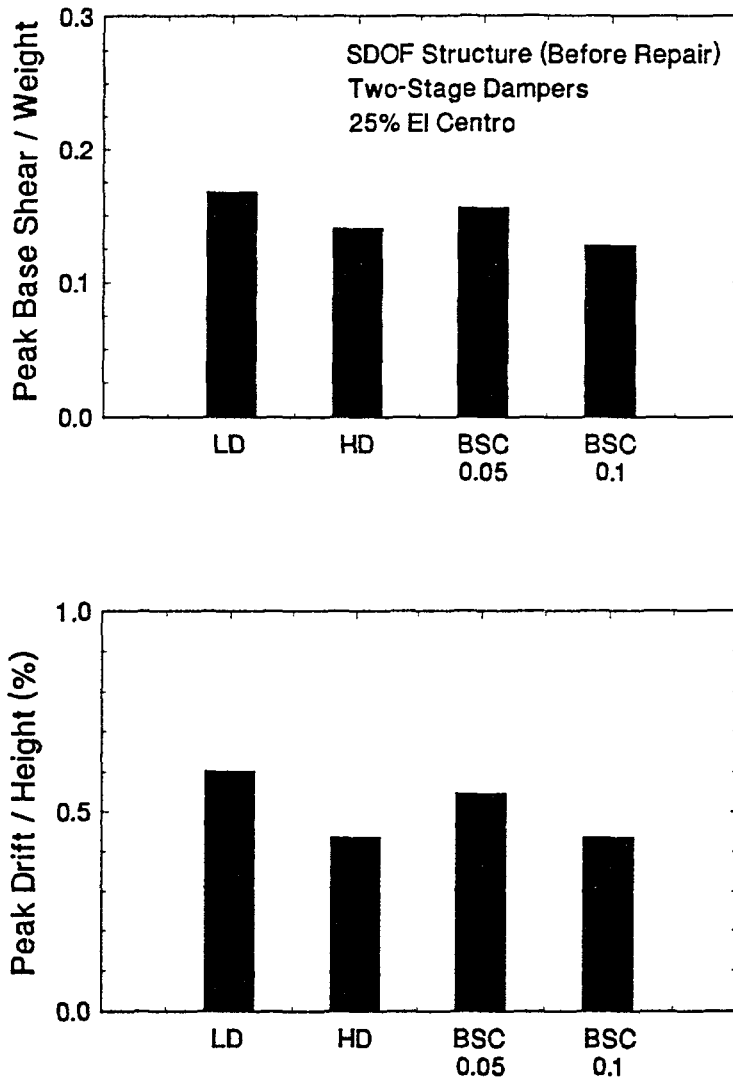


Figure 9-9 Comparisons of Peak Response of the Stiff One-Story Structure with Two-Stage Dampers Subjected to 25% El Centro Motion

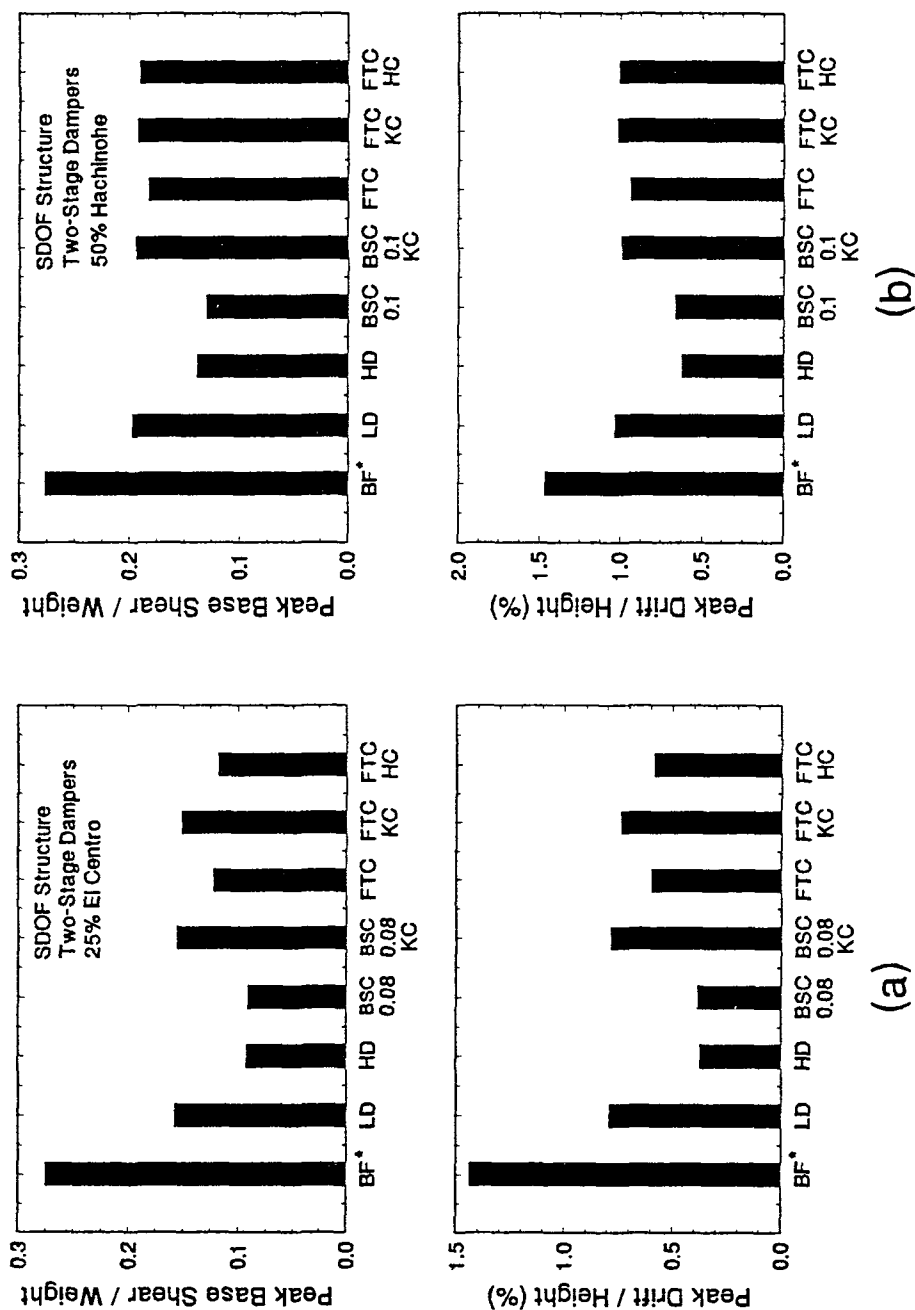


Figure 9-10 Comparisons of Peak Response of the Flexible One-Story Structure with Two-Stage Dampers Subjected to a) 25% EI Centro Motion and b) 50% Hachinohe Motion

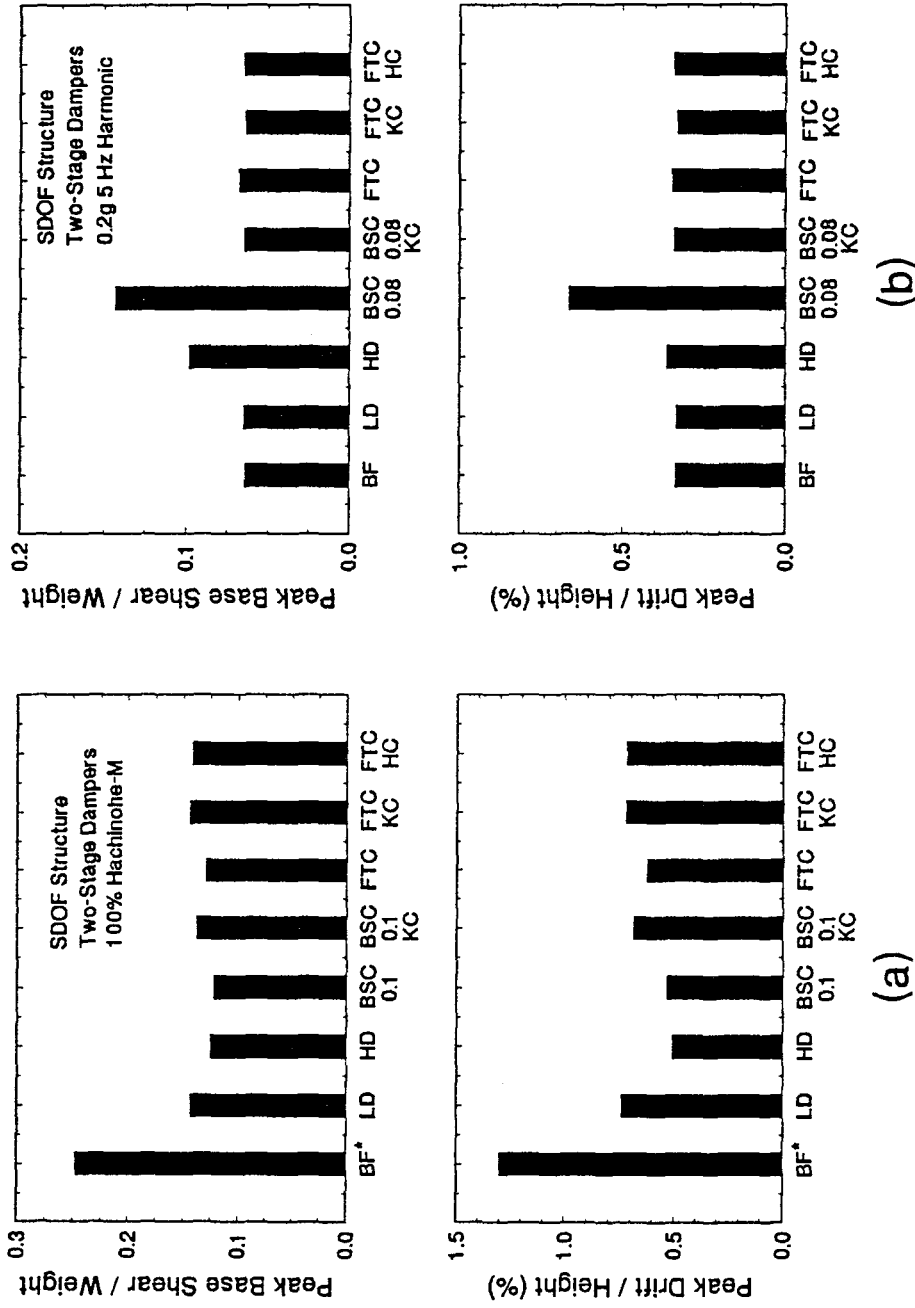


Figure 9-11 Comparisons of Peak Response of Flexible One-Story Structure with Two-Stage Dampers Subjected to a) 100% Modified Hachinohe Motion and b) Harmonic Motion

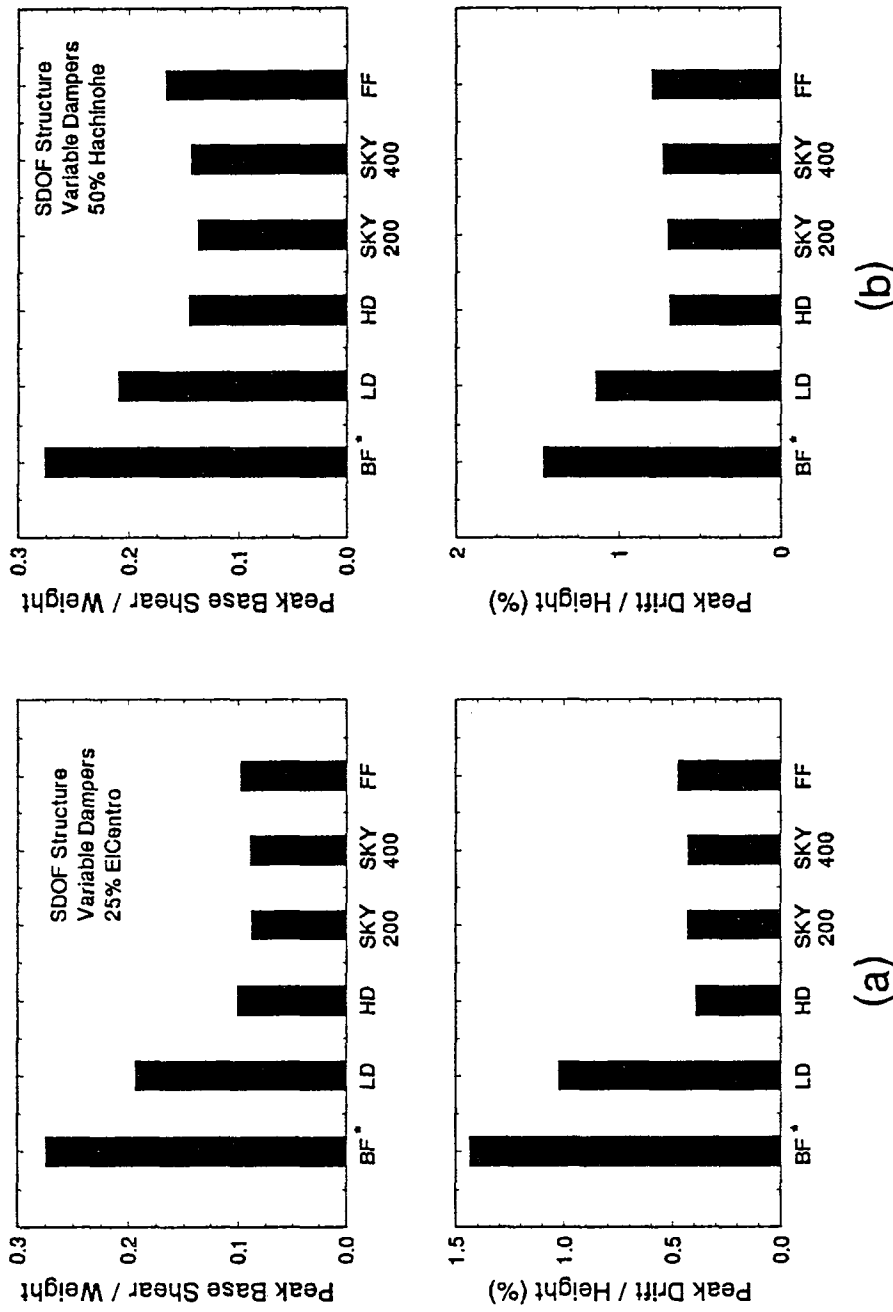


Figure 9-12 Comparisons of Peak Response of Flexible One-Story Structure with Variable Dampers Subjected to a) 25% El Centro Motion and b) 50% Hachinohe Motion

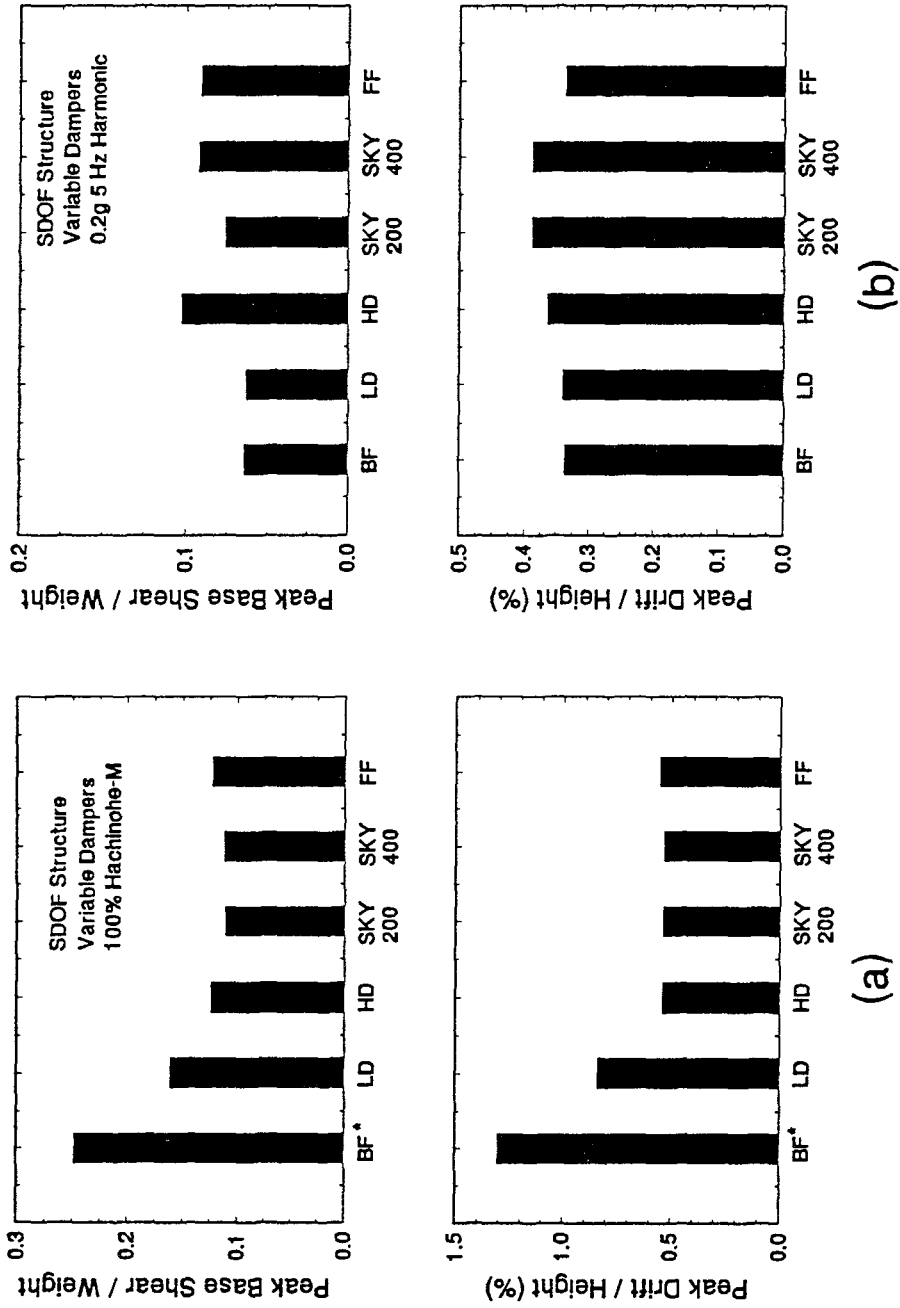


Figure 9-13 Comparisons of Peak Response of Flexible One-Story Structure with Variable Dampers Subjected to a) 100% Modified Hachinohe Motion and b) Harmonic Motion

control tests. Furthermore, the peak response for the semi-active control test is significantly less than the extrapolated peak response for the bare frame tests.

In the case of harmonic loading, Figures 9-11(b) and 9-13(b) show that the peak response with low damping passive control is less than with high damping passive control. This is expected since the frequency ratio (ratio of driving frequency to natural frequency) is approximately 2 and therefore the displacement transmissibility increases with an increase in damping (see Figure 7-2).

A large, unexpected response was observed in one of the tests on the one-story flexible structure with two-stage dampers subjected to harmonic loading (see Figure 9-11(b)). In this case the base shear coefficient control algorithm was used with a base shear coefficient limit of 0.08. Figure 9-14 shows base shear versus drift loops for the low damping, high damping, and semi-active damping (base shear coefficient control) tests corresponding to Figure 9-11(b). Apparently, the semi-actively controlled structure response was larger than that obtained with both the low and high damping passive control systems. This behavior can be explained with reference to Figure 9-2.

All of the semi-active control tests begin with the valves closed (i.e., high damping). The drift time history of Figure 9-2(c) builds up steadily (under high damping) and then, when the base shear coefficient exceeds 0.08, the valves open, initiating a bi-harmonic motion. The bi-harmonic motion is clearly present in the drift time history and in the Fourier

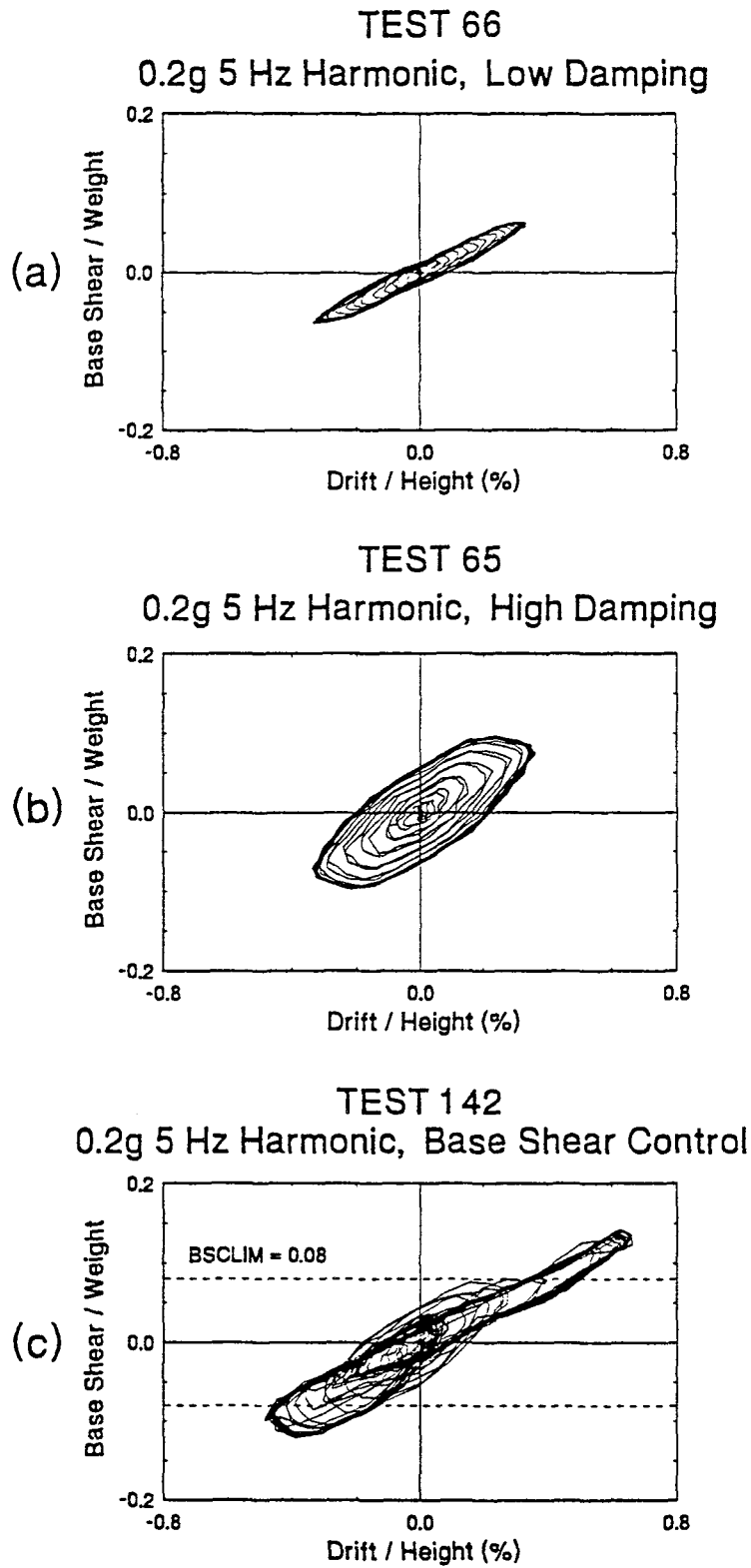


Figure 9-14 Comparison of Response of One-Story Flexible Structure with Two-Stage Dampers Subjected to Harmonic Motion and Controlled by a) Low Damping Passive Control System, b) High Damping Passive Control System, and c) Base Shear Coefficient Control Algorithm

amplitude spectra of the drift (Figure 9-2(e)). The two harmonics that are present in the response correspond to the driving frequency of the input (5 Hz) and the natural frequency of the structure (about 2.5 Hz). The frequency of the steady-state response of the structure with low and high damping passive control systems (Figure 9-14(a) and (b)) was found to be, as expected, 5 Hz. Apparently, the modification of damping during the semi-active control test initiates, in addition to the steady-state response at the frequency of the input, a transient response corresponding to the natural frequency of the structure. The bi-harmonic response of Figure 9-2 was not observed in any other shaking table tests. A further discussion on this test is presented in Section 10.4.1.

9.3.1.2 Three-Story Structure

Figures 9-15 through 9-20 present response profiles of the three-story structure subjected to the four different shaking table motions described in Section 5.3 and controlled by the semi-active variable dampers using the control algorithms described in Section 7.4. The values corresponding to the peak response at each floor or story in Figures 9-15 through 9-20 are available in Tables 9-IV, 9-V(a), and 9-V(b). For each of Figures 9-15 through 9-18, part (a) compares response profiles of the bare frame structure, the structure with a low damping passive control system, and the structure with a high damping passive control system. Part (b) compares response profiles of the bare frame structure with the structure controlled according to two of the semi-active control algorithms. Part (c) compares response profiles of the structure with a high damping passive control system to

Excitation: 25% El Centro

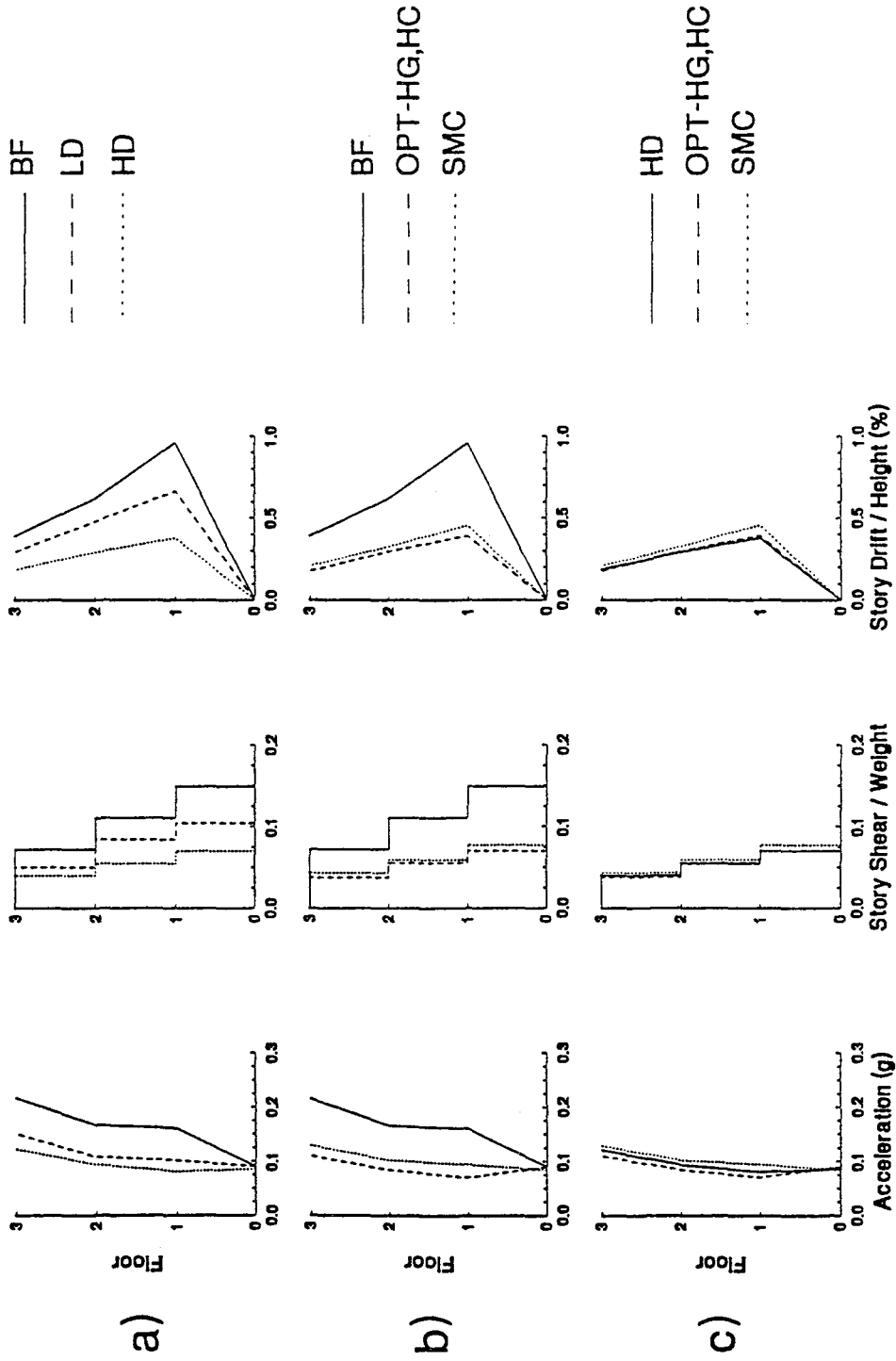


Figure 9-15 Comparison of Peak Response Profiles for Three-Story Structure Subjected to 25% El Centro Motion and Controlled by Various Control Systems

Excitation: 50% Hachinohe

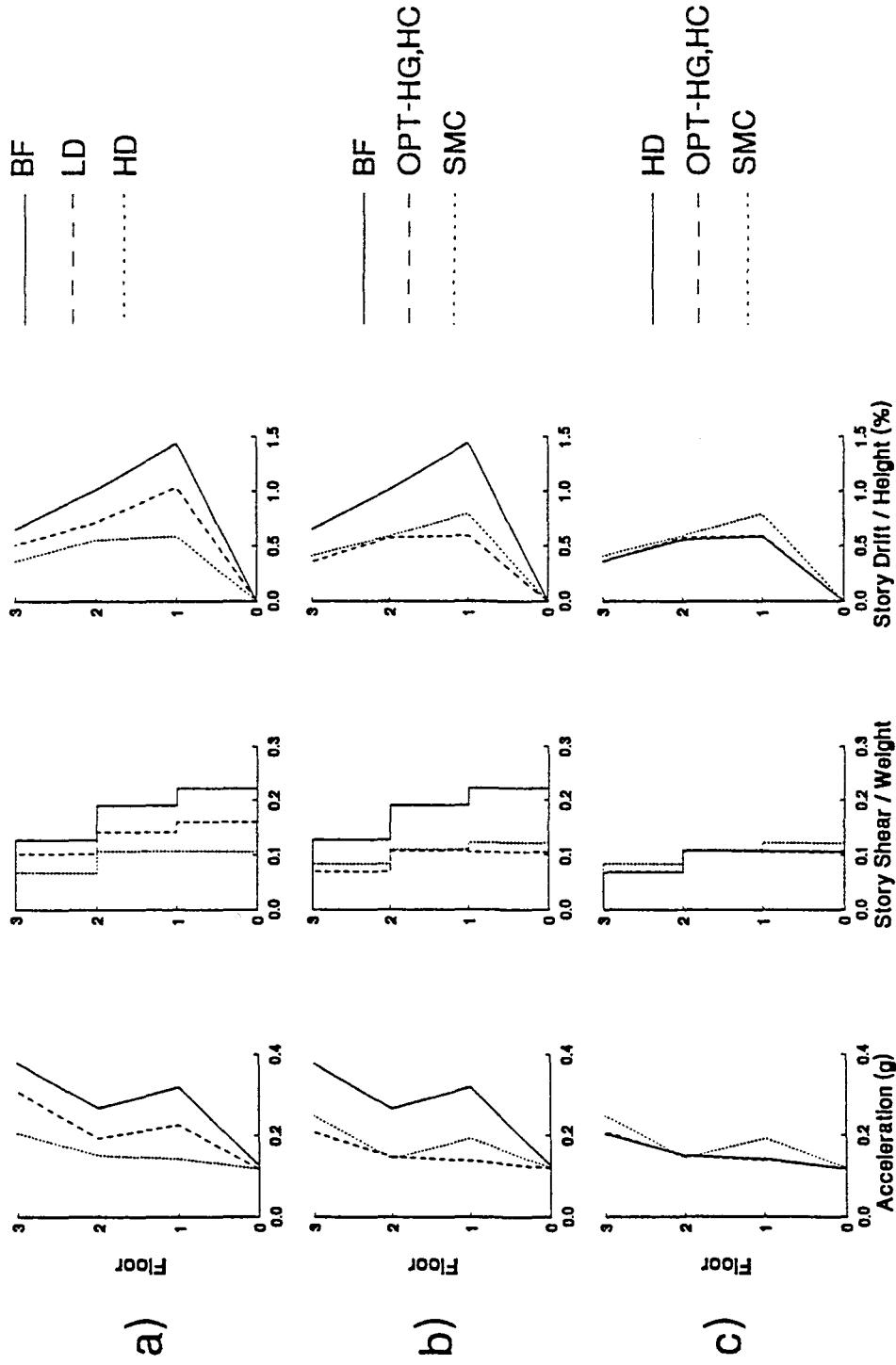


Figure 9-16 Comparison of Peak Response Profiles for Three-Story Structure Subjected to 50% Hachinohe Motion and Controlled by Various Control Systems

Excitation: 100% Hachinohe-M

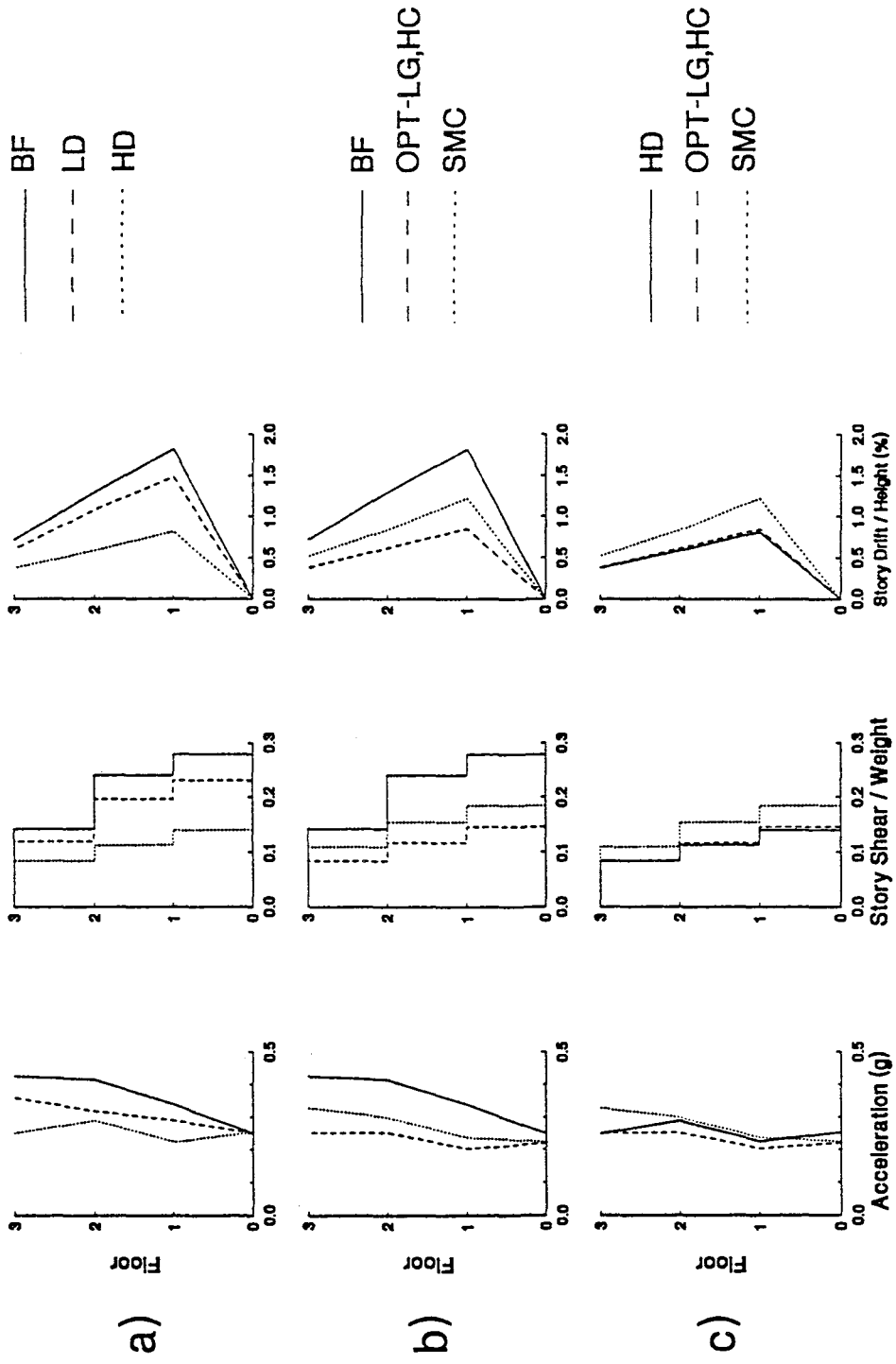


Figure 9-17 Comparison of Peak Response Profiles for Three-Story Structure Subjected to 100% Modified Hachinohe Motion and Controlled by Various Control Systems

Excitation: 0.4g 5 Hz Harmonic

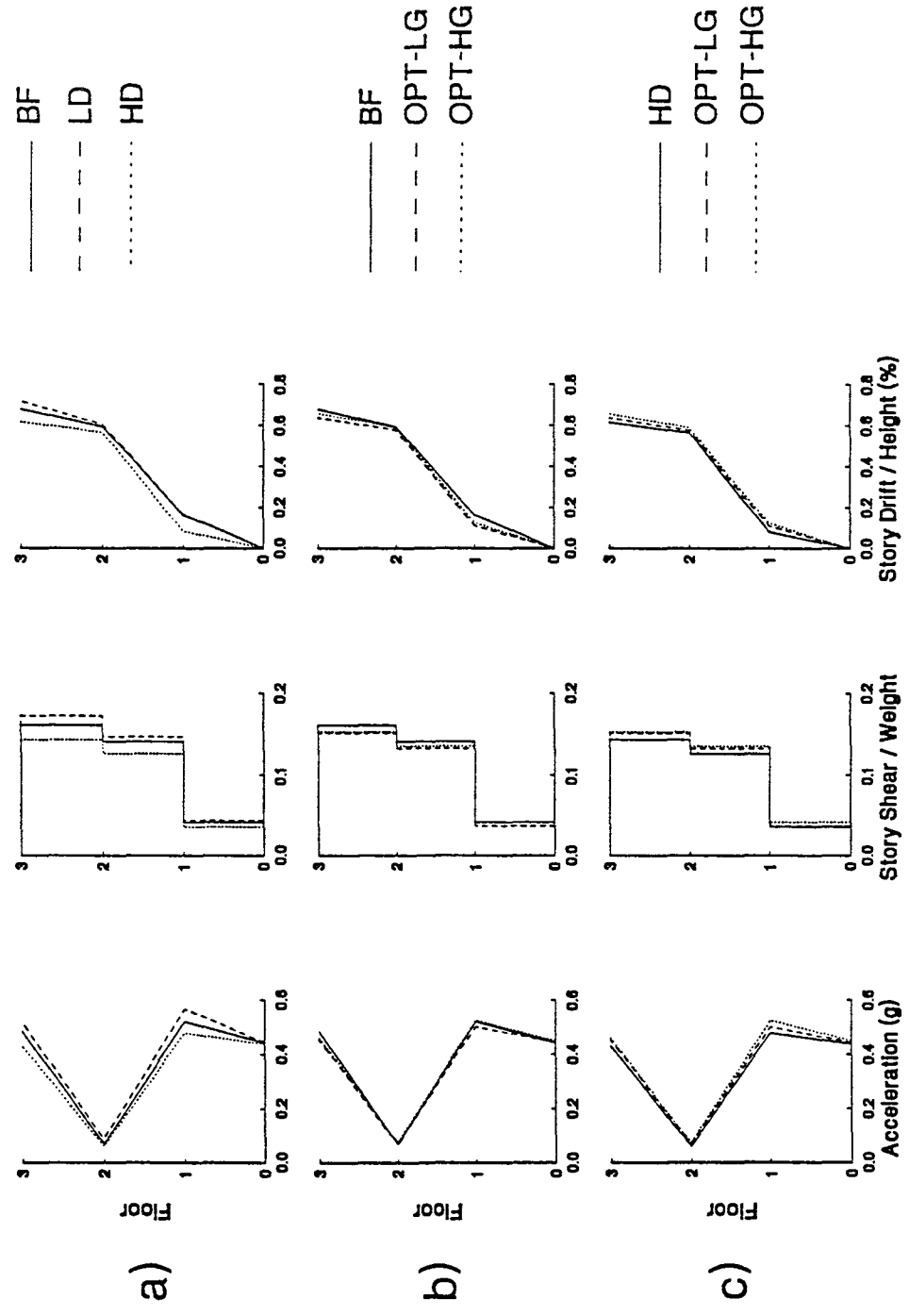


Figure 9-18 Comparison of Peak Response Profiles for Three-Story Structure Subjected to Harmonic Motion and Controlled by Various Control Systems

Excitation: 25% El Centro

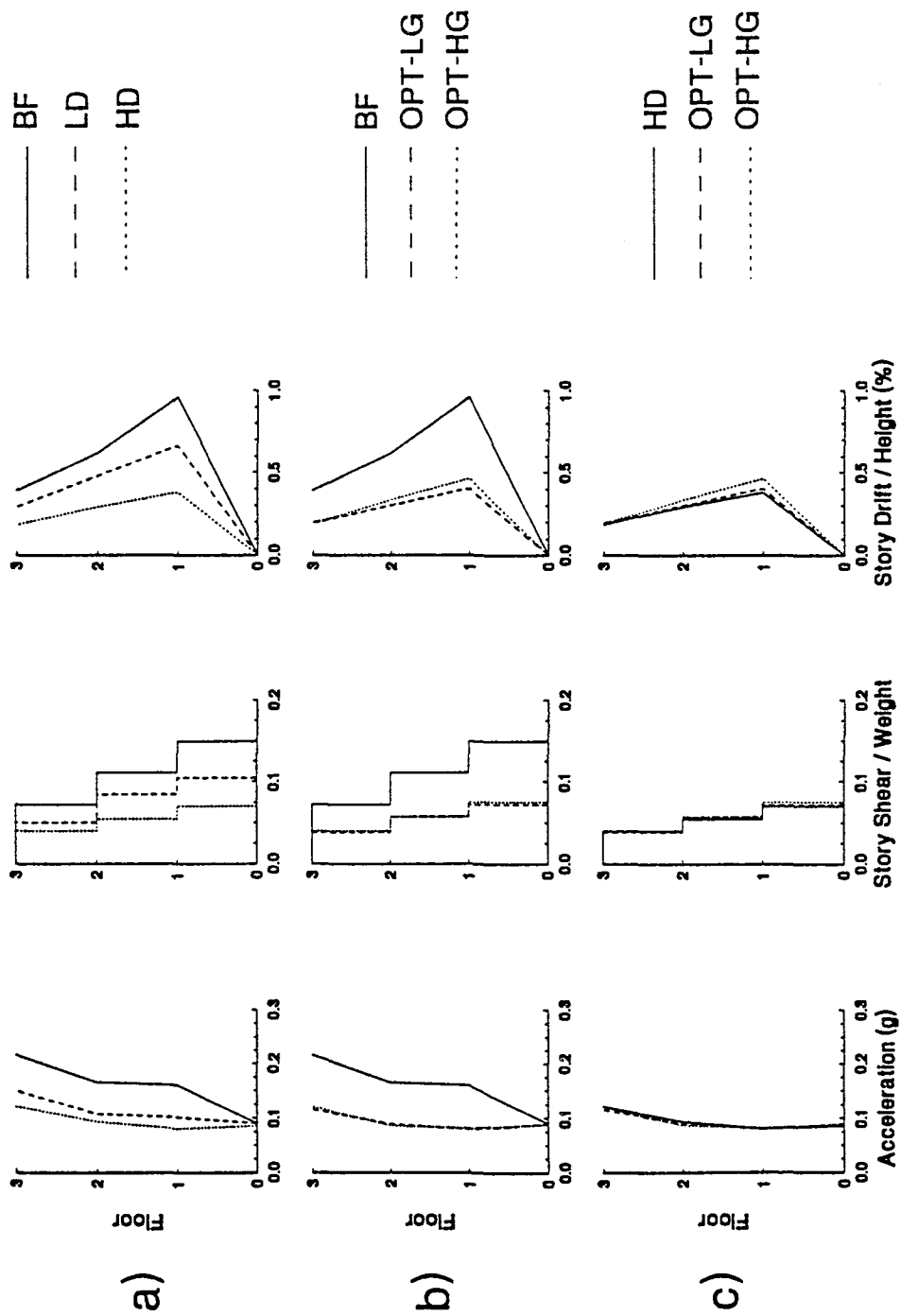


Figure 9-19 Comparison of Peak Response Profiles for Three-Story Structure Subjected to 25% El Centro Motion and Controlled by Various Control Systems

Excitation: 50% Hachinohe

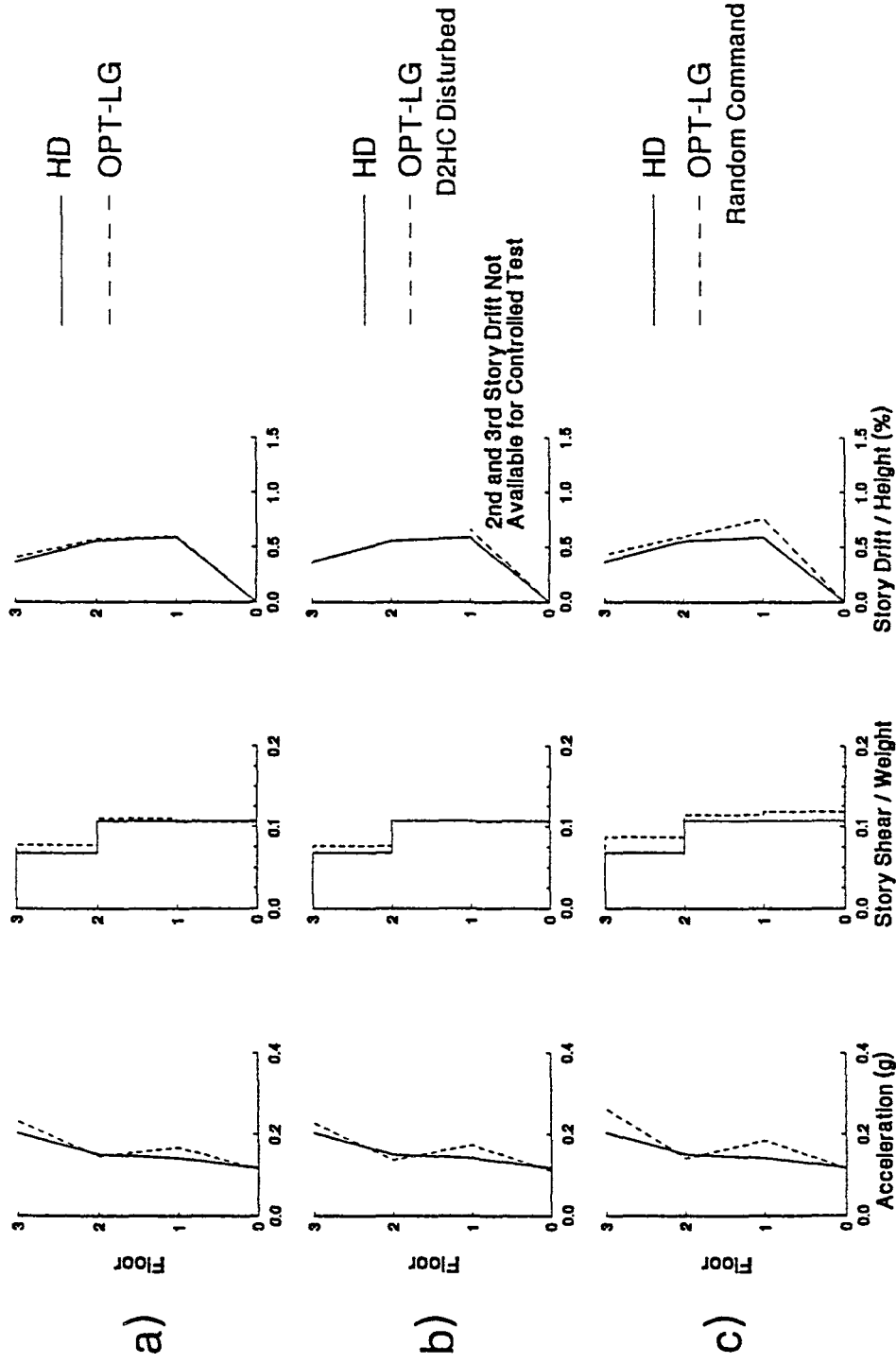


Figure 9-20 Comparison of Peak Response Profiles for Three-Story Structure Subjected to 50% Hachinohe Motion and Controlled by Various Control Systems

the structure controlled according to the same two semi-active control algorithms which are presented in part (b).

The two semi-active control algorithms used in the comparisons of Figure 9-15 through 9-18 were selected based on which algorithms produced the maximum and minimum response reduction for a given ground motion. For example, in Figure 9-15(b), the bare frame response is compared with the response of the semi-active control test using the optimal control algorithm with high gains and harmonic compensation. For this particular earthquake (25% El Centro), the optimal control algorithm with high gains and harmonic compensation produced the maximum response reduction for any of the semi-active control tests performed with this earthquake. Furthermore, in Figure 9-15(b), the bare frame response is compared with the response of the semi-active control test using the sliding mode control algorithm. For this particular earthquake (25% El Centro), the sliding mode control algorithm produced the minimum response reduction for any of the semi-active control tests performed with this earthquake.

The experimental results for the three-story structure subjected to earthquake input (Figures 9-15 through 9-17) reveal that:

- 1) The response of the bare frame structure is significantly reduced with the addition of the passive high damping control system (see part (a) of the figures).
- 2) The response of the bare frame structure is significantly reduced with the addition of the semi-active control systems (see part (b) of the figures).

- 3) The response of the structure with the passive high damping control system is typically less than or nearly the same as the response obtained with the semi-active control systems (see part (c) of the figures).

Evidently, the use of semi-active control systems offered no significant advantage over the use of a high damping passive control system. Similar conclusions were made by Polak (1994) in a numerical study on a three-story structure with a semi-active damping system. However, the authors of that study note that, under certain special conditions, a semi-active damping system may be warranted.

The response profiles of the three-story structure subjected to harmonic ground motion are presented in Figure 9-18. Note that the shape of the response profiles is very different from those corresponding to the earthquake ground motions (Figures 9-15 through 9-17). For example, under harmonic loading the peak drift of the first story is very small in comparison to the second and third story peak drifts whereas, under earthquake loading, the peak drift of the first story is larger than the second and third story peak drifts. This difference in response under the two different types of ground motion is related to the frequency of vibration in each case. Under earthquake loading, the three-story structure primarily vibrates at the fundamental frequency in the first mode of vibration. For the tested structure, the first mode of vibration produces larger drifts in the first story than in the second or third story. Recall that the three-story structure behaves as a shear type building with the lowest stiffness in the first story (the height of the first story columns (81.3 cm) is larger than that of the second and third story columns (76.2 cm)). Under

harmonic loading, the structure vibrates primarily at a frequency corresponding to the second mode of vibration (the driving frequency is 5 Hz and the natural frequency in the second mode of vibration is about 5.8 Hz (see Table 6-II)). For the tested structure, vibration in the second mode produces the smallest drifts in the first story. Note that the response profiles of all the tests in Figure 9-18 are very similar. This is because the installation of dampers in the first story had very little effect on the response since the first story drift was so small and therefore the damper stroke was minimal, preventing any appreciable energy dissipation.

It is interesting to note that in each of Figures 9-15, 9-16, and 9-17, the maximum response reduction for the semi-active control system was consistently produced by the optimal control algorithm while the minimum response reduction was consistently produced by the sliding mode control algorithm. This observation can be explained in two ways. First, the sliding mode control algorithm was originally developed for a SDOF structure and then adapted to a MDOF structure (see Section 7.4.2). Secondly, the sliding mode control algorithm requires measurement of the ground acceleration (see Equation 7-82) whereas the optimal control algorithm does not (see Equation (7-55)). In general, control algorithms which require acceleration measurements are more sensitive to measurement errors than algorithms which do not require such measurements.

A comparison of test results for the semi-actively controlled structure subjected to the 25% El Centro earthquake and controlled by the optimal control algorithm is shown in

Figure 9-19. Results from both the low gain and high gain optimal control algorithm are presented. Recall that the high gain control was developed as a result of reducing the values within the control force weighting matrix (see Section 7.4.1). The acceleration and story shear profiles are nearly identical for the two sets of control gains while the drift profile of the low gain control is marginally less than that corresponding to the high gain control. Apparently, for the two different optimal control gain sets used in this study, no significant difference in response was obtained for this particular excitation. The same conclusion can be shown to apply to other tests in which different excitations were used.

Any control algorithm utilized in an active or semi-active control system should be robust with respect to measurement errors. This issue was explored in a test on the three-story structure subjected to the 50% Hachinohe ground motion (see Figure 9-20). In Figure 9-20(a), a comparison is made between the passive high damping control system response and the semi-active control system response using the optimal control algorithm with low gains. As discussed previously, the response of the three-story structure with a semi-active control system is nearly the same as the response with a passive high damping control system (see Figure 9-20(a)). In Figure 9-20(b), the same comparison is made as in Figure 9-20(a) but with the second floor total displacement signal disturbed during the test (the disturbance was caused by randomly moving the external magnet assembly of the linear displacement transducer during the shaking table test). Recall that analog differentiators are used to obtain the total velocity at each floor level. Therefore, both the second floor displacement and velocity were affected by the disturbance. It is apparent

from Figure 9-20(b) that the measurement errors caused by the disturbance did not adversely affect the response of the structure (maximum peak acceleration increase of about 4%, no increase in peak shear force, and a peak drift increase at the first story of about 11%). A different disturbance was produced by randomly adjusting the command signal to the variable damper valves during the semi-active control test (see Figure 9-20(c)). A valve command signal was generated by the control computer but the power supply to the valve control circuits was turned on and off randomly to allow or not allow, respectively, the valve command signal to be sent to the valve. The effect of the random command was to increase peak accelerations and peak shear forces by about 12% and peak drifts by about 28%.

Robust behavior may also be considered with respect to the control algorithm. Tests were performed on the one-story structure in which the feedforward control algorithm was intentionally modified (see Table 9-III, Tests 322 and 323). The feedforward control algorithm was modified by simply negating the desired damping coefficient of Equation (7-13). In the case of the 50% Hachinohe ground motion, the negated control algorithm resulted in a 6% increase in peak shear force and a 24% increase in peak drift as compared with the correct application of the control algorithm. Furthermore, in the case of the 50% El Centro ground motion, the negated control algorithm resulted in a 16% increase in peak shear force and a 28% increase in peak drift as compared with the correct application of the control algorithm.

9.3.2 Time Delay Compensation

Two different methods of time delay compensation were described in Section 8. The effectiveness of semi-active control with and without time delay compensation is examined in this section. Note that the implementation of time delay compensation requires a good estimate of the time delays associated with each component of the control system. The time delays associated with response measurements had well defined values (see Table 8-I). In contrast, the semi-active damper time delays were not as well defined and average values from command signal saturation tests (see Tables 3-VI, 3-VII, and 8-I) were used in the tests with time delay compensation.

9.3.2.1 One-Story Structure

Figures 9-21 through 9-23 show the effect of time delay compensation for the one-story structure subjected to various ground motions and controlled by the semi-active two-stage dampers using various control algorithms. The value of the height of each bar in these figures is available in Table 9-II. In Figures 9-21 and 9-22, the effect of kinematic compensation is examined whereas in Figure 9-23, the effect of harmonic compensation is examined. The percentage figures shown in Figures 9-21 through 9-23 indicate the increase or decrease in peak response obtained through the use of time delay compensation.

For nearly all of the tests on the one-story structure with earthquake ground motion, the use of control algorithms with time delay compensation degraded the response in terms of

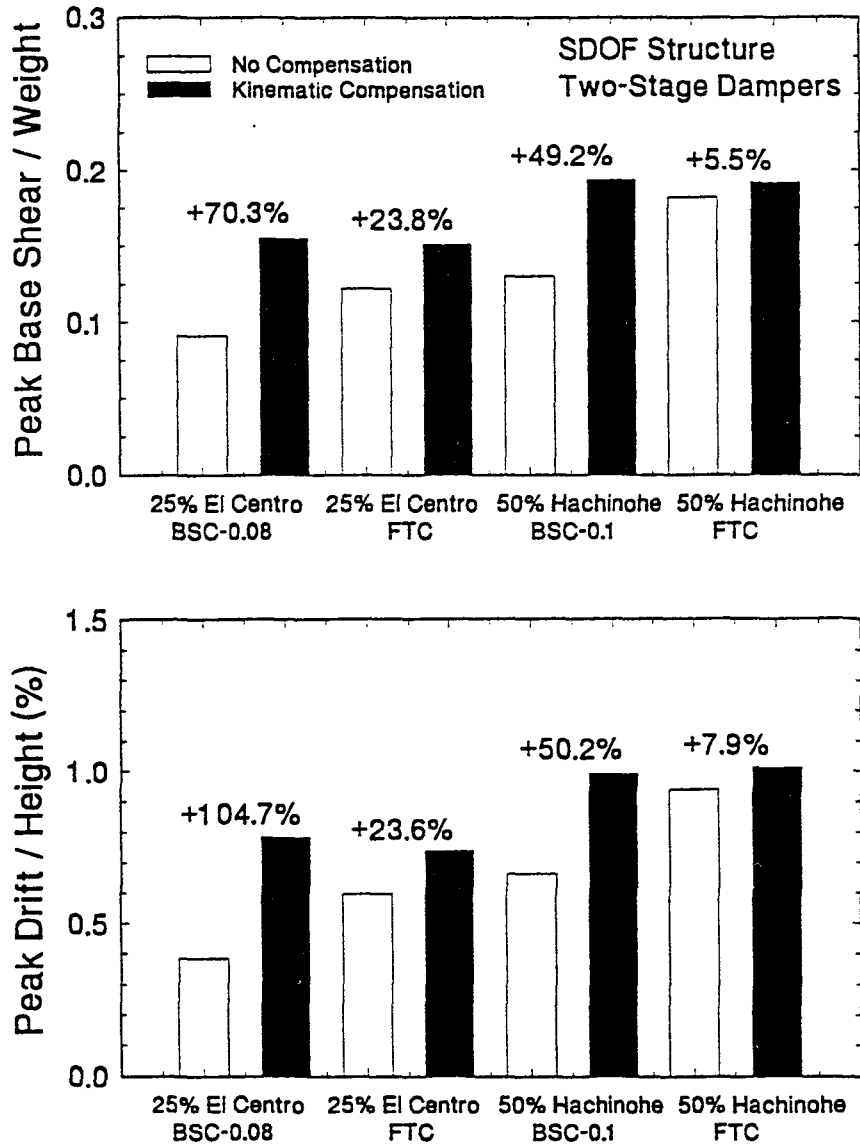


Figure 9-21 Peak Response of One-Story Flexible Structure with Two-Stage Dampers Subjected to 25% El Centro and 50% Hachinohe Motions and Controlled with and without Kinematic Compensation Applied to Control Algorithms

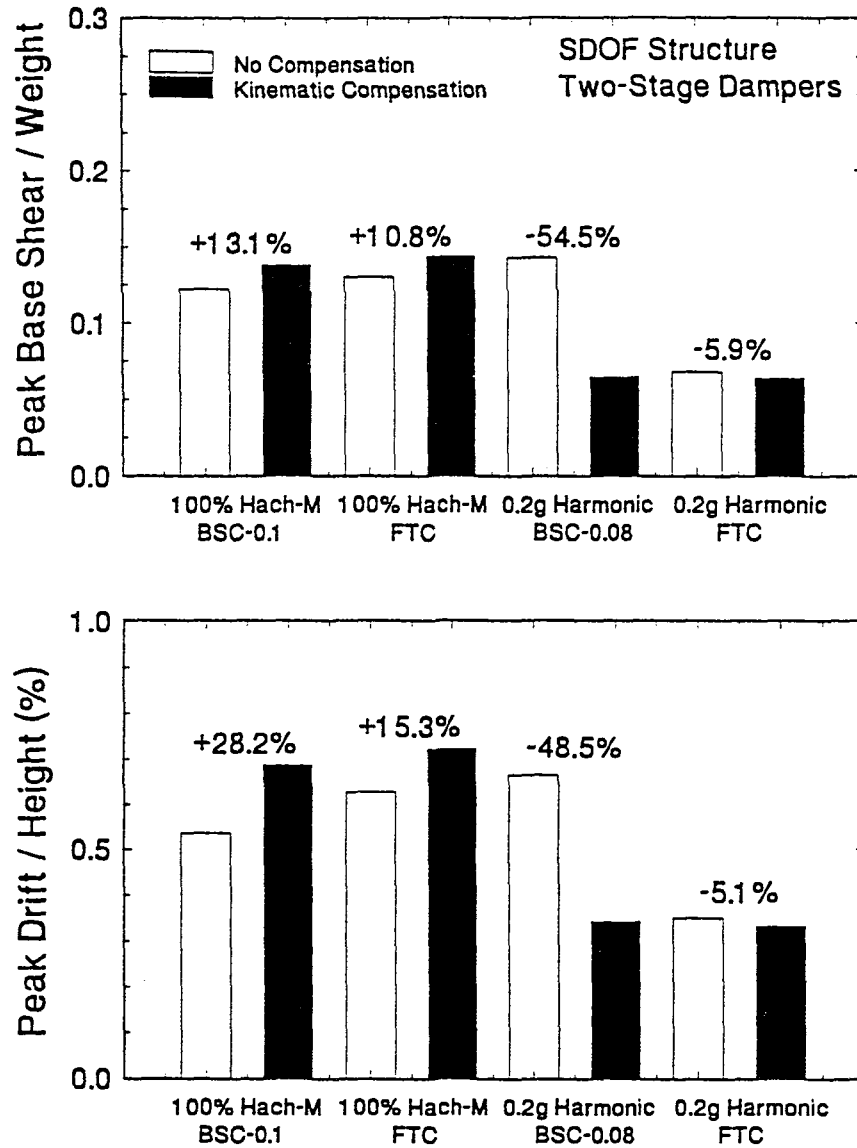


Figure 9-22 Peak Response of One-Story Flexible Structure with Two-Stage Dampers Subjected to 100% Modified Hachinohe Motion and Harmonic Motion and Controlled with and without Kinematic Compensation Applied to Control Algorithms

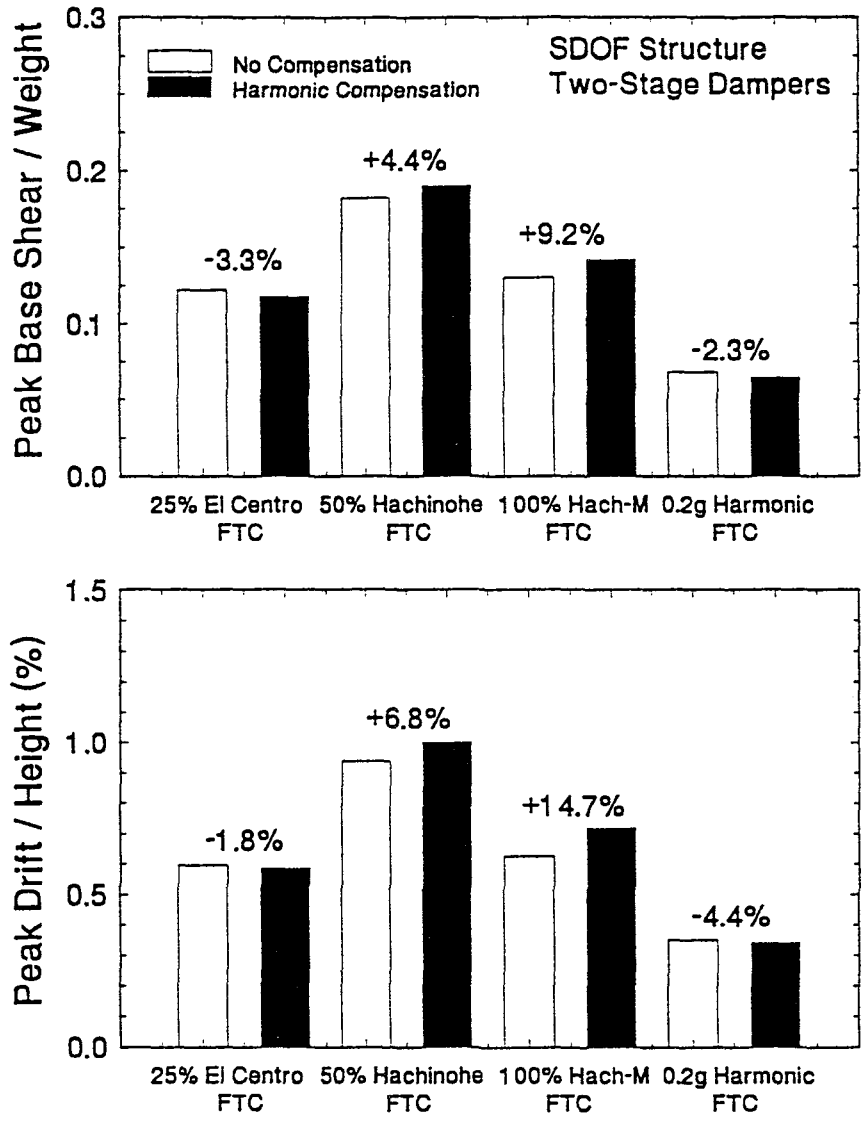


Figure 9-23 Peak Response of One-Story Flexible Structure with Two-Stage Dampers Subjected to Various Ground Motions and Controlled with and without Harmonic Compensation Applied to the Control Algorithms

peak base shear and peak drift. The effect of compensation for the tests with earthquake input is also evaluated in Figure 9-24 in the form of base shear versus drift loops.

As shown in Figures 9-22 and 9-23, in the tests with harmonic ground motion, the application of control algorithms with time delay compensation produced dramatic reductions in the response (about 50% reduction in peak base shear and in peak drift in one case) or minor reductions (between 2 and 5% reduction in the peak response quantities for two different cases). The effect of time delay compensation for the tests with harmonic input is also evaluated in Figure 9-25 in the form of base shear versus drift loops. Recall from Section 8 that the kinematic compensation method is based on a Taylor series expansion of the response and the harmonic compensation method is based on the assumption of undamped free vibration response during the total time delay τ (see Figure 8-1). Both of these time delay compensation methods are most suitable when the excitation is smooth over the time interval τ . The earthquake ground motions are significantly more erratic (contain a wide range of frequencies and varying peak amplitude) than the harmonic ground motion (contains a single frequency with a constant peak amplitude). To some extent, the different characteristics of the ground motions played a role in determining the effectiveness of the time delay compensation methods utilized in the experiments.

The effect of time delay compensation methods for tests with harmonic ground motion can be explored further in Figure 9-25. Figures 9-25(a) and (c) and Figures 9-25(b) and (d)

NO COMPENSATION

COMPENSATION APPLIED

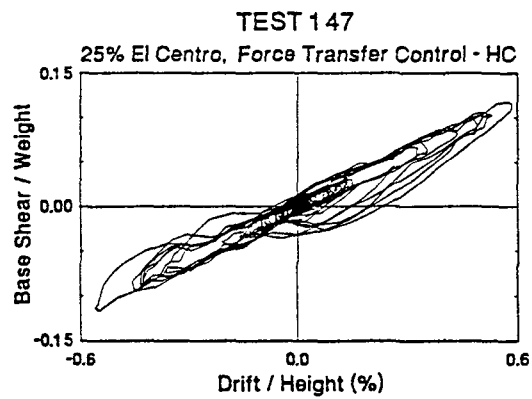
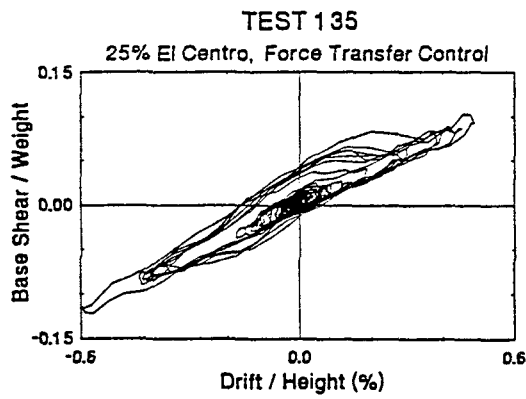
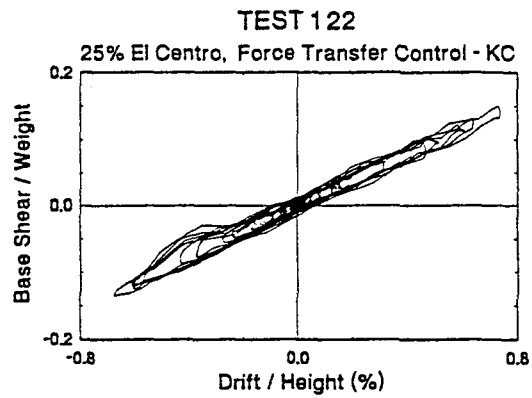
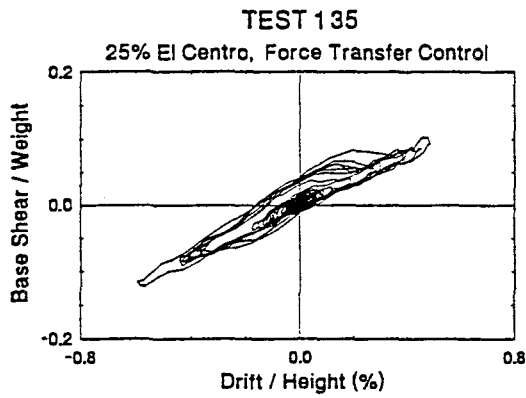
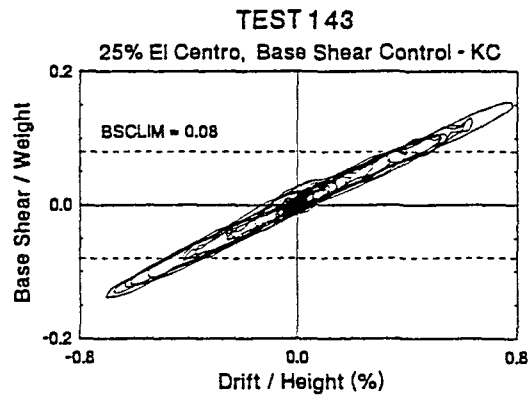
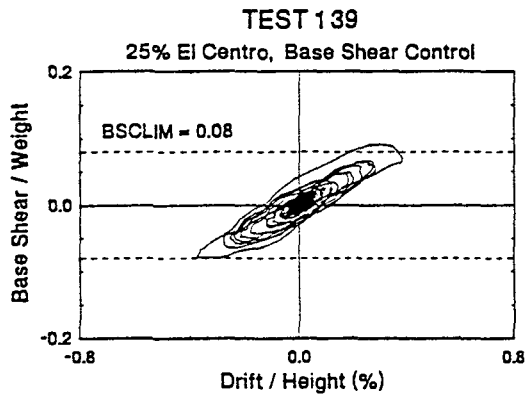


Figure 9-24 Effect of Time Delay Compensation on Response of One-Story Structure Subjected to 25% El Centro

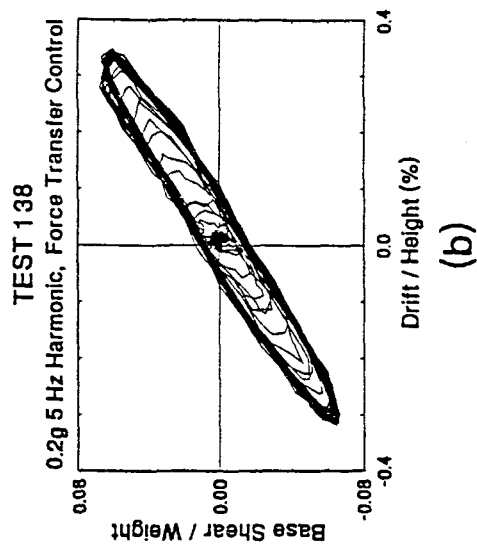
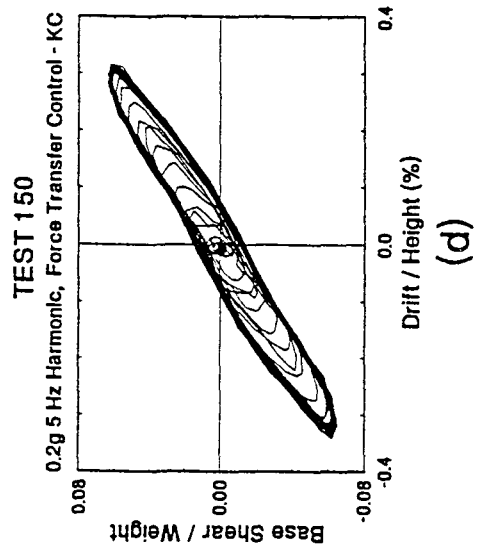
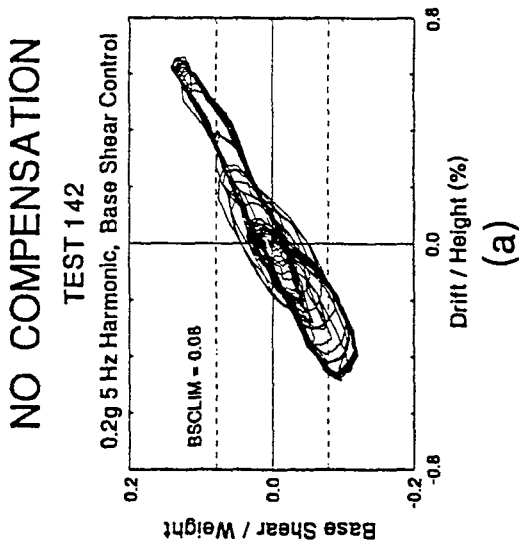
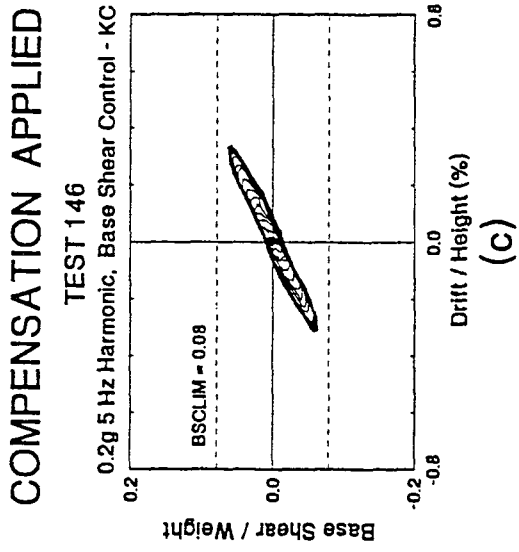


Figure 9-25 Comparison of Response of One-Story Structure Subjected to Harmonic Motion and Controlled with and without Time Delay Compensation

indicate that the control algorithm with time delay compensation was very successful or marginally successful, respectively, in reducing the response as compared with the uncompensated test (also, see Figure 9-22 which shows data for the same tests). The large reduction in response for the base shear control algorithm with compensation (Figure 9-25(a) and (c)) can be explained with reference to Figure 9-26 which shows a more detailed description of test results for Figure 9-25(c). The measured acceleration, shown in Figure 9-26(d), does not exceed 0.08g which corresponds to the base shear coefficient limit of 0.08. Therefore, according to the base shear coefficient control algorithm (see Section 7.2.1), the damping level should be high at all times. However, the compensated (predicted) acceleration (Figure 9-26(e)) exceeds the limit of 0.08 to such an extent that the valve is on (low damping) for a large portion of the test (see Figure 9-26(f) which shows the filtered command signal). Therefore, the damping is essentially low at all times, producing the controlled base shear versus drift loop of Figure 9-26(a). Note that the drift response (Figure 9-26(b)) is very smooth and contains a single dominant frequency corresponding to the frequency of the input (Figure 9-26(c)) while the drift response of the uncompensated test (Figure 9-2(c)) is bi-harmonic in nature.

In summary, the improvement in response with time delay compensation occurs as a result of an incorrectly predicted acceleration which induces low damping over a large portion of the test. If the time delay compensated control algorithm had predicted the acceleration correctly, the damping would have been high at all times which would have been detrimental to the response in comparison to the low damping case since the frequency

TEST 146
0.2g 5 Hz Harmonic, Base Shear Control - KC

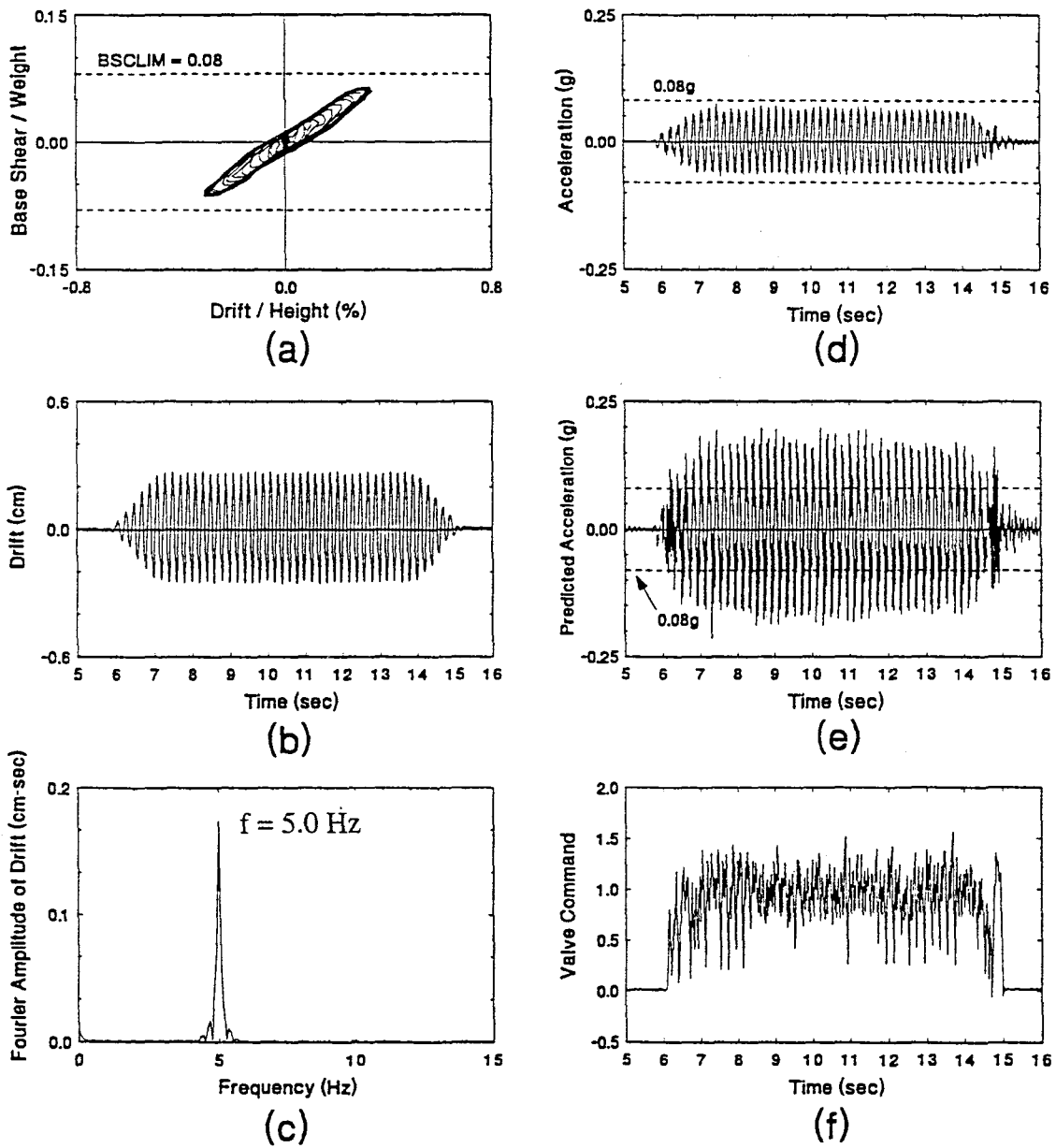


Figure 9-26 Test Results for One-Story Structure with Two-Stage Dampers Subjected to Harmonic Motion and Controlled by Base Shear Coefficient Control Algorithm with Kinematic Compensation

ratio (ratio of input frequency to natural frequency) is approximately 2 (see Figure 7-2). Furthermore, the compensated test appears to be successful since comparisons are made with test results from an uncompensated control algorithm in which a bi-harmonic response occurred producing excessive base shear and story drift.

As Figure 9-25(b) shows, the response of the structure under the force transfer control algorithm with no compensation does not exhibit the bi-harmonic response exhibited in Figure 9-25(a). Therefore, the comparison with the compensated test (Figure 9-25(d)), although showing a marginal improvement, is much less dramatic.

9.3.2.2 Three-Story Structure

The effect of the harmonic time delay compensation method on the response of the three-story structure is examined in Figures 9-27 through 9-30 in the form of peak response profiles. The peak values of the response of each floor or story is available in Tables 9-V(a) and 9-V(b). The effect of compensation for tests in which earthquake ground motion was used (Figures 9-27 through 9-29) appears to be, in general, a minor improvement or minor degradation in the various response profiles. The absence of significant response reductions with the implementation of time delay compensation may be attributed to the approximate nature of the experimentally measured semi-active damper time delays as well as the simplifying assumptions used in developing the time delay compensation methods. Under harmonic excitation (Figure 9-30), there is essentially no change in the response when compensation is utilized. Recall that, under

Excitation: 25% El Centro

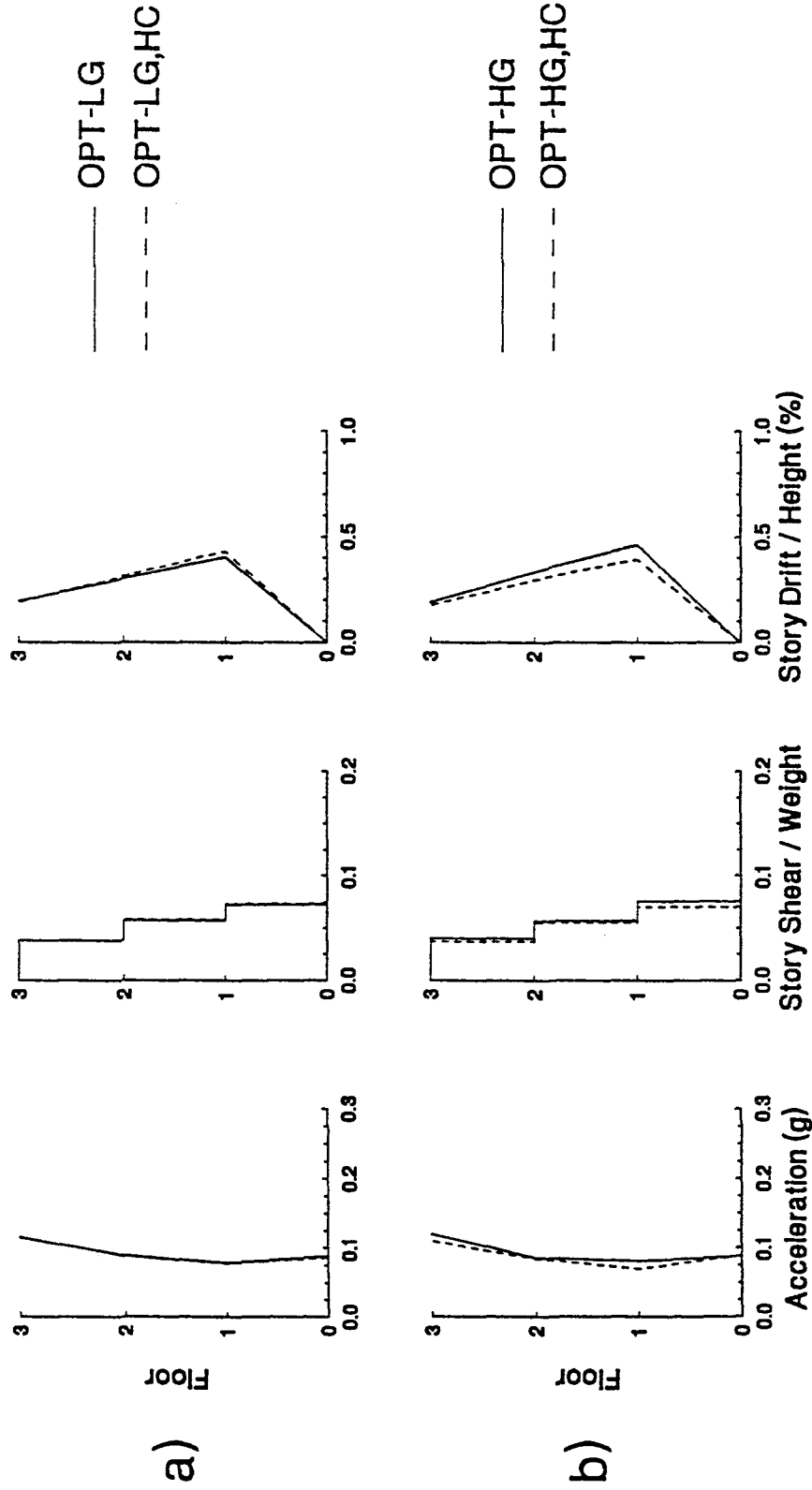


Figure 9-27 Comparison of Peak Response Profiles of Three-Story Structure Subjected to 25% El Centro and Controlled by Optimal Control Algorithm with and without Harmonic Compensation

Excitation: 50% Hachinohe

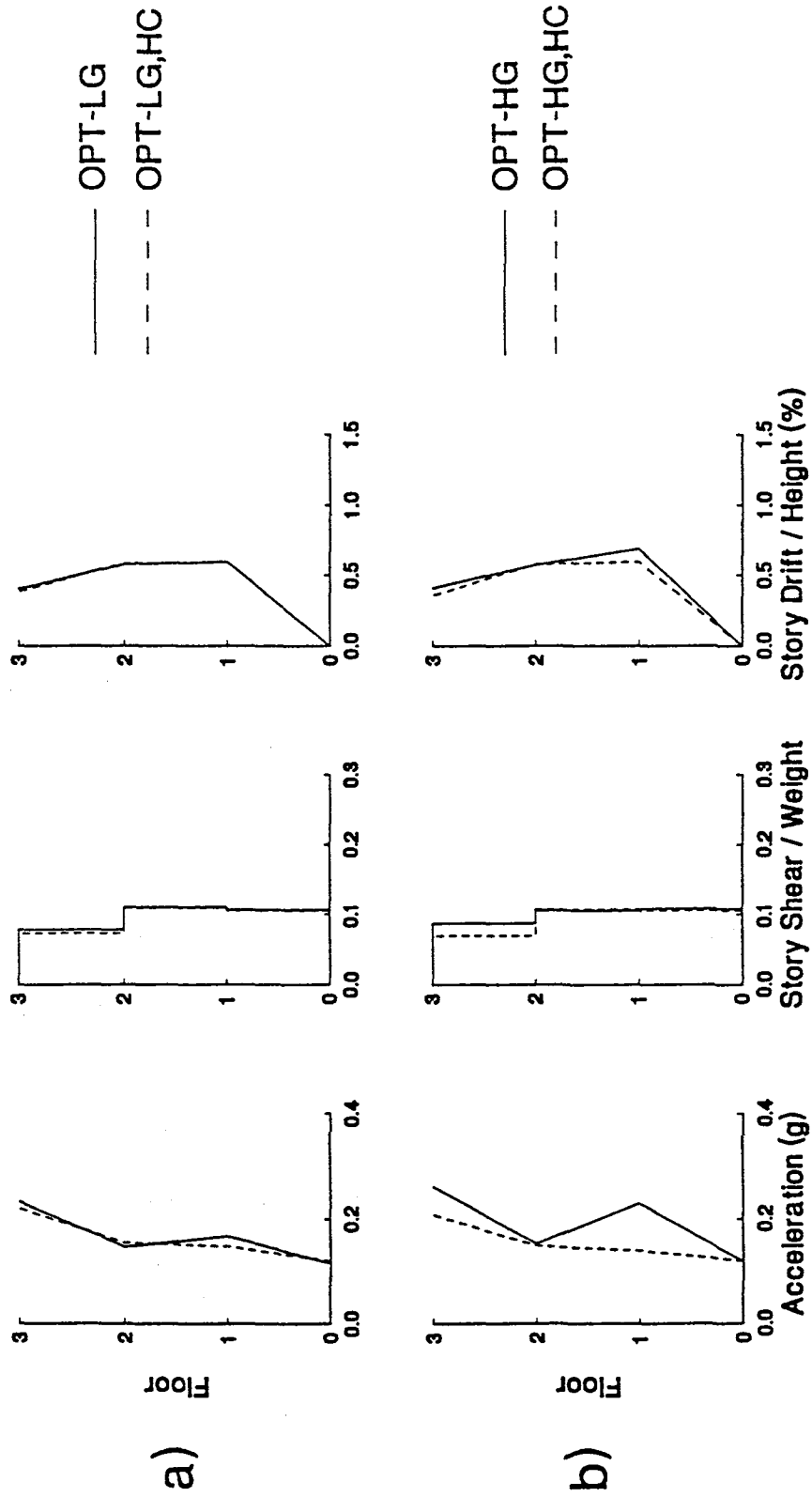


Figure 9-28 Comparison of Peak Response Profiles of Three-Story Structure Subjected to 50% Hachinohe Motion and Controlled by Optimal Control Algorithm with and without Harmonic Compensation

Excitation: 100% Hachinohe-M

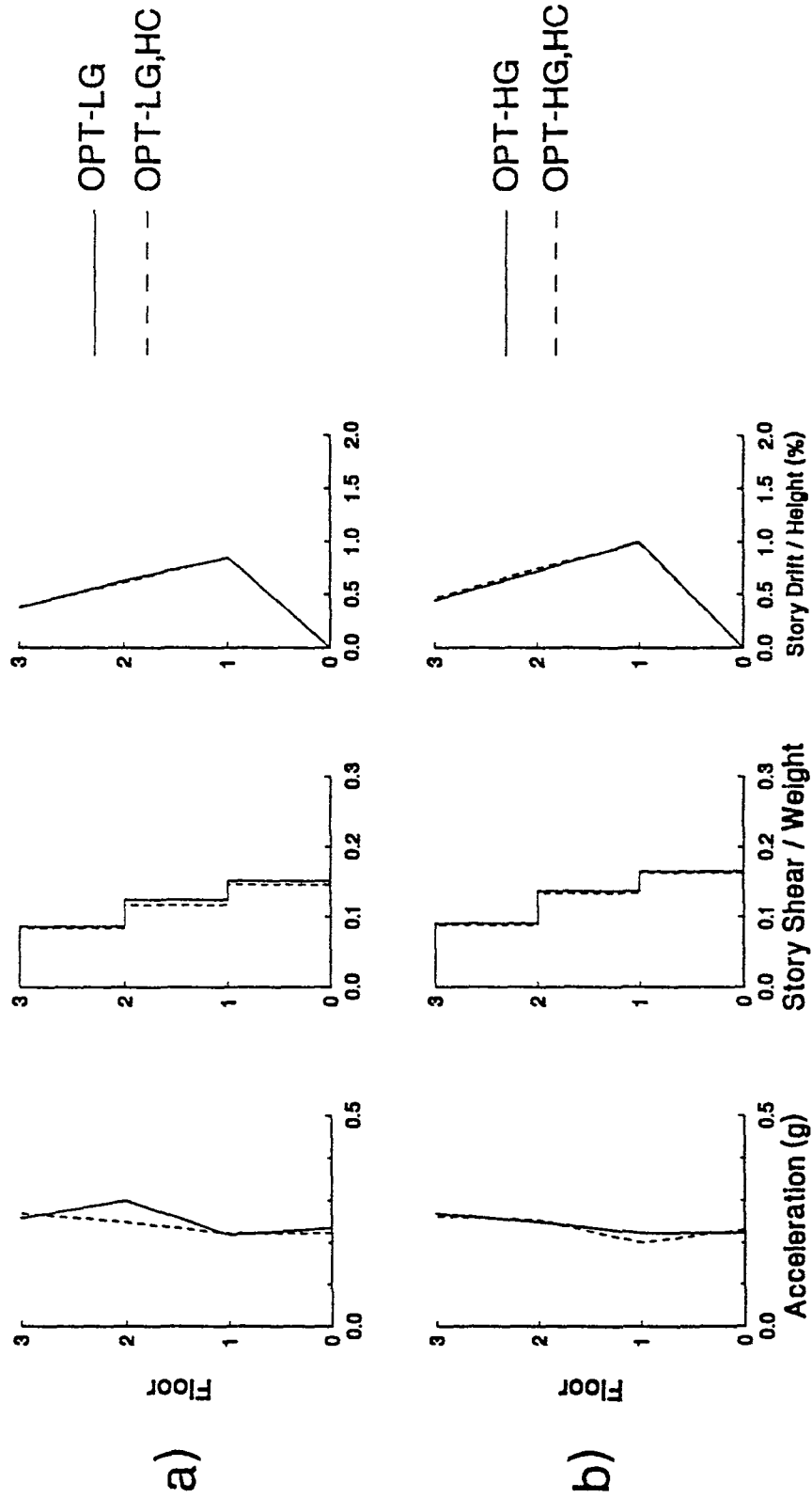


Figure 9-29 Comparison of Peak Response Profiles of Three-Story Structure Subjected to 100% Modified Hachinohe Motion and Controlled by Optimal Control Algorithm with and without Harmonic Compensation

Excitation: 0.4g 5 Hz Harmonic

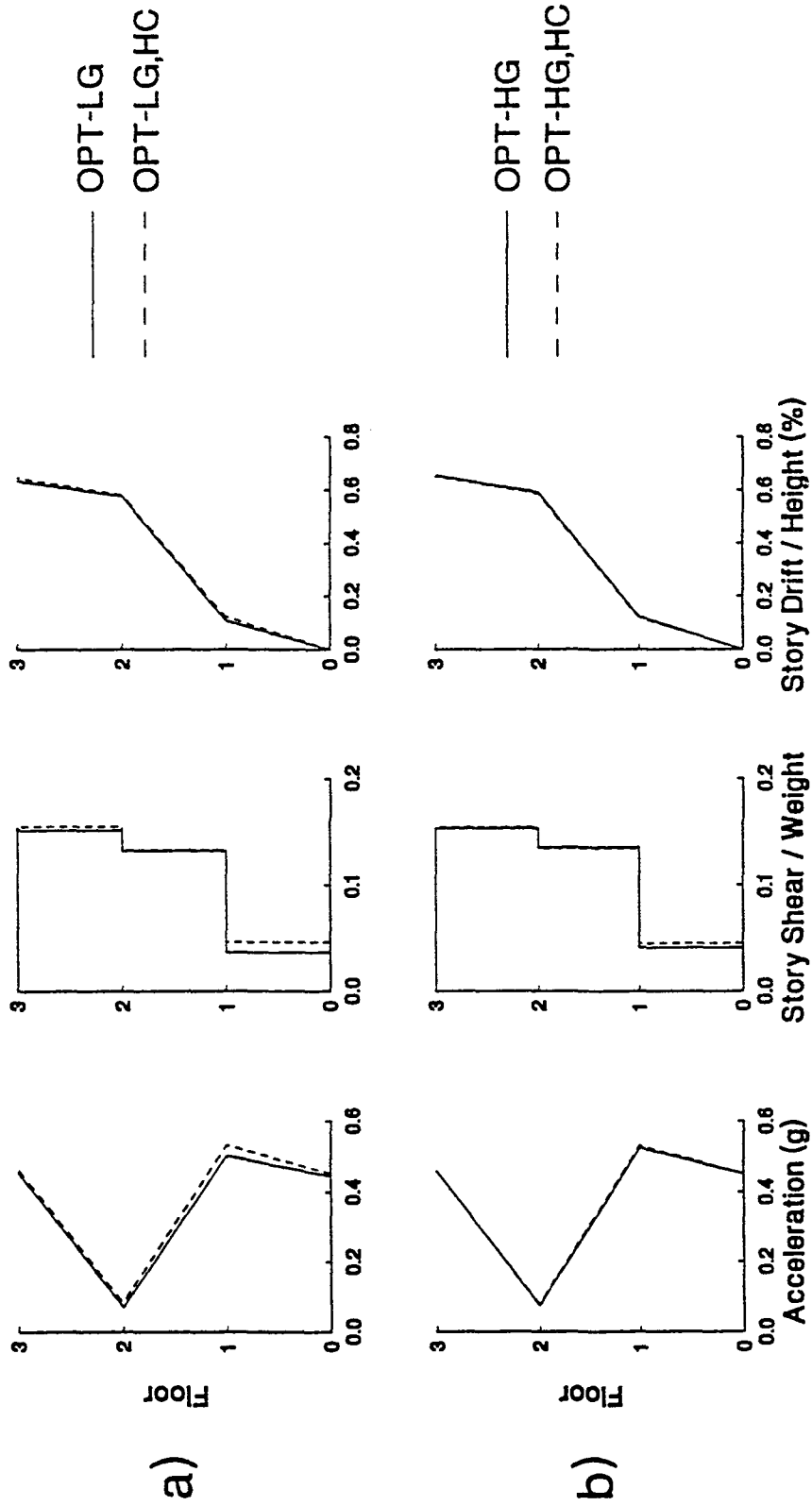


Figure 9-30 Comparison of Peak Response Profiles of Three-Story Structure Subjected to Harmonic Motion and Controlled by Optimal Control Algorithm with and without Harmonic Compensation

harmonic loading, the structure vibrates primarily at a frequency corresponding to the second mode of vibration. For the tested structure, vibration in the second mode produces the smallest drifts in the first story which limits the stroke of the dampers, preventing any appreciable energy dissipation.

After the shaking table tests were completed, an error was discovered in the value of the coefficients used in the MDOF harmonic compensation equation for relative velocity (similar to Equation (8-17)). The error was on the order of 150% of the correct values of the coefficients. It is clear from Figures 9-27 through 9-30 that the error in harmonic compensation had no adverse effect on the controlled response of the three-story structure.

9.4 Comparison with an Active Control System

The three-story structure utilized in the shaking table tests has been tested previously by others for active control research. A comparison can be made between the results from the semi-active control tests described in this report and previous results obtained from tests in which an active tendon system was used to control the structure through linear optimal control algorithms similar to that described in Section 7.4.1 (Chung 1989, Soong 1994 and 1990). The results are compared in tabular form in Table 9-VII and in graphical form in Figure 9-31 for the 25% El Centro ground motion. The percentage figures shown in Figure 9-31 indicate the peak response reduction in comparison with the bare frame structure response. Figure 9-31(a) shows that the active tendon system significantly

Table 9-VII Comparison of Experimental Results from Active and Semi-Active Control Tests

Active Control Tests	CONTROL SYSTEM	SYSTEM PARAMETERS						EXCITATION	PEAK ACCELERATION (g)			PEAK DRIFT / HEIGHT (%)		
		Frequency (Hz)			Damping Ratio (%)				1st floor	2nd floor	3rd floor	1st story	2nd story	3rd story
		Mode 1	Mode 2	Mode 3	Mode 1	Mode 2	Mode 3							
Active Control Tests	Bare Frame	2.2	6.8	11.5	1.60	0.39	0.36	25% El Centro S00E P.G.A. = 0.085g	0.16	0.22	0.32	0.67	0.87	0.60
	Active Tendon System	2.28	6.94	11.56	12.77	12.27	5.45	25% El Centro S00E P.G.A. = 0.085g	0.14	0.14	0.20	0.39	0.59	0.41
Semi-Active Control Tests	Bare Frame	1.8	5.8	11.4	1.74	0.76	0.34	25% El Centro S00E P.G.A. = 0.090g	0.16	0.17	0.22	0.96	0.62	0.39
	Variable Dampers: High Damping	1.85	6.04	11.48	14.41	18.79	4.83	25% El Centro S00E P.G.A. = 0.085g	0.08	0.09	0.12	0.38	0.29	0.18
	Variable Dampers: Optimal Control - LG	--	--	--	--	--	--	25% El Centro S00E P.G.A. = 0.089g	0.08	0.09	0.12	0.40	0.30	0.19

Excitation: 25% El Centro

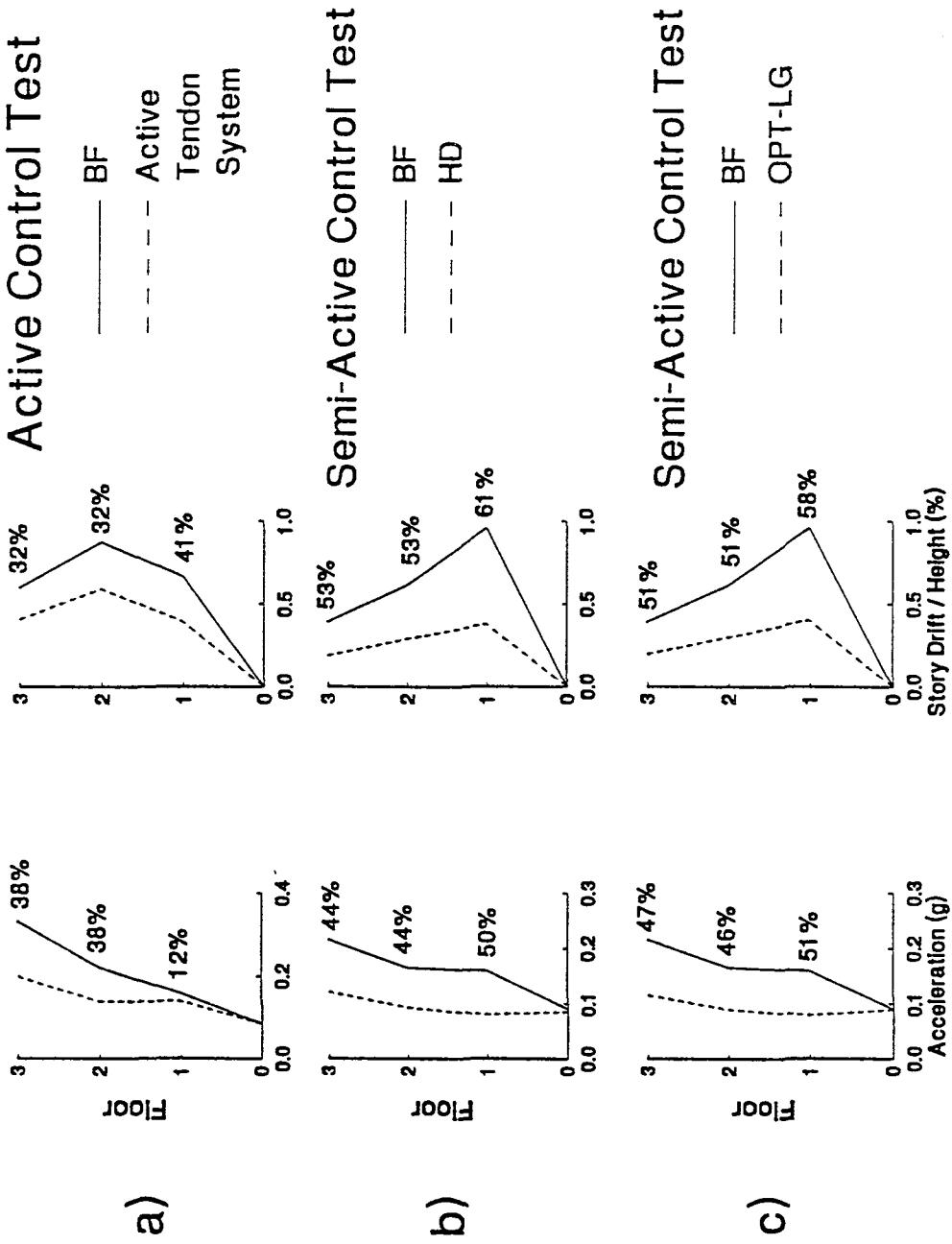


Figure 9-31 Comparison of Peak Response Profiles for Three-Story Structure Subjected to 25% El Centro Ground Motion and Controlled by Active Control System and Semi-Active Control System

reduces the peak response as compared with the bare frame structure. Further, Figure 9-31(b) shows that the peak response of the structure with the high damping passive control system is significantly less than that obtained with the bare frame and surpasses the reduction obtained with the active tendon system. Finally, Figure 9-31(c) shows results for the semi-active control system in which the optimal control algorithm was utilized with low gains.

Recalling Section 7.4.1, the optimal control algorithm used in the semi-active control test of Figure 9-31(c) is identical to that used in the active tendon control test of Figure 9-31(a) (i.e., the control gain matrix of Equation (7-49) is exactly the same for the two control algorithms) except that the semi-active control damping coefficient is bounded according to Equation (7-6). The results of Figure 9-31(a) and (c) indicate that the semi-active control system was capable of achieving larger reductions in peak response in comparison to the active control system in which the same control algorithm was utilized. This was simply the result of larger effective damping in the semi-active control system.

Interestingly, the semi-active control system produced peak response reductions which are nearly identical to those obtained with the high damping passive control system (compare Figure 9-31(b) and (c)). This is further demonstrated in Figure 9-32 in which the story shear versus drift loops of the first story of the structure are shown for a semi-active optimal control test and a passive high damping control test under the 50% El Centro ground motion. The similarity of the loops is apparent. A ten point moving average on

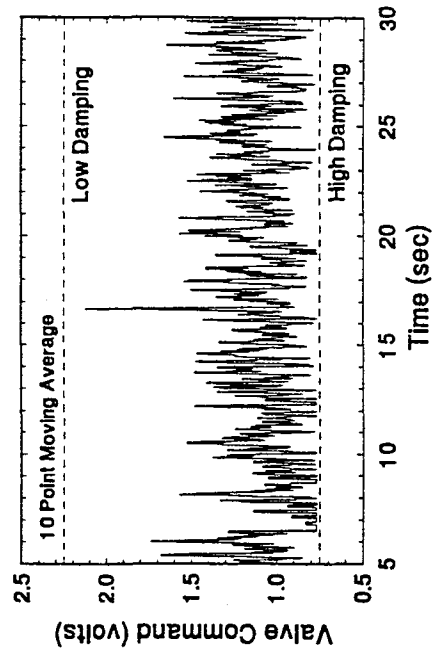
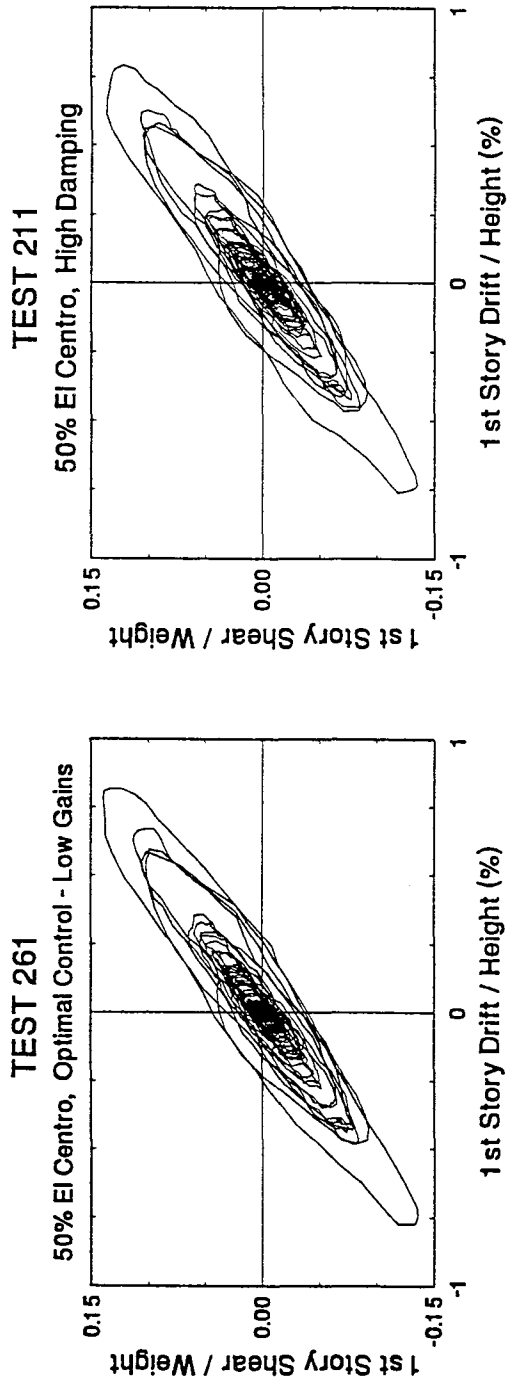


Figure 9-32 Comparison of Semi-Active Optimal Control Test Results with High Damping Passive Control Test Results for Three-Story Structure Subjected to 50% El Centro Motion

the unfiltered valve command signal for the semi-active control test is also presented in Figure 9-32 and demonstrates that the optimal control algorithm tends to drive the semi-active dampers toward the high damping configuration. Apparently, the high damping passive control system was more efficient than the active or semi-active control systems for this particular structure, excitation, and control algorithm.

SECTION 10

ANALYTICAL PREDICTION OF SEISMIC SIMULATION TEST RESULTS

10.1 Instantaneous Control Predictions

Analytical predictions of the shaking table test results for the one-story and three-story structure were obtained using two different methods. One method assumes that, at each time step in the analysis, the response is measured instantaneously, a command signal is determined instantaneously, and the semi-active dampers respond instantaneously. This type of control is ideal but cannot be realized in the laboratory. The analytical predictions associated with this method are designated as "instantaneous" control predictions.

10.2 Predictions Including the Effect of Time Delays

A second method for analytical predictions was developed to take into the account the inherent time delays associated with dynamic control systems. This method assumes that, at each time step in the analysis, the response is measured with a time delay, the command signal is generated based on the delayed response, and the semi-active dampers respond with both a static and dynamic time delay (recall Section 3.4 for a discussion of semi-active damper time delays). Further, it is assumed that the semi-active control valves are not capable of responding to a command signal if they are currently responding to a previous command signal.

The time delays utilized in analysis of the one-story and three-story structure with semi-active dampers are based on the data provided in Tables 3-VI, 3-VII, and 8-I and are given in Table 10-I for the one-story structure with two-stage dampers and in Table 10-II for the one-story and three-story structure with variable dampers. The time delays are expressed as multiples of the time step of the numerical analysis (10 msec). In Section 10.4, predictions which include the effect of time delays are shown to produce results that are in closer agreement with the experimentally measured results than the predictions obtained under the assumption of instantaneous control.

10.3 Time History Response Analysis

The general procedure for obtaining analytical predictions was as follows:

- 1) At each time step, calculate the response of the structure.
- 2) Check if valve is currently responding to a previous command signal. If so, allow the valve to respond and continue to next time step. Otherwise, proceed to step 3.
- 3) Using one of the control algorithms described in Section 7, calculate the required damping coefficient, C_{SA} , for each semi-active damper (e.g., see Equation (7-11)).
- 4) Check if the required damping coefficient is within the range of allowable values for the semi-active damper damping coefficient (see Equation (7-6)). If outside acceptable range, set the damping coefficient equal to the appropriate limit (i.e., C_{max} or C_{min}).
- 5) Adjust the damping coefficient according to either the instantaneous (Section 10.1) or delayed (Section 10.2) control method.

Table 10-I Time Delays for Numerical Analysis of Response of One-Story Structure with Two-Stage Dampers (with reference to Figure 8-1)

QUANTITY	NOTATION	APPROXIMATE DELAY (msec)	NUMBER OF TIME STEPS
Measurement and Computation Delays	τ_1	30	3
Damper Delays (High to Low)	τ_2 - HL - S τ_2 - HL - D	10	0 - Static 1 - Dynamic
Damper Delays (Low to High)	τ_2 - LH - S τ_2 - LH - D	50	3 - Static 2 - Dynamic

Notes: HL = High to Low Damping
 LH = Low to High Damping
 S = Static Damper Response
 D = Dynamic Damper Response
 Time step of numerical analysis = 10 msec

Table 10-II Time Delays for Numerical Analysis of Response of One-Story and Three-Story Structure with Variable Dampers (with reference to Figure 8-1)

QUANTITY	NOTATION	APPROXIMATE DELAY (msec)	NUMBER OF TIME STEPS
Measurement and Computation Delays	τ_1	30	3
Damper Delays (High to Low)	τ_2 - HL - S τ_2 - HL - D	20	1 Static 1 Dynamic
Damper Delays (Low to High)	τ_2 - LH - S τ_2 - LH - D	20	1 Static 1 Dynamic

Notes: HL = High to Low Damping
 LH = Low to High Damping
 S = Static Damper Response
 D = Dynamic Damper Response
 Time step of numerical analysis = 10 msec

10.3.1 One-Story Structure

The time history analysis of the one-story structure with semi-active dampers begins with the equation of motion given by Equation (6-1) and the equation describing the semi-active damper behavior (Equation 6-2)

$$m\ddot{u} + c_u \dot{u} + ku + 2P_d = -m\ddot{u}_g \quad (10-1)$$

$$P_d + \lambda \dot{P}_d = C_{SA} \cos^2 \theta \dot{u} \quad (10-2)$$

where the number of dampers, η , has been set equal to two. Equations (10-1) and (10-2) are written as a set of first order differential equations

$$\{\dot{Z}\} = [A]\{Z\} + \{H\}\ddot{u}_g \quad (10-3)$$

where

$$\{Z\} = \begin{Bmatrix} \dot{u} \\ u \\ P_d \end{Bmatrix} \quad (10-4)$$

$$[A] = \begin{bmatrix} -2\xi_u \omega_n & -\omega_n^2 & -2m^{-1} \\ 1 & 0 & 0 \\ \lambda^{-1} C_{SA} \cos^2 \theta & 0 & -\lambda^{-1} \end{bmatrix} \quad (10-5)$$

and

$$\{H\} = \begin{Bmatrix} 1 \\ 0 \\ 0 \end{Bmatrix} \quad (10-6)$$

Analytical predictions for the one-story structure were obtained by numerically solving the set of differential equations described by Equation (10-3) (e.g., IMSL 1987). The numerical solution provides the time history of the quantities in vector $\{Z\}$ (i.e., the

relative displacement, relative velocity, and horizontal component of force in each semi-active damper). The total acceleration is computed from Equation (10-1) and is used in calculation of the base shear force.

10.3.2 Three-Story Structure

The time-history analysis of the three-story structure follows the same approach as described in the previous section for the one-story structure. The equations of motion of the structure with semi-active dampers at the first story and the equation describing the damper behavior are given by Equations (6-17), (6-18), and (6-19)

$$[M]\{\ddot{u}\} + [C_u]\{\dot{u}\} + [K]\{u\} + \{P_d\} = -[M]\{1\}\ddot{u}_g \quad (10-7)$$

$$\{P_d\} = \begin{Bmatrix} 0 \\ 0 \\ 2P_1 \end{Bmatrix} \quad (10-8)$$

$$P_1 + \lambda \dot{P}_1 = C_{SA} \cos^2 \theta_1 \dot{u}_1 \quad (10-9)$$

where the number of dampers in the first story, η_1 , has been set equal to two. Equations (10-7), (10-8), and (10-9) can be written as a set of first order differential equations

$$\{\dot{Z}\} = [A]\{Z\} + [H]\{f\} \quad (10-10)$$

where

$$\{Z\} = \begin{Bmatrix} \{\dot{u}\} \\ \{u\} \\ \{P_d\} \end{Bmatrix} \quad (10-11)$$

$$[A] = \begin{bmatrix} -[M]^{-1}[C_u] & -[M]^{-1}[K] & -[M]^{-1} \\ [I] & 0 & 0 \\ \lambda^{-1}[C] & 0 & -\lambda^{-1}[I] \end{bmatrix} \quad (10-12)$$

$$[H] = \begin{bmatrix} [I] \\ [0] \\ [0] \end{bmatrix} \quad (10-13)$$

and

$$\{f\} = \{1\}\ddot{u}_g \quad (10-14)$$

Note that matrix $[C]$ is obtained from Equation (6-38)

$$[C] = \begin{bmatrix} 0 & 0 & 0 \\ 0 & 0 & 0 \\ 0 & 0 & 2C_{SA}\cos^2\theta \end{bmatrix} \quad (10-15)$$

Analytical predictions for the three-story structure were obtained by numerically solving the set of differential equations described by Equation (10-10) (e.g., IMSL 1987). The stiffness and damping matrix of the structure, $[K]$ and $[C_v]$ in Equation (10-7), were obtained from experimentally determined frequencies, damping ratios, and mode shapes (see Section 6.4.2). The numerical solution provides the time history of the quantities in vector $\{Z\}$ (i.e., the relative displacement vector, the relative velocity vector, and the vector of horizontal component of force from the semi-active dampers). The total acceleration vector is computed from Equation (10-7) and is used in calculation of the story shear forces.

10.4 Comparison of Experimental Results and Analytical Predictions

10.4.1 One-Story Structure

Experimental results are compared with analytical predictions in Figures 10-1 through 10-11 for the one-story structure with semi-active two-stage dampers. The comparisons are presented in the form of base shear force versus story drift loops.

Figure 10-1 shows comparisons for the low and high damping passive control systems. Note that friction is clearly present in the experimental low damping test. Although the analytical model does not account for the friction between the piston rod and piston rod seal, the analytical prediction compares quite well with the experimental results. This is because the analytical model of semi-active damper behavior (Equation 6-2) was calibrated using experimental data in which friction was not explicitly accounted for (see Section 3.3) but was implicitly included (i.e., the friction force was not extracted from the damper force-displacement loops prior to determining the mechanical properties). The analytical results for the high damping passive control system also compare very well with the experimental data, indicating that the mathematical models describing the structure (Equation (10-1)) and the dampers (Equation (10-2)) are valid.

Figures 10-2 through 10-11 show comparisons of experimental and analytical base shear versus story drift loops for the one-story structure with two-stage dampers using three different analytical methods. The plot shown at the top of each figure presents analytical results based on the assumption of instantaneous control (see Section 10.1). Although

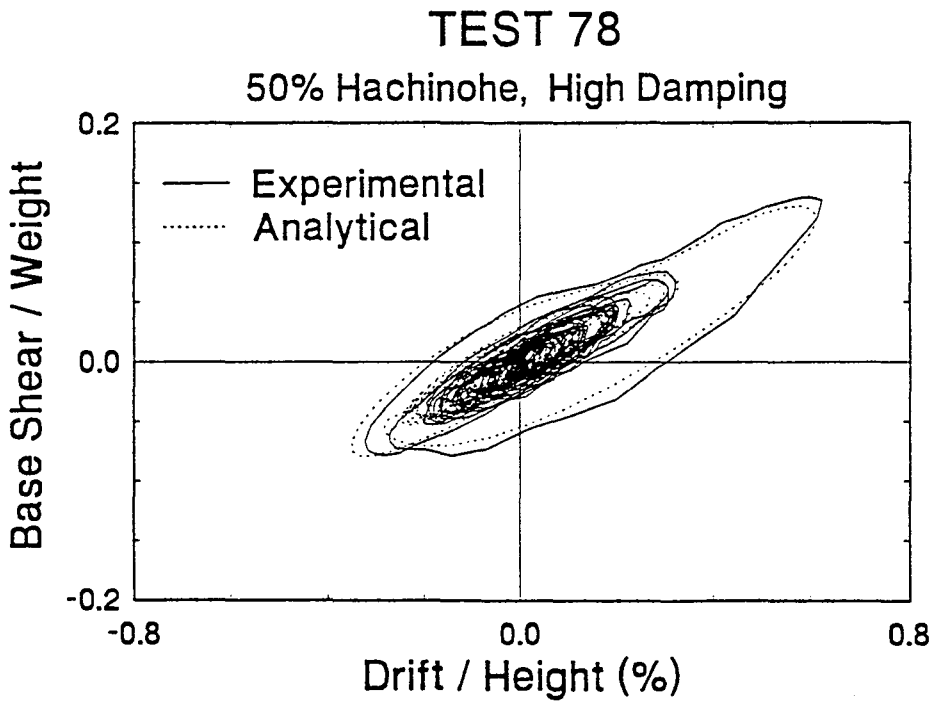
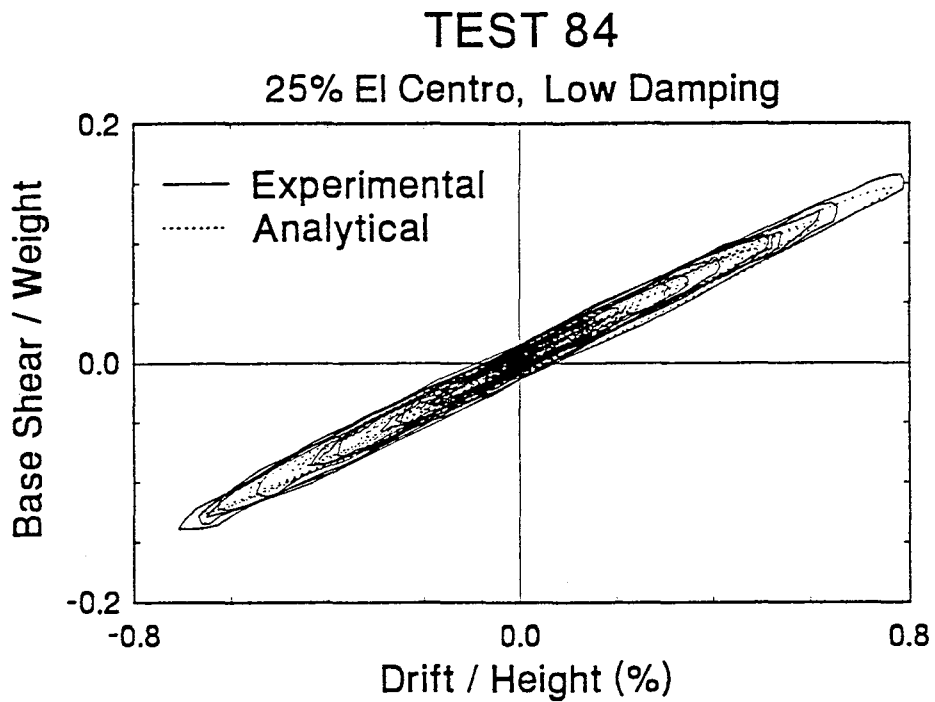


Figure 10-1 Comparison of Experimental and Analytical Base Shear Versus Drift Loops of the One-Story Flexible Structure with Two-Stage Dampers Set to Low and High Damping

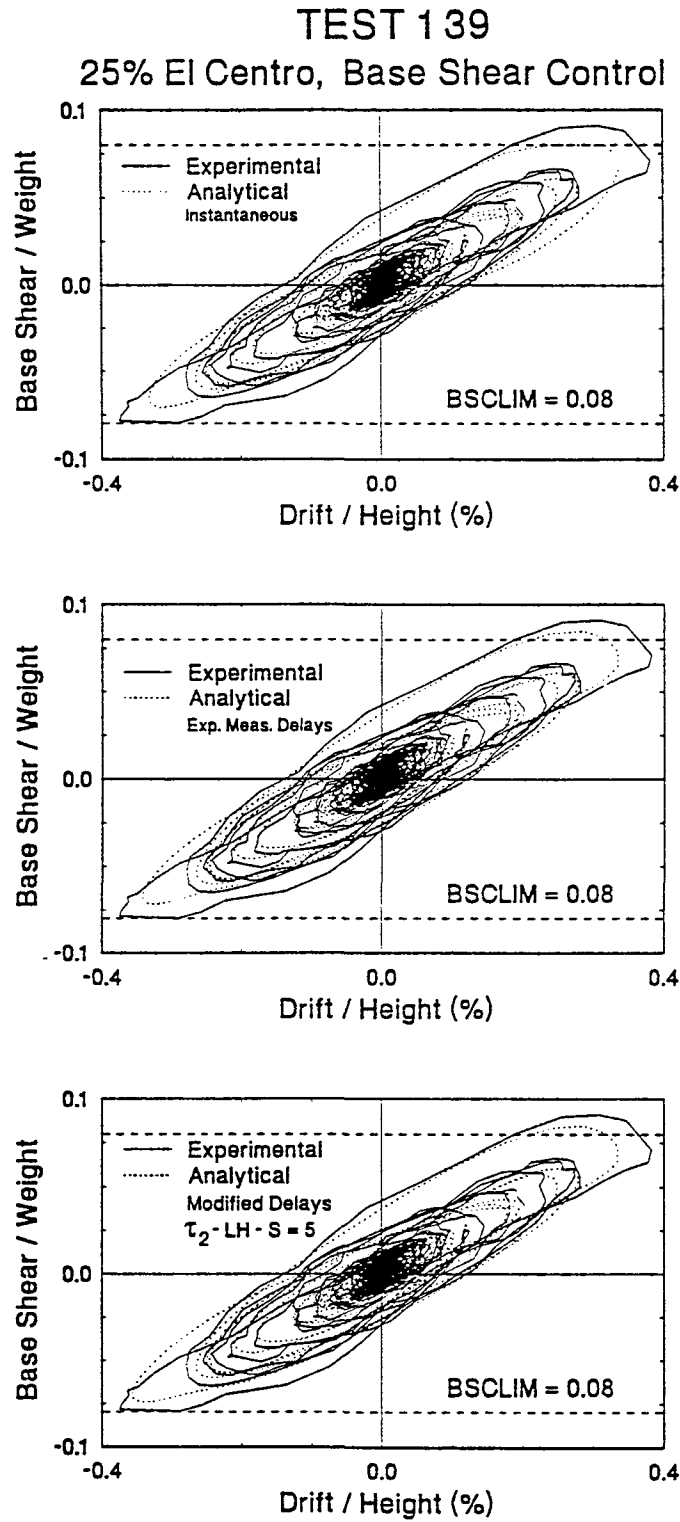


Figure 10-2 Comparison of Experimental and Analytical Base Shear Versus Drift Loops of One-Story Flexible Structure with Two-Stage Dampers Subjected to 25% El Centro Motion and Controlled by Base Shear Coefficient Control Algorithm

TEST 140
50% Hachinohe, Base Shear Control

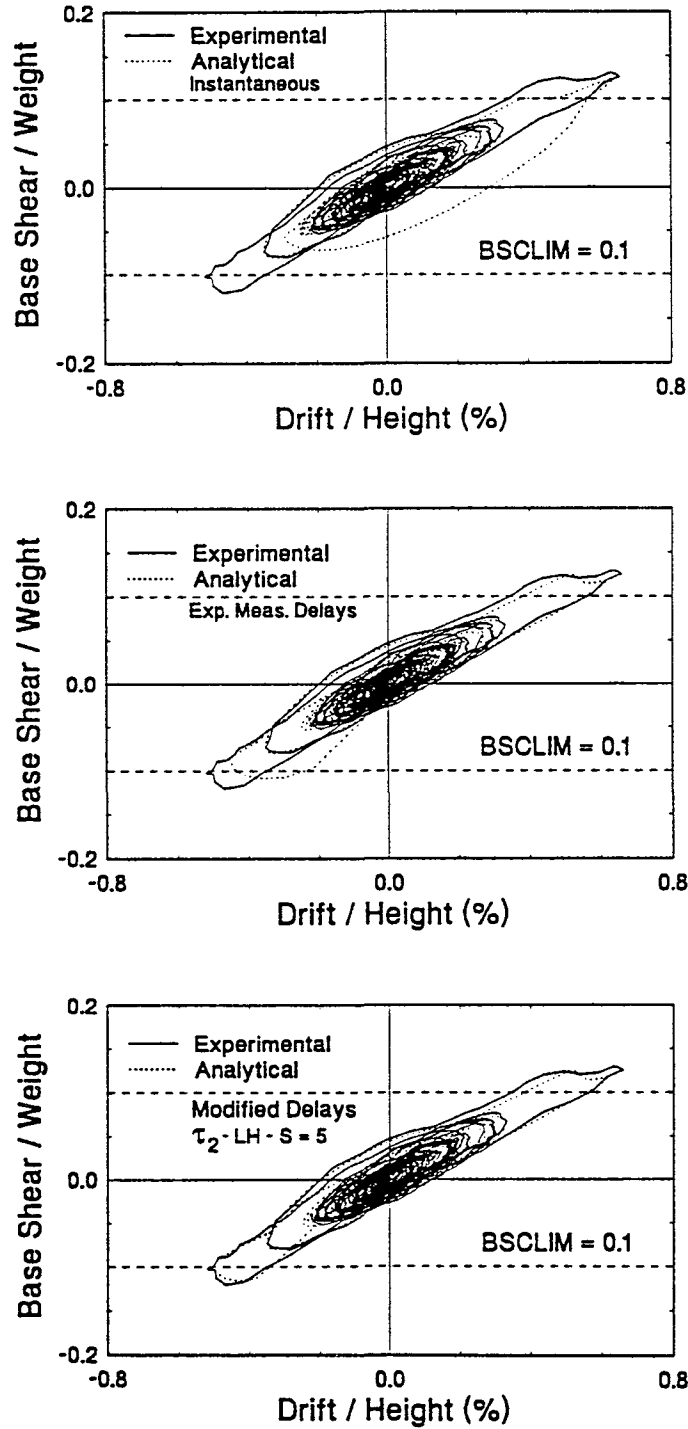


Figure 10-3 Comparison of Experimental and Analytical Base Shear Versus Drift Loops of One-Story Flexible Structure with Two-Stage Dampers Subjected to 50% Hachinohe Motion and Controlled by Base Shear Coefficient Control Algorithm

TEST 142
 0.2g 5 Hz Harmonic, Base Shear Control

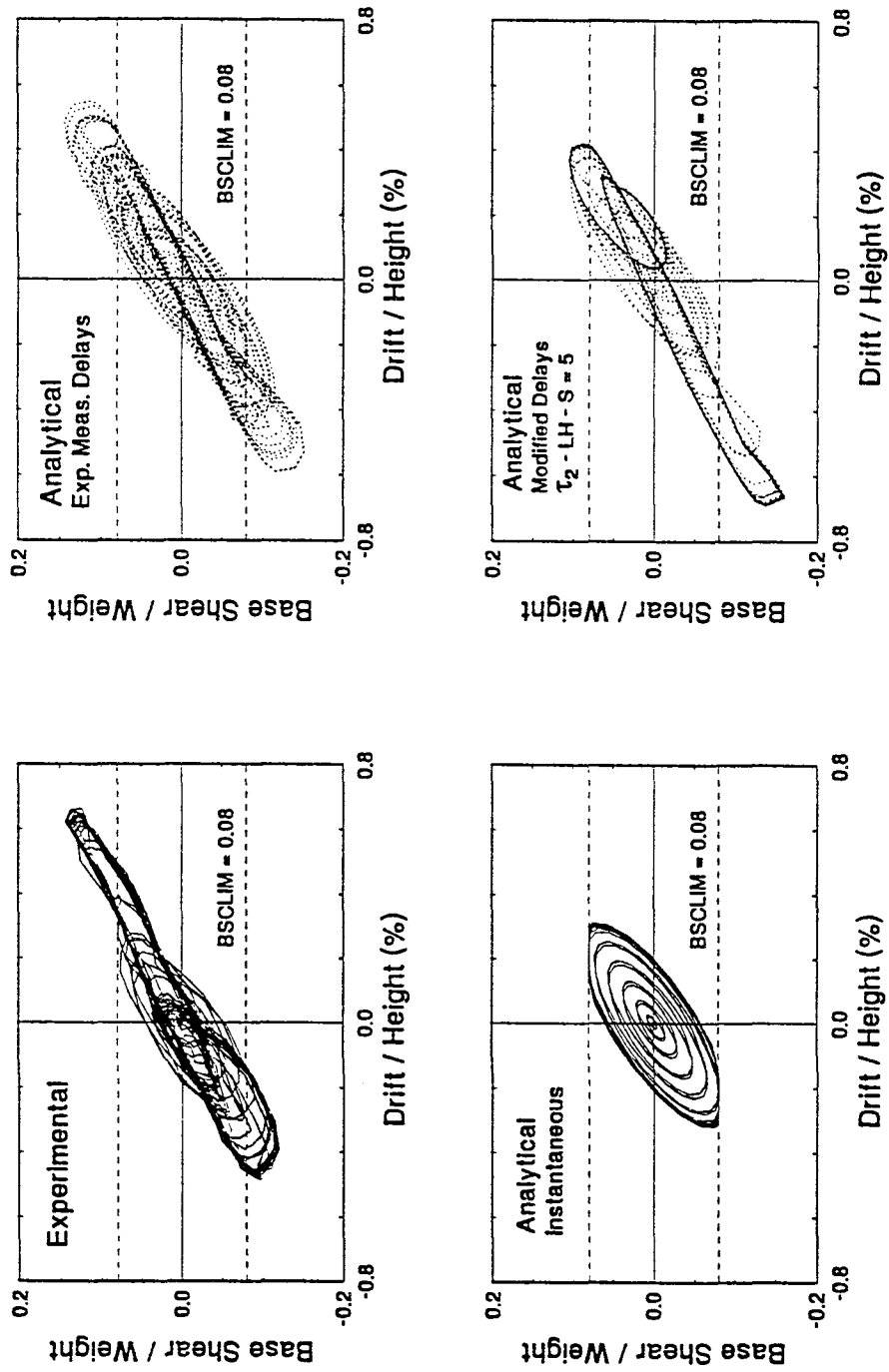


Figure 10-4 Comparison of Experimental and Analytical Base Shear Versus Drift Loops of One-Story Flexible Structure with Two-Stage Dampers Subjected to Harmonic Motion and Controlled by Base Shear Coefficient Control Algorithm

TEST 135
25% El Centro, Force Transfer Control

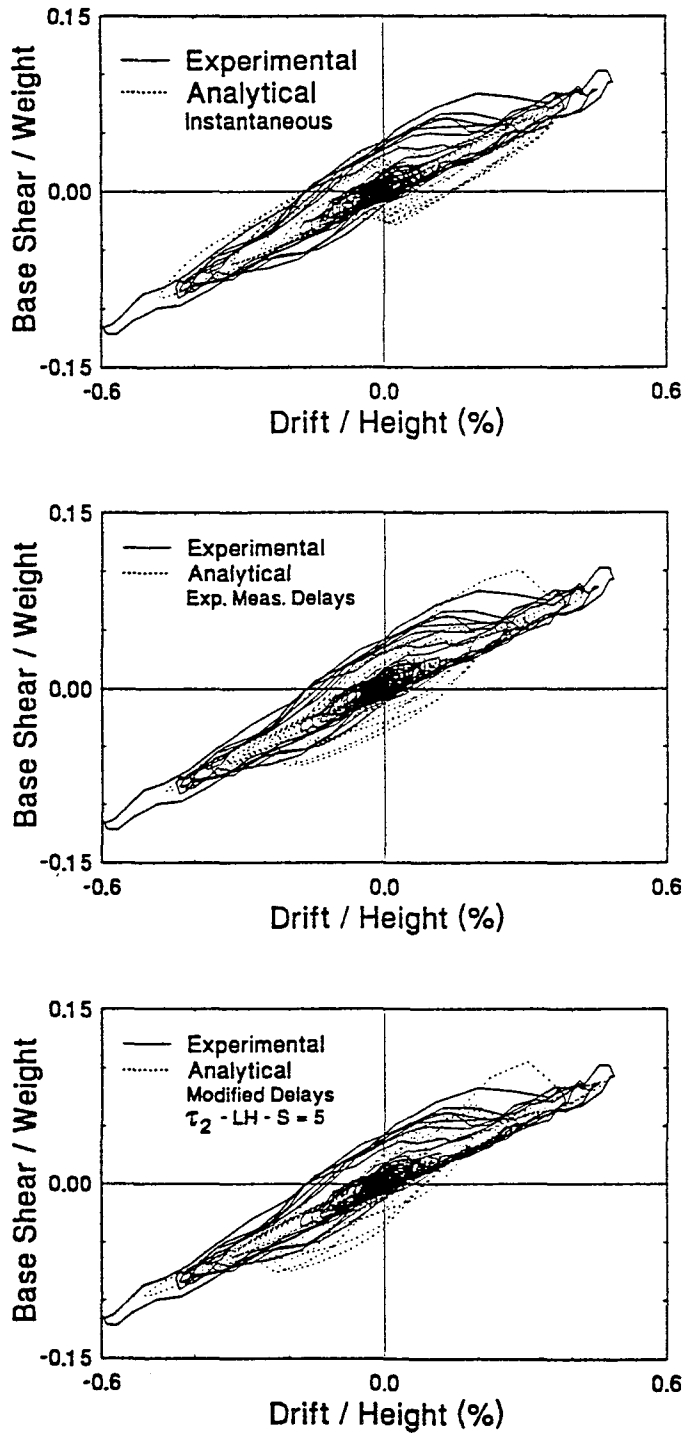


Figure 10-5 Comparison of Experimental and Analytical Base Shear Versus Drift Loops of One-Story Flexible Structure with Two-Stage Dampers Subjected to 25% El Centro Motion and Controlled by Force Transfer Control Algorithm

TEST 136
50% Hachinohe, Force Transfer Control

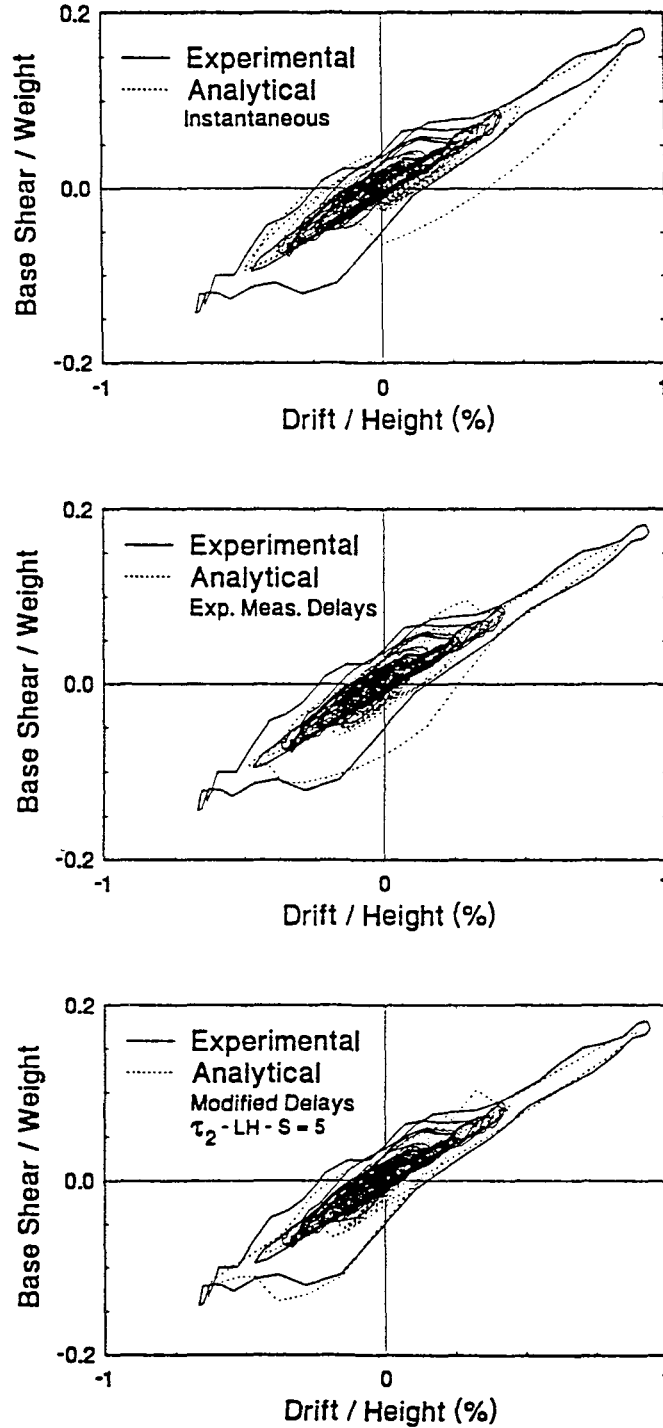


Figure 10-6 Comparison of Experimental and Analytical Base Shear Versus Drift Loops of One-Story Flexible Structure with Two-Stage Dampers Subjected to 50% Hachinohe Motion and Controlled by Force Transfer Control Algorithm

TEST 146
0.2g 5 Hz Harmonic, Base Shear Control - KC

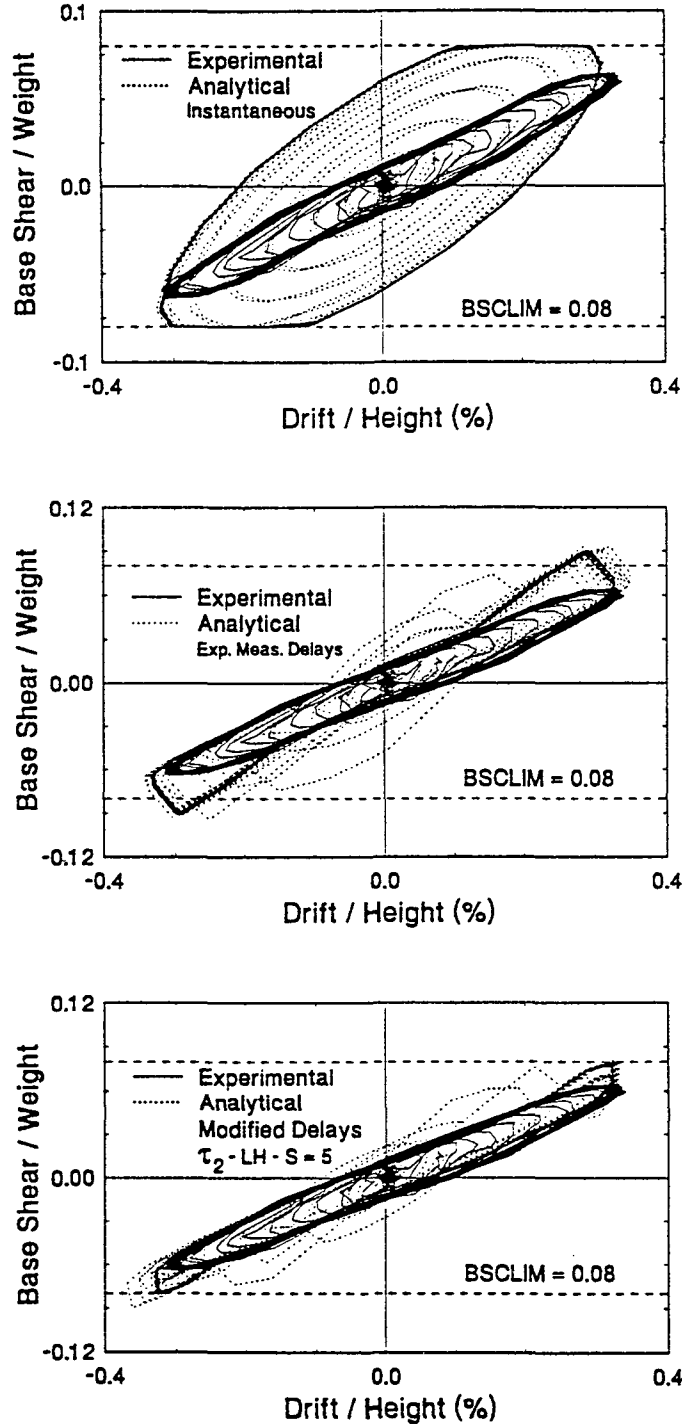


Figure 10-7 Comparison of Experimental and Analytical Base Shear Versus Drift Loops of One-Story Flexible Structure with Two-Stage Dampers Subjected to Harmonic Motion and Controlled by Base Shear Coefficient Control Algorithm with Kinematic Compensation

TEST 125
50% Hachinohe, Force Transfer Control - KC

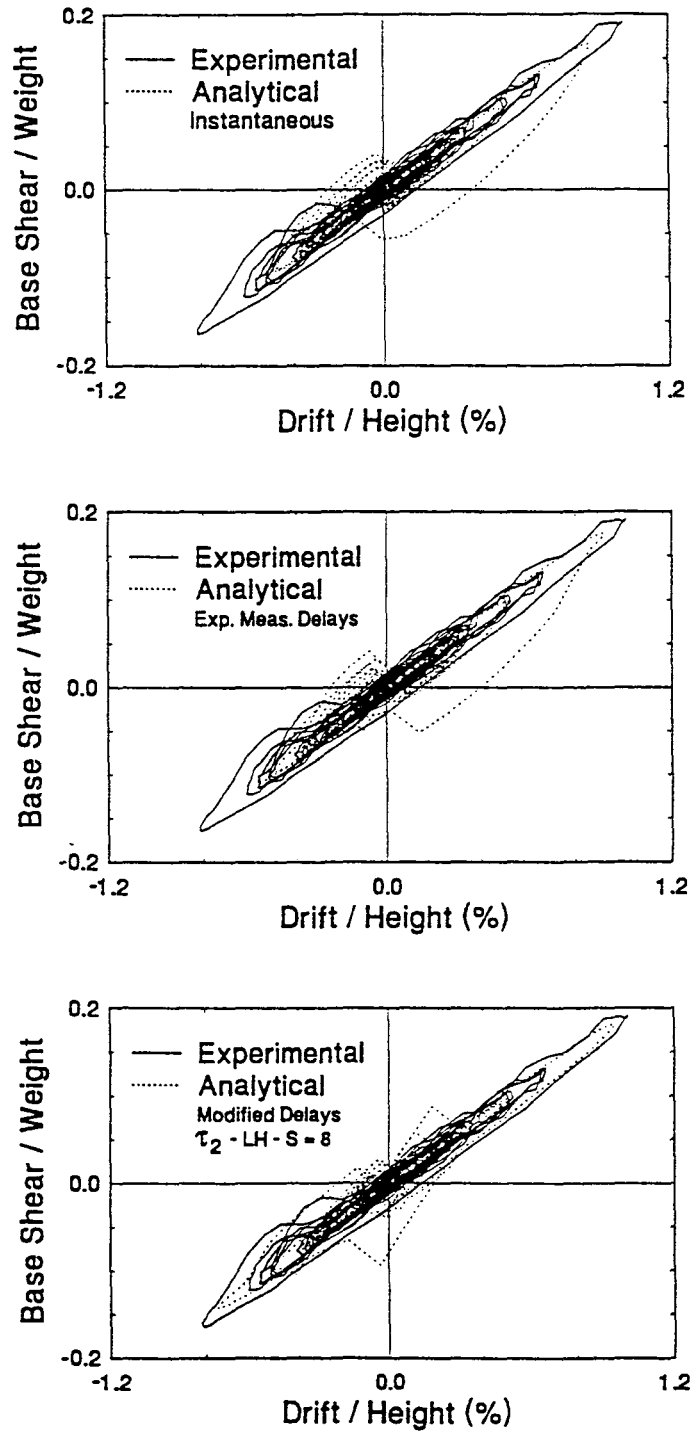


Figure 10-8 Comparison of Experimental and Analytical Base Shear Versus Drift Loops of One-Story Flexible Structure with Two-Stage Dampers Subjected to 50% Hachinohe Motion and Controlled by Force Transfer Control Algorithm with Kinematic Compensation

TEST 148
50% Hachinohe, Force Transfer Control - HC

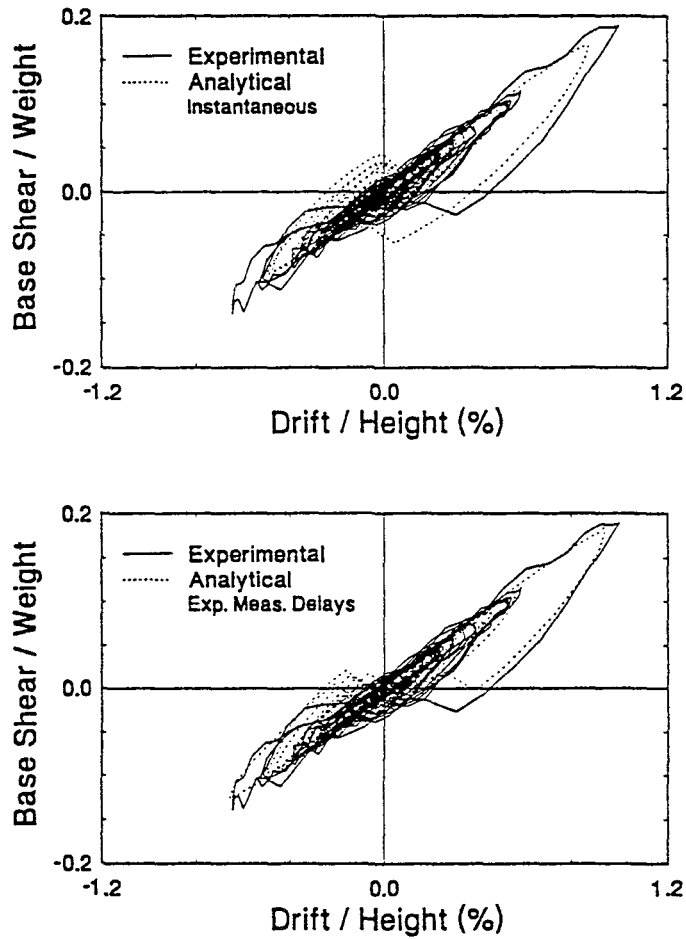


Figure 10-9 Comparison of Experimental and Analytical Base Shear Versus Drift Loops of One-Story Flexible Structure with Two-Stage Dampers Subjected to 50% Hachinohe Motion and Controlled by Force Transfer Control Algorithm with Kinematic Compensation

TEST 149

100% Hachinohe-M, Force Transfer Control - HC

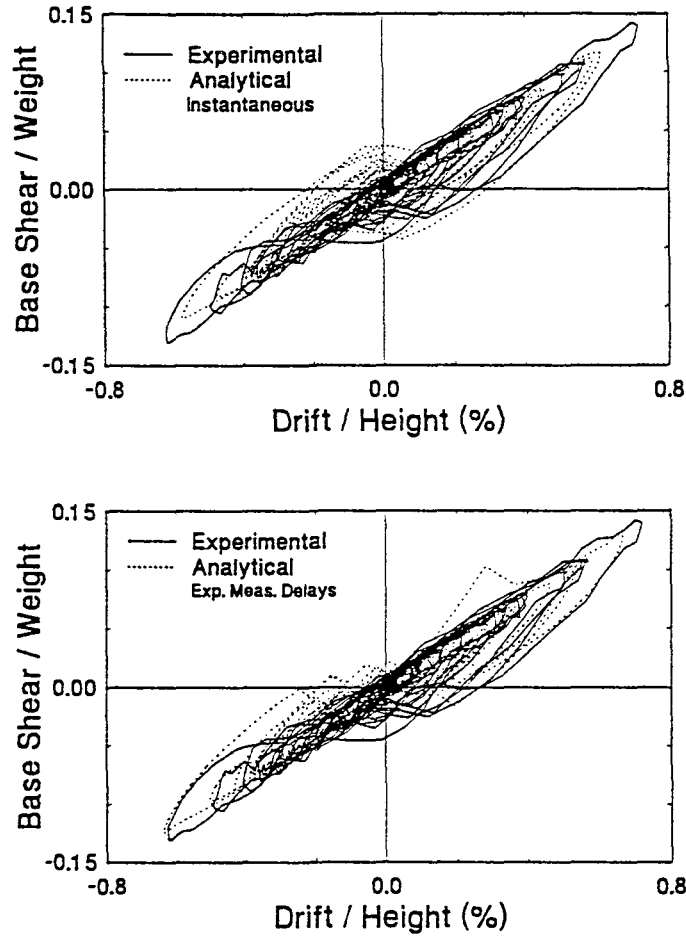


Figure 10-10 Comparison of Experimental and Analytical Base Shear Versus Drift Loop of One-Story Flexible Structure with Two-Stage Dampers Subjected to 100% Modified Hachinohe Motion and Controlled by Force Transfer Control Algorithm with Harmonic Compensation

TEST 150
0.2g 5 Hz Harmonic, Force Transfer Control - HC

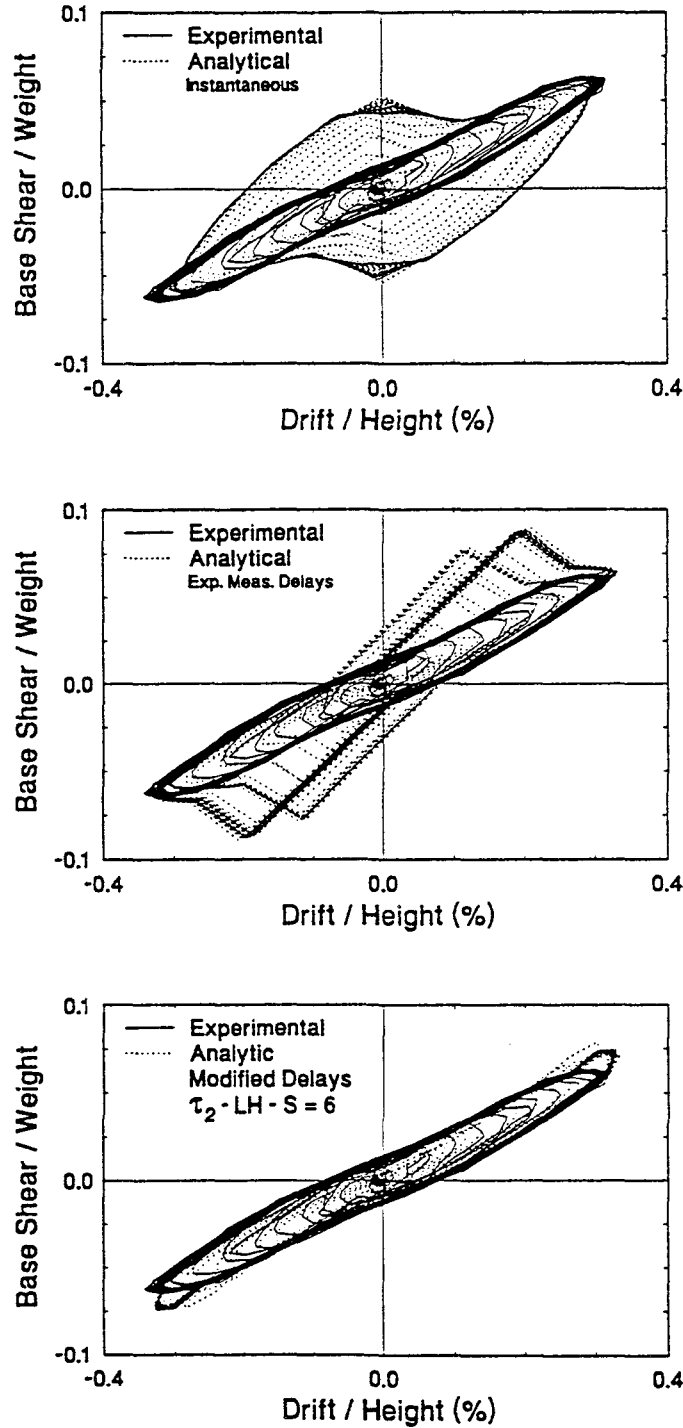


Figure 10-11 Comparison of Experimental and Analytical Base Shear Versus Drift Loops of One-Story Flexible Structure with Two-Stage Dampers Subjected to Harmonic Motion and Controlled by Force Transfer Control Algorithm with Harmonic Compensation

instantaneous control cannot be realized in the laboratory, it does represent the ideal response for the given semi-active control algorithm. The plot shown in the center of Figures 10-2 through 10-11 shows analytical results which utilize the experimentally measured delays (see Section 10.2). Of course, the experimentally measured delays for the semi-active dampers were obtained in saturated command signal tests in which a single command signal was applied to the control valve (see Section 3.4). In contrast, during the shaking table tests, the command signal to the control valves was updated at time intervals of approximately 2 to 6 ms. Lack of knowledge regarding the behavior of the control valves under such high frequency command signals produced analytical results that are not generally in close agreement with the experimental results. In an effort to further improve the analytical predictions, some of the time delays shown in Tables 10-I and 10-II were modified. The plot shown at the bottom of Figures 10-2 through 10-11 presents analytical predictions which are based on modified time delays. For example, the response in Figure 10-2 was calculated with a modified time delay model in which all parameters were maintained as given in Table 10-I except for the static low to high damper delay which was increased from 3 to 5 time steps ($\tau_2 - LH - S = 5$ rather than $\tau_2 - LH - S = 3$). In general, the modification of a single time delay parameter results in a significant improvement in the analytical prediction. The notation used in the modified time delay plots may be interpreted according to Tables 10-I and 10-II.

An interesting prediction is presented in Figure 10-4 for the one-story structure with two-stage dampers subjected to harmonic ground motion and controlled according to the

base shear coefficient control algorithm. The experimental results were discussed previously in Section 9.3.1.1 where the bi-harmonic nature of the response was described. The analytical prediction based on modified time delays appears to contain the bi-harmonic response but the large drifts occur in the opposite direction compared to the experimental results. This situation is explored in further detail in Figure 10-12 in which time histories of experimental and analytical response quantities are presented. The bi-harmonic response is clearly evident in the time histories. The experimental and analytical drift time histories are superimposed in Figure 10-13 over the complete duration of the test and over the initial portion of the test. Note that the experimental and analytical drift response start out in unison but reach a point where the two results diverge, one with large positive drifts (experimental) and one with large negative drifts (analytical). This behavior is also evident in the time history of damper force shown at the bottom of Figure 10-13. The divergence in the experimental and analytical results may have occurred as the result of minor differences between the parameters of the mathematical model of the structure/semi-active damper system and the actual properties of the system. Recall from Section 9.3.1.1 that the bi-harmonic response contains a driving frequency component related to the steady-state harmonic ground motion and a natural frequency component related to the transient response. The transient response is apparently induced by the semi-active damper control activity wherein time delays play an important role (compare the instantaneous and modified time delay response shown in Figure 10-4; the bi-harmonic response can be predicted only if time delays are included in the analysis).

0.2g 5 Hz Harmonic, Base Shear Control

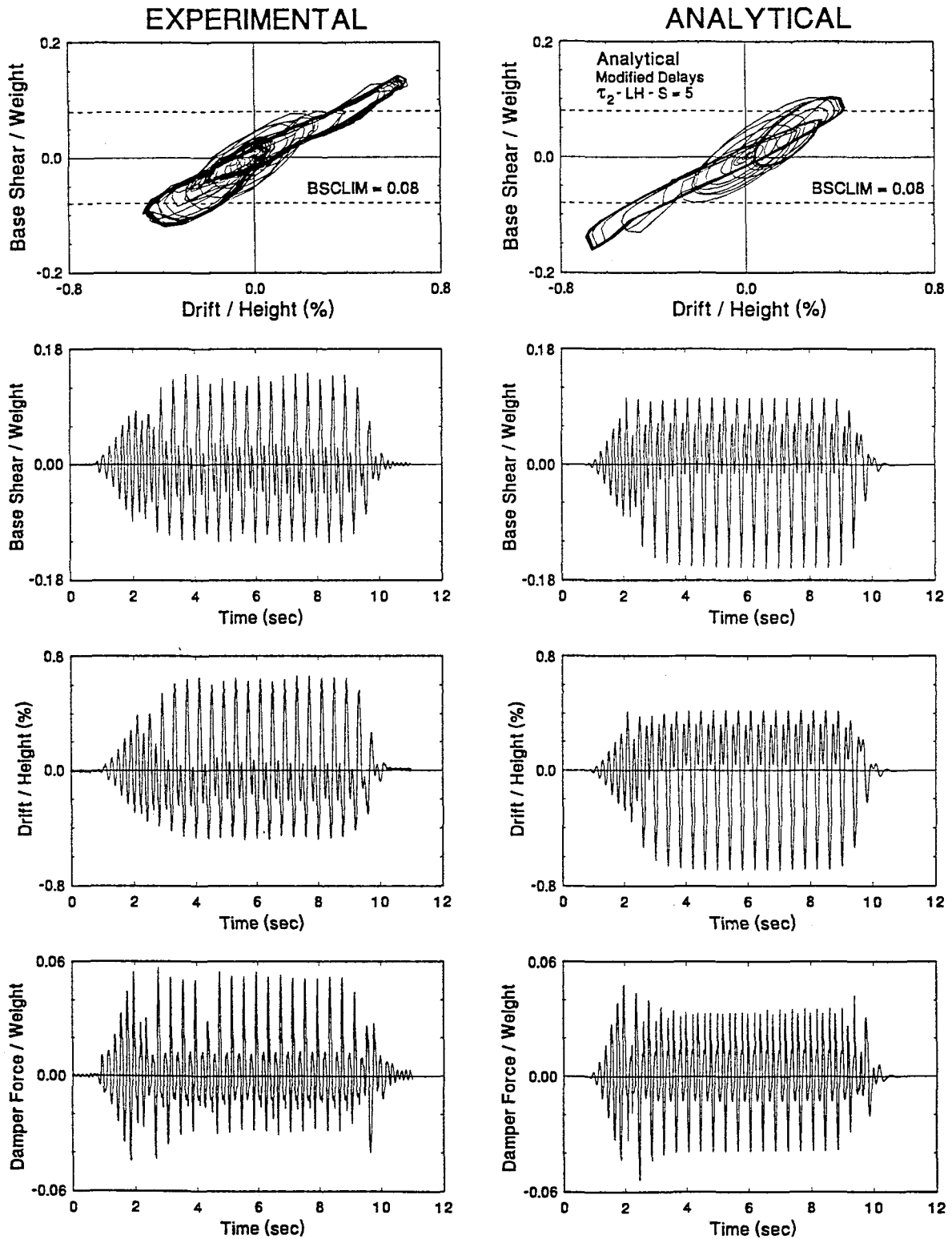


Figure 10-12 Experimental and Analytical Time Histories of Various Response Quantities of One-Story Flexible Structure with Two-Stage Dampers Subjected to Harmonic Motion and Controlled by Base Shear Coefficient Control Algorithm

TEST 142

0.2g 5 Hz Harmonic, Base Shear Control

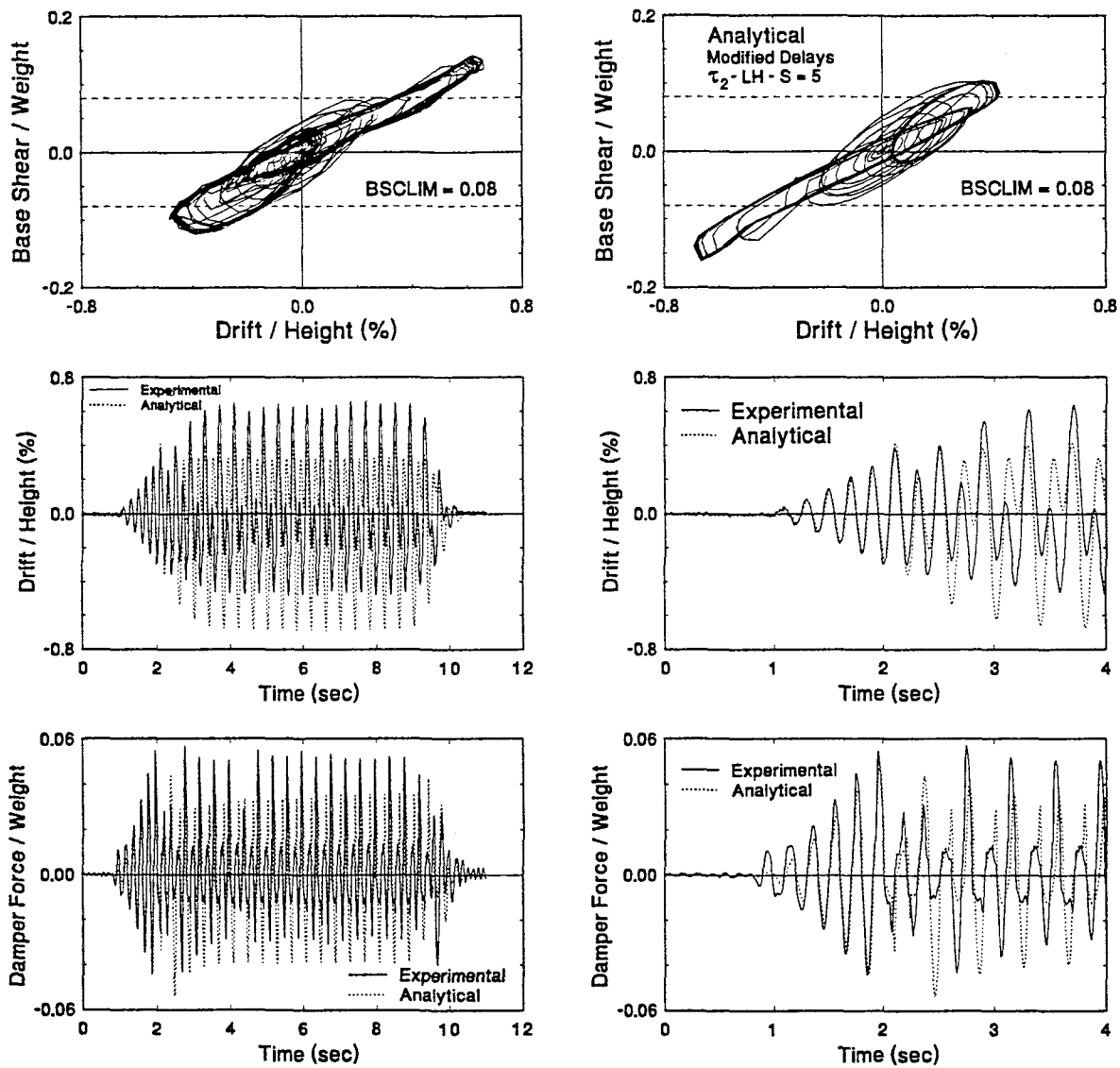


Figure 10-13 Comparisons of Experimental and Analytical Response of One-Story Flexible Structure with Two-Stage Dampers Subjected to Harmonic Motion and Controlled by Base Shear Coefficient Control Algorithm

The objective of the experimental time delay compensation methods is to achieve control which approaches the instantaneous control described in Section 10.1. Verification of this is provided in the test results shown in Figures 10-6 and 10-9 where it is clear that the use of harmonic compensation (for the particular ground motion and control algorithm utilized in the two tests) resulted in an experimental response which approaches the analytical prediction based on the assumption of instantaneous control.

Experimental results are compared with analytical predictions in Figures 10-14 through 10-16 for the one-story structure with semi-active variable dampers. Figure 10-14 shows comparisons for the low and high damping passive control systems. The same discussion in the beginning of this section regarding the presence of friction in the low damping case with two-stage dampers is also applicable to the variable dampers. The experimental and analytical loops in the high damping case do not compare well in terms of the peak values of base shear and drift. This is apparently the result of the difference in the experimental value of the damping coefficient in each variable damper unit and the value used in the analysis (see Figure 7-1).

There is a clear improvement in the analytical prediction with modified time delays for the feedforward control test shown in Figure 10-16. Note that two of the five time delay parameters (see Table 10-II) were modified for this particular analysis. The experimental and analytical results for this test are examined in further detail in Figure 10-17. In Figure 10-17(c), the experimental command signal (filtered) and experimental spool displacement

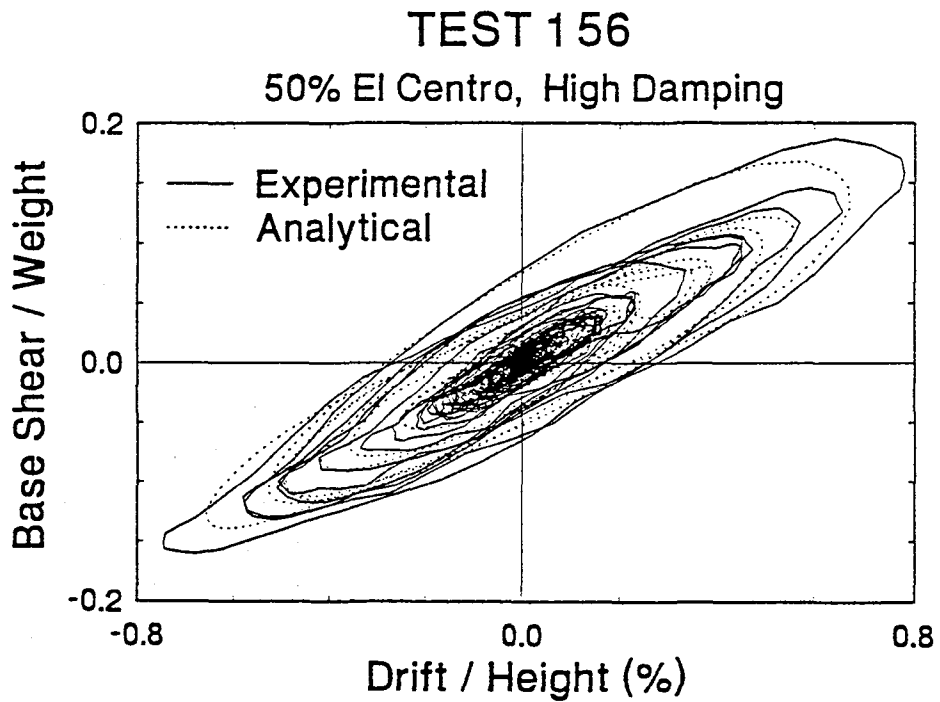
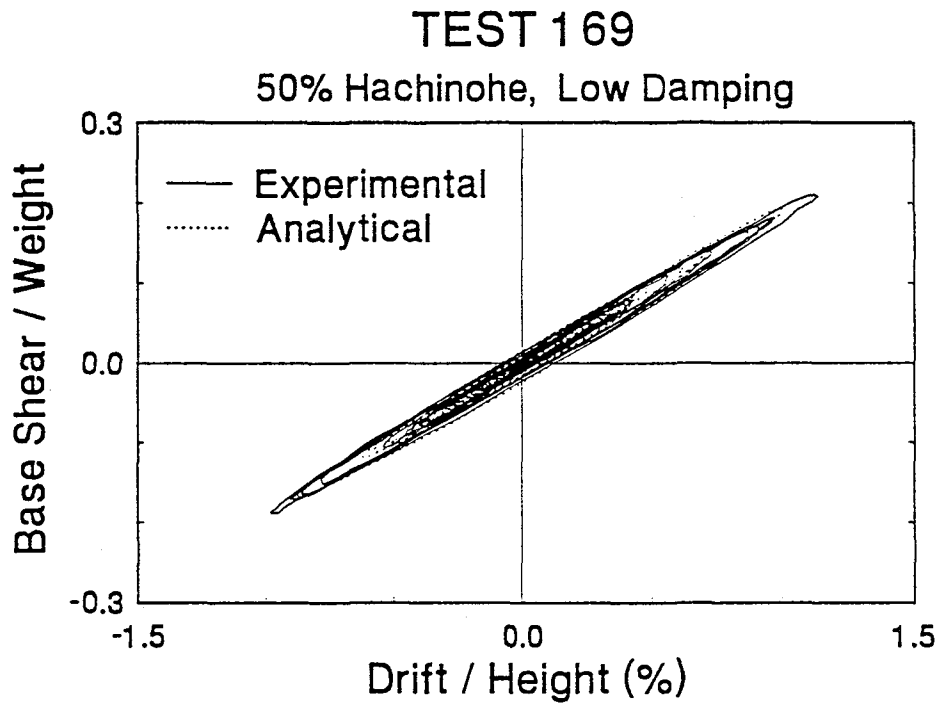


Figure 10-14 Comparison of Experimental and Analytical Base Shear Versus Drift Loops of the One-Story Flexible Structure with Variable Dampers Set to Low and High Damping

TEST 287

25% El Centro, Skyhook Damping

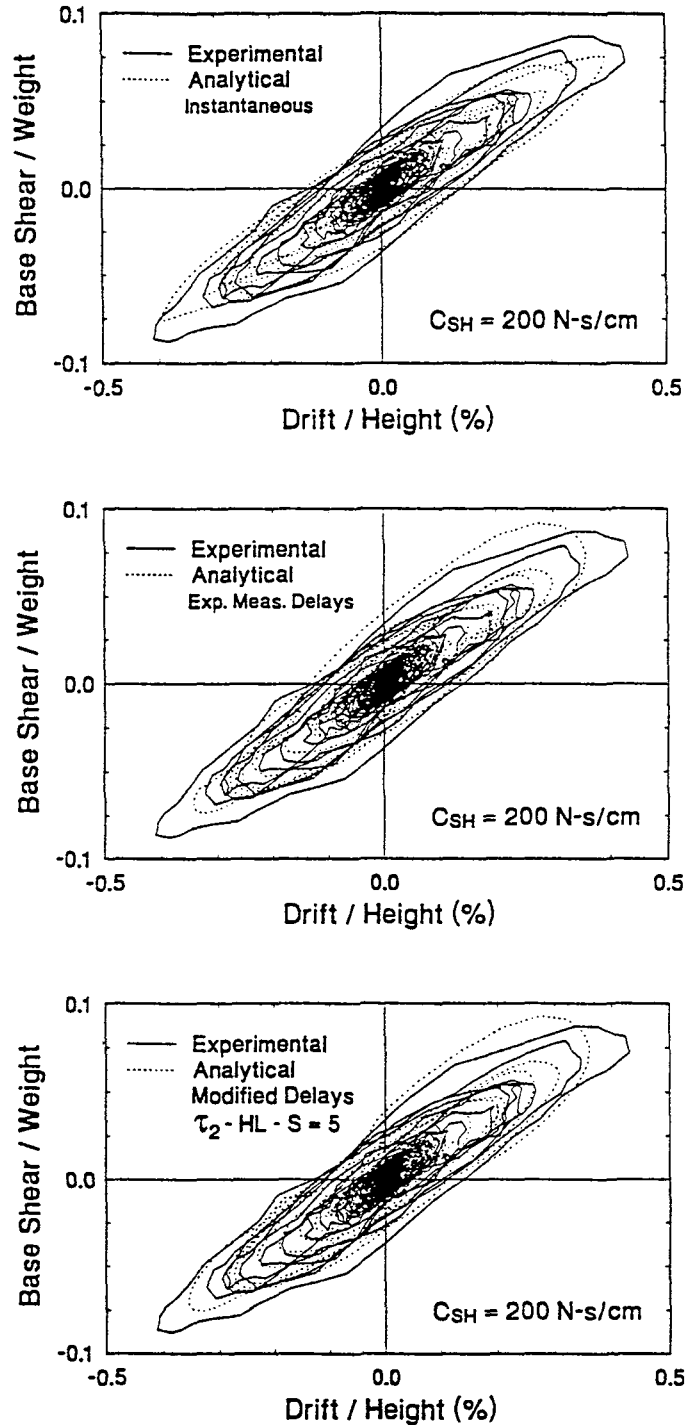


Figure 10-15 Comparison of Experimental and Analytical Base Shear Versus Drift Loops of One-Story Flexible Structure with Variable Dampers Subjected to 25% El Centro Motion and Controlled by Skyhook Damping Algorithm

TEST 315

75% Hachinohe, Feedforward Control

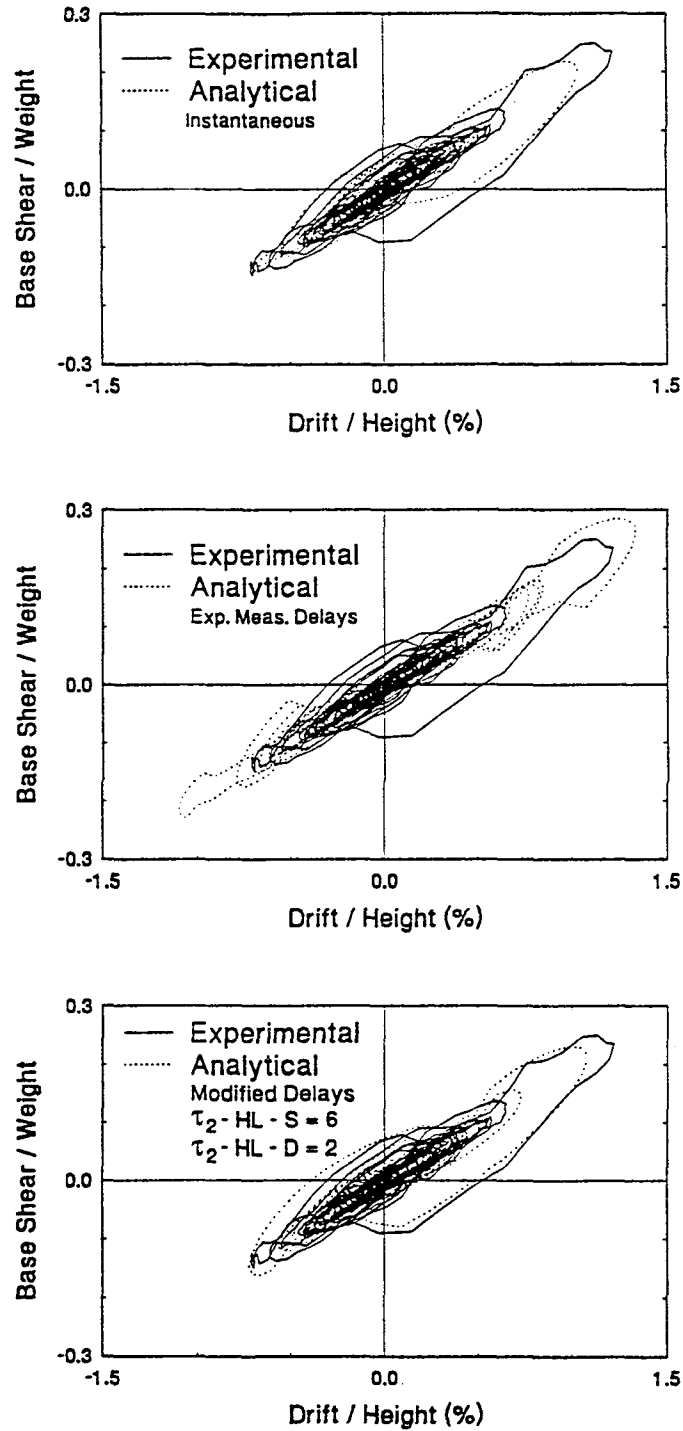


Figure 10-16 Comparison of Experimental and Analytical Base Shear Versus Drift Loops of One-Story Flexible Structure with Variable Dampers Subjected to 75% Hachinohe Motion and Controlled by Feedforward Control Algorithm

TEST 315
75% Hachinohe, Feedforward Control

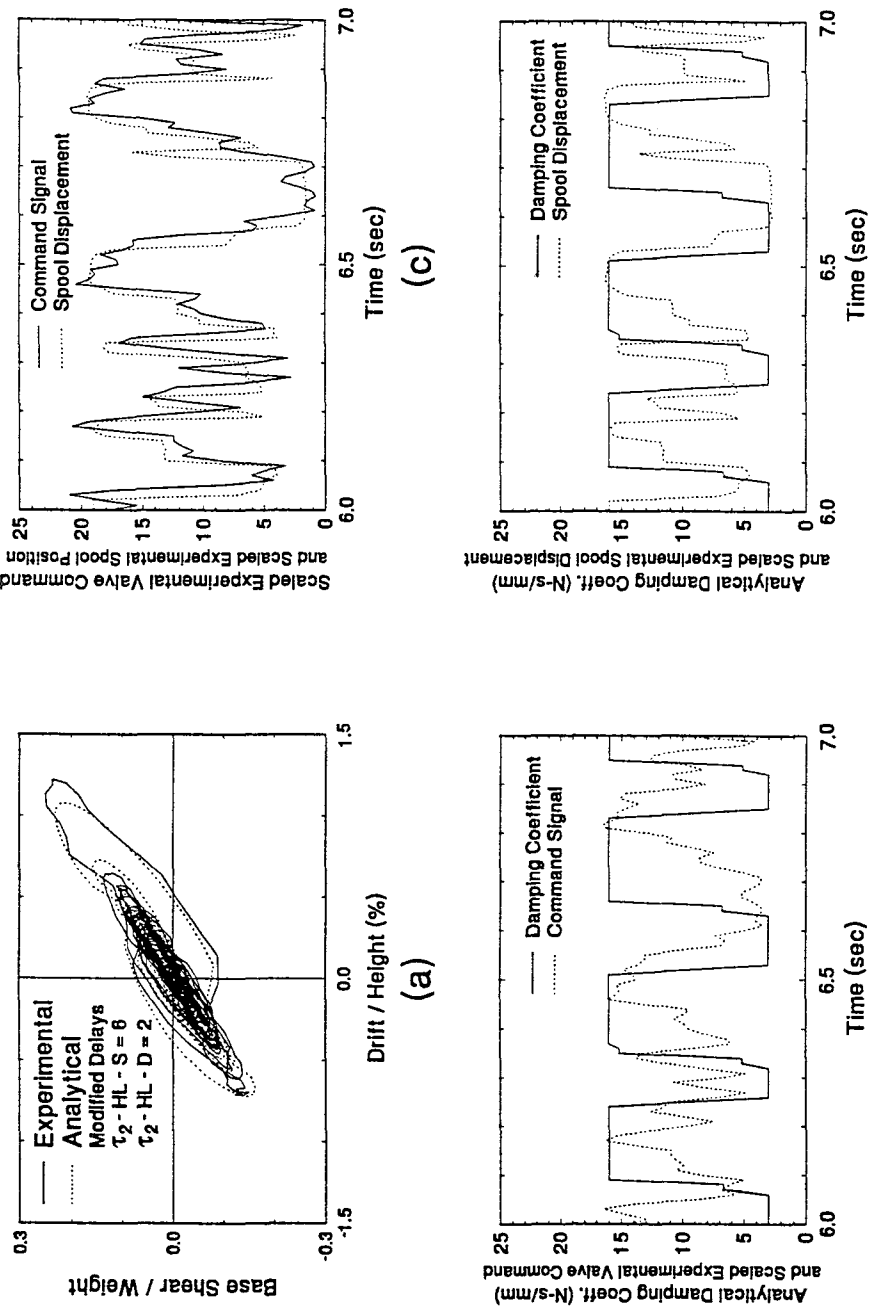


Figure 10-17 Comparison of Experimental and Analytical Results for One-Story Flexible Structure with Variable Dampers Subjected to 75% Hachinohe Motion and Controlled by Feedforward Control Algorithm

(filtered) are superimposed for one of the variable damper valves over a time interval of one second. Note that the spool is able to follow the command signal in a global sense but cannot follow the high frequency localized fluctuations. This is due to the dynamics of the spool as well as the effect that fluid pressure changes have on the spool motion. The analytically determined damping coefficient that was used to obtain the loop of Figure 10-17(a) does not follow the experimental valve command signal (see Figure 10-17(b)) quite as well as it follows the experimental spool displacement (see Figure 10-17(d)). Recall that the command signal and spool displacement are directly related to the damping coefficient (see Figures 3-10 and 7-1). It can be inferred, therefore, that the use of modified time delays in the analysis accounts, in an approximate way, for the unmodeled dynamics of the valve spool. For example, when two successive command signals are sent to the spool within a time interval which is less than the response time measured in the command signal saturation tests of Section 3.4, it is not clear how the spool responds to the second command signal (i.e., the dynamics of the spool under such conditions have not been investigated).

10.4.2 Three-Story Structure

Experimental results are compared with analytical predictions in Figures 10-18 through 10-25 for the three-story structure with semi-active variable dampers. The comparisons are presented in the form of story shear force over total weight ratio versus story drift over story height ratio.

TEST 224

25% Hachinohe, Low Damping

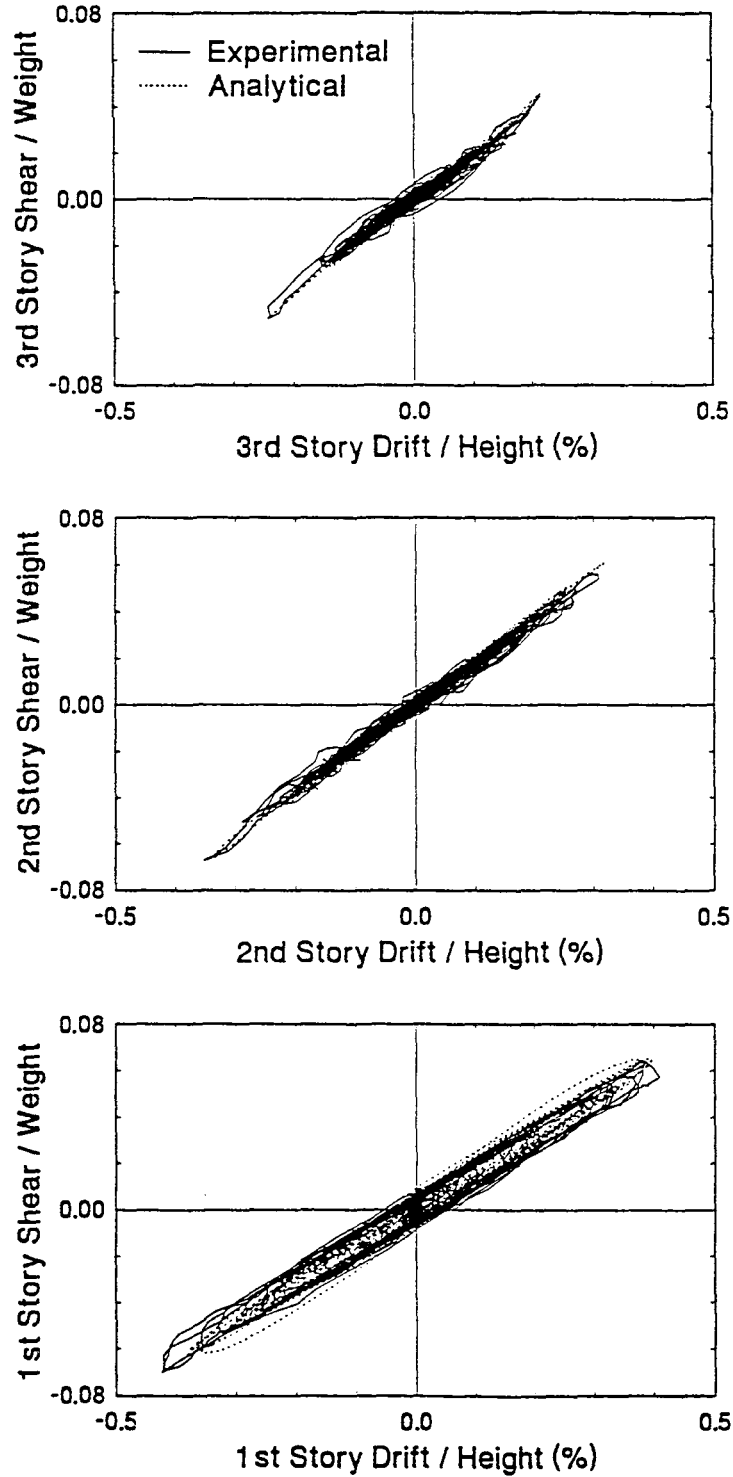


Figure 10-18 Comparison of Experimental and Analytical Story Shear Versus Story Drift Loops for Three-Story Structure Subjected to 25% Hachinohe Motion with Variable Dampers Set to Low Damping

TEST 211

50% El Centro, High Damping

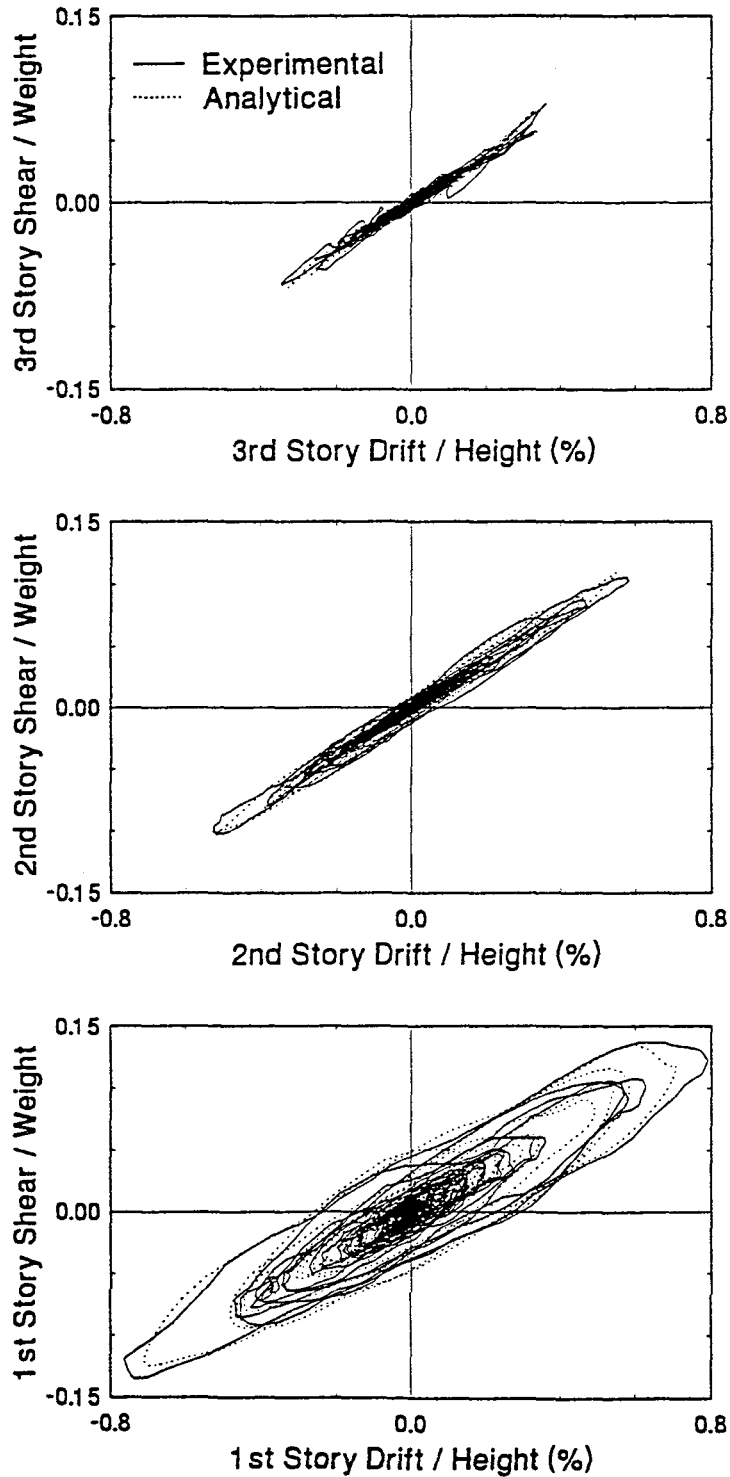


Figure 10-19 Comparison of Experimental and Analytical Story Shear Versus Story Drift Loops for Three-Story Structure Subjected to 50% El Centro Motion with Variable Dampers Set to High Damping

TEST 261

50% El Centro, Optimal Control - Low Gains

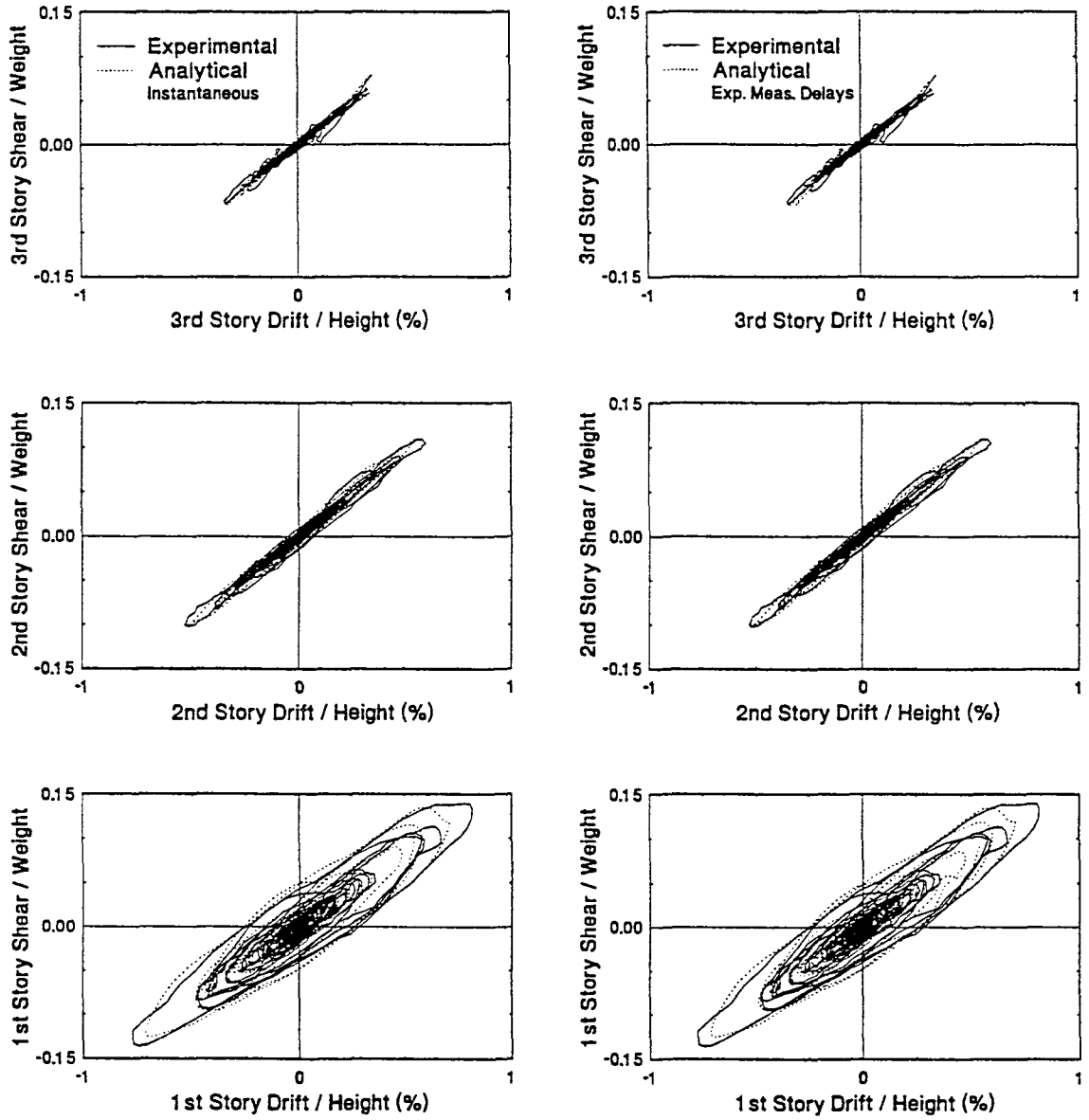


Figure 10-20 Comparison of Experimental and Analytical Story Shear Versus Story Drift Loops for Three-Story Structure Subjected to 50% El Centro Motion with Variable Dampers Controlled by Optimal Control Algorithm with Low Gains

TEST 388

50% El Centro, Optimal Control - High Gains

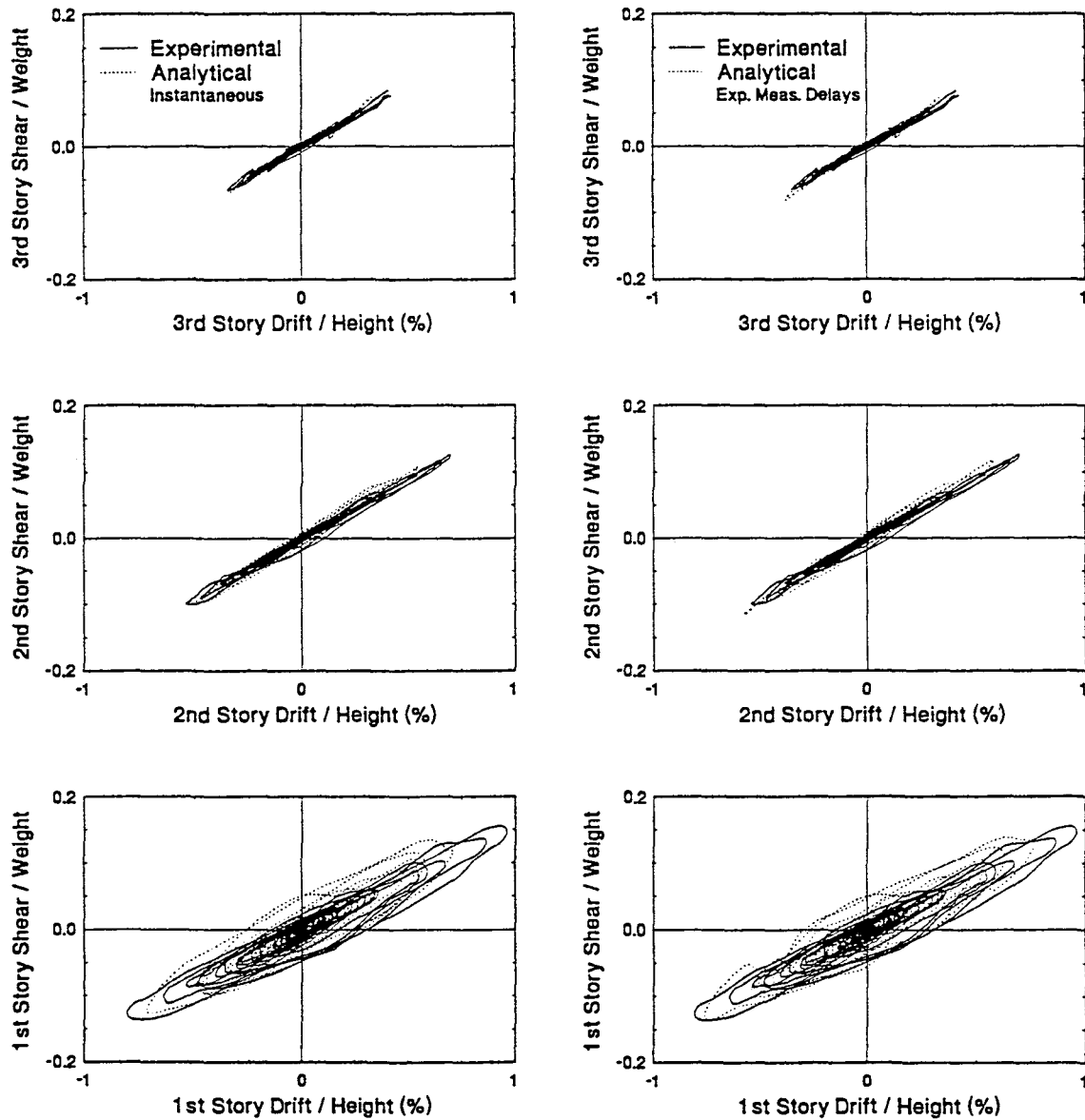


Figure 10-21 Comparison of Experimental and Analytical Story Shear Versus Story Drift Loops for Three-Story Structure Subjected to 50% El Centro Motion with Variable Dampers Controlled by Optimal Control Algorithm with High Gains

TEST 438

50% El Centro, Optimal Control - Low Gains - HC

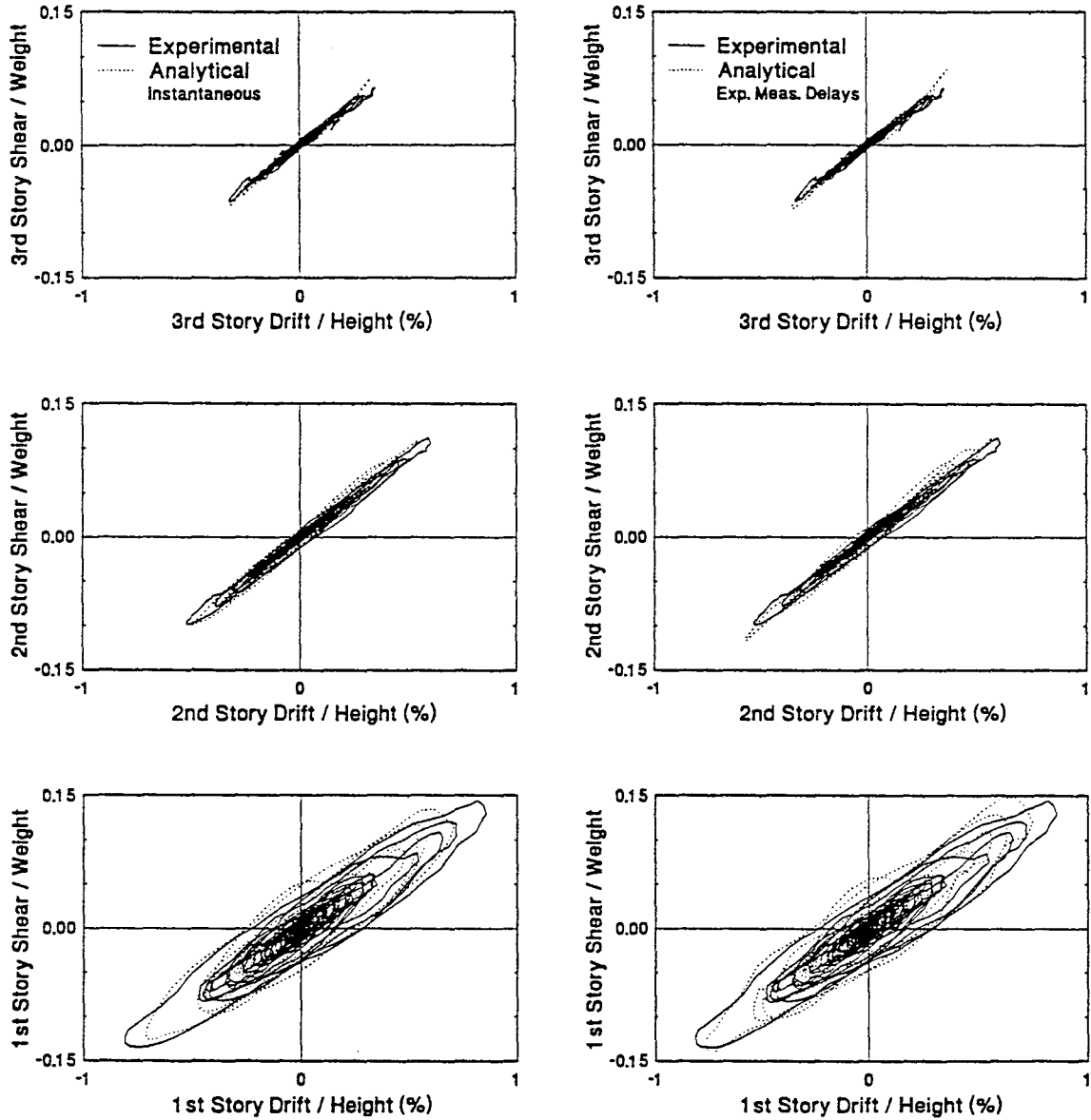


Figure 10-22 Comparison of Experimental and Analytical Story Shear Versus Story Drift Loops for Three-Story Structure Subjected to 50% El Centro Motion with Variable Dampers Controlled by Optimal Control Algorithm with Low Gains and Harmonic Compensation

TEST 436

0.4g 5 Hz Harmonic, Optimal Control - High Gains - HC

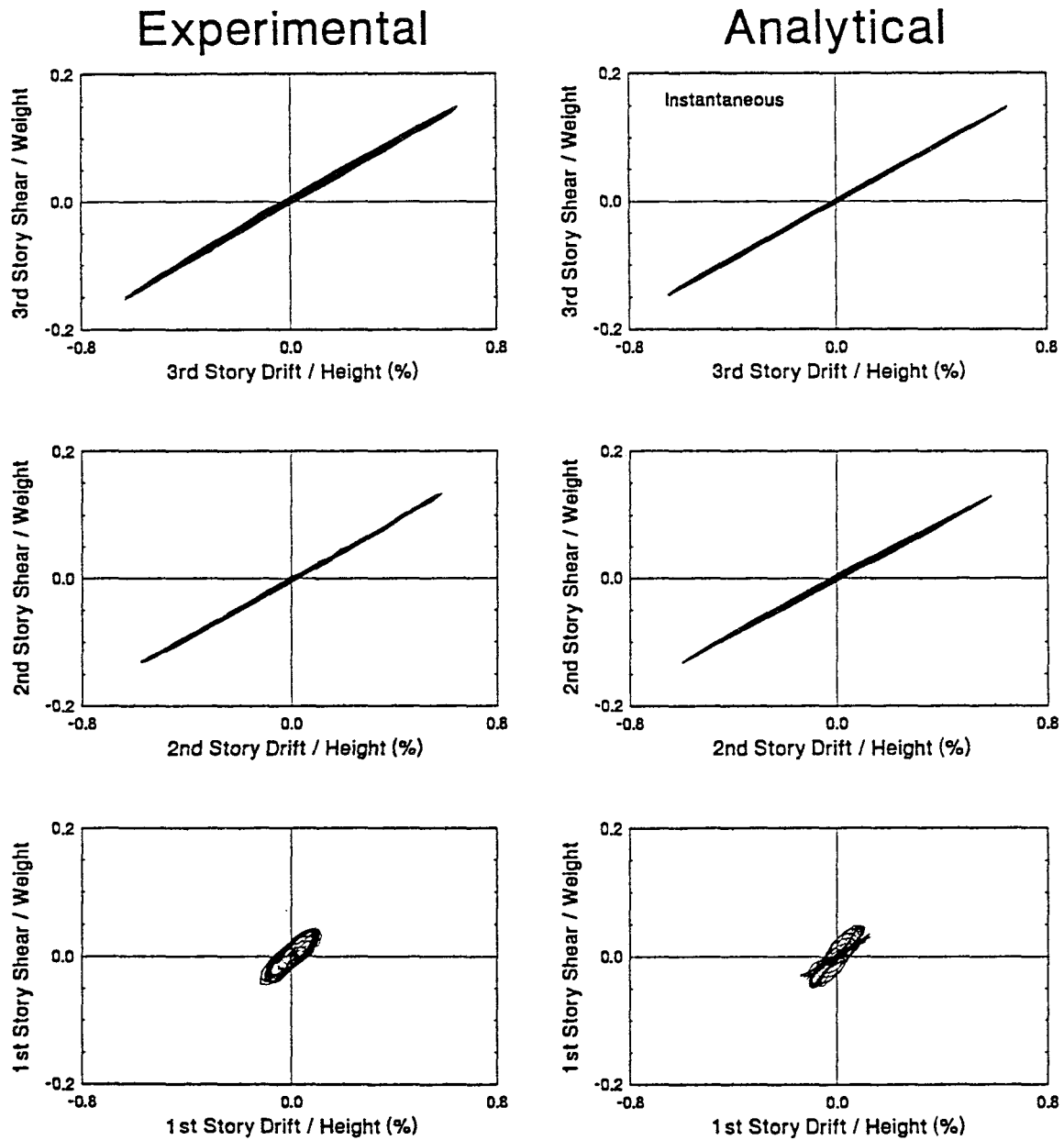


Figure 10-23 Comparison of Experimental and Analytical Story Shear Versus Story Drift Loops for Three-Story Structure Subjected to Harmonic Motion with Variable Dampers Controlled by Optimal Control Algorithm with High Gains and Harmonic Compensation

TEST 436

0.4g 5 Hz Harmonic, Optimal Control - High Gains - HC

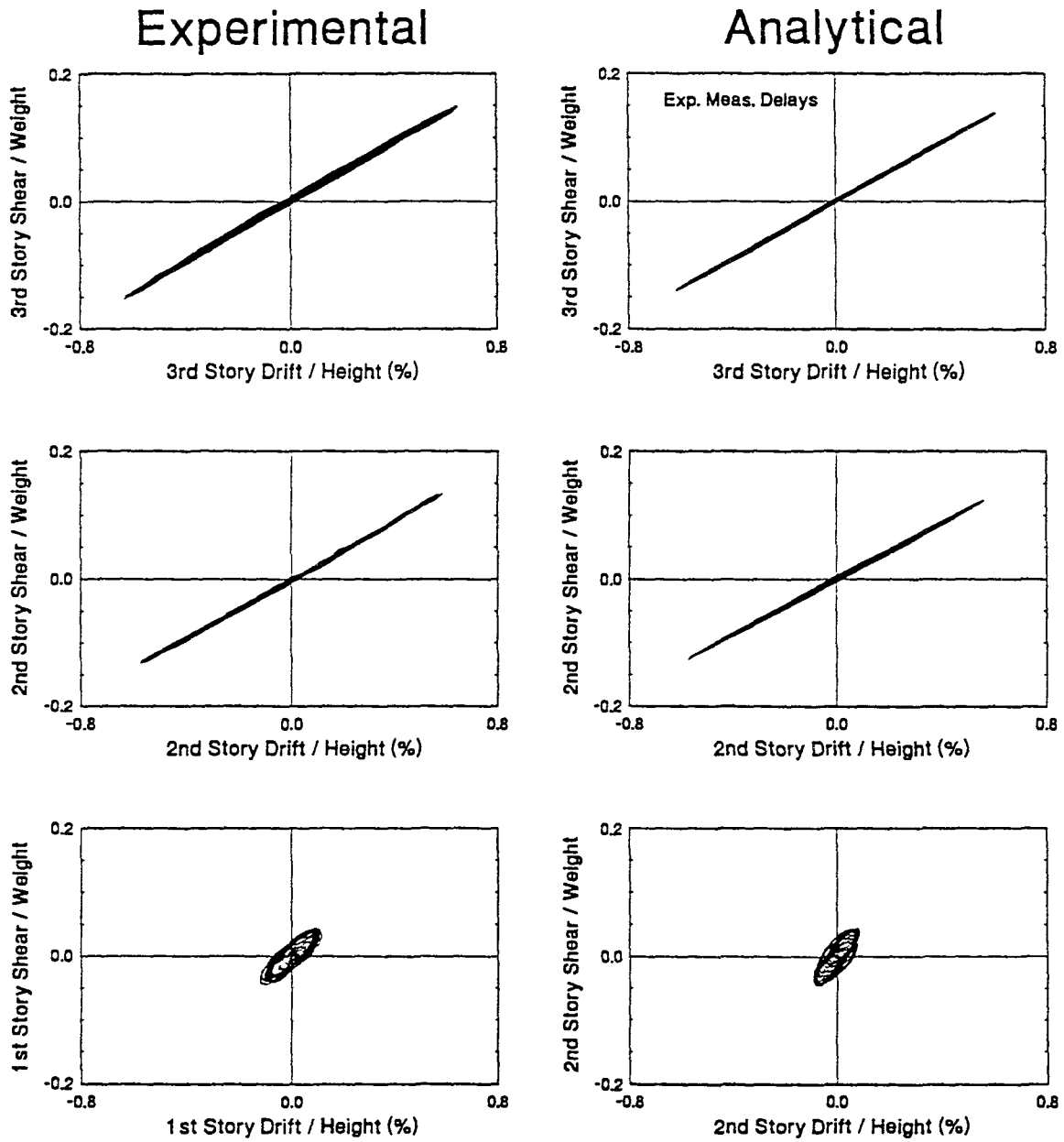


Figure 10-23 Cont'd

TEST 378

75% El Centro, Sliding Mode Control

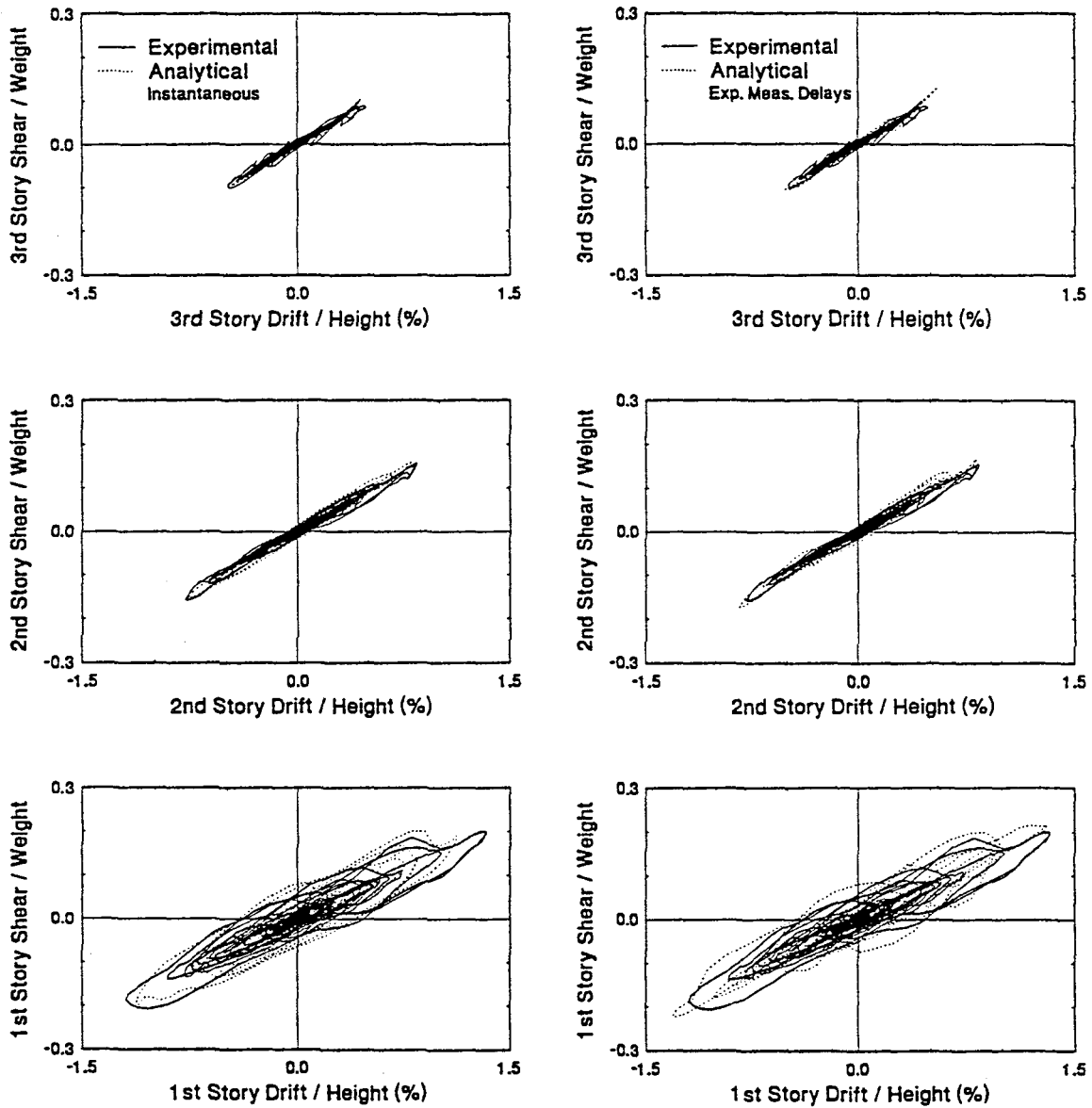


Figure 10-24 Comparison of Experimental and Analytical Story Shear Versus Story Drift Loops for Three-Story Structure Subjected to 75% El Centro Motion with Variable Dampers Controlled by Sliding Mode Control Algorithm

TEST 381

75% Hachinohe, Sliding Mode Control

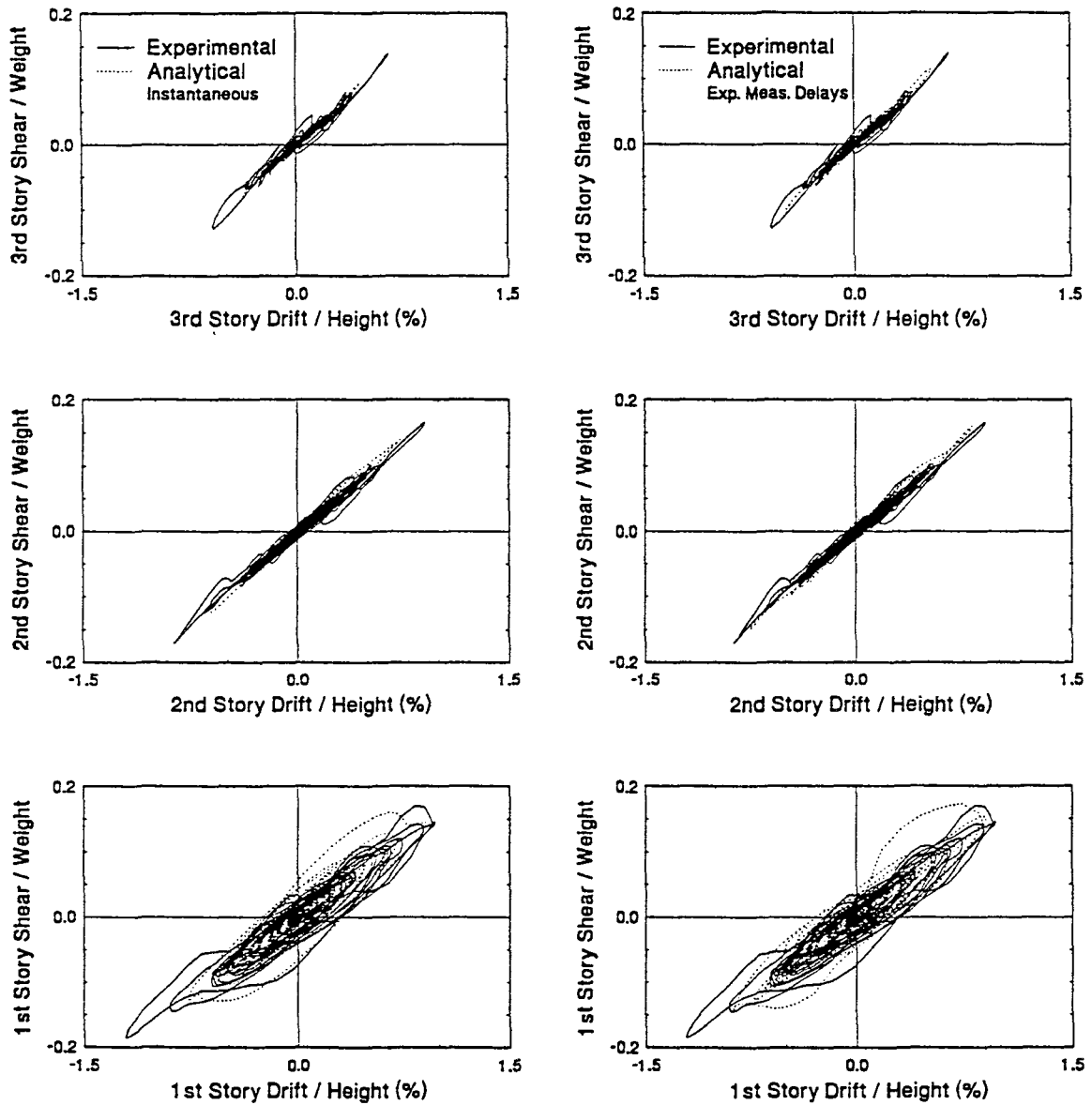


Figure 10-25 Comparison of Experimental and Analytical Story Shear Versus Story Drift Loops for Three-Story Structure Subjected to 75% Hachinohe Motion with Variable Dampers Controlled by Sliding Mode Control Algorithm

Figures 10-18 and 10-19 show comparisons for the low and high passive damping control systems. As was observed in tests on the one-story structure, the low damping test results provide a clear indication of frictional energy dissipation in the semi-active dampers. Furthermore, the low and high damping comparisons are quite good, confirming the validity of the mathematical models describing the behavior of the structure and dampers. Recall that the properties of the three-story bare frame structure were not determined directly from transfer functions due to the presence of torsional motion (see Section 6.5).

Figures 10-20 through 10-25 show comparisons of experimental and analytical story shear versus story drift loops for the three-story structure with variable dampers using two different analytical methods. In the first method, instantaneous control was assumed (see Section 10.1) and in the second method, experimentally measured time delays were utilized (see Section 10.2). The two methods of analytical prediction produce very similar results and, in most cases, compare reasonably well with the experimental results. An effort was made to further improve the analytical predictions by modifying some of the time delays used in the analysis. However, no significant improvements in the predictions were achieved through this method. As mentioned previously, the analytical predictions may be further improved by developing a model for the semi-active damper that explicitly accounts for valve dynamics.

The analytical predictions for the test with harmonic motion and semi-active optimal control (Figure 10-23) compare very well with the experimental response. In fact, the

analytical and experimental results are not superimposed as in the tests with earthquake motion because the two sets of data would be nearly indistinguishable. The analytical data was obtained using a mathematical model of the structure in which the properties of stiffness and damping were determined from a shear type representation of the structure (recall that the bare frame structure exhibited torsional response and the properties of the frame were not obtained directly from the transfer functions; see Section 6.5). According to the results of Figure 10-23, the mathematical model of the structure is quite good.

A different model of the structure was initially developed and used to obtain analytical predictions. The model utilized the mode shapes and damping ratios from previous testing of the model in which torsional response was not observed (Constantinou 1993b and 1992b) and the estimated frequencies from the experimental transfer functions (see Table 6-II). Figure 10-26 shows analytical predictions of the response of the structure subjected to harmonic excitation and low damping passive control. Clearly, the analytical response does not agree well with the experimental data. Not only is the stiffness in the second and third story unpredictable, but the analytical response at the first story is significantly larger than the results from the experimental data. Similar discrepancies were observed in predictions of the response of the structure subjected to seismic motion. Evidently, a reasonably accurate representation of the structural properties is required to reliably predict the response.

TEST 231

0.4g 5 Hz Harmonic, Low Damping

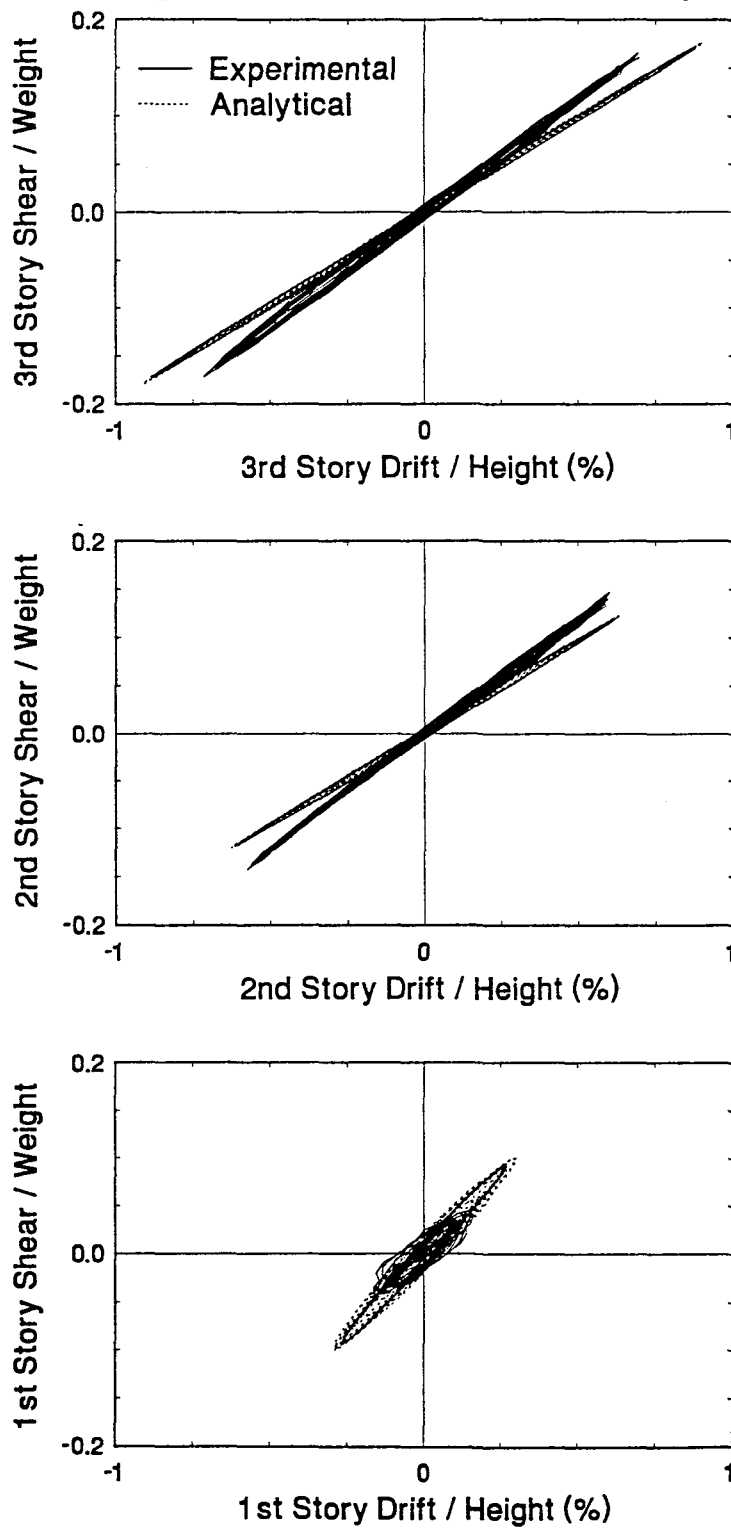


Figure 10-26 Comparison of Experimental and Analytical Story Shear Versus Story Drift Loops for Three-Story Structure Subjected to Harmonic Motion with Variable Dampers Set to Low Damping and Analytical Predictions Based on Alternate Model of Structure

Experimental and analytical results for the sliding mode control test of Figure 10-25 is presented in further detail in Figure 10-27. Recall that, in the sliding mode control algorithm the parameters defining the structural system are updated continuously beginning with an initial estimate. The initial estimates were obtained using Equations (7-102) through (7-104) and are shown in Table 7-I. In both the experimental and analytical results of Figure 10-27, the estimated parameters of mass and stiffness do not change significantly over the duration of the test. However, the experimental estimation of the damping coefficient is reduced significantly from its initial estimate while the analytical estimate only reduces slightly. The reason for this difference is related to the methods by which the estimates are calculated. In the experimental case, the estimates are a function of the response of the structure (see Equations 7-77 through 7-79) and therefore may vary considerably depending upon how well the structural system is initially modeled. In the analytical case, the estimates are also a function of the response but the response is based on a model which is exactly known as far as the numerical analysis is concerned (i.e., the parameters within the equation of motion are defined precisely). The fact that the experimental estimate becomes negative is of no concern; it simply means that the assumed model of the structure is not exact. Finally, the experimental and analytical time histories of combined error (Equation 7-58) compare reasonably well over the duration of the test.

TEST 381

75% Hachinohe, Sliding Mode Control

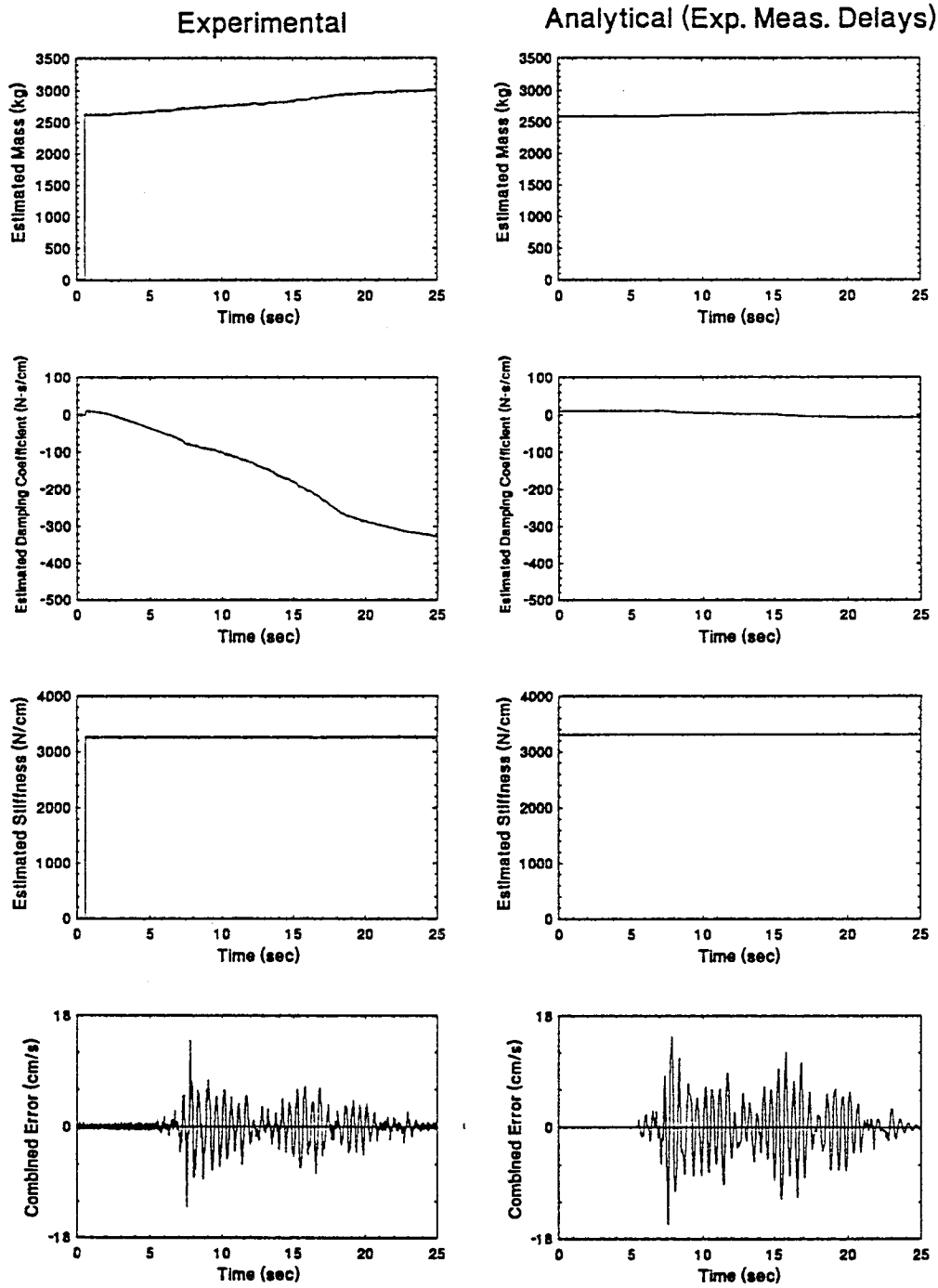


Figure 10-27 Comparison of Experimental and Analytical Results for Three-Story Structure Subjected to 75% Hachinohe Motion with Variable Dampers Controlled by Sliding Mode Control Algorithm

SECTION 11

CONCLUSIONS

This study involved the development and testing of semi-active damping devices for the seismic protection of structures. The devices take the form of a fluid damper in combination with an external control valve for adjustment of mechanical properties. Specifically, a variable damper was developed which utilizes a servovalve and is thus capable of developing a wide range of damping characteristics. A two-stage damper was also developed which utilizes a solenoid valve and is thus capable of developing only two distinct levels of damping.

The semi-active dampers operate on the principle of fluid orificing and have mechanical properties that are relatively insensitive to temperature. The mechanical properties of the devices and time delays associated with operation of the external control valve were determined through dynamic component tests. The dampers were shown to exhibit essentially linear viscous behavior below a certain cut-off frequency which was about 4 Hz for the tested dampers.

Three different analytical models of varying degrees of sophistication were presented for describing the dynamic behavior of the semi-active dampers. One of the models was a relatively complex fluid mechanics based model which was shown to predict the experimental behavior of the variable damper with reasonable accuracy.

A small moment-resisting structural frame outfitted with the semi-active fluid dampers was tested with seismic ground motion supplied by a large shaking table. The structure was tested in both a one-story and three-story configuration both with and without the semi-active dampers. A number of control algorithms were developed for operation of the semi-active dampers. Furthermore, time delay compensation methods were investigated to accommodate the inherent time delays associated with any feedback control system (i.e., measurement of response, calculation of command signal, application of control force, etc.). Finally, time history analyses were performed in which time delays were taken into account in an approximate way.

The results from shaking table tests on the one-story and three-story structure subjected to seismic excitation demonstrated the following:

- 1) The response of the structure with no dampers (bare frame) was dramatically improved with the addition of a semi-active damper control system.
- 2) The response reductions achieved with the semi-active control systems were comparable to those obtained with a high damping passive control system (as measured by peak response quantities). It is expected that further response reductions beyond those afforded by a passive control system can be achieved through improved control algorithms, improved semi-active damper hardware, and improved methods of accounting for time delays either directly through improved modeling of the dynamics of the control system or indirectly through improved time delay compensation methods. Furthermore, this study was limited to a specific type of structural system which was subjected to a limited range of ground

motion characteristics. There may be other conditions in which the use of semi-active dampers may prove advantageous.

- 3) The semi-active damper control system produced larger response reductions in the three-story structure compared to those obtained with an active tendon control system wherein both control systems were designed according to optimal control theory. The difference in response of the semi-active and active control systems is simply the result of larger effective damping in the semi-active control system.
- 4) The tested time delay compensation methods typically produced minor improvements in the response and, in some cases, degraded the response. The implementation of time delay compensation in a feedback control system requires a good estimate of the time delays associated with each component of the control system. The time delays associated with response measurements (i.e., signal filtering, signal differentiating, and data acquisition) had well defined values. In contrast, the semi-active damper time delays were not as well defined and average values from command signal saturation tests were used in the time delay compensation tests. Moreover, the time delay compensation methods utilized in this study were based on certain simplifying assumptions and thus were approximate in nature. This may explain those cases in which a degradation of response was observed.
- 5) The response of the structure was predictable but was strongly dependent upon the time delays within the control system. In some of the analytical predictions, the best results were obtained by incorporating time delays which were different from the experimentally measured time delays. The reason for the improved predictions is related to the fact that command signal saturation tests in which a single command was issued to the control valve were utilized for obtaining measurements of time delays in the semi-active damper system. In contrast, during shaking table tests the valve command signal is updated at time intervals which are

much smaller than the measured time delays. Therefore, a lack of knowledge exists regarding the dynamic behavior of the semi-active damper valve under high frequency command signals. The modified time delays used in the analytical predictions accounted, in an approximate way, for the unmodeled dynamics of the valve.

- 6) The semi-active control system was robust with respect to measurement disturbances and command signal disturbances in the sense that the structural system did not become unstable as a result of the disturbances. Stability is generally not a concern in control systems which can only extract energy from the structural system. In contrast, the servohydraulic actuators used within active control systems are capable of supplying energy to the structural system and thus the issue of stability must be addressed.

- 7) In contrast to the above mentioned comments on stability, there was one test performed on the one-story structure with two-stage dampers which indicated that, although the damper must always extract energy from the system, the modulation of damping can induce unexpectedly large responses under certain special conditions. In this case, the excitation was a steady-state harmonic signal having a frequency of about twice the natural frequency of the structure. The response was composed of two harmonics, one steady-state component corresponding to the excitation frequency and one transient component corresponding to the natural frequency of the structure. Apparently, the modulation of damping introduced the unexpected transient response wherein time delays played an important role.

SECTION 12

REFERENCES

Abdel-Rohman, M. (1985). "Structural Control Considering Time Delay Effect," Transactions of the Canadian Society of Mechanical Engineers, 9(4), 224-227.

ATC (1994). "Guidelines and Commentary for the Seismic Rehabilitation of Buildings," Report No. 33-02, Applied Technology Council, Redwood City, CA.

ATC (1993). "Proceedings of Seminar on Seismic Isolation, Passive Energy Dissipation, and Active Control", Report No. ATC-17-1, Applied Technology Council, San Francisco, CA, March.

Akbay, Z. and Aktan, H.M. (1991). "Actively Regulated Friction Slip Braces," Sixth Canadian Conf. on Earthquake Engrg., Toronto, Canada, June, 367-374.

Alanoly, J. and Sankar, S. (1987). "A New Concept in Semi-Active Vibration Isolation," J. of Mechanisms, Transmissions, and Automation in Design, Vol. 109, 242-247.

Chung, L.L., Lin, R.C., Soong, T.T. and Reinhorn, A.M. (1989). "Experimental Study of Active Control for MDOF Seismic Structures," J. of Engrg. Mech., ASCE, 115 (8), 1609-1627.

Clough, R.W. and Penzien, J. (1975). Dynamics of Structures, McGraw Hill, New York.

Constantinou, M.C. and Symans, M.D. (1993a). "Seismic Response of Buildings with Supplemental Damping," J. of Structural Design of Tall Buildings, Vol. 2, 77-92.

Constantinou, M.C. and Symans, M.D. (1993b). "Experimental Study of Seismic Response of Buildings with Supplemental Fluid Dampers," J. of Structural Design of Tall Buildings, Vol. 2, 93-132.

Constantinou, M.C., Fujii, S., Tsopelas, P. and Okamoto, S. (1992a). "University at Buffalo-Taisei Corporation Research Project on Bridge Seismic Isolation Systems," Third Workshop on Engineering Research in Progress, La Jolla, CA, Nov., 235-238.

Constantinou, M.C. and Symans, M.D. (1992b). "Seismic Response of Structures with Supplemental Fluid Viscous Dampers," Report No. NCEER 92-0032, National Center for Earthquake Engineering Research, Buffalo, NY.

Crolla, D.A., Horton, D.N.L., Pitcher, R.H. and Lines, J.A. (1987). "Active Suspension Control for an Off-Road Vehicle," Proc. Instn. Mech. Engrs., Vol. 201, No. D1, 1-10.

- Duchnowski, L.J. and Hann, S.A. (1989). "Modeling and Analysis of an Automobile Semi-Active Suspension," *Advanced Automotive Technologies*, ASME, DSC-Vol. 13, WAM, San Francisco, CA, Dec., 321-334.
- Dyke, S.J., Spencer, Jr., B.F., Quast, P., Sain, M.K. and Kaspari, D.C. (1994). "Experimental Verification of Acceleration Feedback Control Strategies for an Active Tendon System," Report No. NCEER 94-0024, National Center for Earthquake Engineering Research, Buffalo, NY.
- EERI (1993). "Theme Issue: Passive Energy Dissipation," *Earthquake Spectra*, 9 (3), August.
- EERI (1990). "Theme Issue: Seismic Isolation," *Earthquake Spectra*, 6 (2), May.
- Feng, M.Q. and Shinozuka, M. (1992). "Experimental and Analytical Study of a Hybrid Isolation System Using Friction Controllable Sliding Bearings," Report No. NCEER 92-0009, National Center for Earthquake Engineering Research, Buffalo, NY.
- Fujita, T., Shimazaki, M., Hayamizu, Y., Aizawa, S., Higashino, M. and Nobuyoshi, H. (1994). "Semiactive Seismic Isolation System Using Controllable Friction Damper," *Bull. of Earthquake Resistant Structure Research Center*, No. 27, March, 21-31.
- Gavin, H.P., Hose, Y.D. and Hanson, R.D. (1994). "Design and Control of Electrorheological Dampers," *Proc. of First World Conf. on Structural Control*, Los Angeles, CA, August, WP3-83 to WP3-92.
- Ghanem, R. and Bujakov, M. (1994). "Adaptive Control of Non-linear Dynamical Systems with Uncertainties," *Proc. of First World Conf. on Structural Control*, Los Angeles, CA, August, TA4-23 to TA4-32.
- Hamilton, J.M. (1985). "Computer-Optimized Adaptive Suspension Technology (COAST)," *IEEE Trans. on Industrial Electronics*, Vol. IE-32, No. 4, 355-363.
- Hasewaga, K. and Kelly, J.M. (1992). "Application of a Mass Damping System to Bridge Structures," Report No. UCB/EERC - 92/12, Earthquake Engineering Research Center, University of California, Berkeley.
- Hrovat, D., Barak, P. and Rabins, M. (1983). "Semi-Active Versus Passive or Active Tuned Mass Dampers for Structural Control," *J. of Engrg. Mech.*, 109 (3), 691-705.
- IMSL (1987). *International Mathematical and Statistical Library*, Subroutine IVPAG and GVCRCG, Houston, TX.
- International Association for Structural Control (1994). "Proc. of First World Conf. on Structural Control ", Los Angeles, CA, August.

- Ivers, D.E. and Miller, L.R. (1991). "Semi-Active Suspension Technology: An Evolutionary View," *Advanced Automotive Technologies*, ASME, DE-Vol. 40, WAM, Atlanta, GA, Dec., 327-346.
- Karnopp, D. (1990). "Design Principles for Vibration Control Systems Using Semi-Active Dampers," *J. of Dynamic Systems, Measurement, and Control*, Vol. 112, 448-455.
- Karnopp, D., Crosby, M.J. and Harwood, R.A. (1974). "Vibration Control Using Semi-Active Force Generators," *J. of Engrg. for Industry*, 96 (2), 619-626.
- Kawashima, K., Unjoh, S., IIDA, H. and Mukai, H. (1992). "Effectiveness of the Variable Damper for Reducing Seismic Response of Highway Bridges," *Second U.S.-Japan Workshop on Earthquake Protective Systems for Bridges*, PWRI, Tsukuba Science City, Japan, Dec., 479-493.
- Kelly, J.M. (1993). Earthquake-Resistant Design with Rubber, Springer-Verlag, London.
- Kobori, T., Takahashi, M., Nasu, T. and Niwa, N. (1993). "Seismic Response Controlled Structure with Active Variable Stiffness," *Earthquake Engrg. and Structural Dynamics*, Vol. 22, 925-941.
- Makris, N., Hill, D., Burton, S. and Jordan, M. (1995). "Electrorheological Fluid Damper for Seismic Protection of Structures," *Smart Structures and Materials Conf.*, San Diego, CA, Feb, 184-194.
- MATLAB (1990). The Mathworks Inc., Natick, Ma.
- McCloy, D. and Martin, H.R. (1980). Control of Fluid Power: Analysis and Design, 2nd (revised) edition, Ellis Horwood Limited, Chichester.
- McGreevy, S., Soong, T.T. and Reinhorn, A.M. (1988). "An Experimental Study of Time Delay Compensation in Active Structural Control," *Proc. of the Sixth Int. Modal Analysis Conf.*, Vol. 1, Orlando, FL, 733-739.
- Mizuno, T., Kobori, T., Hirai, J., Yoshinori, M. and Niwa, N. (1992). "Development of Adjustable Hydraulic Damper for Seismic Response Control of Large Structures," *PVP-Vol. 229, DOE Facilities Programs, Systems Interaction, and Active/Inactive Damping*, ASME, New Orleans, LA, June, 163-170.
- Patten, W.N., Kuo, C.C., He, Q., Liu, L. and Sack, R.L. (1994). "Seismic Structural Control Via Hydraulic Semi-active Vibration Dampers (SAVD)", *Proc. of First World Conf. on Structural Control*, Los Angeles, CA, August, FA2-83 to FA2-89.

- Polak, E., Meeker, G., Yamada, K. and Kurata, N. (1994). "Evaluation of an Active Variable-Damping Structure," *Earthquake Engrg. and Structural Dynamics*, Vol. 23, 1259-1274.
- Rakheja, S. and Sankar, S. (1985). "Vibration and Shock Isolation Performance of a Semi-Active "On-Off" Damper," *J. of Vibration, Acoustics, Stress, and Reliability in Design*, Vol. 107, 98-403.
- Reinhorn, A.M., Soong, T.T., Lin, R.C., Riley, M.A., Wang, Y.P., Aizawa, S. and Higashino, M. (1992). "Active Bracing System: A Full Scale Implementation of Active Control," Report No. NCEER 92-0020, National Center for Earthquake Engineering Research, Buffalo, NY.
- Riley, M.A., Reinhorn, A.M., Nagarajaiah, S. and Subramaniam, R. (1994). "Control Algorithms for Structures with Hybrid Isolation Systems," Fifth U.S. National Conf. on Earthquake Engrg., Chicago, IL, July, 981-990.
- Sack, R.L. and Patten, W.N. (1993). "Semiactive Hydraulic Structural Control," Proc. of Int. Workshop on Structural Control, Honolulu, Hawaii, August, 417-431.
- Sage, A.P. and White, C.C. (1977). Optimum Systems Control, Prentice Hall, Englewood Cliffs, NJ.
- Slotine, J. and Li, W. (1991). Applied Nonlinear Control, Prentice Hall, Englewood Cliffs, NJ.
- Shinozuka, M., Constantinou, M.C. and Ghanem, R. (1992). "Passive and Active Fluid Dampers in Structural Applications," U.S./China/Japan Workshop on Structural Control, Shanghai, China, Oct., 507-516.
- Skinner, R.I., Robinson, W.H. and McVerry, G.H. (1993). An Introduction to Seismic Isolation, J. Wiley & Sons, Chichester.
- Soong, T.T. and Constantinou, M.C. (1994). Passive and Active Structural Vibration Control in Civil Engineering, Springer-Verlag, Wien-New York.
- Soong, T.T., Masri, S.F. and Housner, G.W. (1991). "An Overview of Active Structural Control Under Seismic Loads," *Earthquake Spectra*, 7 (3), 483-505.
- Soong, T.T. (1990). Active Structural Control: Theory and Practice, Longman, New York.
- Soong, T.T., Reinhorn, A.M. and Yang, J.N. (1987). "A Standardized Model for Structural Control Experiments and Some Experimental Results," Proc. of Second Int. Symp. on Structural Control, 1985, Waterloo, Canada, 669-693.

Taylor Devices (1991). "Compressible Fluid Strut for Wheeled Vehicles," Report No. 67R-14808-1, David Taylor Research Center, Bethesda, MD.

Watton, J. (1989). Fluid Power Systems: Modeling, Simulation, Analog and Microcomputer Control, Prentice Hall International (UK) Ltd.

Wylie, E.B., Suo, L., Bruckman, R. and Kerastas, M. (1989). "Numerical Modeling of a Damper with a Semi-Active Valve," Advanced Automotive Technologies, ASME, DSC-Vol. 13, WAM, San Francisco, CA, Dec., 291-303.

APPENDIX A

Data Acquisition and Instrumentation Specifications

Table A-I Data Acquisition Channel Specifications

CHANNEL	NOTATION	CALIBRATION FACTOR	FULL-SCALE VOLTAGE	FULL-SCALE MEASUREMENT	MINIMUM RESOLUTION
1	AFHE	0.2 g/volt	±10	±2 g	0.00006 g
2	AFHW	0.2 g/volt	±10	±2 g	0.00006 g
3	AIHE	0.2 g/volt	±10	±2 g	0.00006 g
4	AIHW	0.2 g/volt	±10	±2 g	0.00006 g
5	A2HE	0.2 g/volt	±10	±2 g	0.00006 g
6	A2HW	0.2 g/volt	±10	±2 g	0.00006 g
7	A3HE	0.2 g/volt	±10	±2 g	0.00006 g
8	A3HW	0.2 g/volt	±10	±2 g	0.00006 g
9	DFHC	2.54 cm/volt	±10	±25.4 cm	0.00078 cm
10	DIHC	2.54 cm/volt	±10	±25.4 cm	0.00078 cm
11	D2HC	2.54 cm/volt	±10	±25.4 cm	0.00078 cm
12	D3HC	2.54 cm/volt	±10	±25.4 cm	0.00078 cm
13	DDAE	0.508 cm/volt	±10	±5.08 cm	0.00015 cm
14	DDAW	0.508 cm/volt	±10	±5.08 cm	0.00015 cm
15	LCAE	2,225.0 N/volt	±10	±22,250 N	0.67902 N
16	LCAW	2,225.0 N/volt	±10	±22,250 N	0.67902 N
17	DIHW	0.122 cm/volt	±10	±1.22 cm	0.00004 cm
18	DLAT	1.524 cm/volt	±10	±15.24 cm	0.00047 cm
19	ALAT	0.2 g/volt	±10	±2 g	0.00006 g
20	DROL	1.524 cm/volt	±10	±15.24 cm	0.00047 cm
21	AROL	0.4 g/volt	±10	±4 g	0.00012 g
22	VAR-A	0.254 mm/volt	±10	±2.54 mm	0.000078 mm

Table A-I Cont'd

CHANNEL	NOTATION	CALIBRATION FACTOR	FULL-SCALE VOLTAGE	FULL-SCALE MEASUREMENT	MINIMUM RESOLUTION
23	VAR-B	0.254 mm/volt	±10	±2.54 mm	0.000078 mm
24	VFHC	125.17 cm/s/volt	±10	1251.7 cm/s	0.03820 cm/s
25	V1HC	164.95 cm/s/volt	±10	1649.5 cm/s	0.05034 cm/s
26	V2HC	127.69 cm/s/volt	±10	1276.9 cm/s	0.03897 cm/s
27	V3HC	204.88 cm/s/volt	±10	2048.8 cm/s	0.06252 cm/s
28	DCOM	1.0 volt/volt	±10	±10 volts	0.00031 volts
29	DCOM2	1.0 volt/volt	±10	±10 volts	0.00031 volts
30	MEST	3,000 kg/volt	±10	30,000 kg	0.91553 kg
31	KEST	8,000 N/cm/volt	±10	80,000 N/cm	2.44141 N/cm
32	CEST	100 N-s/cm/volt	±10	1,000 N-s/cm	0.03052 N-s/cm
33	CUNB	1,000 N-s/cm/volt	±10	10,000 N-s/cm	0.30518 N-s/cm
34	JERK	10.053 g/s/volt	±10	100.53 g/s	0.00307 g/s

Table A-II Instrumentation Specifications for Transducers Located on the Model Structure (with reference to Figure 5-16)

CHANNEL	NOTATION	MANUFACTURER	MODEL / SERIAL #	FULL-SCALE MEASUREMENT
1	AFHE	KULITE	GAD-813-25 / 10326	±2 g
2	AFHW	KULITE	GAD-813-25 / 9665	±2 g
3	A1HE	KULITE	GAD-813-25 / 10319	±2 g
4	A1HW	KULITE	GAD-813-25 / 10327	±2 g
5	A2HE	KULITE	GAD-813-25 / 10325 GAD-813-25 / 9049*	±2 g
6	A2HW	KULITE	GAD-813-25 / 10321	±2 g
7	A3HE	KULITE	GAD-813-25 / 9673	±2 g
8	A3HW	KULITE	GAD-813-25 / 9668	±2 g
9	DFHC	TEMPOSONICS	11020050109 / 14412-04-001P	±25.4 cm
10	D1HC	TEMPOSONICS	11020050109 / 14412-04-002P	±25.4 cm
11	D2HC	TEMPOSONICS	11020050109 / 14412-04-003P	±25.4 cm
12	D3HC	TEMPOSONICS	11020050109 / 14412-04-004P	±25.4 cm
13	DDAE	TEMPOSONICS	11004050209 / 14412-01-007N	±5.08 cm
14	DDAW	TEMPOSONICS	DCTH-4002-?? / 12577-01-002N	±5.08 cm
15	LCAE	A.L. DESIGN	871090	±22,250 N
16	LCAW	A.L. DESIGN	871092	±22,250 N
17	DIHW	MEASUREMENTS GROUP	---	±1.22 cm

* AFTER TEST 285

Table A-III Strain Gage Signal Conditioner Specifications

CHANNEL	NOTATION	TRANSDUCER	CONDITIONER MODEL / SERIAL #	GAIN	BRIDGE EXCITATION (volts)	FILTER
1	AFHE	ACCELEROMETER	2310 / 88779	435.8	10	WIDE BAND
2	AFHW	ACCELEROMETER	2310 / 72366	493	10	WIDE BAND
3	A1HE	ACCELEROMETER	2310 / 72495	507.5	10	WIDE BAND
4	A1HW	ACCELEROMETER	2310 / 72463	501.8	10	WIDE BAND
5	A2HE	ACCELEROMETER	2310 / 88780	475.5	10	WIDE BAND
6	A2HW	ACCELEROMETER	2310 / 72556	504.2	10	WIDE BAND
7	A3HE	ACCELEROMETER	2310 / 88776	450	10	WIDE BAND
8	A3HW	ACCELEROMETER	2310 / 72312	464.2	10	WIDE BAND
9	LCAE	LOAD CELL	2310 / 72578	408.2	10	WIDE BAND
10	LCAW	LOAD CELL	2310 / 72494	411.7	10	WIDE BAND
11	DIHW	STRAIN GAGE	2310 / 88784	481	10	WIDE BAND

Note: All conditioners manufactured by Measurements Group, Inc.

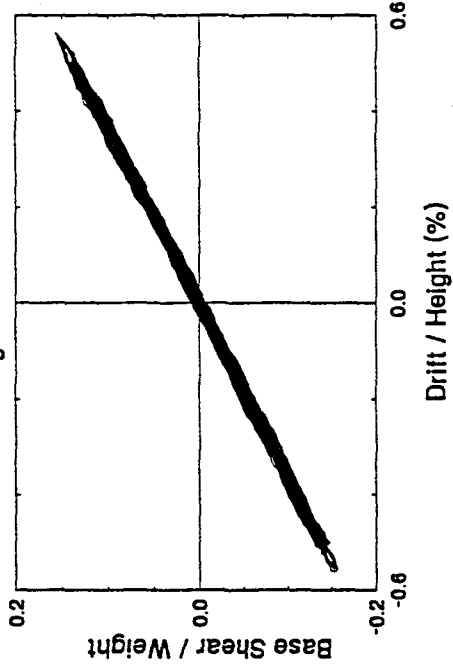
APPENDIX B

Shaking Table Test Results:

One-Story Structure with No Dampers (Bare Frame)

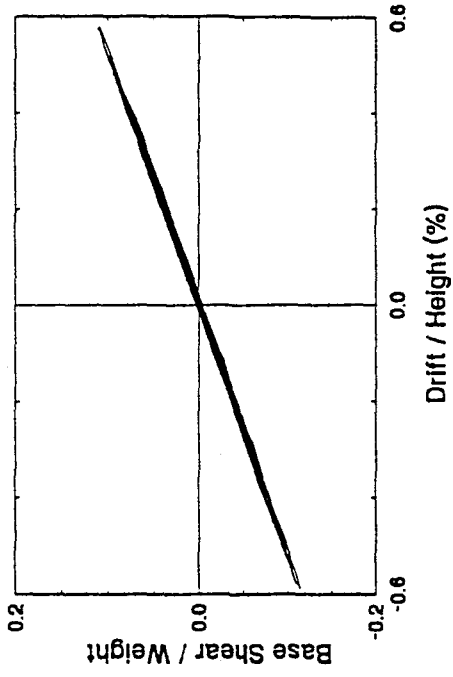
TEST 3

0.05g White Noise



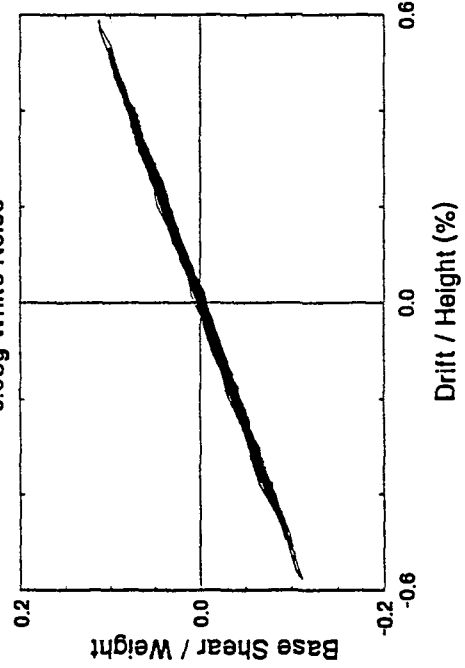
TEST 178

10% El Centro



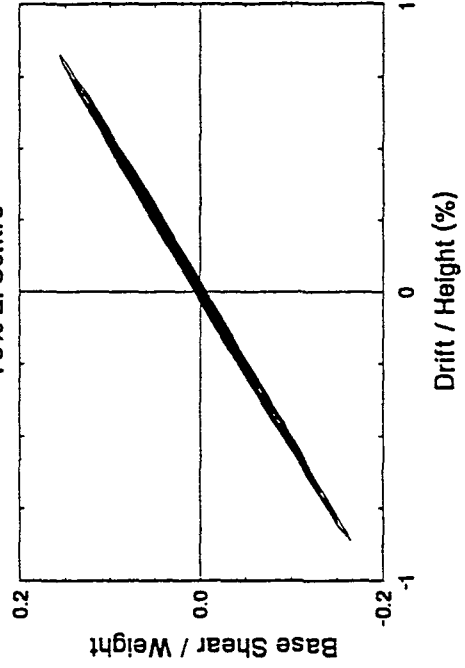
TEST 177

0.05g White Noise



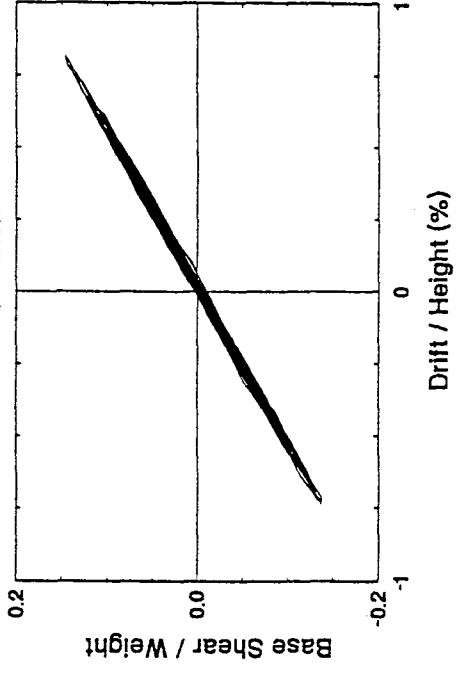
TEST 179

15% El Centro



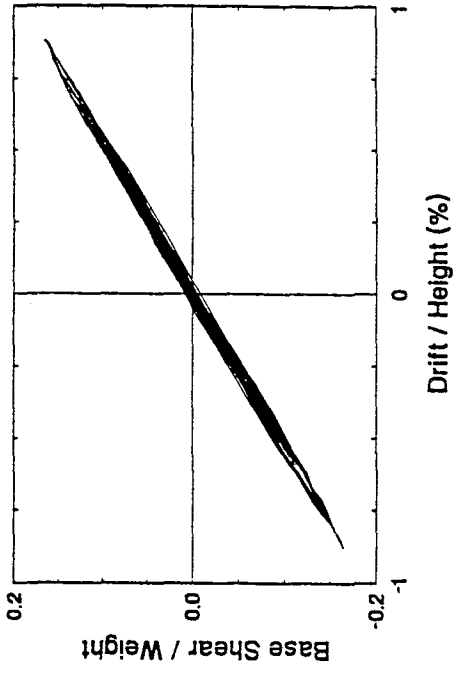
TEST 324

25% Hachinohe



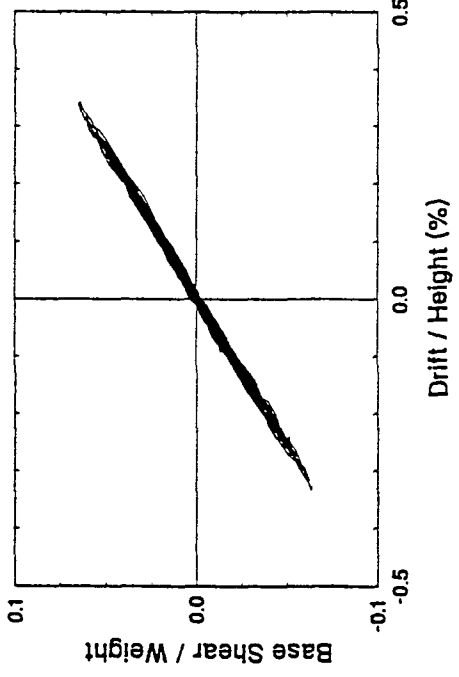
TEST 182

30% Hachinohe



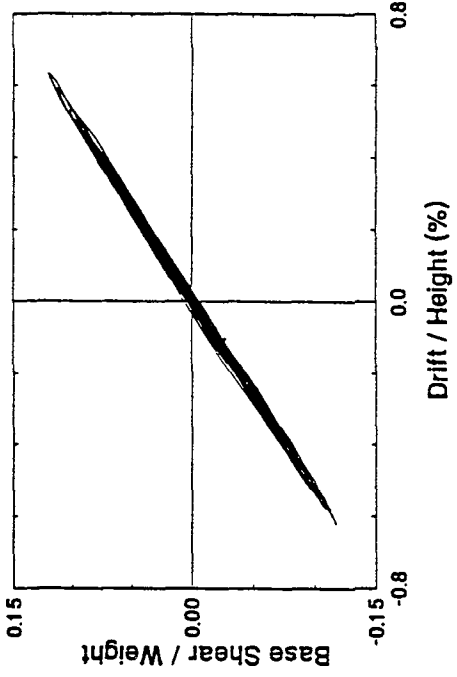
TEST 180

10% Hachinohe



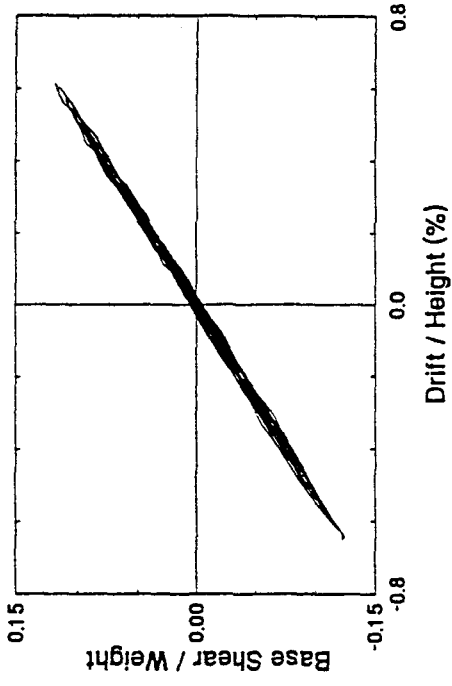
TEST 181

20% Hachinohe



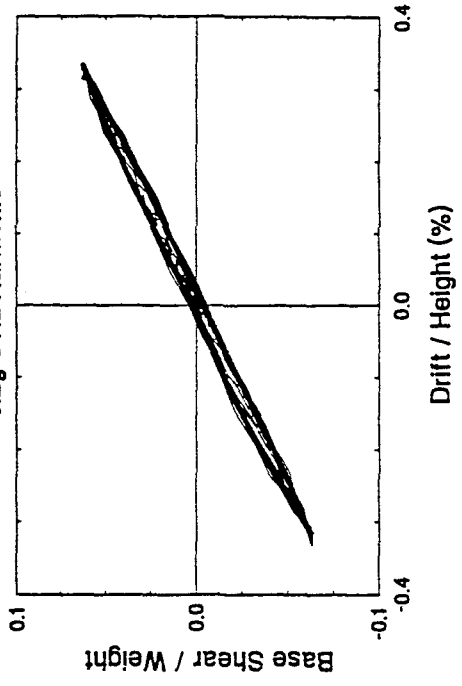
TEST 185

50% Hachinohe-M



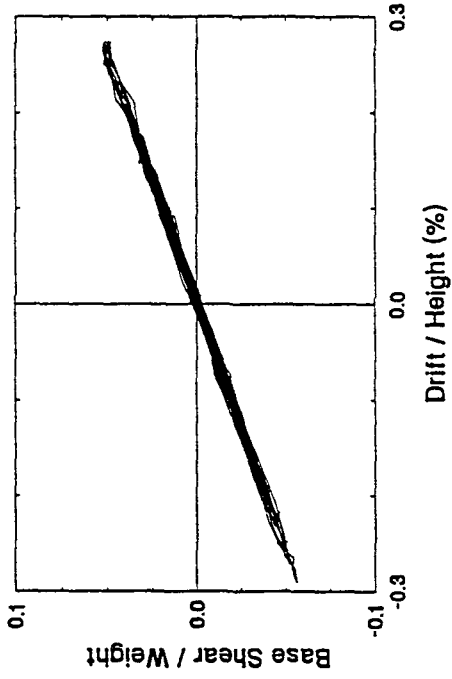
TEST 187

0.2g 5 Hz Harmonic



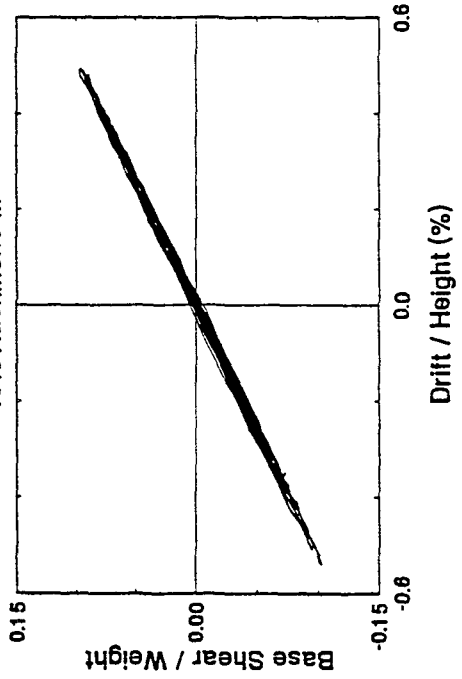
TEST 183

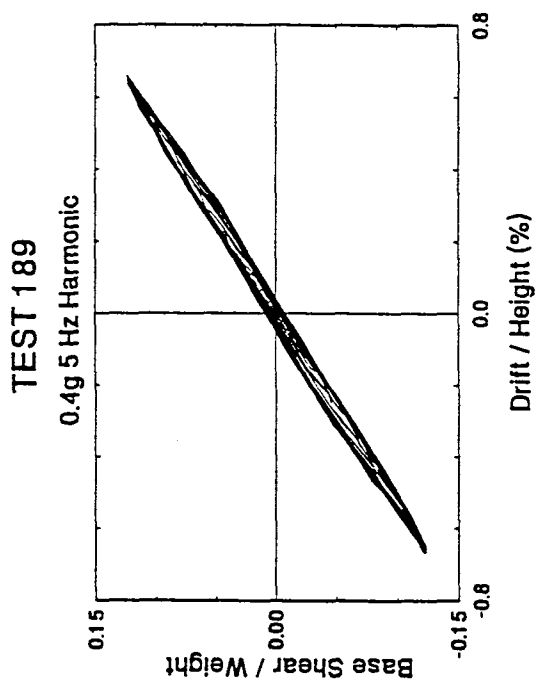
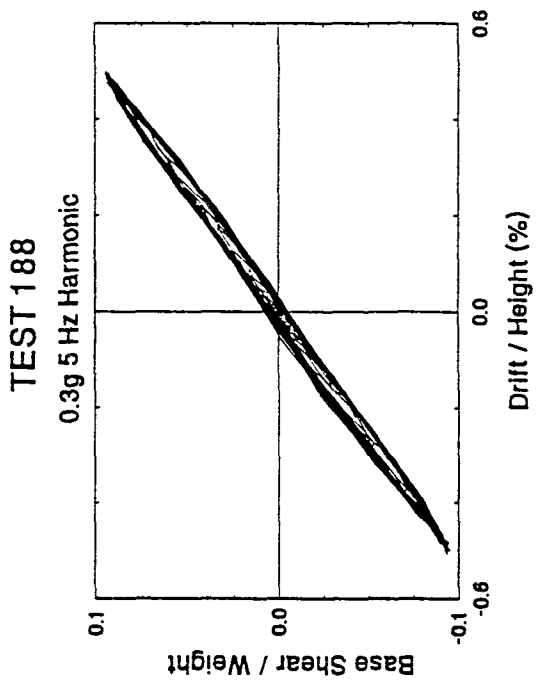
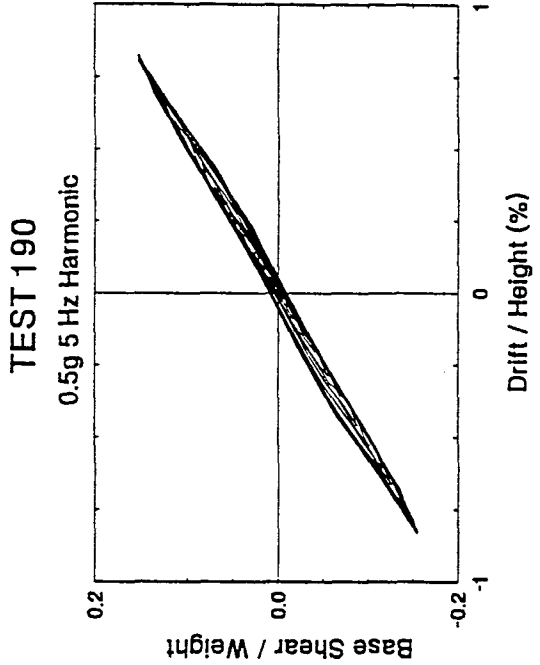
20% Hachinohe-M



TEST 184

40% Hachinohe-M





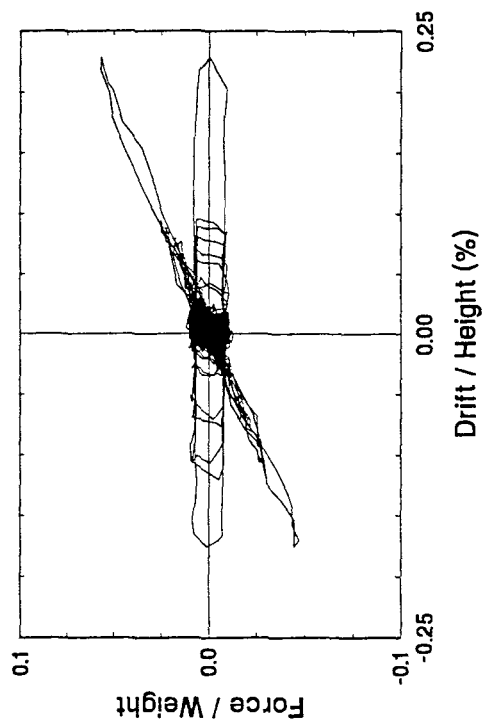
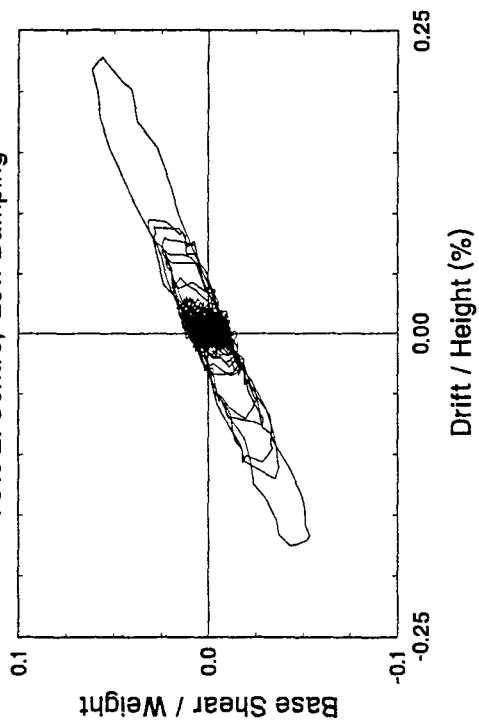
APPENDIX C

Shaking Table Test Results:

One-Story Structure with Two-Stage Dampers

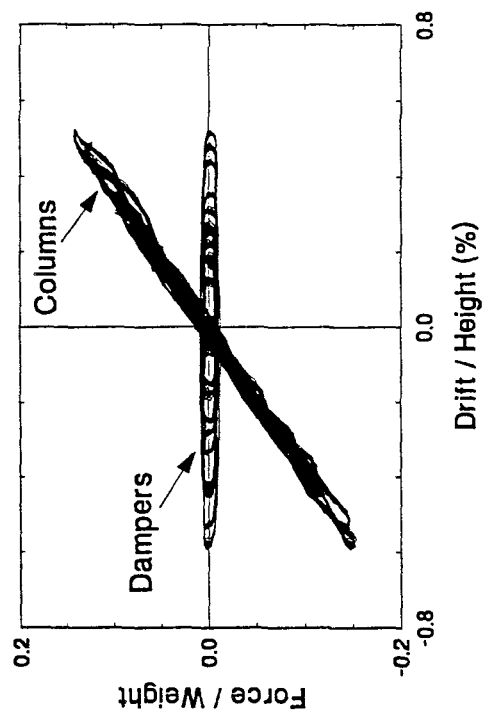
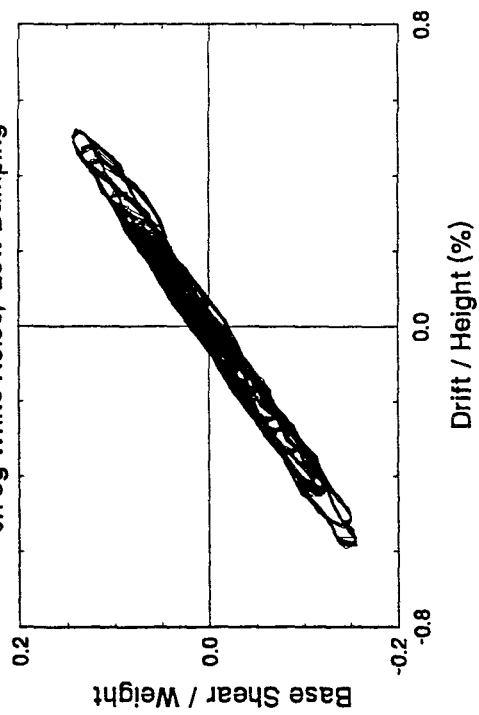
TEST 19

10% EI Centro, Low Damping



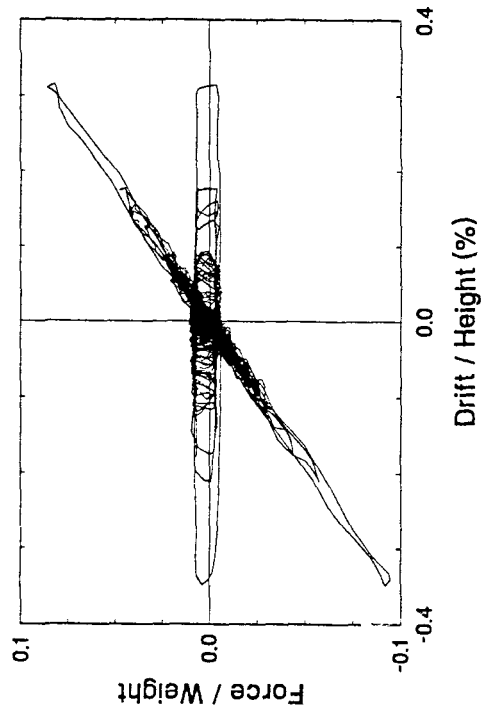
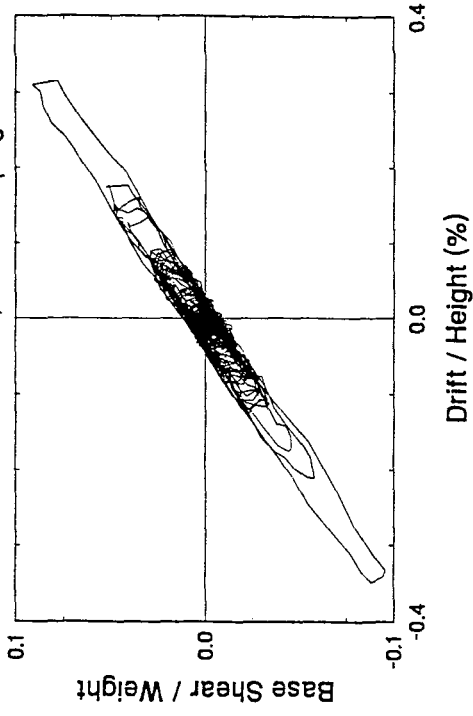
TEST 43

0.15g White Noise, Low Damping



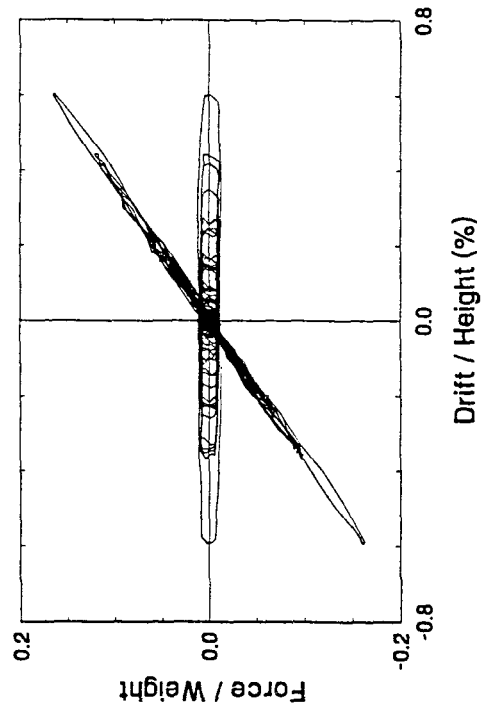
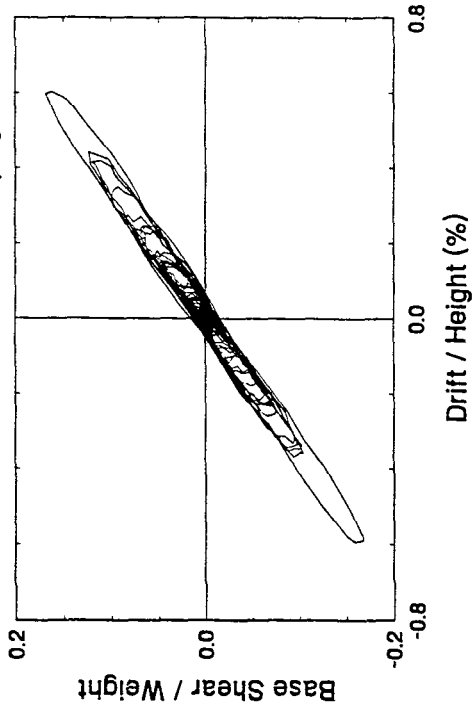
TEST 49

25% Hachinohe, Low Damping



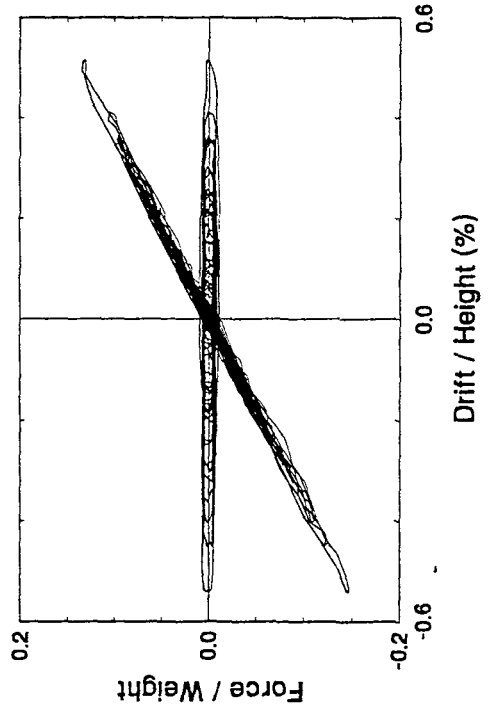
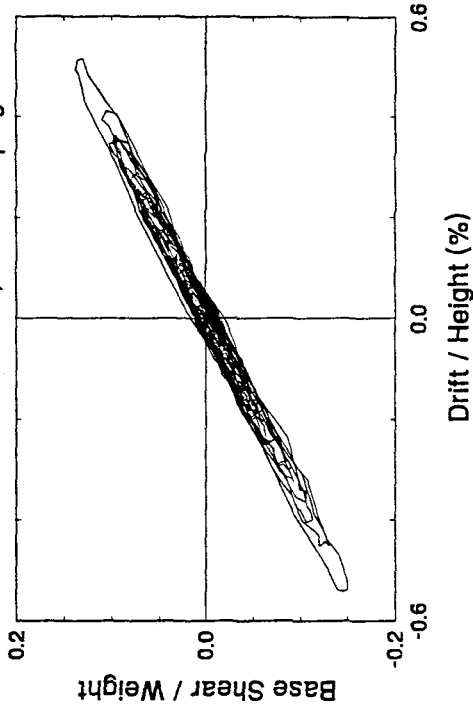
TEST 20

25% El Centro, Low Damping



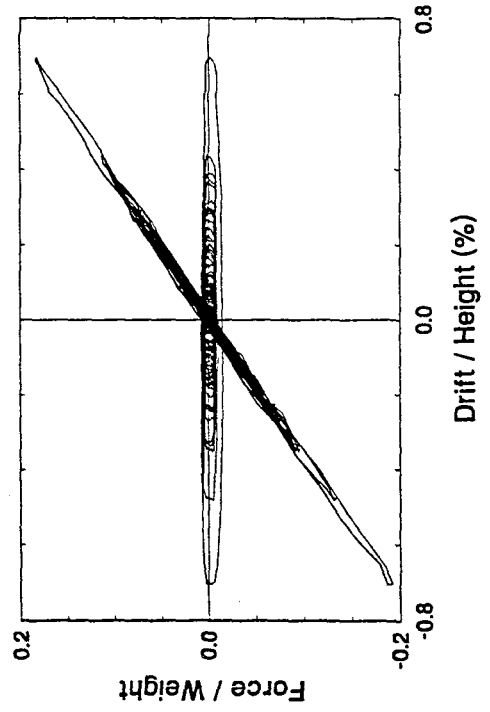
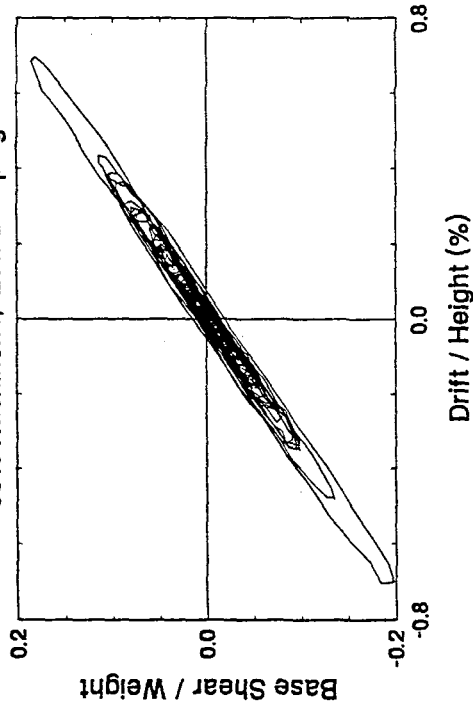
TEST 34

100% Hachinohe-M, Low Damping



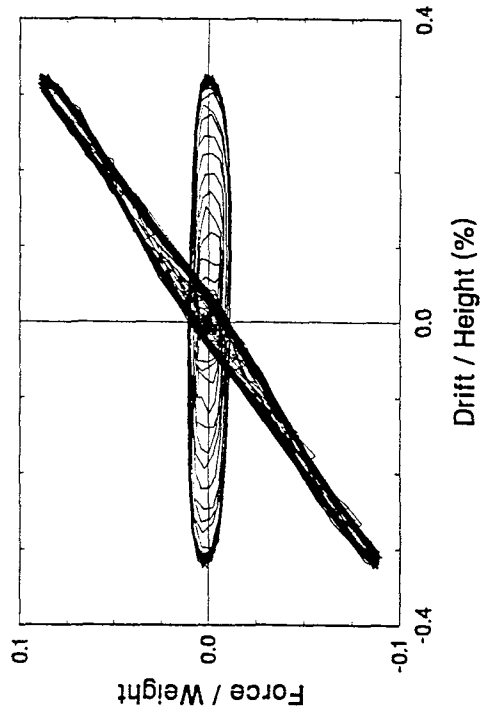
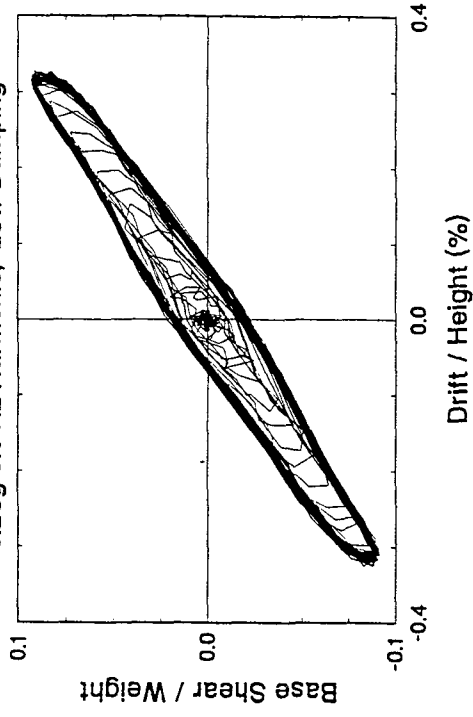
TEST 50

50% Hachinohe, Low Damping



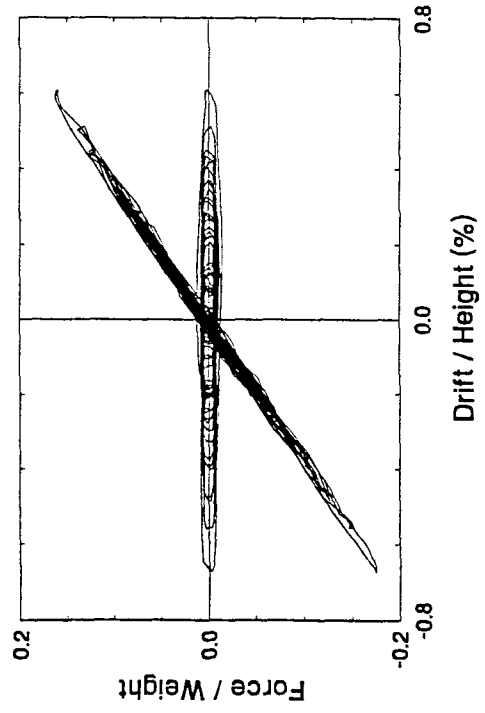
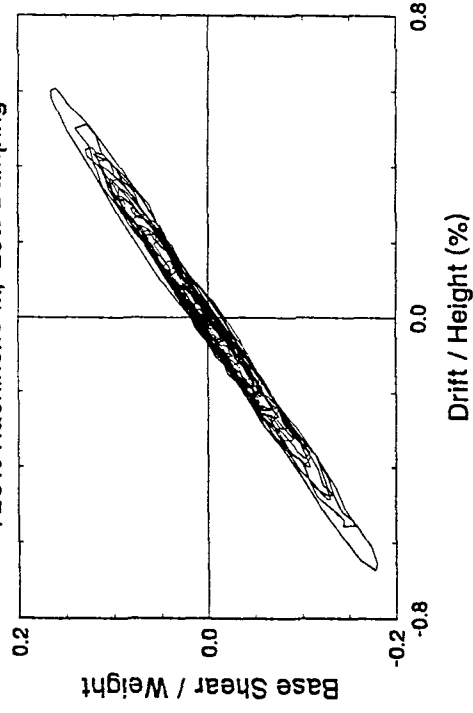
TEST 37

0.25g 5.6 Hz Harmonic, Low Damping



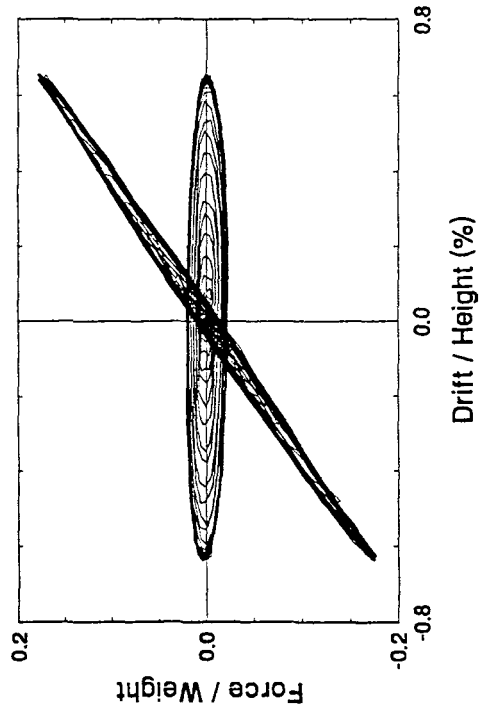
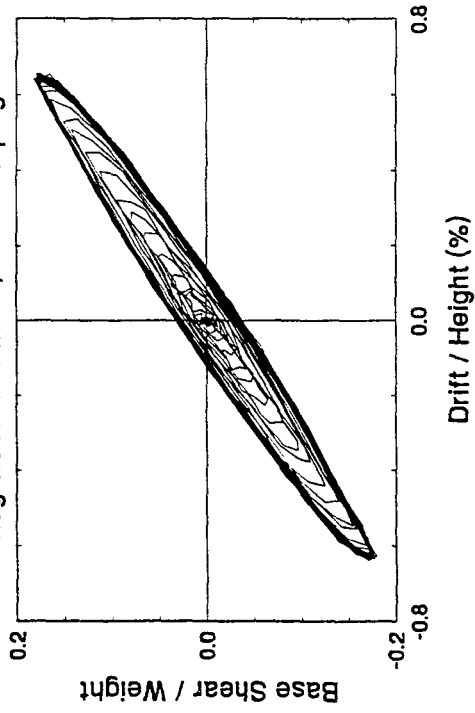
TEST 48

125% Hachinohe-M, Low Damping



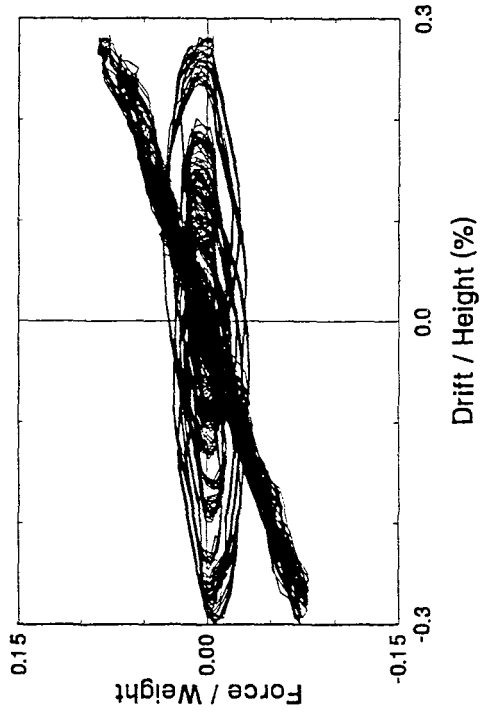
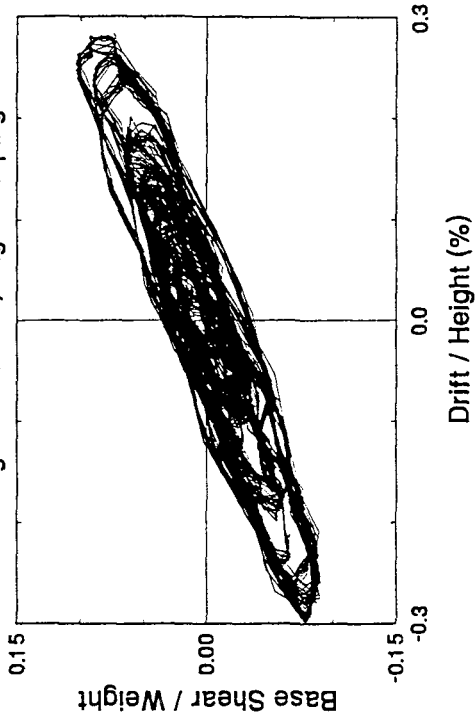
TEST 39

0.5g 5.6 Hz Harmonic, Low Damping



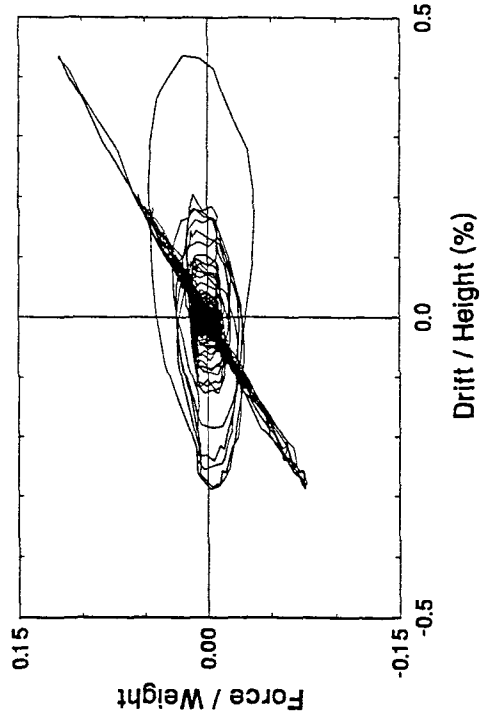
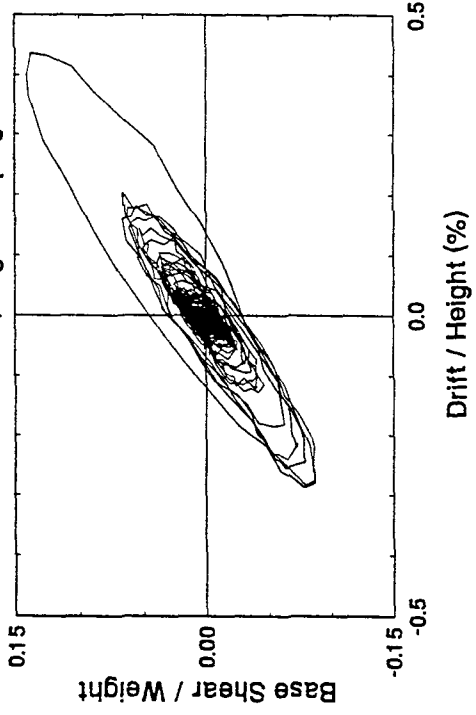
TEST 44

0.15g White Noise, High Damping



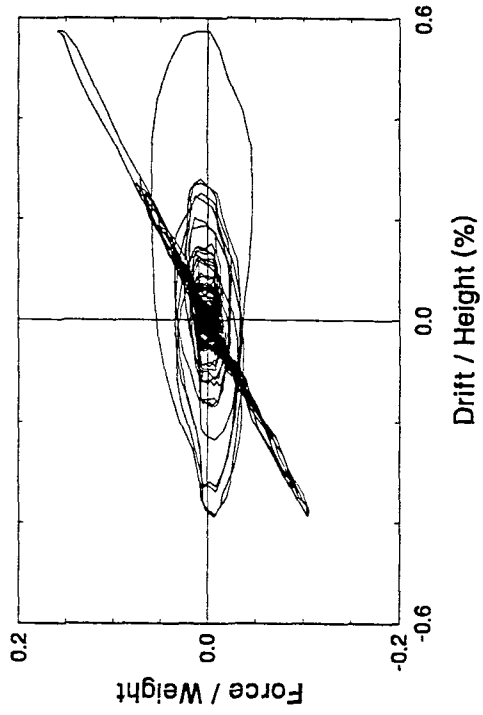
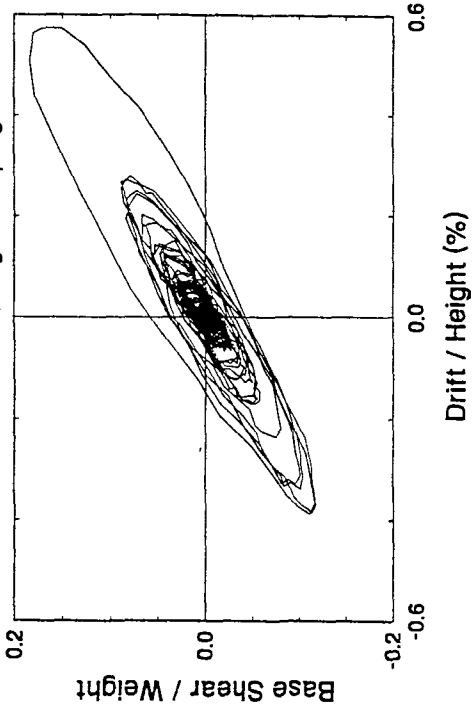
TEST 17

25% El Centro, High Damping



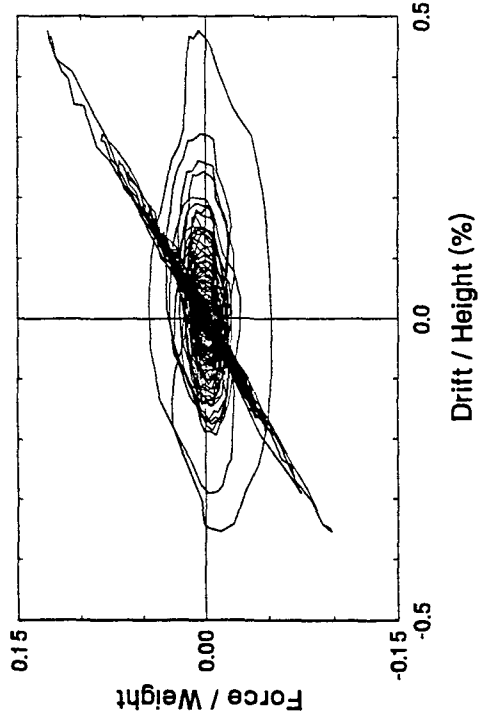
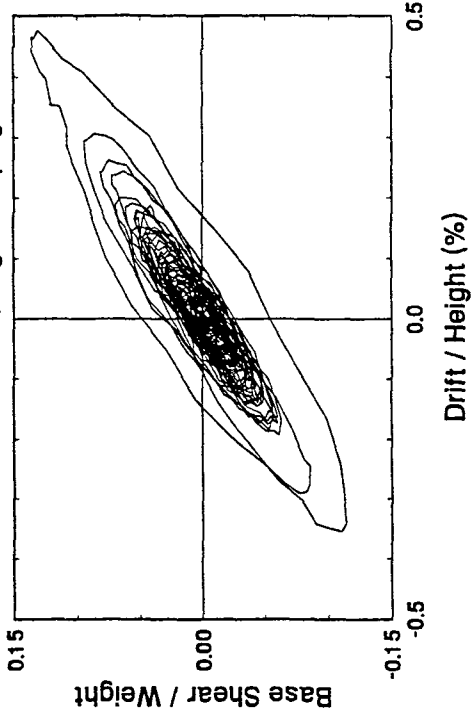
TEST 18

33.3% El Centro, High Damping



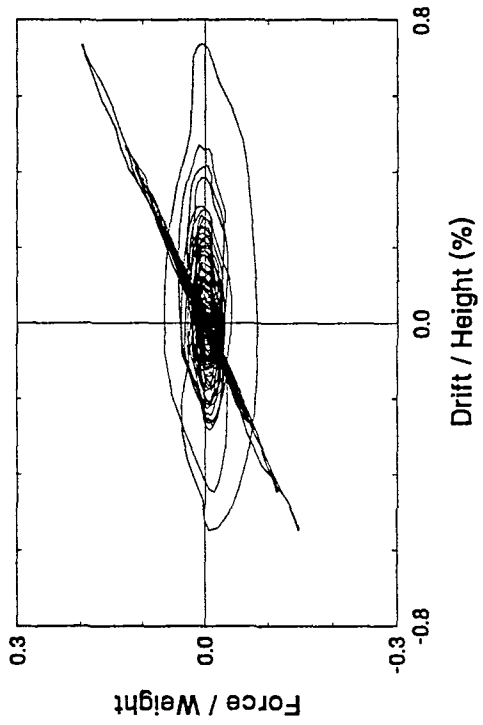
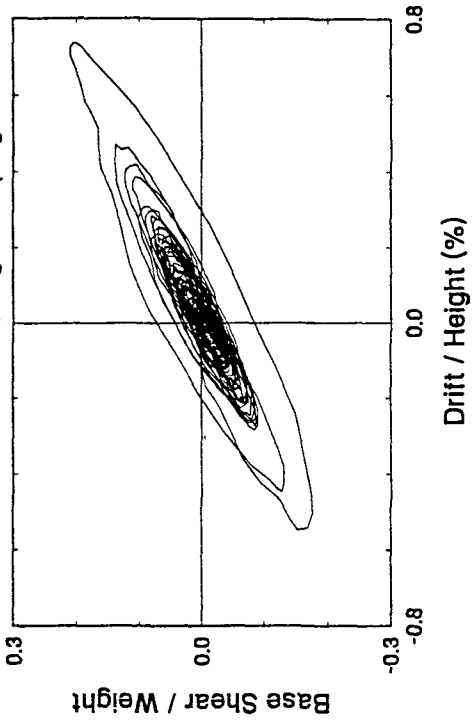
TEST 46

50% Hachinohe, High Damping



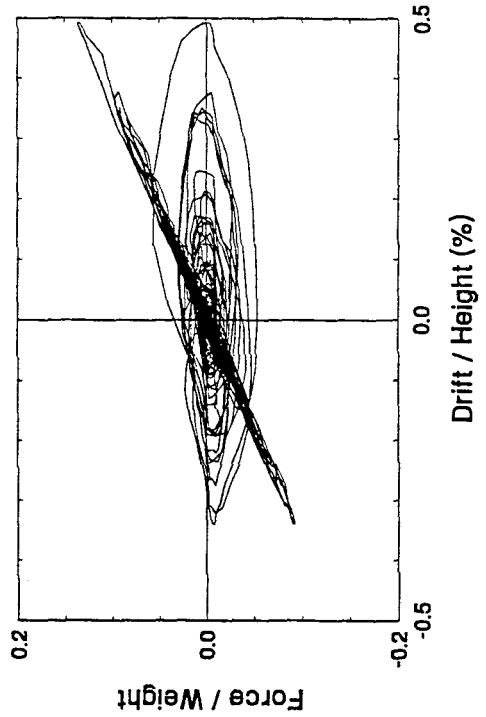
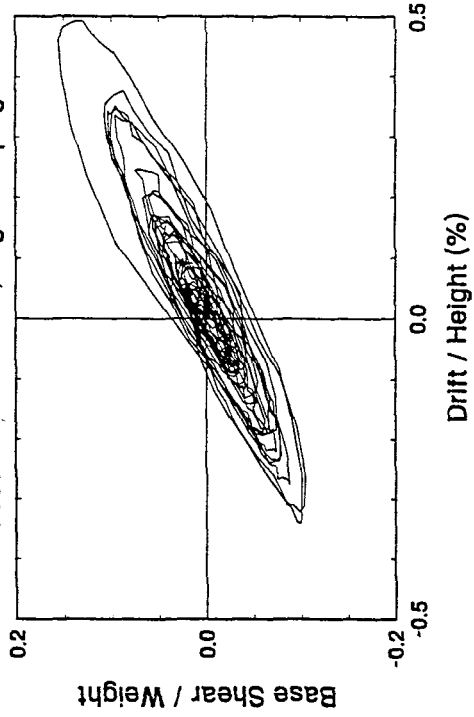
TEST 47

75% Hachinohe, High Damping



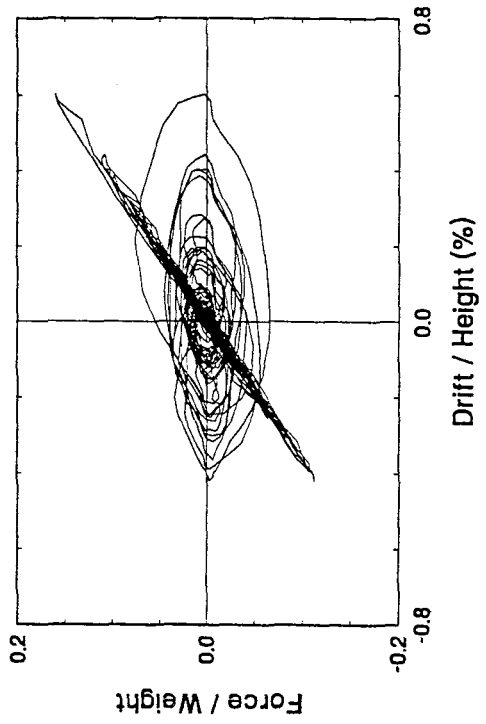
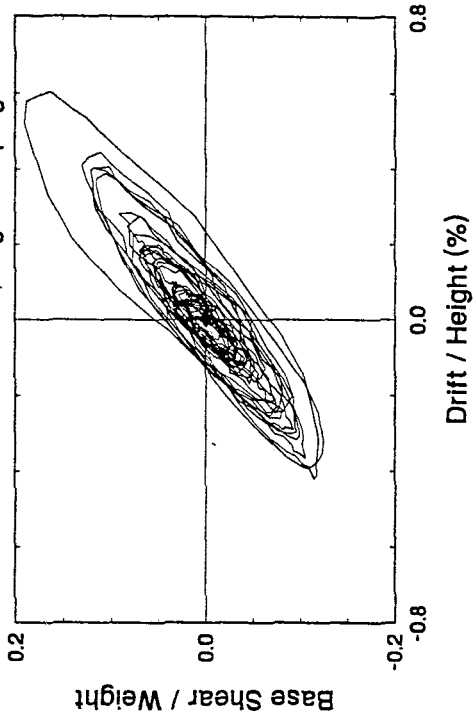
TEST 35

100% Hachinohe-M, High Damping



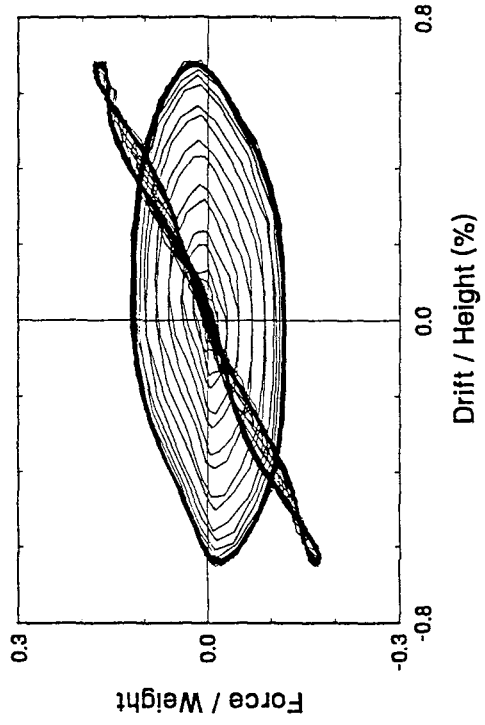
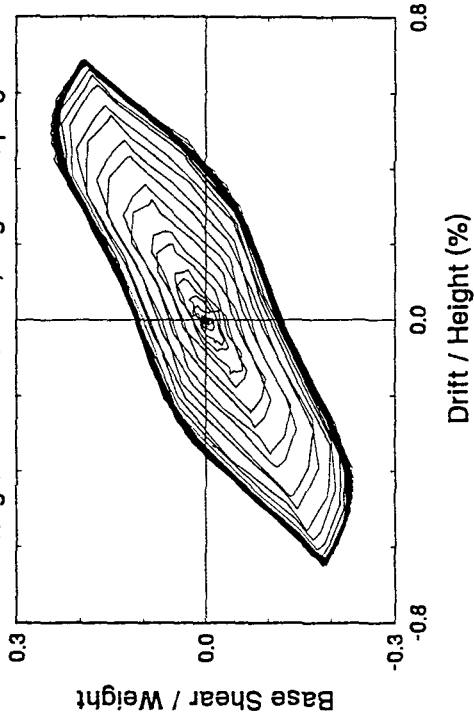
TEST 45

125% Hachinohe-M, High Damping



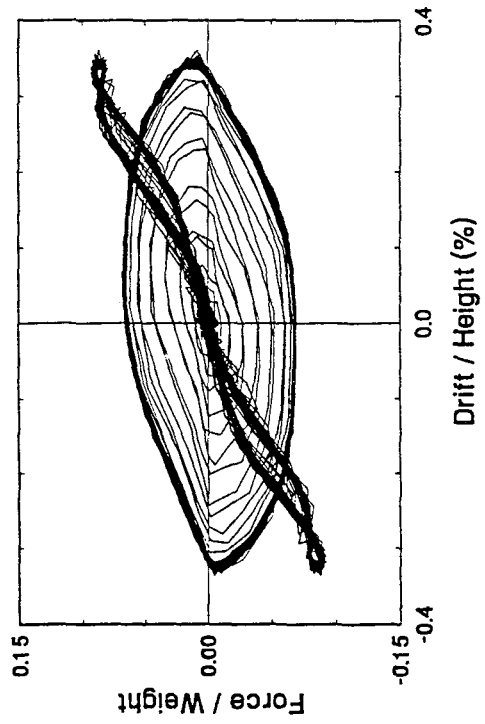
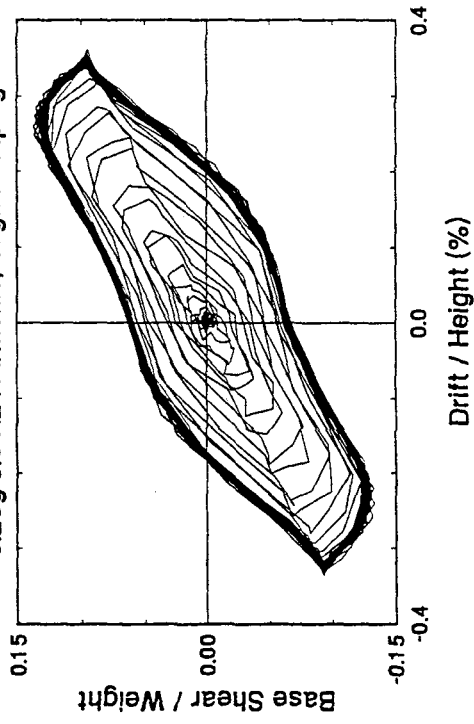
TEST 42

0.5g 5.6 Hz Harmonic, High Damping

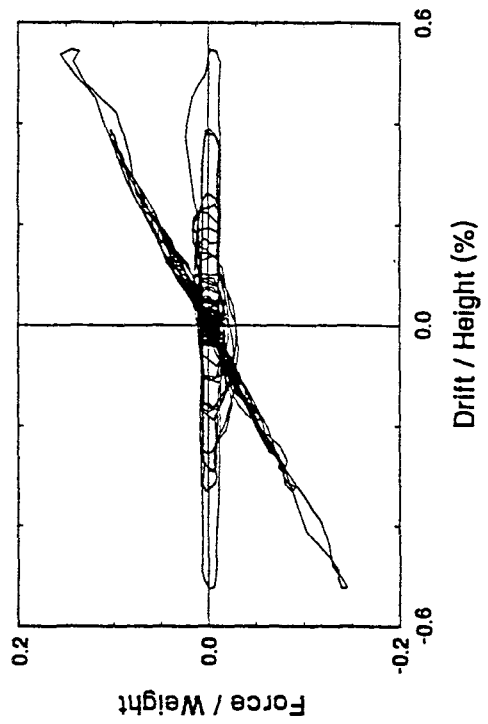
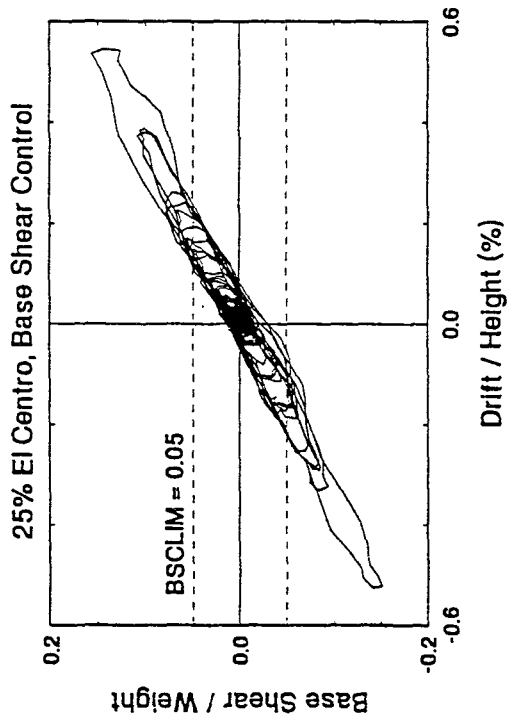


TEST 40

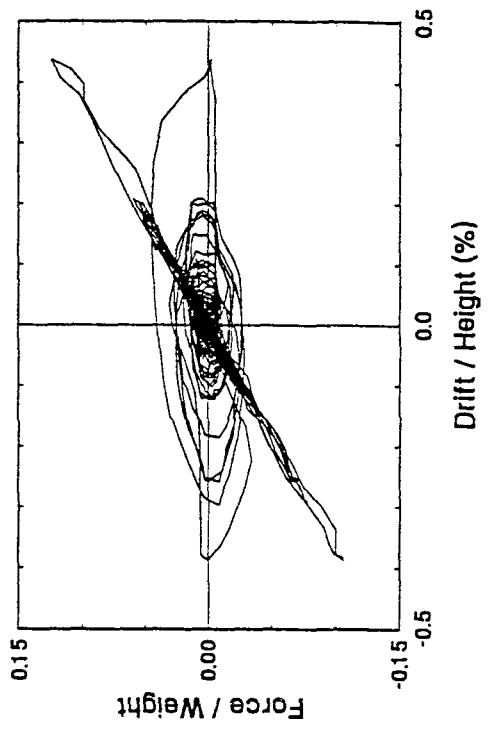
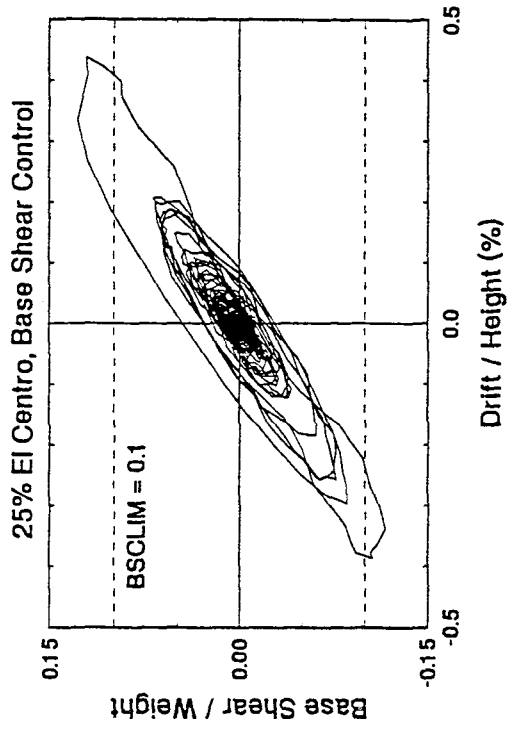
0.25g 5.6 Hz Harmonic, High Damping



TEST 29

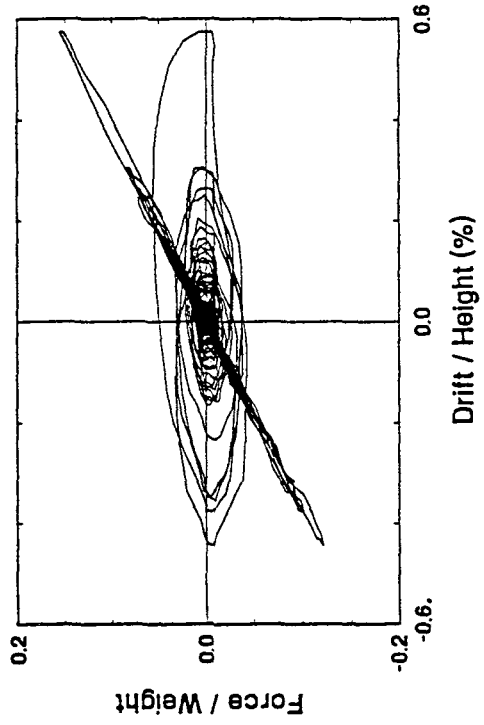
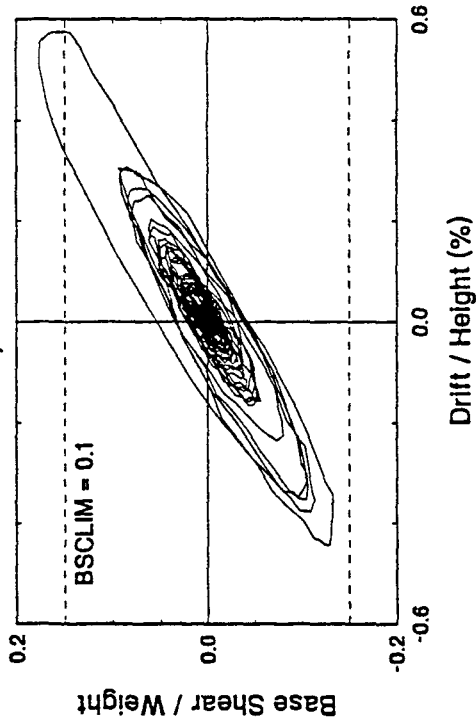


TEST 51



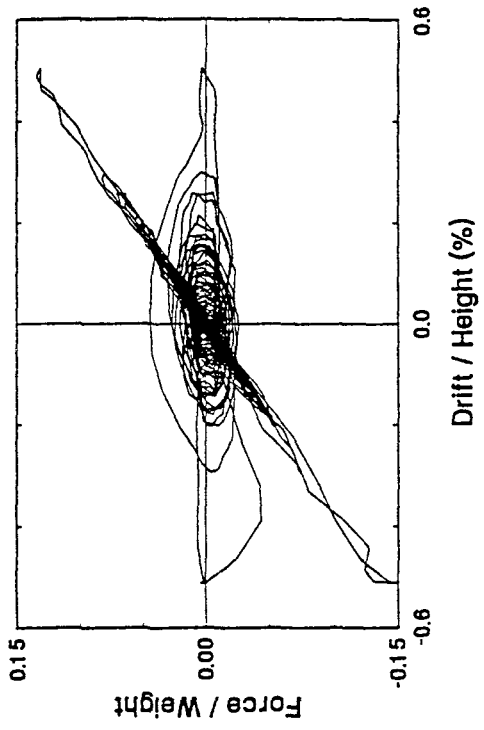
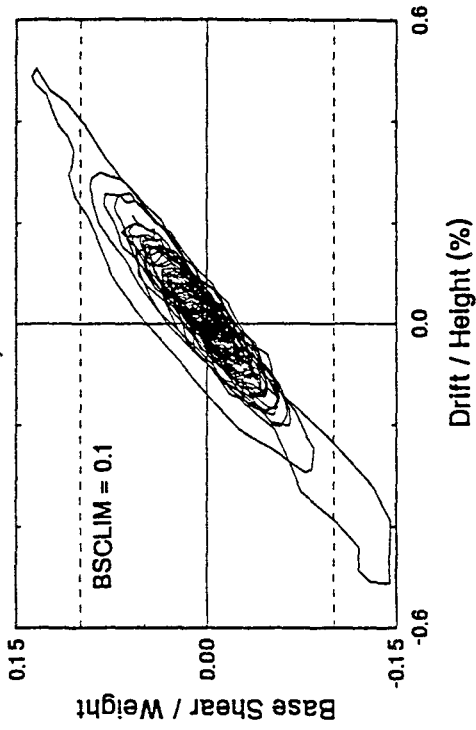
TEST 52

33.3% El Centro, Base Shear Control



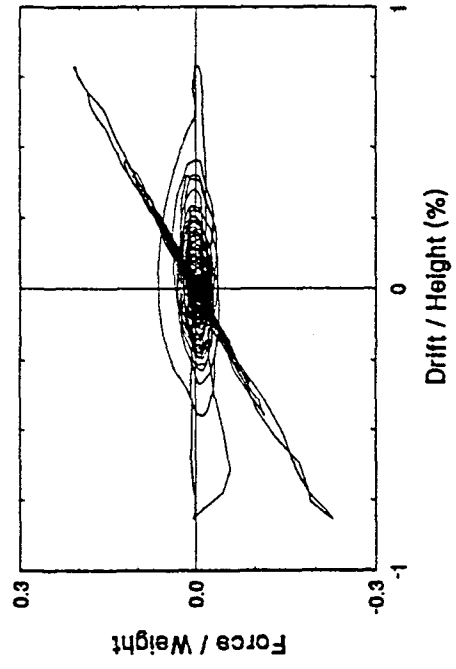
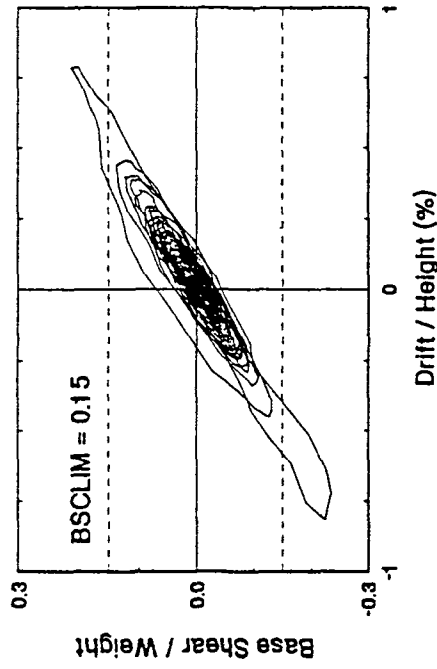
TEST 55

50% Hachinohe, Base Shear Control



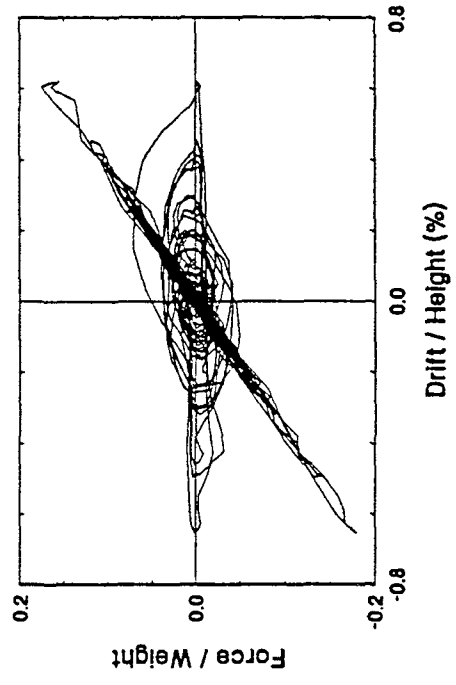
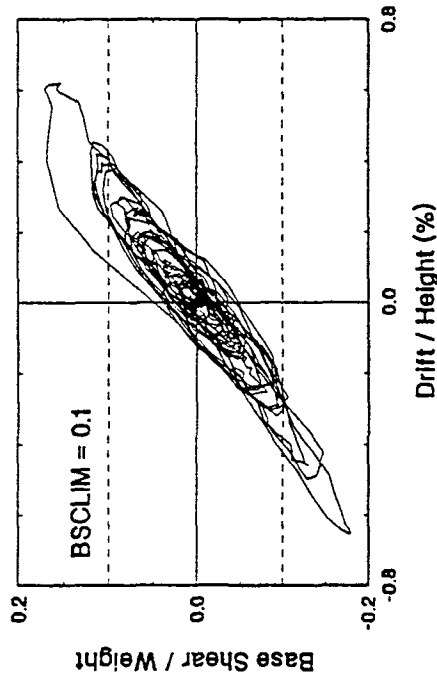
TEST 56

75% Hachinohe, Base Shear Control



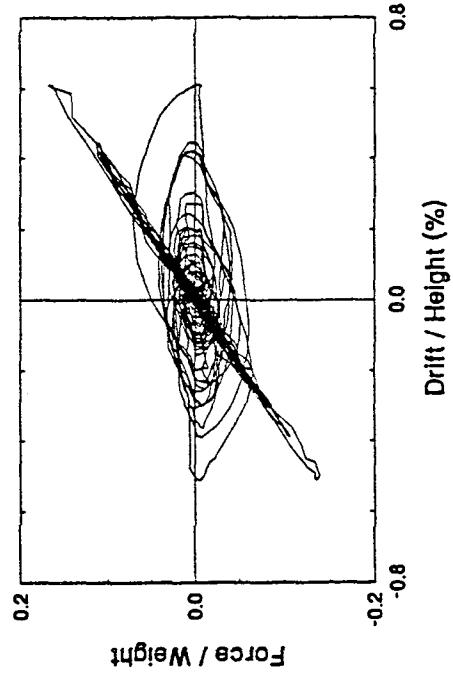
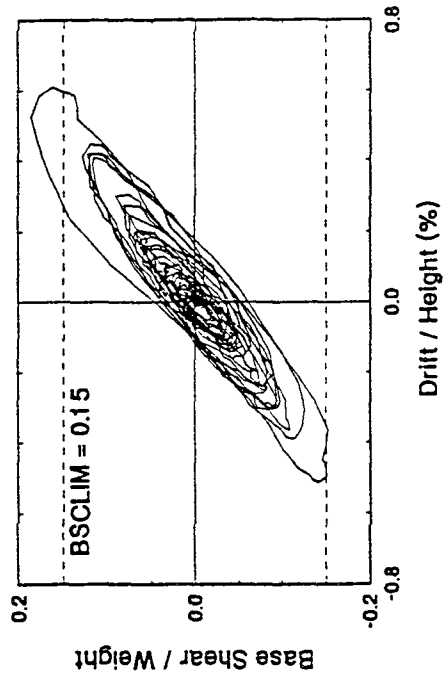
TEST 53

125% Hachinohe-M, Base Shear Control



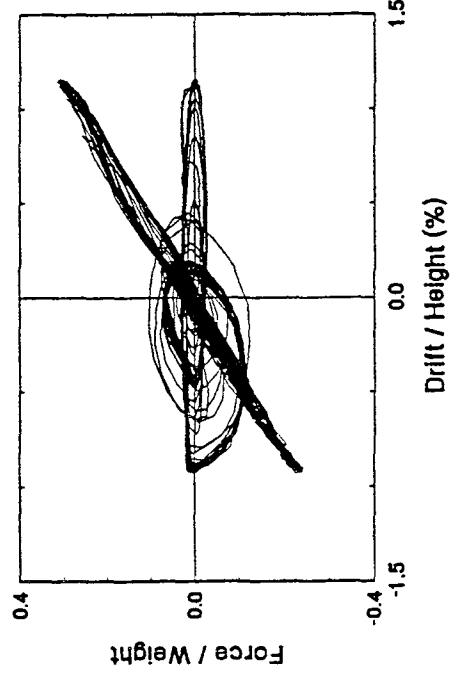
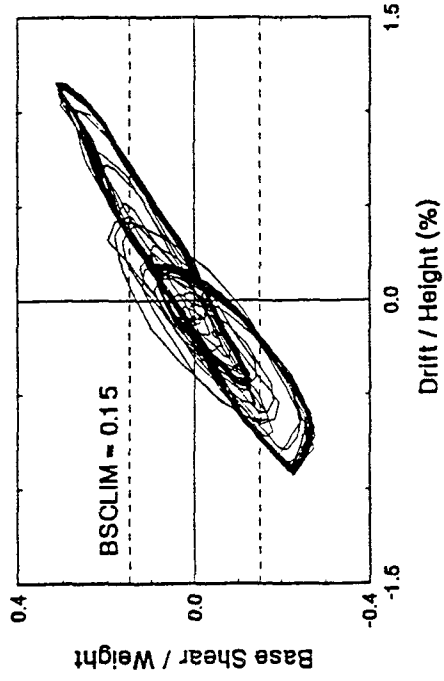
TEST 54

125% Hachinohe-M, Base Shear Control



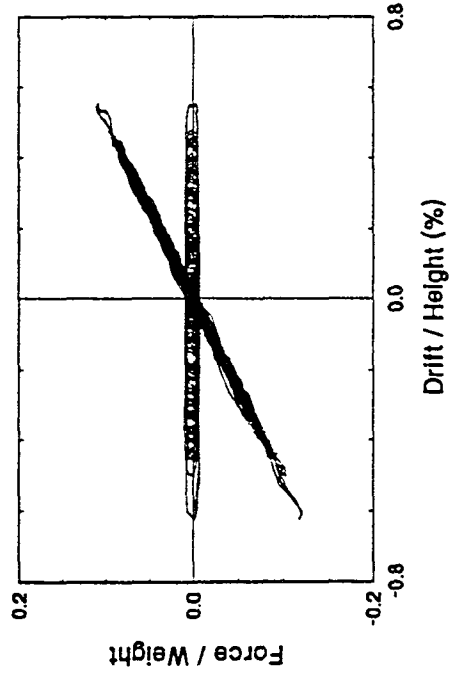
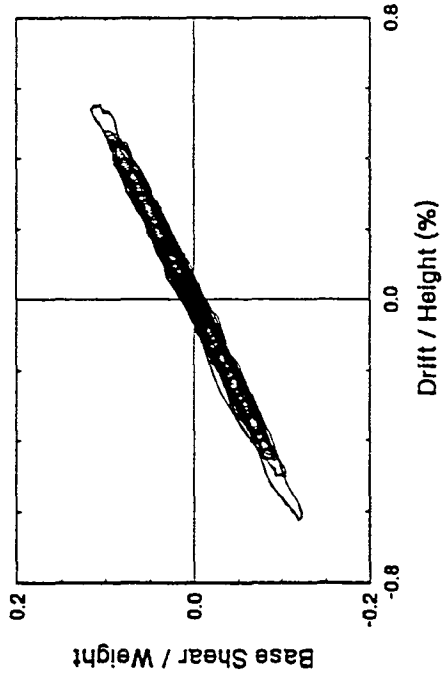
TEST 57

0.5g 5.6 Hz Harmonic, Base Shear Control



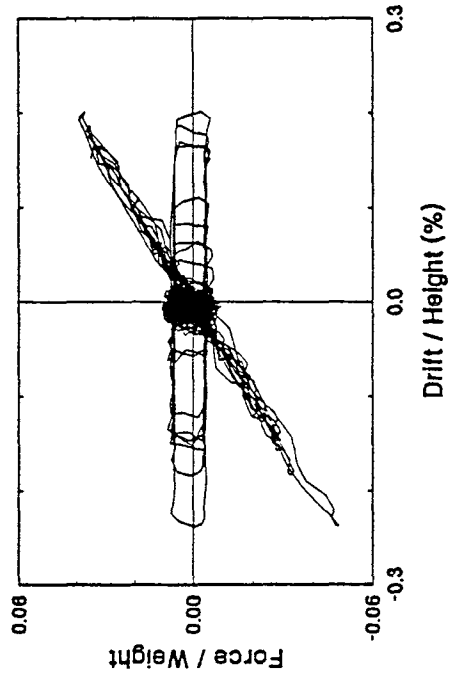
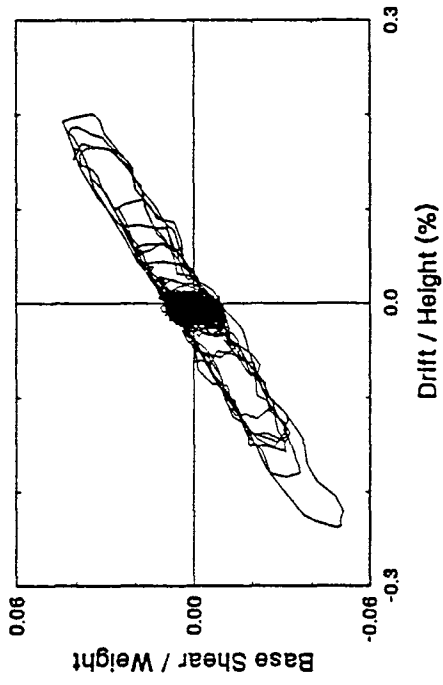
TEST 59

0.1 g White Noise, Low Damping



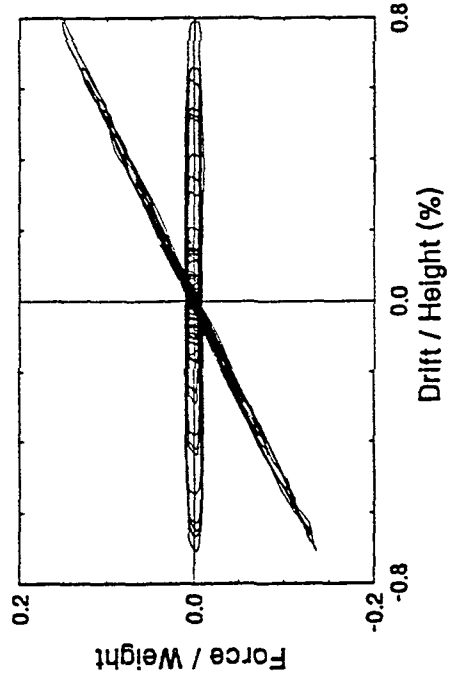
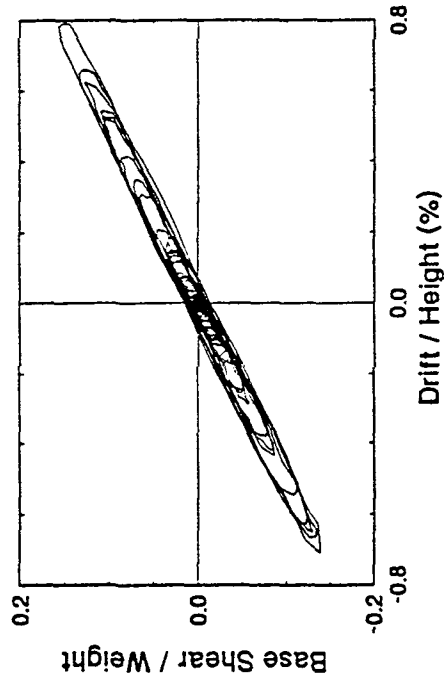
TEST 83

10% El Centro, Low Damping



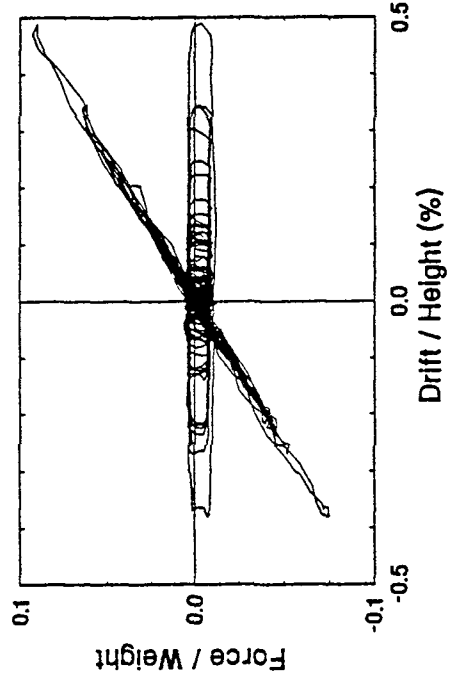
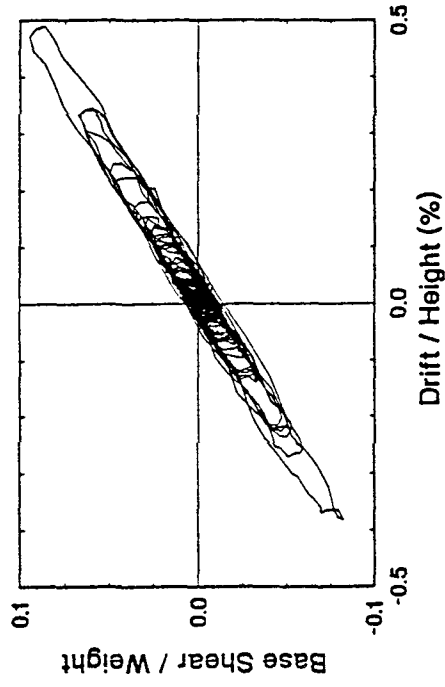
TEST 84

25% El Centro, Low Damping



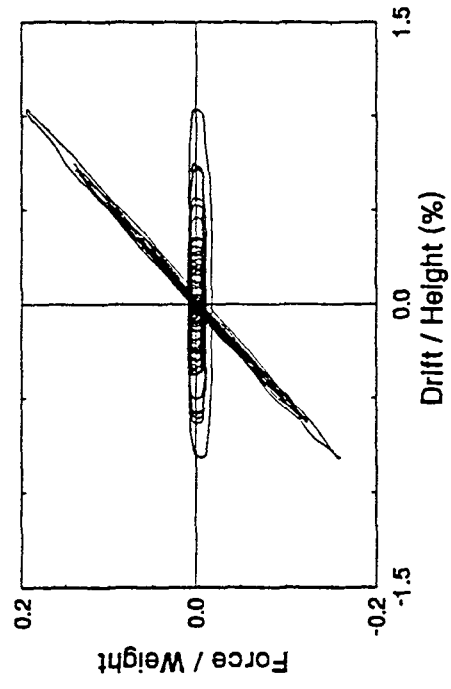
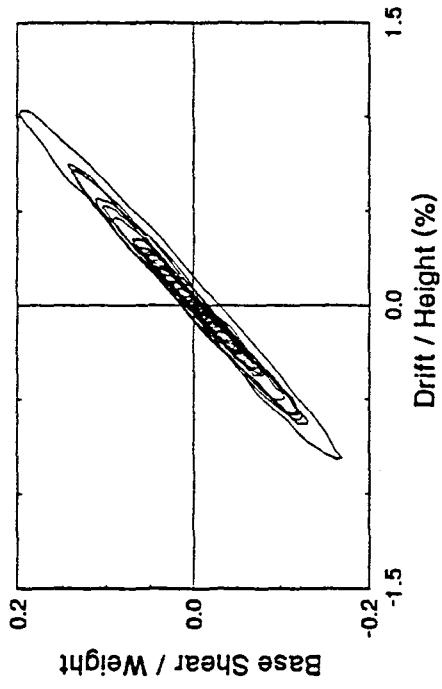
TEST 86

25% Hachinohe, Low Damping



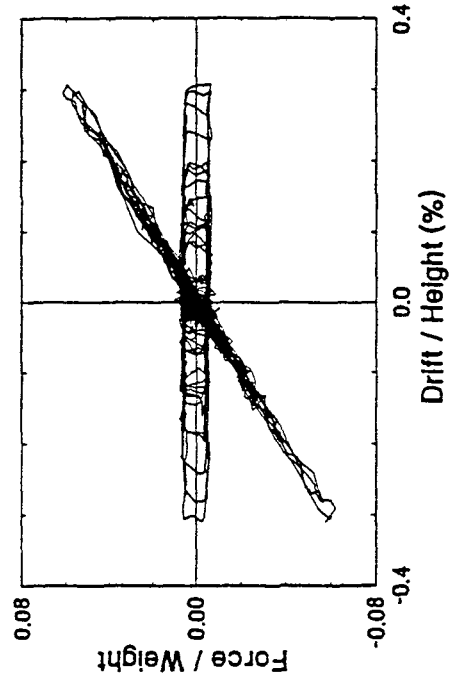
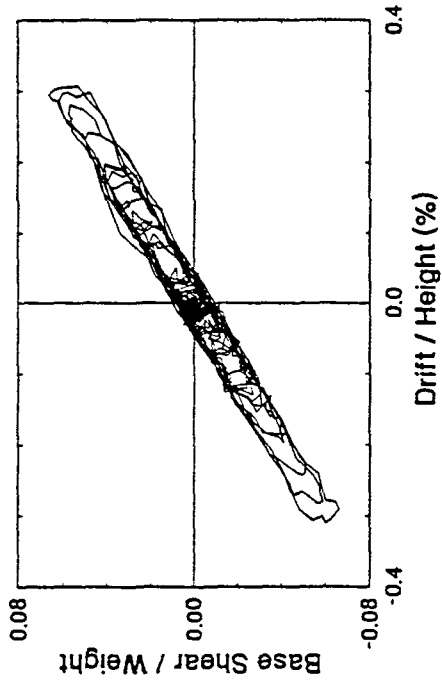
TEST 85

50% Hachinohe, Low Damping



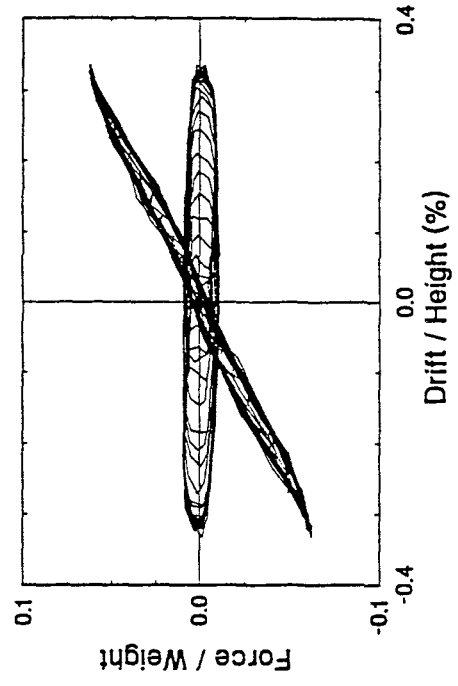
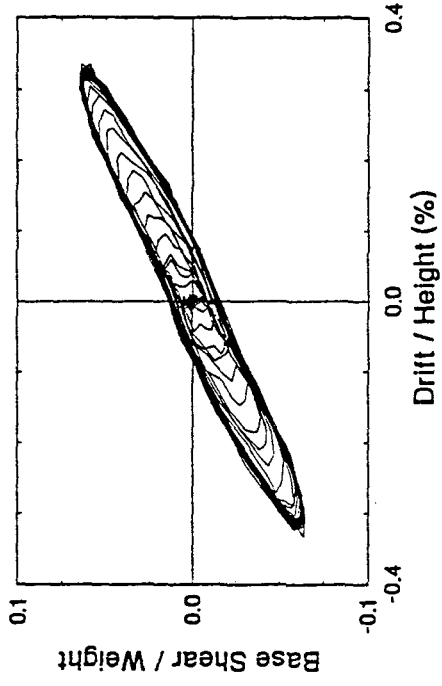
TEST 87

50% Hachinohe-M, Low Damping



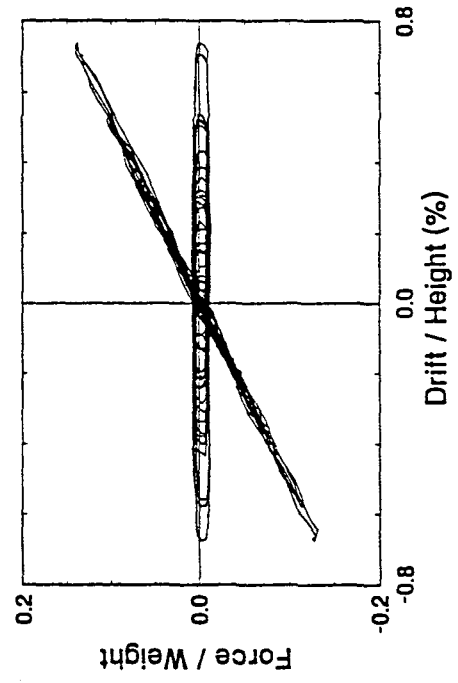
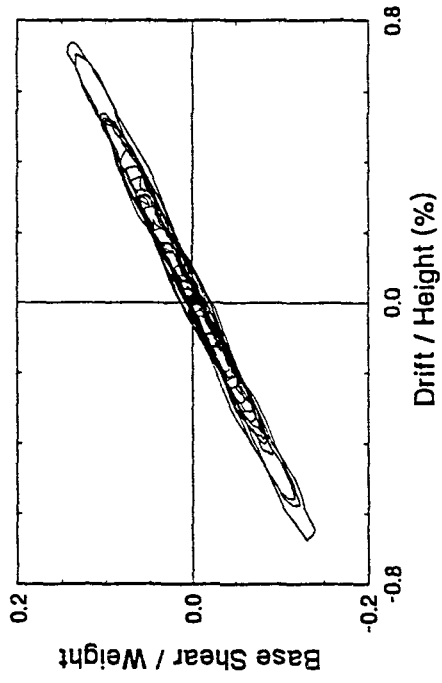
TEST 66

0.2g 5 Hz Harmonic, Low Damping



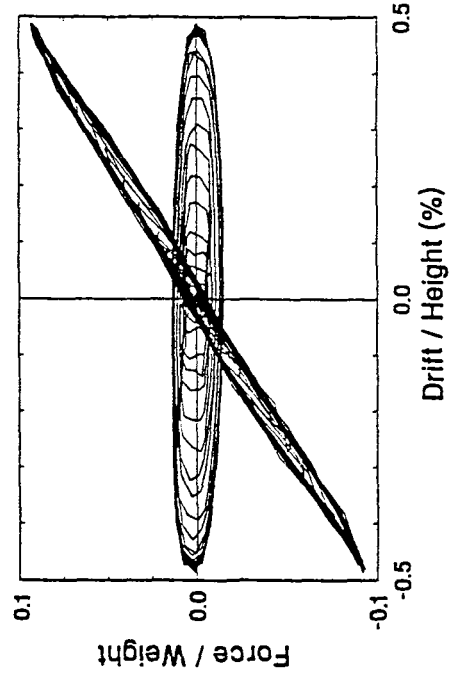
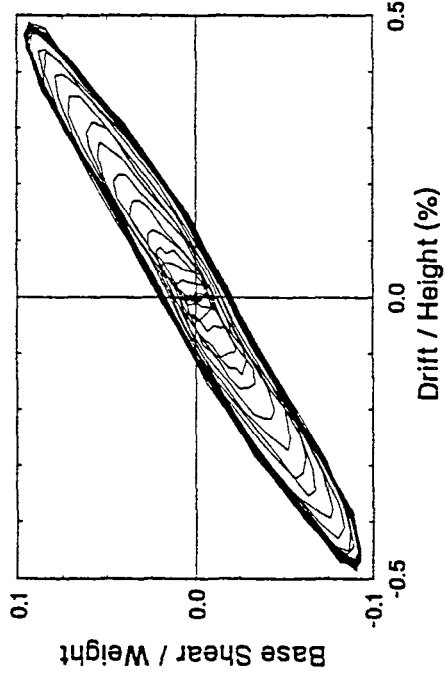
TEST 88

100% Hachinohe-M, Low Damping



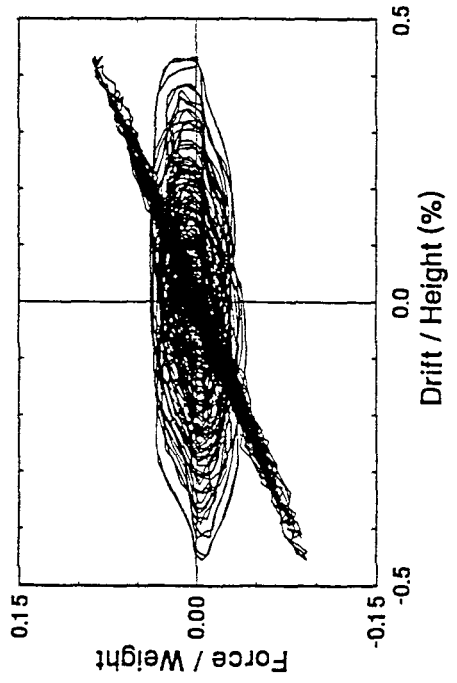
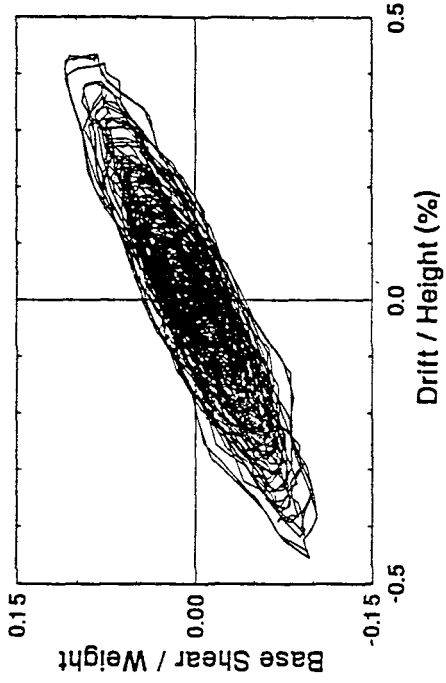
TEST 62

0.3g 5 Hz Harmonic, Low Damping



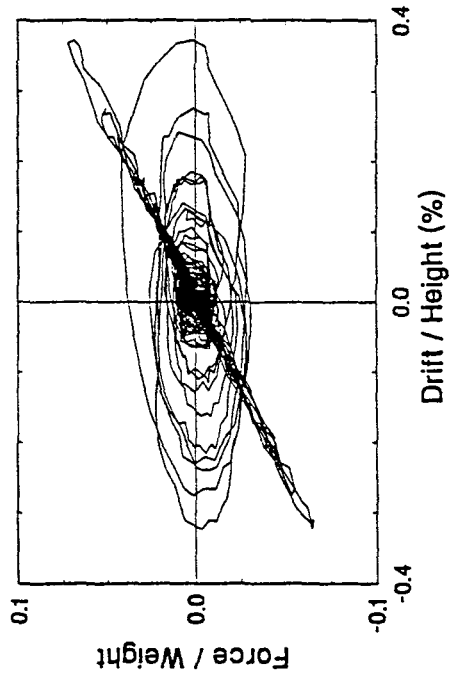
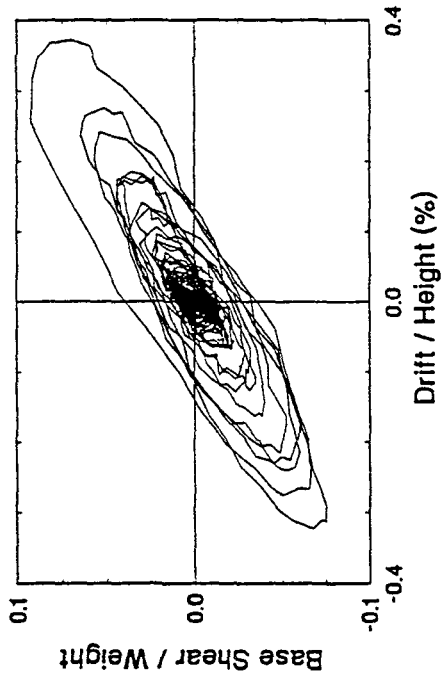
TEST 60

0.15g White Noise, High Damping



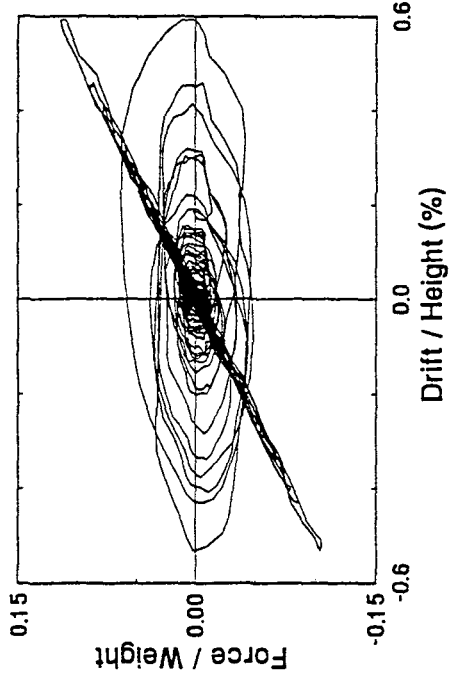
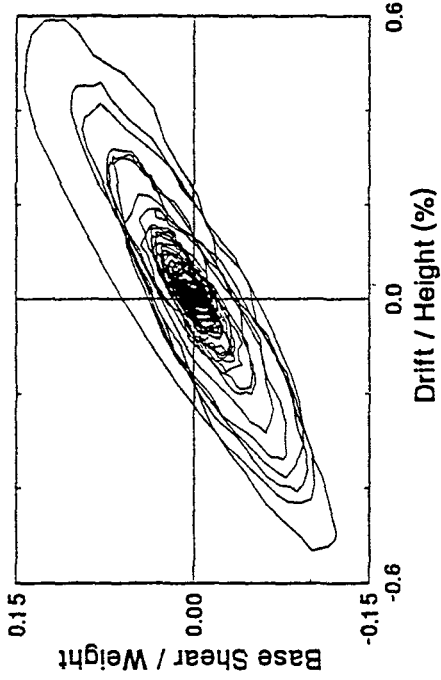
TEST 75

25% El Centro, High Damping



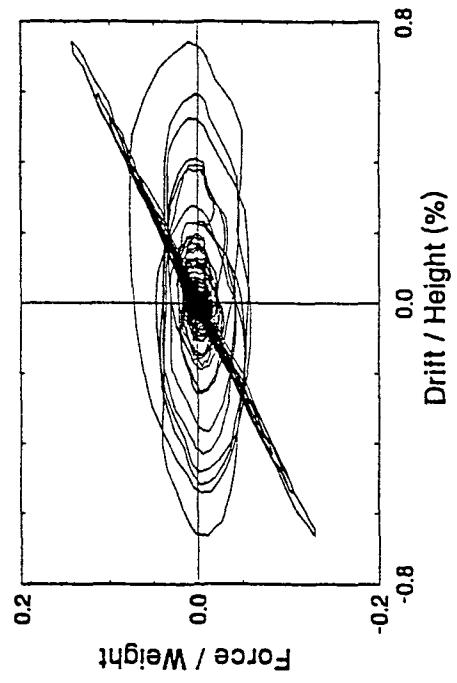
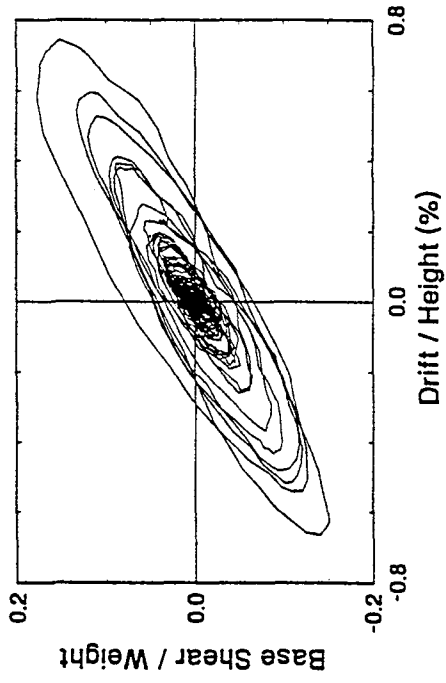
TEST 76

40% El Centro, High Damping



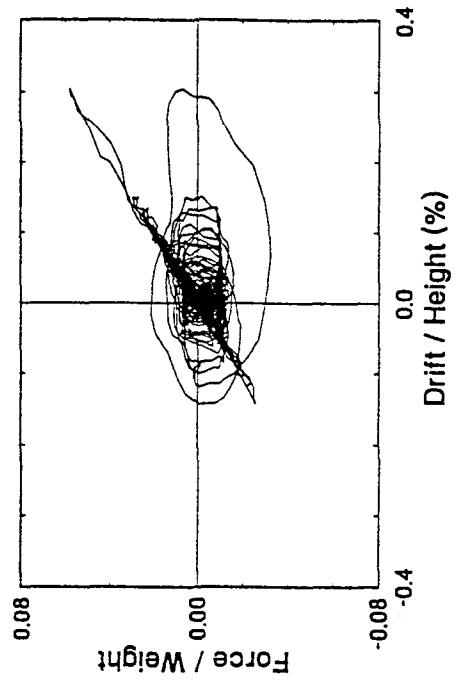
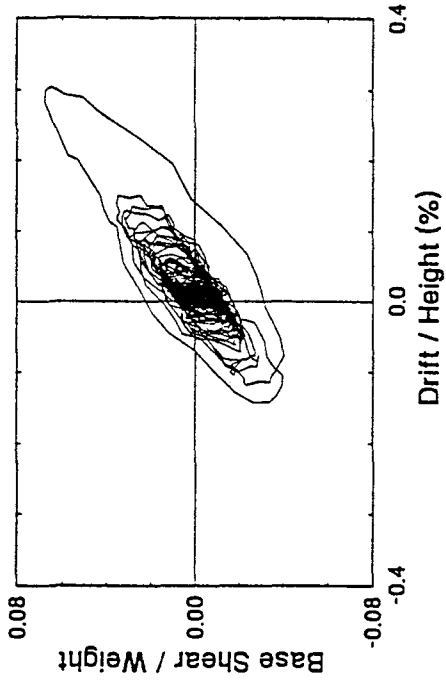
TEST 77

50% El Centro, High Damping



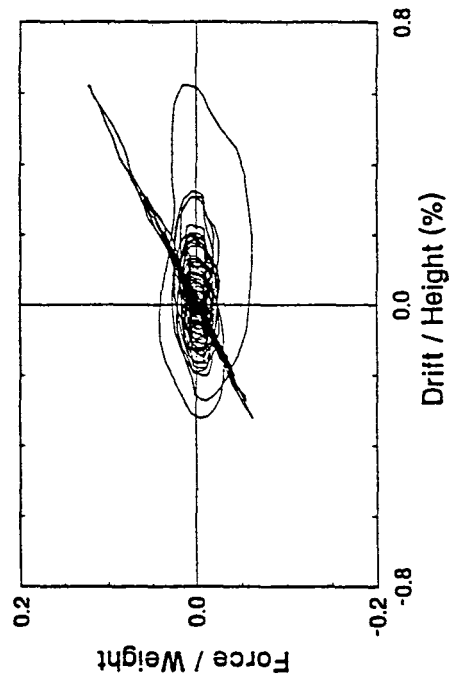
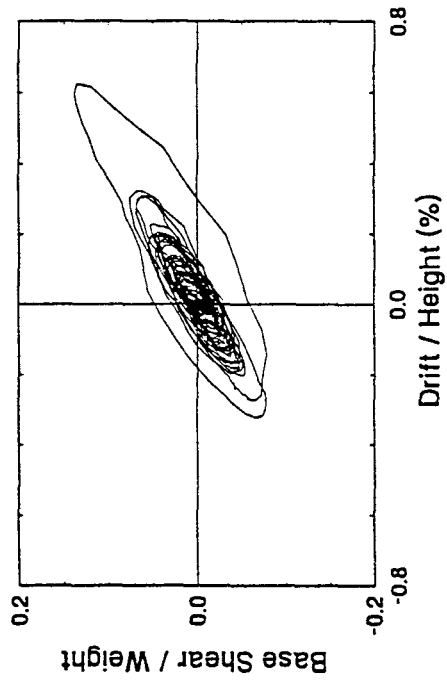
TEST 79

25% Hachinohe, High Damping



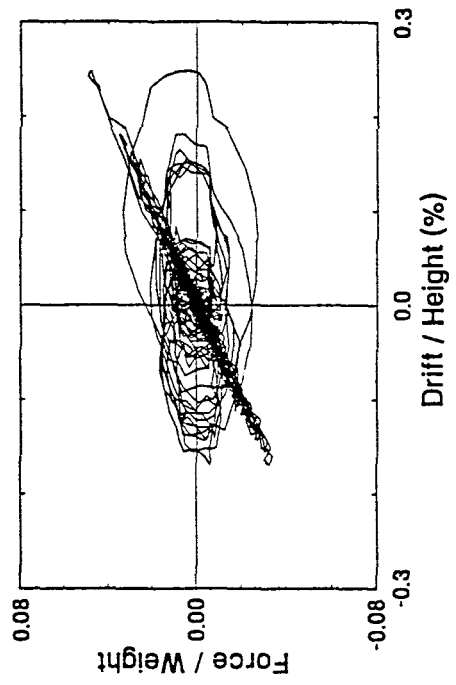
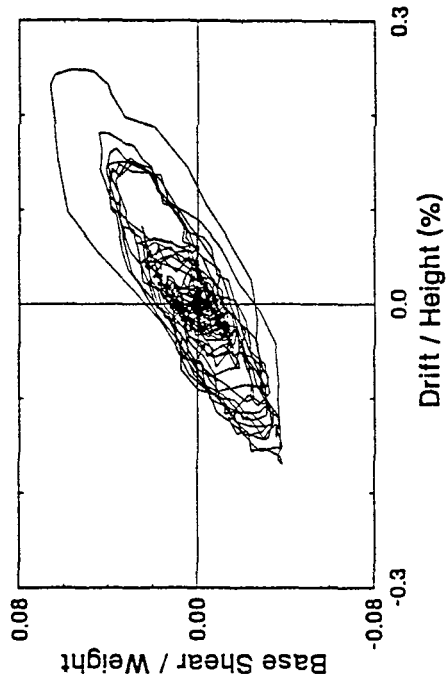
TEST 78

50% Hachinohe, High Damping



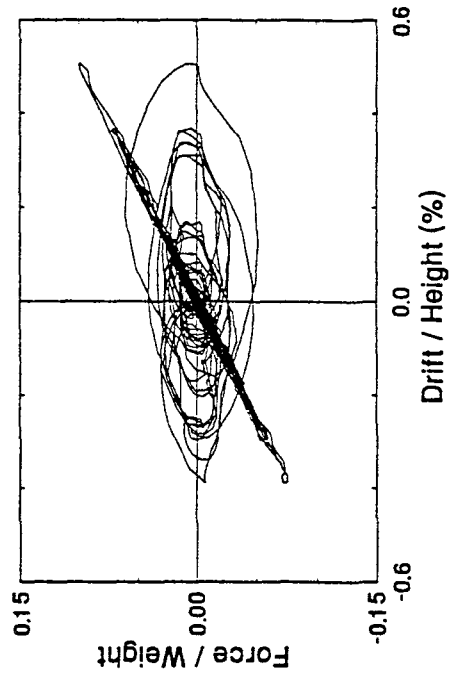
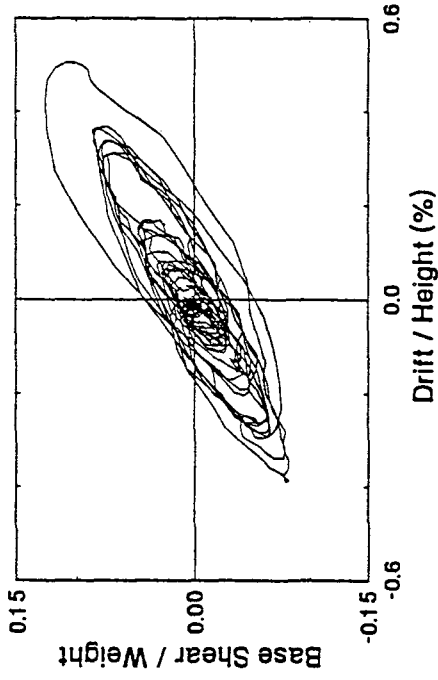
TEST 80

50% Hachinohe-M, High Damping



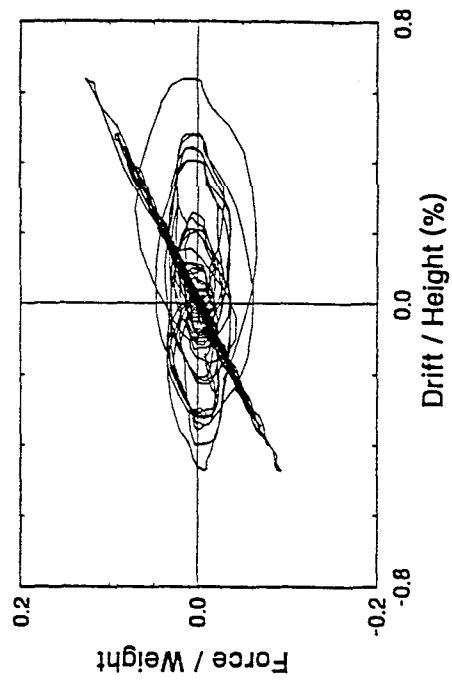
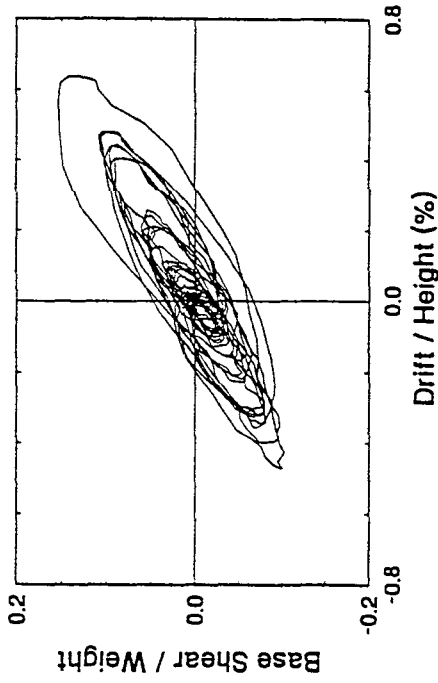
TEST 81

100% Hachinohe-M, High Damping



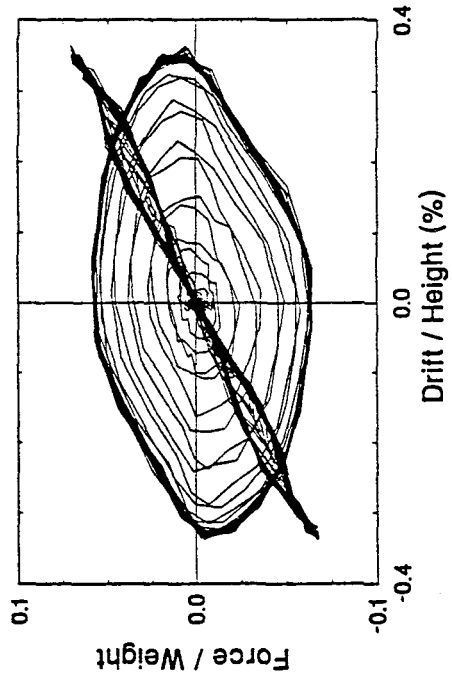
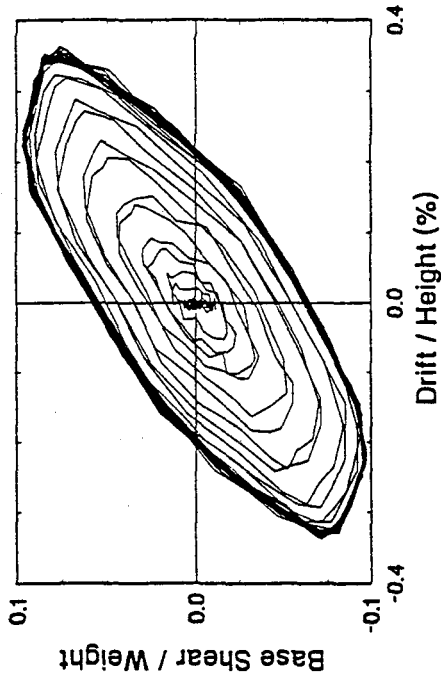
TEST 82

125% Hachinohe-M, High Damping



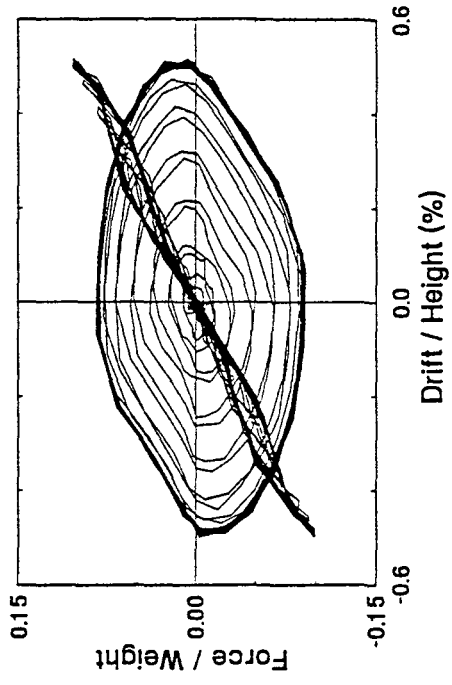
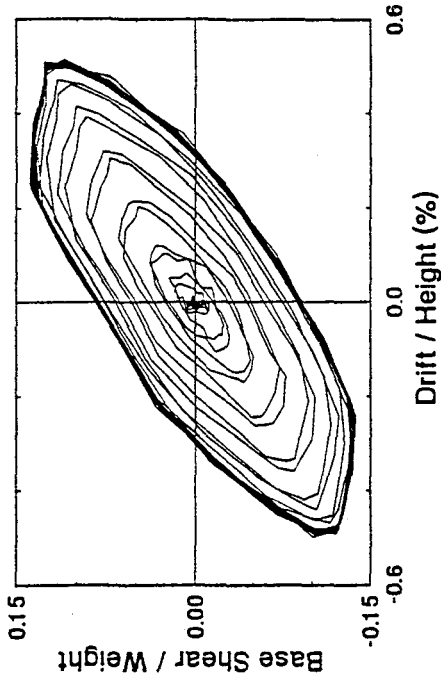
TEST 65

0.2g 5 Hz Harmonic, High Damping



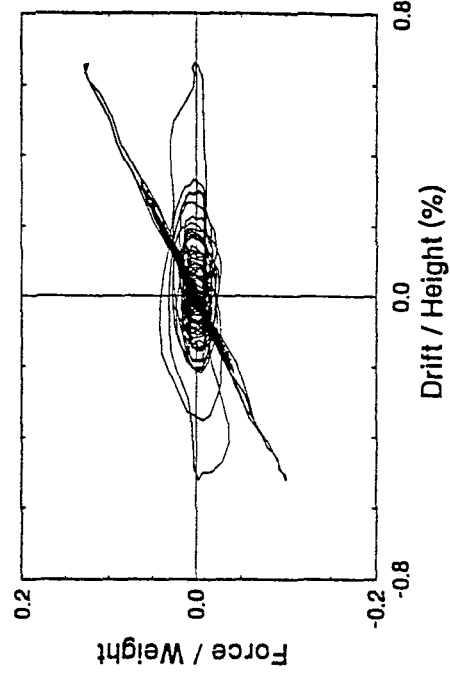
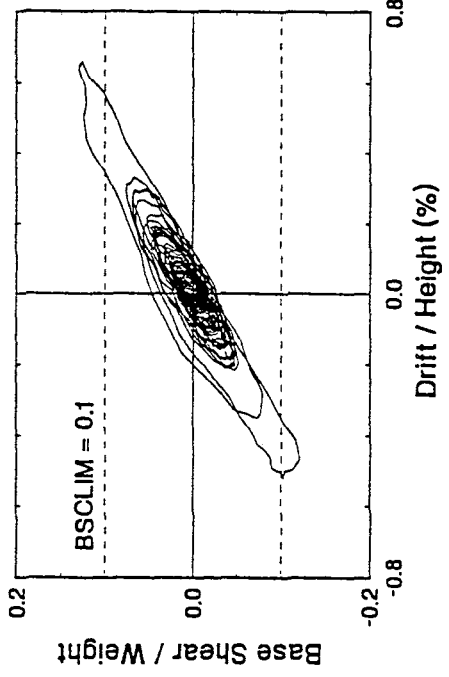
TEST 61

0.3g 5 Hz Harmonic, High Damping



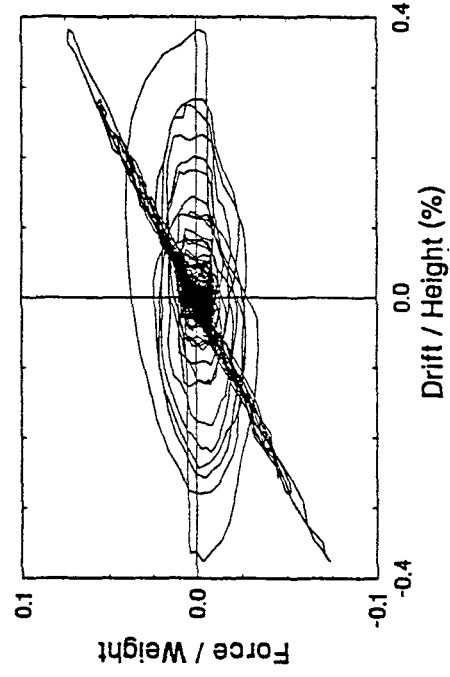
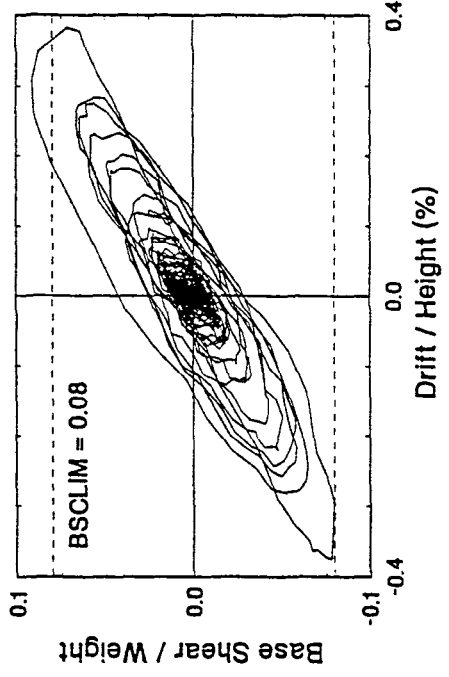
TEST 140

50% Hachinohe, Base Shear Control



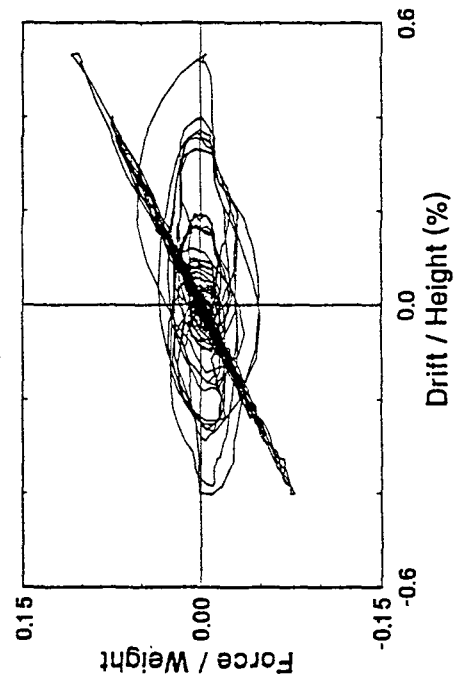
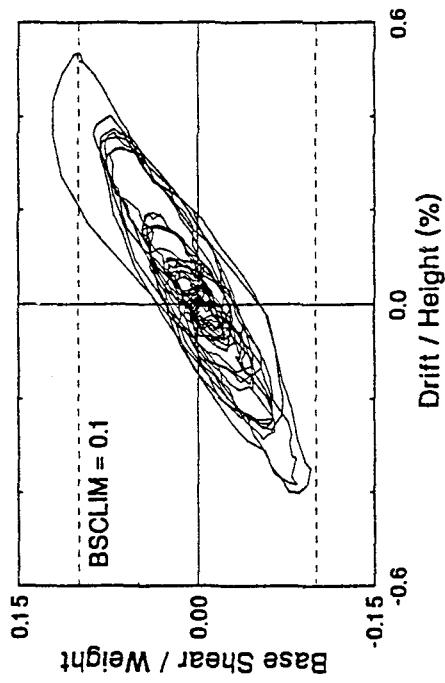
TEST 139

25% El Centro, Base Shear Control



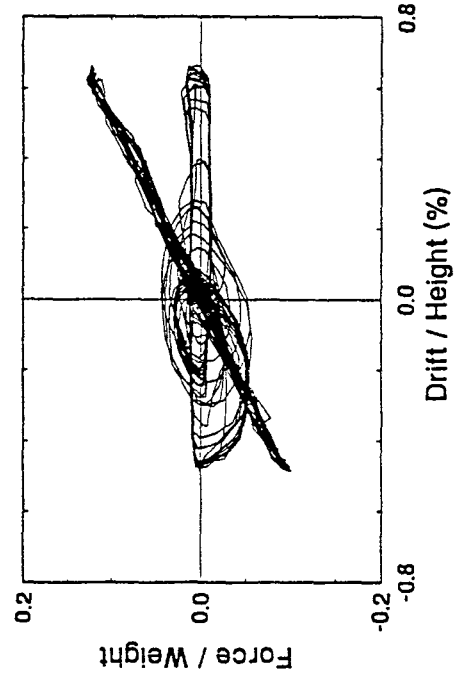
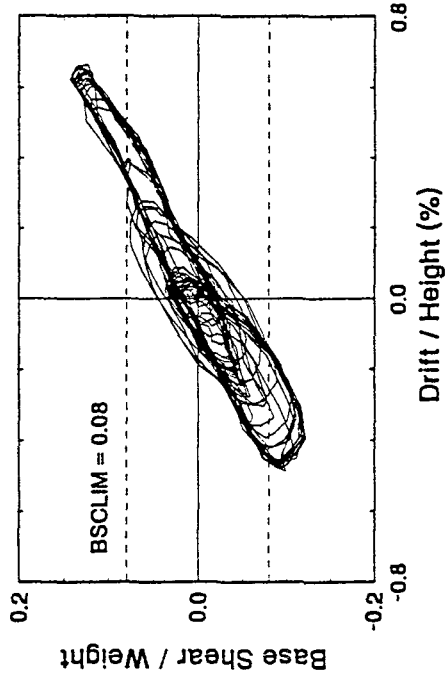
TEST 141

100% Hachinohe-M, Base Shear Control



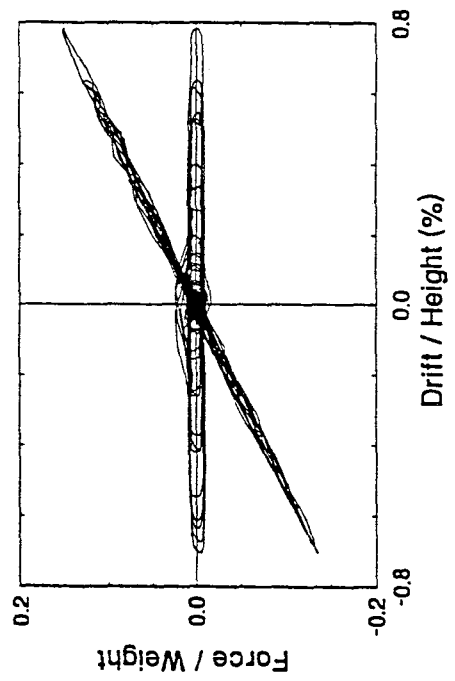
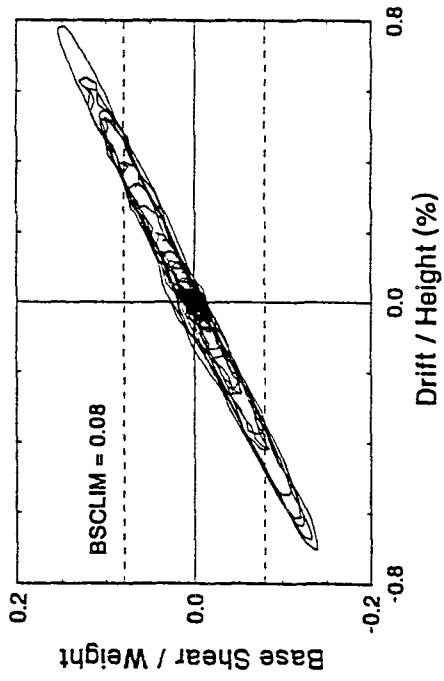
TEST 142

0.2g 5 Hz Harmonic, Base Shear Control



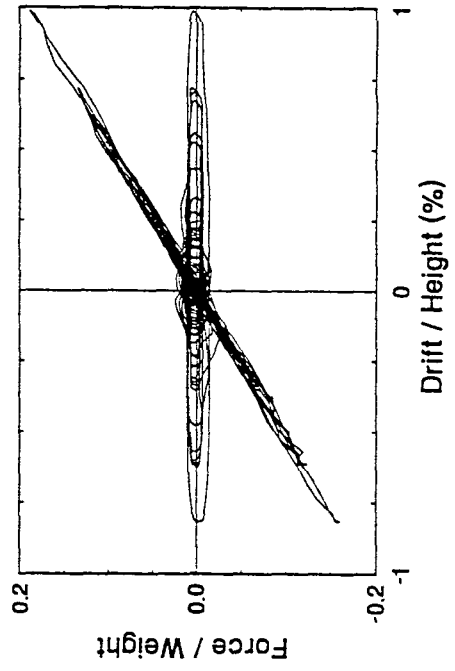
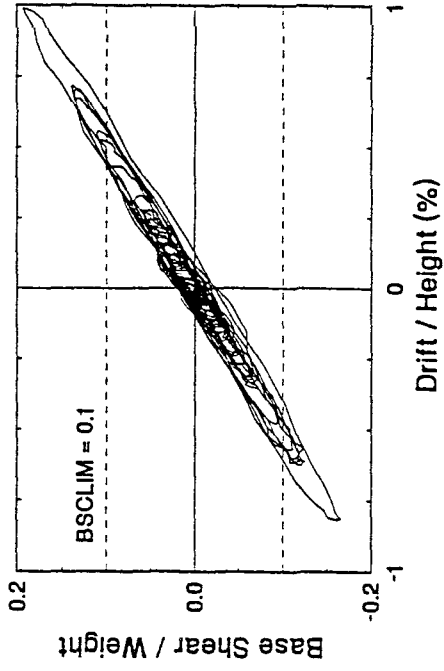
TEST 143

25% El Centro, Base Shear Control - KC



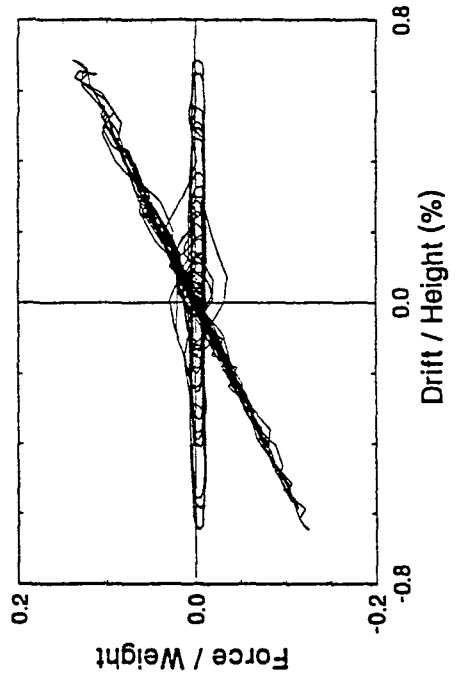
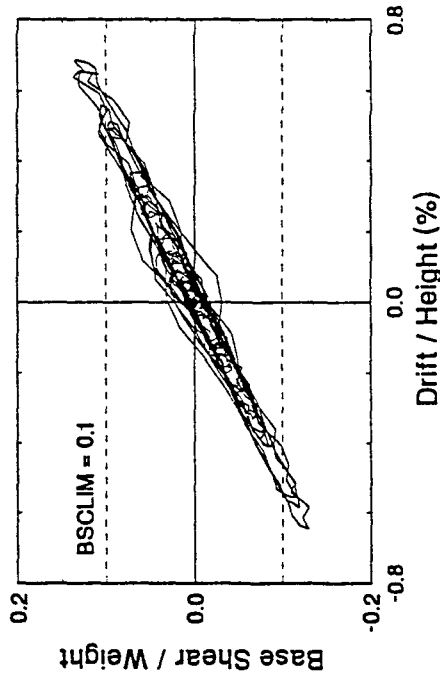
TEST 144

50% Hachinohe, Base Shear Control - KC



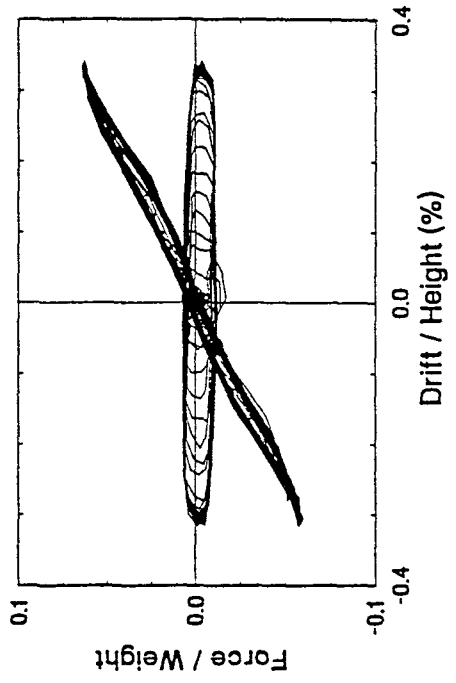
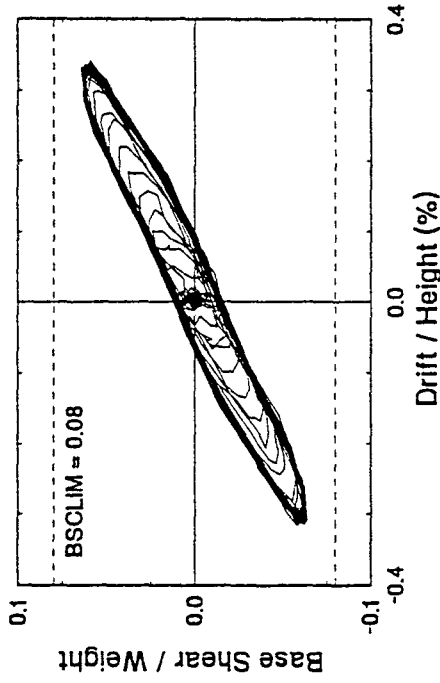
TEST 145

100% Hachinohe-M, Base Shear Control - KC



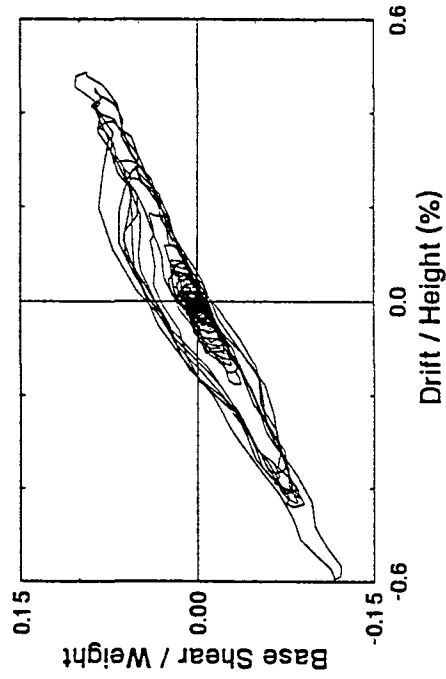
TEST 146

0.2g 5 Hz Harmonic, Base Shear Control - KC



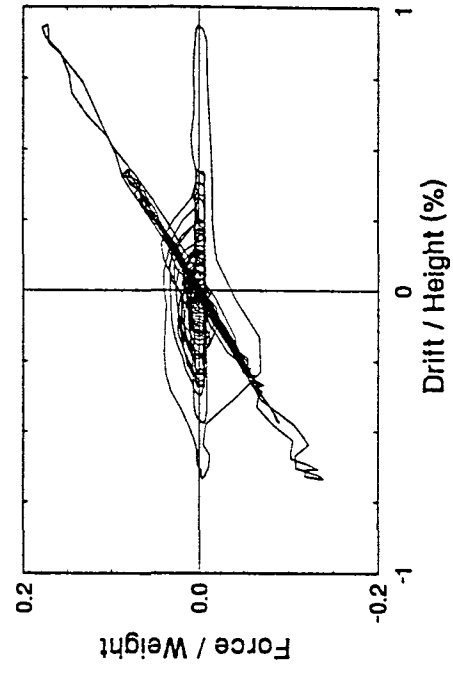
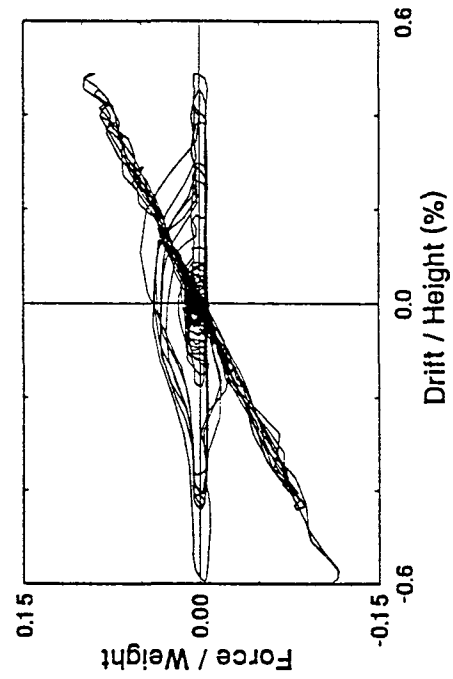
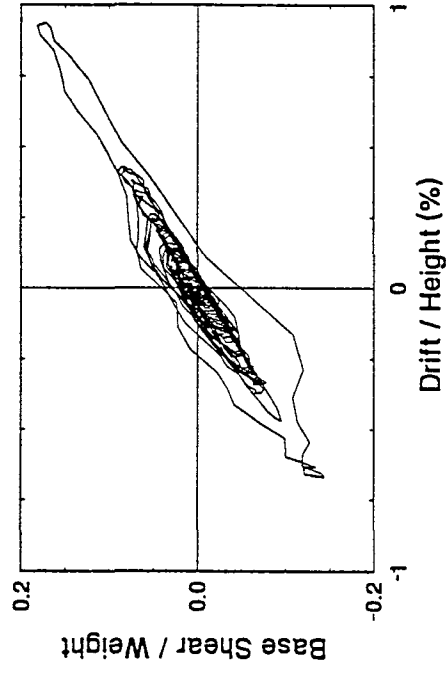
TEST 135

25% El Centro, Force Transfer Control



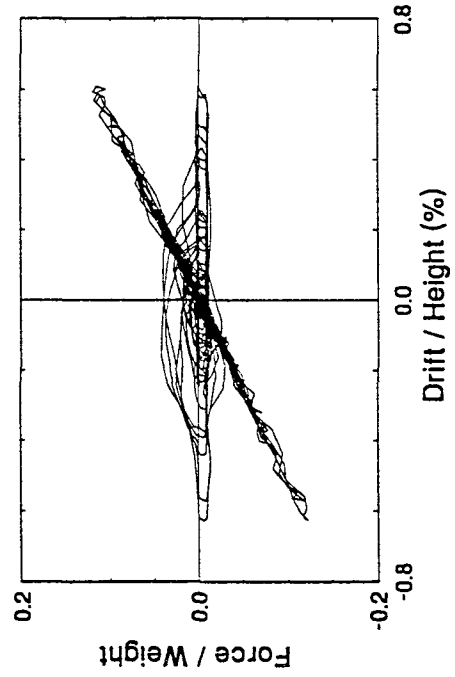
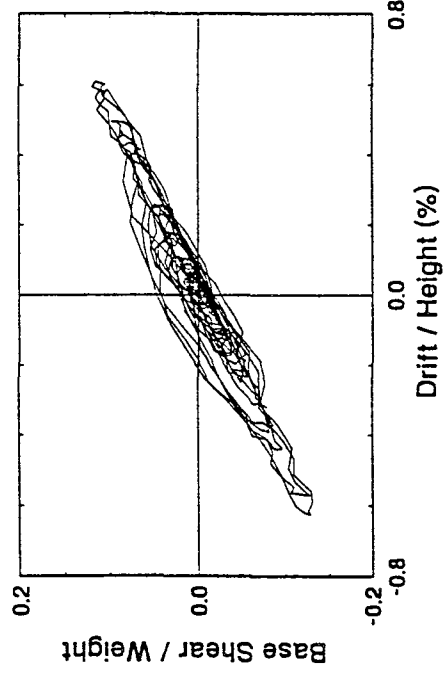
TEST 136

50% Hachinohe, Force Transfer Control



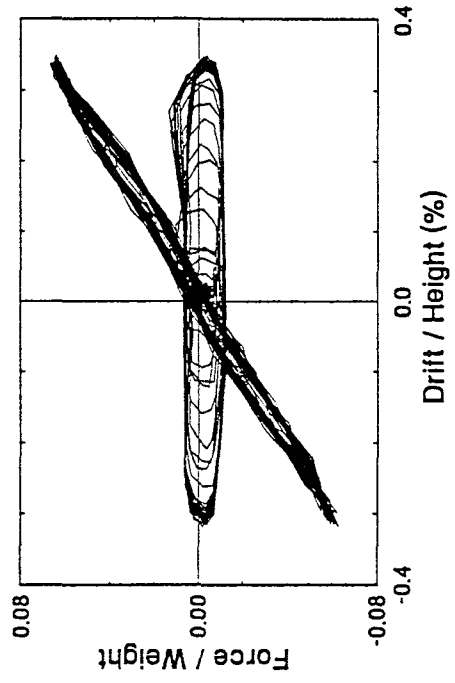
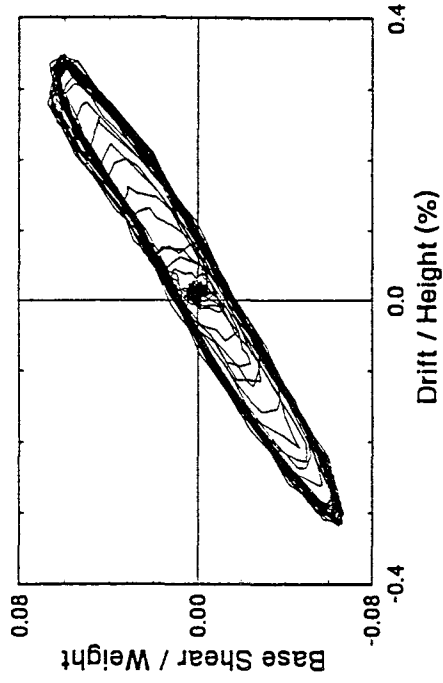
TEST 137

100% Hachinohe-M, Force Transfer Control



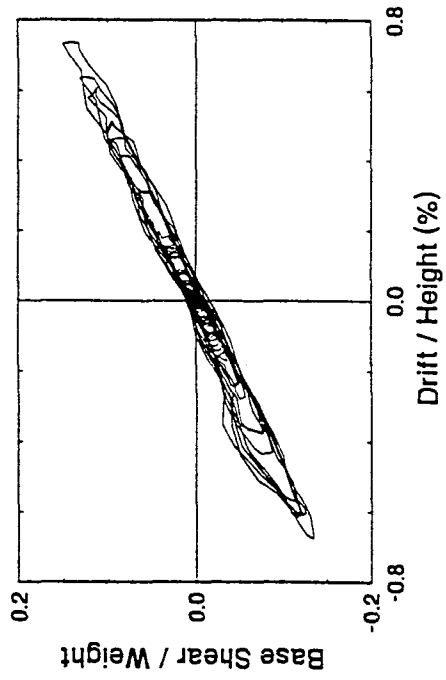
TEST 138

0.2g 5 Hz Harmonic, Force Transfer Control



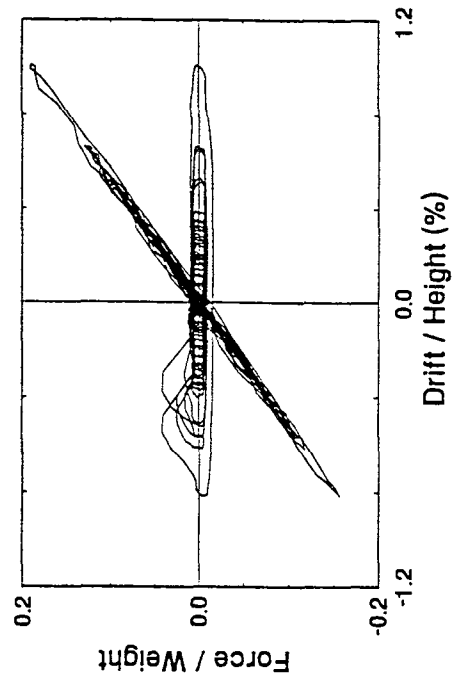
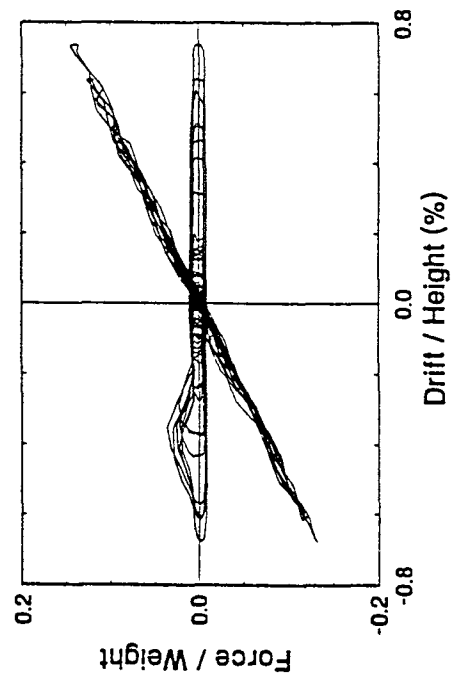
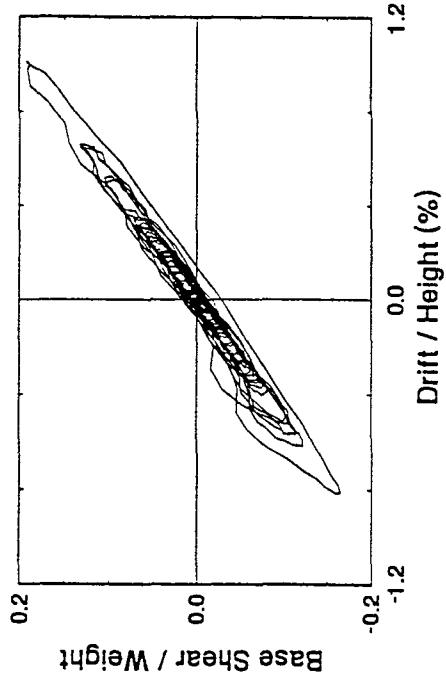
TEST 122

25% El Centro, Force Transfer Control - KC

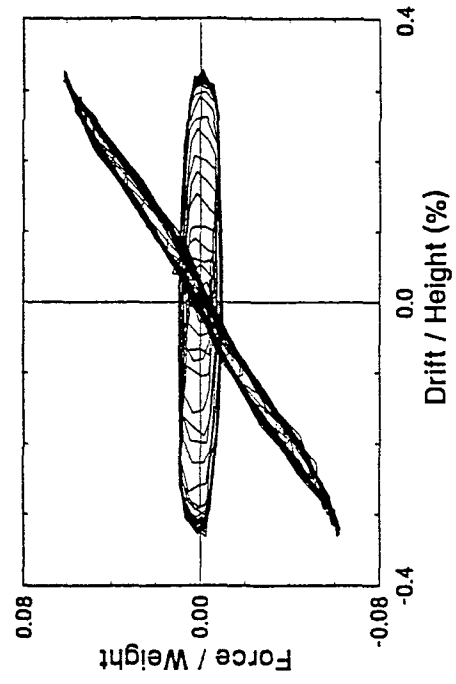
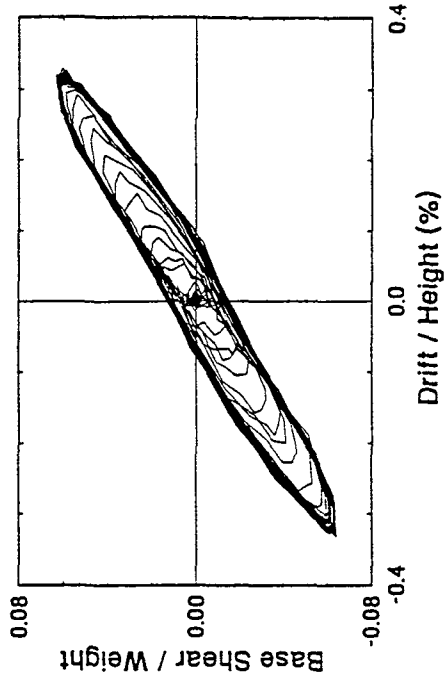


TEST 125

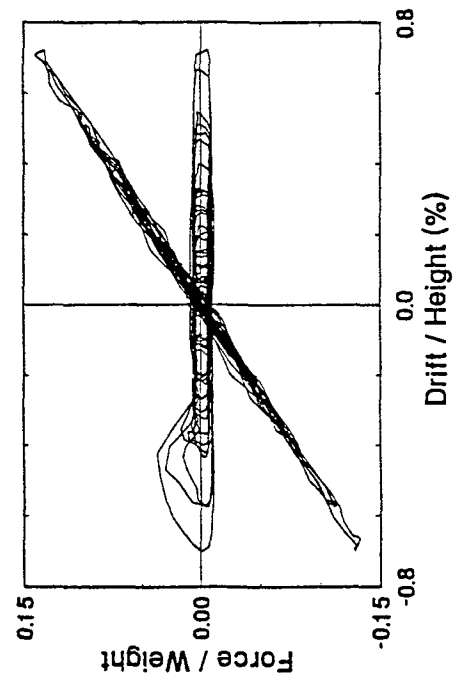
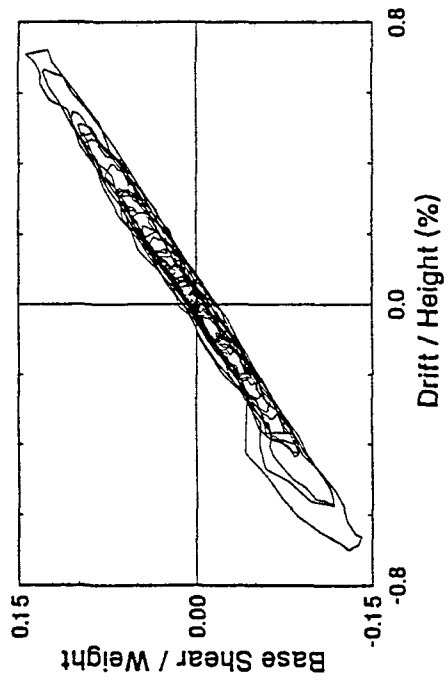
50% Hachinohe, Force Transfer Control - KC



TEST 124
 0.2g 5 Hz Harmonic
 Force Transfer Control - KC

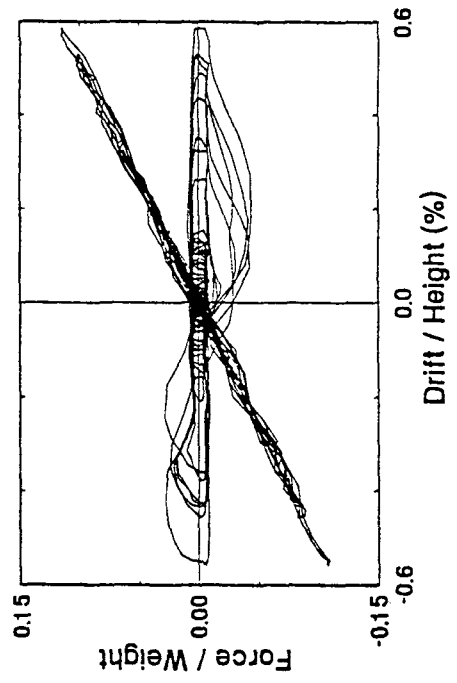
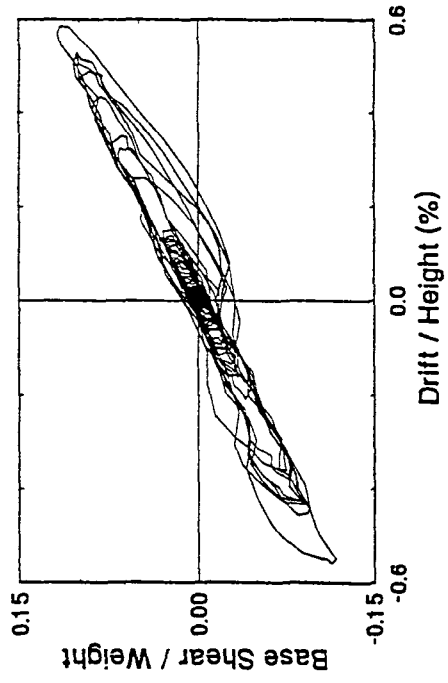


TEST 126
 100% Hachinohe-M
 Force Transfer Control - KC



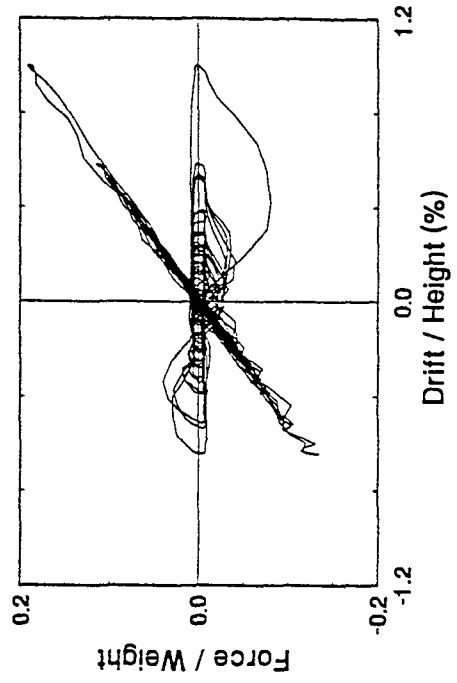
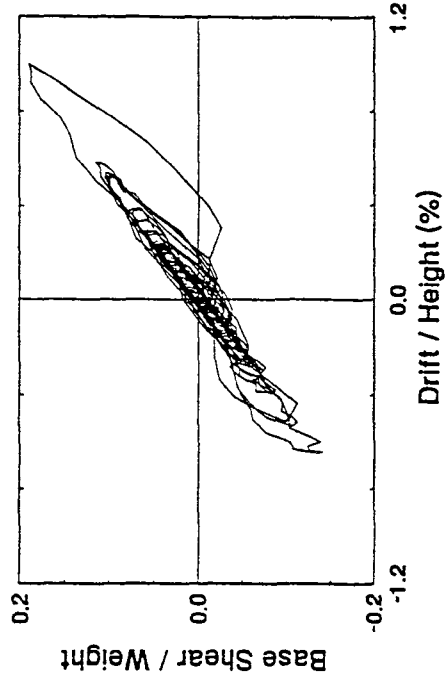
TEST 147

25% El Centro, Force Transfer Control - HC

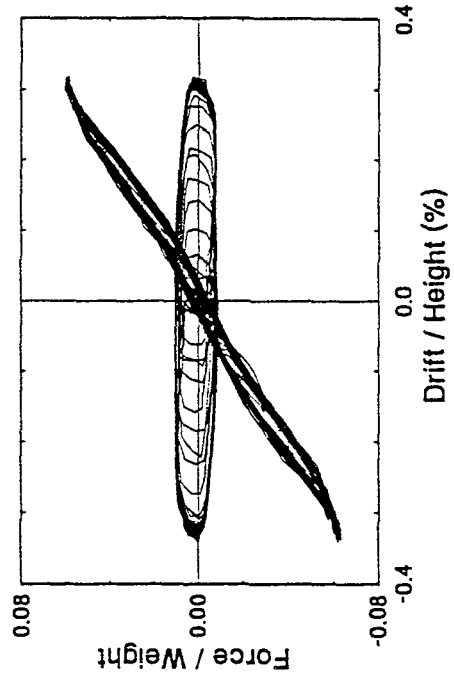
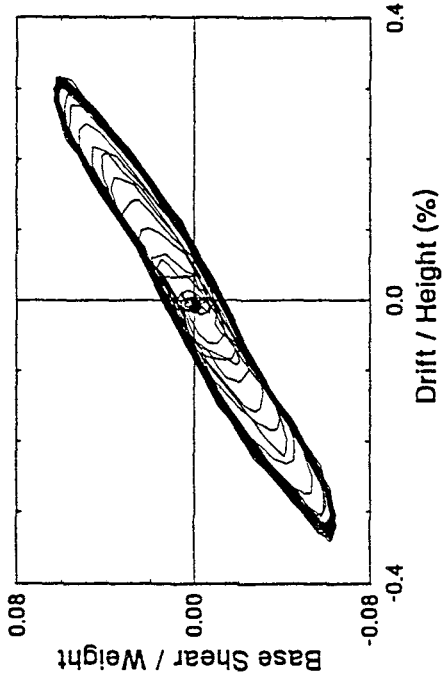


TEST 148

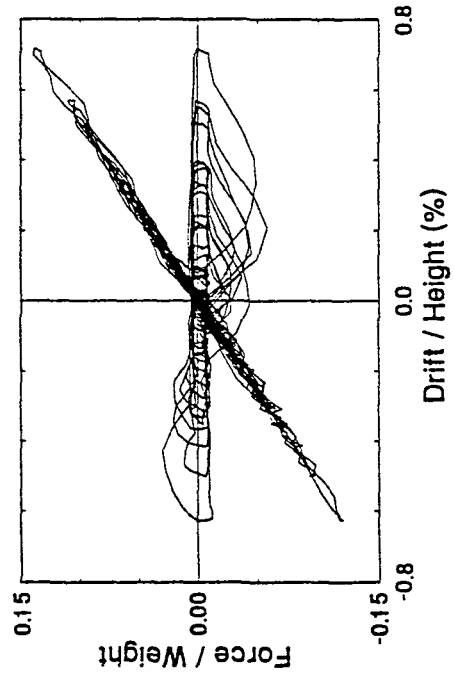
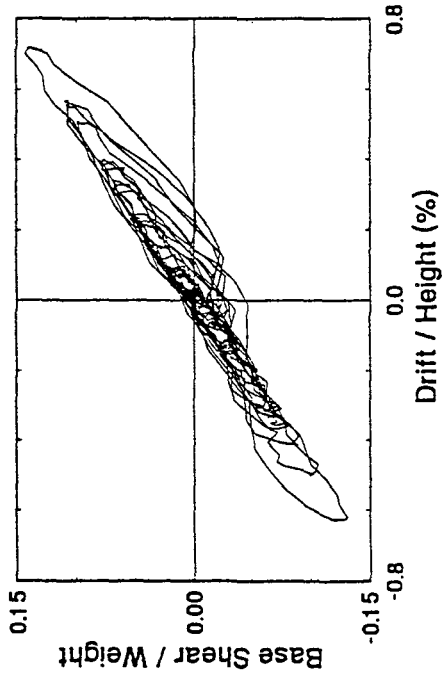
50% Hachinohe, Force Transfer Control - HC



TEST 150
0.2g 5 Hz Harmonic
Force Transfer Control - HC



TEST 149
100% Hachinohe-M
Force Transfer Control - HC



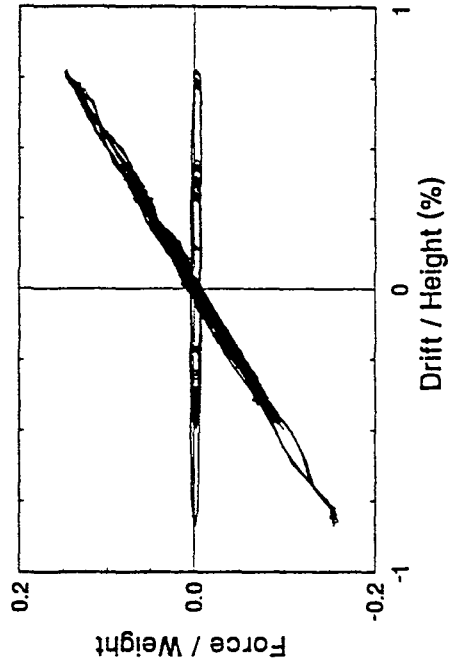
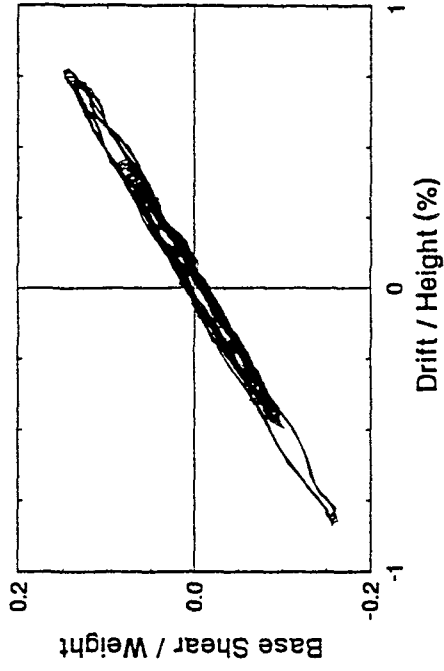
APPENDIX D

Shaking Table Test Results:

One-Story Structure with Variable Dampers

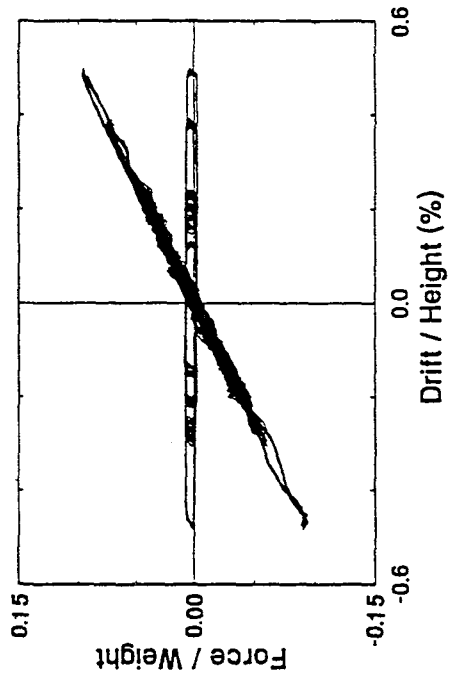
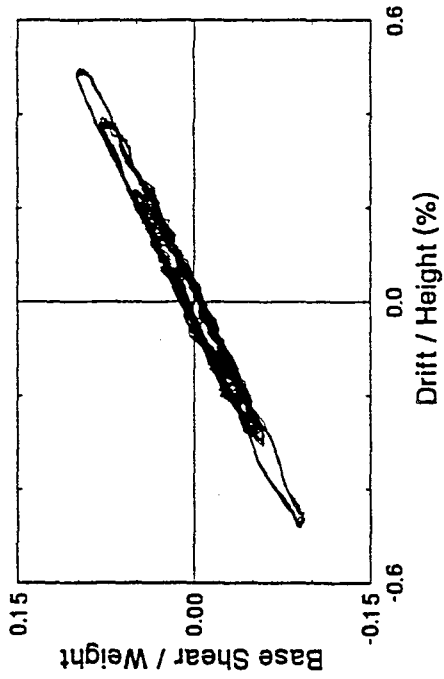
TEST 154

0.15g White Noise, Low Damping



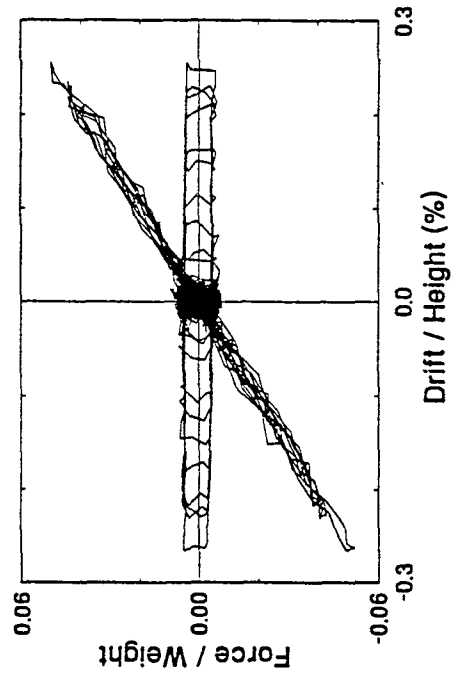
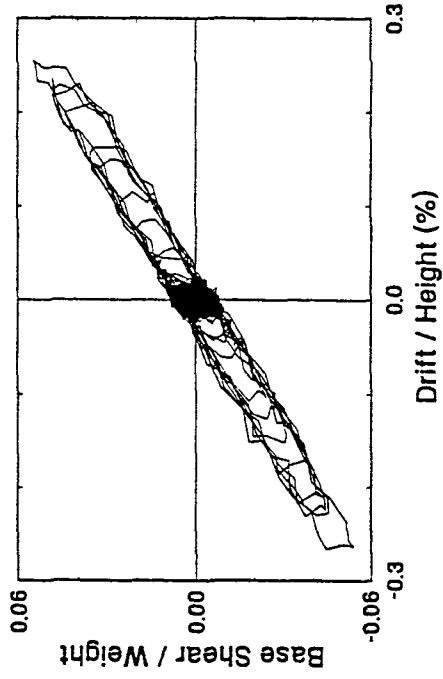
TEST 153

0.1g White Noise, Low Damping



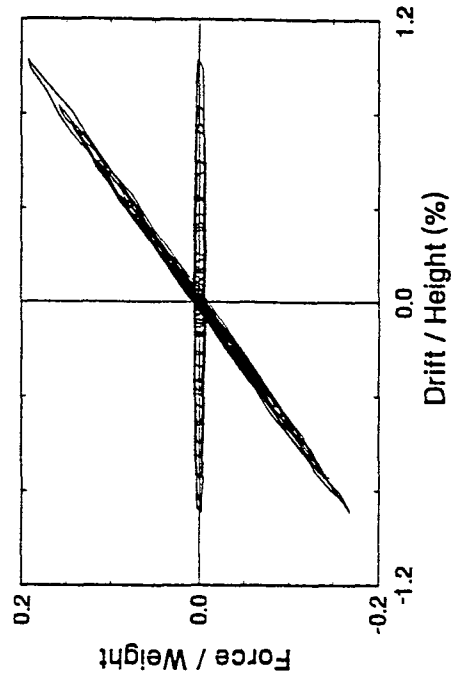
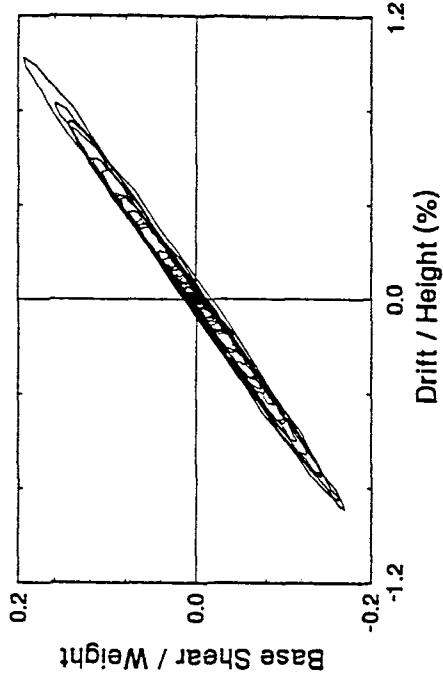
TEST 165

10% EI Centro, Low Damping



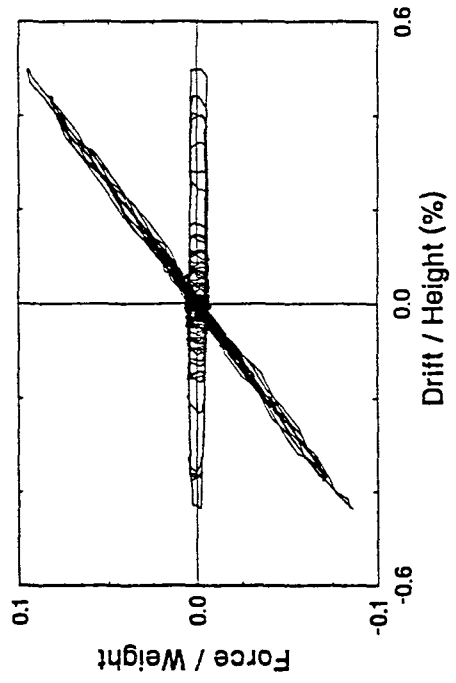
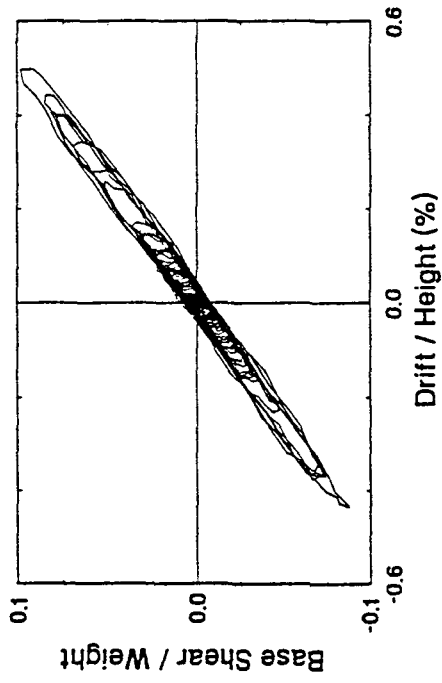
TEST 166

25% EI Centro, Low Damping



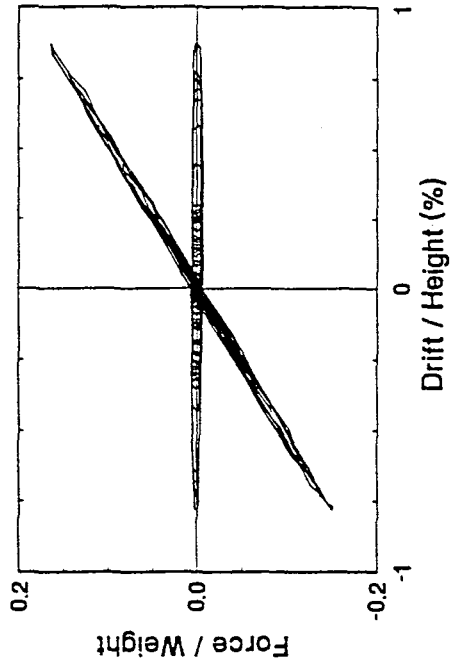
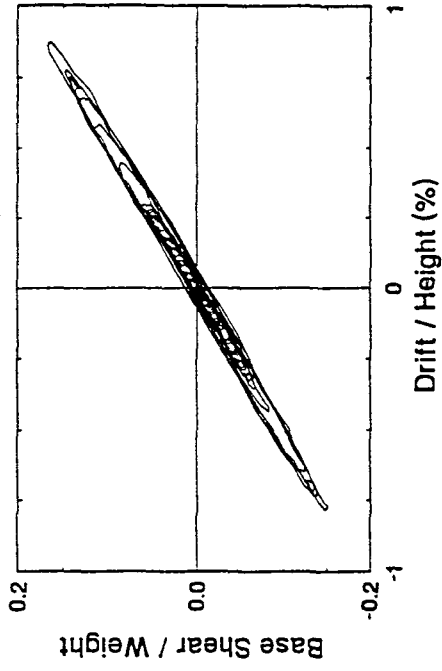
TEST 167

25% Hachinohe, Low Damping



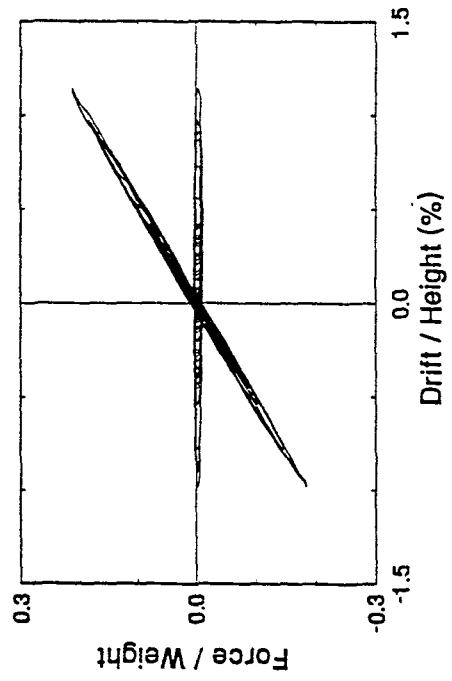
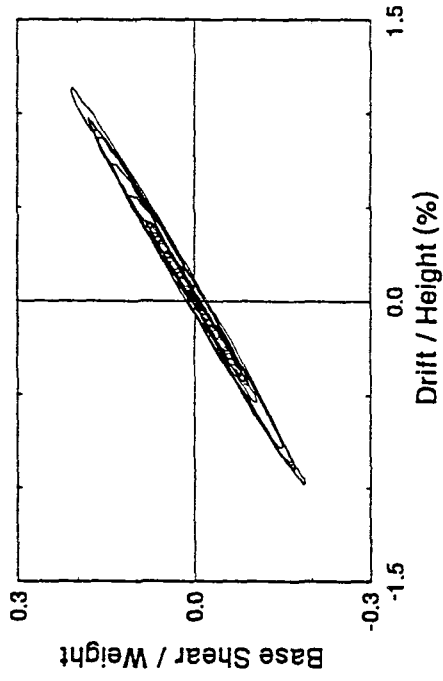
TEST 168

40% Hachinohe, Low Damping



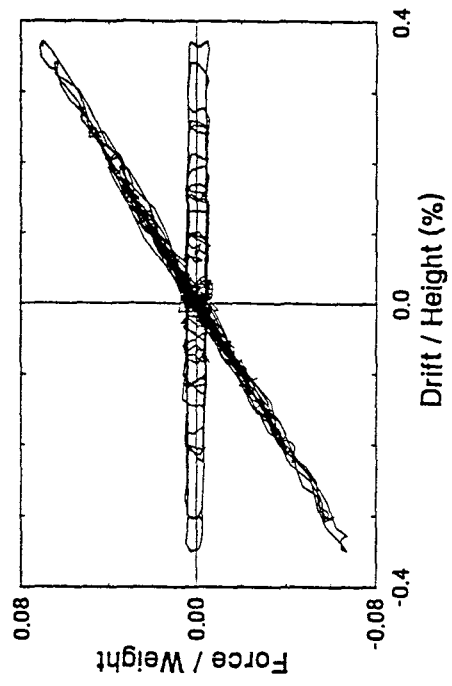
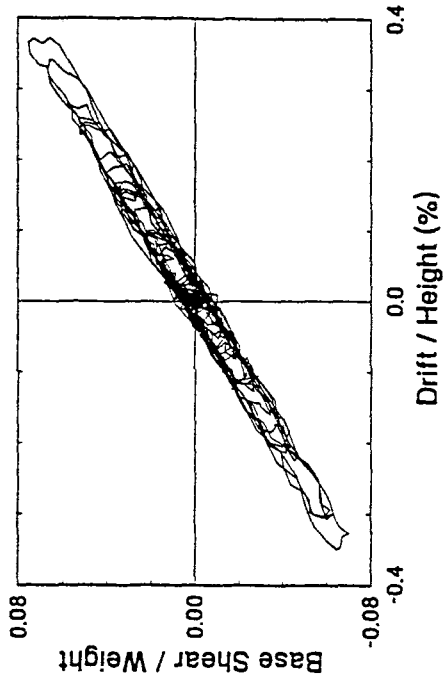
TEST 169

50% Hachinohe, Low Damping



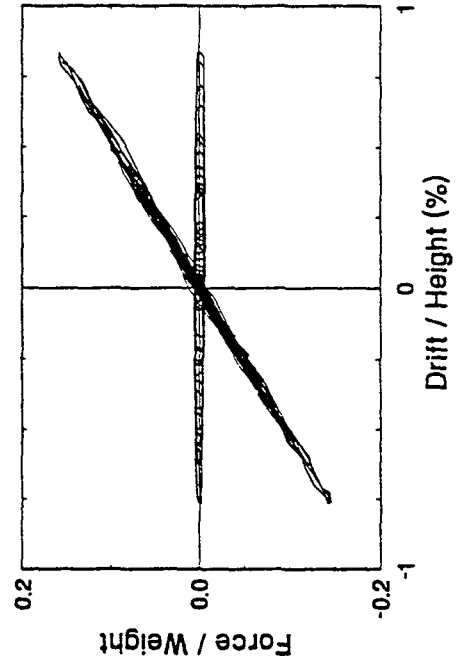
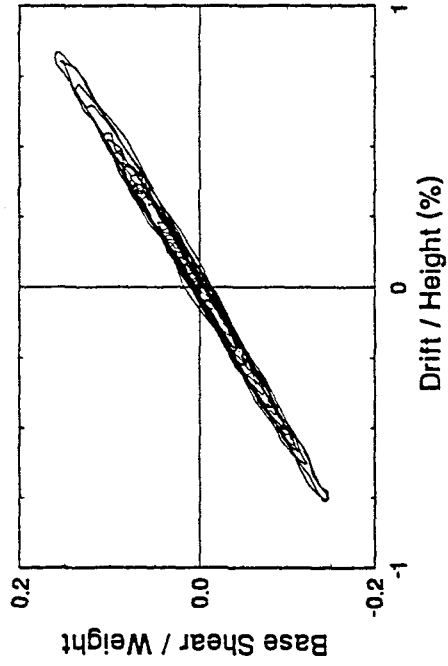
TEST 170

50% Hachinohe-M, Low Damping



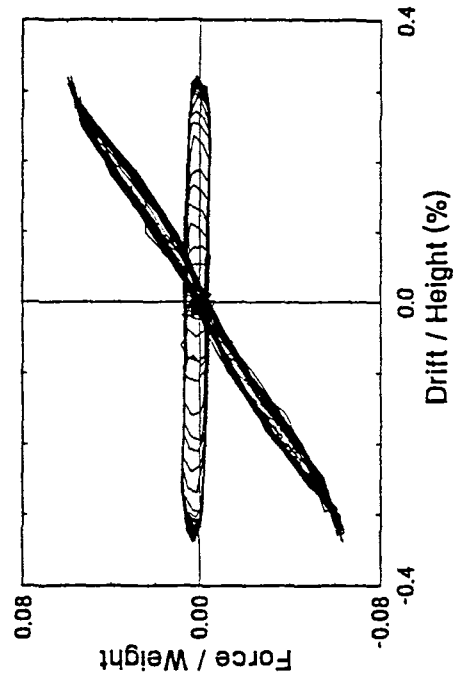
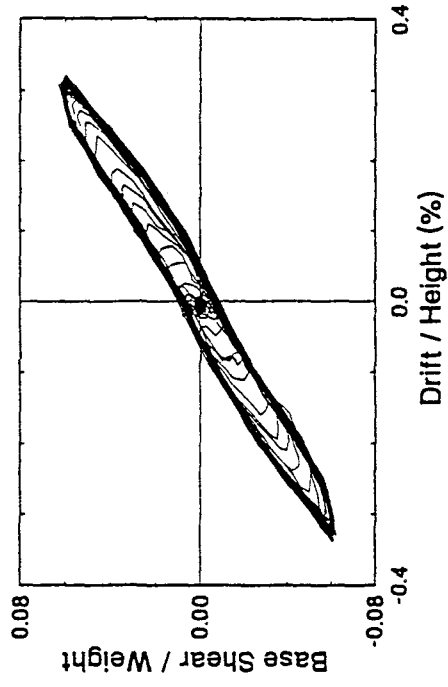
TEST 171

100% Hachinohe, Low Damping



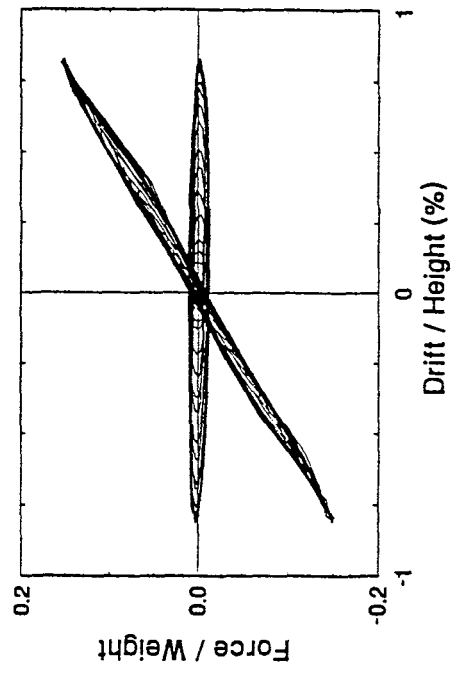
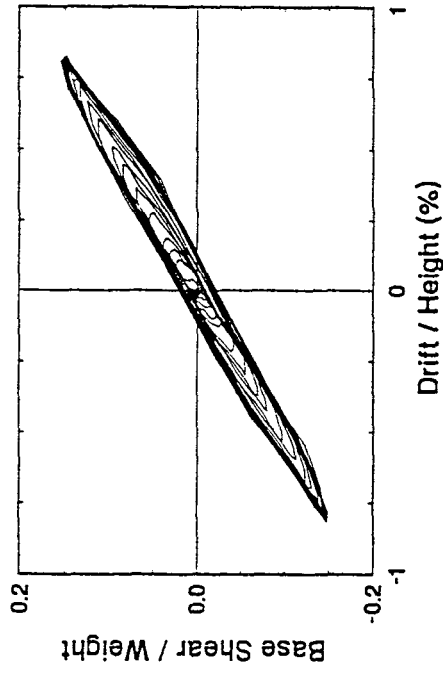
TEST 172

0.2g 5 Hz Harmonic, Low Damping



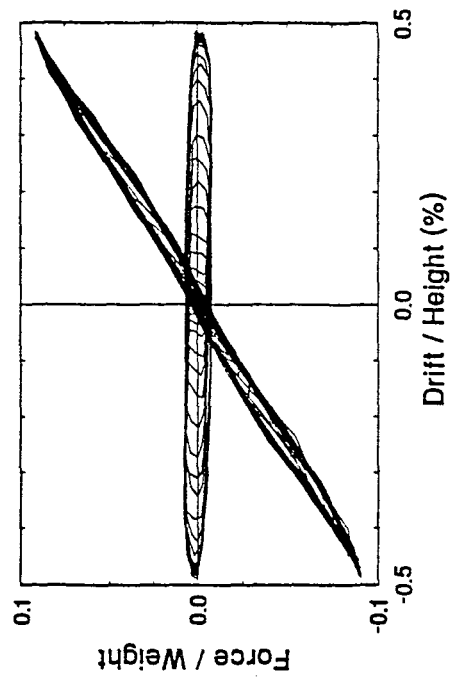
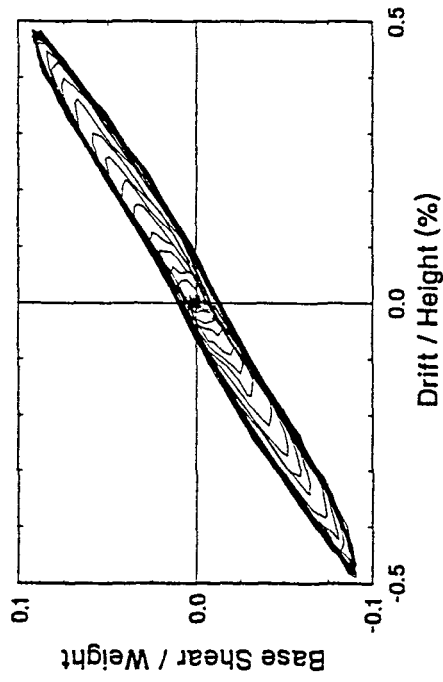
TEST 174

0.5g 5 Hz Harmonic, Low Damping



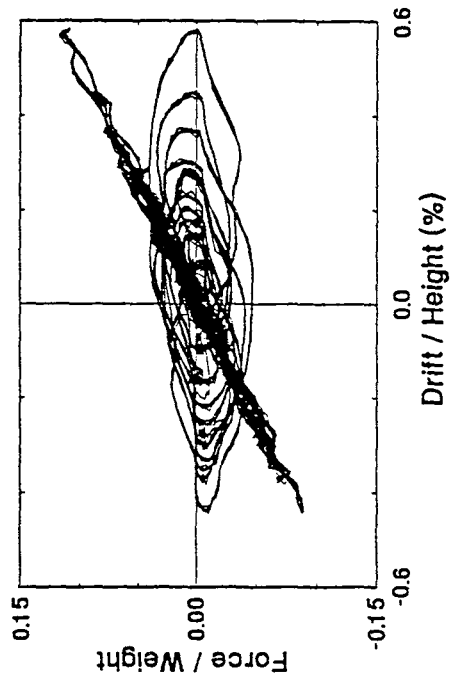
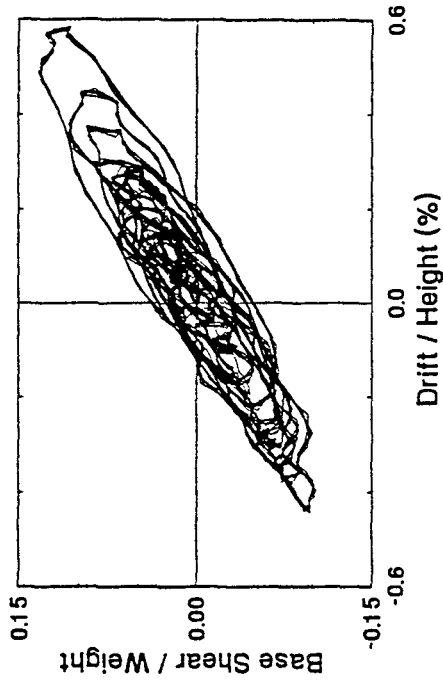
TEST 173

0.3g 5 Hz Harmonic, Low Damping



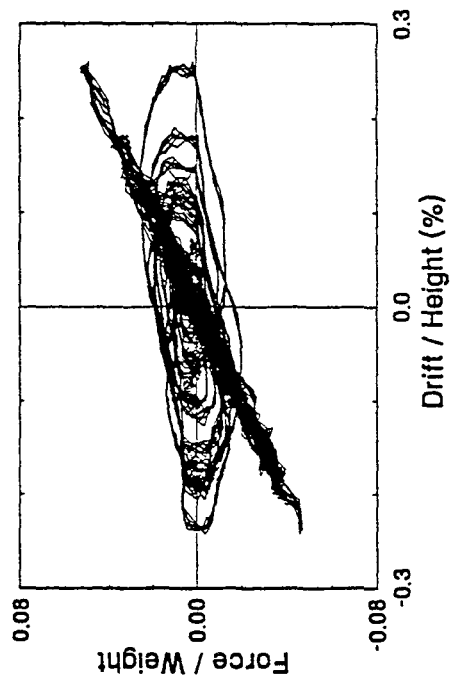
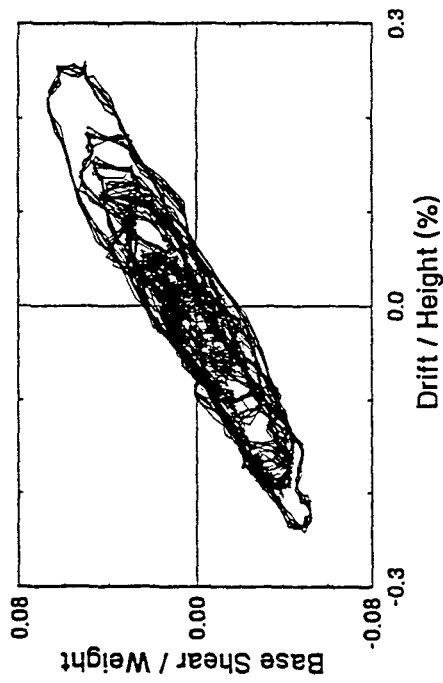
TEST 152

0.2g White Noise, High Damping



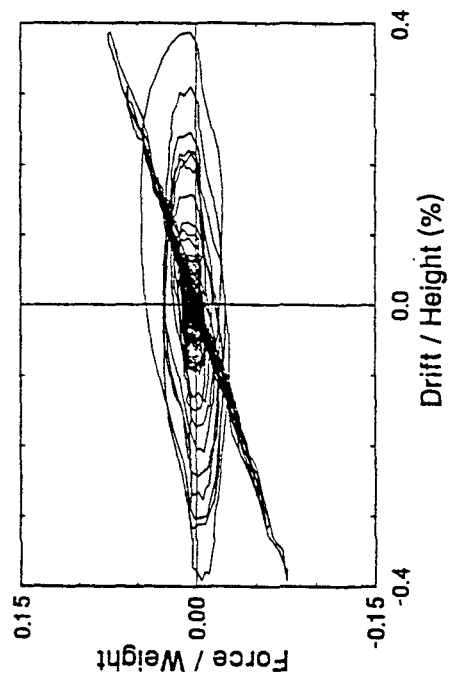
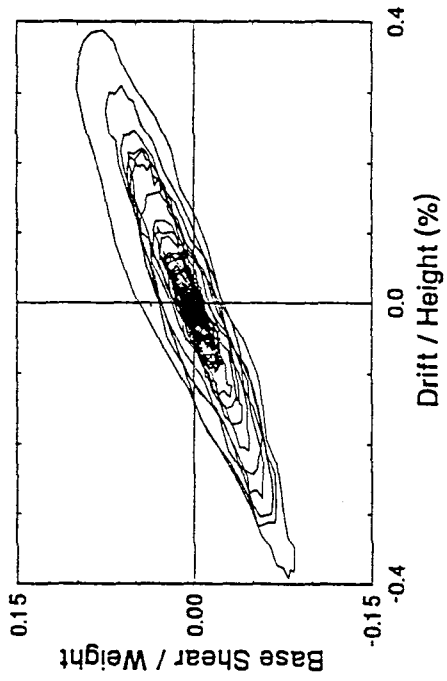
TEST 151

0.1g White Noise, High Damping



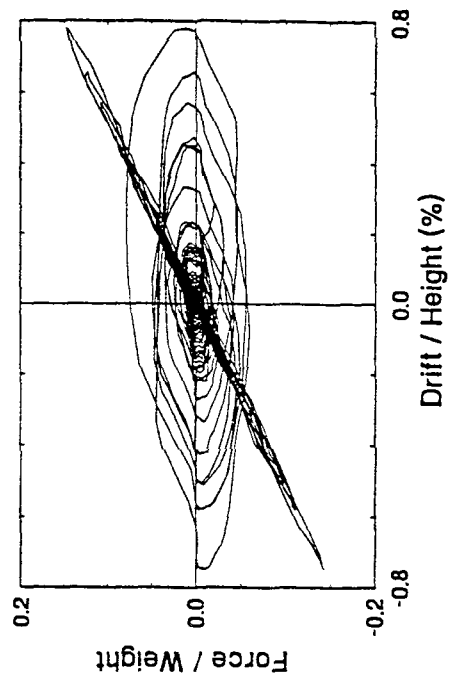
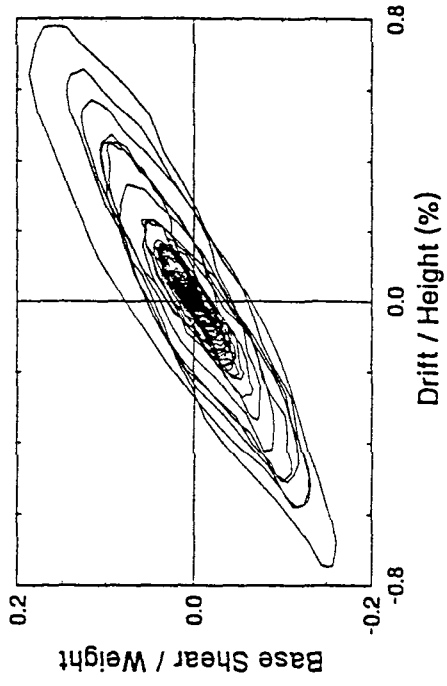
TEST 155

25% El Centro, High Damping



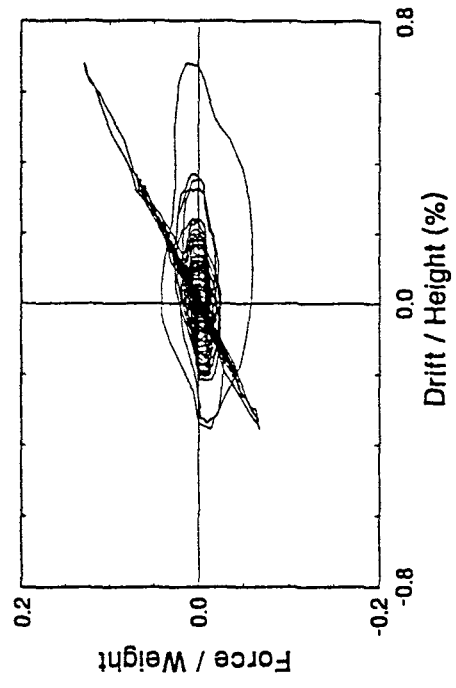
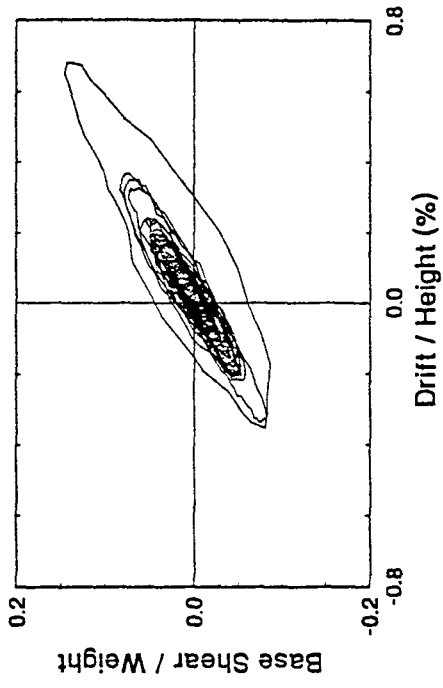
TEST 156

50% El Centro, High Damping



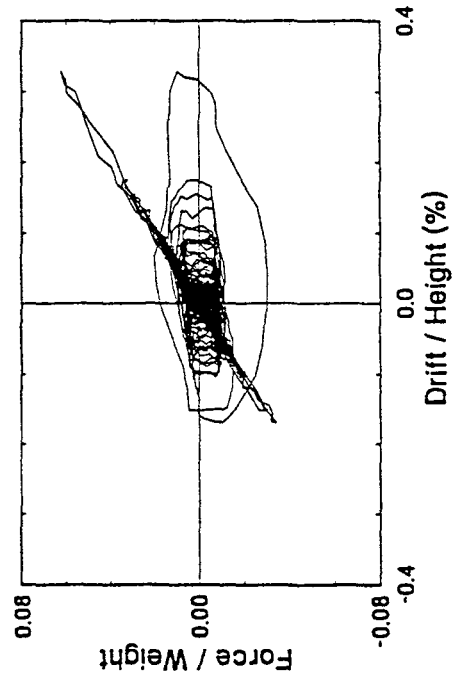
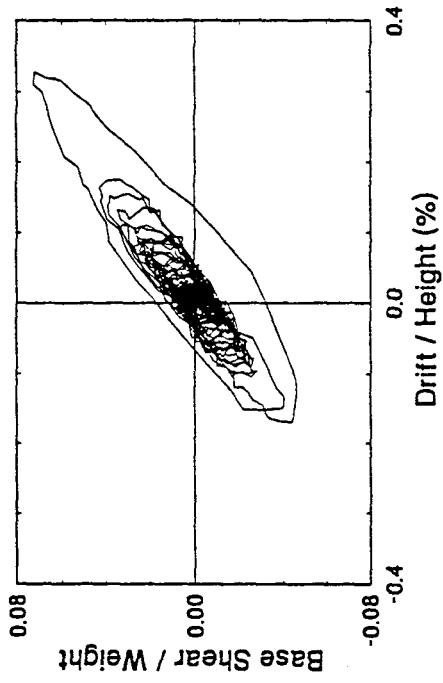
TEST 157

50% Hachinohe, High Damping



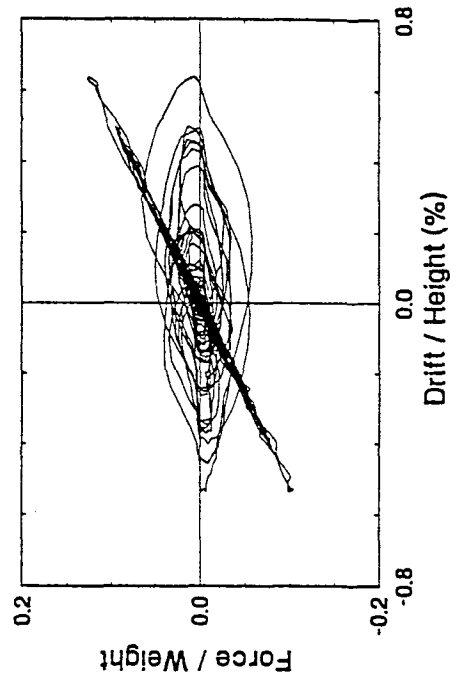
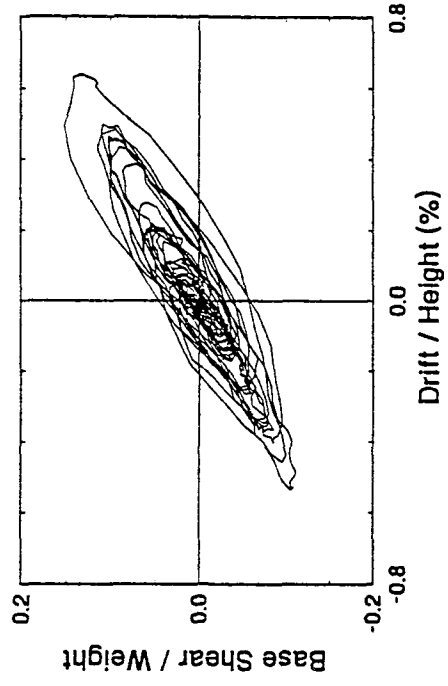
TEST 158

25% Hachinohe, High Damping



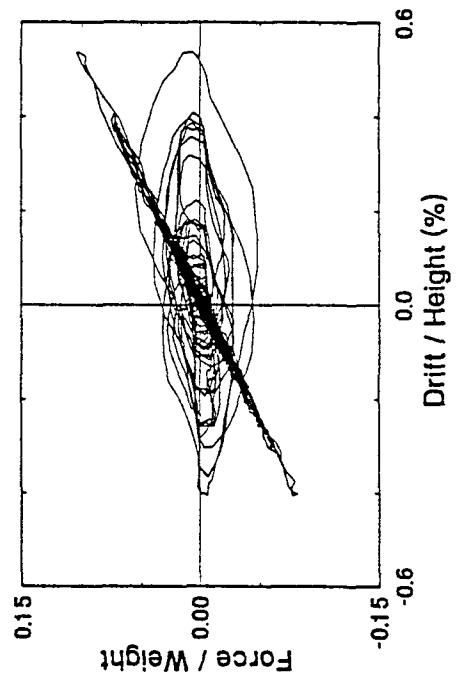
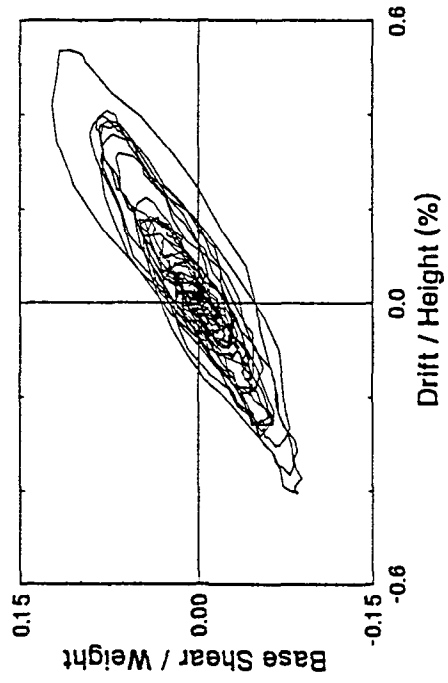
TEST 160

125% Hachinohe-M, High Damping



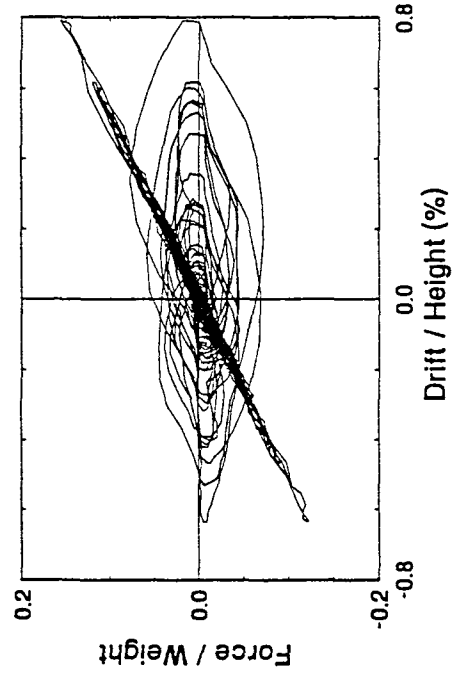
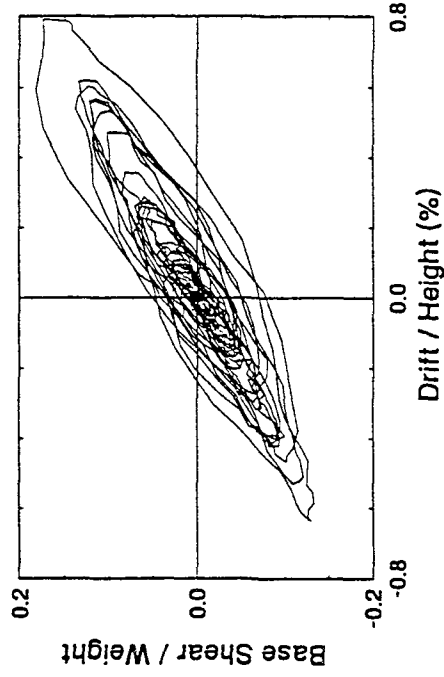
TEST 159

100% Hachinohe-M, High Damping



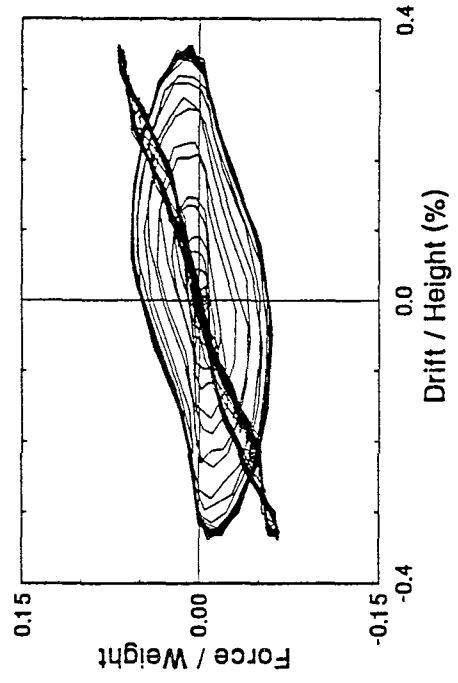
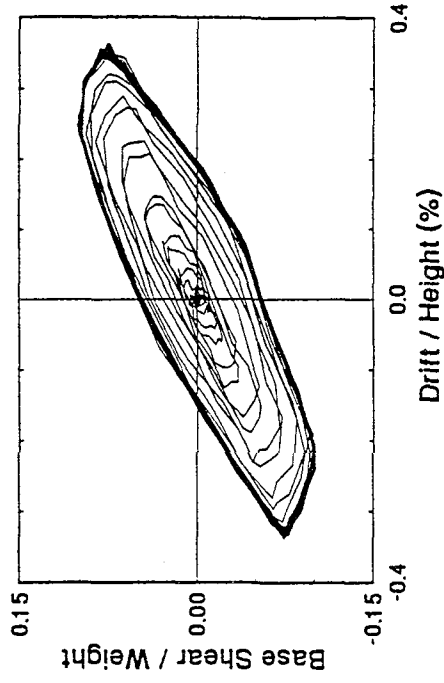
TEST 161

150% Hachinohe-M, High Damping



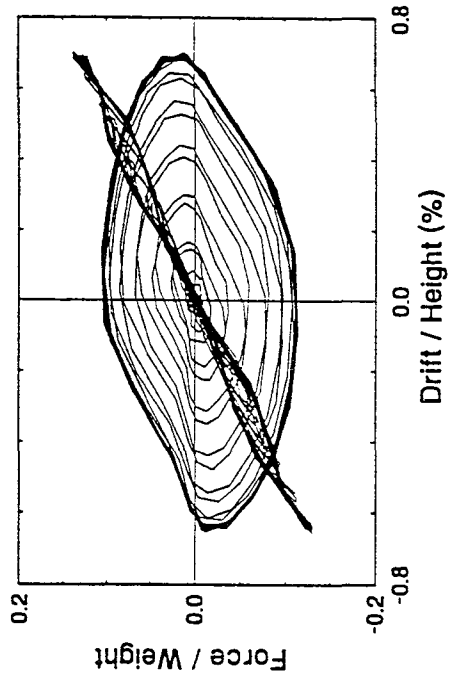
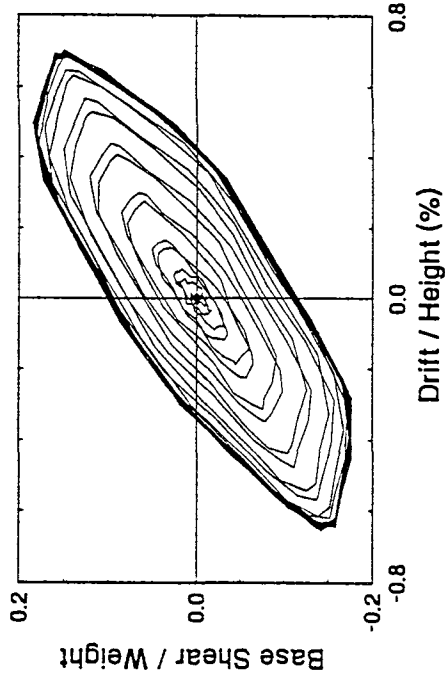
TEST 162

0.2g 5 Hz Harmonic, High Damping



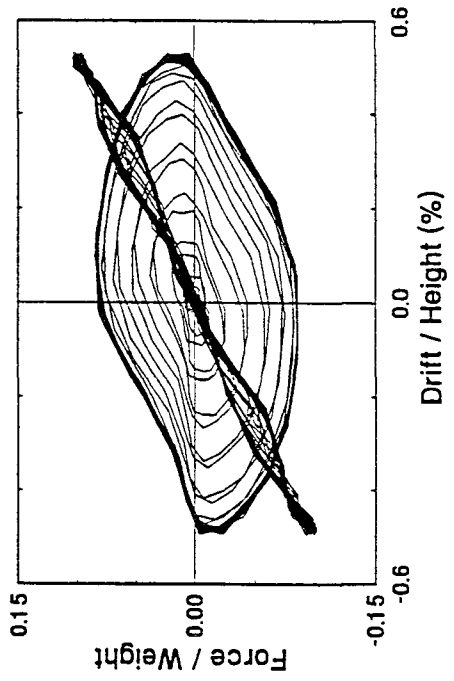
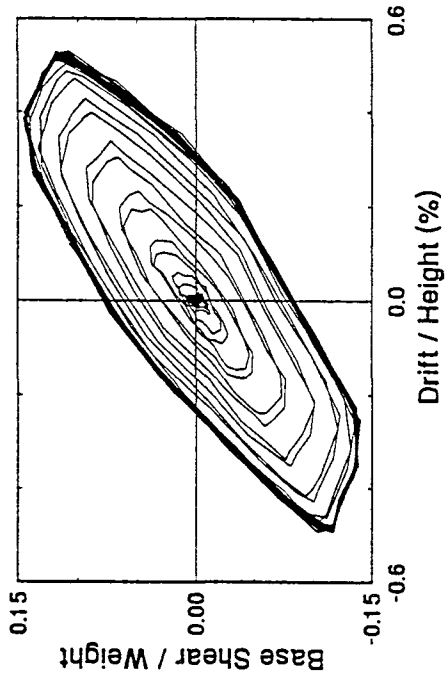
TEST 175

0.4g 5 Hz Harmonic, Low Damping



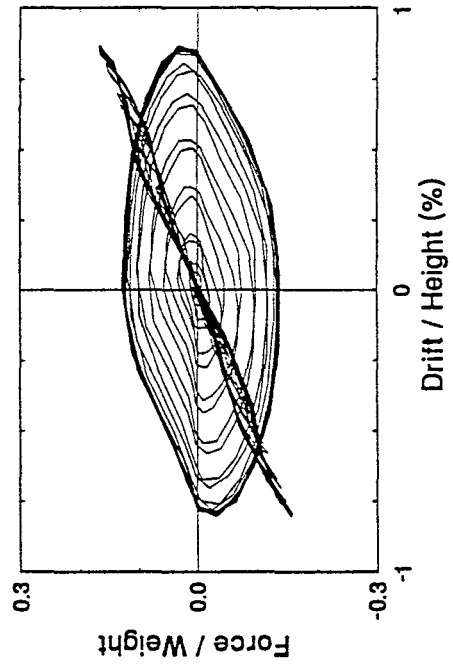
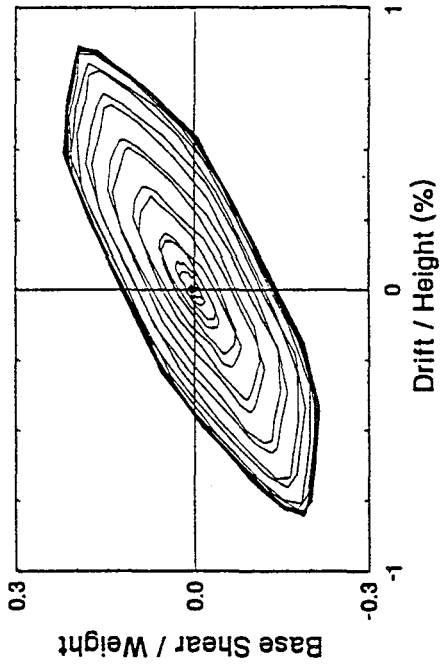
TEST 164

0.3g 5 Hz Harmonic, Low Damping



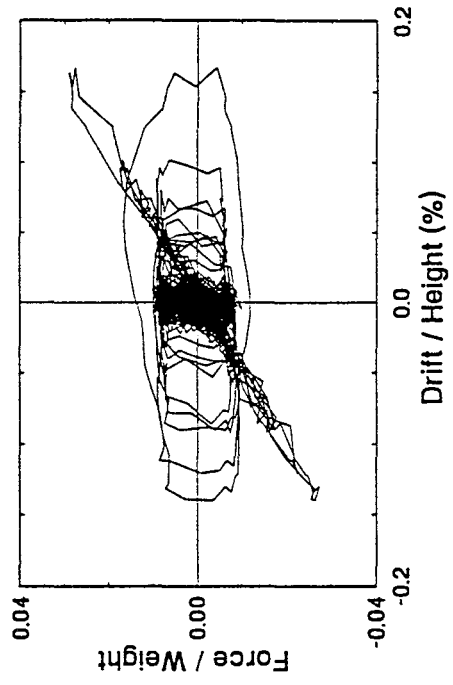
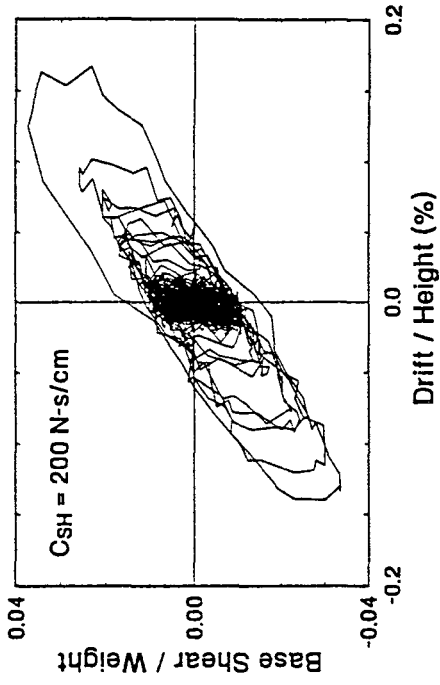
TEST 176

0.5g 5 Hz Harmonic, High Damping



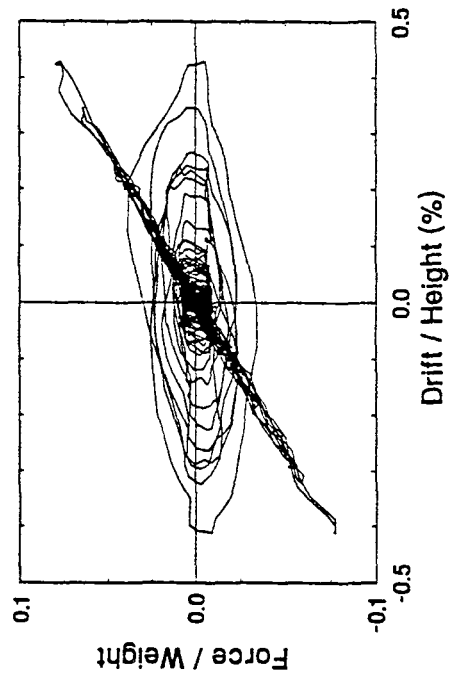
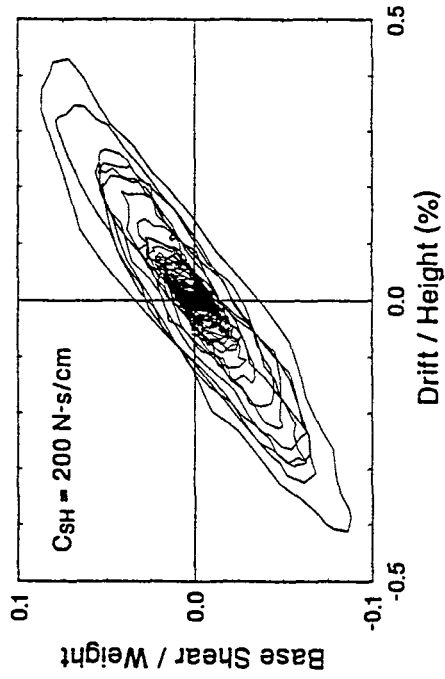
TEST 286

10% El Centro, Skyhook Damping



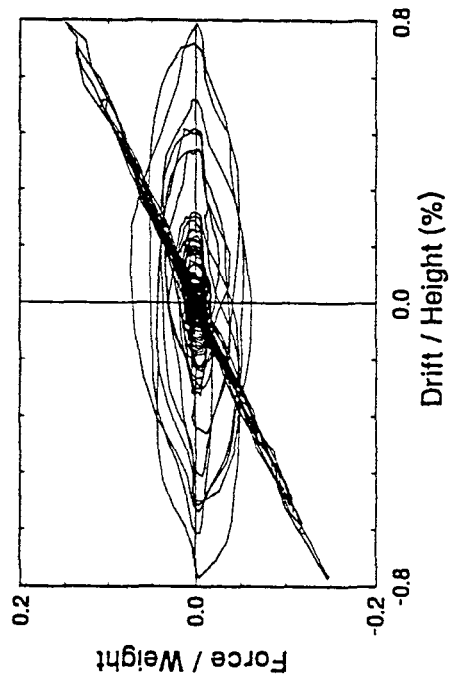
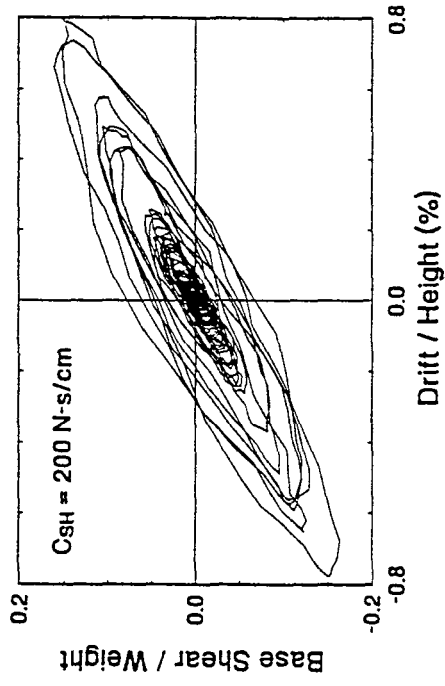
TEST 287

25% El Centro, Skyhook Damping



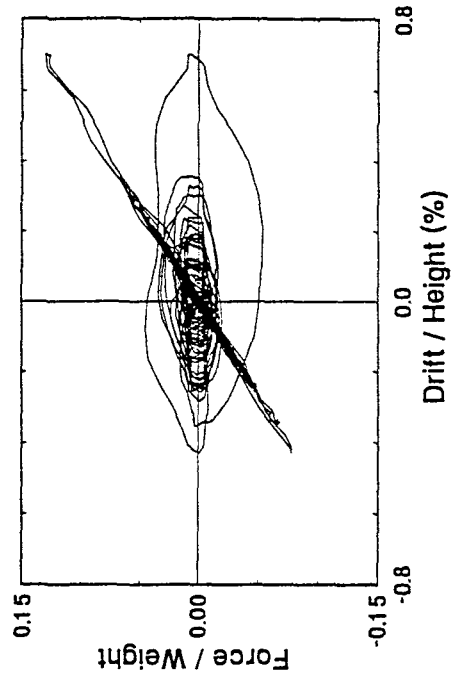
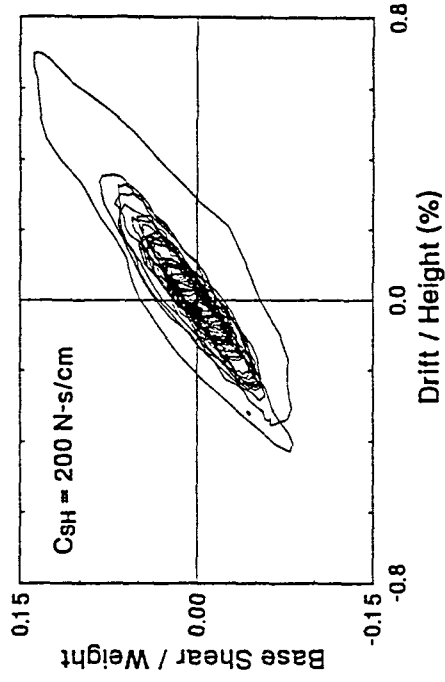
TEST 288

50% El Centro, Skyhook Damping



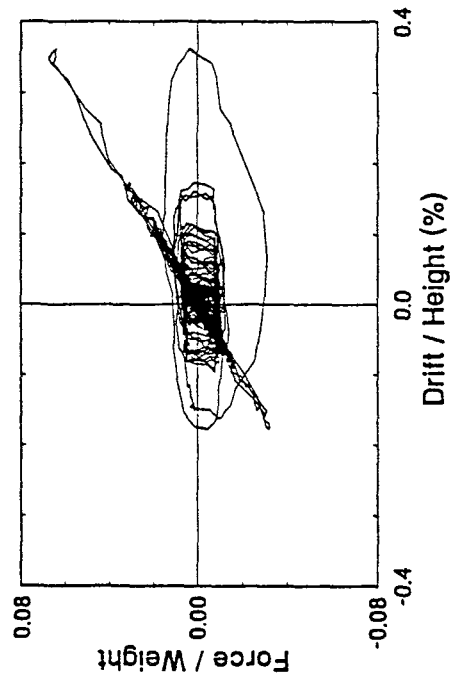
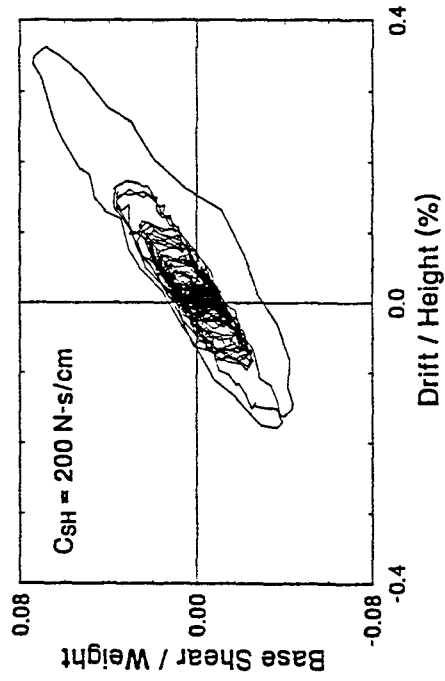
TEST 290

50% Hachinohe, Skyhook Damping



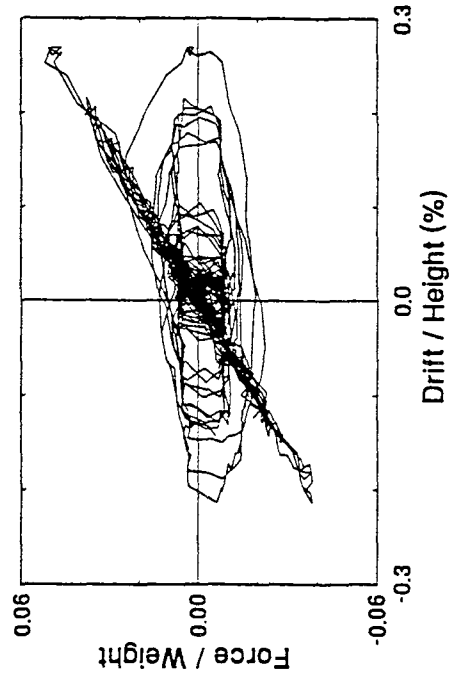
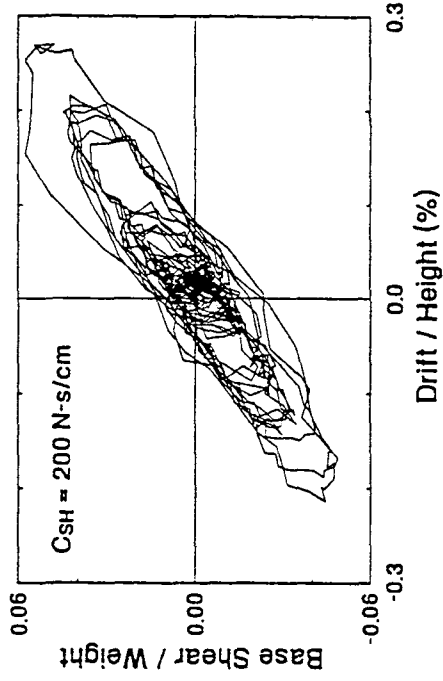
TEST 289

25% Hachinohe, Skyhook Damping



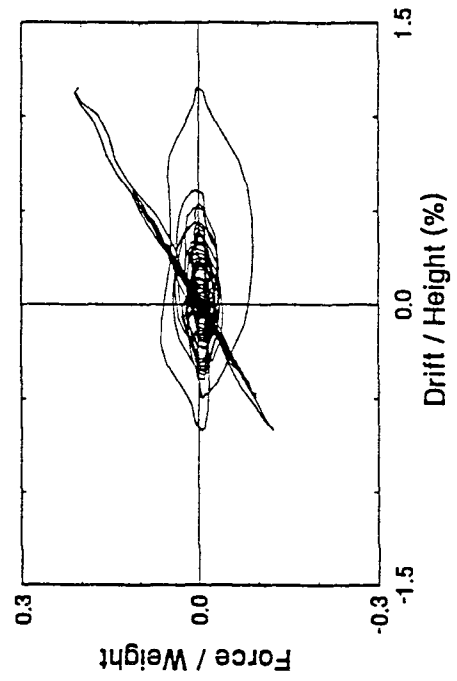
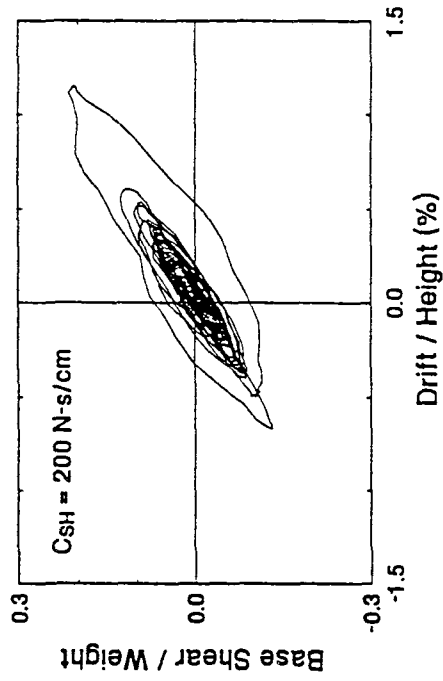
TEST 292

50% Hachinohe-M, Skyhook Damping



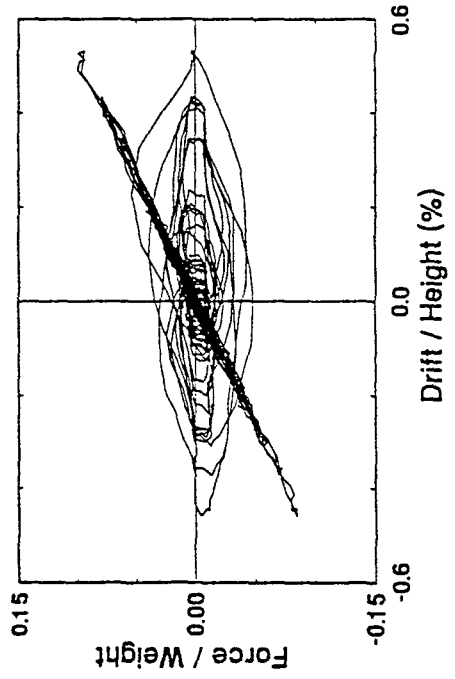
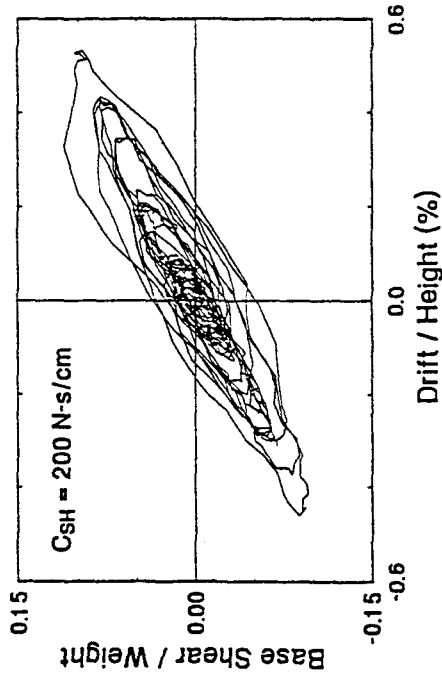
TEST 291

75% Hachinohe, Skyhook Damping



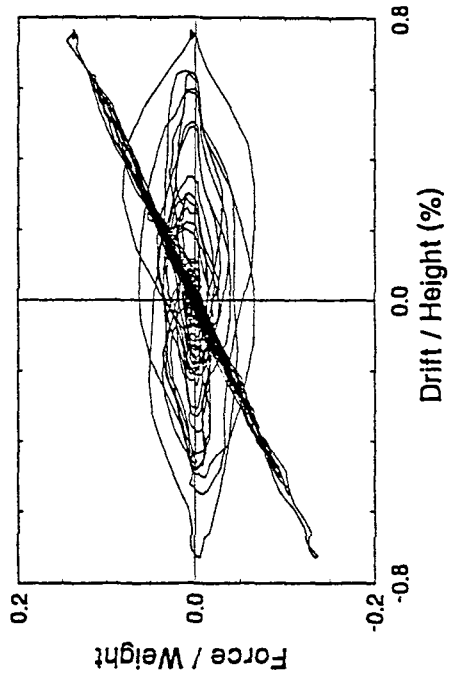
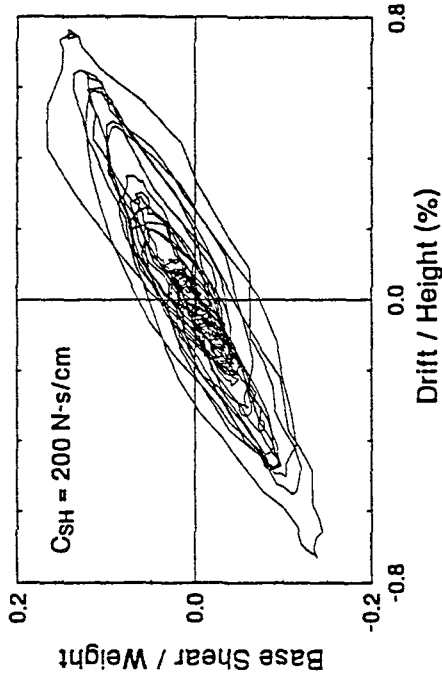
TEST 293

100% Hachinohe-M, Skyhook Damping



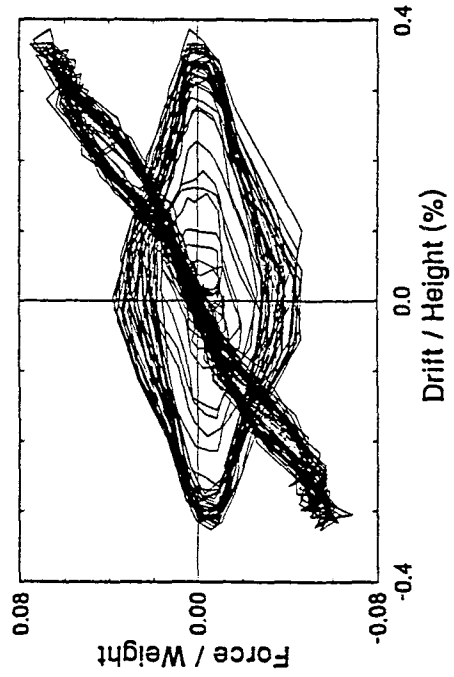
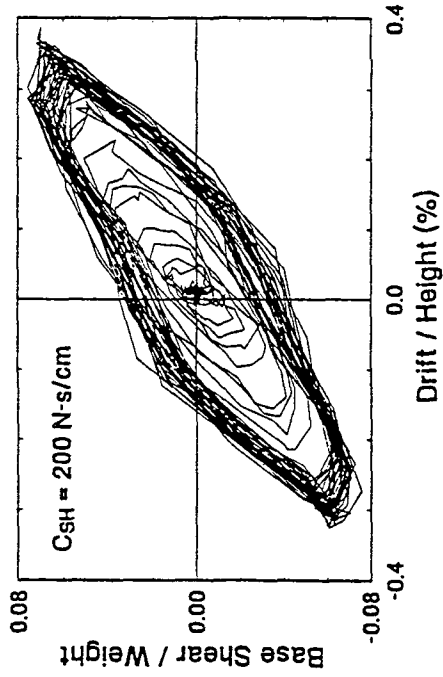
TEST 294

150% Hachinohe-M, Skyhook Damping



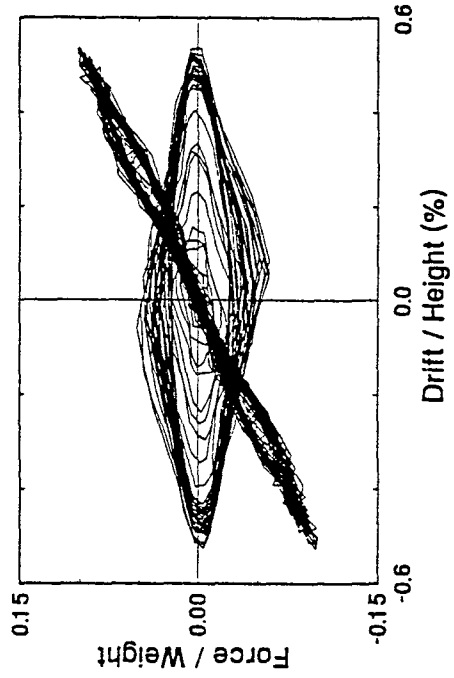
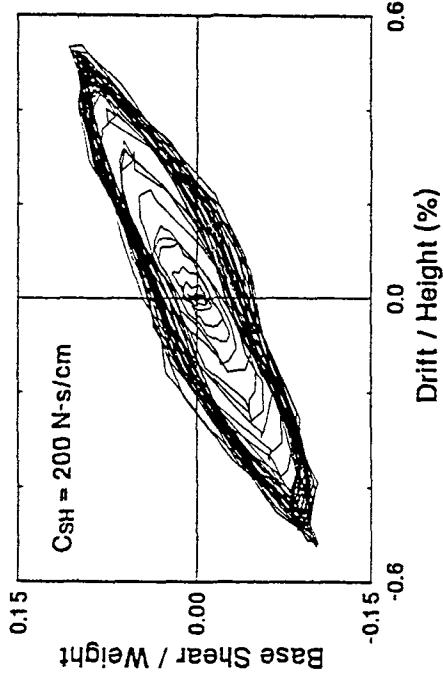
TEST 295

0.2g 5 Hz Harmonic, Skyhook Damping



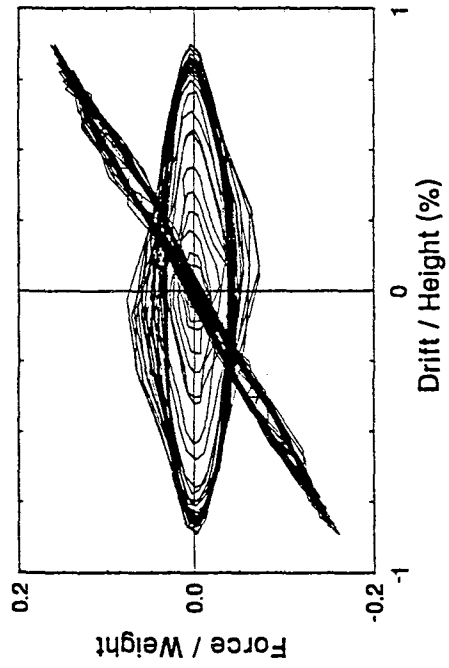
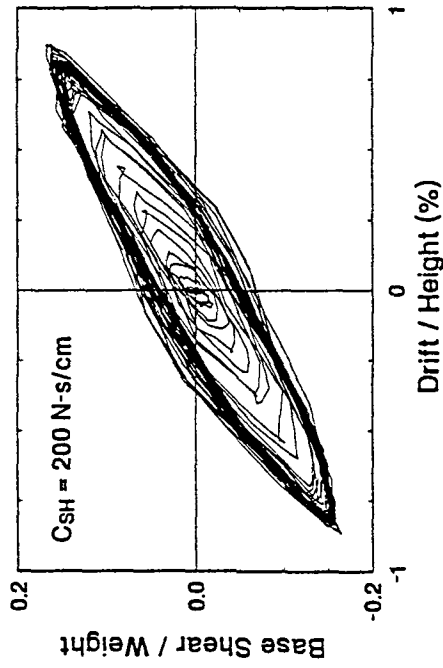
TEST 296

0.3g 5 Hz Harmonic, Skyhook Damping



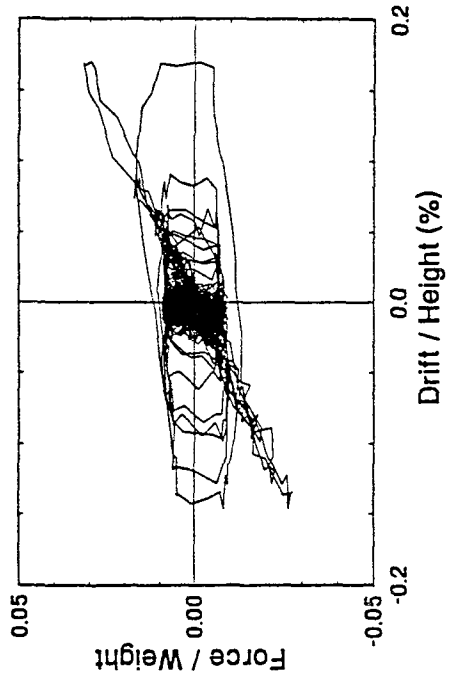
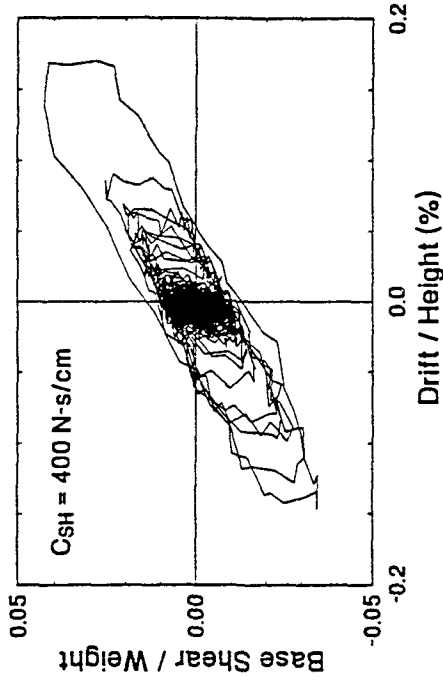
TEST 297

0.5g 5 Hz Harmonic, Skyhook Damping



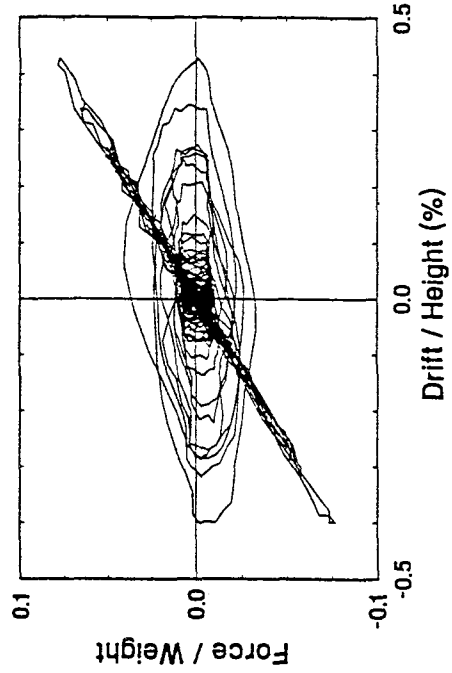
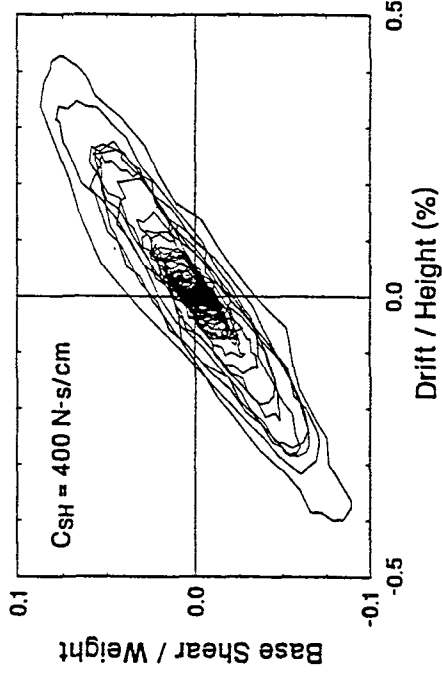
TEST 298

10% El Centro, Skyhook Damping



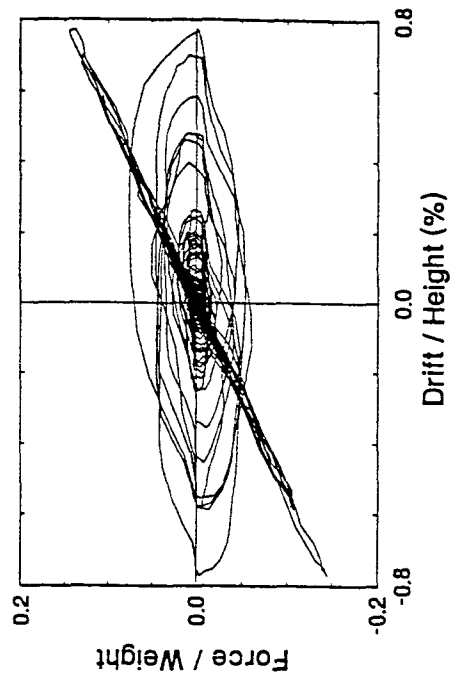
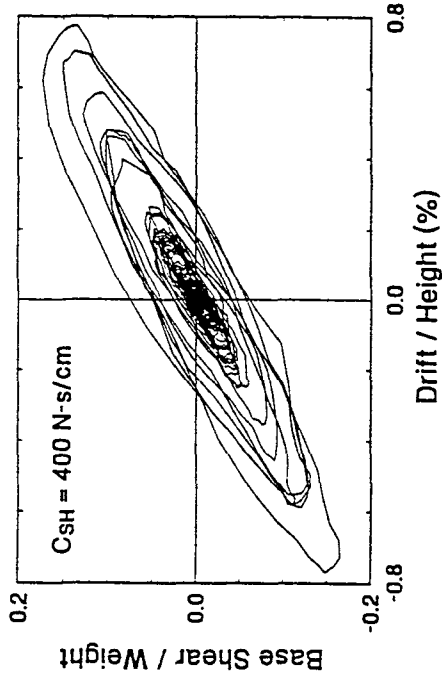
TEST 299

25% El Centro, Skyhook Damping



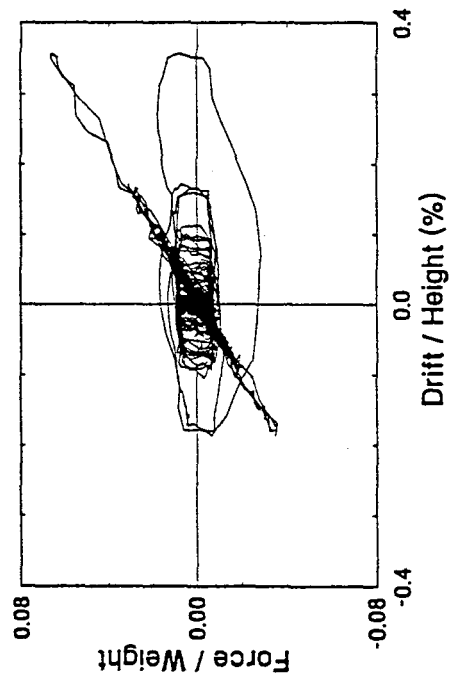
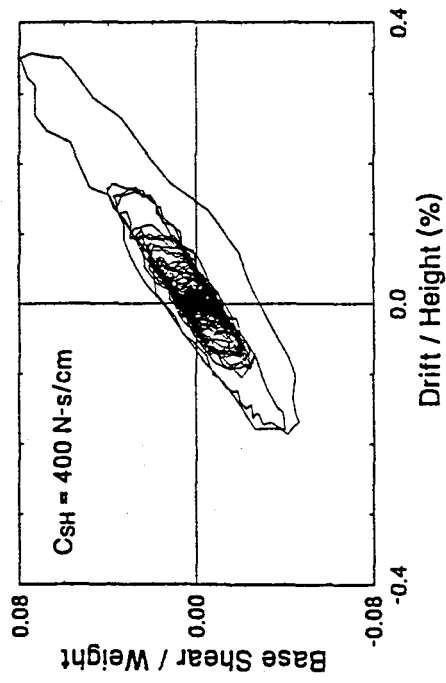
TEST 300

50% El Centro, Skyhook Damping



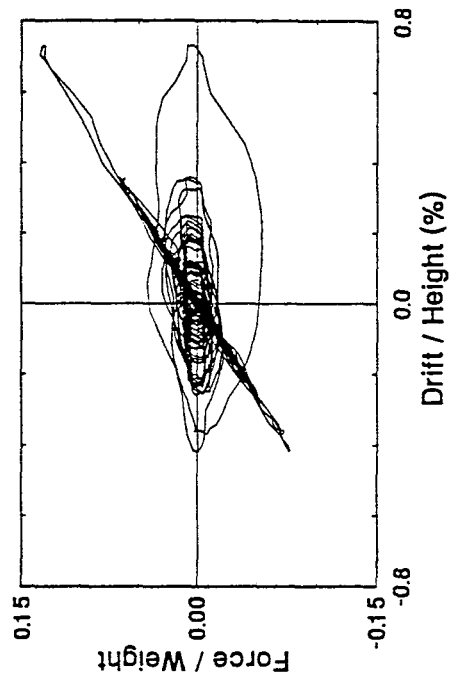
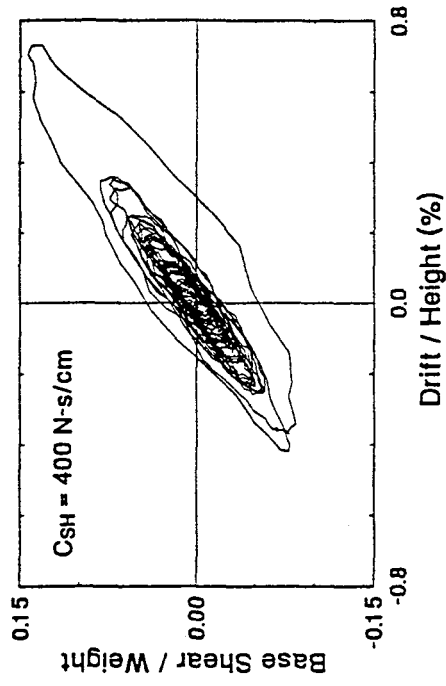
TEST 301

25% Hachinohe, Skyhook Damping



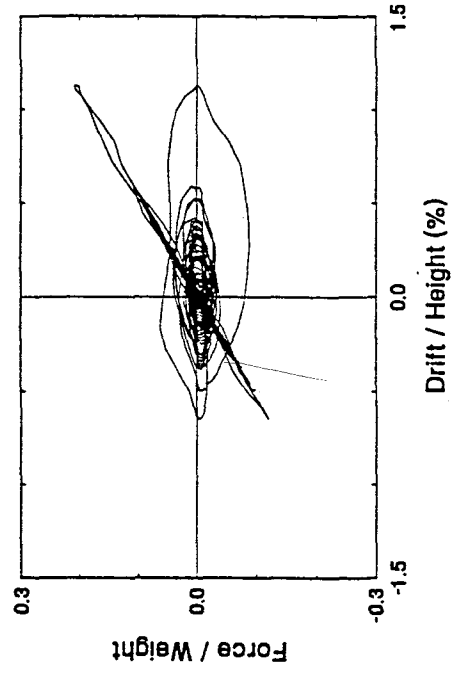
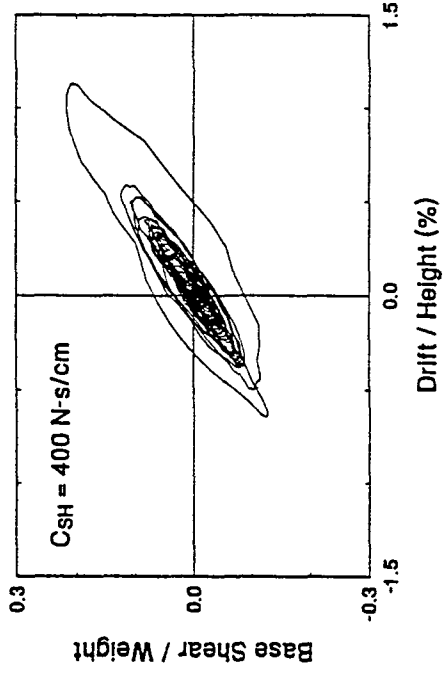
TEST 302

50% Hachinohe, Skyhook Damping



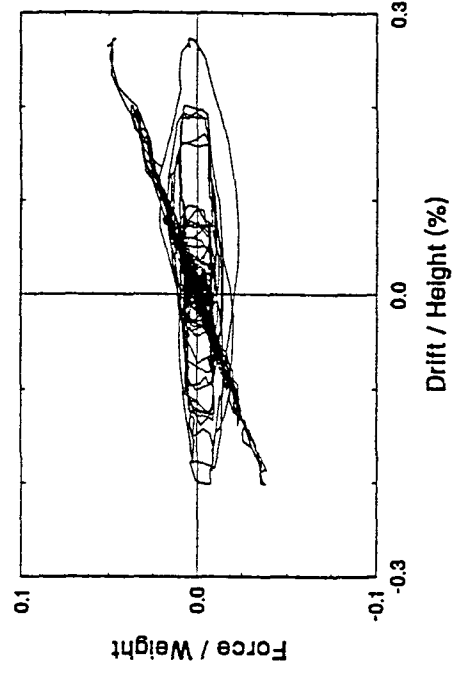
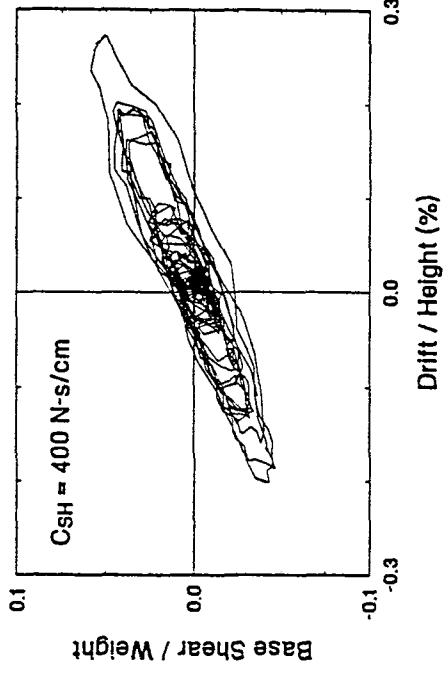
TEST 303

75% Hachinohe, Skyhook Damping



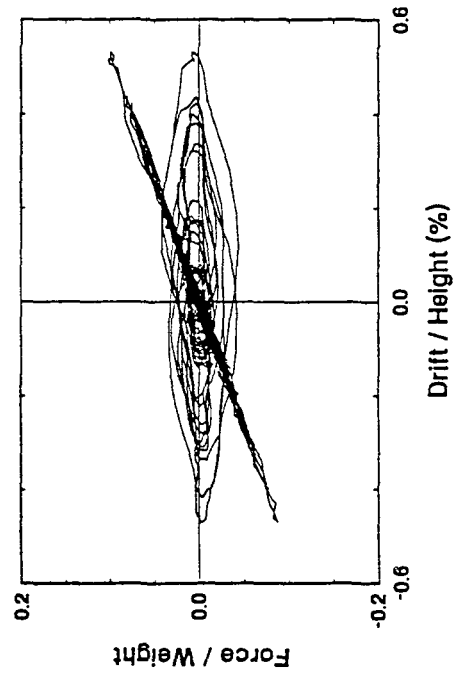
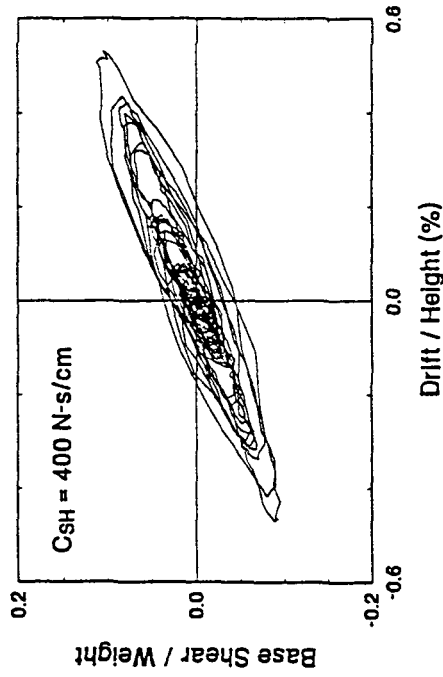
TEST 304

50% Hachinohe-M, Skyhook Damping



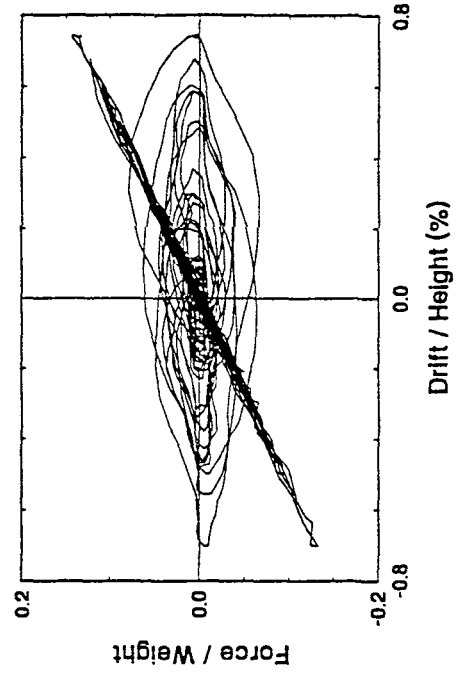
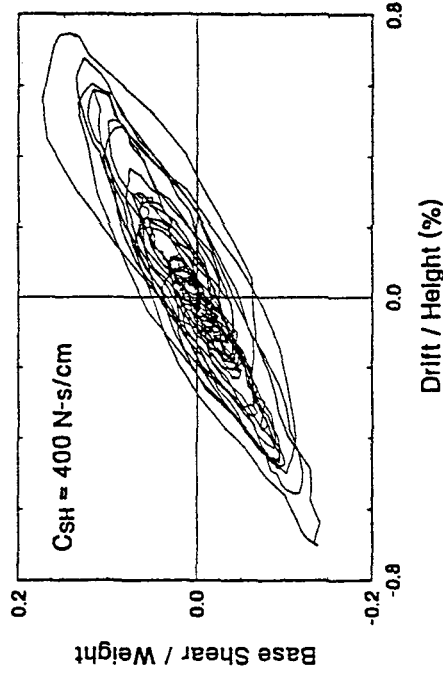
TEST 305

100% Hachinohe-M, Skyhook Damping



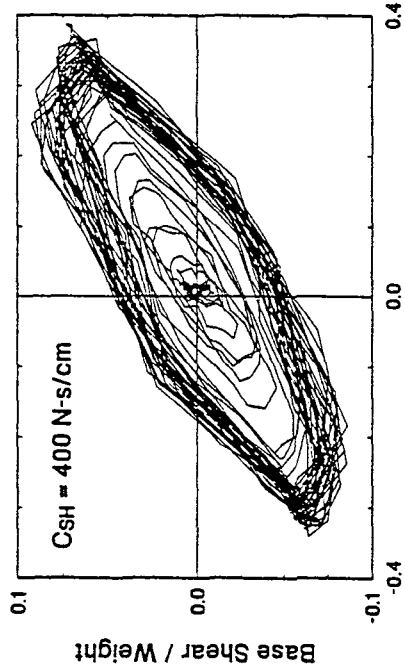
TEST 306

150% Hachinohe-M, Skyhook Damping



TEST 307

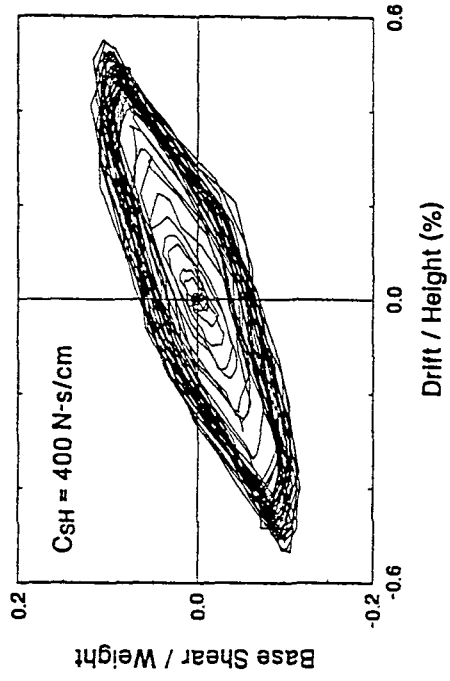
0.2g 5 Hz Harmonic, Skyhook Damping



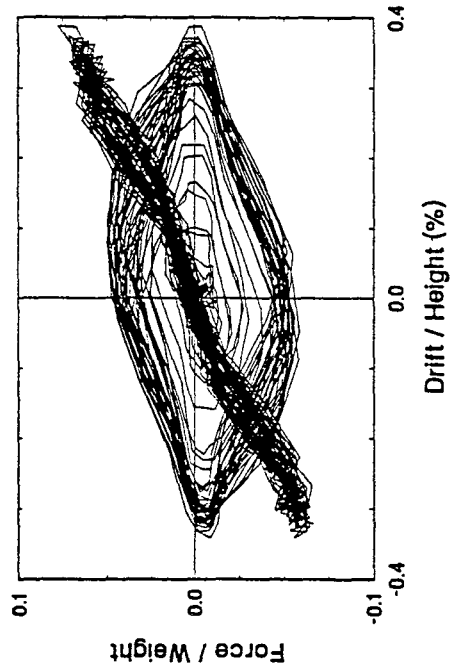
Drift / Height (%)

TEST 308

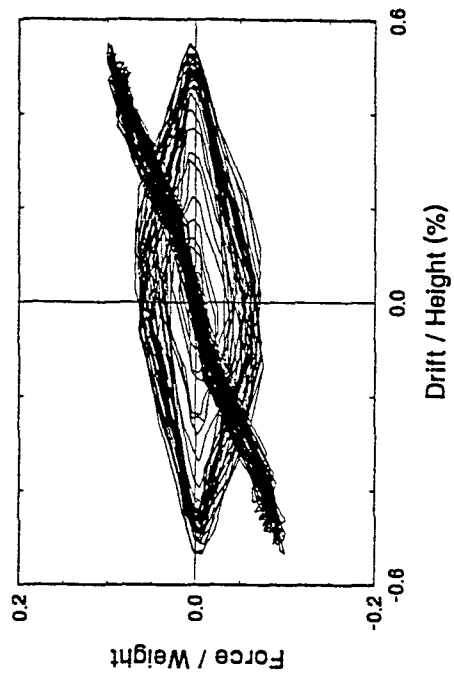
0.3g 5 Hz Harmonic, Skyhook Damping



Drift / Height (%)



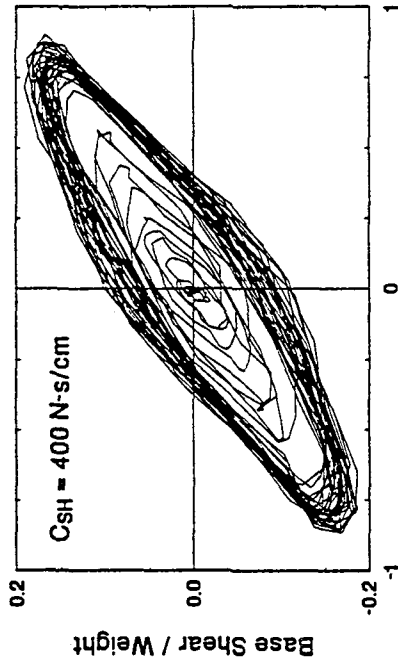
Drift / Height (%)



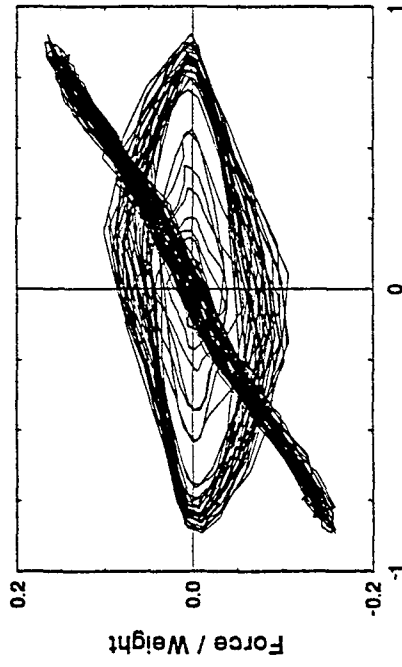
Drift / Height (%)

TEST 309

0.5g 5 Hz Harmonic, Skyhook Damping



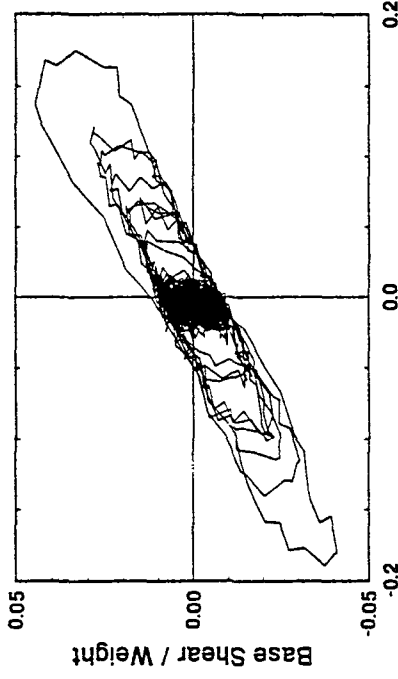
Drift / Height (%)



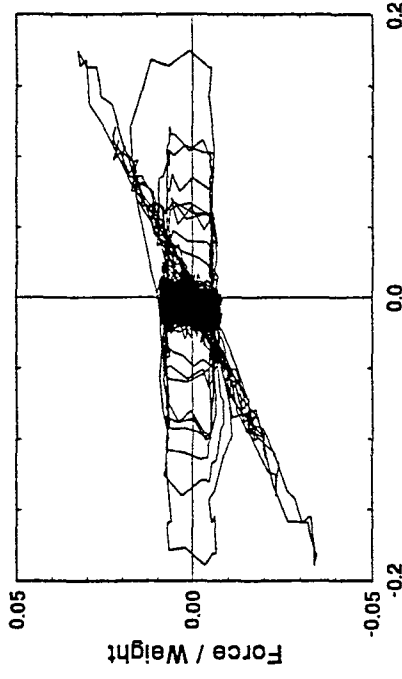
Drift / Height (%)

TEST 310

10% El Centro, Feedforward Control



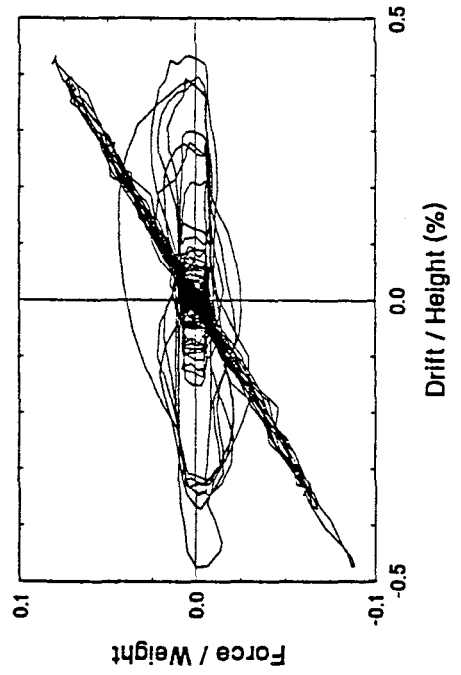
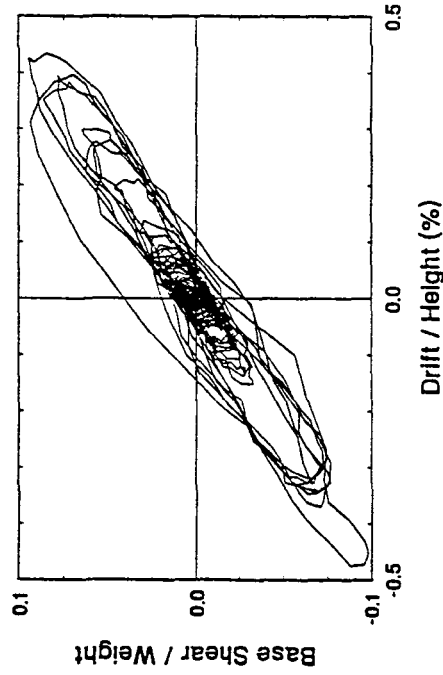
Drift / Height (%)



Drift / Height (%)

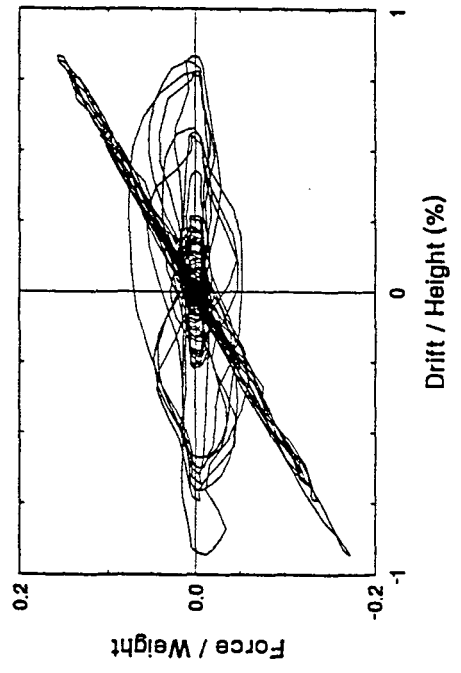
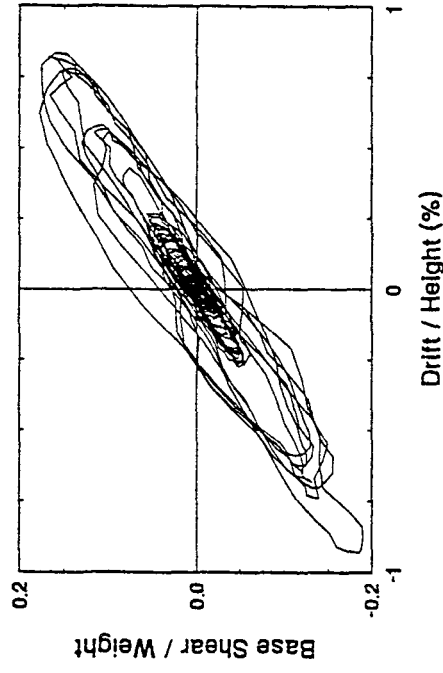
TEST 311

25% El Centro, Feedforward Control



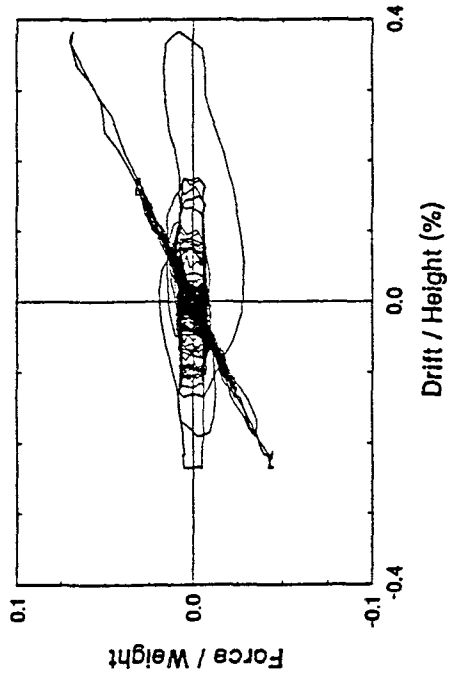
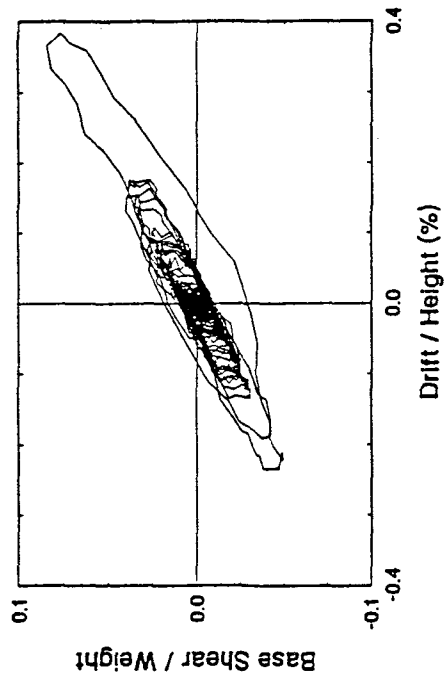
TEST 312

50% El Centro, Feedforward Control



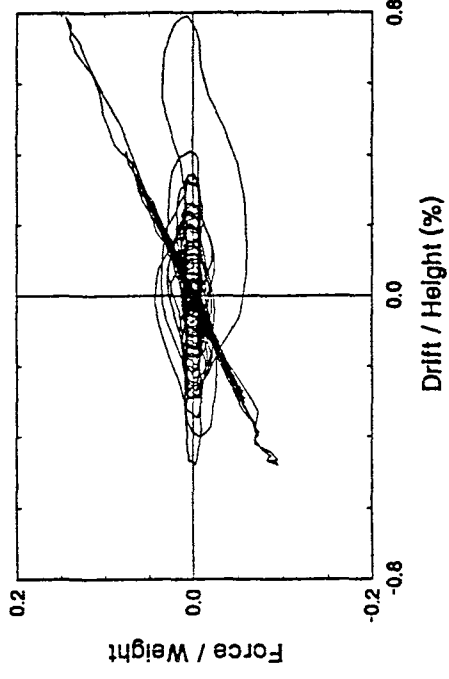
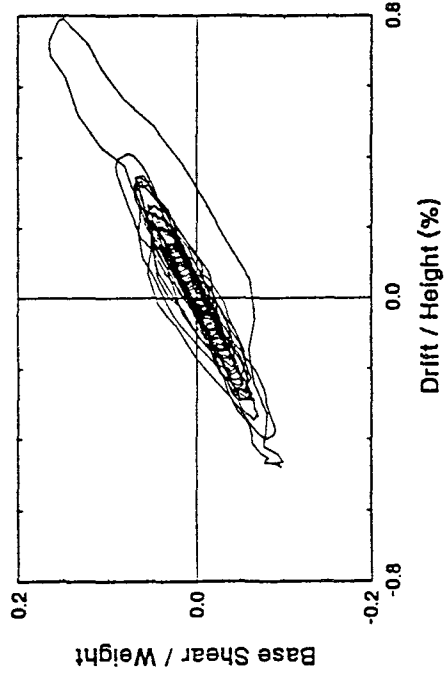
TEST 313

25% Hachinohe, Feedforward Control



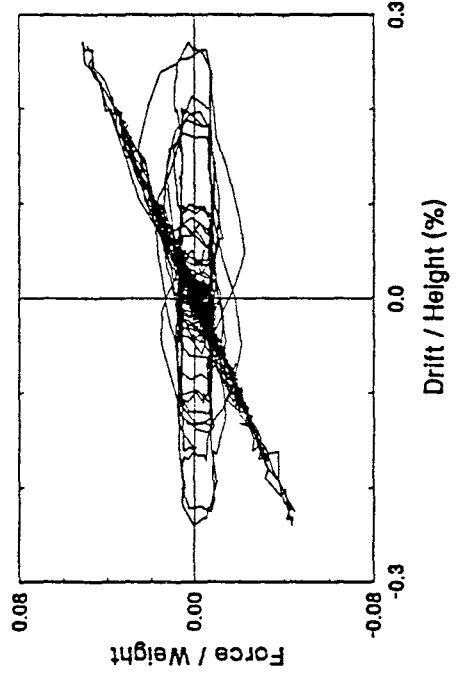
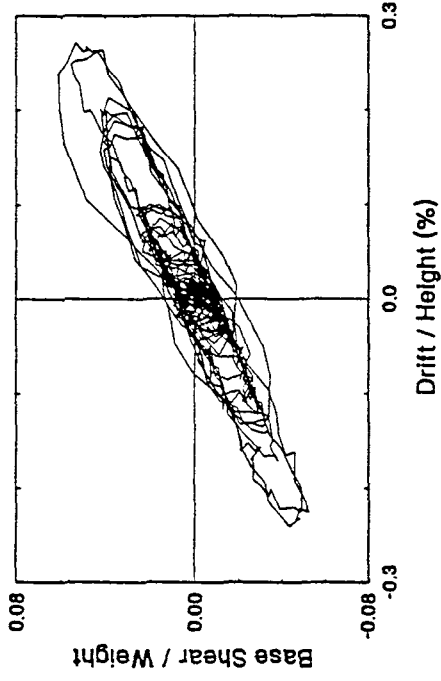
TEST 314

50% Hachinohe, Feedforward Control



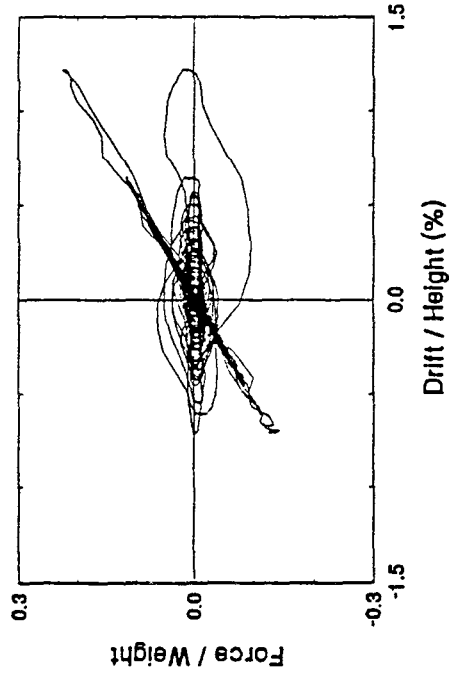
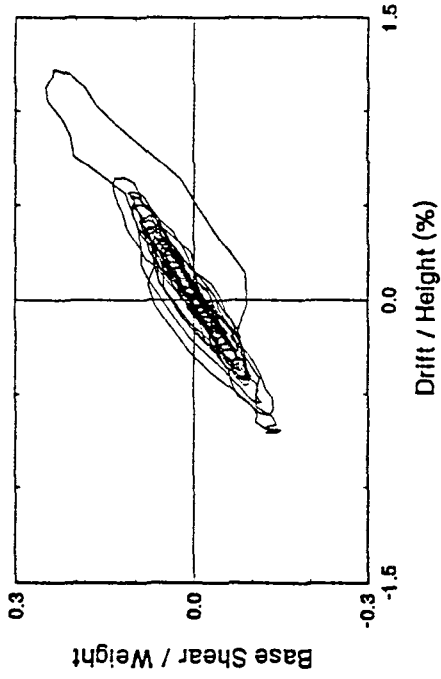
TEST 316

50% Hachinohe-M, Feedforward Control



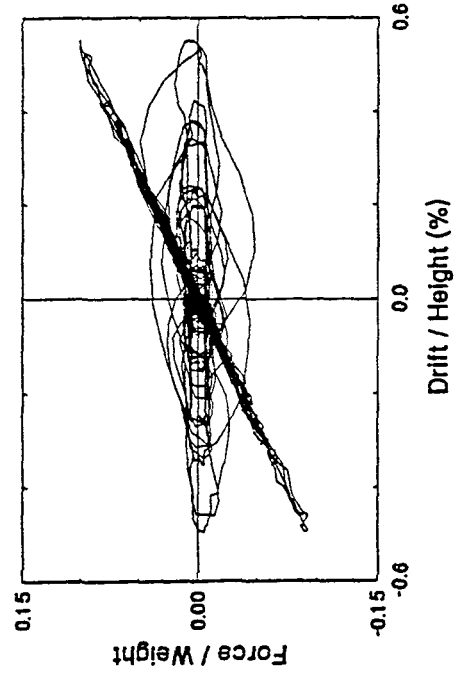
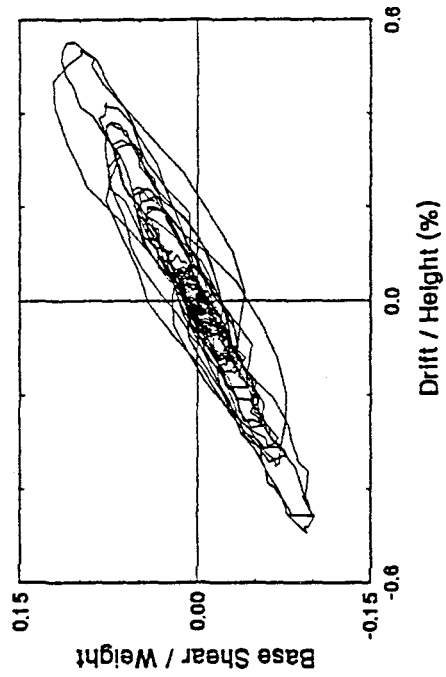
TEST 315

75% Hachinohe, Feedforward Control



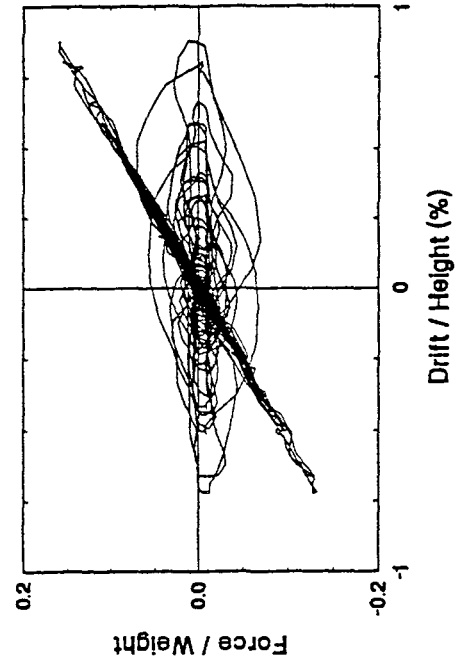
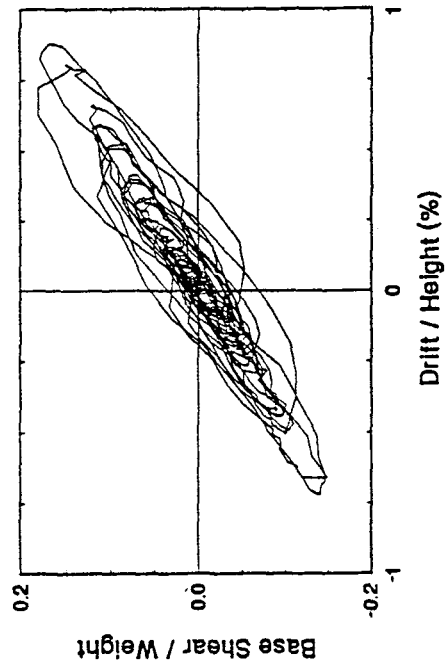
TEST 317

100% Hachinohe-M, Feedforward Control



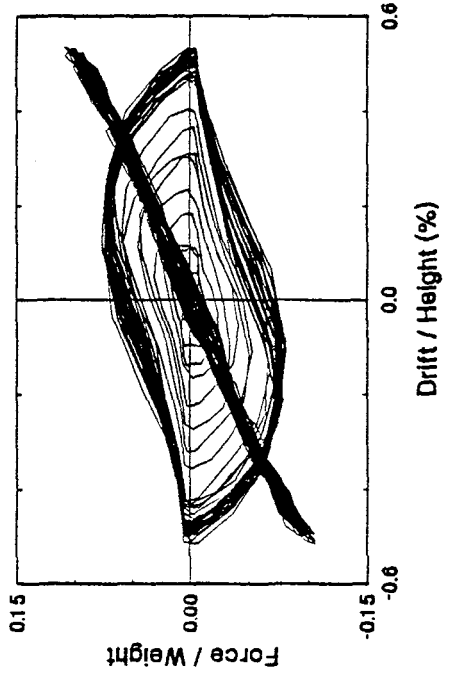
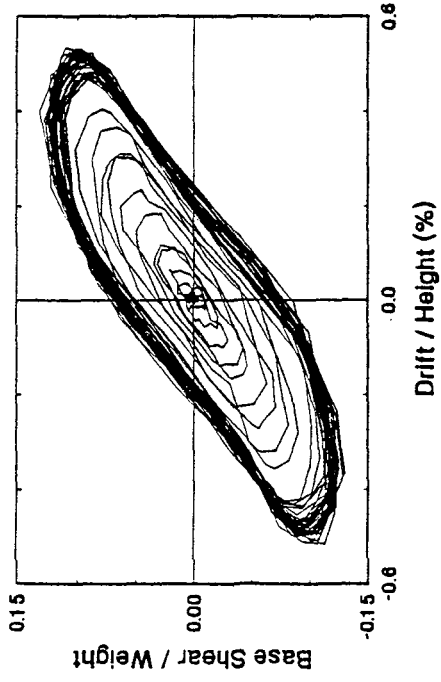
TEST 318

125% Hachinohe-M, Feedforward Control



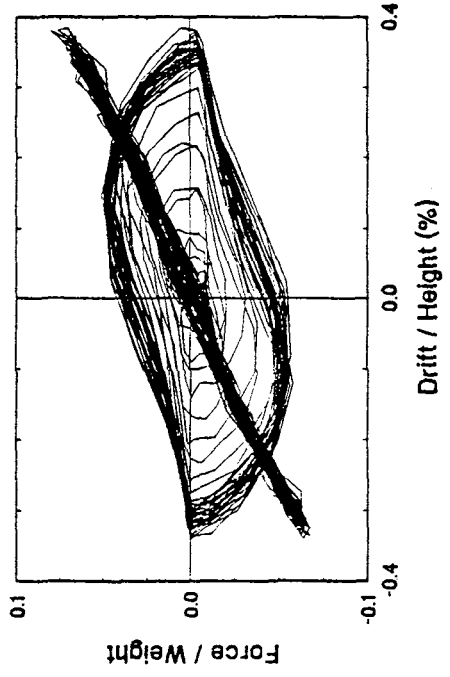
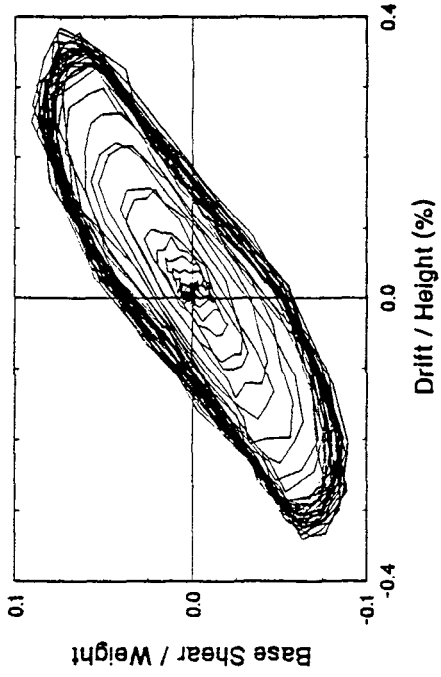
TEST 320

0.3g 5 Hz Harmonic, Feedforward Control



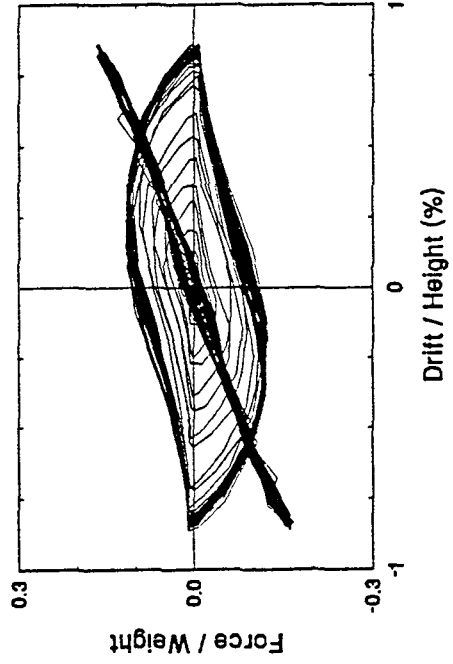
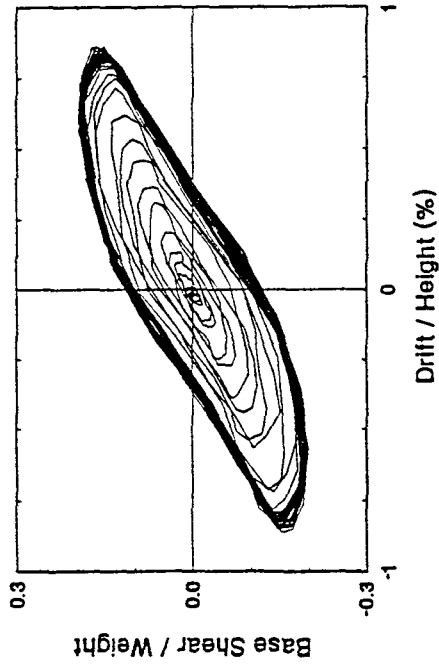
TEST 319

0.2g 5 Hz Harmonic, Feedforward Control



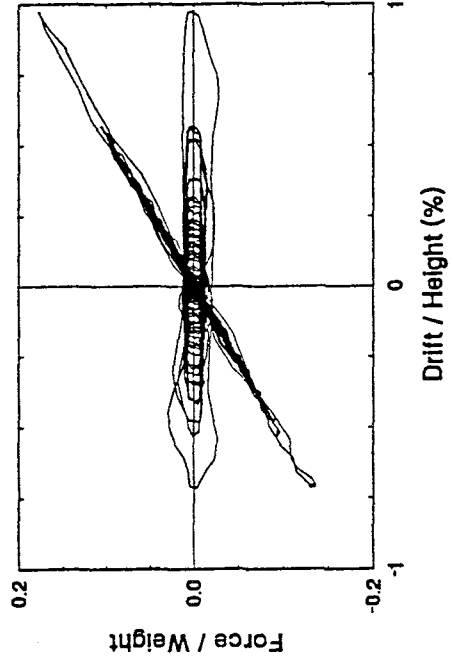
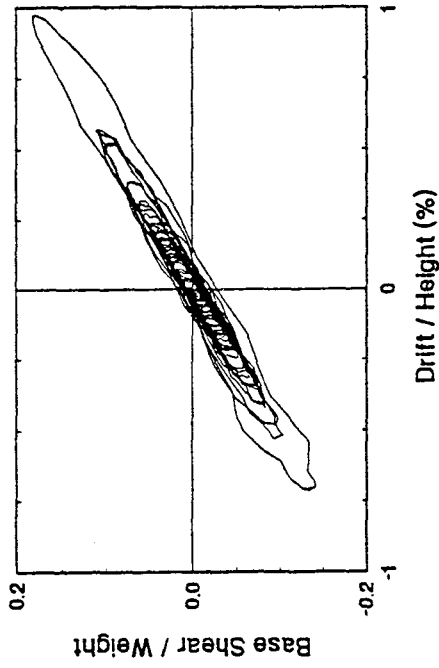
TEST 321

0.5g 5 Hz Harmonic, Feedforward Control



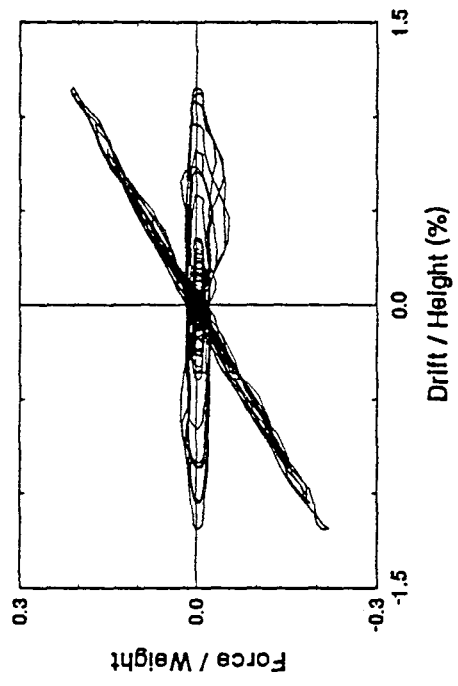
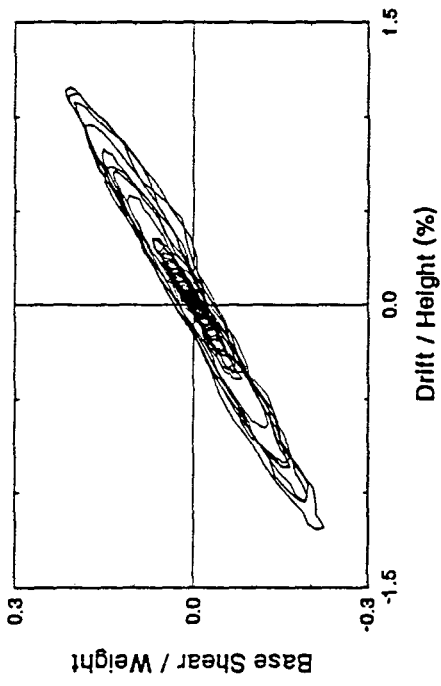
TEST 322

50% Hachinohe, Feedforward-Neg Control



TEST 323

50% El Centro, Feedforward-Neg Control

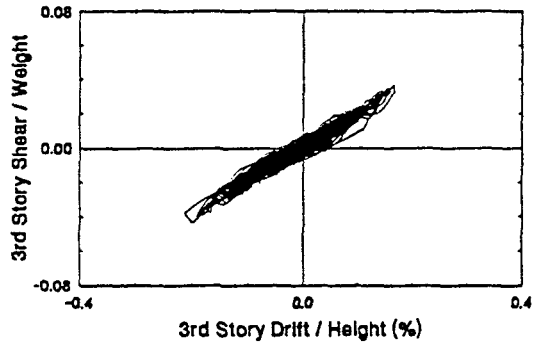


APPENDIX E

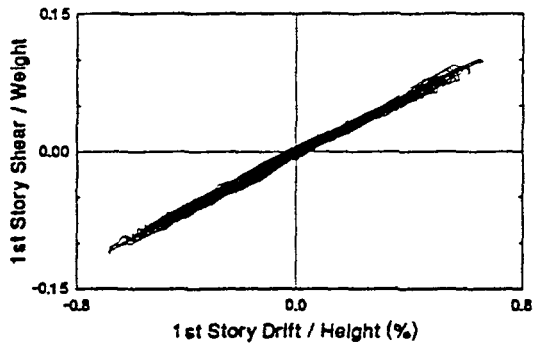
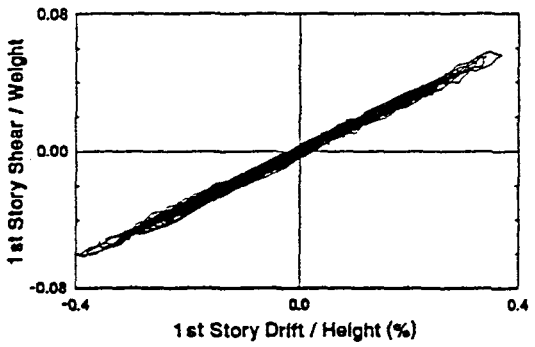
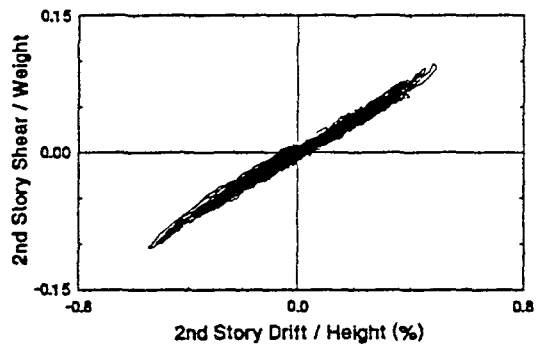
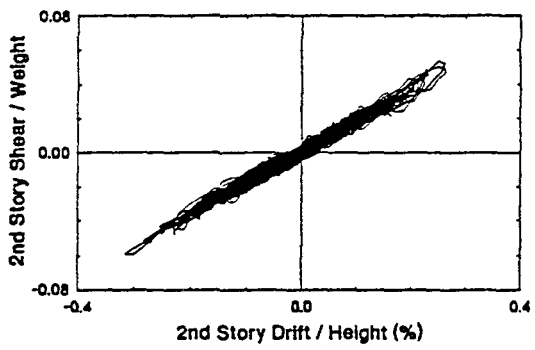
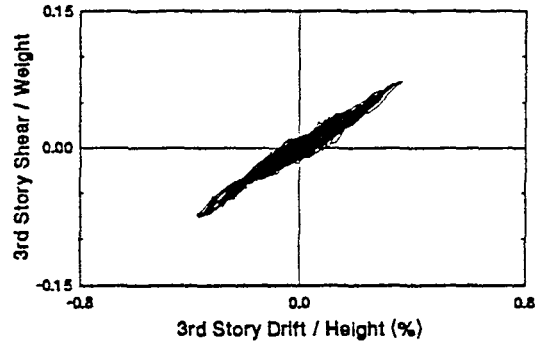
Shaking Table Test Results:

Three-Story Structure with No Dampers (Bare Frame)

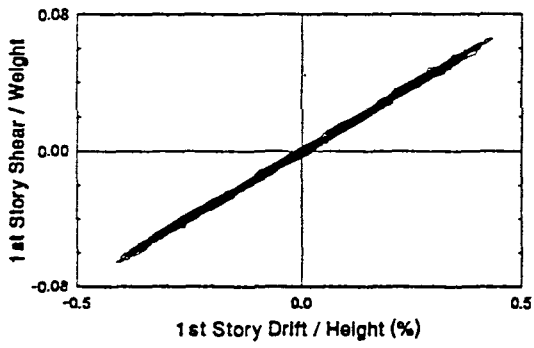
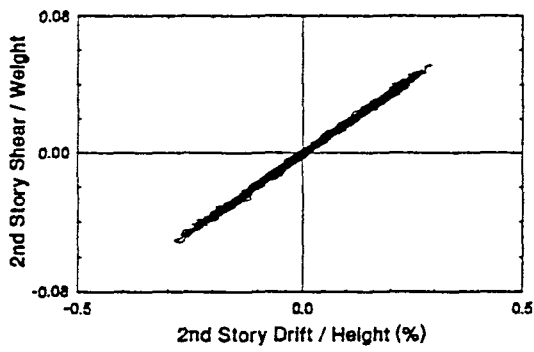
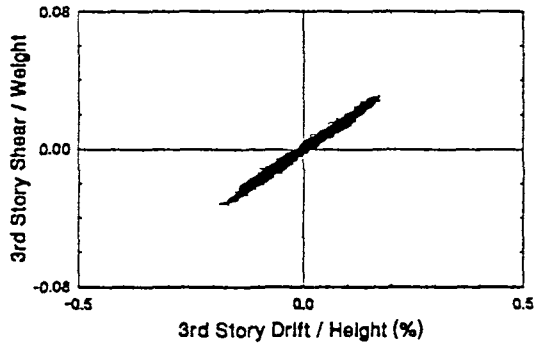
TEST 191
0.05g White Noise



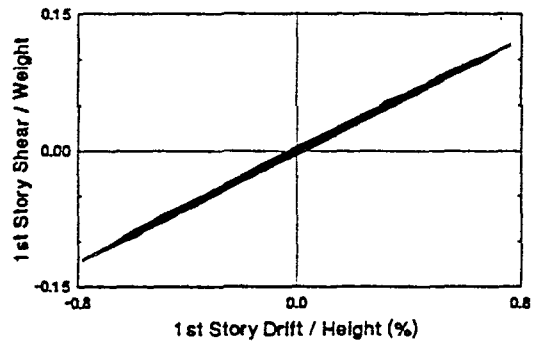
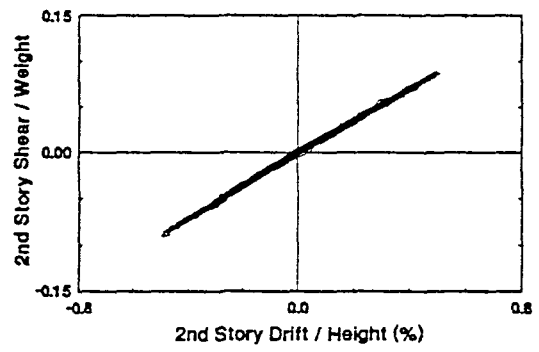
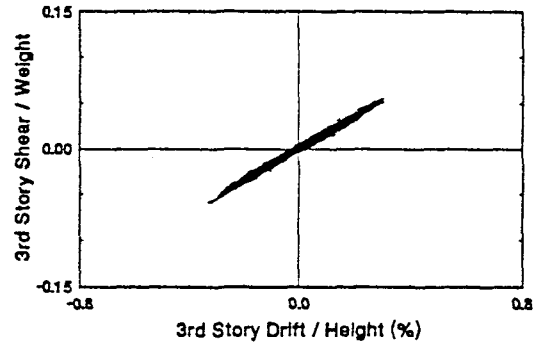
TEST 192
0.1g White Noise



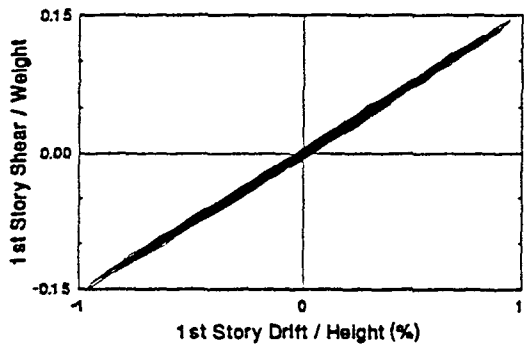
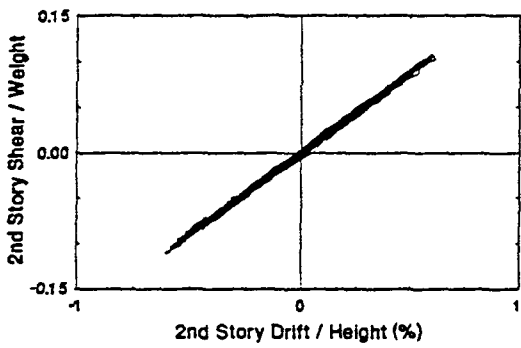
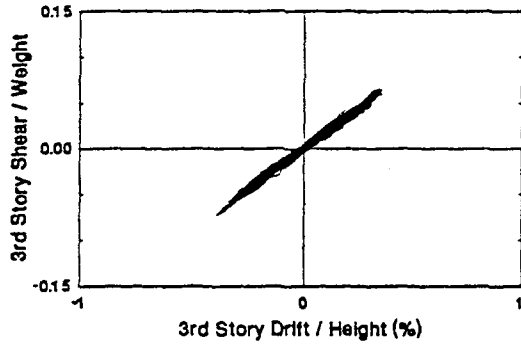
TEST 193
10% El Centro



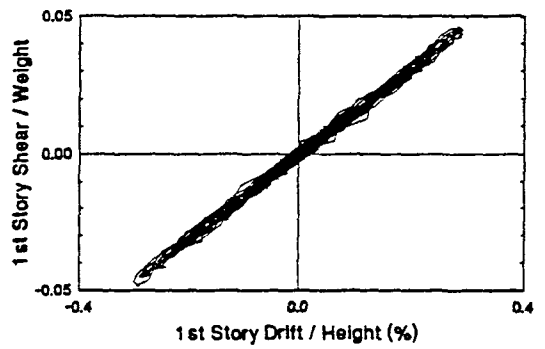
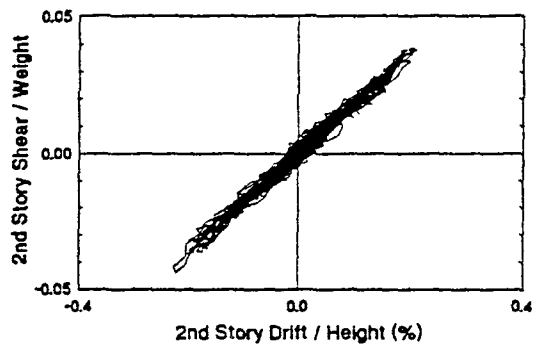
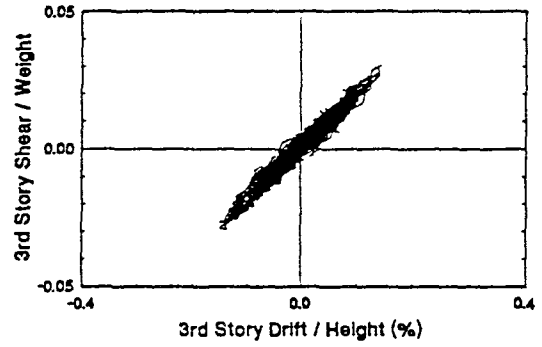
TEST 194
20% El Centro



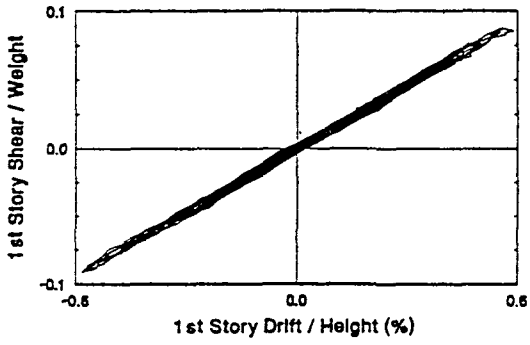
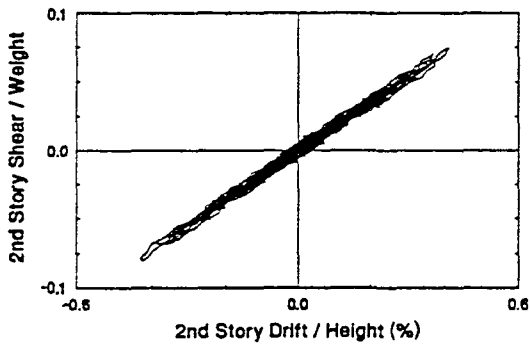
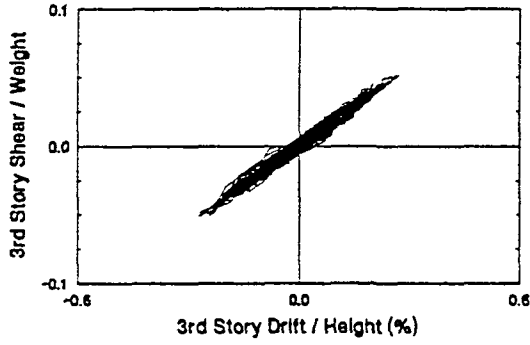
TEST 195
25% El Centro



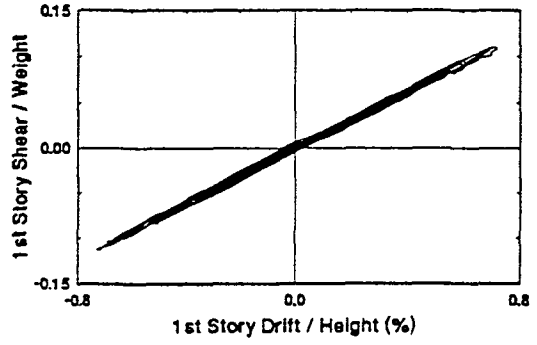
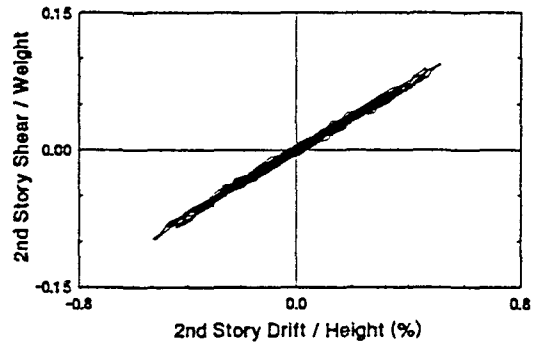
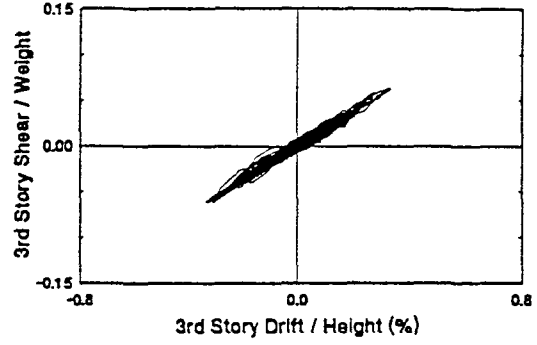
TEST 196
10% Hachinohe



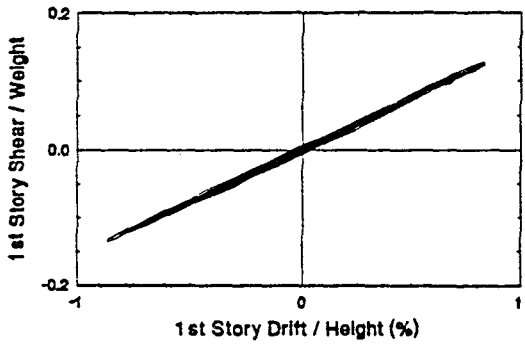
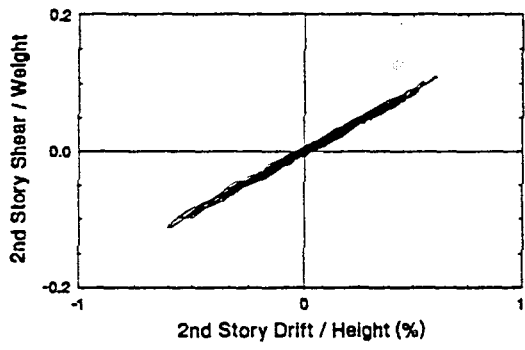
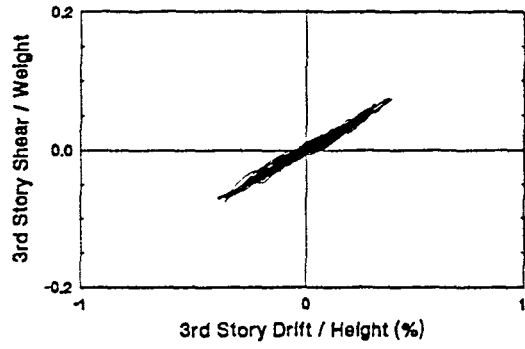
TEST 197
20% Hachinohe



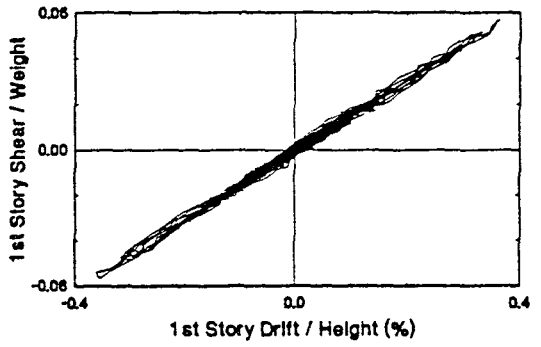
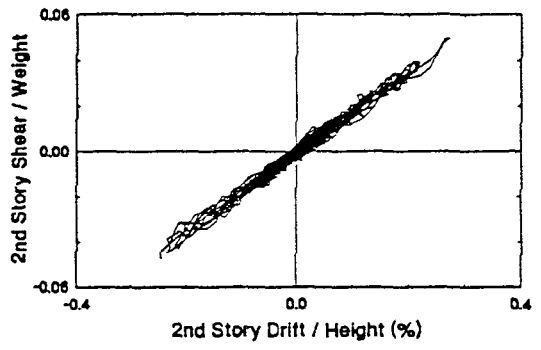
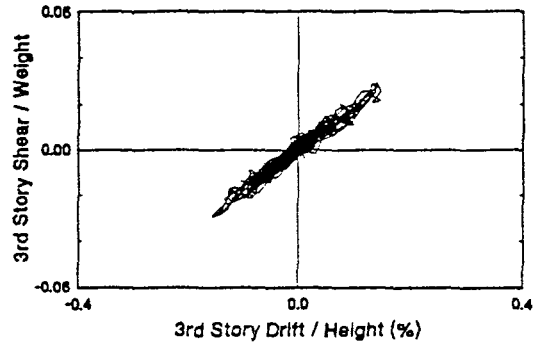
TEST 198
25% Hachinohe



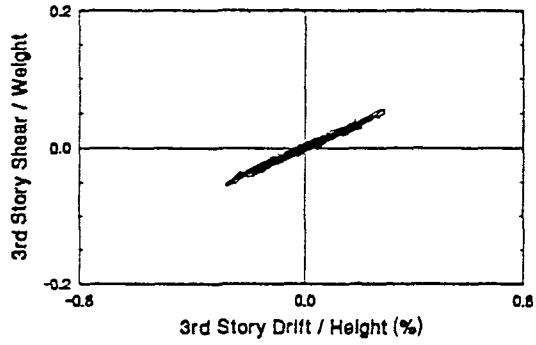
TEST 199
30% Hachinohe



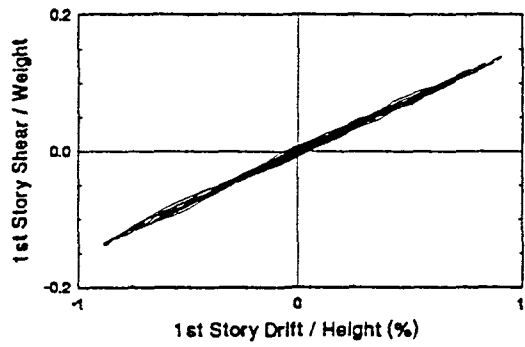
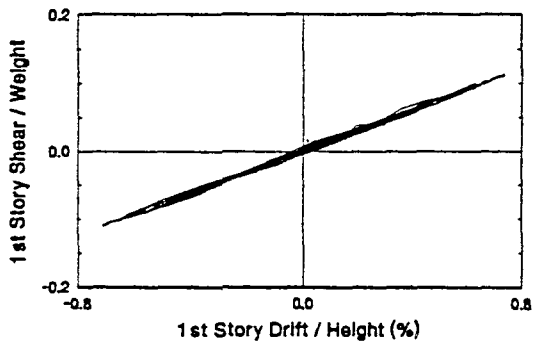
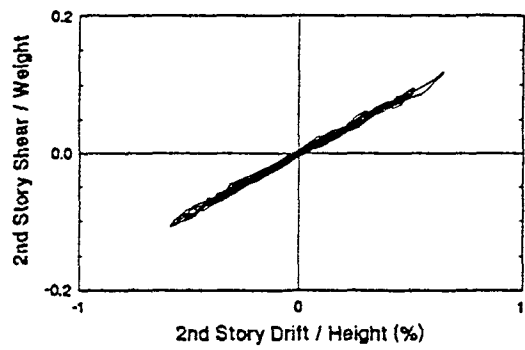
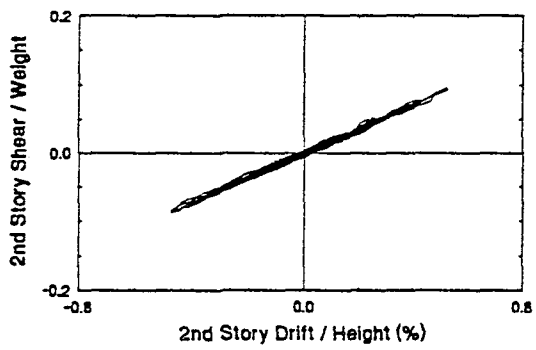
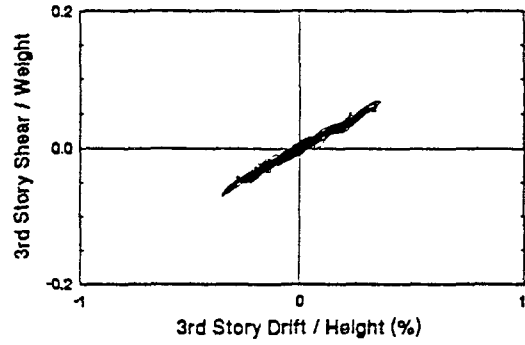
TEST 200
20% Hachinohe-M



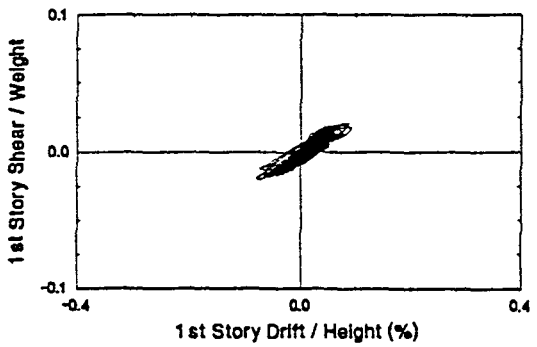
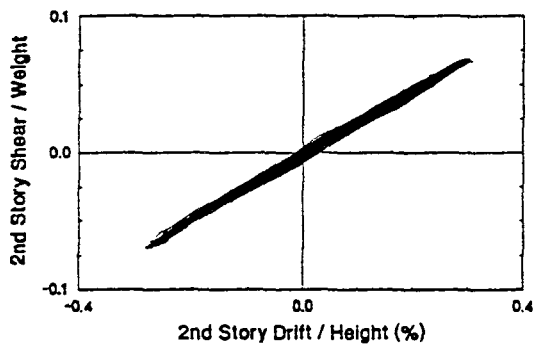
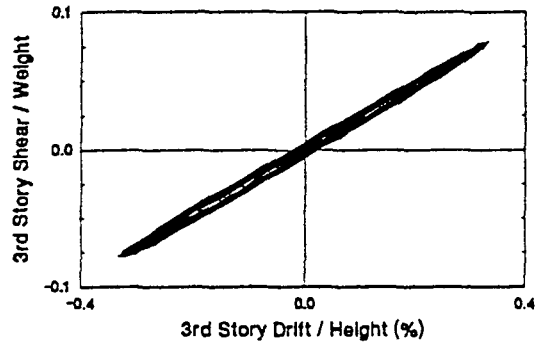
TEST 201
40% Hachinohe-M



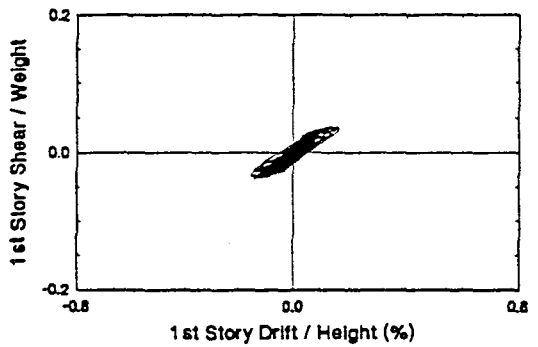
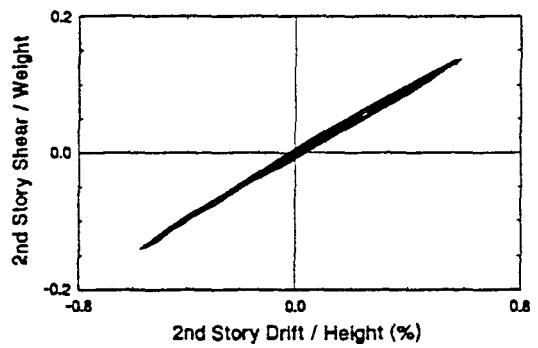
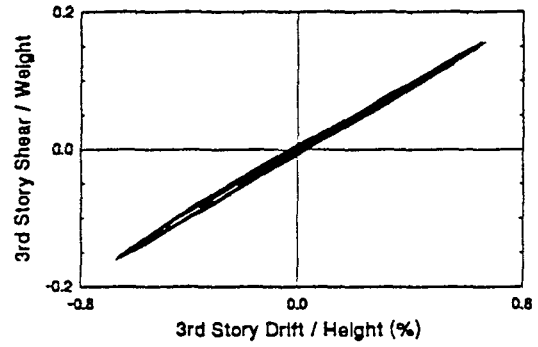
TEST 202
50% Hachinohe-M



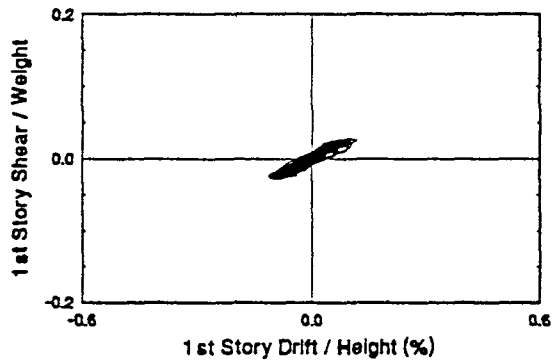
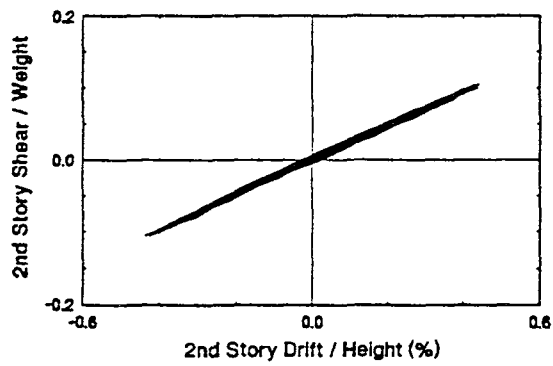
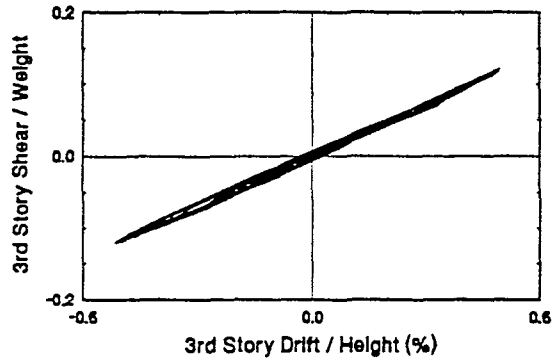
TEST 203
0.2g 5 Hz Harmonic



TEST 204
0.4g 5 Hz Harmonic



TEST 205
0.3g 5 Hz Harmonic



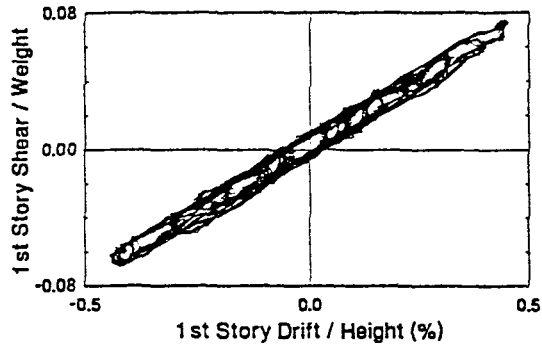
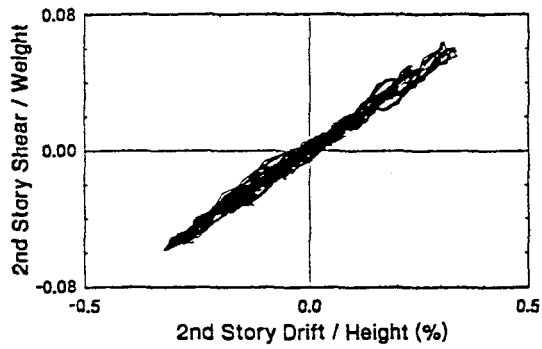
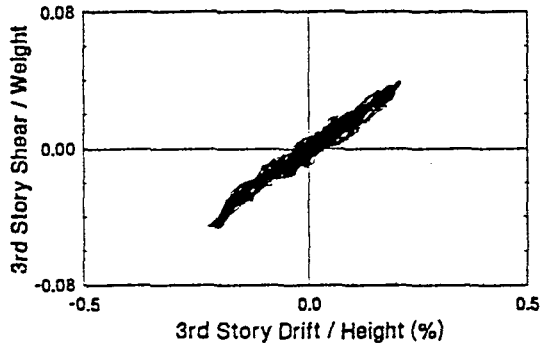
APPENDIX F

Shaking Table Test Results:

Three-Story Structure with Variable Dampers

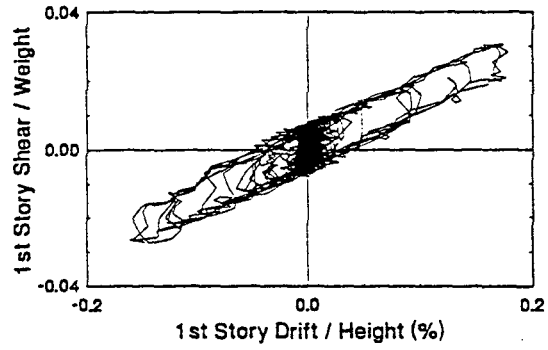
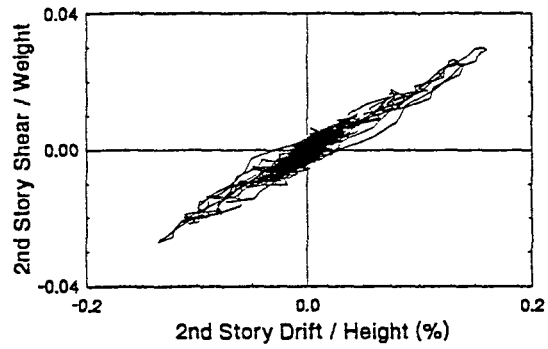
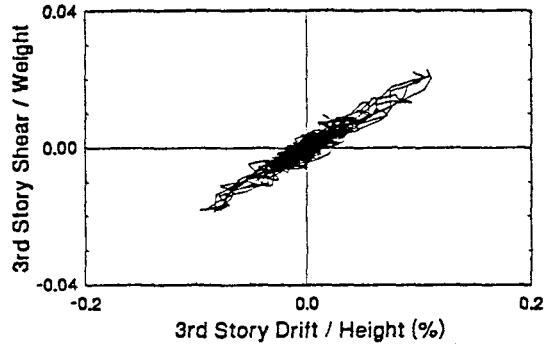
TEST 209

0.1 g White Noise, Low Damping



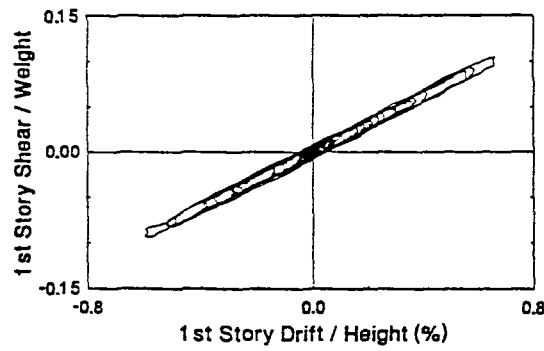
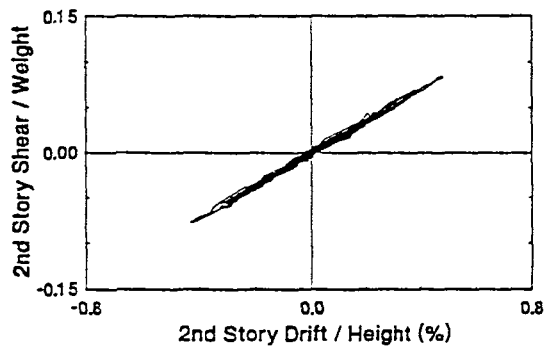
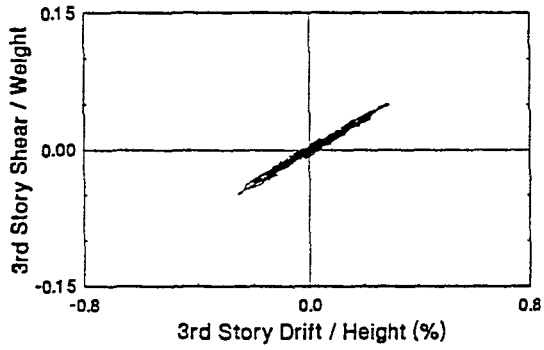
TEST 220

10% El Centro, Low Damping



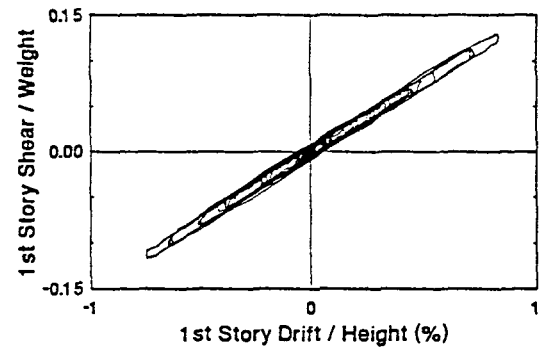
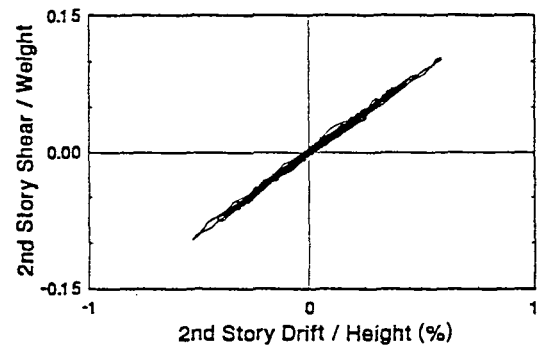
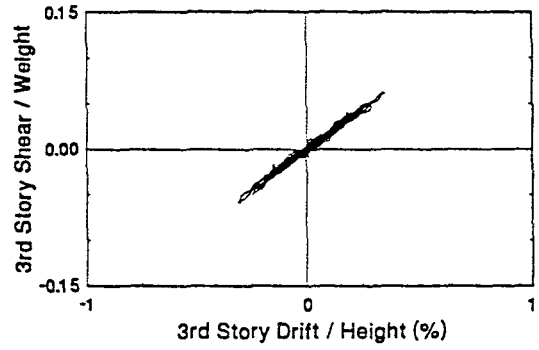
TEST 221

25% El Centro, Low Damping



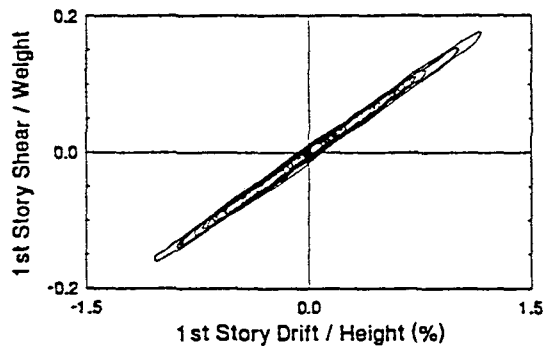
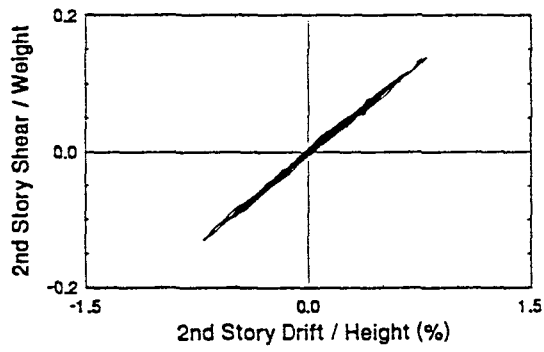
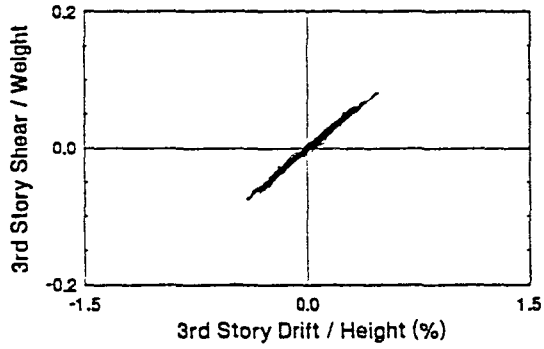
TEST 222

30% El Centro, Low Damping



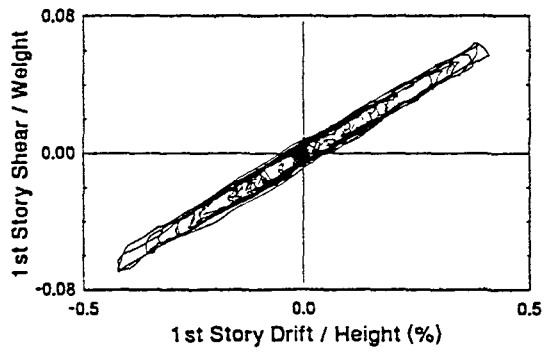
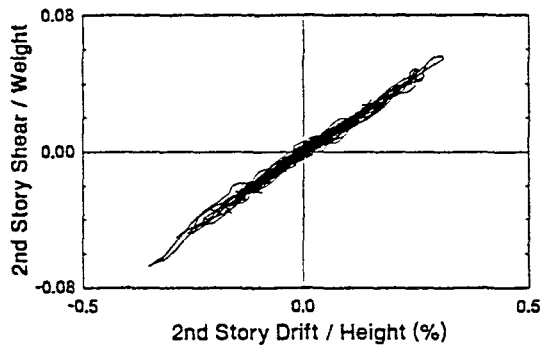
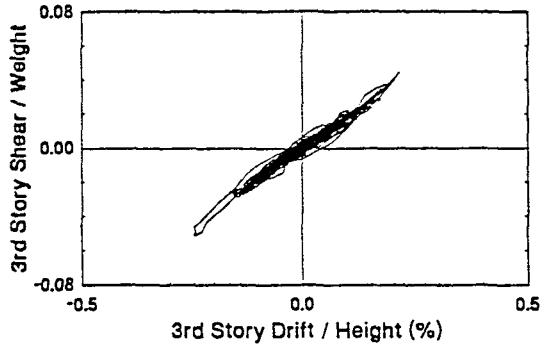
TEST 223

40% El Centro, Low Damping



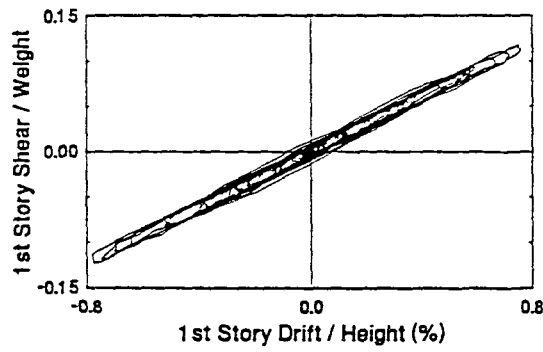
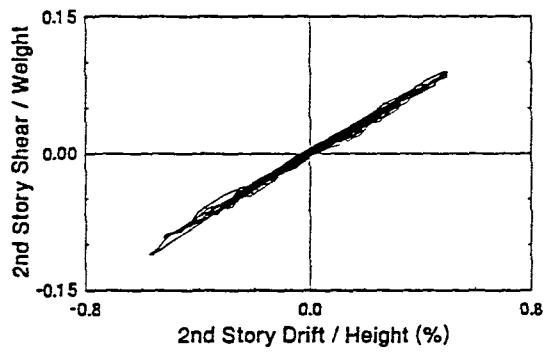
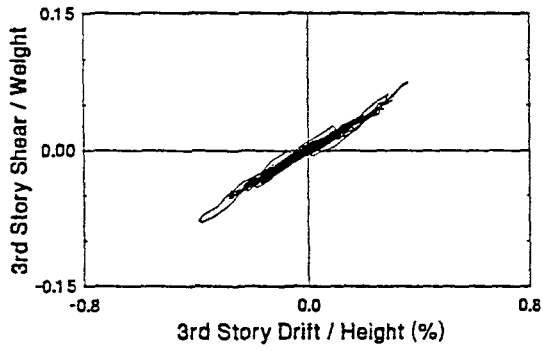
TEST 224

25% Hachinohe, Low Damping



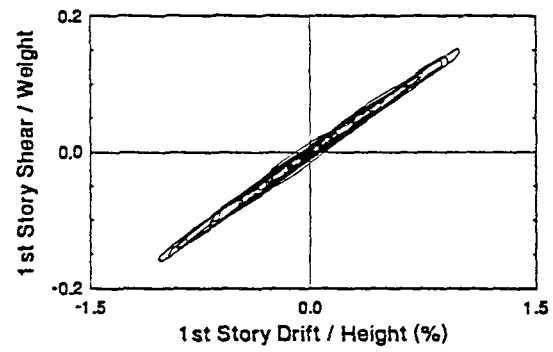
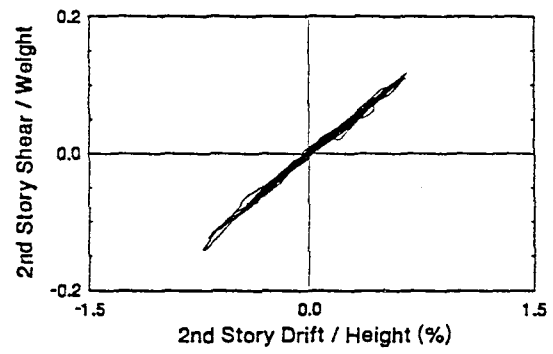
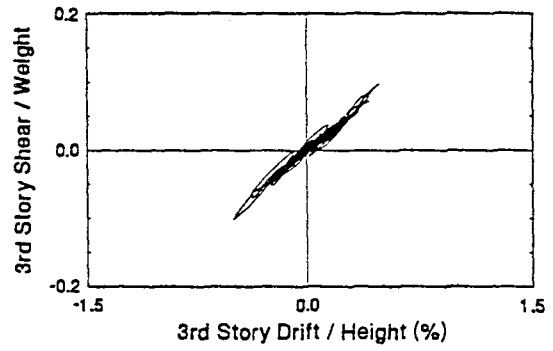
TEST 225

40% Hachinohe, Low Damping



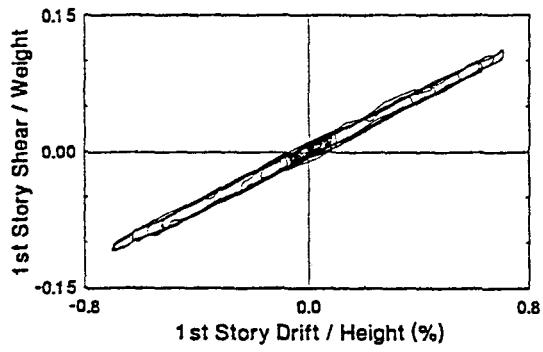
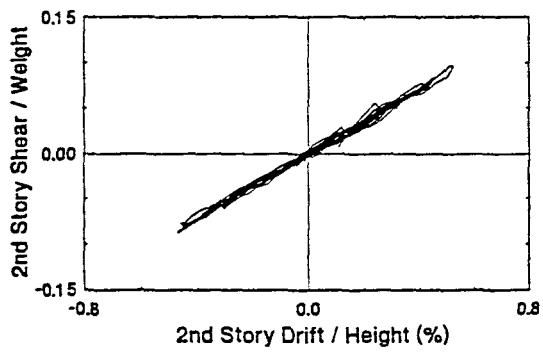
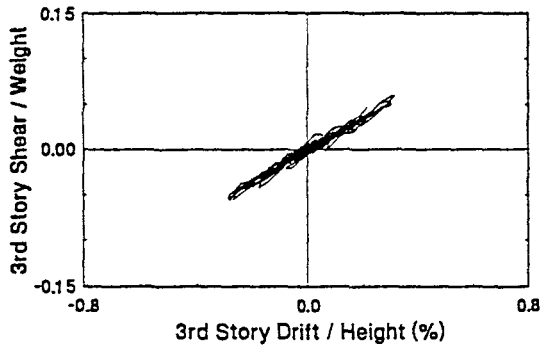
TEST 226

50% Hachinohe, Low Damping



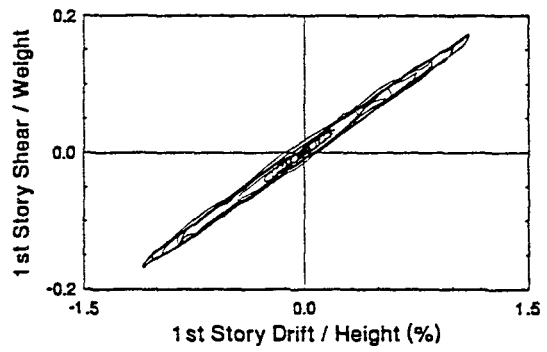
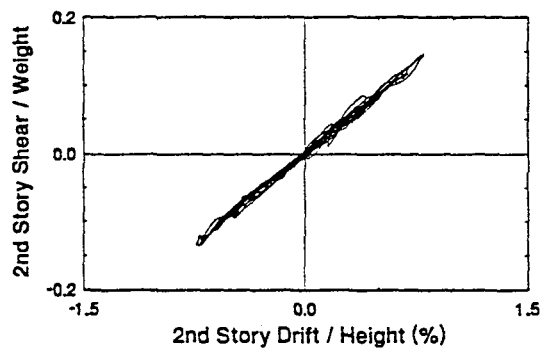
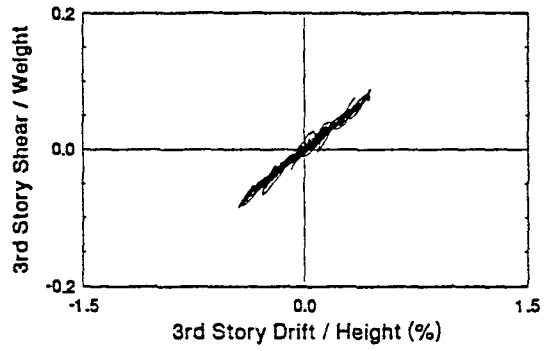
TEST 227

50% Hachinohe-M, Low Damping



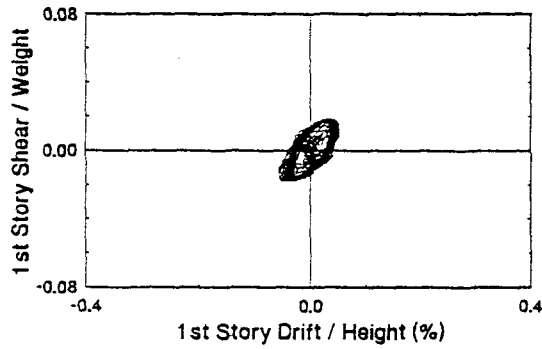
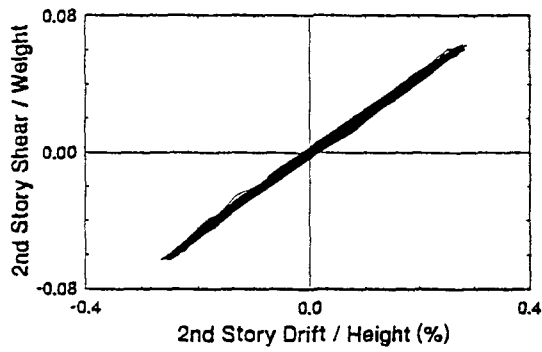
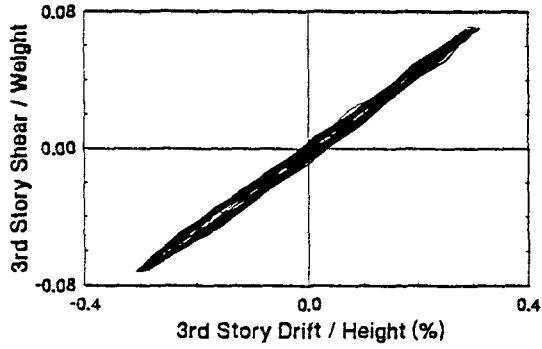
TEST 228

75% Hachinohe-M, Low Damping



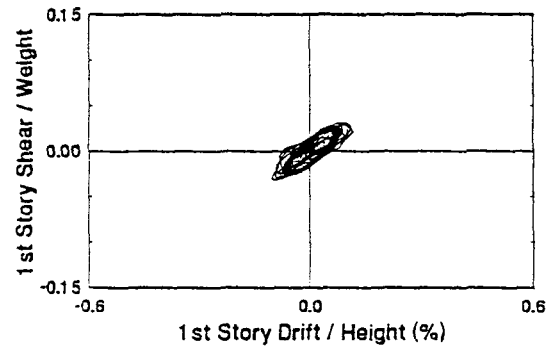
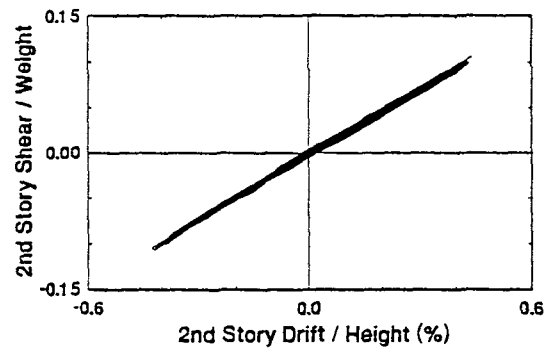
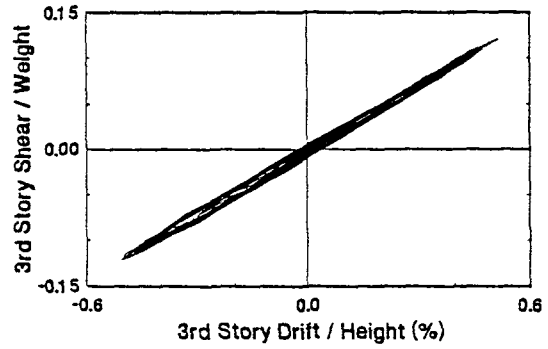
TEST 229

0.2g 5 Hz Harmonic, Low Damping



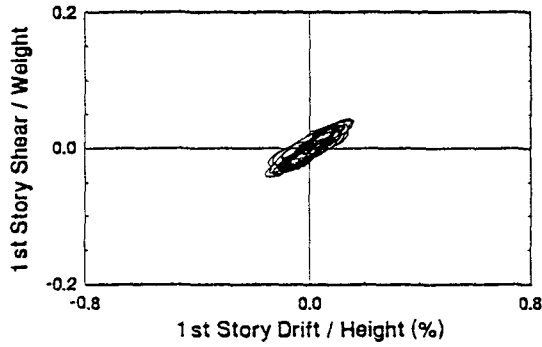
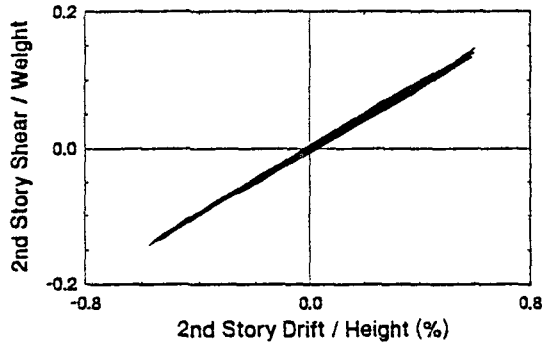
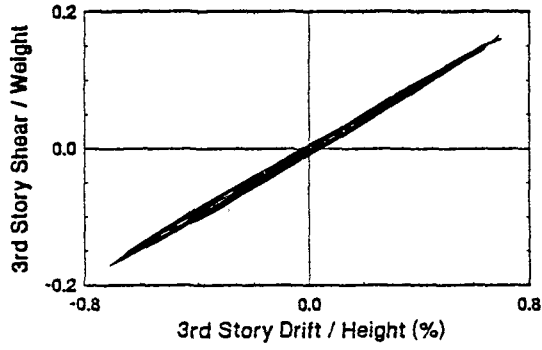
TEST 230

0.3g 5 Hz Harmonic, Low Damping



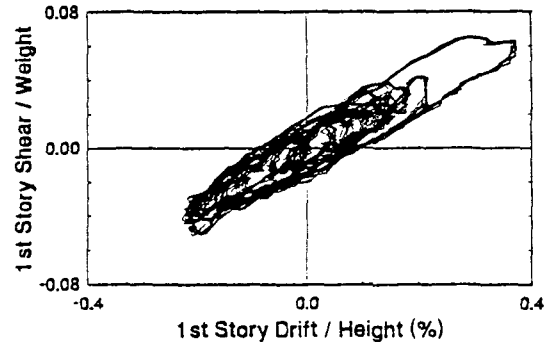
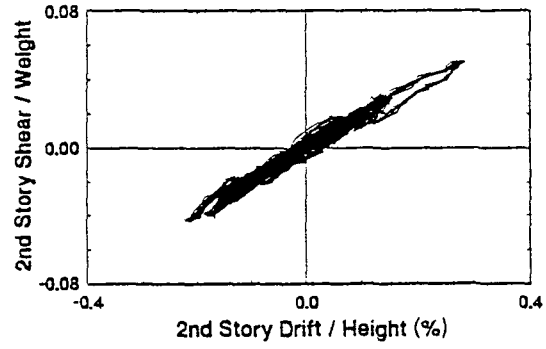
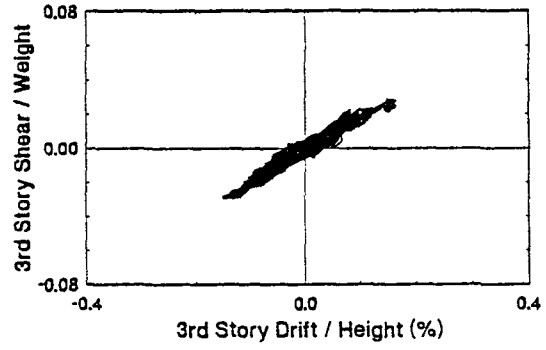
TEST 231

0.4g 5 Hz Harmonic, Low Damping



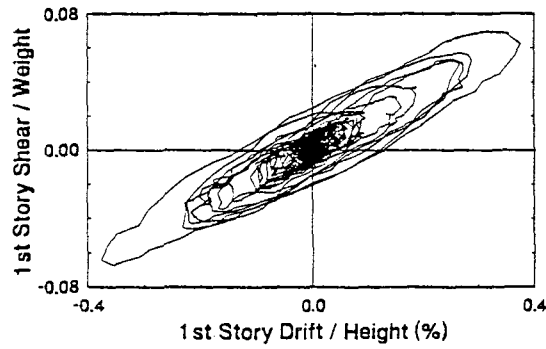
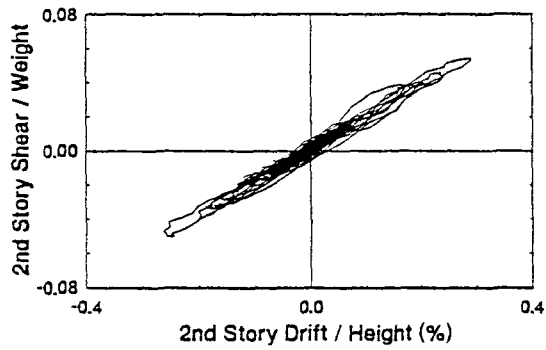
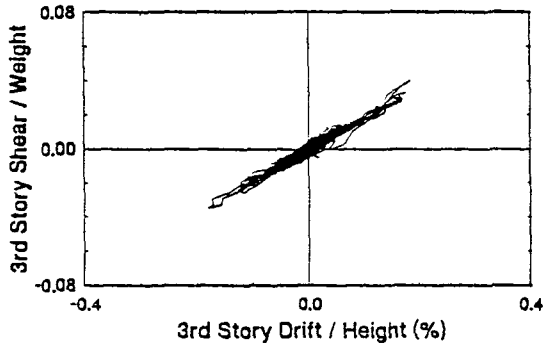
TEST 207

0.1 g White Noise, High Damping



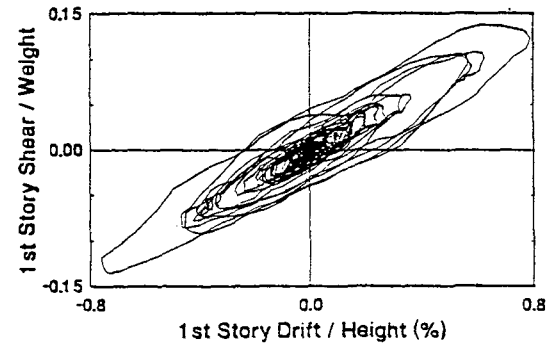
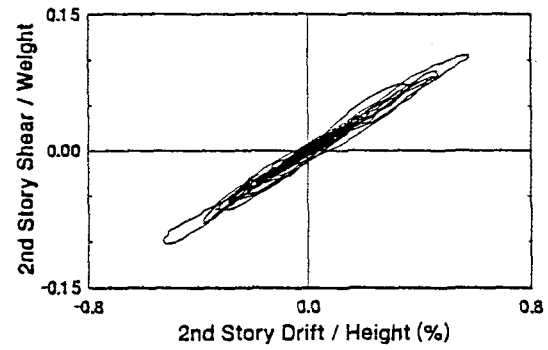
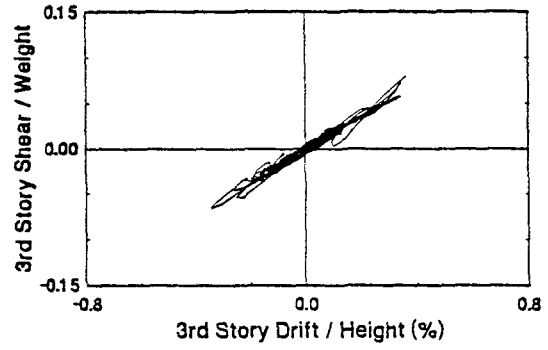
TEST 210

25% El Centro, High Damping



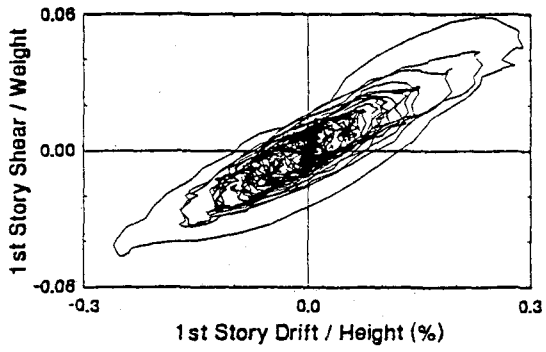
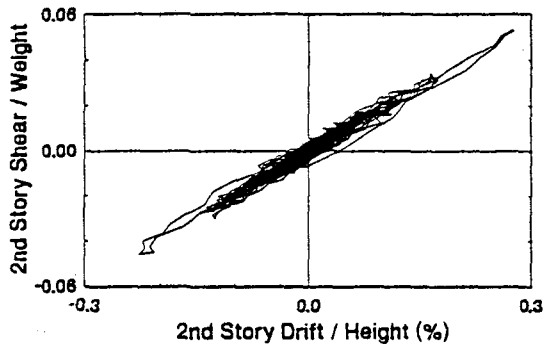
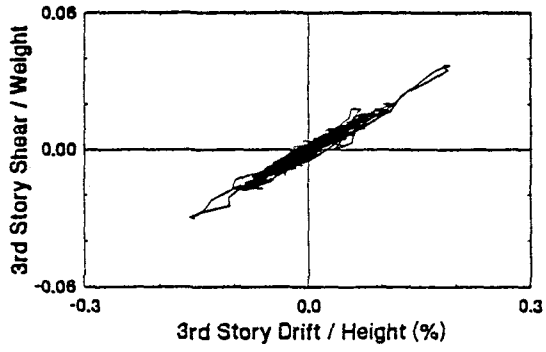
TEST 211

50% El Centro, High Damping



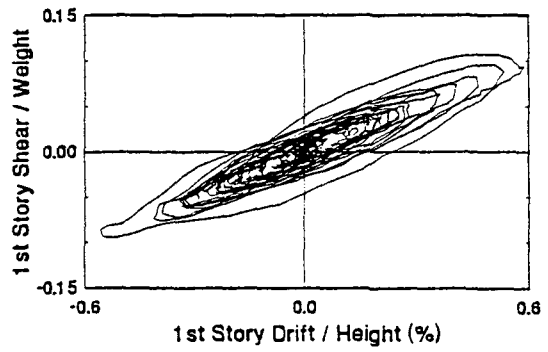
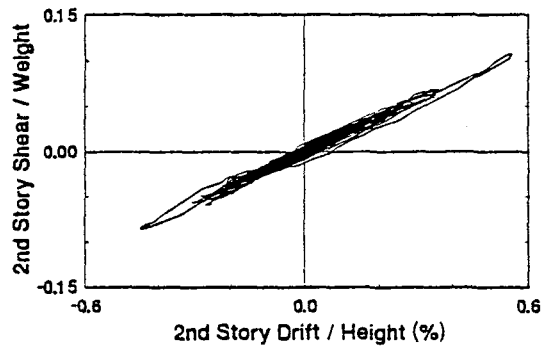
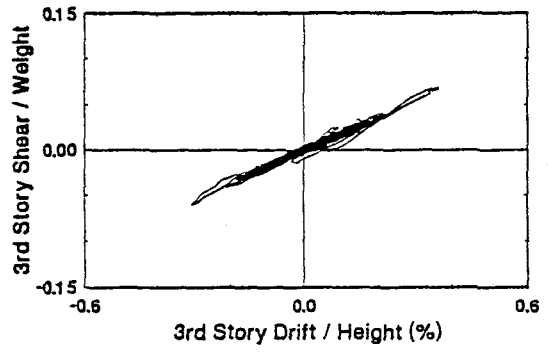
TEST 212

25% Hachinohe, High Damping



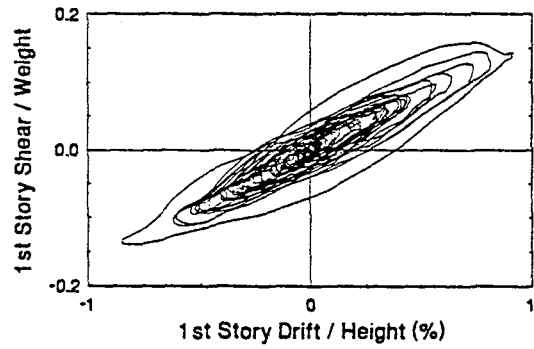
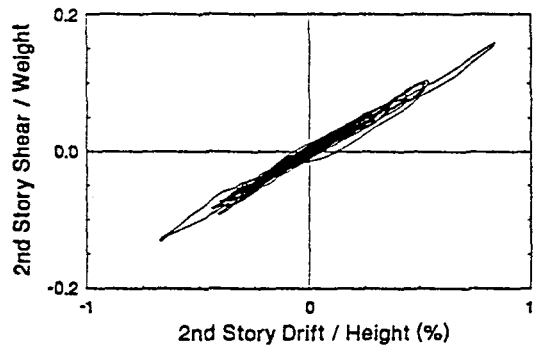
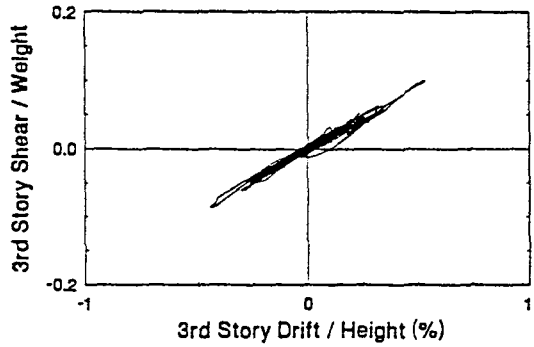
TEST 213

50% Hachinohe, High Damping



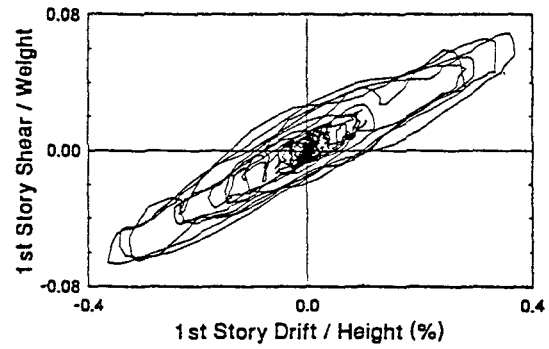
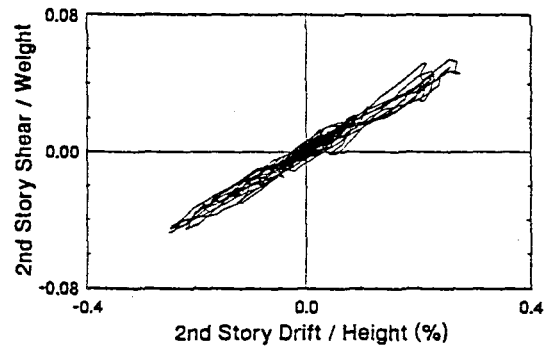
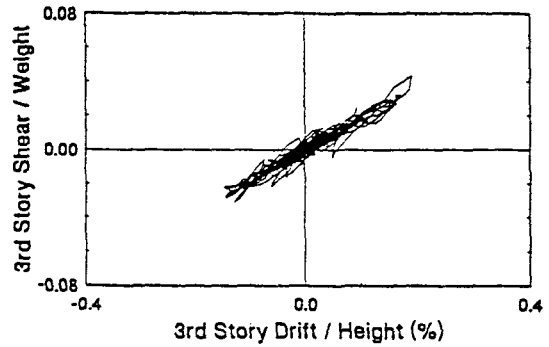
TEST 214

75% Hachinohe, High Damping



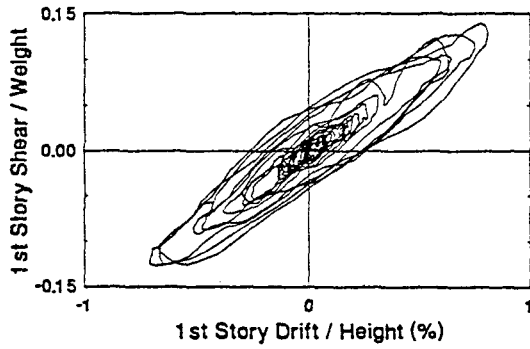
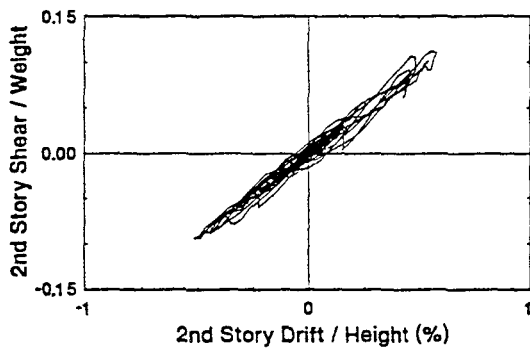
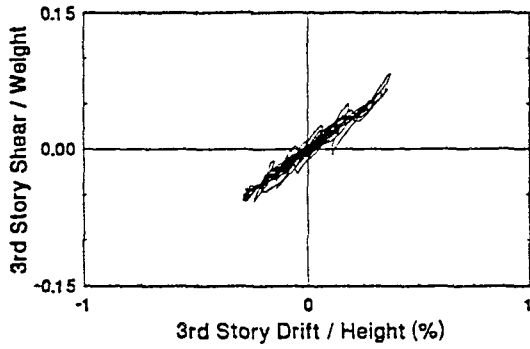
TEST 285

50% Hachinohe-M, High Damping



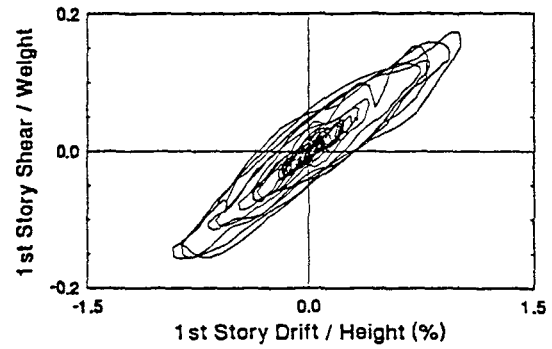
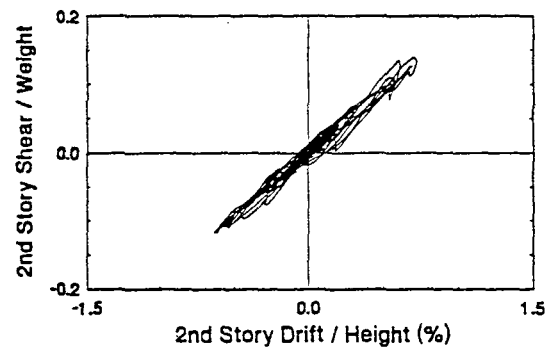
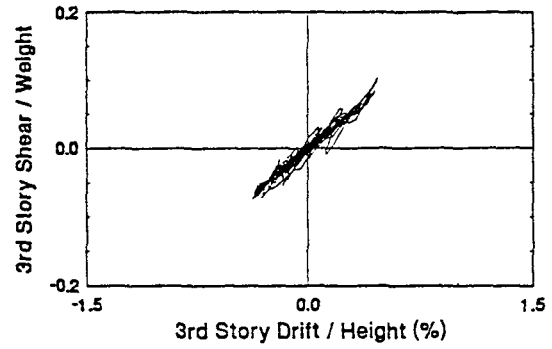
TEST 215

100% Hachinohe-M, High Damping



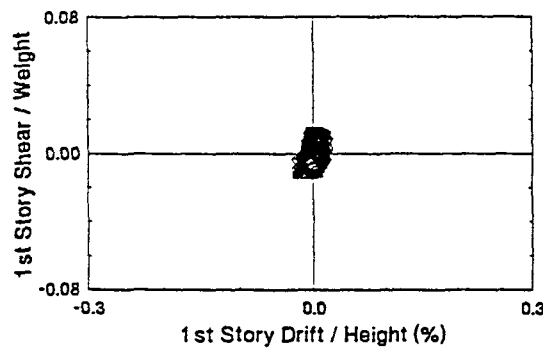
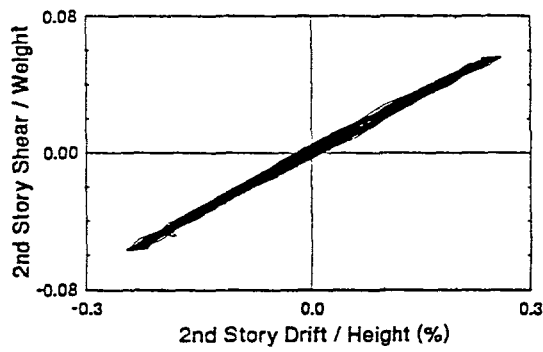
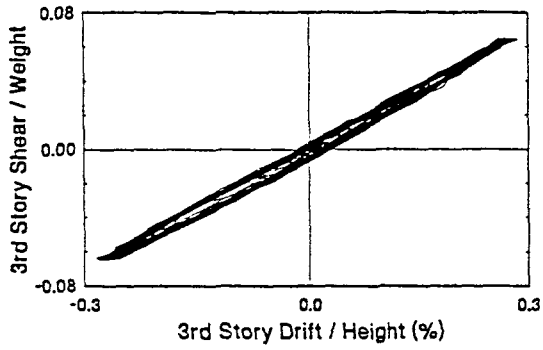
TEST 216

125% Hachinohe-M, High Damping



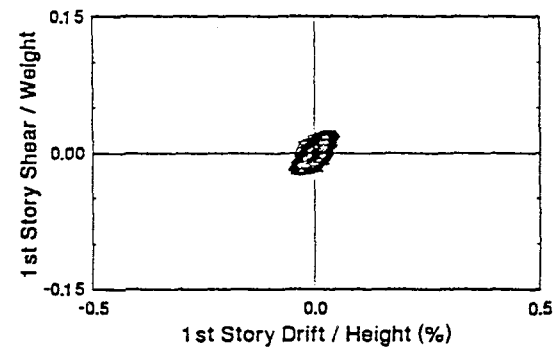
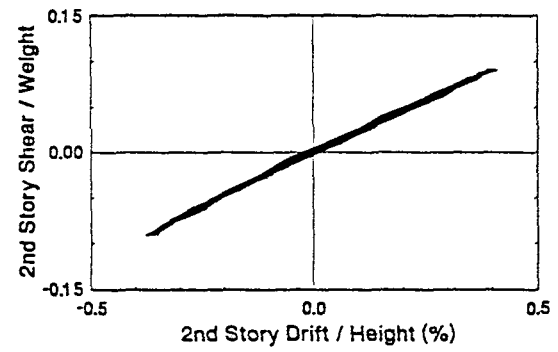
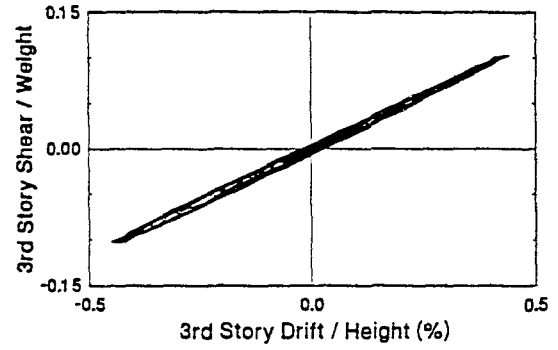
TEST 217

0.2g 5 Hz Harmonic, High Damping



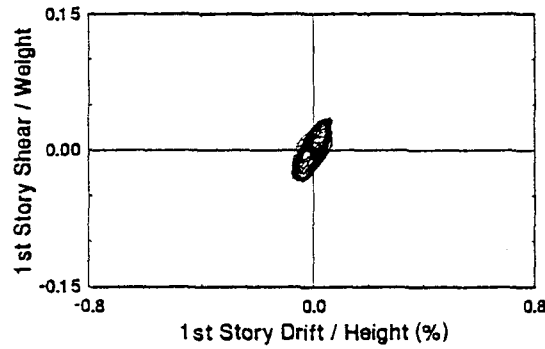
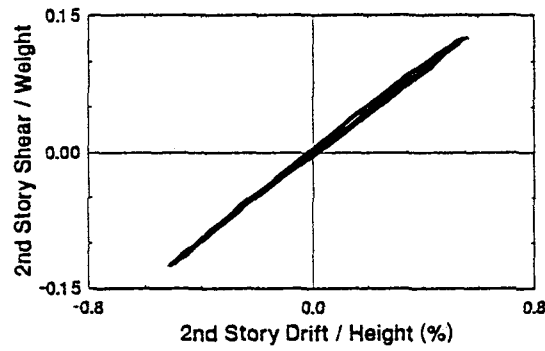
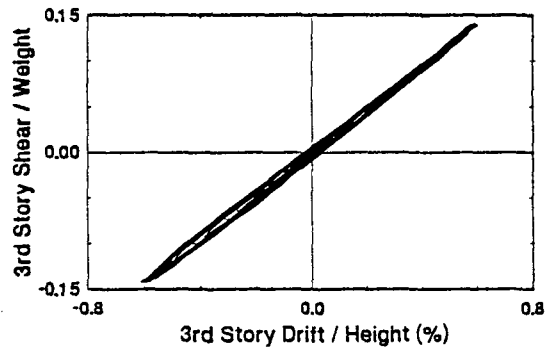
TEST 218

0.3g 5 Hz Harmonic, High Damping



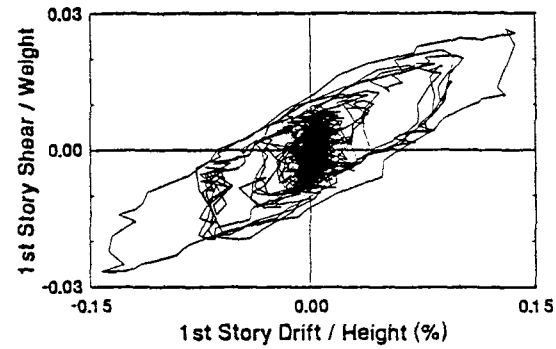
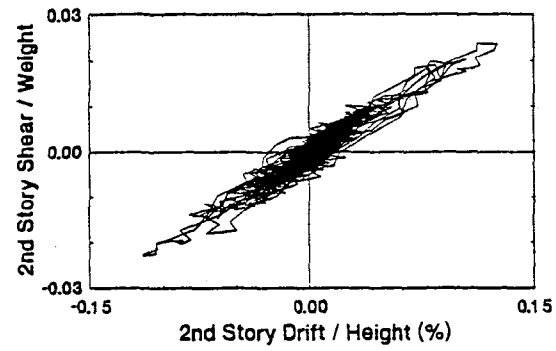
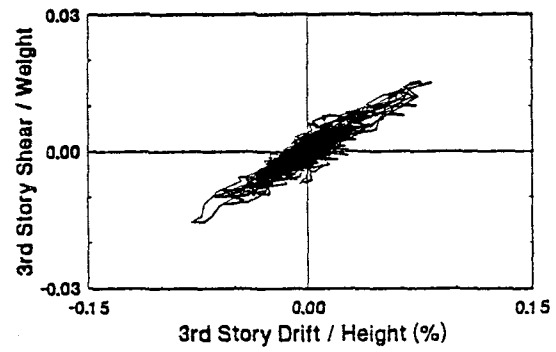
TEST 219

0.4g 5 Hz Harmonic, High Damping

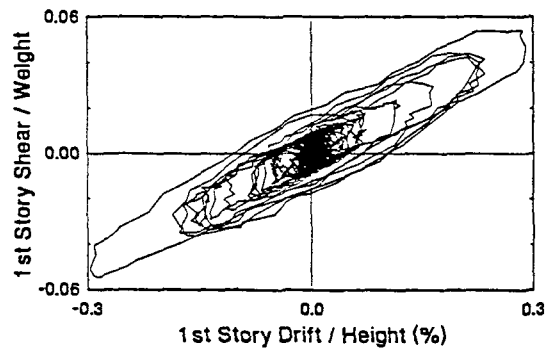
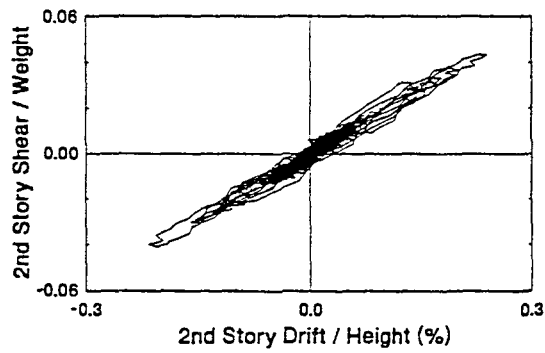
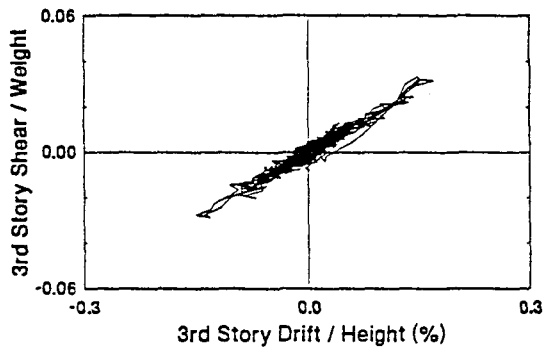


TEST 256

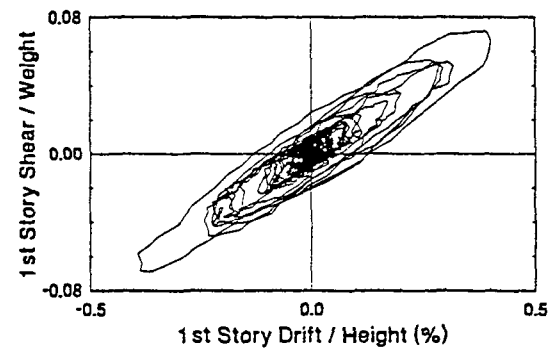
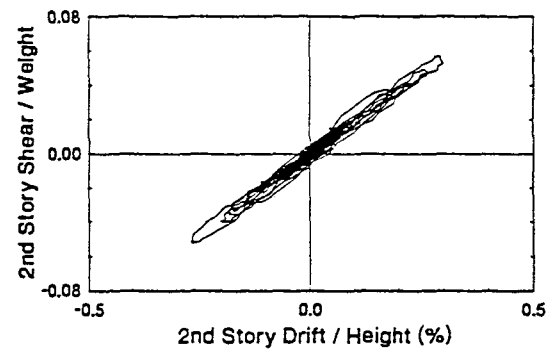
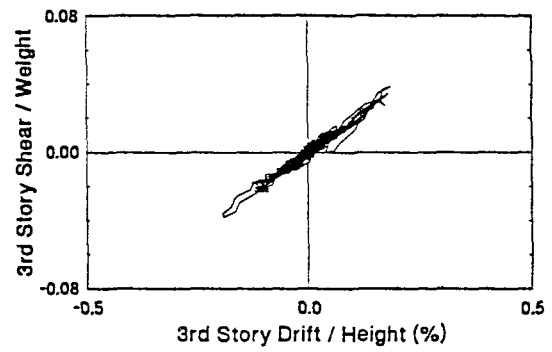
10% El Centro, Optimal Control - LG



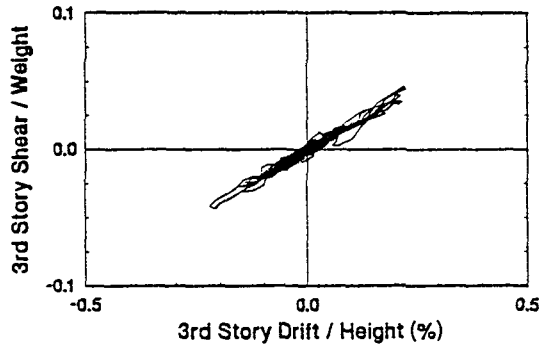
TEST 257
20% El Centro
Optimal Control - LG



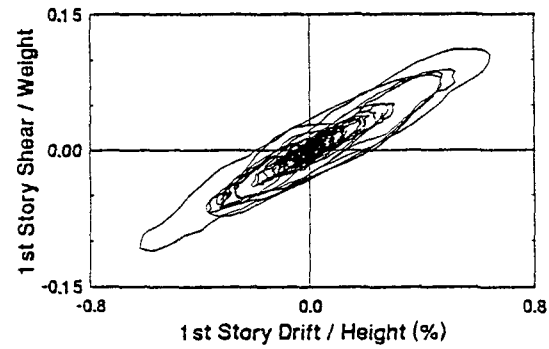
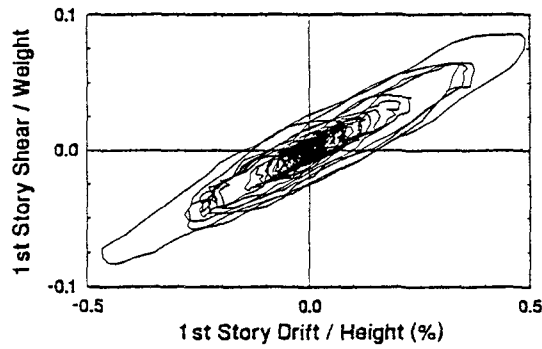
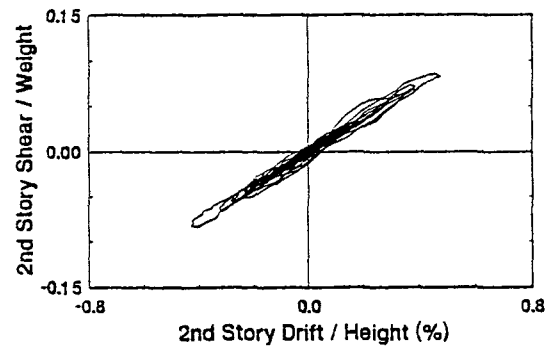
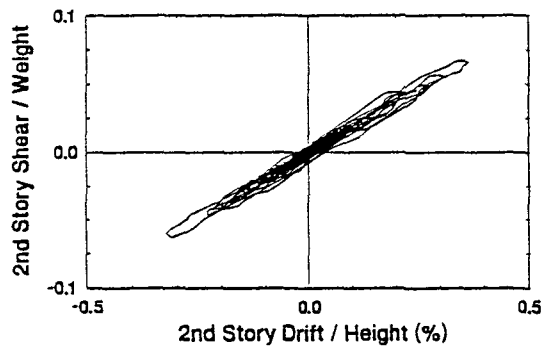
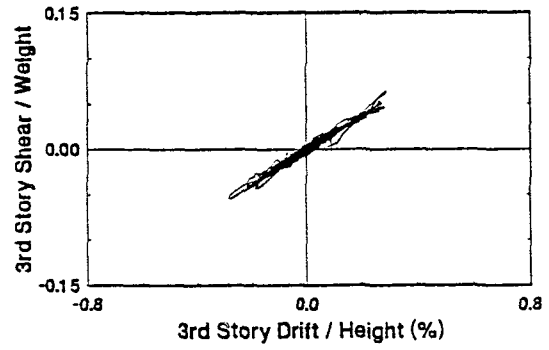
TEST 258
25% El Centro
Optimal Control - LG



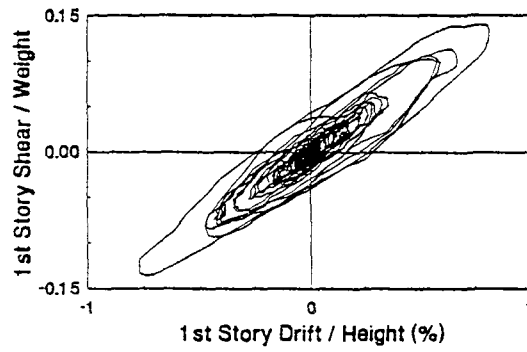
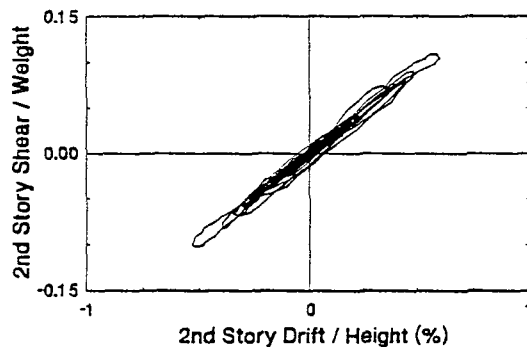
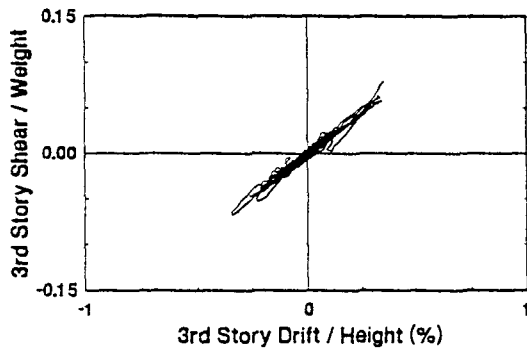
TEST 259
30% El Centro
Optimal Control - LG



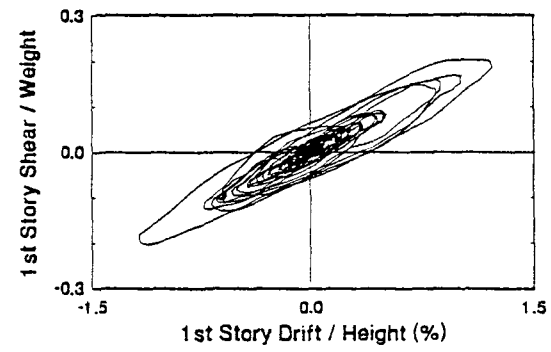
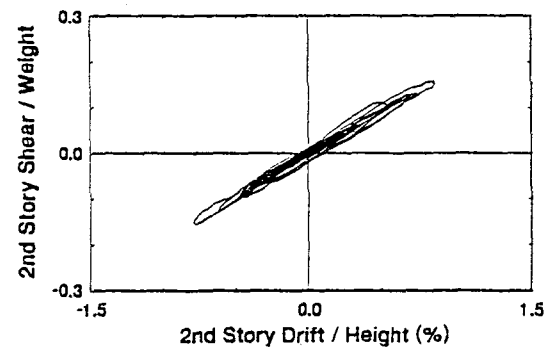
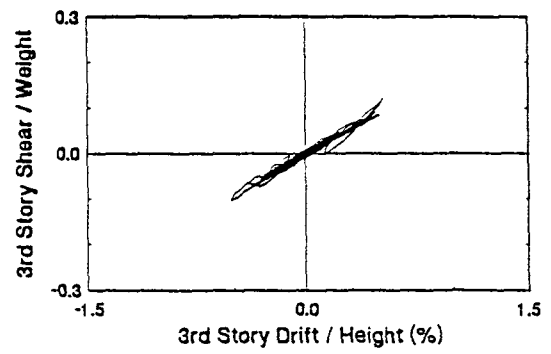
TEST 260
40% El Centro
Optimal Control - LG



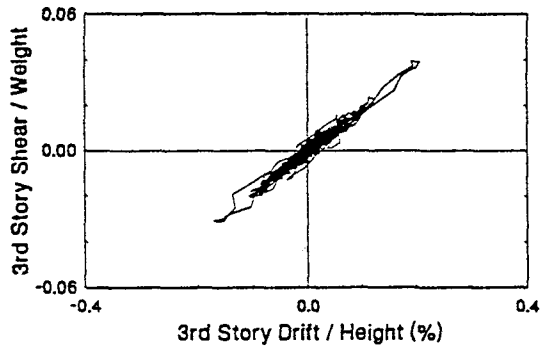
TEST 261
50% El Centro
Optimal Control - LG



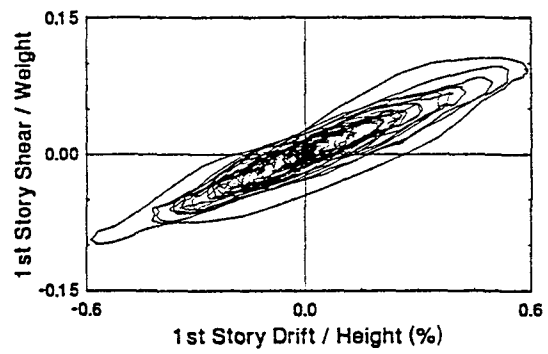
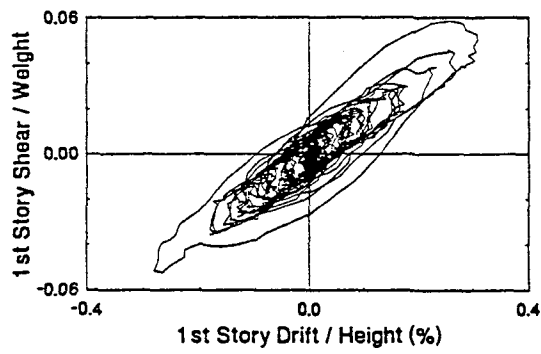
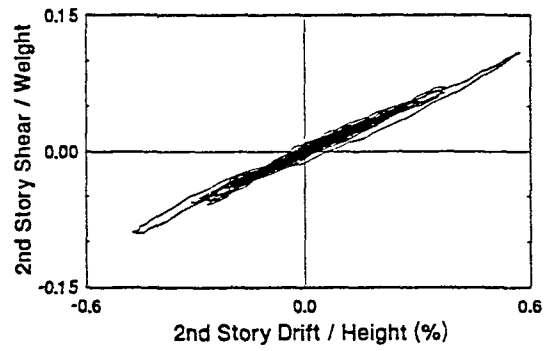
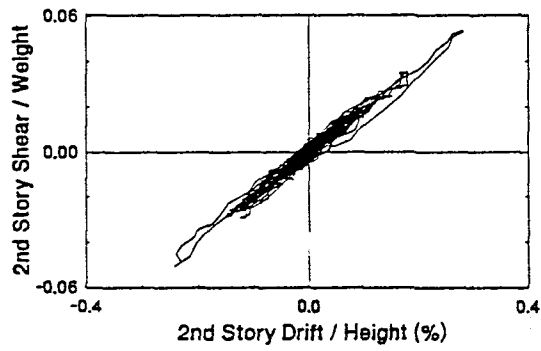
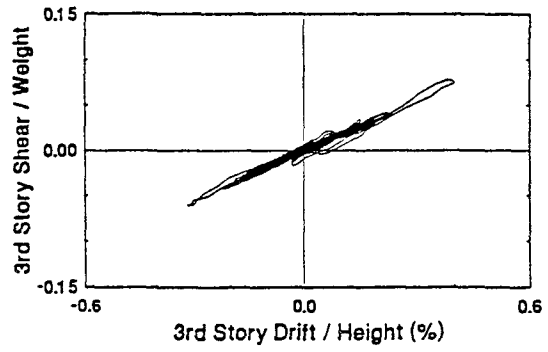
TEST 262
75% El Centro
Optimal Control - LG



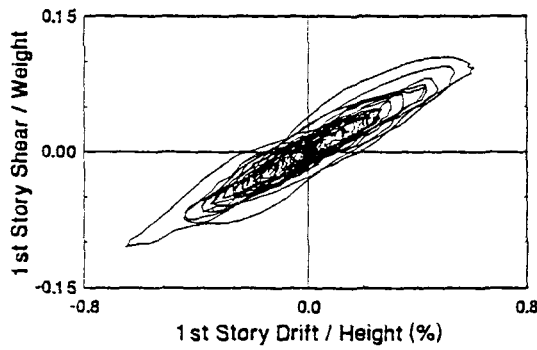
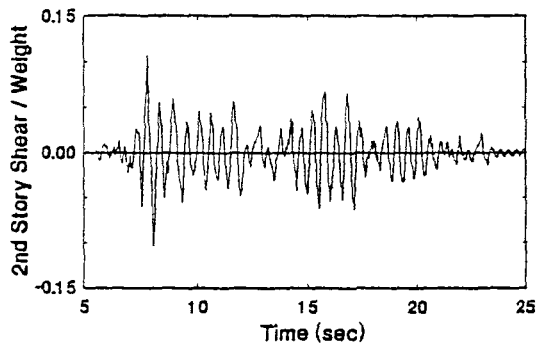
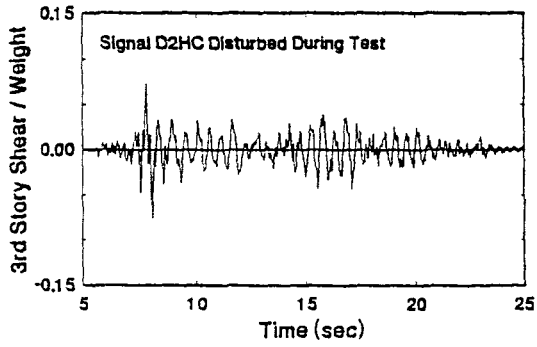
TEST 263
25% Hachinohe
Optimal Control - LG



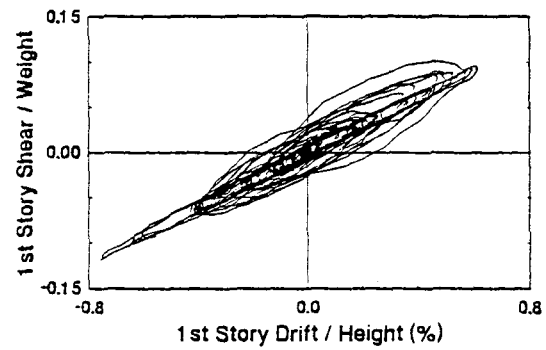
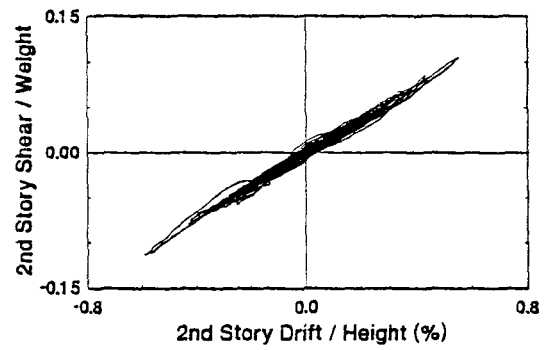
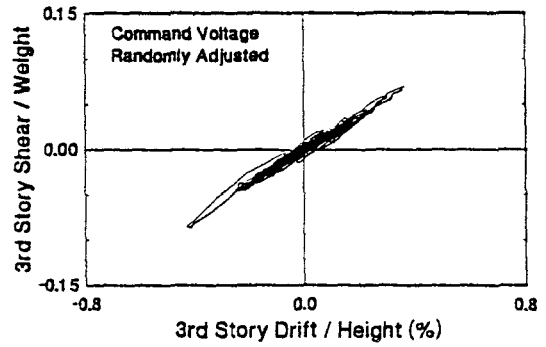
TEST 264
50% Hachinohe
Optimal Control - LG



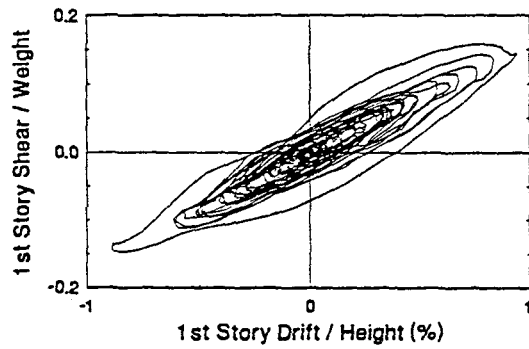
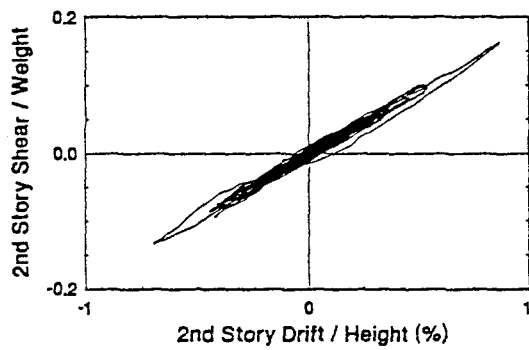
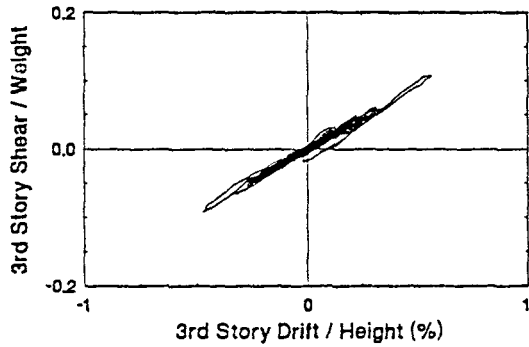
TEST 265
50% Hachinohe
Optimal Control - LG



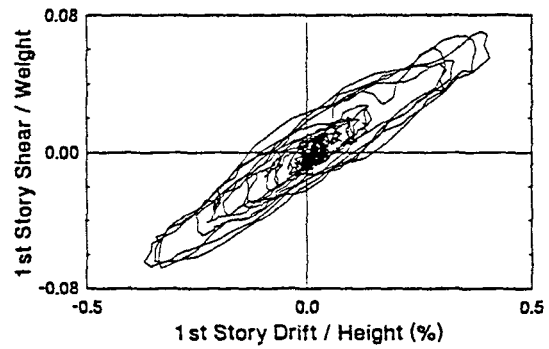
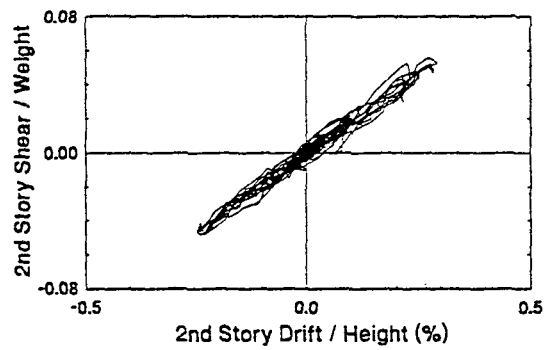
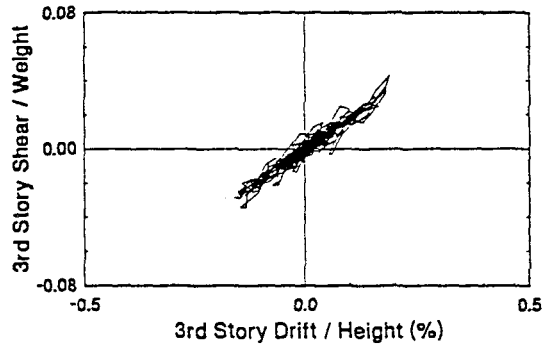
TEST 266
50% Hachinohe
Optimal Control - LG



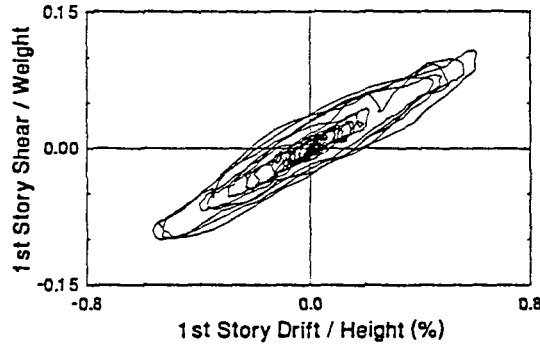
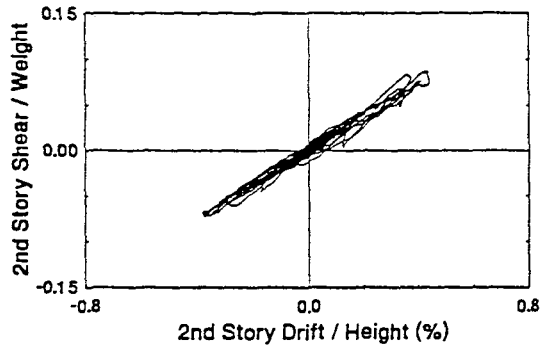
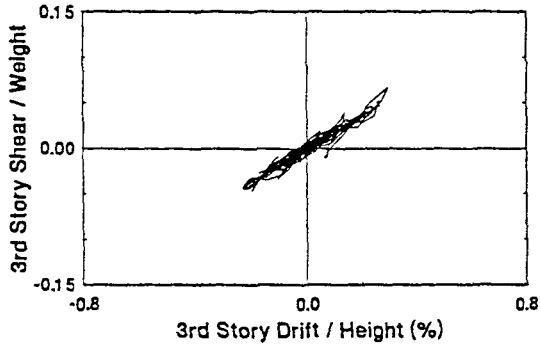
TEST 248
75% Hachinohe
Optimal Control - LG



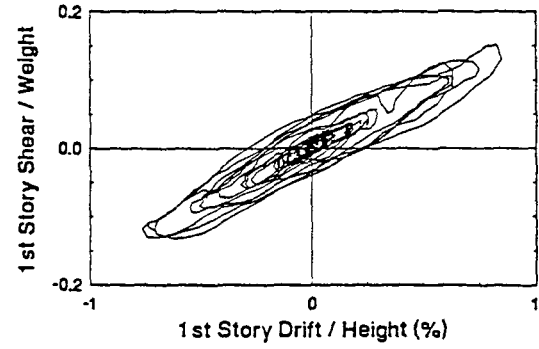
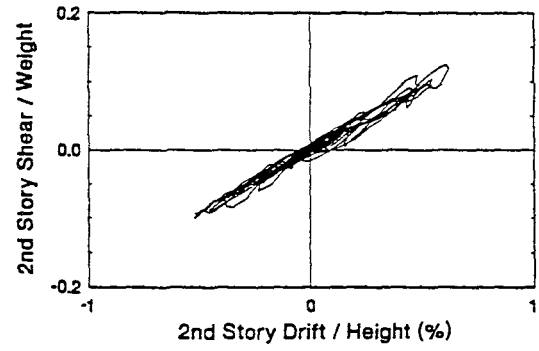
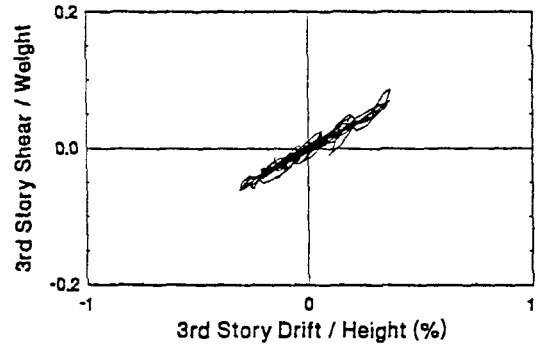
TEST 249
50% Hachinohe-M
Optimal Control - LG



TEST 250
75% Hachinohe-M
Optimal Control - LG



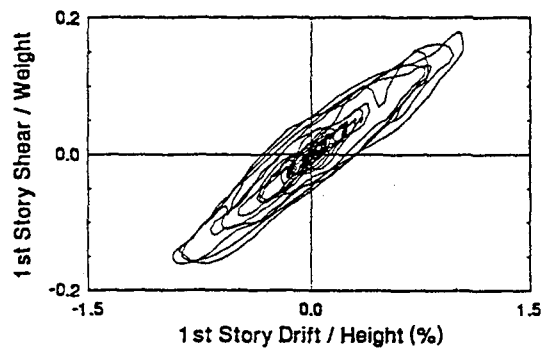
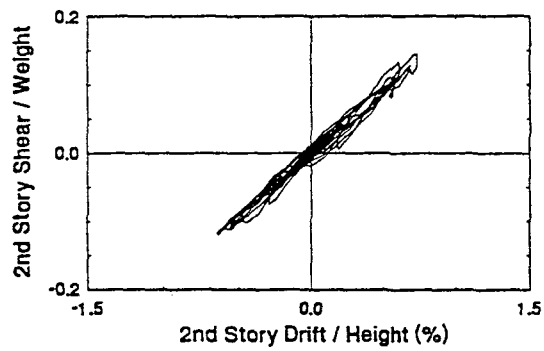
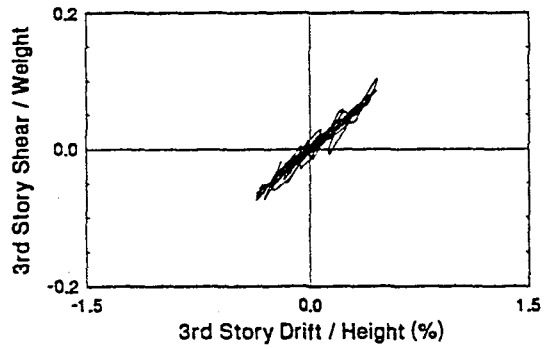
TEST 251
100% Hachinohe-M
Optimal Control - LG



TEST 252

1 25% Hachinohe-M

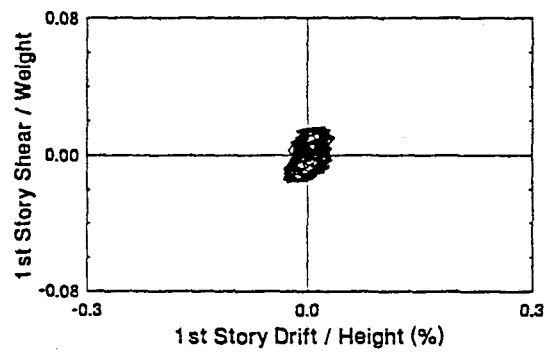
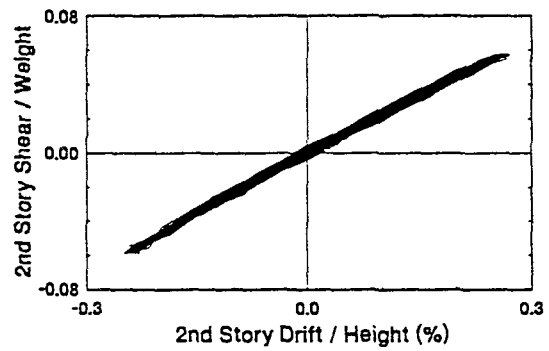
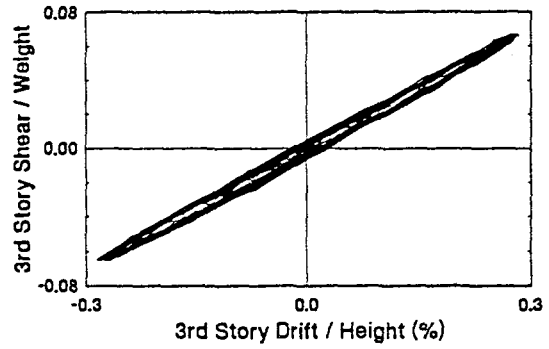
Optimal Control - LG



TEST 253

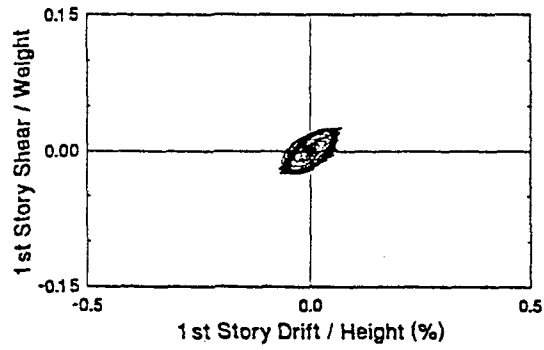
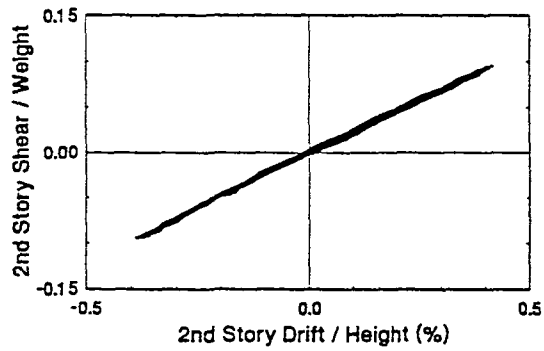
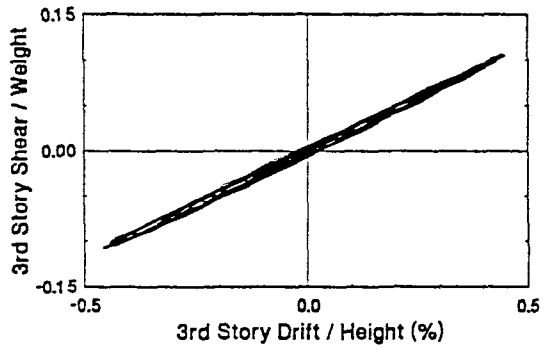
0.2g 5 Hz Harmonic

Optimal Control - LG



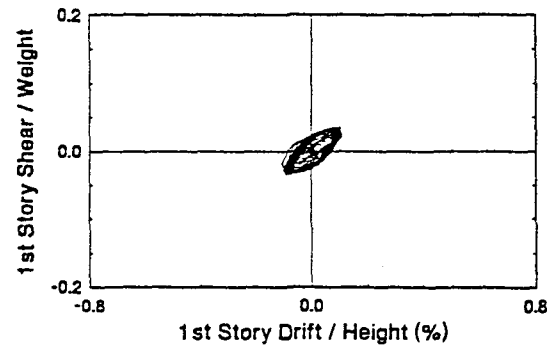
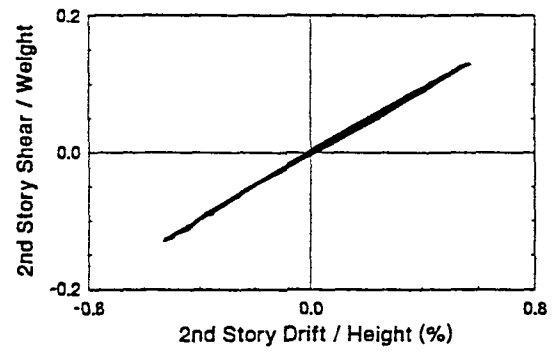
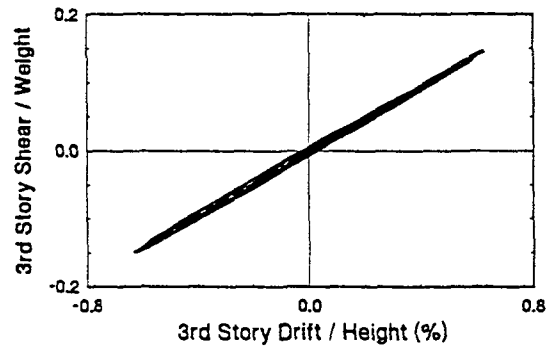
TEST 254

0.3g 5 Hz Harmonic
Optimal Control - LG



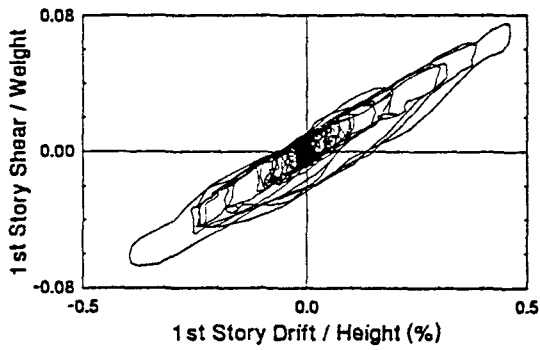
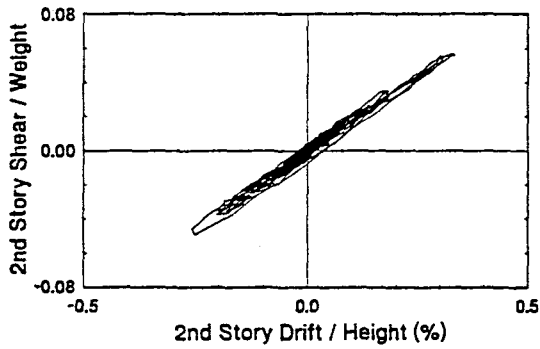
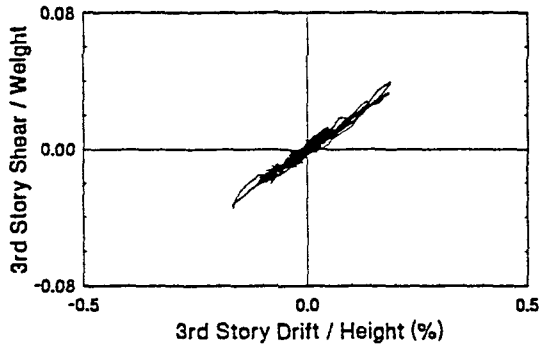
TEST 255

0.4g 5 Hz Harmonic
Optimal Control - LG



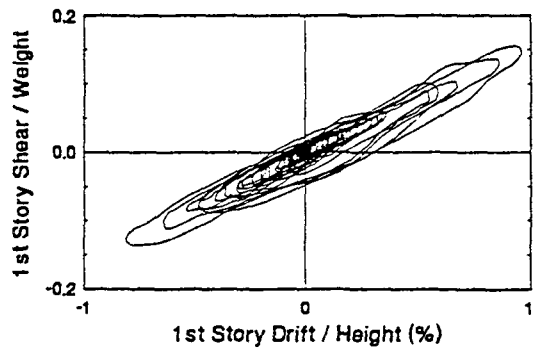
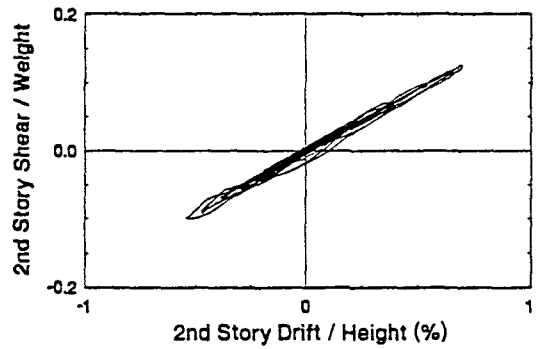
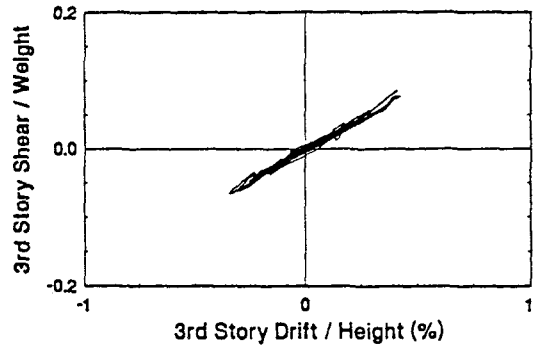
TEST 387

25% El Centro
Optimal Control - HG

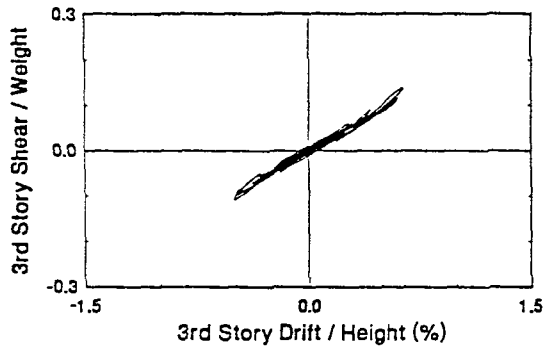


TEST 388

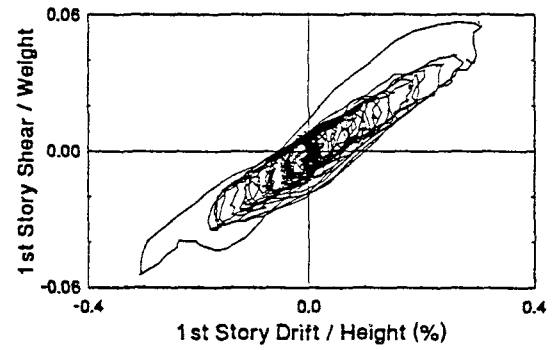
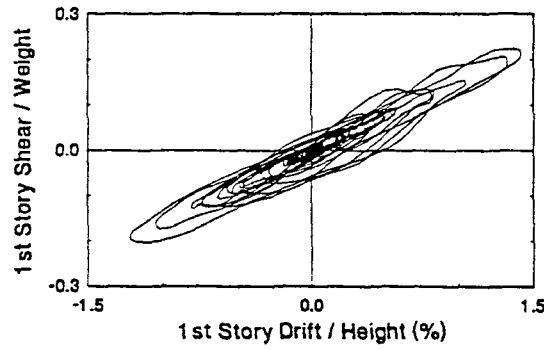
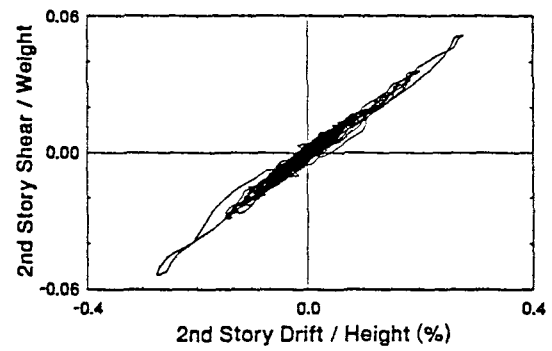
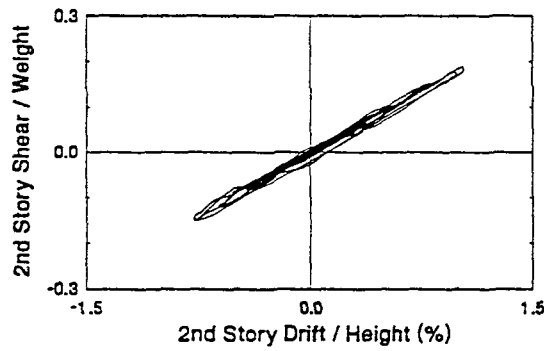
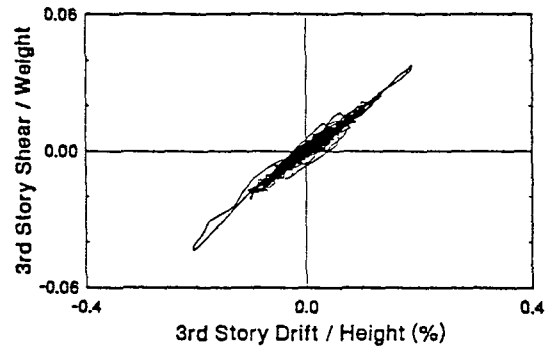
50% El Centro
Optimal Control - HG



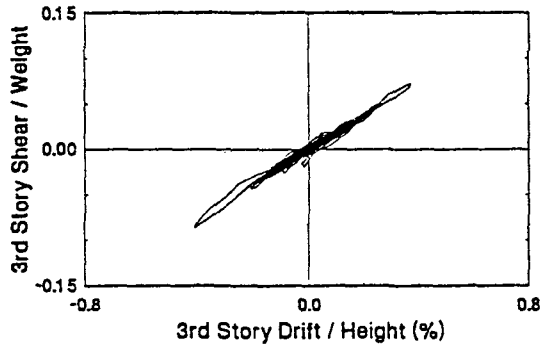
TEST 389
75% El Centro
Optimal Control - HG



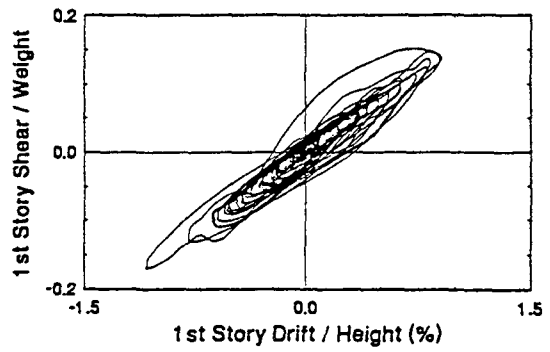
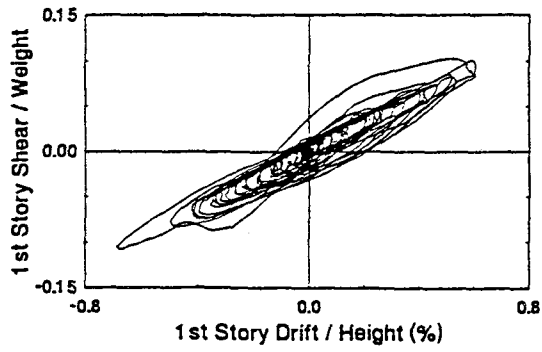
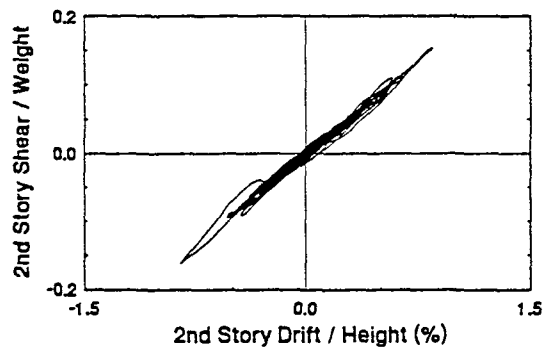
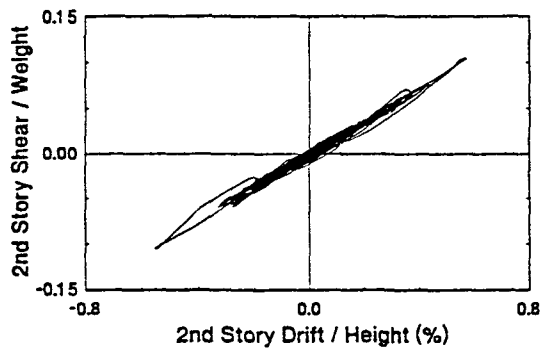
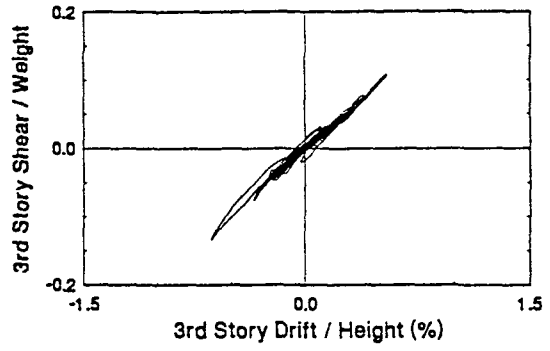
TEST 390
25% Hachinohe
Optimal Control - HG



TEST 391
50% Hachinohe
Optimal Control - HG



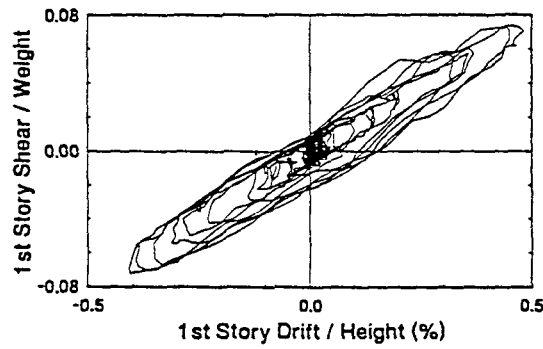
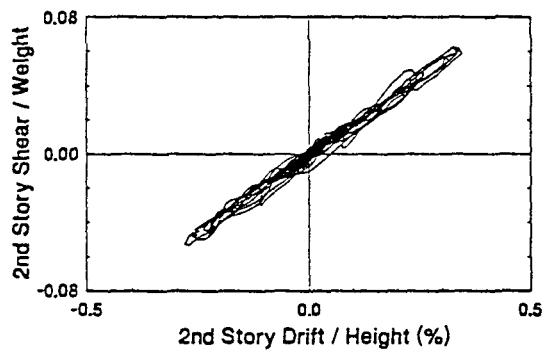
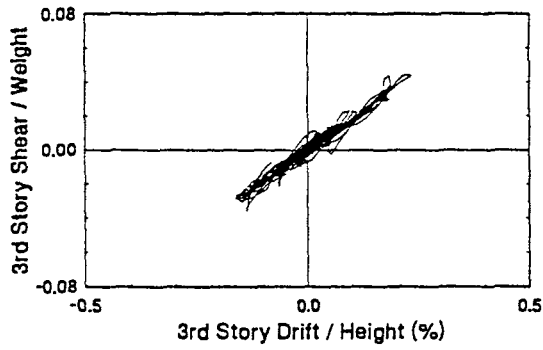
TEST 392
75% Hachinohe
Optimal Control - HG



TEST 393

50% Hachinohe-M

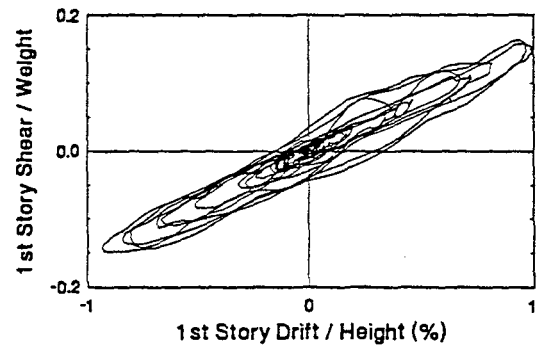
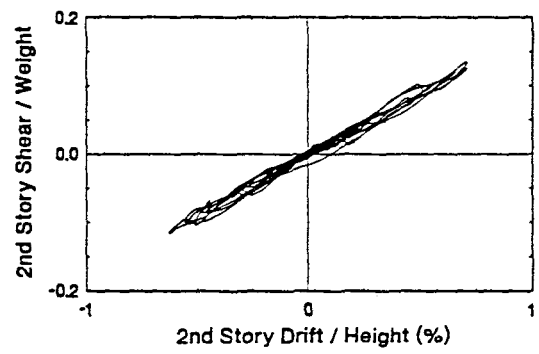
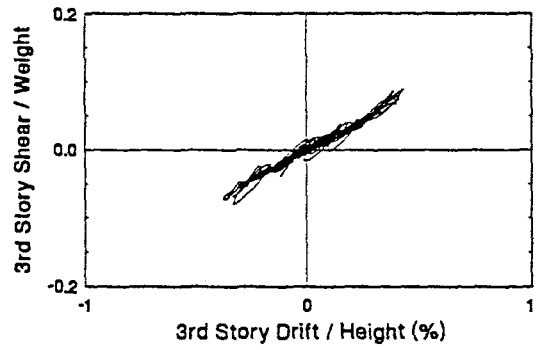
Optimal Control - HG



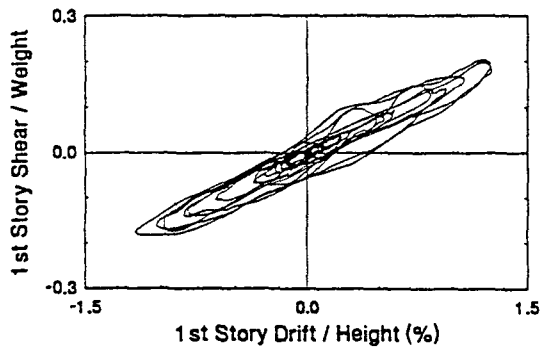
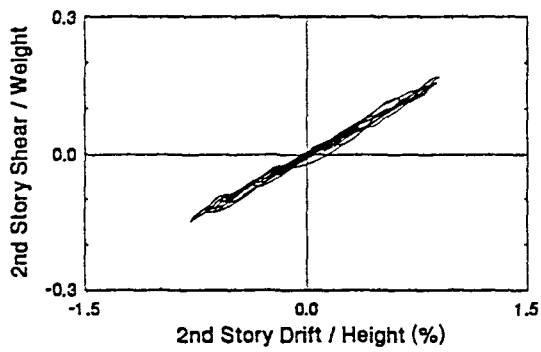
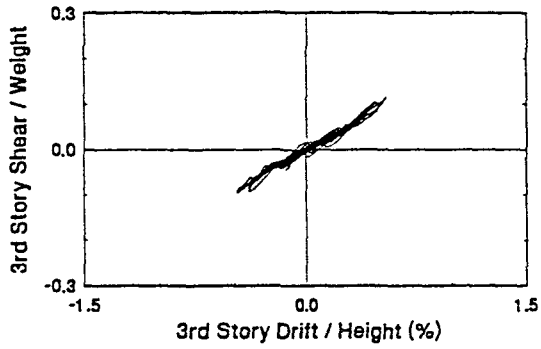
TEST 394

100% Hachinohe-M

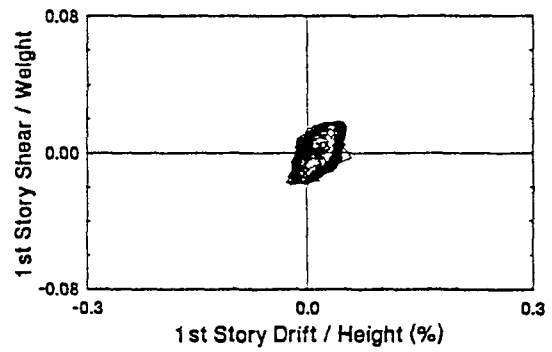
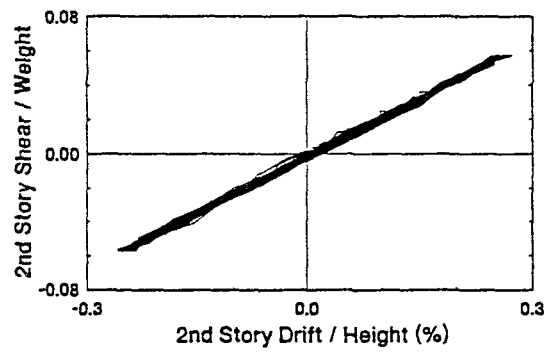
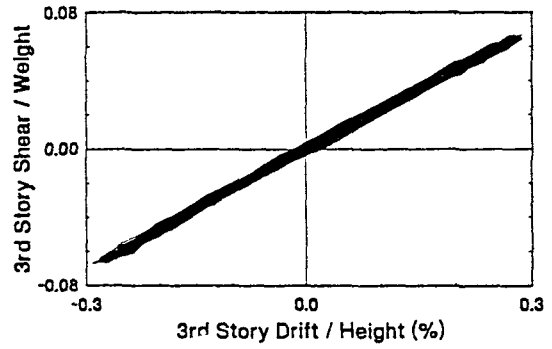
Optimal Control - HG



TEST 395
125% Hachinohe-M
Optimal Control - HG

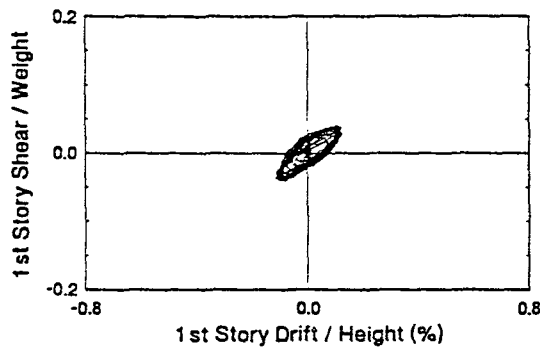
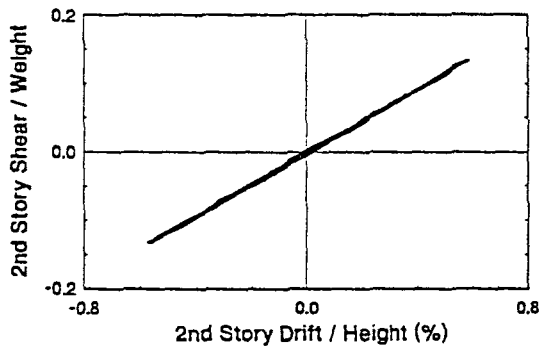
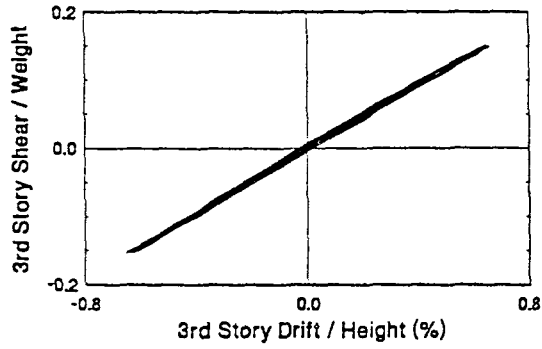


TEST 396
0.2g 5 Hz Harmonic
Optimal Control - HG



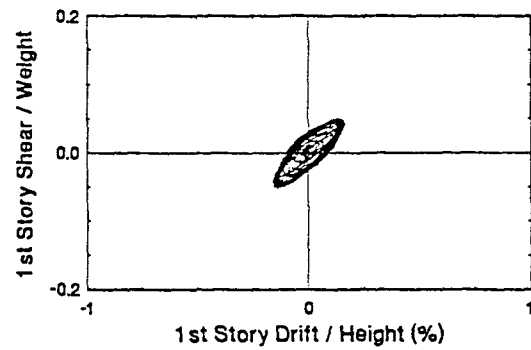
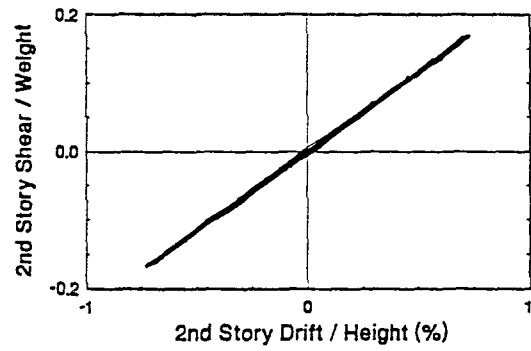
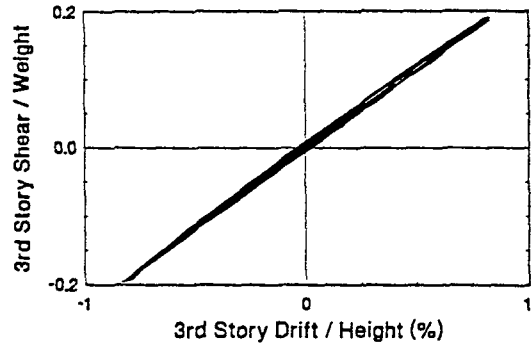
TEST 397

0.4g 5 Hz Harmonic
Optimal Control - HG

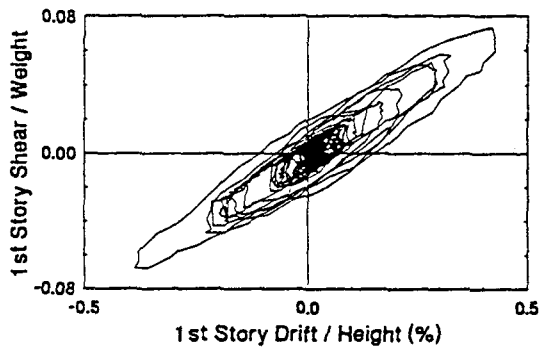
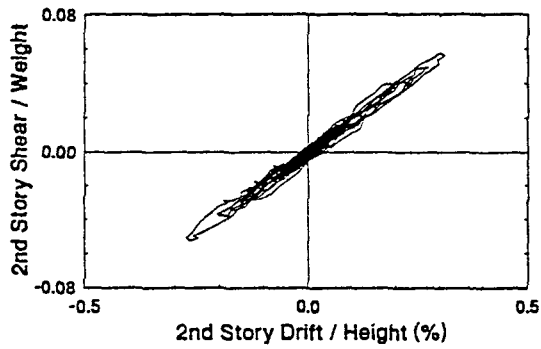
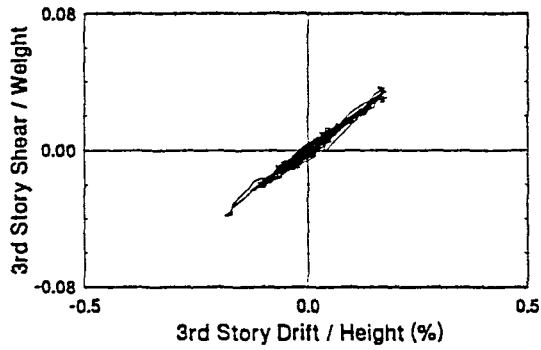


TEST 398

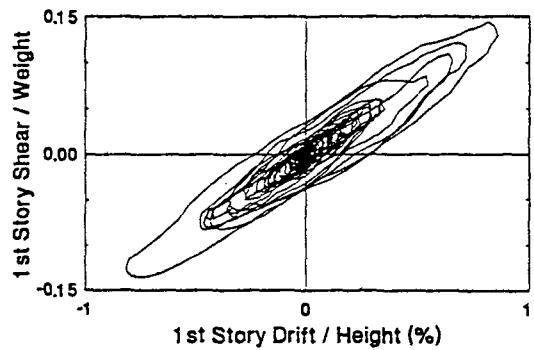
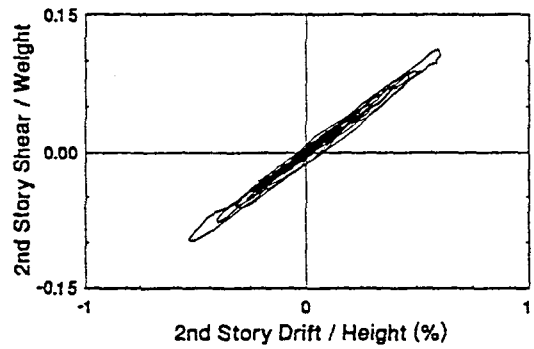
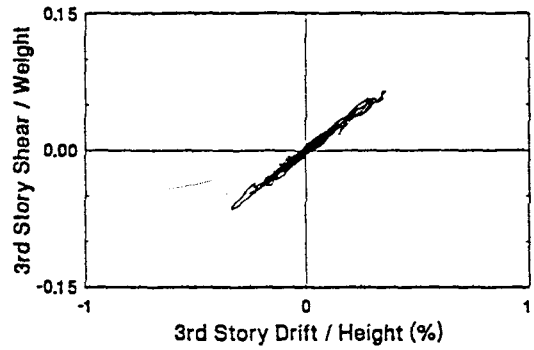
0.5g 5 Hz Harmonic
Optimal Control - HG



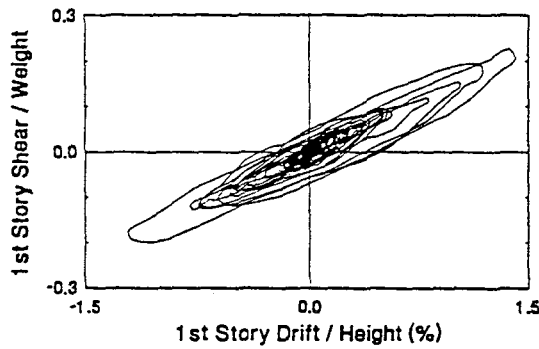
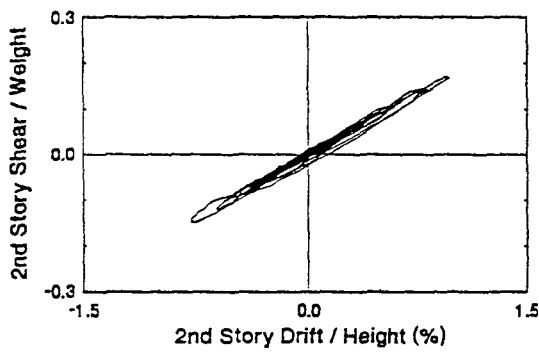
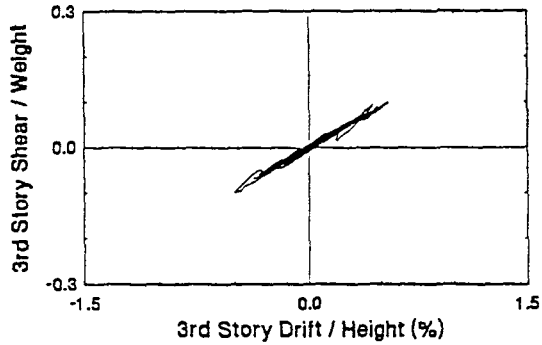
TEST 437
25% El Centro
Optimal Control - LG, HC



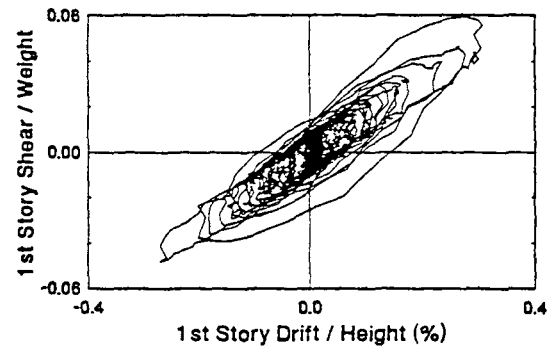
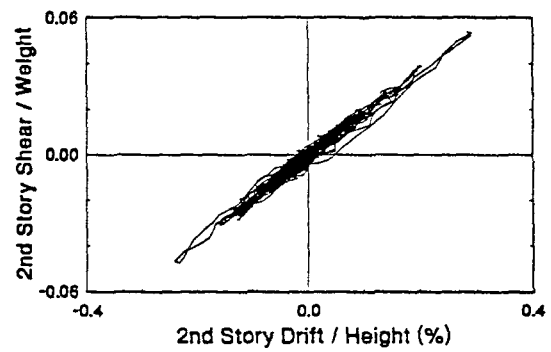
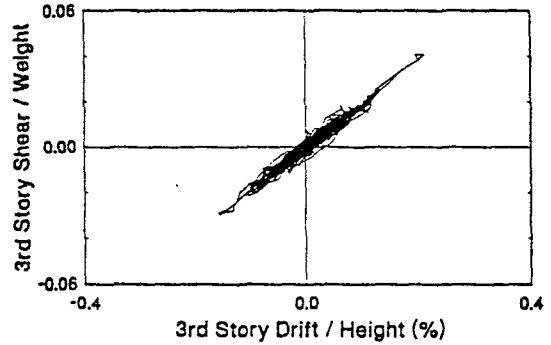
TEST 438
50% El Centro
Optimal Control - LG, HC



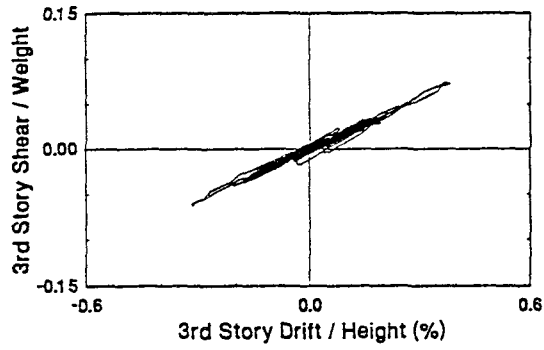
TEST 439
75% El Centro
Optimal Control - LG, HC



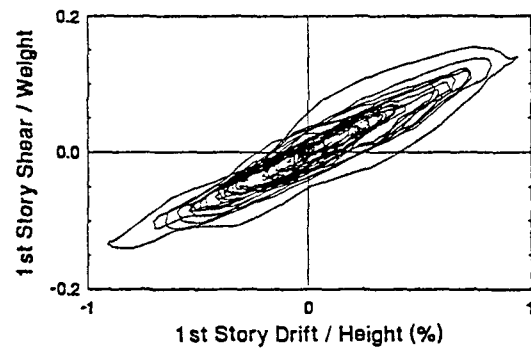
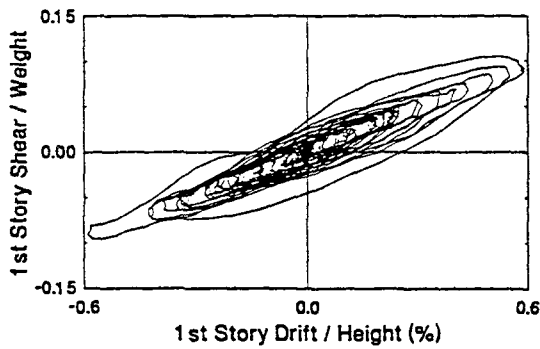
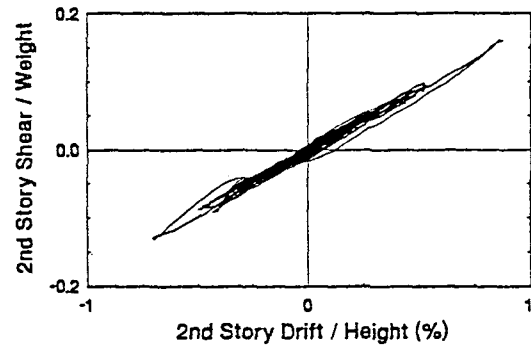
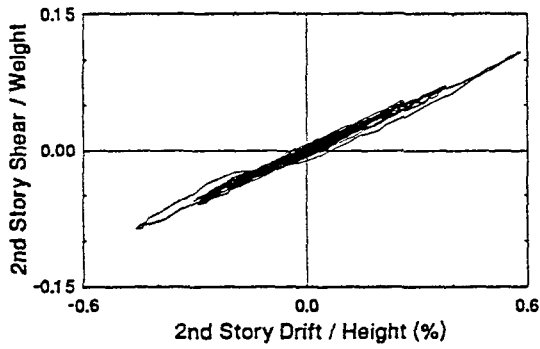
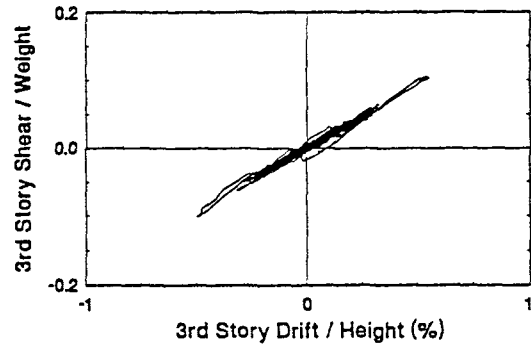
TEST 440
25% Hachinohe
Optimal Control - LG, HC



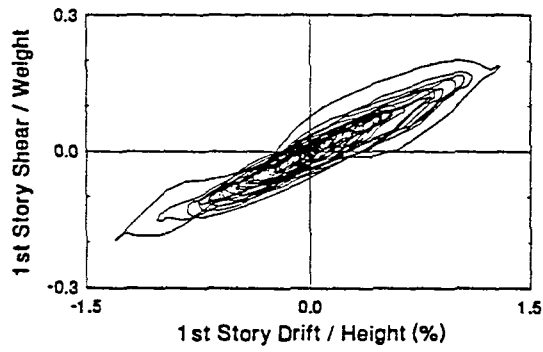
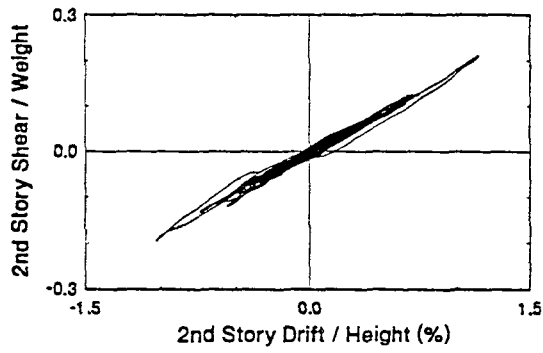
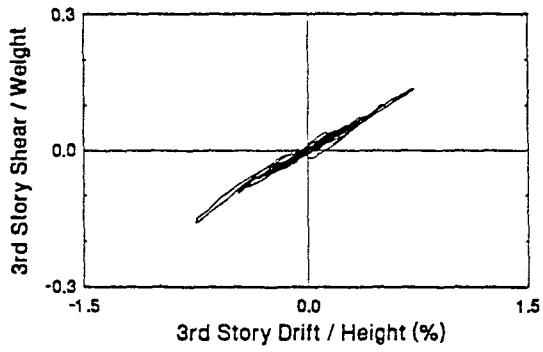
TEST 441
50% Hachinohe
Optimal Control - LG, HC



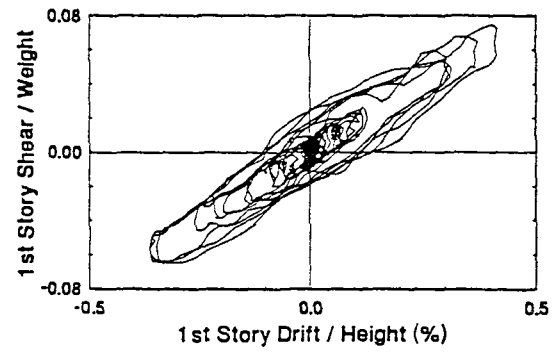
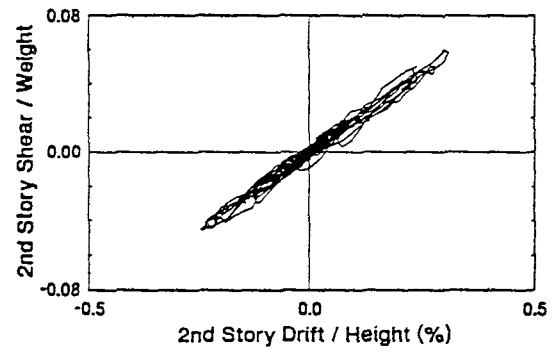
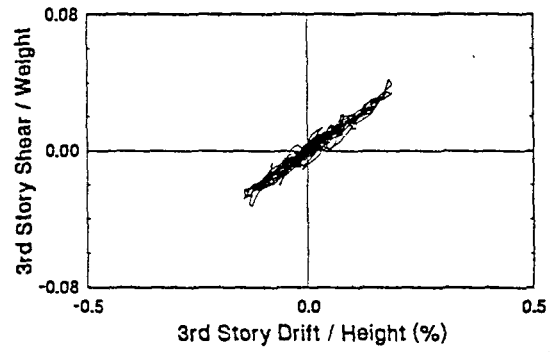
TEST 442
75% Hachinohe
Optimal Control - LG, HC



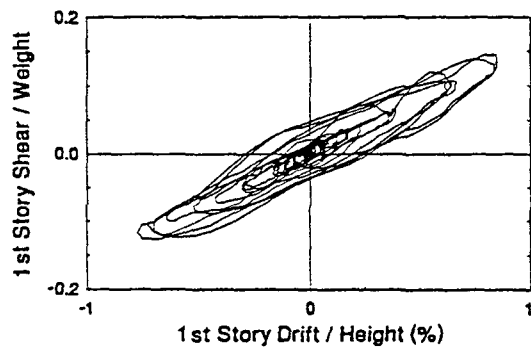
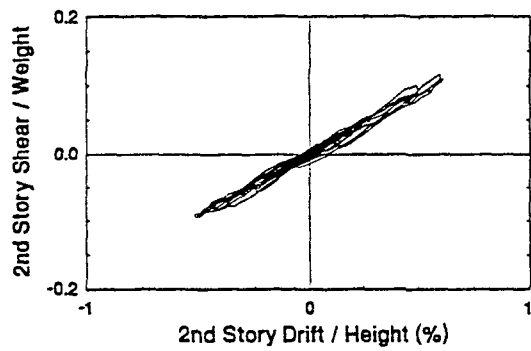
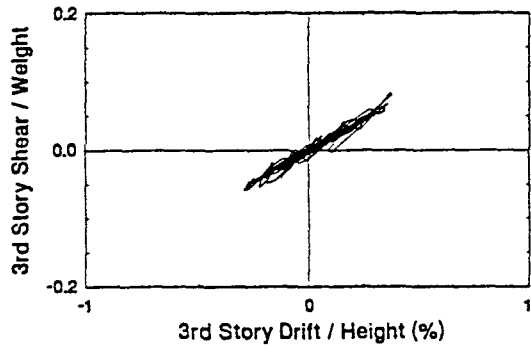
TEST 443
100% Hachinohe
Optimal Control - LG, HC



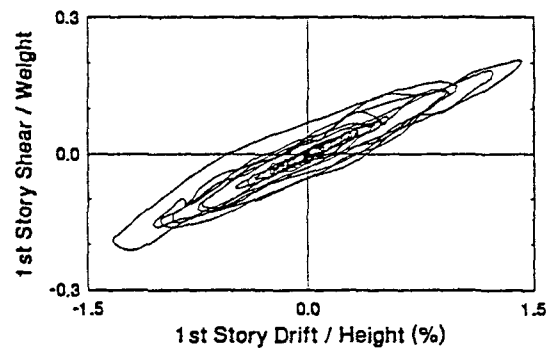
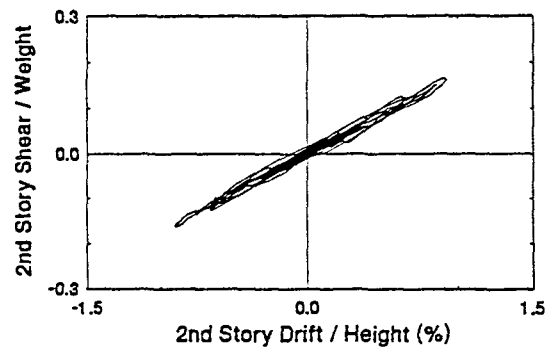
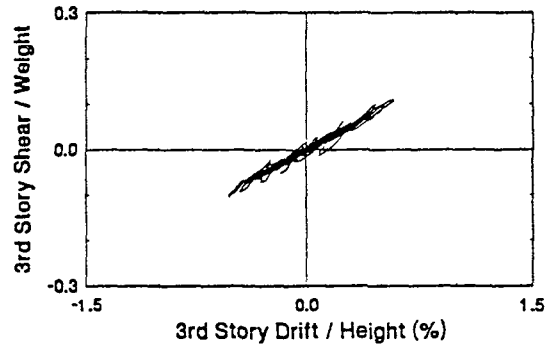
TEST 444
50% Hachinohe-M
Optimal Control - LG, HC



TEST 445
100% Hachinohe-M
Optimal Control - LG, HC

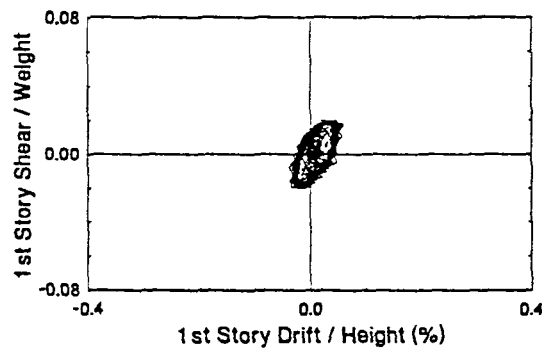
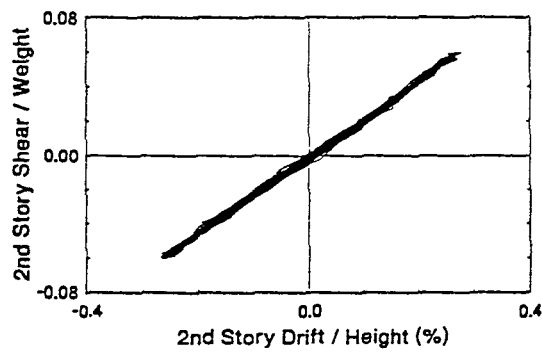
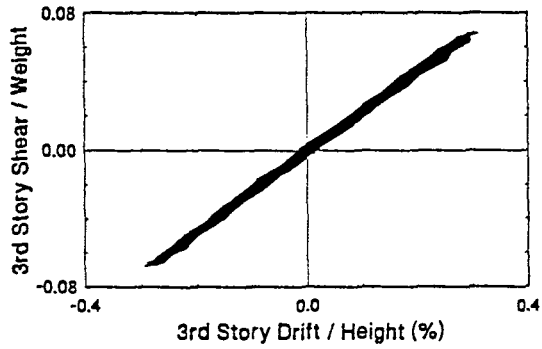


TEST 446
125% Hachinohe-M
Optimal Control - LG, HC



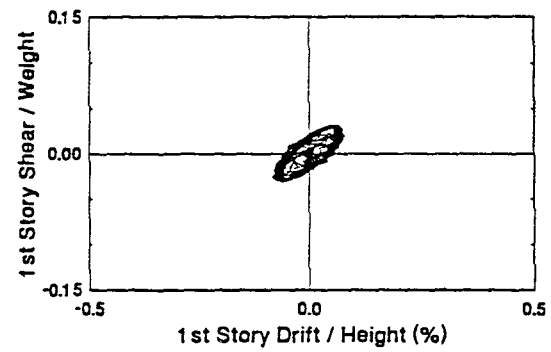
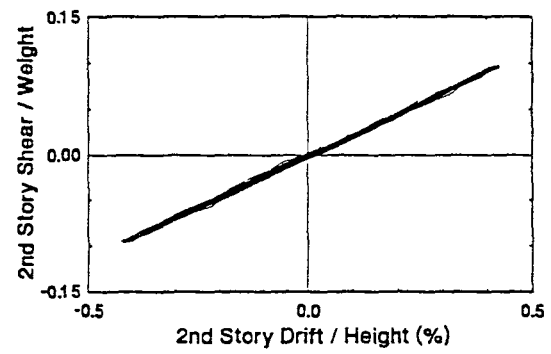
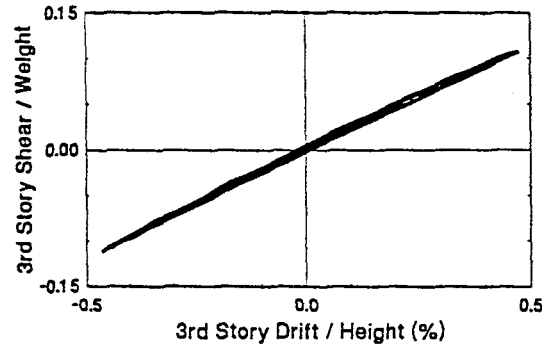
TEST 447

0.2g 5 Hz Harmonic
Optimal Control - LG, HC



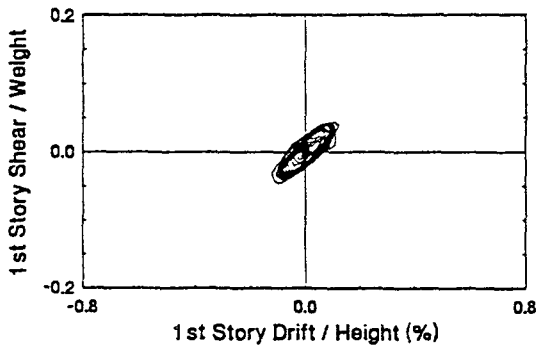
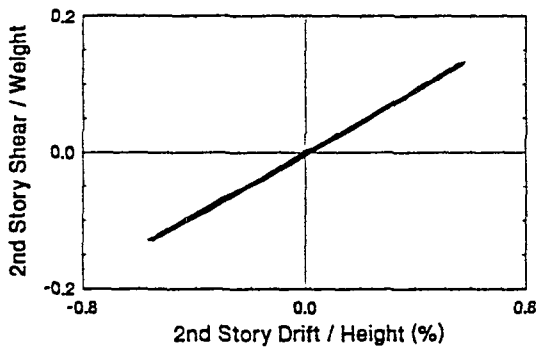
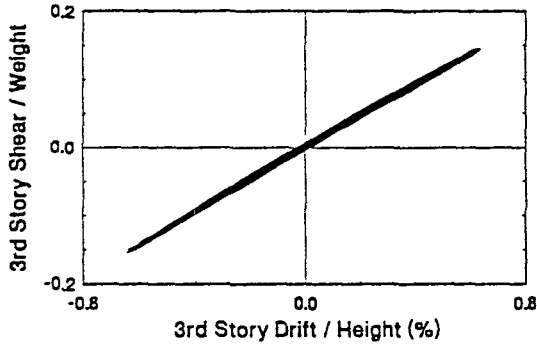
TEST 448

0.3g 5 Hz Harmonic
Optimal Control - LG, HC



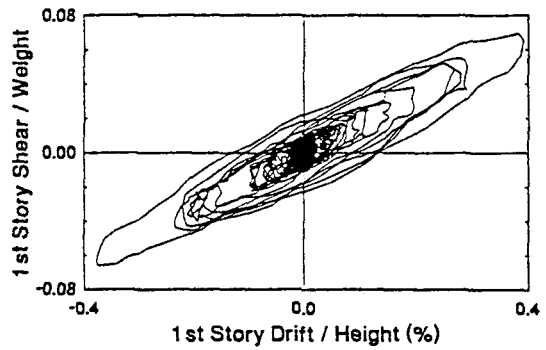
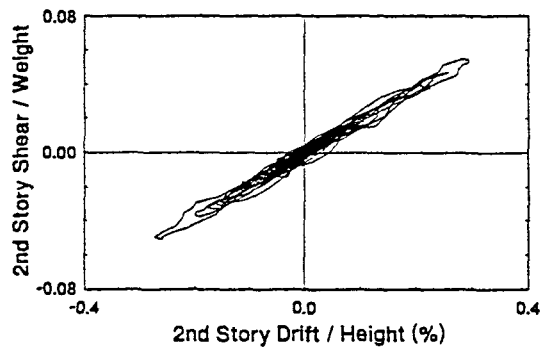
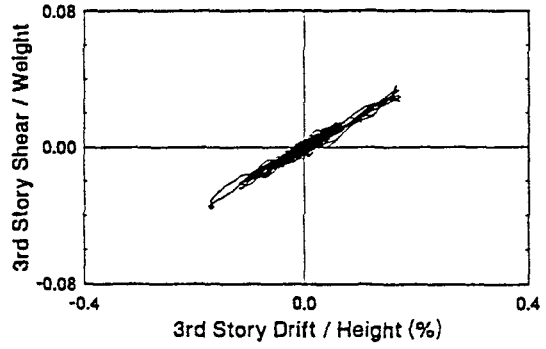
TEST 449

0.4g 5 Hz Harmonic
Optimal Control - LG, HC

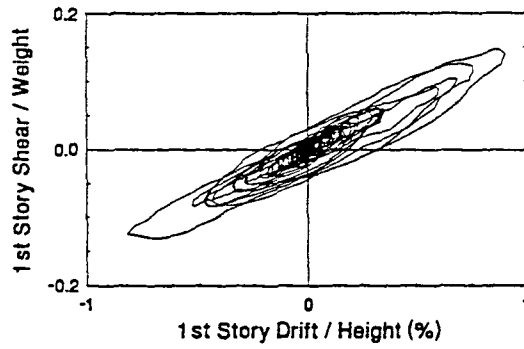
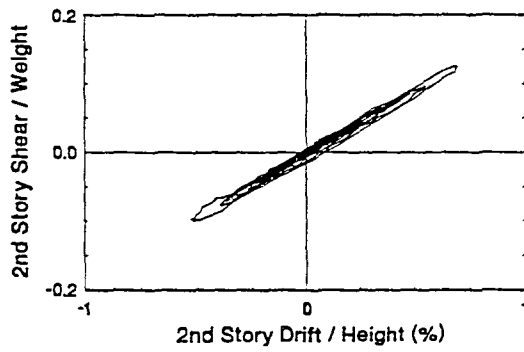
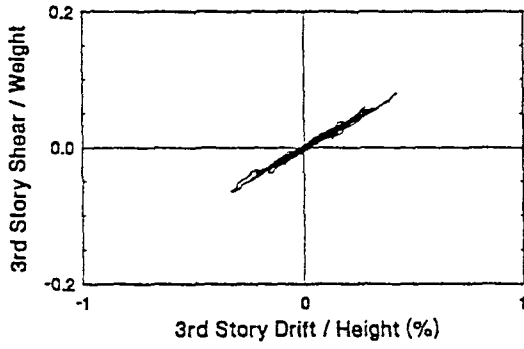


TEST 425

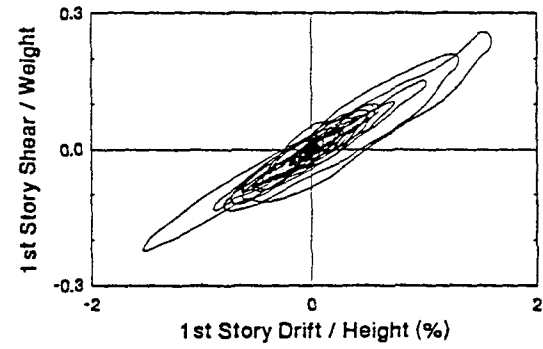
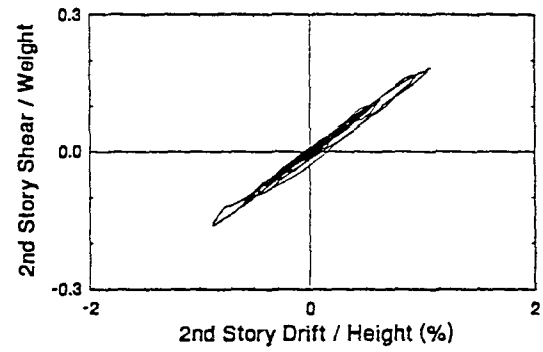
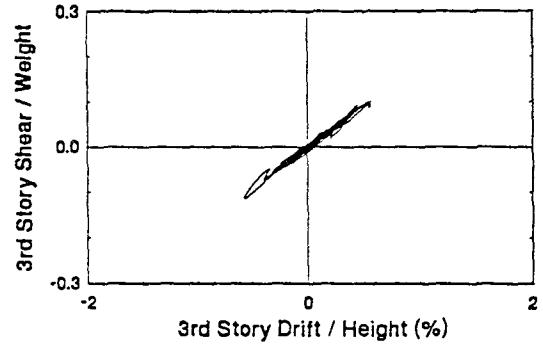
25% EI Centro
Optimal Control - HG, HC



TEST 426
50% El Centro
Optimal Control - HG, HC

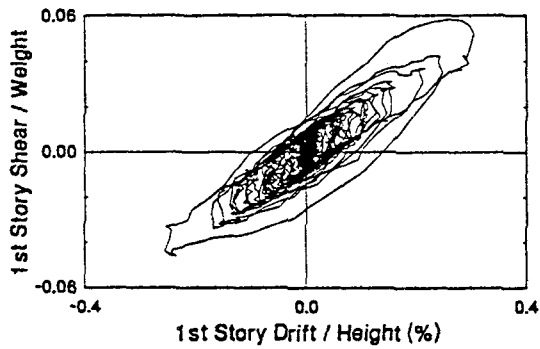
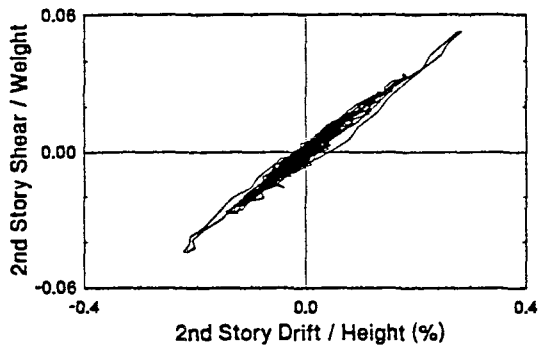
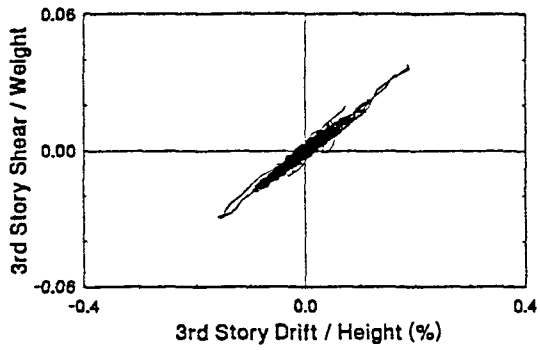


TEST 427
75% El Centro
Optimal Control - HG, HC



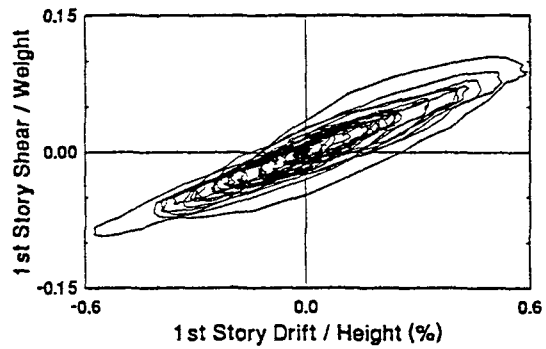
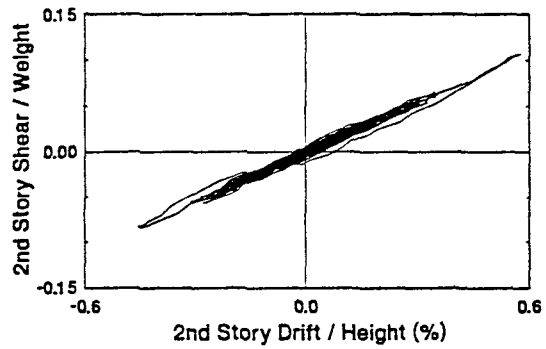
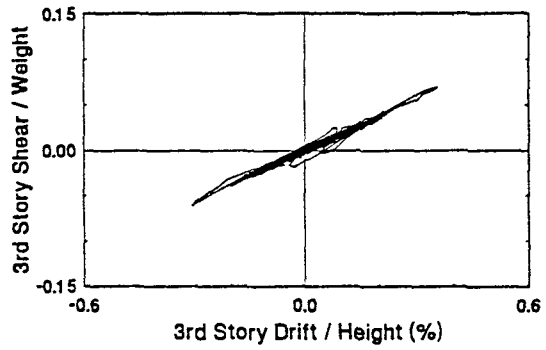
TEST 428

25% Hachinohe
Optimal Control - HG, HC

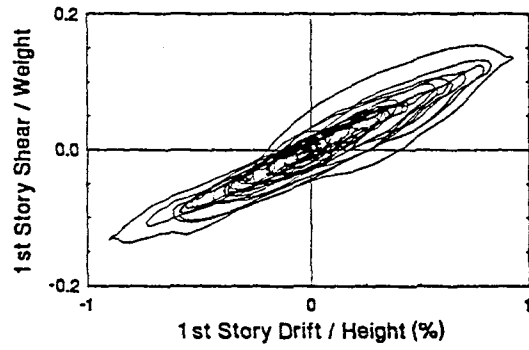
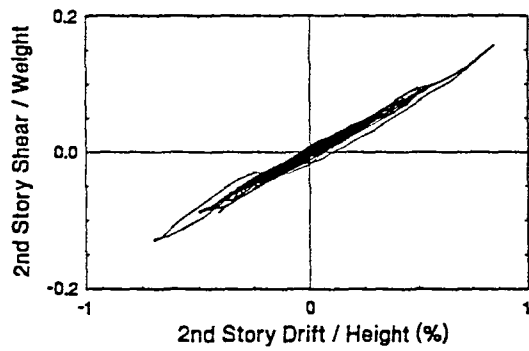
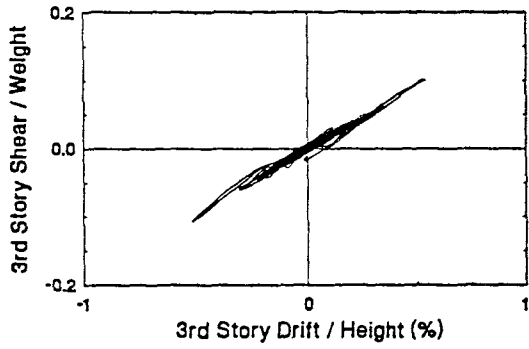


TEST 429

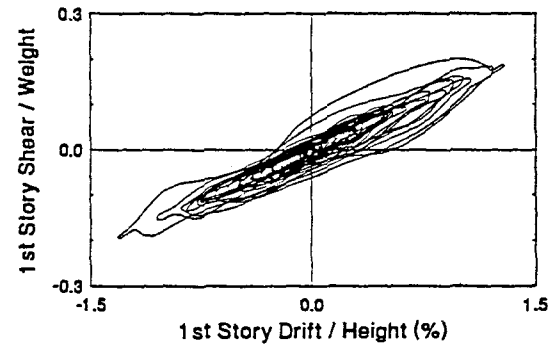
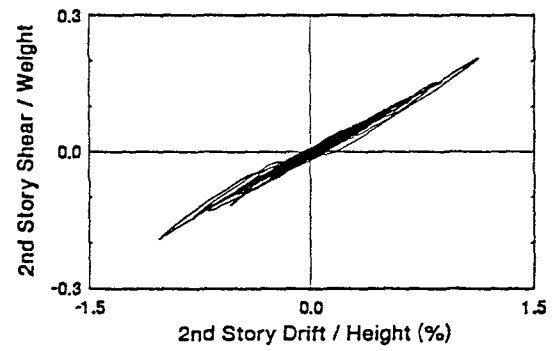
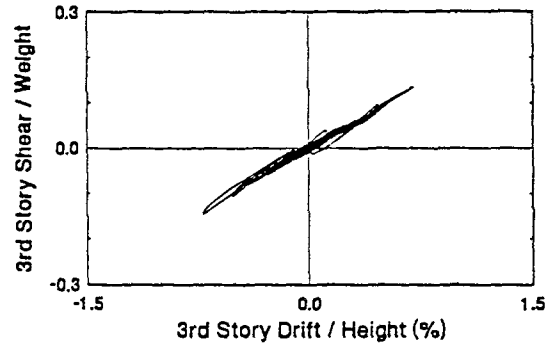
50% Hachinohe
Optimal Control - HG, HC



TEST 430
75% Hachinohe
Optimal Control - HG, HC

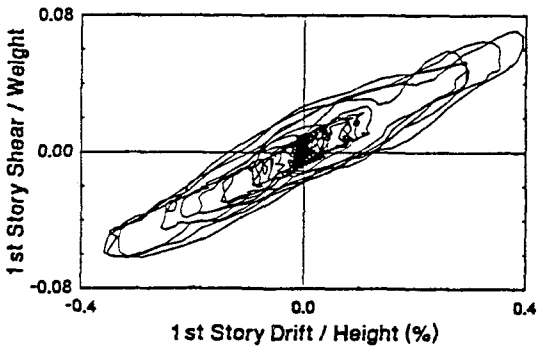
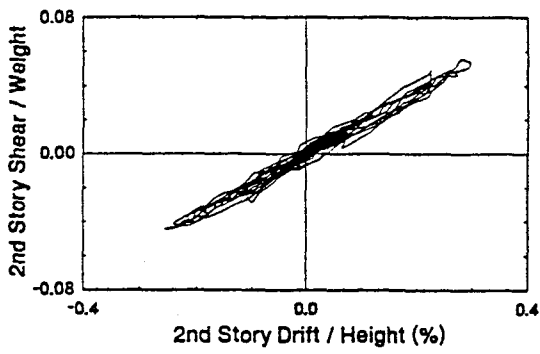
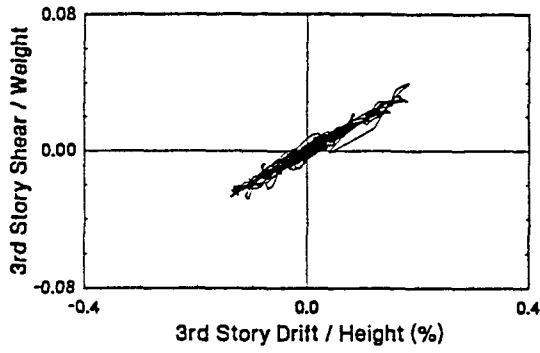


TEST 431
100% Hachinohe
Optimal Control - HG, HC



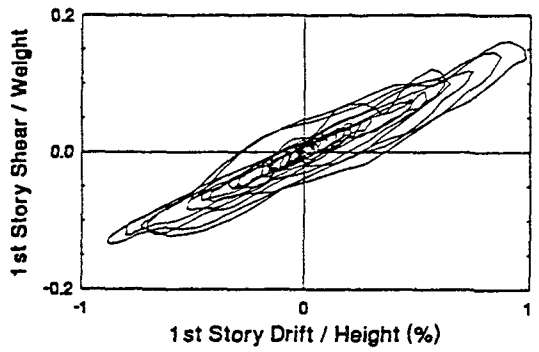
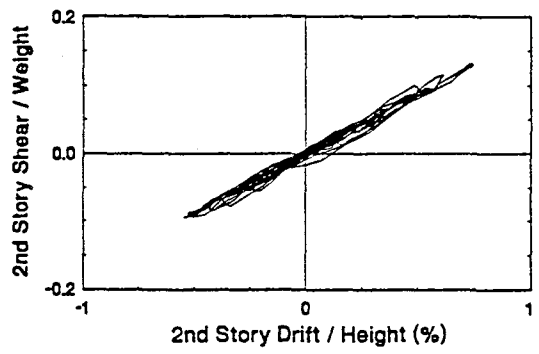
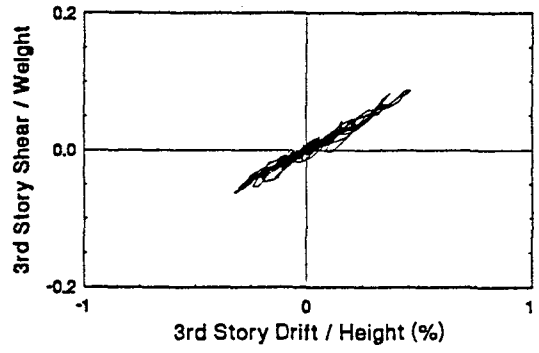
TEST 432

50% Hachinohe-M
Optimal Control - HG, HC



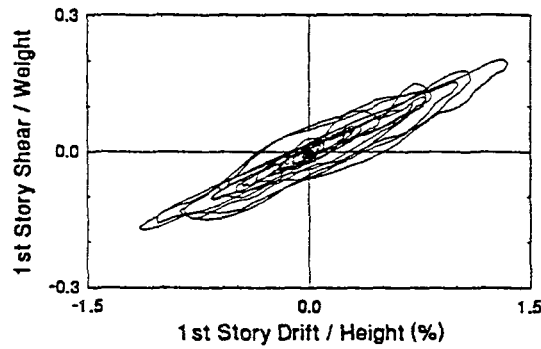
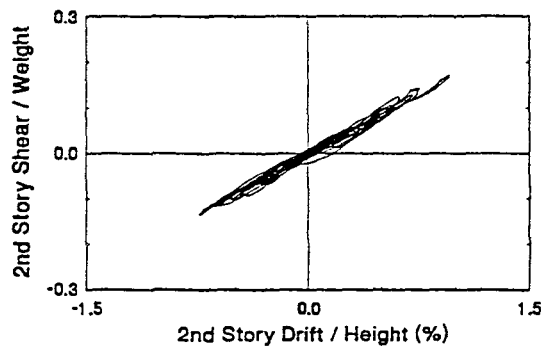
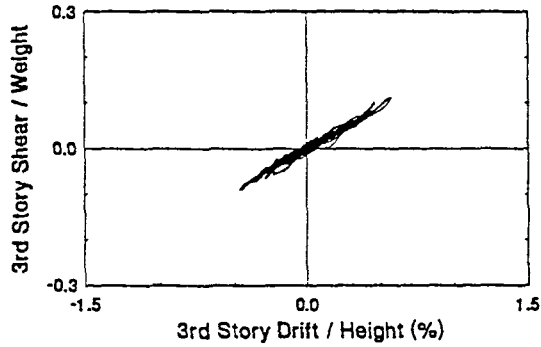
TEST 450

100% Hachinohe-M
Optimal Control - HG, HC



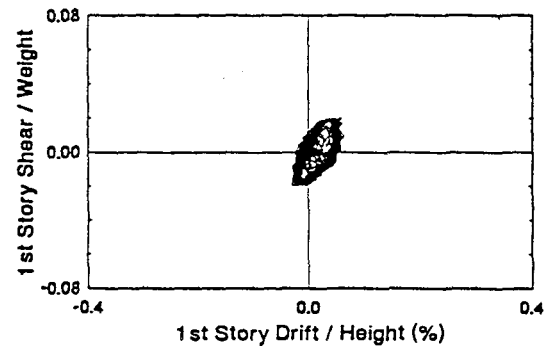
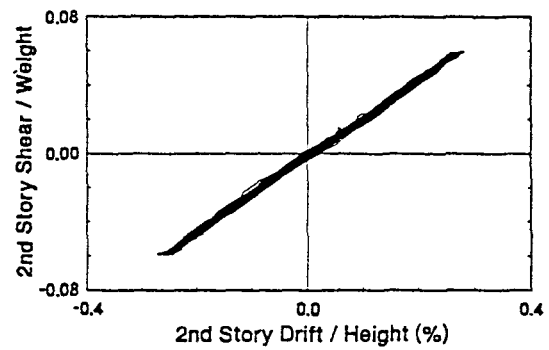
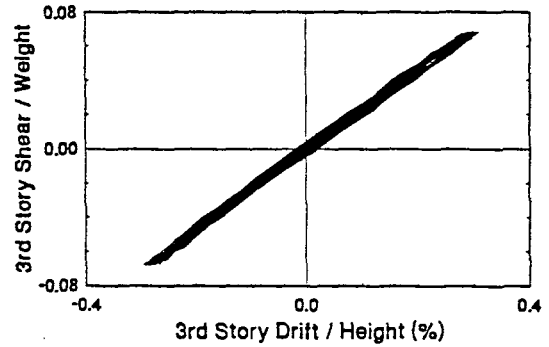
TEST 451

125% Hachinohe-M
Optimal Control - HG, HC



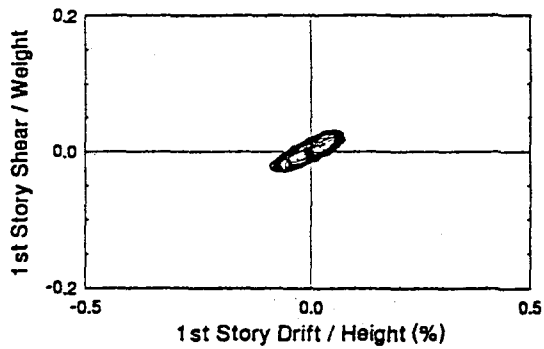
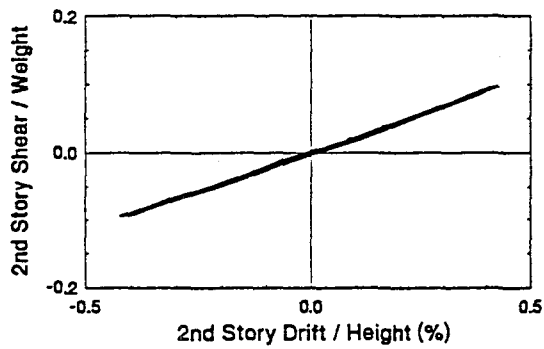
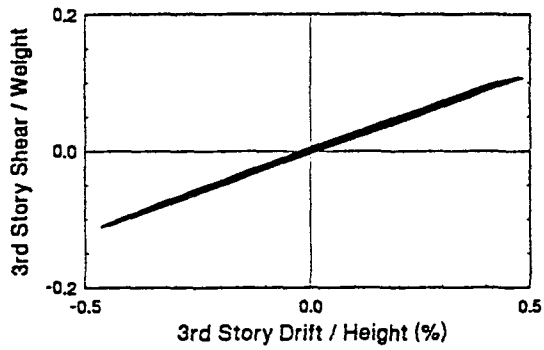
TEST 434

0.2g 5 Hz Harmonic
Optimal Control - HG, HC



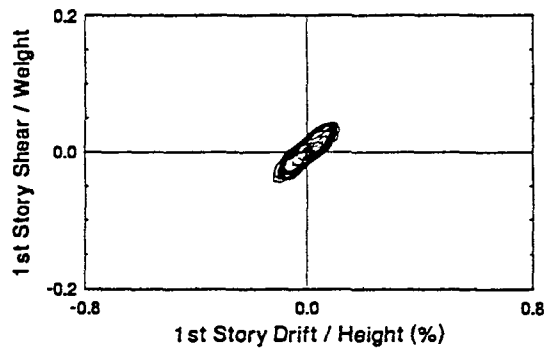
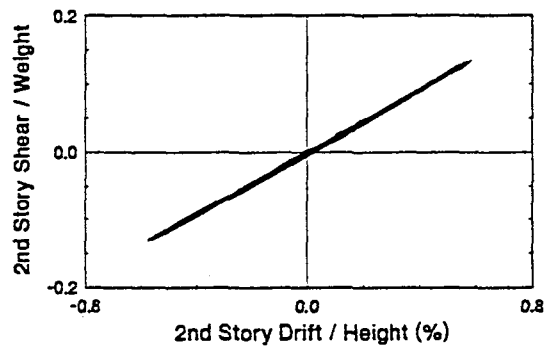
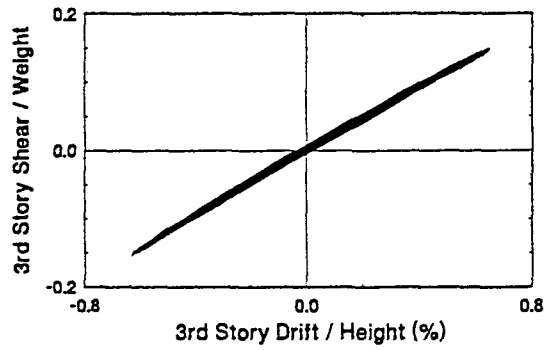
TEST 435

0.3g 5 Hz Harmonic
Optimal Control - HG, HC

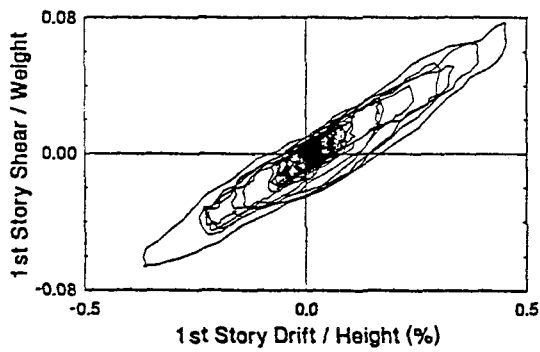
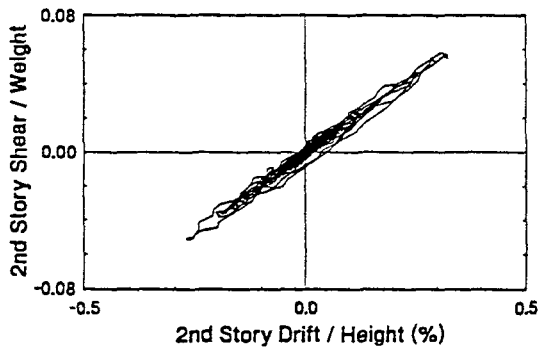
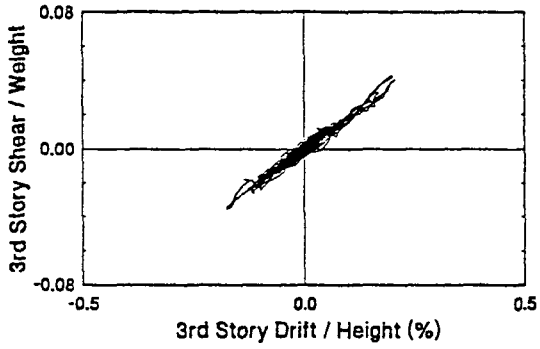


TEST 436

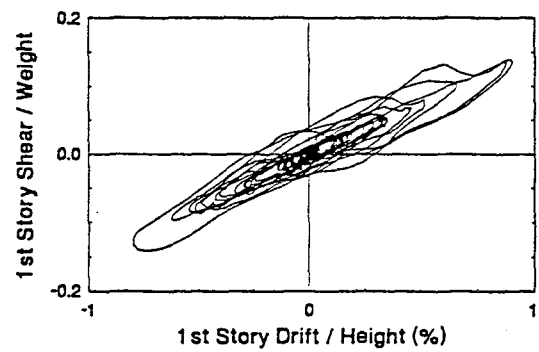
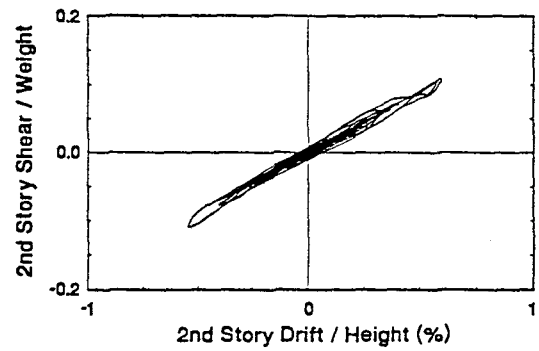
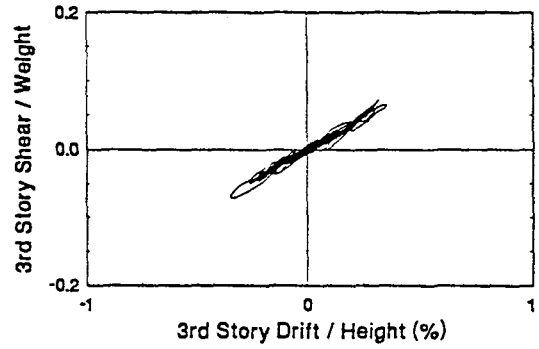
0.4g 5 Hz Harmonic
Optimal Control - HG, HC



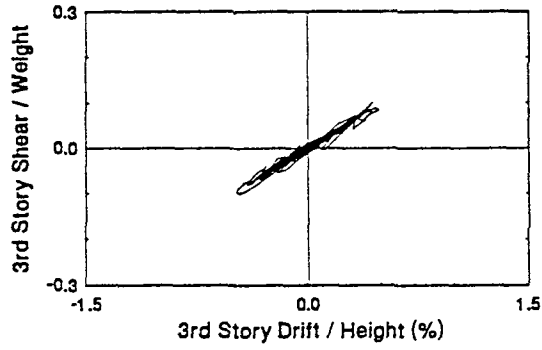
TEST 376
25% El Centro
Sliding Mode Control



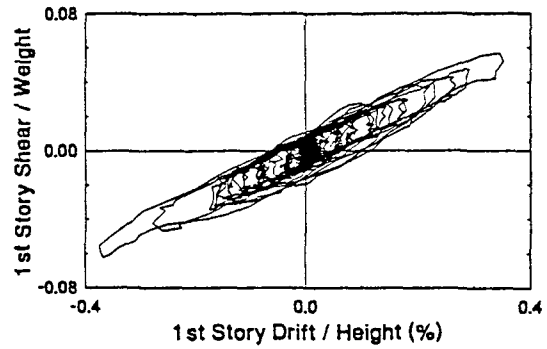
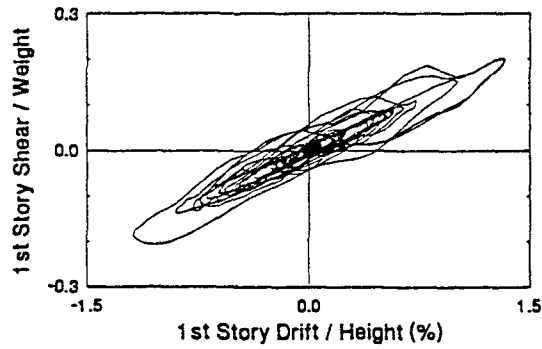
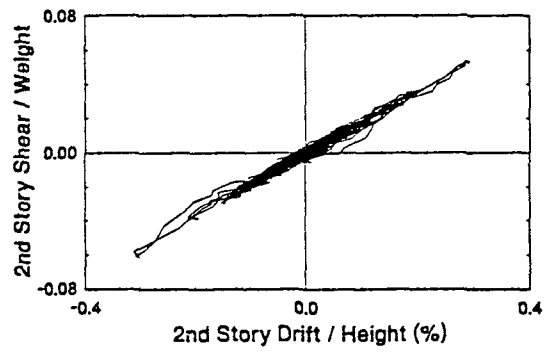
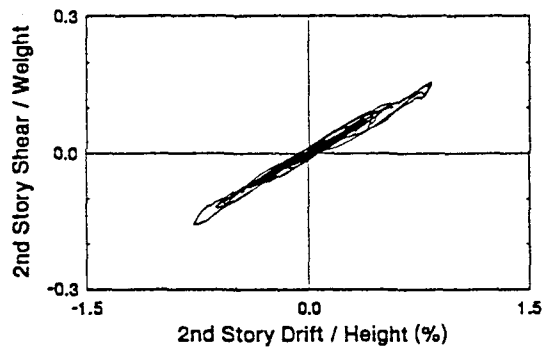
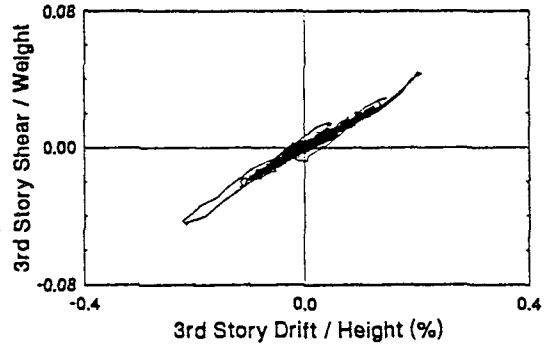
TEST 377
50% El Centro
Sliding Mode Control



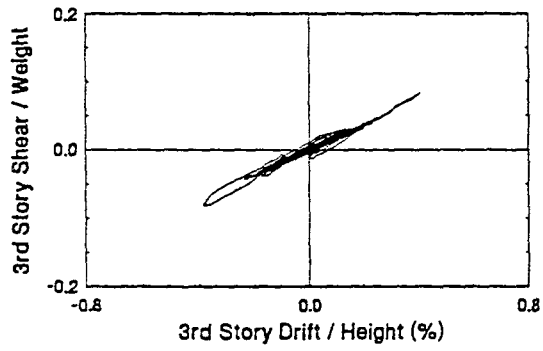
TEST 378
75% El Centro
Sliding Mode Control



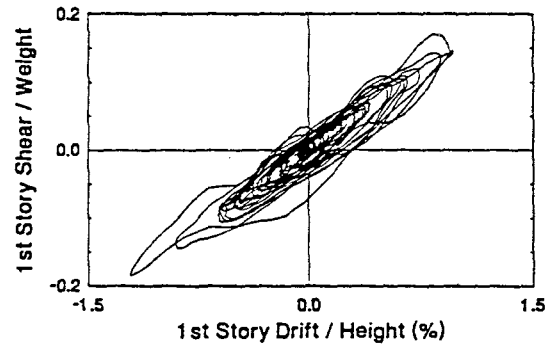
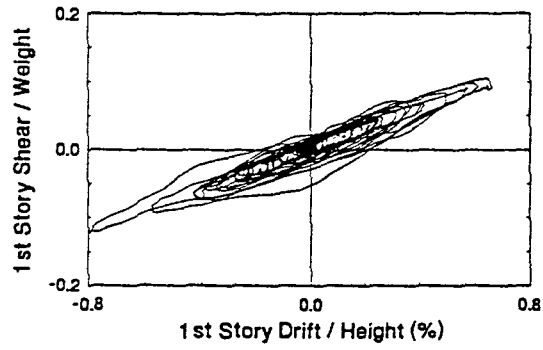
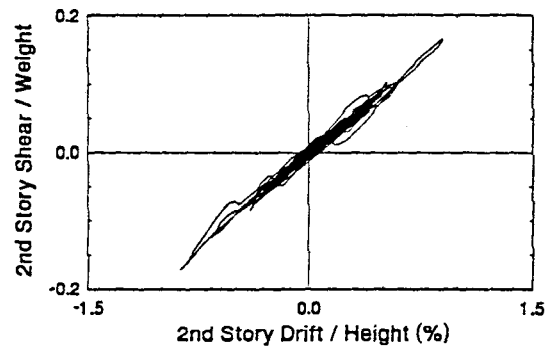
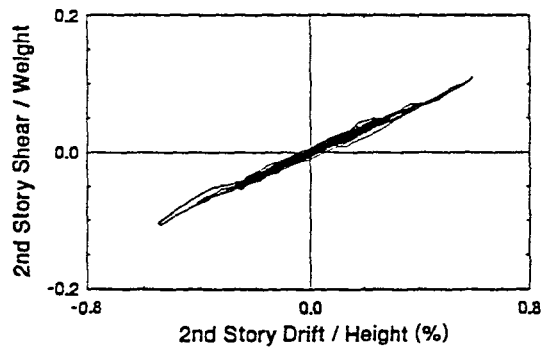
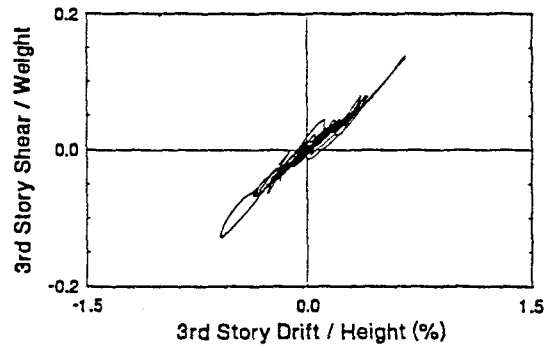
TEST 379
25% Hachinohe
Sliding Mode Control



TEST 380
50% Hachinohe
Sliding Mode Control

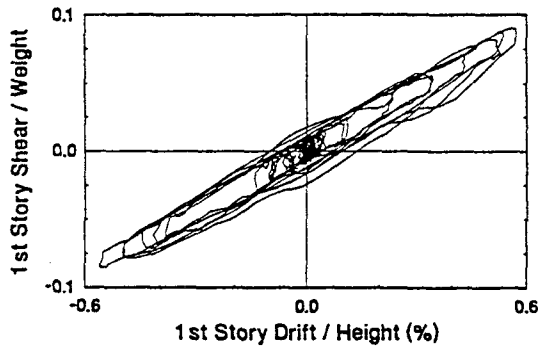
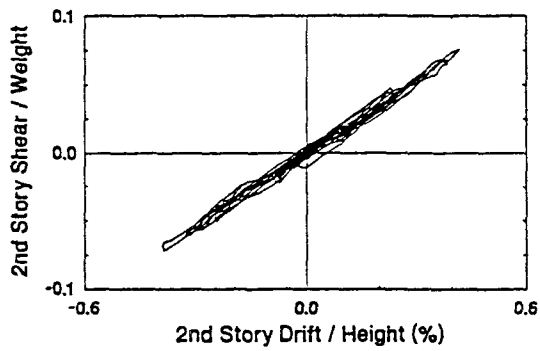
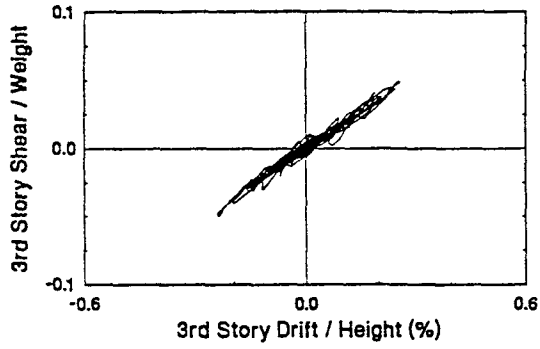


TEST 381
75% Hachinohe
Sliding Mode Control



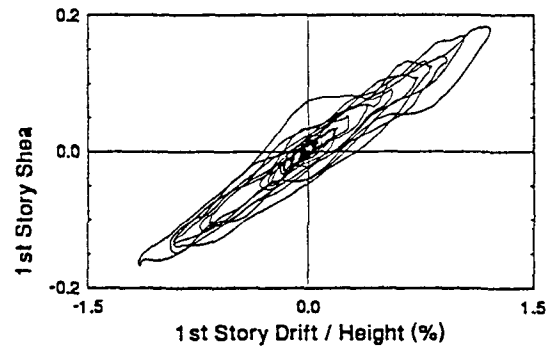
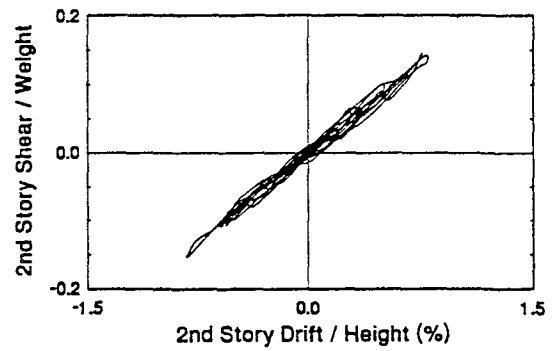
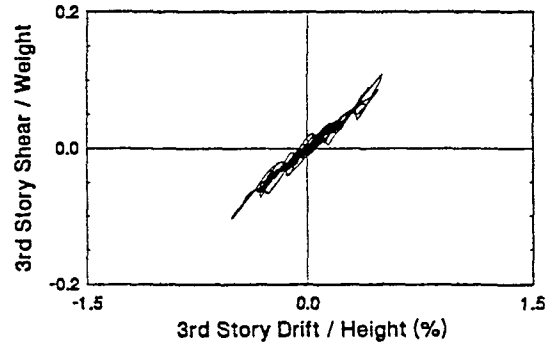
TEST 382

50% Hachinohe-M
Sliding Mode Control



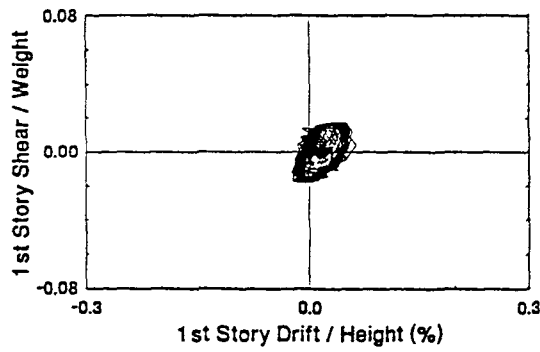
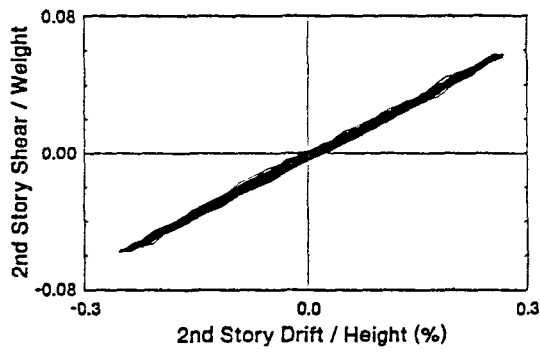
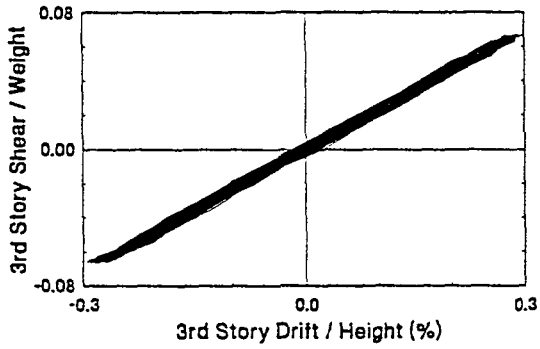
TEST 383

100% Hachinohe-M
Sliding Mode Control



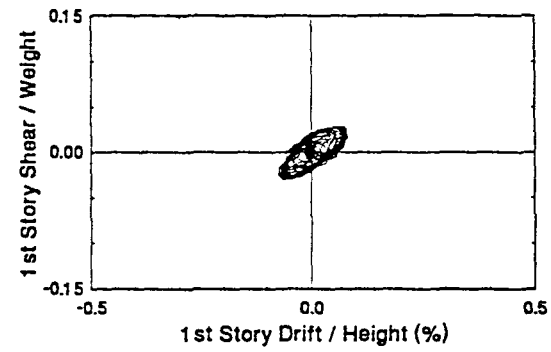
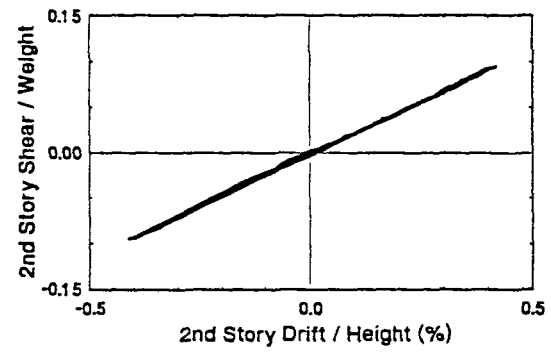
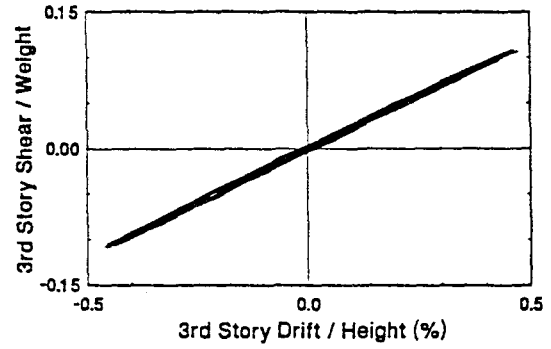
TEST 384

0.2g 5 Hz Harmonic
Sliding Mode Control



TEST 385

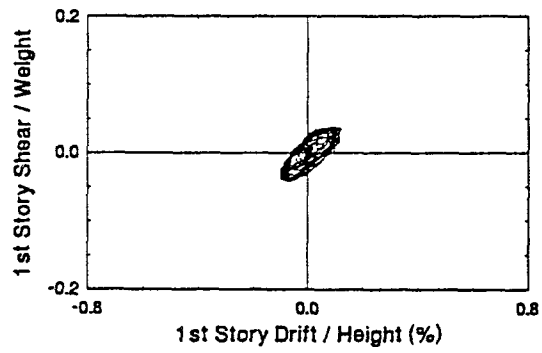
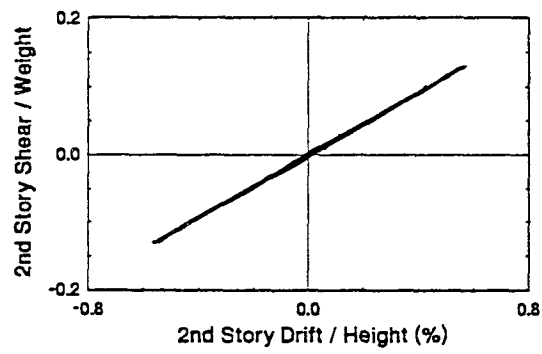
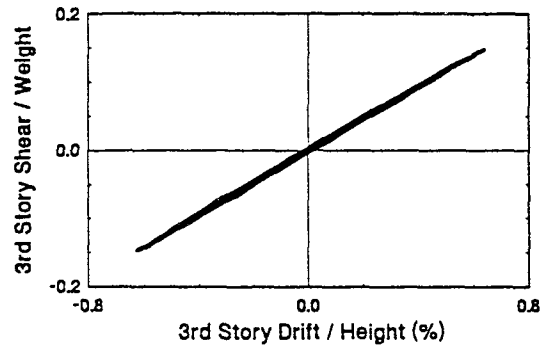
0.3g 5 Hz Harmonic
Sliding Mode Control



TEST 386

0.4g 5 Hz Harmonic

Sliding Mode Control



**NATIONAL CENTER FOR EARTHQUAKE ENGINEERING RESEARCH
LIST OF TECHNICAL REPORTS**

The National Center for Earthquake Engineering Research (NCEER) publishes technical reports on a variety of subjects related to earthquake engineering written by authors funded through NCEER. These reports are available from both NCEER's Publications Department and the National Technical Information Service (NTIS). Requests for reports should be directed to the Publications Department, National Center for Earthquake Engineering Research, State University of New York at Buffalo, Red Jacket Quadrangle, Buffalo, New York 14261. Reports can also be requested through NTIS, 5285 Port Royal Road, Springfield, Virginia 22161. NTIS accession numbers are shown in parenthesis, if available.

- NCEER-87-0001 "First-Year Program in Research, Education and Technology Transfer," 3/5/87, (PB88-134275).
- NCEER-87-0002 "Experimental Evaluation of Instantaneous Optimal Algorithms for Structural Control," by R.C. Lin, T.T. Soong and A.M. Reinhorn, 4/20/87, (PB88-134341).
- NCEER-87-0003 "Experimentation Using the Earthquake Simulation Facilities at University at Buffalo," by A.M. Reinhorn and R.L. Ketter, to be published.
- NCEER-87-0004 "The System Characteristics and Performance of a Shaking Table," by J.S. Hwang, K.C. Chang and G.C. Lee, 6/1/87, (PB88-134259). This report is available only through NTIS (see address given above).
- NCEER-87-0005 "A Finite Element Formulation for Nonlinear Viscoplastic Material Using a Q Model," by O. Gyebi and G. Dasgupta, 11/2/87, (PB88-213764).
- NCEER-87-0006 "Symbolic Manipulation Program (SMP) - Algebraic Codes for Two and Three Dimensional Finite Element Formulations," by X. Lee and G. Dasgupta, 11/9/87, (PB88-218522).
- NCEER-87-0007 "Instantaneous Optimal Control Laws for Tall Buildings Under Seismic Excitations," by J.N. Yang, A. Akbarpour and P. Ghaemmaghami, 6/10/87, (PB88-134333). This report is only available through NTIS (see address given above).
- NCEER-87-0008 "IDARC: Inelastic Damage Analysis of Reinforced Concrete Frame - Shear-Wall Structures," by Y.J. Park, A.M. Reinhorn and S.K. Kunnath, 7/20/87, (PB88-134325).
- NCEER-87-0009 "Liquefaction Potential for New York State: A Preliminary Report on Sites in Manhattan and Buffalo," by M. Budhu, V. Vijayakumar, R.F. Giese and L. Baumgras, 8/31/87, (PB88-163704). This report is available only through NTIS (see address given above).
- NCEER-87-0010 "Vertical and Torsional Vibration of Foundations in Inhomogeneous Media," by A.S. Veletsos and K.W. Dotson, 6/1/87, (PB88-134291).
- NCEER-87-0011 "Seismic Probabilistic Risk Assessment and Seismic Margins Studies for Nuclear Power Plants," by Howard H.M. Hwang, 6/15/87, (PB88-134267).
- NCEER-87-0012 "Parametric Studies of Frequency Response of Secondary Systems Under Ground-Acceleration Excitations," by Y. Yong and Y.K. Lin, 6/10/87, (PB88-134309).
- NCEER-87-0013 "Frequency Response of Secondary Systems Under Seismic Excitation," by J.A. HoLung, J. Cai and Y.K. Lin, 7/31/87, (PB88-134317).
- NCEER-87-0014 "Modelling Earthquake Ground Motions in Seismically Active Regions Using Parametric Time Series Methods," by G.W. Ellis and A.S. Cakmak, 8/25/87, (PB88-134283).
- NCEER-87-0015 "Detection and Assessment of Seismic Structural Damage," by E. DiPasquale and A.S. Cakmak, 8/25/87, (PB88-163712).

- NCEER-87-0016 "Pipeline Experiment at Parkfield, California," by J. Isenberg and E. Richardson, 9/15/87, (PB88-163720). This report is available only through NTIS (see address given above).
- NCEER-87-0017 "Digital Simulation of Seismic Ground Motion," by M. Shinozuka, G. Deodatis and T. Harada, 8/31/87, (PB88-155197). This report is available only through NTIS (see address given above).
- NCEER-87-0018 "Practical Considerations for Structural Control: System Uncertainty, System Time Delay and Truncation of Small Control Forces," J.N. Yang and A. Akbarpour, 8/10/87, (PB88-163738).
- NCEER-87-0019 "Modal Analysis of Nonclassically Damped Structural Systems Using Canonical Transformation," by J.N. Yang, S. Sarkani and F.X. Long, 9/27/87, (PB88-187851).
- NCEER-87-0020 "A Nonstationary Solution in Random Vibration Theory," by J.R. Red-Horse and P.D. Spanos, 11/3/87, (PB88-163746).
- NCEER-87-0021 "Horizontal Impedances for Radially Inhomogeneous Viscoelastic Soil Layers," by A.S. Veletsos and K.W. Dotson, 10/15/87, (PB88-150859).
- NCEER-87-0022 "Seismic Damage Assessment of Reinforced Concrete Members," by Y.S. Chung, C. Meyer and M. Shinozuka, 10/9/87, (PB88-150867). This report is available only through NTIS (see address given above).
- NCEER-87-0023 "Active Structural Control in Civil Engineering," by T.T. Soong, 11/11/87, (PB88-187778).
- NCEER-87-0024 "Vertical and Torsional Impedances for Radially Inhomogeneous Viscoelastic Soil Layers," by K.W. Dotson and A.S. Veletsos, 12/87, (PB88-187786).
- NCEER-87-0025 "Proceedings from the Symposium on Seismic Hazards, Ground Motions, Soil-Liquefaction and Engineering Practice in Eastern North America," October 20-22, 1987, edited by K.H. Jacob, 12/87, (PB88-188115).
- NCEER-87-0026 "Report on the Whittier-Narrows, California, Earthquake of October 1, 1987," by J. Pantelic and A. Reinhorn, 11/87, (PB88-187752). This report is available only through NTIS (see address given above).
- NCEER-87-0027 "Design of a Modular Program for Transient Nonlinear Analysis of Large 3-D Building Structures," by S. Srivastav and J.F. Abel, 12/30/87, (PB88-187950).
- NCEER-87-0028 "Second-Year Program in Research, Education and Technology Transfer," 3/8/88, (PB88-219480).
- NCEER-88-0001 "Workshop on Seismic Computer Analysis and Design of Buildings With Interactive Graphics," by W. McGuire, J.F. Abel and C.H. Conley, 1/18/88, (PB88-187760).
- NCEER-88-0002 "Optimal Control of Nonlinear Flexible Structures," by J.N. Yang, F.X. Long and D. Wong, 1/22/88, (PB88-213772).
- NCEER-88-0003 "Substructuring Techniques in the Time Domain for Primary-Secondary Structural Systems," by G.D. Manolis and G. Juhn, 2/10/88, (PB88-213780).
- NCEER-88-0004 "Iterative Seismic Analysis of Primary-Secondary Systems," by A. Singhal, L.D. Lutes and P.D. Spanos, 2/23/88, (PB88-213798).
- NCEER-88-0005 "Stochastic Finite Element Expansion for Random Media," by P.D. Spanos and R. Ghanem, 3/14/88, (PB88-213806).
- NCEER-88-0006 "Combining Structural Optimization and Structural Control," by F.Y. Cheng and C.P. Pantelides, 1/10/88, (PB88-213814).

- NCEER-88-0007 "Seismic Performance Assessment of Code-Designed Structures," by H.H-M. Hwang, J-W. Jaw and H-J. Shau, 3/20/88, (PB88-219423).
- NCEER-88-0008 "Reliability Analysis of Code-Designed Structures Under Natural Hazards," by H.H-M. Hwang, H. Ushiba and M. Shinozuka, 2/29/88, (PB88-229471).
- NCEER-88-0009 "Seismic Fragility Analysis of Shear Wall Structures," by J-W Jaw and H.H-M. Hwang, 4/30/88, (PB89-102867).
- NCEER-88-0010 "Base Isolation of a Multi-Story Building Under a Harmonic Ground Motion - A Comparison of Performances of Various Systems," by F-G Fan, G. Ahmadi and I.G. Tadjbakhsh, 5/18/88, (PB89-122238).
- NCEER-88-0011 "Seismic Floor Response Spectra for a Combined System by Green's Functions," by F.M. Lavelle, L.A. Bergman and P.D. Spanos, 5/1/88, (PB89-102875).
- NCEER-88-0012 "A New Solution Technique for Randomly Excited Hysteretic Structures," by G.Q. Cai and Y.K. Lin, 5/16/88, (PB89-102883).
- NCEER-88-0013 "A Study of Radiation Damping and Soil-Structure Interaction Effects in the Centrifuge," by K. Weissman, supervised by J.H. Prevost, 5/24/88, (PB89-144703).
- NCEER-88-0014 "Parameter Identification and Implementation of a Kinematic Plasticity Model for Frictional Soils," by J.H. Prevost and D.V. Griffiths, to be published.
- NCEER-88-0015 "Two- and Three- Dimensional Dynamic Finite Element Analyses of the Long Valley Dam," by D.V. Griffiths and J.H. Prevost, 6/17/88, (PB89-144711).
- NCEER-88-0016 "Damage Assessment of Reinforced Concrete Structures in Eastern United States," by A.M. Reinhorn, M.J. Seidel, S.K. Kunnath and Y.J. Park, 6/15/88, (PB89-122220).
- NCEER-88-0017 "Dynamic Compliance of Vertically Loaded Strip Foundations in Multilayered Viscoelastic Soils," by S. Ahmad and A.S.M. Israil, 6/17/88, (PB89-102891).
- NCEER-88-0018 "An Experimental Study of Seismic Structural Response With Added Viscoelastic Dampers," by R.C. Lin, Z. Liang, T.T. Soong and R.H. Zhang, 6/30/88, (PB89-122212). This report is available only through NTIS (see address given above).
- NCEER-88-0019 "Experimental Investigation of Primary - Secondary System Interaction," by G.D. Manolis, G. Juhn and A.M. Reinhorn, 5/27/88, (PB89-122204).
- NCEER-88-0020 "A Response Spectrum Approach For Analysis of Nonclassically Damped Structures," by J.N. Yang, S. Sarkani and F.X. Long, 4/22/88, (PB89-102909).
- NCEER-88-0021 "Seismic Interaction of Structures and Soils: Stochastic Approach," by A.S. Veletsos and A.M. Prasad, 7/21/88, (PB89-122196).
- NCEER-88-0022 "Identification of the Serviceability Limit State and Detection of Seismic Structural Damage," by E. DiPasquale and A.S. Cakmak, 6/15/88, (PB89-122188). This report is available only through NTIS (see address given above).
- NCEER-88-0023 "Multi-Hazard Risk Analysis: Case of a Simple Offshore Structure," by B.K. Bhartia and E.H. Vanmarcke, 7/21/88, (PB89-145213).
- NCEER-88-0024 "Automated Seismic Design of Reinforced Concrete Buildings," by Y.S. Chung, C. Meyer and M. Shinozuka, 7/5/88, (PB89-122170). This report is available only through NTIS (see address given above).

- NCEER-88-0025 "Experimental Study of Active Control of MDOF Structures Under Seismic Excitations," by L.L. Chung, R.C. Lin, T.T. Soong and A.M. Reinhorn, 7/10/88, (PB89-122600).
- NCEER-88-0026 "Earthquake Simulation Tests of a Low-Rise Metal Structure," by J.S. Hwang, K.C. Chang, G.C. Lee and R.L. Ketter, 8/1/88, (PB89-102917).
- NCEER-88-0027 "Systems Study of Urban Response and Reconstruction Due to Catastrophic Earthquakes," by F. Kozin and H.K. Zhou, 9/22/88, (PB90-162348).
- NCEER-88-0028 "Seismic Fragility Analysis of Plane Frame Structures," by H.H-M. Hwang and Y.K. Low, 7/31/88, (PB89-131445).
- NCEER-88-0029 "Response Analysis of Stochastic Structures," by A. Kardara, C. Bucher and M. Shinozuka, 9/22/88, (PB89-174429).
- NCEER-88-0030 "Nonnormal Accelerations Due to Yielding in a Primary Structure," by D.C.K. Chen and L.D. Lutes, 9/19/88, (PB89-131437).
- NCEER-88-0031 "Design Approaches for Soil-Structure Interaction," by A.S. Veletsos, A.M. Prasad and Y. Tang, 12/30/88, (PB89-174437). This report is available only through NTIS (see address given above).
- NCEER-88-0032 "A Re-evaluation of Design Spectra for Seismic Damage Control," by C.J. Turkstra and A.G. Tallin, 11/7/88, (PB89-145221).
- NCEER-88-0033 "The Behavior and Design of Noncontact Lap Splices Subjected to Repeated Inelastic Tensile Loading," by V.E. Sagan, P. Gergely and R.N. White, 12/8/88, (PB89-163737).
- NCEER-88-0034 "Seismic Response of Pile Foundations," by S.M. Mamoon, P.K. Banerjee and S. Ahmad, 11/1/88, (PB89-145239).
- NCEER-88-0035 "Modeling of R/C Building Structures With Flexible Floor Diaphragms (IDARC2)," by A.M. Reinhorn, S.K. Kunnath and N. Panahshahi, 9/7/88, (PB89-207153).
- NCEER-88-0036 "Solution of the Dam-Reservoir Interaction Problem Using a Combination of FEM, BEM with Particular Integrals, Modal Analysis, and Substructuring," by C-S. Tsai, G.C. Lee and R.L. Ketter, 12/31/88, (PB89-207146).
- NCEER-88-0037 "Optimal Placement of Actuators for Structural Control," by F.Y. Cheng and C.P. Pantelides, 8/15/88, (PB89-162846).
- NCEER-88-0038 "Teflon Bearings in Aseismic Base Isolation: Experimental Studies and Mathematical Modeling," by A. Mokha, M.C. Constantinou and A.M. Reinhorn, 12/5/88, (PB89-218457). This report is available only through NTIS (see address given above).
- NCEER-88-0039 "Seismic Behavior of Flat Slab High-Rise Buildings in the New York City Area," by P. Weidlinger and M. Ettouney, 10/15/88, (PB90-145681).
- NCEER-88-0040 "Evaluation of the Earthquake Resistance of Existing Buildings in New York City," by P. Weidlinger and M. Ettouney, 10/15/88, to be published.
- NCEER-88-0041 "Small-Scale Modeling Techniques for Reinforced Concrete Structures Subjected to Seismic Loads," by W. Kim, A. El-Attar and R.N. White, 11/22/88, (PB89-189625).
- NCEER-88-0042 "Modeling Strong Ground Motion from Multiple Event Earthquakes," by G.W. Ellis and A.S. Cakmak, 10/15/88, (PB89-174445).

- NCEER-88-0043 "Nonstationary Models of Seismic Ground Acceleration," by M. Grigoriu, S.E. Ruiz and E. Rosenblueth, 7/15/88, (PB89-189617).
- NCEER-88-0044 "SARCF User's Guide: Seismic Analysis of Reinforced Concrete Frames," by Y.S. Chung, C. Meyer and M. Shinozuka, 11/9/88, (PB89-174452).
- NCEER-88-0045 "First Expert Panel Meeting on Disaster Research and Planning," edited by J. Pantelic and J. Stoye, 9/15/88, (PB89-174460).
- NCEER-88-0046 "Preliminary Studies of the Effect of Degrading Infill Walls on the Nonlinear Seismic Response of Steel Frames," by C.Z. Chrysostomou, P. Gergely and J.F. Abel, 12/19/88, (PB89-208383).
- NCEER-88-0047 "Reinforced Concrete Frame Component Testing Facility - Design, Construction, Instrumentation and Operation," by S.P. Pessiki, C. Conley, T. Bond, P. Gergely and R.N. White, 12/16/88, (PB89-174478).
- NCEER-89-0001 "Effects of Protective Cushion and Soil Compliancy on the Response of Equipment Within a Seismically Excited Building," by J.A. HoLung, 2/16/89, (PB89-207179).
- NCEER-89-0002 "Statistical Evaluation of Response Modification Factors for Reinforced Concrete Structures," by H.H-M. Hwang and J-W. Jaw, 2/17/89, (PB89-207187).
- NCEER-89-0003 "Hysteretic Columns Under Random Excitation," by G-Q. Cai and Y.K. Lin, 1/9/89, (PB89-196513).
- NCEER-89-0004 "Experimental Study of `Elephant Foot Bulge' Instability of Thin-Walled Metal Tanks," by Z-H. Jia and R.L. Ketter, 2/22/89, (PB89-207195).
- NCEER-89-0005 "Experiment on Performance of Buried Pipelines Across San Andreas Fault," by J. Isenberg, E. Richardson and T.D. O'Rourke, 3/10/89, (PB89-218440). This report is available only through NTIS (see address given above).
- NCEER-89-0006 "A Knowledge-Based Approach to Structural Design of Earthquake-Resistant Buildings," by M. Subramani, P. Gergely, C.H. Conley, J.F. Abel and A.H. Zaghaw, 1/15/89, (PB89-218465).
- NCEER-89-0007 "Liquefaction Hazards and Their Effects on Buried Pipelines," by T.D. O'Rourke and P.A. Lane, 2/1/89, (PB89-218481).
- NCEER-89-0008 "Fundamentals of System Identification in Structural Dynamics," by H. Imai, C-B. Yun, O. Maruyama and M. Shinozuka, 1/26/89, (PB89-207211).
- NCEER-89-0009 "Effects of the 1985 Michoacan Earthquake on Water Systems and Other Buried Lifelines in Mexico," by A.G. Ayala and M.J. O'Rourke, 3/8/89, (PB89-207229).
- NCEER-89-R010 "NCEER Bibliography of Earthquake Education Materials," by K.E.K. Ross, Second Revision, 9/1/89, (PB90-125352).
- NCEER-89-0011 "Inelastic Three-Dimensional Response Analysis of Reinforced Concrete Building Structures (IDARC-3D), Part I - Modeling," by S.K. Kunnath and A.M. Reinhorn, 4/17/89, (PB90-114612).
- NCEER-89-0012 "Recommended Modifications to ATC-14," by C.D. Poland and J.O. Malley, 4/12/89, (PB90-108648).
- NCEER-89-0013 "Repair and Strengthening of Beam-to-Column Connections Subjected to Earthquake Loading," by M. Corazao and A.J. Durrani, 2/28/89, (PB90-109885).
- NCEER-89-0014 "Program EXKAL2 for Identification of Structural Dynamic Systems," by O. Maruyama, C-B. Yun, M. Hoshiya and M. Shinozuka, 5/19/89, (PB90-109877).

- NCEER-89-0015 "Response of Frames With Bolted Semi-Rigid Connections, Part I - Experimental Study and Analytical Predictions," by P.J. DiCorso, A.M. Reinhorn, J.R. Dickerson, J.B. Radzinski and W.L. Harper, 6/1/89, to be published.
- NCEER-89-0016 "ARMA Monte Carlo Simulation in Probabilistic Structural Analysis," by P.D. Spanos and M.P. Mignolet, 7/10/89, (PB90-109893).
- NCEER-89-P017 "Preliminary Proceedings from the Conference on Disaster Preparedness - The Place of Earthquake Education in Our Schools," Edited by K.E.K. Ross, 6/23/89, (PB90-108606).
- NCEER-89-0017 "Proceedings from the Conference on Disaster Preparedness - The Place of Earthquake Education in Our Schools," Edited by K.E.K. Ross, 12/31/89, (PB90-207895). This report is available only through NTIS (see address given above).
- NCEER-89-0018 "Multidimensional Models of Hysteretic Material Behavior for Vibration Analysis of Shape Memory Energy Absorbing Devices, by E.J. Graesser and F.A. Cozzarelli, 6/7/89, (PB90-164146).
- NCEER-89-0019 "Nonlinear Dynamic Analysis of Three-Dimensional Base Isolated Structures (3D-BASIS)," by S. Nagarajaiah, A.M. Reinhorn and M.C. Constantinou, 8/3/89, (PB90-161936). This report is available only through NTIS (see address given above).
- NCEER-89-0020 "Structural Control Considering Time-Rate of Control Forces and Control Rate Constraints," by F.Y. Cheng and C.P. Pantelides, 8/3/89, (PB90-120445).
- NCEER-89-0021 "Subsurface Conditions of Memphis and Shelby County," by K.W. Ng, T-S. Chang and H-H.M. Hwang, 7/26/89, (PB90-120437).
- NCEER-89-0022 "Seismic Wave Propagation Effects on Straight Jointed Buried Pipelines," by K. Elhadi and M.J. O'Rourke, 8/24/89, (PB90-162322).
- NCEER-89-0023 "Workshop on Serviceability Analysis of Water Delivery Systems," edited by M. Grigoriu, 3/6/89, (PB90-127424).
- NCEER-89-0024 "Shaking Table Study of a 1/5 Scale Steel Frame Composed of Tapered Members," by K.C. Chang, J.S. Hwang and G.C. Lee, 9/18/89, (PB90-160169).
- NCEER-89-0025 "DYNA1D: A Computer Program for Nonlinear Seismic Site Response Analysis - Technical Documentation," by Jean H. Prevost, 9/14/89, (PB90-161944). This report is available only through NTIS (see address given above).
- NCEER-89-0026 "1:4 Scale Model Studies of Active Tendon Systems and Active Mass Dampers for Aseismic Protection," by A.M. Reinhorn, T.T. Soong, R.C. Lin, Y.P. Yang, Y. Fukao, H. Abe and M. Nakai, 9/15/89, (PB90-173246).
- NCEER-89-0027 "Scattering of Waves by Inclusions in a Nonhomogeneous Elastic Half Space Solved by Boundary Element Methods," by P.K. Hadley, A. Askar and A.S. Cakmak, 6/15/89, (PB90-145699).
- NCEER-89-0028 "Statistical Evaluation of Deflection Amplification Factors for Reinforced Concrete Structures," by H.H.M. Hwang, J-W. Jaw and A.L. Ch'ng, 8/31/89, (PB90-164633).
- NCEER-89-0029 "Bedrock Accelerations in Memphis Area Due to Large New Madrid Earthquakes," by H.H.M. Hwang, C.H.S. Chen and G. Yu, 11/7/89, (PB90-162330).
- NCEER-89-0030 "Seismic Behavior and Response Sensitivity of Secondary Structural Systems," by Y.Q. Chen and T.T. Soong, 10/23/89, (PB90-164658).

- NCEER-89-0031 "Random Vibration and Reliability Analysis of Primary-Secondary Structural Systems," by Y. Ibrahim, M. Grigoriu and T.T. Soong, 11/10/89, (PB90-161951).
- NCEER-89-0032 "Proceedings from the Second U.S. - Japan Workshop on Liquefaction, Large Ground Deformation and Their Effects on Lifelines, September 26-29, 1989," Edited by T.D. O'Rourke and M. Hamada, 12/1/89, (PB90-209388).
- NCEER-89-0033 "Deterministic Model for Seismic Damage Evaluation of Reinforced Concrete Structures," by J.M. Bracci, A.M. Reinhorn, J.B. Mander and S.K. Kunnath, 9/27/89.
- NCEER-89-0034 "On the Relation Between Local and Global Damage Indices," by E. DiPasquale and A.S. Cakmak, 8/15/89, (PB90-173865).
- NCEER-89-0035 "Cyclic Undrained Behavior of Nonplastic and Low Plasticity Silts," by A.J. Walker and H.E. Stewart, 7/26/89, (PB90-183518).
- NCEER-89-0036 "Liquefaction Potential of Surficial Deposits in the City of Buffalo, New York," by M. Budhu, R. Giese and L. Baumgrass, 1/17/89, (PB90-208455).
- NCEER-89-0037 "A Deterministic Assessment of Effects of Ground Motion Incoherence," by A.S. Veletsos and Y. Tang, 7/15/89, (PB90-164294).
- NCEER-89-0038 "Workshop on Ground Motion Parameters for Seismic Hazard Mapping," July 17-18, 1989, edited by R.V. Whitman, 12/1/89, (PB90-173923).
- NCEER-89-0039 "Seismic Effects on Elevated Transit Lines of the New York City Transit Authority," by C.J. Costantino, C.A. Miller and E. Heymsfield, 12/26/89, (PB90-207887).
- NCEER-89-0040 "Centrifugal Modeling of Dynamic Soil-Structure Interaction," by K. Weissman, Supervised by J.H. Prevost, 5/10/89, (PB90-207879).
- NCEER-89-0041 "Linearized Identification of Buildings With Cores for Seismic Vulnerability Assessment," by I-K. Ho and A.E. Aktan, 11/1/89, (PB90-251943).
- NCEER-90-0001 "Geotechnical and Lifeline Aspects of the October 17, 1989 Loma Prieta Earthquake in San Francisco," by T.D. O'Rourke, H.E. Stewart, F.T. Blackburn and T.S. Dickerman, 1/90, (PB90-208596).
- NCEER-90-0002 "Nonnormal Secondary Response Due to Yielding in a Primary Structure," by D.C.K. Chen and L.D. Lutes, 2/28/90, (PB90-251976).
- NCEER-90-0003 "Earthquake Education Materials for Grades K-12," by K.E.K. Ross, 4/16/90, (PB91-251984).
- NCEER-90-0004 "Catalog of Strong Motion Stations in Eastern North America," by R.W. Busby, 4/3/90, (PB90-251984).
- NCEER-90-0005 "NCEER Strong-Motion Data Base: A User Manual for the GeoBase Release (Version 1.0 for the Sun3)," by P. Friberg and K. Jacob, 3/31/90 (PB90-258062).
- NCEER-90-0006 "Seismic Hazard Along a Crude Oil Pipeline in the Event of an 1811-1812 Type New Madrid Earthquake," by H.H.M. Hwang and C-H.S. Chen, 4/16/90(PB90-258054).
- NCEER-90-0007 "Site-Specific Response Spectra for Memphis Sheahan Pumping Station," by H.H.M. Hwang and C.S. Lee, 5/15/90, (PB91-108811).
- NCEER-90-0008 "Pilot Study on Seismic Vulnerability of Crude Oil Transmission Systems," by T. Ariman, R. Dobry, M. Grigoriu, F. Kozin, M. O'Rourke, T. O'Rourke and M. Shinozuka, 5/25/90, (PB91-108837).

- NCEER-90-0009 "A Program to Generate Site Dependent Time Histories: EQGEN," by G.W. Ellis, M. Srinivasan and A.S. Cakmak, 1/30/90, (PB91-108829).
- NCEER-90-0010 "Active Isolation for Seismic Protection of Operating Rooms," by M.E. Talbott, Supervised by M. Shinozuka, 6/8/9, (PB91-110205).
- NCEER-90-0011 "Program LINEARID for Identification of Linear Structural Dynamic Systems," by C-B. Yun and M. Shinozuka, 6/25/90, (PB91-110312).
- NCEER-90-0012 "Two-Dimensional Two-Phase Elasto-Plastic Seismic Response of Earth Dams," by A.N. Yiagos, Supervised by J.H. Prevost, 6/20/90, (PB91-110197).
- NCEER-90-0013 "Secondary Systems in Base-Isolated Structures: Experimental Investigation, Stochastic Response and Stochastic Sensitivity," by G.D. Manolis, G. Juhn, M.C. Constantinou and A.M. Reinhorn, 7/1/90, (PB91-110320).
- NCEER-90-0014 "Seismic Behavior of Lightly-Reinforced Concrete Column and Beam-Column Joint Details," by S.P. Pessiki, C.H. Conley, P. Gergely and R.N. White, 8/22/90, (PB91-108795).
- NCEER-90-0015 "Two Hybrid Control Systems for Building Structures Under Strong Earthquakes," by J.N. Yang and A. Danielians, 6/29/90, (PB91-125393).
- NCEER-90-0016 "Instantaneous Optimal Control with Acceleration and Velocity Feedback," by J.N. Yang and Z. Li, 6/29/90, (PB91-125401).
- NCEER-90-0017 "Reconnaissance Report on the Northern Iran Earthquake of June 21, 1990," by M. Mehraïn, 10/4/90, (PB91-125377).
- NCEER-90-0018 "Evaluation of Liquefaction Potential in Memphis and Shelby County," by T.S. Chang, P.S. Tang, C.S. Lee and H. Hwang, 8/10/90, (PB91-125427).
- NCEER-90-0019 "Experimental and Analytical Study of a Combined Sliding Disc Bearing and Helical Steel Spring Isolation System," by M.C. Constantinou, A.S. Mokha and A.M. Reinhorn, 10/4/90, (PB91-125385).
- NCEER-90-0020 "Experimental Study and Analytical Prediction of Earthquake Response of a Sliding Isolation System with a Spherical Surface," by A.S. Mokha, M.C. Constantinou and A.M. Reinhorn, 10/11/90, (PB91-125419).
- NCEER-90-0021 "Dynamic Interaction Factors for Floating Pile Groups," by G. Gazetas, K. Fan, A. Kaynia and E. Kausel, 9/10/90, (PB91-170381).
- NCEER-90-0022 "Evaluation of Seismic Damage Indices for Reinforced Concrete Structures," by S. Rodriguez-Gomez and A.S. Cakmak, 9/30/90, PB91-171322).
- NCEER-90-0023 "Study of Site Response at a Selected Memphis Site," by H. Desai, S. Ahmad, E.S. Gazetas and M.R. Oh, 10/11/90, (PB91-196857).
- NCEER-90-0024 "A User's Guide to Strongmo: Version 1.0 of NCEER's Strong-Motion Data Access Tool for PCs and Terminals," by P.A. Friberg and C.A.T. Susch, 11/15/90, (PB91-171272).
- NCEER-90-0025 "A Three-Dimensional Analytical Study of Spatial Variability of Seismic Ground Motions," by L-L. Hong and A.H.-S. Ang, 10/30/90, (PB91-170399).
- NCEER-90-0026 "MUMOID User's Guide - A Program for the Identification of Modal Parameters," by S. Rodriguez-Gomez and E. DiPasquale, 9/30/90, (PB91-171298).
- NCEER-90-0027 "SARCF-II User's Guide - Seismic Analysis of Reinforced Concrete Frames," by S. Rodriguez-Gomez, Y.S. Chung and C. Meyer, 9/30/90, (PB91-171280).

- NCEER-90-0028 "Viscous Dampers: Testing, Modeling and Application in Vibration and Seismic Isolation," by N. Makris and M.C. Constantinou, 12/20/90 (PB91-190561).
- NCEER-90-0029 "Soil Effects on Earthquake Ground Motions in the Memphis Area," by H. Hwang, C.S. Lee, K.W. Ng and T.S. Chang, 8/2/90, (PB91-190751).
- NCEER-91-0001 "Proceedings from the Third Japan-U.S. Workshop on Earthquake Resistant Design of Lifeline Facilities and Countermeasures for Soil Liquefaction, December 17-19, 1990," edited by T.D. O'Rourke and M. Hamada, 2/1/91, (PB91-179259).
- NCEER-91-0002 "Physical Space Solutions of Non-Proportionally Damped Systems," by M. Tong, Z. Liang and G.C. Lee, 1/15/91, (PB91-179242).
- NCEER-91-0003 "Seismic Response of Single Piles and Pile Groups," by K. Fan and G. Gazetas, 1/10/91, (PB92-174994).
- NCEER-91-0004 "Damping of Structures: Part 1 - Theory of Complex Damping," by Z. Liang and G. Lee, 10/10/91, (PB92-197235).
- NCEER-91-0005 "3D-BASIS - Nonlinear Dynamic Analysis of Three Dimensional Base Isolated Structures: Part II," by S. Nagarajaiah, A.M. Reinhorn and M.C. Constantinou, 2/28/91, (PB91-190553).
- NCEER-91-0006 "A Multidimensional Hysteretic Model for Plasticity Deforming Metals in Energy Absorbing Devices," by E.J. Graesser and F.A. Cozzarelli, 4/9/91, (PB92-108364).
- NCEER-91-0007 "A Framework for Customizable Knowledge-Based Expert Systems with an Application to a KBES for Evaluating the Seismic Resistance of Existing Buildings," by E.G. Ibarra-Anaya and S.J. Fenves, 4/9/91, (PB91-210930).
- NCEER-91-0008 "Nonlinear Analysis of Steel Frames with Semi-Rigid Connections Using the Capacity Spectrum Method," by G.G. Deierlein, S-H. Hsieh, Y-J. Shen and J.F. Abel, 7/2/91, (PB92-113828).
- NCEER-91-0009 "Earthquake Education Materials for Grades K-12," by K.E.K. Ross, 4/30/91, (PB91-212142).
- NCEER-91-0010 "Phase Wave Velocities and Displacement Phase Differences in a Harmonically Oscillating Pile," by N. Makris and G. Gazetas, 7/8/91, (PB92-108356).
- NCEER-91-0011 "Dynamic Characteristics of a Full-Size Five-Story Steel Structure and a 2/5 Scale Model," by K.C. Chang, G.C. Yao, G.C. Lee, D.S. Hao and Y.C. Yeh, 7/2/91, (PB93-116648).
- NCEER-91-0012 "Seismic Response of a 2/5 Scale Steel Structure with Added Viscoelastic Dampers," by K.C. Chang, T.T. Soong, S-T. Oh and M.L. Lai, 5/17/91, (PB92-110816).
- NCEER-91-0013 "Earthquake Response of Retaining Walls; Full-Scale Testing and Computational Modeling," by S. Alampalli and A-W.M. Elgamal, 6/20/91, to be published.
- NCEER-91-0014 "3D-BASIS-M: Nonlinear Dynamic Analysis of Multiple Building Base Isolated Structures," by P.C. Tsopelas, S. Nagarajaiah, M.C. Constantinou and A.M. Reinhorn, 5/28/91, (PB92-113885).
- NCEER-91-0015 "Evaluation of SEAOC Design Requirements for Sliding Isolated Structures," by D. Theodossiou and M.C. Constantinou, 6/10/91, (PB92-114602).
- NCEER-91-0016 "Closed-Loop Modal Testing of a 27-Story Reinforced Concrete Flat Plate-Core Building," by H.R. Somaprasad, T. Toksoy, H. Yoshiyuki and A.E. Aktan, 7/15/91, (PB92-129980).
- NCEER-91-0017 "Shake Table Test of a 1/6 Scale Two-Story Lightly Reinforced Concrete Building," by A.G. El-Attar, R.N. White and P. Gergely, 2/28/91, (PB92-222447).

- NCEER-91-0018 "Shake Table Test of a 1/8 Scale Three-Story Lightly Reinforced Concrete Building," by A.G. El-Attar, R.N. White and P. Gergely, 2/28/91, (PB93-116630).
- NCEER-91-0019 "Transfer Functions for Rigid Rectangular Foundations," by A.S. Veletsos, A.M. Prasad and W.H. Wu, 7/31/91.
- NCEER-91-0020 "Hybrid Control of Seismic-Excited Nonlinear and Inelastic Structural Systems," by J.N. Yang, Z. Li and A. Danielians, 8/1/91, (PB92-143171).
- NCEER-91-0021 "The NCEER-91 Earthquake Catalog: Improved Intensity-Based Magnitudes and Recurrence Relations for U.S. Earthquakes East of New Madrid," by L. Seeber and J.G. Armbruster, 8/28/91, (PB92-176742).
- NCEER-91-0022 "Proceedings from the Implementation of Earthquake Planning and Education in Schools: The Need for Change - The Roles of the Changemakers," by K.E.K. Ross and F. Winslow, 7/23/91, (PB92-129998).
- NCEER-91-0023 "A Study of Reliability-Based Criteria for Seismic Design of Reinforced Concrete Frame Buildings," by H.H.M. Hwang and H-M. Hsu, 8/10/91, (PB92-140235).
- NCEER-91-0024 "Experimental Verification of a Number of Structural System Identification Algorithms," by R.G. Ghanem, H. Gavin and M. Shinozuka, 9/18/91, (PB92-176577).
- NCEER-91-0025 "Probabilistic Evaluation of Liquefaction Potential," by H.H.M. Hwang and C.S. Lee, 11/25/91, (PB92-143429).
- NCEER-91-0026 "Instantaneous Optimal Control for Linear, Nonlinear and Hysteretic Structures - Stable Controllers," by J.N. Yang and Z. Li, 11/15/91, (PB92-163807).
- NCEER-91-0027 "Experimental and Theoretical Study of a Sliding Isolation System for Bridges," by M.C. Constantinou, A. Kartoum, A.M. Reinhorn and P. Bradford, 11/15/91, (PB92-176973).
- NCEER-92-0001 "Case Studies of Liquefaction and Lifeline Performance During Past Earthquakes, Volume 1: Japanese Case Studies," Edited by M. Hamada and T. O'Rourke, 2/17/92, (PB92-197243).
- NCEER-92-0002 "Case Studies of Liquefaction and Lifeline Performance During Past Earthquakes, Volume 2: United States Case Studies," Edited by T. O'Rourke and M. Hamada, 2/17/92, (PB92-197250).
- NCEER-92-0003 "Issues in Earthquake Education," Edited by K. Ross, 2/3/92, (PB92-222389).
- NCEER-92-0004 "Proceedings from the First U.S. - Japan Workshop on Earthquake Protective Systems for Bridges," Edited by I.G. Buckle, 2/4/92, (PB94-142239, A99, MF-A06).
- NCEER-92-0005 "Seismic Ground Motion from a Haskell-Type Source in a Multiple-Layered Half-Space," A.P. Theoharis, G. Deodatis and M. Shinozuka, 1/2/92, to be published.
- NCEER-92-0006 "Proceedings from the Site Effects Workshop," Edited by R. Whitman, 2/29/92, (PB92-197201).
- NCEER-92-0007 "Engineering Evaluation of Permanent Ground Deformations Due to Seismically-Induced Liquefaction," by M.H. Baziar, R. Dobry and A-W.M. Elgamal, 3/24/92, (PB92-222421).
- NCEER-92-0008 "A Procedure for the Seismic Evaluation of Buildings in the Central and Eastern United States," by C.D. Poland and J.O. Malley, 4/2/92, (PB92-222439).
- NCEER-92-0009 "Experimental and Analytical Study of a Hybrid Isolation System Using Friction Controllable Sliding Bearings," by M.Q. Feng, S. Fujii and M. Shinozuka, 5/15/92, (PB93-150282).
- NCEER-92-0010 "Seismic Resistance of Slab-Column Connections in Existing Non-Ductile Flat-Plate Buildings," by A.J. Durrani and Y. Du, 5/18/92.

- NCEER-92-0011 "The Hysteretic and Dynamic Behavior of Brick Masonry Walls Upgraded by Ferrocement Coatings Under Cyclic Loading and Strong Simulated Ground Motion," by H. Lee and S.P. Prawel, 5/11/92, to be published.
- NCEER-92-0012 "Study of Wire Rope Systems for Seismic Protection of Equipment in Buildings," by G.F. Demetriades, M.C. Constantinou and A.M. Reinhorn, 5/20/92.
- NCEER-92-0013 "Shape Memory Structural Dampers: Material Properties, Design and Seismic Testing," by P.R. Witting and F.A. Cozzarelli, 5/26/92.
- NCEER-92-0014 "Longitudinal Permanent Ground Deformation Effects on Buried Continuous Pipelines," by M.J. O'Rourke, and C. Nordberg, 6/15/92.
- NCEER-92-0015 "A Simulation Method for Stationary Gaussian Random Functions Based on the Sampling Theorem," by M. Grigoriu and S. Balopoulou, 6/11/92, (PB93-127496).
- NCEER-92-0016 "Gravity-Load-Designed Reinforced Concrete Buildings: Seismic Evaluation of Existing Construction and Detailing Strategies for Improved Seismic Resistance," by G.W. Hoffmann, S.K. Kunnath, A.M. Reinhorn and J.B. Mander, 7/15/92, (PB94-142007, A08, MF-A02).
- NCEER-92-0017 "Observations on Water System and Pipeline Performance in the Limón Area of Costa Rica Due to the April 22, 1991 Earthquake," by M. O'Rourke and D. Ballantyne, 6/30/92, (PB93-126811).
- NCEER-92-0018 "Fourth Edition of Earthquake Education Materials for Grades K-12," Edited by K.E.K. Ross, 8/10/92.
- NCEER-92-0019 "Proceedings from the Fourth Japan-U.S. Workshop on Earthquake Resistant Design of Lifeline Facilities and Countermeasures for Soil Liquefaction," Edited by M. Hamada and T.D. O'Rourke, 8/12/92, (PB93-163939).
- NCEER-92-0020 "Active Bracing System: A Full Scale Implementation of Active Control," by A.M. Reinhorn, T.T. Soong, R.C. Lin, M.A. Riley, Y.P. Wang, S. Aizawa and M. Higashino, 8/14/92, (PB93-127512).
- NCEER-92-0021 "Empirical Analysis of Horizontal Ground Displacement Generated by Liquefaction-Induced Lateral Spreads," by S.F. Bartlett and T.L. Youd, 8/17/92, (PB93-188241).
- NCEER-92-0022 "IDARC Version 3.0: Inelastic Damage Analysis of Reinforced Concrete Structures," by S.K. Kunnath, A.M. Reinhorn and R.F. Lobo, 8/31/92, (PB93-227502, A07, MF-A02).
- NCEER-92-0023 "A Semi-Empirical Analysis of Strong-Motion Peaks in Terms of Seismic Source, Propagation Path and Local Site Conditions, by M. Kamiyama, M.J. O'Rourke and R. Flores-Berrones, 9/9/92, (PB93-150266).
- NCEER-92-0024 "Seismic Behavior of Reinforced Concrete Frame Structures with Nonductile Details, Part I: Summary of Experimental Findings of Full Scale Beam-Column Joint Tests," by A. Beres, R.N. White and P. Gergely, 9/30/92, (PB93-227783, A05, MF-A01).
- NCEER-92-0025 "Experimental Results of Repaired and Retrofitted Beam-Column Joint Tests in Lightly Reinforced Concrete Frame Buildings," by A. Beres, S. El-Borgi, R.N. White and P. Gergely, 10/29/92, (PB93-227791, A05, MF-A01).
- NCEER-92-0026 "A Generalization of Optimal Control Theory: Linear and Nonlinear Structures," by J.N. Yang, Z. Li and S. Vongchavalitkul, 11/2/92, (PB93-188621).
- NCEER-92-0027 "Seismic Resistance of Reinforced Concrete Frame Structures Designed Only for Gravity Loads: Part I - Design and Properties of a One-Third Scale Model Structure," by J.M. Bracci, A.M. Reinhorn and J.B. Mander, 12/1/92, (PB94-104502, A08, MF-A02).

- NCEER-92-0028 "Seismic Resistance of Reinforced Concrete Frame Structures Designed Only for Gravity Loads: Part II - Experimental Performance of Subassemblages," by L.E. Aycardi, J.B. Mander and A.M. Reinhorn, 12/1/92, (PB94-104510, A08, MF-A02).
- NCEER-92-0029 "Seismic Resistance of Reinforced Concrete Frame Structures Designed Only for Gravity Loads: Part III - Experimental Performance and Analytical Study of a Structural Model," by J.M. Bracci, A.M. Reinhorn and J.B. Mander, 12/1/92, (PB93-227528, A09, MF-A01).
- NCEER-92-0030 "Evaluation of Seismic Retrofit of Reinforced Concrete Frame Structures: Part I - Experimental Performance of Retrofitted Subassemblages," by D. Choudhuri, J.B. Mander and A.M. Reinhorn, 12/8/92, (PB93-198307, A07, MF-A02).
- NCEER-92-0031 "Evaluation of Seismic Retrofit of Reinforced Concrete Frame Structures: Part II - Experimental Performance and Analytical Study of a Retrofitted Structural Model," by J.M. Bracci, A.M. Reinhorn and J.B. Mander, 12/8/92, (PB93-198315, A09, MF-A03).
- NCEER-92-0032 "Experimental and Analytical Investigation of Seismic Response of Structures with Supplemental Fluid Viscous Dampers," by M.C. Constantinou and M.D. Symans, 12/21/92, (PB93-191435).
- NCEER-92-0033 "Reconnaissance Report on the Cairo, Egypt Earthquake of October 12, 1992," by M. Khater, 12/23/92, (PB93-188621).
- NCEER-92-0034 "Low-Level Dynamic Characteristics of Four Tall Flat-Plate Buildings in New York City," by H. Gavin, S. Yuan, J. Grossman, E. Pekelis and K. Jacob, 12/28/92, (PB93-188217).
- NCEER-93-0001 "An Experimental Study on the Seismic Performance of Brick-Infilled Steel Frames With and Without Retrofit," by J.B. Mander, B. Nair, K. Wojtkowski and J. Ma, 1/29/93, (PB93-227510, A07, MF-A02).
- NCEER-93-0002 "Social Accounting for Disaster Preparedness and Recovery Planning," by S. Cole, E. Pantoja and V. Razak, 2/22/93, (PB94-142114, A12, MF-A03).
- NCEER-93-0003 "Assessment of 1991 NEHRP Provisions for Nonstructural Components and Recommended Revisions," by T.T. Soong, G. Chen, Z. Wu, R-H. Zhang and M. Grigoriu, 3/1/93, (PB93-188639).
- NCEER-93-0004 "Evaluation of Static and Response Spectrum Analysis Procedures of SEAOC/UBC for Seismic Isolated Structures," by C.W. Winters and M.C. Constantinou, 3/23/93, (PB93-198299).
- NCEER-93-0005 "Earthquakes in the Northeast - Are We Ignoring the Hazard? A Workshop on Earthquake Science and Safety for Educators," edited by K.E.K. Ross, 4/2/93, (PB94-103066, A09, MF-A02).
- NCEER-93-0006 "Inelastic Response of Reinforced Concrete Structures with Viscoelastic Braces," by R.F. Lobo, J.M. Bracci, K.L. Shen, A.M. Reinhorn and T.T. Soong, 4/5/93, (PB93-227486, A05, MF-A02).
- NCEER-93-0007 "Seismic Testing of Installation Methods for Computers and Data Processing Equipment," by K. Kosar, T.T. Soong, K.L. Shen, J.A. HoLung and Y.K. Lin, 4/12/93, (PB93-198299).
- NCEER-93-0008 "Retrofit of Reinforced Concrete Frames Using Added Dampers," by A. Reinhorn, M. Constantinou and C. Li, to be published.
- NCEER-93-0009 "Seismic Behavior and Design Guidelines for Steel Frame Structures with Added Viscoelastic Dampers," by K.C. Chang, M.L. Lai, T.T. Soong, D.S. Hao and Y.C. Yeh, 5/1/93, (PB94-141959, A07, MF-A02).
- NCEER-93-0010 "Seismic Performance of Shear-Critical Reinforced Concrete Bridge Piers," by J.B. Mander, S.M. Waheed, M.T.A. Chaudhary and S.S. Chen, 5/12/93. (PB93-227494, A08, MF-A02).

- NCEER-93-0011 "3D-BASIS-TABS: Computer Program for Nonlinear Dynamic Analysis of Three Dimensional Base Isolated Structures," by S. Nagarajaiah, C. Li, A.M. Reinhorn and M.C. Constantinou, 8/2/93, (PB94-141819, A09, MF-A02).
- NCEER-93-0012 "Effects of Hydrocarbon Spills from an Oil Pipeline Break on Ground Water," by O.J. Helweg and H.H.M. Hwang, 8/3/93, (PB94-141942, A06, MF-A02).
- NCEER-93-0013 "Simplified Procedures for Seismic Design of Nonstructural Components and Assessment of Current Code Provisions," by M.P. Singh, L.E. Suarez, E.E. Matheu and G.O. Maldonado, 8/4/93, (PB94-141827, A09, MF-A02).
- NCEER-93-0014 "An Energy Approach to Seismic Analysis and Design of Secondary Systems," by G. Chen and T.T. Soong, 8/6/93, (PB94-142767, A11, MF-A03).
- NCEER-93-0015 "Proceedings from School Sites: Becoming Prepared for Earthquakes - Commemorating the Third Anniversary of the Loma Prieta Earthquake," Edited by F.E. Winslow and K.E.K. Ross, 8/16/93.
- NCEER-93-0016 "Reconnaissance Report of Damage to Historic Monuments in Cairo, Egypt Following the October 12, 1992 Dahshur Earthquake," by D. Sykora, D. Look, G. Croci, E. Karaesmen and E. Karaesmen, 8/19/93, (PB94-142221, A08, MF-A02).
- NCEER-93-0017 "The Island of Guam Earthquake of August 8, 1993," by S.W. Swan and S.K. Harris, 9/30/93, (PB94-141843, A04, MF-A01).
- NCEER-93-0018 "Engineering Aspects of the October 12, 1992 Egyptian Earthquake," by A.W. Elgamal, M. Amer, K. Adalier and A. Abul-Fadl, 10/7/93, (PB94-141983, A05, MF-A01).
- NCEER-93-0019 "Development of an Earthquake Motion Simulator and its Application in Dynamic Centrifuge Testing," by I. Krstelj, Supervised by J.H. Prevost, 10/23/93, (PB94-181773, A-10, MF-A03).
- NCEER-93-0020 "NCEER-Taisei Corporation Research Program on Sliding Seismic Isolation Systems for Bridges: Experimental and Analytical Study of a Friction Pendulum System (FPS)," by M.C. Constantinou, P. Tsopelas, Y-S. Kim and S. Okamoto, 11/1/93, (PB94-142775, A08, MF-A02).
- NCEER-93-0021 "Finite Element Modeling of Elastomeric Seismic Isolation Bearings," by L.J. Billings, Supervised by R. Shepherd, 11/8/93, to be published.
- NCEER-93-0022 "Seismic Vulnerability of Equipment in Critical Facilities: Life-Safety and Operational Consequences," by K. Porter, G.S. Johnson, M.M. Zadeh, C. Scawthorn and S. Eder, 11/24/93, (PB94-181765, A16, MF-A03).
- NCEER-93-0023 "Hokkaido Nansei-oki, Japan Earthquake of July 12, 1993, by P.I. Yanev and C.R. Scawthorn, 12/23/93, (PB94-181500, A07, MF-A01).
- NCEER-94-0001 "An Evaluation of Seismic Serviceability of Water Supply Networks with Application to the San Francisco Auxiliary Water Supply System," by I. Markov, Supervised by M. Grigoriu and T. O'Rourke, 1/21/94.
- NCEER-94-0002 "NCEER-Taisei Corporation Research Program on Sliding Seismic Isolation Systems for Bridges: Experimental and Analytical Study of Systems Consisting of Sliding Bearings, Rubber Restoring Force Devices and Fluid Dampers," Volumes I and II, by P. Tsopelas, S. Okamoto, M.C. Constantinou, D. Ozaki and S. Fujii, 2/4/94, (PB94-181740, A09, MF-A02 and PB94-181757, A12, MF-A03).
- NCEER-94-0003 "A Markov Model for Local and Global Damage Indices in Seismic Analysis," by S. Rahman and M. Grigoriu, 2/18/94.

- NCEER-94-0004 "Proceedings from the NCEER Workshop on Seismic Response of Masonry Infills," edited by D.P. Abrams, 3/1/94, (PB94-180783, A07, MF-A02).
- NCEER-94-0005 "The Northridge, California Earthquake of January 17, 1994: General Reconnaissance Report," edited by J.D. Goltz, 3/11/94, (PB193943, A10, MF-A03).
- NCEER-94-0006 "Seismic Energy Based Fatigue Damage Analysis of Bridge Columns: Part I - Evaluation of Seismic Capacity," by G.A. Chang and J.B. Mander, 3/14/94, (PB94-219185, A11, MF-A03).
- NCEER-94-0007 "Seismic Isolation of Multi-Story Frame Structures Using Spherical Sliding Isolation Systems," by T.M. Al-Hussaini, V.A. Zayas and M.C. Constantinou, 3/17/94, (PB193745, A09, MF-A02).
- NCEER-94-0008 "The Northridge, California Earthquake of January 17, 1994: Performance of Highway Bridges," edited by I.G. Buckle, 3/24/94, (PB94-193851, A06, MF-A02).
- NCEER-94-0009 "Proceedings of the Third U.S.-Japan Workshop on Earthquake Protective Systems for Bridges," edited by I.G. Buckle and I. Friedland, 3/31/94, (PB94-195815, A99, MF-MF).
- NCEER-94-0010 "3D-BASIS-ME: Computer Program for Nonlinear Dynamic Analysis of Seismically Isolated Single and Multiple Structures and Liquid Storage Tanks," by P.C. Tsopelas, M.C. Constantinou and A.M. Reinhorn, 4/12/94.
- NCEER-94-0011 "The Northridge, California Earthquake of January 17, 1994: Performance of Gas Transmission Pipelines," by T.D. O'Rourke and M.C. Palmer, 5/16/94.
- NCEER-94-0012 "Feasibility Study of Replacement Procedures and Earthquake Performance Related to Gas Transmission Pipelines," by T.D. O'Rourke and M.C. Palmer, 5/25/94, (PB94-206638, A09, MF-A02).
- NCEER-94-0013 "Seismic Energy Based Fatigue Damage Analysis of Bridge Columns: Part II - Evaluation of Seismic Demand," by G.A. Chang and J.B. Mander, 6/1/94, (PB95-18106, A08, MF-A02).
- NCEER-94-0014 "NCEER-Taisei Corporation Research Program on Sliding Seismic Isolation Systems for Bridges: Experimental and Analytical Study of a System Consisting of Sliding Bearings and Fluid Restoring Force/Damping Devices," by P. Tsopelas and M.C. Constantinou, 6/13/94, (PB94-219144, A10, MF-A03).
- NCEER-94-0015 "Generation of Hazard-Consistent Fragility Curves for Seismic Loss Estimation Studies," by H. Hwang and J-R. Huo, 6/14/94, (PB95-181996, A09, MF-A02).
- NCEER-94-0016 "Seismic Study of Building Frames with Added Energy-Absorbing Devices," by W.S. Pong, C.S. Tsai and G.C. Lee, 6/20/94, (PB94-219136, A10, A03).
- NCEER-94-0017 "Sliding Mode Control for Seismic-Excited Linear and Nonlinear Civil Engineering Structures," by J. Yang, J. Wu, A. Agrawal and Z. Li, 6/21/94, (PB95-138483, A06, MF-A02).
- NCEER-94-0018 "3D-BASIS-TABS Version 2.0: Computer Program for Nonlinear Dynamic Analysis of Three Dimensional Base Isolated Structures," by A.M. Reinhorn, S. Nagarajah, M.C. Constantinou, P. Tsopelas and R. Li, 6/22/94, (PB95-182176, A08, MF-A02).
- NCEER-94-0019 "Proceedings of the International Workshop on Civil Infrastructure Systems: Application of Intelligent Systems and Advanced Materials on Bridge Systems," Edited by G.C. Lee and K.C. Chang, 7/18/94.
- NCEER-94-0020 "Study of Seismic Isolation Systems for Computer Floors," by V. Lambrou and M.C. Constantinou, 7/19/94, (PB95-138533, A10, MF-A03).

- NCEER-94-0021 "Proceedings of the U.S.-Italian Workshop on Guidelines for Seismic Evaluation and Rehabilitation of Unreinforced Masonry Buildings," Edited by D.P. Abrams and G.M. Calvi, 7/20/94, (PB95-138749, A13, MF-A03).
- NCEER-94-0022 "NCEER-Taisei Corporation Research Program on Sliding Seismic Isolation Systems for Bridges: Experimental and Analytical Study of a System Consisting of Lubricated PTFE Sliding Bearings and Mild Steel Dampers," by P. Tsopelas and M.C. Constantinou, 7/22/94, (PB95-182184, A08, MF-A02).
- NCEER-94-0023 "Development of Reliability-Based Design Criteria for Buildings Under Seismic Load," by Y.K. Wen, H. Hwang and M. Shinozuka, 8/1/94, (PB95-211934, A08, MF-A02).
- NCEER-94-0024 "Experimental Verification of Acceleration Feedback Control Strategies for an Active Tendon System," by S.J. Dyke, B.F. Spencer, Jr., P. Quast, M.K. Sain, D.C. Kaspari, Jr. and T.T. Soong, 8/29/94, (PB95-212320, A05, MF-A01).
- NCEER-94-0025 "Seismic Retrofitting Manual for Highway Bridges," Edited by I.G. Buckle and I.F. Friedland, to be published.
- NCEER-94-0026 "Proceedings from the Fifth U.S.-Japan Workshop on Earthquake Resistant Design of Lifeline Facilities and Countermeasures Against Soil Liquefaction," Edited by T.D. O'Rourke and M. Hamada, 11/7/94, (PB95-220802, A99, MF-E08).
- NCEER-95-0001 "Experimental and Analytical Investigation of Seismic Retrofit of Structures with Supplemental Damping: Part I - Fluid Viscous Damping Devices," by A.M. Reinhorn, C. Li and M.C. Constantinou, 1/3/95.
- NCEER-95-0002 "Experimental and Analytical Study of Low-Cycle Fatigue Behavior of Semi-Rigid Top-And-Seat Angle Connections," by G. Pekcan, J.B. Mander and S.S. Chen, 1/5/95.
- NCEER-95-0003 "NCEER-ATC Joint Study on Fragility of Buildings," by T. Anagnos, C. Rojahn and A.S. Kiremidjian, 1/20/95, (PB95-220026, A06, MF-A02).
- NCEER-95-0004 "Nonlinear Control Algorithms for Peak Response Reduction," by Z. Wu, T.T. Soong, V. Gattulli and R.C. Lin, 2/16/95.
- NCEER-95-0005 "Pipeline Replacement Feasibility Study: A Methodology for Minimizing Seismic and Corrosion Risks to Underground Natural Gas Pipelines," by R.T. Eguchi, H.A. Seligson and D.G. Honegger, 3/2/95.
- NCEER-95-0006 "Evaluation of Seismic Performance of an 11-Story Frame Building During the 1994 Northridge Earthquake," by F. Naeim, R. DiSulio, K. Benuska, A. Reinhorn and C. Li, to be published.
- NCEER-95-0007 "Prioritization of Bridges for Seismic Retrofitting," by N. Basöz and A.S. Kiremidjian, 4/24/95, (PB95-252300, A08, MF-A02).
- NCEER-95-0008 "Method for Developing Motion Damage Relationships for Reinforced Concrete Frames," by A. Singhal and A.S. Kiremidjian, 5/11/95.
- NCEER-95-0009 "Experimental and Analytical Investigation of Seismic Retrofit of Structures with Supplemental Damping: Part II - Friction Devices," by C. Li and A.M. Reinhorn, 7/6/95, to be published.
- NCEER-95-0010 "Experimental Performance and Analytical Study of a Non-Ductile Reinforced Concrete Frame Structure Retrofitted with Elastomeric Spring Dampers," by G. Pekcan, J.B. Mander and S.S. Chen, 7/14/95, to be published.
- NCEER-95-0011 "Development and Experimental Study of Semi-Active Fluid Damping Devices for Seismic Protection of Structures," by M.D. Symans and M.C. Constantinou, 8/3/95.

